

พีริโวลิตินิลเพปไทด์นิวคลีอิกแอซิดที่มีคอนฟอร์เมชันถูกจำกัด: หน้าที่ใหม่และการประยุกต์ใช้ (DPG5780002)

ภาคผนวก 2

Reprint ของบทความที่ได้รับการตีพิมพ์

The base discriminating potential of pyrrolidinyl PNA demonstrated by magnetic Fe_xO_y particles†

Claudia Stubinitzky,^a Tirayut Vilaivan^{*b} and Hans-Achim Wagenknecht^{*a}

Cite this: *Org. Biomol. Chem.*, 2014, 12, 3586

Received 4th March 2014

Accepted 8th April 2014

DOI: 10.1039/c4ob00487f

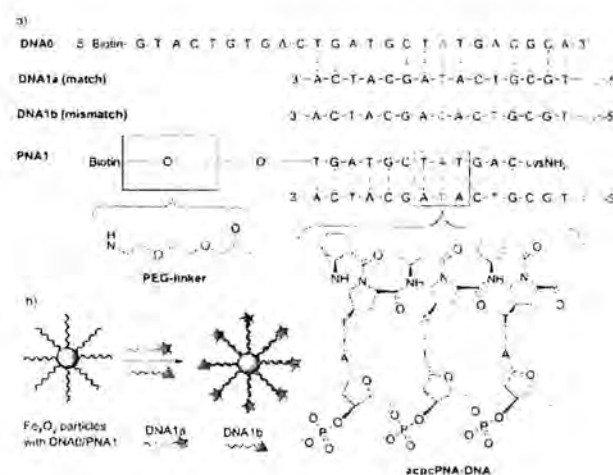
www.rsc.org/obc

Pyrrolidinyl PNA was immobilized on Fe_xO_y magnetic particles and was able to capture and thereby discriminate single base alterations in DNA counterstrands better than DNA. The selectivities of matched vs. mismatched oligonucleotides measured by the absorption differences were up to 10–12 which are remarkable values for linear probes.

Among several peptide nucleic acids (PNA)^{1,2} described as DNA analogues to date, the acpcPNA system consisting of 4'-substituted proline units with (2*R*,4'*R*) configuration in combination with (1*S*)-amino-cyclopentane-(1*S*)-carboxylic acids plays a unique role for the following reasons:^{3–5} (i) acpcPNA oligos form stable hybrids with complementary DNA but much less stable hybrids with RNA. (ii) acpcPNA recognition of DNA occurs highly sequence selectively. (iii) No self-pairing hybrids can be obtained. Fluorescence dyes such as 5-(1-pyrenyl)uracil and thiazole orange have recently been synthetically incorporated into acpcPNA to visualize the sequence selectivity with DNA by means of fluorescence.⁶ Only the fully complementary acpcPNA-DNA hybrid showed a significant fluorescence intensity increase.

Chip-based arrays as well as soluble assays with PNA allow the single nucleotide discrimination in the target DNA.^{7–9} Furthermore, the applications of DNA and PNA on inorganic particles have emerging significance as carrier systems for therapeutic purposes.^{9–17} Herein we demonstrate the potential of pyrrolidinyl PNA immobilized on inorganic magnetic particles (Fe_xO_y) for single base discrimination in capturing oligonucleotides.

The investigations started with a random acpcPNA sequence (PNA1) that carries a biotin anchor tethered *via* a short PEG linker to the N-terminus. The corresponding conventional DNA sequence (DNA0) contains a biotin group at the 5'-end. PNA1 is shorter than DNA0 to avoid solubility issues and to obtain melting temperatures (*T_m*) in a comparable range. Successful immobilization of the biotinylated oligonucleotides on streptavidin-coated Fe_xO_y magnetic particles was confirmed by the loss of absorption at 260 nm (see ESI†). In order to test and compare the base discriminating potential of PNA1 with DNA0, two DNA counterstrands were mixed in an equimolar ratio: DNA1a is fully complementary and was labeled with Cy3, whereas DNA1b contains a single mismatch and was labeled with Cy5 (Scheme 1a). Both dyes exhibit extremely high extinction coefficients that allow following the capture of oligonucleotides simply by absorption measurements. The Cy3 (550 nm) and Cy5 (645 nm) absorptions were each normalized at the beginning to obtain a comparable



Scheme 1 (a) Sequences of biotinylated DNA0 and PNA1, modified DNA counterstrands DNA1a, DNA1b and the structure of acpcPNA hybrids in detail; (b) description for single base mismatch discrimination using DNA- or PNA-immobilized Fe_xO_y-particles.

^aInstitute of Organic Chemistry, Karlsruhe Institute of Technology (KIT), Fritz-Haber-Weiz 6, 76131 Karlsruhe, Germany. E-mail: Wagenknecht@kit.edu; Fax: +49-721-608-44825; Tel: +49-721-608-47486

^bOrganic Synthesis Research Unit, Department of Chemistry, Faculty of Science, Chulalongkorn University, Phuyathai Road, Patumwan, Bangkok 10330, Thailand. E-mail: vilayut@chula.ac.th; Fax: +66-2-2187598; Tel: +66-2-2187627

† Electronic supplementary information (ESI) available: Details of synthesis of PNA1–PNA5, all DNA and PNA sequences, melting temperatures and spectroscopic analysis of the capture experiments. See DOI: 10.1039/c4ob00487f

readout. The absorbance loss at 550 nm (Cy3) and at 645 nm (Cy5) was monitored until 60 min after the addition of the magnetic particles that were previously immobilized with PNA1 (or DNA0). In both cases it was impossible to capture the corresponding oligonucleotides quantitatively, which may reflect limited accessibility of the immobilized PNA/DNA probes. A control experiment showed that the amount of the finally captured acpcPNA-DNA hybrid is comparable (i) if the acpcPNA is immobilized on the particle and subsequently annealed with the complementary DNA strand (68%) or (ii) if the acpcPNA-DNA hybrid is first annealed in solution and then immobilized on the particle (73%) (see Fig. S8 in the ESI†). As expected, immobilized DNA0 does not allow discriminating between DNA1a and DNA1b at ambient temperature (50 mM Na-P_i buffer, pH 7, with 250 mM NaCl). In fact, the selectivity of approximately 0.6 shows that the mismatched DNA1b was captured slightly more efficiently (Fig. 1). Employing a slight excess of DNA1a/DNA1b (1.2 equiv.) did not change the capture selectivity. Control capture experiments with arbitrarily chosen Cy3 and Cy5 labeled DNA using streptavidin-coated magnetic beads in the absence and presence of immobilized DNA exclude non-specific binding (see Fig. S9 in the ESI†).

In contrast, immobilized PNA1 yields a selectivity of 5-6 and thereby illustrates the base discriminating potential of

acpcPNA compared to normal DNA as a linear probe. Although the lengths of the PNA and DNA used are different, this comparison is still valid as the discrimination experiments were carried out under the situation that the relevant PNA and DNA hybrids were of comparable thermal stabilities. This experiment is complemented by considering the melting temperatures of the PNA-DNA1a/b hybrids which show remarkable differences compared to the DNA0-DNA1a/b duplexes (Table 1): (i) the T_m of the fully matched hybrid PNA1-DNA1a is significantly higher (77.5 °C) compared to the duplex DNA0-DNA1a (63.5 °C), although the sequence of PNA1 is much shorter than that of DNA0. This result shows the extraordinary stabilizing effect of acpcPNA for hybridization with DNA. The cyclic, five-membered ring spacer locks the conformation of the acpcPNA that is optimal for DNA binding.⁵ The principle of incorporating conformational rigidity into the PNA backbone to improve the binding affinity especially to DNA is the result of decreased entropy loss upon hybridization.^{9,16,17} (ii) The T_m difference of the PNA1-DNA1a (match) and PNA1-DNA1b (mismatch) hybrids is 41.0 °C. This is an astonishingly high value given the fact that the two hybrids are only differing by a single base in the DNA part, but this is fully consistent with previous studies on acpcPNA.⁴

In order to give the investigations a background that is biologically more relevant, we synthesized two pairs of acpcPNA sequences that bear the R175H mutation (CGC in PNA2 vs. CAC in PNA3)¹⁸ and the R248Q mutation (C \overline{C} G in PNA4 vs. CAG in PNA5)¹³ within the p53 gene (Scheme 2).¹⁹ DNA2 to DNA5 were used as counterstrands that either match completely (e.g. PNA2-DNA2) or form a single mismatch in the PNA-DNA hybrid (e.g. PNA2-DNA3). In all four cases, the T_m values (Table 1) of the matched PNA-DNA hybrids are significantly higher than that of the corresponding mismatched ones. However one can notice significantly less discrimination in the case of mismatches with X = G and Y = T (PNA2-DNA3, PNA2-DNA7, PNA4-DNA5, PNA4-DNA9) (ΔT_m in the range of 11.4–15.5 °C) when compared to other mismatches (ΔT_m in the range of 23.1–38.0 °C). The unusually high stability of GT mismatch is well known in the DNA field but was unexpected with respect to acpcPNA-DNA hybrids.²⁰

The capture experiments have been performed with PNA2-5 as described above. PNA3 and PNA5 discriminate the single base mismatches successfully and showed selectivities of 4–5.

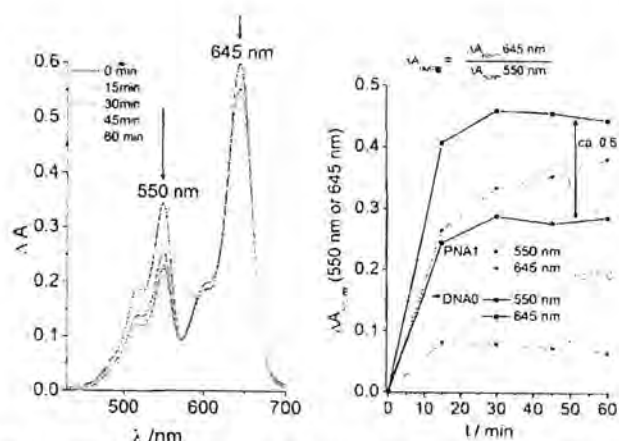
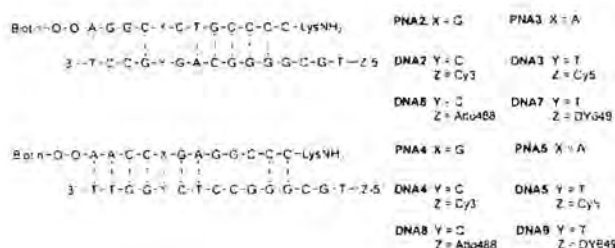


Fig. 1 (Left) UV/Vis absorption of DNA1a and DNA1b hybridized with PNA1 bearing Fe₃O₄ particles, 50 mM Na-P_i buffer, pH 7, 250 mM NaCl; (right) selectivity ΔA_{norm} of DNA0 and PNA1 towards DNA1a (complementary) and DNA1b (mismatch).

Table 1 Melting temperatures (T_m) of PNA-DNA hybrids and DNA-DNA duplexes

| Strand | Codon | Match | Codon | T_m (°C) | Mismatch | Codon | T_m (°C) | ΔT_m (°C) |
|--------|--------------------|-------|--------------------|------------|----------|--------------------|------------|-------------------|
| DNA0 | — | DNA1a | — | 63.5 | DNA1b | — | 52.5 | 11.0 |
| PNA1 | — | DNA1a | — | 77.5 | DNA1b | — | 36.5 | 41.0 |
| PNA2 | C \overline{C} G | DNA2 | G \overline{C} C | 65.1 | DNA3 | G \overline{T} G | 49.6 | 15.5 |
| PNA3 | CAC | DNA3 | G \overline{T} G | 64.1 | DNA2 | G \overline{C} C | 29.3 | 34.8 |
| PNA4 | C \overline{C} G | DNA4 | G \overline{C} C | 70.7 | DNA5 | G \overline{T} C | 55.6 | 15.1 |
| PNA5 | CAG | DNA5 | G \overline{T} C | 68.8 | DNA4 | G \overline{C} C | 43.3 | 25.5 |
| PNA2 | C \overline{C} G | DNA6 | G \overline{C} C | 67.4 | DNA7 | G \overline{T} G | 56.0 | 11.4 |
| PNA3 | CAC | DNA7 | G \overline{T} G | 73.9 | DNA6 | G \overline{C} C | 35.9 | 38.0 |
| PNA4 | C \overline{C} G | DNA8 | G \overline{C} C | 70.5 | DNA9 | G \overline{T} C | 57.1 | 13.4 |
| PNA5 | CAG | DNA9 | G \overline{T} C | 69.4 | DNA8 | G \overline{C} C | 46.3 | 23.1 |



Scheme 2 Sequences of PNA2–PNA4 and DNA2–DNA9.

5–6 for the matched PNA–DNA hybrids. In contrast, the capture experiments with immobilized PNA2 and PNA4 failed as the selectivities were approximately 1 or even lower (Fig. 2).

In principle, there are three differences between the capture experiments that showed selectivity and the unselective ones: (i) the sequence mainly differs by the match/mismatch A–T/A–C pairs in the hybrids of PNA3 and PNA5 compared to the G–C/G–T pairs in the hybrids of PNA2 and PNA4. (ii) ΔT_m of PNA3 and PNA5 are >20 °C as described for PNA1, whereas the corresponding T_m differences of the hybrids with PNA2 and PNA4 are lower. Nevertheless in all cases ΔT_m is higher than that of DNA–DNA hybrids containing the same sequence (ESI†). (iii) The modification of complementary counterstrands is different (Cy5 vs. Cy3). The question is whether the observed differences in selectivities have to be mainly attributed to the sequence issues followed by differences in ΔT_m or to undesired dye interactions.

In order to follow this question, the capture experiments of PNA2–PNA5 were repeated with oligonucleotides DNA6/7 and DNA8/9 bearing a different dye combination. The Cy3 dye of DNA2 and DNA4 was replaced by the Atto488 dye in DNA6 and DNA8, and the Cy5 dye of DNA3 and DNA5 was replaced by the DY649 dye in DNA7 and DNA9. Although the optical properties are similar to Cy3 and Cy5, Atto488 and DY649 exhibit negative charges in contrast to the cationic Cy3/Cy5 dyes. The T_m values of this additional set of PNA–DNA hybrids showed similarities

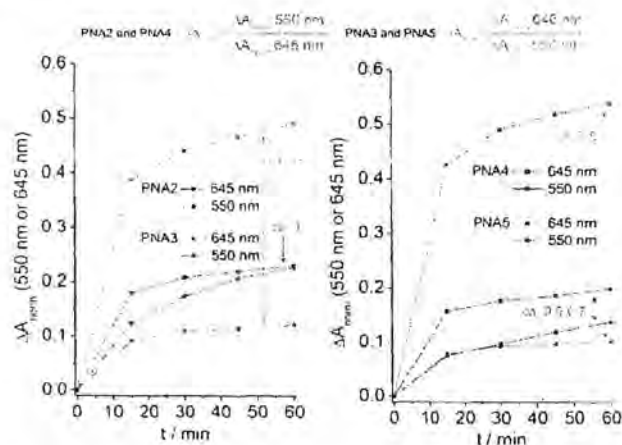


Fig. 2 Selectivity ΔA_{norm} of PNA2/PNA3 (left) and selectivity ΔA_{norm} of PNA4/PNA5 (right) towards matched and mismatched counterstrands.

to the previously described set (Table 1). The T_m were also compared with those of the corresponding duplexes without dyes, which gave similar values (ESI†). This result rules out possible dye interaction that influences the stability of the PNA–DNA duplexes.

Interestingly, the selectivities in the capture experiments that were obtained were improved with PNA3 and PNA5 from values of 4–5/5–6 to 9–10/11–12 (15 min after the addition of the magnetic particles to the oligonucleotide mixture) (Fig. 3). This result seems to be surprising since the T_m values were quite similar and not affected by the dyes. We attribute the selectivity improvement to the charge of the dyes: between the positively charged Cy3 and Cy5 dyes, heterodimeric and homodimeric interactions occur that let the oligonucleotides bind to each other and interfere with binding to the immobilized PNA strand on the particle. Typically, such excitonic interactions are indicated by the ratios of the absorption maxima as given by the (0 → 0/0 → 1 vibronic) fine structure of the dyes. This was successfully demonstrated e.g. for the perylene bisimide^{21,22} and the thiazole orange dye.^{23,24} The absorption ratio between ΔA at 602 nm and ΔA at 645 nm for the Cy5 decreases during the capture experiments of PNA3 and PNA5 with DNA3/DNA2 and DNA5/DNA4, respectively (see Fig. S10 in the ESI†). This indicates that the Cy5 dyes as terminal labels of the corresponding oligonucleotides are aggregated and get isolated during the capturing process onto the immobilized PNA. In the case of the negatively charged Atto488 and DY649 dyes, these dye–dye interactions were not observed as the corresponding absorption ratio at 610 nm and 652 nm for the Dy649 dye remains unchanged. Nevertheless, a selective capture of the completely matched oligonucleotide is still not possible for PNA2 and PNA4. This clearly shows that the differences between PNA2/PNA4 and PNA3/PNA5 have to be attributed to their sequential context, most likely to the high stability of the GT mismatch.²⁵

Furthermore the negatively charged dyes Atto488 and DY649 enable a fully reversible annealing and dehybridisation of DNA strands to PNA4 and PNA5 that has not been possible with the corresponding Cy3- and Cy5-labeled oligonucleotides DNA2 and DNA3. By heating up the particles to 80 °C for

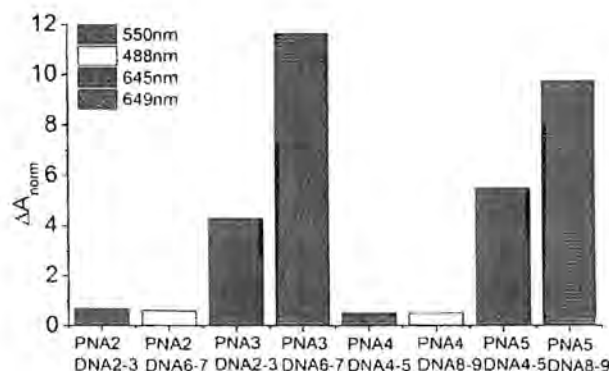


Fig. 3 Selectivity ΔA_{norm} of PNA2–5 towards complementary DNA labeled counterstrands 15 min after the addition of the magnetic particles to the oligonucleotide mixture.

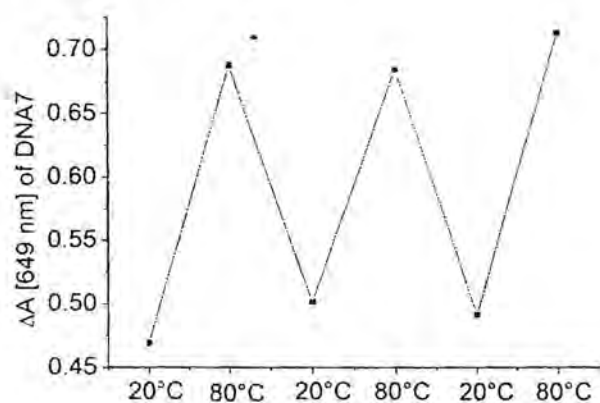


Fig. 4 Absorption differences by release and capture of DNA7 using particles bearing immobilized PNA3.

10 min the Atto488- or DY649-labeled DNA counterstrands can be fully released and subsequently recaptured (Fig. 4). This again supports the interpretation mentioned above that the negative charge of the dyes inhibits dye-dye interactions that interfere with selective capturing.

In conclusion we showed that acpcPNA can be immobilized on Fe_3O_4 magnetic particles and is potentially able to reversibly discriminate single base alterations in DNA counterstrands better than DNA itself. This can be followed by absorption and potentially also by fluorescence. The selectivities of matched vs. mismatched oligonucleotides measured by the absorption differences were up to 10–12. These values are remarkable for linear probes. The rates of hybridization of a matched vs. a mismatched DNA target were nearly the same in our experiments. Hence, the selectivity of the oligonucleotide capturing seems to primarily be driven by thermodynamics and the relative stability of the acpcPNA-DNA hybrid. A ΔT_m of at least 20 °C is required to obtain selectivity. Such ΔT_m differences can be easily obtained in acpcPNA-DNA hybrids (except the GT mismatch) and clearly show the base discriminating potential of this pyrrolidinyl PNA.

Acknowledgements

Financial support by the Deutsche Forschungsgemeinschaft (DFG), KJT and the Thailand Research Fund (DPG5780002) is gratefully acknowledged. Claudia Stubinitzky thanks the Karlsruhe House of Young Scientists (KHYS) for a short-term doctoral fellowship. Tirayut Vilaivan received a research fellowship under the support of the Alexander von Humboldt Foundation.

Notes and references

- P. E. Nielsen, M. Egholm, R. H. Berg and O. Buchardt, *Science*, 1991, **254**, 1497–1500; M. Egholm, O. Buchardt, L. Christensen, C. Behrens, S. M. Freier, D. A. Driver, R. H. Berg, S. K. Kim, B. Norden and P. E. Nielsen, *Nature*, 1993, **365**, 566–568.
- B. Hyrup and P. E. Nielsen, *Bioorg. Med. Chem.*, 1996, **4**, 5–23.
- T. Vilaivan and G. Lowe, *J. Am. Chem. Soc.*, 2002, **124**, 9326–9327.
- T. Vilaivan and C. Srisuwannaket, *Org. Lett.*, 2006, **8**, 1879–1900; C. Vilaivan, C. Srisuwannaket, C. Ananthanawat, C. Suparpprom, J. Kawakami, Y. Yamaguchi, Y. Tanaka and T. Vilaivan, *Artif. DNA PNA XNA*, 2011, **2**, 50–59.
- W. Mansawat, C. Vilaivan, Á. Balázs, D. J. Aitken and T. Vilaivan, *Org. Lett.*, 2012, **14**, 1440–1443.
- C. Boonlua, C. Vilaivan, H.-A. Wagenknecht and T. Vilaivan, *Chem. – Asian J.*, 2011, **12**, 3251–3259; B. Ditmangklo, C. Boonlua, C. Suparpprom and T. Vilaivan, *Bioconjugate Chem.*, 2013, **24**, 614–625.
- K. Matsumoto, E. Nakata, T. Tamura, I. Saito, Y. Aizawa and T. Morii, *Chem. – Eur. J.*, 2013, **19**, 5034–5504.
- M. F. Ali, R. Kirby, A. P. Goodey, M. D. Rodriguez, A. D. Ellington, D. P. Neikirk and J. T. McDevitt, *Anal. Chem.*, 2013, **75**, 4732–4739.
- J. K. Pokorski, M. A. Witschi, B. L. Purnell and D. H. Appella, *J. Am. Chem. Soc.*, 2004, **126**, 15067–15073; C. M. Micklitsch, B. Y. Oqu岸, C. Zhao and D. H. Appella, *Anal. Chem.*, 2013, **85**, 251–257.
- A. Rolland, *Advanced Gene Delivery: From Concepts to Pharmaceutical Products*, Harwood, Amsterdam, 1999.
- G. P. H. Dietz and M. Bahr, *Mol. Cell. Neurosci.*, 2004, **27**, 85–131.
- R. Langer and N. A. Peppas, *AIChE J.*, 2003, **49**, 2990–3006.
- W. C. Heiser, *Gene Delivery to Mammalian Cells*, Humana Press, Totowa, New Jersey, 2004.
- V. Sokolova and M. Epple, *Angew. Chem., Int. Ed.*, 2008, **47**, 1382–1395.
- Y. Chen, H. Chen and J. Shi, *Mol. Pharmaceutics*, 2014, DOI: 10.1021/mp400596v.
- V. A. Kumar and K. N. Ganesh, *Acc. Chem. Res.*, 2005, **38**, 404–412.
- R. J. Worthington, A. P. O'Rourke, J. Morral, T. H. S. Tan and J. Mickelfield, *Org. Biomol. Chem.*, 2007, **5**, 249–259.
- A. N. Bullock and A. R. Fersht, *Nat. Rev. Cancer*, 2001, **1**, 68–76.
- P. Lamb and L. Crawford, *Mol. Cell Biol.*, 1986, **6**, 1379–1385.
- S. Pan, X. Sun and J. K. Lee, *Int. J. Mass Spectrom.*, 2006, **253**, 238–248; P. S. Ho, C. A. Frederick, G. J. Quigley, G. A. van der Marel, J. H. van Boom, A. H. Wang and A. Rich, *EMBO J.*, 1985, **4**, 3617–3623.
- P. P. Neelakandan, Z. Pan, M. Hariharan, Y. Zheng, H. Weissman, B. Rybtchinski and F. D. Lewis, *J. Am. Chem. Soc.*, 2010, **132**, 15808–15813.
- D. Baumstark and H.-A. Wagenknecht, *Angew. Chem., Int. Ed.*, 2008, **47**, 2612–2614.
- A. Okamoto, *Chem. Soc. Rev.*, 2011, **40**, 5815–5828.
- S. Berndl and H.-A. Wagenknecht, *Angew. Chem., Int. Ed.*, 2009, **48**, 2418–2421.



Synthesis and optical properties of pyrrolidinyl peptide nucleic acid carrying a clicked Nile red label

Nattawut Yotapan¹, Chayan Charoenpakdee¹, Pawinee Wathanathavorn¹,
Boonsong Ditmangklo¹, Hans-Achim Wagenknecht² and Tirayut Vilaivan^{*1}

Full Research Paper

Address:

¹Organic Synthesis Research Unit, Department of Chemistry, Faculty of Science, Chulalongkorn University, Phayathai Road, Patumwan, Bangkok 10330, Thailand and ²Institute of Organic Chemistry, Karlsruhe Institute of Technology (KIT), Fritz-Haber-Weg 6, 76131 Karlsruhe, Germany

Email:

Hans-Achim Wagenknecht^{*} - wagenknecht@kit.edu;
Tirayut Vilaivan^{*} - tvilaivan@chula.ac.th

^{*} Corresponding author

Keywords:

click chemistry; deoxyribonucleic acid; DNA bulge; fluorescence; nucleic acids; solvatochromism

Beilstein J. Org. Chem. 2014, 10, 2166–2174.

doi:10.3762/bjoc.10.224

Received: 08 May 2014

Accepted: 19 August 2014

Published: 11 September 2014

This article is part of the Thematic Series "Nucleic acid chemistry".

Associate Editor: S. Flitsch

© 2014 Yotapan et al; licensee Beilstein-Institut.

License and terms: see end of document.

Abstract

DNA or its analogues with an environment-sensitive fluorescent label are potentially useful as a probe for studying the structure and dynamics of nucleic acids. In this work, pyrrolidinyl peptide nucleic acid (acpcPNA) was labeled at its backbone with Nile red, a solvatochromic benzophenoxazine dye, by means of click chemistry. The optical properties of the Nile red-labeled acpcPNA were investigated by UV–vis and fluorescence spectroscopy in the absence and in the presence of DNA. In contrast to the usual quenching observed in Nile red-labeled DNA, the hybridization with DNA resulted in blue shifting and an enhanced fluorescence regardless of the neighboring bases. More pronounced blue shifts and fluorescence enhancements were observed when the DNA target carried a base insertion in close proximity to the Nile red label. The results indicate that the Nile red label is located in a more hydrophobic environment in acpcPNA–DNA duplexes than in the single-stranded acpcPNA. The different fluorescence properties of the acpcPNA hybrids of complementary DNA and DNA carrying a base insertion are suggestive of different interactions between the Nile red label and the duplexes.

Introduction

Fluorescent labels are important tools for investigating the structure and dynamics of biomolecular interactions [1–3]. Traditionally, the biological macromolecules are labeled with two or more dyes which can interact in a conformation/distant-

dependent manner via Förster resonance energy transfer (FRET) [4–6]. Alternatively, the FRET pairs can be replaced by an environmentally sensitive label that can change its fluorescence in response to its altered micro-environment [7–9]. Nile

red is a member of the benzophenoxazine dye family which exhibits several interesting features including a high photostability, high fluorescence quantum yield, broad working pH range, long excitation and emission wavelengths, and solvatochromic properties [10]. Applications of Nile red as a staining dye in histology [11,12] and as a probe for the sensing of polarity and hydrophobicity [13] are well-known. Nile red has been used as a DNA label, either as a base modifier [14–16], a base replacement [17] or a backbone-tethered label [18,19]. However, in most cases the formation of DNA duplexes does not yield significant fluorescence changes in the Nile red, unless it is used in combination with another dye such as pyrene to form an energy transfer pair [20,21]. A related phenoxazine dye – Nile blue – has also been incorporated into DNA as a base replacement, again without showing significant structure-induced fluorescence change [22].

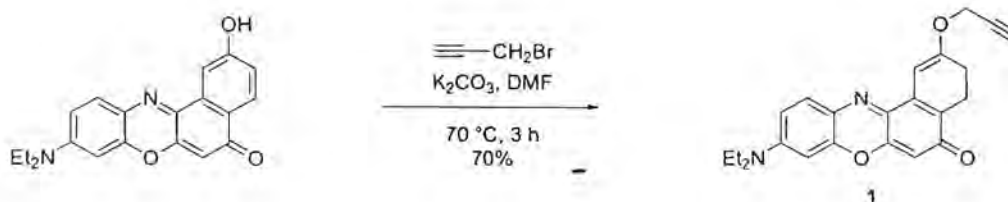
Peptide nucleic acid or PNA is an electrostatically neutral analogue of DNA which can form very stable duplexes with DNA and RNA in a highly sequence specific fashion. PNA–DNA duplexes have different structural morphology and electrostatic potential surfaces from DNA–DNA duplexes and therefore they are interacting differently with DNA-binding dyes [23–25]. We had recently introduced a new conformationally constrained pyrrolidinyl PNA known as acpcPNA that shows several unique properties [26–28]. Its potential applications as a probe for DNA sensing are well-established. For example, we have developed singly labeled acpcPNA probes that can give a fluorescence change in response to hybridization to DNA [29–31]. Due to its solvatochromic properties, Nile red is a potential candidate to be used in combination with PNA to develop a hybridization probe which not only differentiates between complementary and non-complementary DNA, but can also report on local structural variations. Except for an example from our group on the conformation control of Nile red-labeled DNA by acpcPNA [32], no combination of the Nile red label and PNA has yet been reported in the literature. It is therefore our purpose to develop a facile method for synthesizing Nile red-labeled acpcPNA based on the click strategy [33–36] and to investigate its optical properties.

Results and Discussion

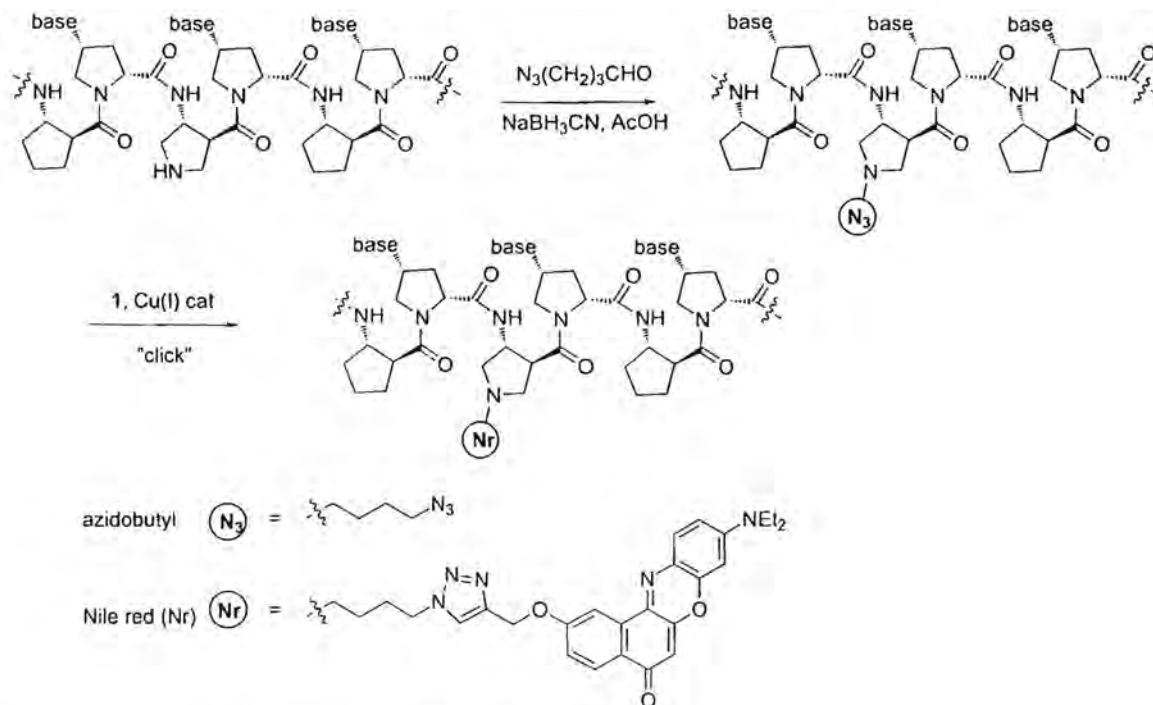
At least two different means to introduce the Nile red label onto DNA by using click chemistry have been reported in the literature. One involves the clicking of in situ generated 5-azido-deoxyuridine-containing DNA with propargyl Nile red [16], the other employs DNA bearing 2'-propargylated nucleotides and azide-modified Nile red [19]. An approach related to the latter was used in this work, although the azide function was placed on the PNA instead of the Nile red, and the clicking was carried out on the solid support rather than in solution phase. The propargylated Nile red label **1** was synthesized in 70% yield by alkylation of the known 2-hydroxy Nile red [37,38] with propargyl bromide in the presence of K_2CO_3 in DMF (Scheme 1).

The alkyne-containing compound **1** was clicked onto the backbone of acpcPNA that had been pre-functionalized with an azidobutyl group by a reductive alkylation strategy previously reported by our group (Scheme 2) [31]. Two lysine residues were incorporated at the N- and C-termini of the acpcPNA to ensure a sufficient solubility in aqueous solution. Five acpcPNA sequences, each of which singly labeled at the backbone with Nile red under different sequence context, were successfully synthesized and characterized by MALDI–TOF MS (Figure 1 and Table 1). Isolated yields in the range of 6–18% were obtained (0.5 μ mol scale), which are typical for solid phase synthesis, whereby the majority of material loss occurred during HPLC purification. All Nile red-labeled acpcPNAs are freely soluble in water (>1 mM), providing a bright blue solution.

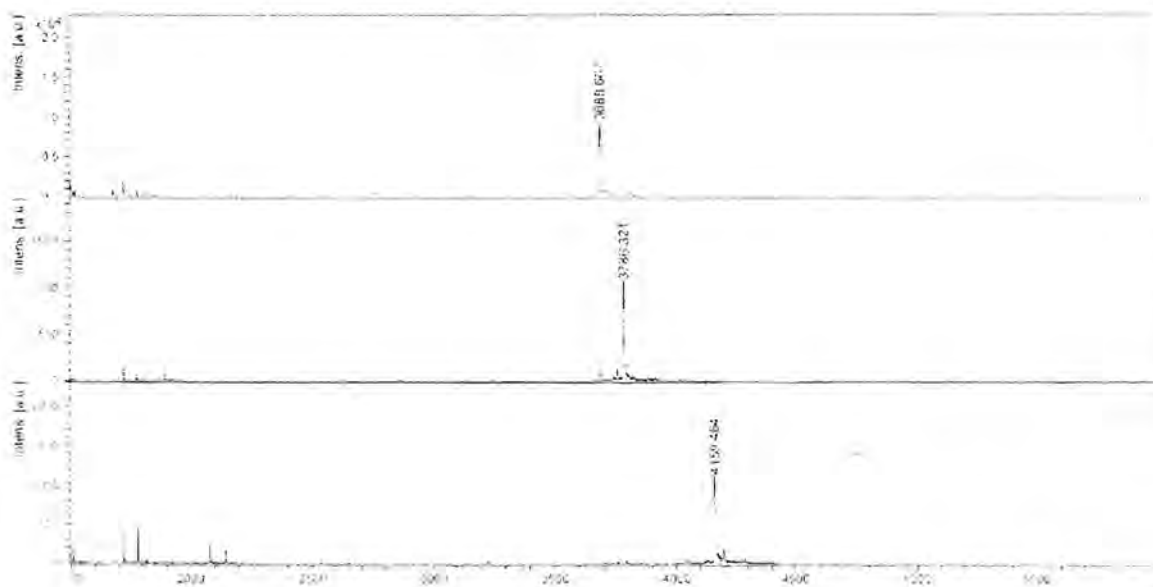
The UV–vis spectrum of the free propargyl Nile red label **1** in acetonitrile (Figure 2a) showed absorption and fluorescence emission maxima at 538 nm and 620 nm, with a fluorescence quantum yield (Φ_F) of 0.65, which is quite comparable to other Nile red derivatives reported in the literature [10]. As the polarity of the solvent increases with the addition of aqueous phosphate buffer, both the absorption and the fluorescence maxima shifted to longer wavelengths with a concomitant decrease in the fluorescence quantum yields (50% MeCN: λ_{abs} 564 nm, λ_{em} 641 nm, Φ_F 0.29; 20% MeCN: λ_{abs} 587 nm, λ_{em}



Scheme 1: Synthesis of propargylated Nile red **1**.



Scheme 2: Synthesis of azidobutyl- and Nile red-modified acpCPNA.

Figure 1: MALDI-TOF mass spectra of the crude 10mer acpCPNA before (top) (calcd m/z 3688.0), and after functionalizing with the azidobutyl group (middle) (calcd m/z 3785.1), and followed by clicking with Nile red (bottom) (calcd m/z 4157.5).

651 nm; Φ_F 0.14). In aqueous phosphate buffer (10 mM, pH 7.0), the Nile red-labeled acpCPNA 10mer-Nr exhibited a broad absorption peak centered at 575 nm and a fluorescence

emission at 656 nm, respectively (Figure 2b). The solvatochromic property of the Nile red-labeled acpCPNA is demonstrated as shown by the progressively blue-shifted absorption

Table 1: Sequence, isolated yield and characterization data of Nile red-labeled acpcPNA.

| PNA | sequence (N to C) ^a | t _R (min) ^b | % yield ^c | m/z ^d (calcd) | m/z ^e (found) |
|------------|--------------------------------|-----------------------------------|----------------------|-----------------------------|-----------------------------|
| 10mer-Nr | GTAGA(Nr)TCACT | 33.6 | 6.3 | 4157.5 | 4155.1 |
| 11merAA-Nr | CATAA(Nr)AATACG | 34.2 | 18.5 | 4491.9 | 4491.1 |
| 11merCC-Nr | CATAC(Nr)CATACG | 34.6 | 11.4 | 4443.9 | 4441.8 |
| 11merGG-Nr | CATAG(Nr)GATACG | 32.8 | 15.2 | 4523.9 | 4523.2 |
| 11merTT-Nr | CATAT(Nr)TATACG | 34.3 | 8.4 | 4473.9 | 4473.0 |

^aAll sequences were end-capped at N- and C-termini with *N*-acetyl-L-lysine and L-lysineamide, respectively. ^bHPLC conditions: C18 column 4.6 × 50 mm, 3 μ, gradient 0.1% TFA in H₂O:MeOH 90:10 for 5 min then linear gradient to 10:90 over 30 min, flow rate 0.5 mL/min, 260 nm. ^cIsolated yield (determined spectrophotometrically) after HPLC purification. ^dAverage mass of [M + H]⁺. ^eMALDI-TOF.

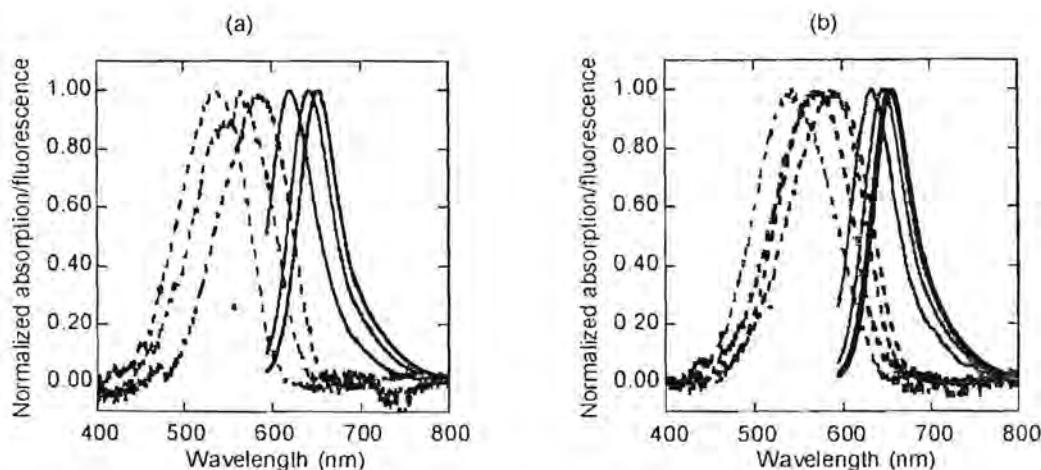


Figure 2: Normalized absorption (---) and fluorescence (—) spectra of (a) propargyl Nile red 1 and (b) Nile red-labeled acpcPNA 10mer-Nr in 10 mM sodium phosphate buffer (pH 7.0):acetonitrile: black = 100:0; blue = 80:20; green = 50:50; red = 0:100. All measurements were carried out in 10 mM sodium phosphate buffer (pH 7.0), [PNA] and [1] = 1.0 μM at 20 °C with λ_{ex} = 580 nm.

and fluorescence emission maxima in the presence of acetonitrile (100% MeCN: λ_{abs} 544 nm, λ_{em} 634 nm; 50% MeCN: λ_{abs} 569 nm, λ_{em} 647 nm; 20% MeCN: λ_{abs} 592 nm, λ_{em} 654 nm). The fluorescence spectrum of the Nile red-labeled acpcPNA is notably red-shifted compared to the fluorescence spectrum of the free Nile red label in the same solvent. This suggests possible interactions between the Nile red label and the PNA base or backbone. Nevertheless, the Nile red in the acpcPNA 10mer-Nr was not quenched as indicated by the quantum yield value being similar to that of the free label (10mer-Nr: Φ_F = 0.16; 1: Φ_F = 0.14 in 20% MeCN). Unfortunately, the value can only be compared in an acetonitrile:water mixture as compound 1 is essentially insoluble in water.

Melting temperature data and optical properties of the Nile red-labeled acpcPNAs and their hybrids with various DNA are summarized in Table 2. Thermal denaturation experiments suggest that the Nile red-labeled acpcPNA 10mer-Nr can form

a stable hybrid with complementary DNA. In contrast to some other labels such as pyrene which usually destabilize acpcPNA–DNA duplexes [30,31], the T_m of the complementary DNA hybrid of Nile red-labeled PNA (58.8 °C by UV or 56.9 °C by fluorescence) was comparable to the T_m of unlabeled acpcPNA with an identical sequence (57.6 °C) [26]. Absorption spectra of 10mer-Nr and its complementary DNA duplex show differences in the Nile red region as shown by the sharpening and red shift of the absorption maxima (λ_{max} = 575 and 598 nm in single stranded and duplex, respectively). Importantly, fluorescence spectra of the duplex showed a pronounced blue shift of the emission maxima (647 nm) compared to the single-stranded PNA (656 nm) as well as a small fluorescence increase (1.36 fold at 643 nm) (Figure 3a,b). The blue-shifted fluorescence maxima and increased quantum yields of Nile red suggest that the Nile red chromophore in complementary PNA–DNA duplexes was placed in a less polar environment compared to its placement in single-stranded PNA. Although

Table 2: T_m and optical properties of Nile red-labeled acpcPNA^a.

| PNA | DNA (5' to 3') ^b | T_m (°C) ^c | λ_{abs} | λ_{em} ^d | Φ_F ^e | F/F_0 ^f |
|------------|-----------------------------|-------------------------|-----------------|-----------------------------|-----------------------|----------------------|
| 10mer-Nr | none | – | 575 | 656 | 0.11 | – |
| | AGT <u>GAT</u> CTAC | 58.8 (56.9) | 598 | 647 | 0.15 | 1.36 |
| | AGT <u>GCT</u> CTAC | 37.5 (36.7) | 585 | 648 | 0.17 | 1.72 |
| | AGT <u>CAT</u> CTAC | 37.7 (37.5) | 589 | 649 | 0.14 | 1.43 |
| | AGT <u>GAC</u> CTAC | 40.8 (41.3) | 592 | 652 | 0.15 | 1.70 |
| | AGT <u>GACT</u> CTAC | 46.9 (52.0) | 589 | 643 | 0.29 | 2.91 |
| | AGT <u>GAAT</u> CTAC | 40.1 (46.7) | 588 | 648 | 0.20 | 2.60 |
| | AGT <u>GATT</u> CTAC | 54.7 (52.7) | 591 | 649 | 0.22 | 2.65 |
| | AGT <u>GAGT</u> CTAC | 42.2 (46.0) | 593 | 645 | 0.20 | 3.31 |
| | AGT <u>CGAT</u> CTAC | N.D. ^g | 591 | 648 | 0.14 | 1.16 |
| | AGT <u>GATC</u> CTAC | N.D. ^g | 597 | 653 | 0.10 | 0.87 |
| | AGT <u>GCC</u> CTAC | N.D. ^g | 585 | 648 | 0.17 | 1.45 |
| | AGT <u>GACC</u> CTAC | N.D. ^g | 593 | 652 | 0.13 | 1.23 |
| | AGT <u>GACTC</u> CAC | N.D. ^g | 585 | 647 | 0.13 | 1.24 |
| 11merAA-Nr | none | – | 598 | 657 | 0.15 | – |
| | CGTATTTATG | 76.0 | 600 | 651 | 0.23 | 1.55 |
| | CGTATTCATG | 74.7 | 593 | 645 | 0.33 | 2.34 |
| 11merCC-Nr | none | – | 594 | 656 | 0.08 | – |
| | CGTATGGTATG | 67.4 | 594 | 646 | 0.19 | 2.49 |
| | CGTATGCGTATG | 71.2 | 598 | 644 | 0.13 | 1.79 |
| 11merGG-Nr | none | – | 599 | 660 | 0.04 | – |
| | CGTATCCTATG | (62.3) | 599 | 655 | 0.15 | 3.27 |
| | CGTATCCCTATG | (62.3) | 599 | 652 | 0.10 | 2.46 |
| 11merTT-Nr | none | – | 588 | 655 | 0.09 | – |
| | CGTATAATATG | 76.6 | 602 | 654 | 0.19 | 2.05 |
| | CGTATACATATG | 76.0 | 590 | 646 | 0.29 | 3.44 |

^aAll measurements were carried out in 10 mM sodium phosphate buffer (pH 7.0), [PNA] = 1.0 μ M; [DNA] = 1.2 μ M at 20 °C. ^bUnderlined and boldface letters in DNA sequences indicate the position of mismatch and base insertion, respectively. ^cDetermined by UV-vis (260 nm) and/or fluorescence spectrophotometry (643 nm, shown in parentheses). ^d λ_{ex} = 580 nm. ^eCresyl violet was used as a standard (Φ = 0.54 in MeOH) [41]. ^f F/F_0 was calculated from the ratio of fluorescence of duplex divided by the single-stranded PNA at 643 nm. ^gNot determined.

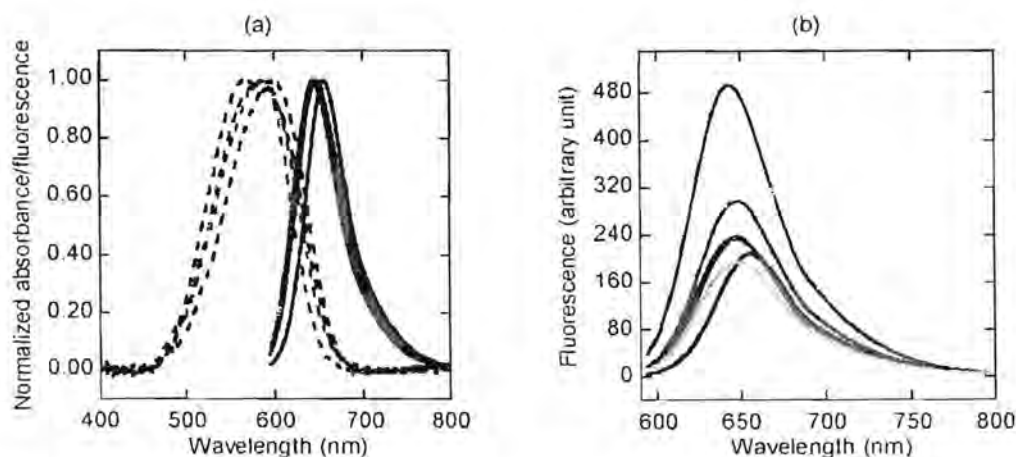


Figure 3: (a) Normalized absorption (—) and fluorescence (---) spectra and (b) fluorescence spectra of Nile red-labeled acpcPNA 10mer-Nr in the absence (black) and presence of various DNA sequences (5'→3'): blue = AGTGATCTAC (complementary); green = AGTGCTCTAC (mismatched); red = AGTGACTCTAC (bulged); pink = AGTGCCCTAC (bulged with mismatch); orange = AGTCGATCTAC (misplaced bulge). All measurements were carried out in 10 mM sodium phosphate buffer (pH 7.0), [PNA] = 1.0 μ M; [DNA] = 1.2 μ M at 20 °C with λ_{ex} = 580 nm.

the related benzophenoxazine dye Nile blue binds to DNA by intercalation, the binding results in a bathochromic shifting and a quenched fluorescence [39,40]. Based on this, together with the fact that PNA–DNA duplexes are not good substrates for intercalative binding [23], we propose that the Nile red is more likely to bind to the groove of the PNA–DNA duplex rather than intercalate into the base stacks.

In the presence of a mismatched base in the DNA strand, the T_m of the duplex was decreased as expected. For example, the mismatched hybrid of **10mer-Nr** with the DNA carrying a mismatched base in close proximity to the position of the Nile red label showed T_m values in the range of 37–41 °C. Fluorescence spectra of these mismatched DNA duplexes showed blue-shifted and enhanced fluorescence emissions similar to the complementary duplex, which ranged from 1.4 to 1.7 fold compared to the one of single-stranded Nile red-labeled acpPNA. This suggests that the Nile red label can still noticeably interact with the mismatched duplexes.

The most remarkable feature of the Nile red-labeled acpPNA **10mer-Nr** is the relatively large fluorescence increase after the hybridization with DNA targets which carry a base insertion in close proximity to the Nile red label. As shown in Table 2, these duplexes showed more pronounced fluorescence increases (2.6–3.3 fold) than the complementary or mismatched duplexes (1.4–1.7 fold relative to the single-stranded **10mer-Nr**). The fluorescence maxima were also further blue-shifted relative to the single-stranded and complementary duplexes of Nile red-labeled acpPNA (Figure 3a,b). These results suggest that the Nile red label in these duplexes adopts a different configuration to the complementary and the single-mismatched duplexes. When the DNA strand carries an extra inserted base, the only way it can form a stable hybrid is to form a bulge on the DNA strand at the insertion site. This is supported by the unusually high T_m values (46–53 °C) for these duplexes. In addition, consistent fluorescence increases were observed regardless of the nature of the inserted base. Based on these findings we propose that the extra DNA base is looped out to form a bulge which can accommodate the Nile red label. A similar binding mode has been proposed earlier for pyrene-labeled DNA [42]. When the inserted base was misplaced, i.e., away from the Nile red label, or when a mismatch base was introduced elsewhere in the DNA strand, the fluorescence change was small (Figure 3b, Figure S11 and Figure S12, Supporting Information File 1), suggesting that the fluorescence increase was due to a specific interaction between the Nile red label and the bulge site. The addition of β -cyclodextrin to the bulged duplexes caused no change in the fluorescence of the Nile red label, whereas a marked blue shift was observed with single-stranded PNA (8 nm) (Figure S17, Supporting Information File 1). This

experiment confirmed that the Nile red label is buried well within the hydrophobic pocket of the bulged duplexes and therefore not available to form an inclusion complex with the cyclodextrins [17]. Less pronounced shifts were observed with complementary and mismatched duplexes (2 and 4 nm, respectively) upon the addition of cyclodextrin, which indicates possible interactions between the groove-bound Nile red and cyclodextrin.

To better understand the effect of neighboring bases on the optical properties of the Nile red-labeled acpPNA and its duplexes with DNA, four Nile red-labeled acpPNA sequences (**11merAA-Nr**, **11merCC-Nr**, **11merGG-Nr**, **11merTT-Nr**) were synthesized. These four Nile red-labeled acpPNA sequence exhibited differences only at the bases flanking the Nile red label. For single-stranded PNA, the order of fluorescence quantum yields was AA > TT ~ CC > GG. This suggests a more efficient quenching of the Nile red label by neighboring G than by other nucleobases. A is almost non-quenching as shown by the high quantum yield of **11merAA-Nr** ($\Phi_F = 0.15$), which is comparable to the high quantum yield of the free Nile red label ($\Phi_F = 0.14$). On the other hand, the presence of two flanking G in **11merGG-Nr** resulted in a decrease of the quantum yield of more than 70% ($\Phi_F = 0.04$). Upon hybridization with complementary DNA targets, the fluorescence quantum yields of all four hybrids were increased to a similar range ($\Phi_F = 0.15$ –0.23). However, since the initial fluorescence of **11merGG-Nr** was low, the fluorescence change was more pronounced (3.27 fold) than other sequences (1.55–2.49 fold). When a bulge was introduced, a larger fluorescence increase was observed in duplexes with neighboring A-T than G-C pairs. Accordingly, the bulged duplexes of **11merAA-Nr** and **11merTT-Nr** became more fluorescent than the corresponding complementary duplexes. Opposite results were observed with **11merCC-Nr** and **11merGG-Nr**, that is, the complementary duplexes exhibited higher fluorescence than the bulged duplexes. In all cases the fluorescence emission maxima of the bulged duplex were at shorter wavelengths than fluorescence emission maxima of the complementary duplexes and single-stranded PNA. These results clearly support our hypothesis of the different placement of the Nile red label in the complementary and bulged duplexes.

Although Nile red has been previously incorporated in DNA either through a base substitution or modification, these Nile red-labeled DNAs do not show appreciable fluorescence changes in response to the hybridization with DNA regardless of the mode of Nile red attachment [14,17,18]. In most cases, the pairing of Nile red-labeled DNA with another DNA strand resulted in unchanged or decreased fluorescence quantum yields. This, together with the red-shifted absorption and fluo-

rescence spectra in comparison to single-stranded DNA, suggests that Nile red may intercalate into the base stack of DNA–DNA duplexes. The behavior of the Nile red label in acpcPNA is completely different, as shown by the consistent increase in the fluorescence quantum yield upon hybridization with complementary DNA irrespective of the nature of the flanking bases. In such duplexes, the Nile red is expected to interact with the PNA–DNA duplexes by means of groove binding, which results in a lower localized polarity around the Nile red chromophore and gives rise to the observed blue shifts and the fluorescence increase. In addition, a larger increase in fluorescence was also observed with DNA targets that can form a bulge in the vicinity of the Nile red label. We propose that the Nile red label is buried within the looped out structure of the bulged duplex, which gives rise to an even more pronounced blue shift and fluorescence increase, except when there are nearby G–C base pairs which may quench the fluorescence.

Conclusion

We successfully synthesized the propargylated Nile red **1** and clicked it onto acpcPNA with an azide-modified backbone. The solvatochromic properties of the Nile red label is retained in the labeled acpcPNA. Quenching of the Nile red label by neighboring bases in acpcPNA increases in the order of A > T – C > G. The hybridization with fully complementary DNA and DNA with an inserted base consistently resulted in blue-shifted and enhanced fluorescence. This indicates that the Nile red label in acpcPNA–DNA duplexes is in a more hydrophobic environment compared to when the Nile red label is in single-stranded acpcPNA. Based on spectroscopic evidence, we propose that either the Nile red label resides within the groove (complementary duplexes) or the hydrophobic pocket formed by the looped-out base (bulged duplexes) rather than intercalating into the base stacks.

Experimental

General remarks

All chemicals were obtained from standard suppliers and used as received. Anhydrous DMF for peptide synthesis was purchased from RCI Labscan (Thailand). All other solvents were AR or HPLC grade and were used without further purification. Oligonucleotides were obtained from Pacific Science (Thailand) or BioDesign (Thailand). The water used in all experiments was obtained from an ultrapure water system fitted with a Millipak® 40 filter unit.

Synthesis of propargyl Nile red **1**

2-Hydroxy Nile red [37] (140.1 mg, 0.41 mmol) was dissolved in anhydrous DMF (5 mL). The solution was cooled in an ice bath followed by the addition of potassium carbonate

(210.7 mg, 1.5 mmol) and propargyl bromide (100 μ L, 1.5 mmol). The mixture was heated at 70 °C and stirred for 3 h. After the removal of the solvent, the residue was purified by column chromatography (EtOAc/hexanes 1:4) to obtain **1** (108.1 mg, 70% yield) as a dark purple solid. ¹H NMR (400 MHz, DMSO-*d*₆) δ 1.17 (t, *J* = 6.9 Hz, 6H, CH₃CH₂), 3.51 (q, *J* = 6.9 Hz, 4H, CH₃CH₂), 3.67 (t, *J* = 2.2 Hz, 1H, =CH), 5.03 (d, *J* = 2.2 Hz, 2H, OCH₂), 6.20 (s, 1H, ArH), 6.65 (d, *J* = 2.6 Hz, 1H, ArH), 6.83 (dd, *J* = 9.1 and 2.6 Hz, 1H, ArH), 7.32 (dd, *J* = 8.7 and 2.5 Hz, 1H, ArH), 7.64 (d, *J* = 9.1 Hz, 1H, ArH), 8.04 (d, *J* = 2.5 Hz, 1H, ArH), 8.08 (d, *J* = 8.7 Hz, 2H, ArH); ¹³C NMR (100 MHz, DMSO-*d*₆) δ 181.3, 159.8, 151.8, 150.9, 146.5, 138.1, 133.5, 131.0, 127.2, 125.5, 124.0, 118.2, 110.1, 107.0, 104.1, 96.0, 78.8, 78.7, 55.9, 44.4, 12.4; IR (ATR) ν_{max} : 3281.7, 3190.3, 2968.3, 2920.4, 2846.4, 1675.4, 1584.0, 1405.6 cm⁻¹; HRMS (ESI–TOF): [M + H]⁺ calcd for C₂₃H₂₁N₂O₃, 373.1552; found, 373.1581; UV (MeOH) λ_{max} (ϵ): 553 (3.2 \times 10⁴).

Synthesis of Nile red-modified acpcPNA

The 3-aminopyrrolidine-4-carboxylic acid (apc) modified acpcPNA was manually synthesized at a 1.5 μ mol scale on Tentagel S-RAM resin (Fluka, 0.24 mmol/g) from the four Fmoc-protected pyrrolidiny PNA monomers (A^{Bz}, T, C^{Bz}, G^{Ibu}) and spacers [Fmoc-(1*S*,2*S*)-2-aminocyclopentanecarboxylic acid or (3*R*,4*S*)-3-(Fmoc-amino)-1-trifluoroacetylpyrrolidine-4-carboxylic acid] [43] according to the previously published protocol [26,27,31]. Lysine was included at both C- and N-termini to improve the water solubility. After the completion of the synthesis, the N-terminal Fmoc group was removed and the free amino group was capped by acetylation. The acpcPNA on the solid support was split to 0.5 μ mol portions for a further labeling experiment and treated with 1:1 dioxane/aqueous NH₃ at 60 °C overnight to remove the nucleobase- and apc-protecting groups. Fully deprotected acpcPNA (0.5 μ mol) was treated with 4-azidobutanol (15 μ mol, 30 equiv) in the presence of NaBH₃CN (30 μ mol, 60 equiv) and HOAc (30 μ mol, 60 equiv) in MeOH (200 μ L) at room temperature overnight. After an exhaustive washing with MeOH, the azide-modified acpcPNA was reacted with **1** (7.5 μ mol, 15 equiv) in the presence of tris[(benzyl-1*H*-1,2,3-triazol-4-yl)methyl]amine [44] (TBTA, 30 μ mol, 60 equiv), tetrakis(acetonitrile) copper(I) hexafluorophosphate (15 μ mol, 30 equiv) and (+)-sodium-L-ascorbate (60 μ mol, 120 equiv) in 3:1 (v/v) DMSO/*t*-BuOH at room temperature overnight. After the reaction was completed, the labeled acpcPNA was cleaved from the solid support with trifluoroacetic acid (500 μ L \times 30 min \times 3). After drying and washing with diethyl ether, the residue was purified by reversed-phase HPLC and characterized by MALDI–TOF mass spectrometry (Microflex, Bruker Daltonics: α -cyano-4-hydroxycinnamic acid matrix, positive linear ion mode).

Spectroscopic studies

Samples for melting temperature, UV-vis, and fluorescence studies were prepared in 10 mM sodium phosphate buffer (pH 7.0) at concentrations of PNA = 1.0 μ M and DNA = 1.2 μ M. UV-vis and thermal denaturation experiments were performed on a CARY 100 UV-vis spectrophotometer (Varian, Australia) equipped with a thermal melting system. Fluorescence spectra were measured on a Cary Eclipse Fluorescence Spectrophotometer (Varian, Australia) at an excitation wavelength of 580 nm with 5 nm excitation and emission slits. Fluorescence melting experiments were performed under the same conditions by measuring the sample that was pre-heated to the specified temperature at 5 °C intervals and left for equilibration at that temperature for at least 5 min. The emission at 643 nm was divided by the emission at 643 nm of the single-stranded acpcPNA at the same temperature and plotted against the temperature to obtain the fluorescence melting curves. Melting temperatures were obtained from the UV or fluorescence melting curves by first derivative plots.

Supporting Information

Supporting Information File 1

* NMR spectra, HPLC chromatogram, mass spectra and additional spectroscopic data.

[<http://www.beilstein-journals.org/bjoc/content/supplementary/1860-5397-10-224-S1.pdf>]

Acknowledgements

Financial support of this work from the Thailand Research Fund (DPG5780002), the Ratchadaphiseksomphot Endowment Fund of the Chulalongkorn University (RES560530126-AM), and the Thai government stimulus package 2 (TKK2555, SP2) under the Project for the Establishment of Comprehensive Center for Innovative Food, Health Products and Agriculture and the Royal Golden Jubilee Ph.D. Program (Grant No. PHD/0316/2550, to NY and TV) is gratefully acknowledged.

References

- Murphy, M. C.; Rasnik, I.; Cheng, W.; Lohman, T. M.; Ha, T. *Biophys. J.* **2004**, *86*, 2530–2537. doi:10.1016/S0006-3495(04)74308-8
- Sindbert, S.; Kalinin, S.; Nguyen, H.; Kiéznler, A.; Clima, L.; Bannwarth, W.; Appel, B.; Müller, S.; Seidel, C. A. M. *J. Am. Chem. Soc.* **2011**, *133*, 2463–2480. doi:10.1021/ja105725e
- Bojesson, K.; Preus, S.; El-Sagheer, A.-H.; Brown, T.; Albinsson, B.; Wilhelmsson, L. M. *J. Am. Chem. Soc.* **2009**, *131*, 4288–4293. doi:10.1021/ja806944w
- Marras, S. A. E. *Mol. Biotechnol.* **2008**, *38*, 247–255. doi:10.1007/s12033-007-9012-9
- Sapsford, K. E.; Berli, L.; Medintz, I. L. *Angew. Chem., Int. Ed.* **2006**, *45*, 4562–4588. doi:10.1002/anie.200503873
- Sahoo, H. J. *Photochem. Photobiol., C* **2011**, *12*, 20–30. doi:10.1016/j.jphotochemrev.2011.05.001
- Lavis, L. D.; Raines, R. T. *ACS Chem. Biol.* **2008**, *3*, 142–155. doi:10.1021/cb700248m
- Waegeler, M. M.; Culik, R. M.; Gai, F. J. *Phys. Chem. Lett.* **2011**, *2*, 2598–2609. doi:10.1021/jz201161b
- Dziuba, D.; Postupalenko, V. Y.; Spadafora, M.; Klymchenko, A. S.; Guérineau, V.; Mely, Y.; Benhida, R.; Burger, A. *J. Am. Chem. Soc.* **2012**, *134*, 10209–10213. doi:10.1021/ja3030388
- Jose, J.; Burgess, K. *Tetrahedron* **2006**, *62*, 11021–11037. doi:10.1016/j.tet.2006.08.056
- Fowler, S. D.; Greenspan, P. J. *Histochem. Cytochem.* **1985**, *33*, 833–836. doi:10.1177/33.8.4020099
- Greenspan, P.; Mayer, E. P.; Fowler, S. D. *J. Cell Biol.* **1985**, *100*, 965–973. doi:10.1083/jcb.100.3.965
- Sackett, D. L.; Wolff, J. *Anal. Biochem.* **1987**, *167*, 228–234. doi:10.1016/0003-2697(87)90157-6
- Varghese, R.; Gajula, P. K.; Chakraborty, T. K.; Wagenknecht, H.-A. *Synlett* **2009**, 3252–3257. doi:10.1055/s-0029-1218384
- Varghese, R.; Wagenknecht, H.-A. *Chem. – Eur. J.* **2010**, *16*, 9040–9046. doi:10.1002/chem.201001136
- Beyer, C.; Wagenknecht, H.-A. *Chem. Commun.* **2010**, *46*, 2230–2231. doi:10.1039/b924471a
- Okamoto, A.; Tainaka, K.; Fujiwara, Y. *J. Org. Chem.* **2006**, *71*, 3592–3598. doi:10.1021/jo060168o
- Prokhorenko, I. A.; Diubankova, N. N.; Korshun, V. A. *Nucleosides, Nucleotides Nucleic Acids* **2004**, *23*, 509–520. doi:10.1081/NCN-120028344
- Wenge, U.; Ehrenschröder, T.; Wagenknecht, H.-A. *Bioconjugate Chem.* **2013**, *24*, 301–304. doi:10.1021/bc300624m
- Varghese, R.; Wagenknecht, H.-A. *Org. Biomol. Chem.* **2010**, *8*, 526–528. doi:10.1039/b918381g
- Varghese, R.; Wagenknecht, H.-A. *Chem. – Eur. J.* **2009**, *15*, 9307–9310. doi:10.1002/chem.200901147
- Lachmann, D.; Berndt, S.; Wolfbeis, O. S.; Wagenknecht, H.-A. *Beilstein J. Org. Chem.* **2010**, *6*, No. 13. doi:10.3762/bjoc.6.13
- Wittung, P.; Kim, S. K.; Buchardt, O.; Nielsen, P.; Nordén, B. *Nucleic Acids Res.* **1994**, *22*, 5371–5377. doi:10.1093/nar/22.24.5371
- Dilek, I.; Madrid, M.; Singh, R.; Urrea, C. P.; Armitage, B. A. *J. Am. Chem. Soc.* **2005**, *127*, 3339–3345. doi:10.1021/ja045145a
- Armitage, B. A. *Top. Curr. Chem.* **2005**, *253*, 55–76. doi:10.1007/b100442
- Vilaivan, T.; Srisuwannaket, C. *Org. Lett.* **2006**, *8*, 1897–1900. doi:10.1021/ol060448q
- Vilaivan, T.; Srisuwannaket, C.; Ananthanawat, C.; Suparpprom, C.; Kawakami, J.; Yamaguchi, Y.; Tanaka, Y.; Vilaivan, T. *Artificial DNA: PNA XNA* **2011**, *2*, 50–59. doi:10.4161/adna.2.2.16340
- Mansawat, W.; Vilaivan, C.; Balázs, Á.; Ailken, D. J.; Vilaivan, T. *Org. Lett.* **2012**, *14*, 1440–1443. doi:10.1021/ol300190u
- Boonlua, C.; Vilaivan, C.; Wagenknecht, H.-A.; Vilaivan, T. *Chem. – Asian J.* **2011**, *6*, 3251–3259. doi:10.1002/asia.201100490
- Boonlua, C.; Diltmangklo, B.; Reenabthue, N.; Suparpprom, C.; Poomsuk, N.; Siritwong, K.; Vilaivan, T. *RSC Adv.* **2014**, *4*, 8817–8827. doi:10.1039/c3ra47997h
- Diltmangklo, B.; Boonlua, C.; Suparpprom, C.; Vilaivan, T. *Bioconjugate Chem.* **2013**, *24*, 614–625. doi:10.1021/bc3005914
- Sezi, S.; Varghese, R.; Vilaivan, T.; Wagenknecht, H.-A. *ChemistryOpen* **2012**, *1*, 173–176. doi:10.1002/open.201200016
- Meldal, M.; Tornøe, C. W. *Chem. Rev.* **2008**, *108*, 2952–3015. doi:10.1021/cr0783479

34. Gramlich, P. M. E.; Wirges, C. T.; Manetto, A.; Carell, T. *Angew. Chem., Int. Ed.* **2008**, *47*, 8350–8358. doi:10.1002/anie.200802077
35. Amblard, F.; Cho, J. H.; Schinazi, R. F. *Chem. Rev.* **2009**, *109*, 4207–4220. doi:10.1021/cr9001462
36. El-Sagheer, A. H.; Brown, T. *Chem. Soc. Rev.* **2010**, *39*, 1388–1405. doi:10.1039/b901971p
37. Briggs, M. S. J.; Bruce, I.; Miller, J. N.; Moody, C. J.; Simmonds, A. C.; Swann, E. J. *Chem. Soc., Perkin Trans. 1* **1997**, 1051–1058. doi:10.1039/a605012c
38. Jose, J.; Burgess, K. *J. Org. Chem.* **2006**, *71*, 7835–7839. doi:10.1021/jo061369v
39. Chen, Q.-y.; Li, D.-h.; Yang, H.-h.; Zhu, Q.-z.; Xu, J.-g.; Zhao, Y. *Analyst* **1999**, *124*, 901–906. doi:10.1039/a901174j
40. Zhao, G.-C.; Zhu, J.-J.; Chen, H.-Y.; Wang, X.-M.; Lu, Z.-H. *Chin. J. Chem.* **2002**, *20*, 57–62. doi:10.1002/cjoc.20020200112
41. Magde, D.; Brannon, J. H.; Cremers, T. L.; Olmsted, J., III. *J. Phys. Chem.* **1979**, *83*, 696–699. doi:10.1021/j100469a012
42. Okamoto, A.; Ichiba, T.; Saito, I. *J. Am. Chem. Soc.* **2004**, *126*, 8364–8365. doi:10.1021/ja049061d
43. Reenabithue, N.; Boonlua, C.; Vilaivan, C.; Vilaivan, T.; Suparpprom, C. *Bioorg. Med. Chem. Lett.* **2011**, *21*, 6465–6469. doi:10.1016/j.bmcl.2011.08.079
44. Chan, T. R.; Hilgraf, R.; Sharpless, K. B.; Fokin, V. V. *Org. Lett.* **2004**, *6*, 2853–2855. doi:10.1021/ol0493094

License and Terms

This is an Open Access article under the terms of the Creative Commons Attribution License (<http://creativecommons.org/licenses/by/2.0>), which permits unrestricted use, distribution, and reproduction in any medium, provided the original work is properly cited.

The license is subject to the *Beilstein Journal of Organic Chemistry* terms and conditions: (<http://www.beilstein-journals.org/bjoc>)

The definitive version of this article is the electronic one which can be found at:
[doi:10.3762/bjoc.10.224](https://doi.org/10.3762/bjoc.10.224)



Pyrrolidinyl peptide nucleic acids immobilised on cellulose paper as a DNA sensor†

Cite this: *RSC Adv.*, 2015, 5, 24110

Nuttapon Jirakittiwut, Nattawadee Panyain, Thanesuan Nuanyai,‡ Tirayut Vilaivan and Thanit Praneenararat*

Received 26th November 2014

Accepted 26th February 2015

DOI: 10.1039/c4ra15287e

www.rsc.org/advances

A new label-free DNA sensor based on pyrrolidinyl peptide nucleic acid on cellulose paper was fabricated. Coupled with straightforward signal detection by cationic dye staining, this sensor has promise as a robust tool for point-of-care DNA detection.

The development of field diagnostics for developing countries remains a challenge that has gained much interest from researchers around the world. In this regard, paper-based analytical devices are of much interest due to several superior properties of cellulose paper such as low cost and biocompatibility.¹ Pioneered by the Whitesides group in the form of paper-based microfluidic devices,^{2–4} several types of paper-based sensors have since been fabricated, leading to various applications such as whole cell biosensors,⁵ or the sensor capable of multiple determinations of metals.^{6,7} Notably, most of these devices used cellulose merely as a platform for physical adsorption of chemical species, whereas covalent immobilisation could allow detection of species that would otherwise be impossible due to the poor retention of the involving counterparts in cellulose material. A notable example includes a study by Yu *et al.* who demonstrated that divinyl sulfone (DVS) could be used to attach various biomolecules having varying retention on cellulose and utilise them as probes.⁸ This paved the way for more economical sensors that can detect various biomolecules including DNA, whose detection can lead to diverse applications such as clinical diagnosis or the detection of pathogens.⁹ Note, however, that DNA as a probe for another DNA strand is subject to enzymatic degradation. Therefore, means to improve the stability, as well as specificity and selectivity, of DNA probes are still desired.

Peptide nucleic acid (PNA),¹⁰ a synthetic DNA mimic, has been extensively studied as a probe for DNA detection due to several advantages including higher binding affinity of PNA–DNA over DNA–DNA, and much greater resistance to enzymatic degradation. This has sparked interest from researchers to utilise PNAs, mostly in the original scaffold called aminoethylglycyl PNA (aegPNA), as probes in a number of sensors with great performance in many aspects such as sensitivity, specificity and robustness.^{11–14}

During the past few years, our group has developed a new class of pyrrolidinyl PNAs, a conformationally rigid PNA. Our pyrrolidinyl PNA consists of a *n*-prolyl-2-amino-cyclopentane-carboxylic acid (acpc) backbone (Fig. 1).^{15,16} This relatively more rigid structure was shown to exhibit certain desirable properties over aegPNA, while maintaining comparable overall binding affinity and sequence specificity. These advantages include the stronger directional preference for antiparallel binding and the higher affinity towards DNA over RNA. Encouraged by the aforementioned features, we have showcased the utility of this PNA as DNA probes in a number of applications.^{17–21}

In the current study, we aimed to immobilise acpcPNA by covalently attaching the PNA onto cellulose paper, and utilising it as a probe for DNA detection. After DNA incubation by capillary method²² and washing, we demonstrated that cationic organic dyes could be used to visualise the binding between

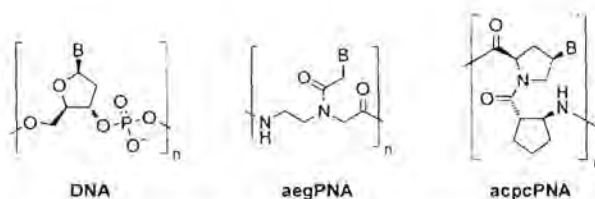


Fig. 1 Chemical structures of DNA, aegPNA, and acpcPNA. B stands for nucleobases (A, T, C, and G).

Department of Chemistry, Faculty of Science, Chulalongkorn University, Phayathai Rd., Pathumwan, Bangkok, 10330, Thailand. E-mail: Thanit.P@chula.ac.th

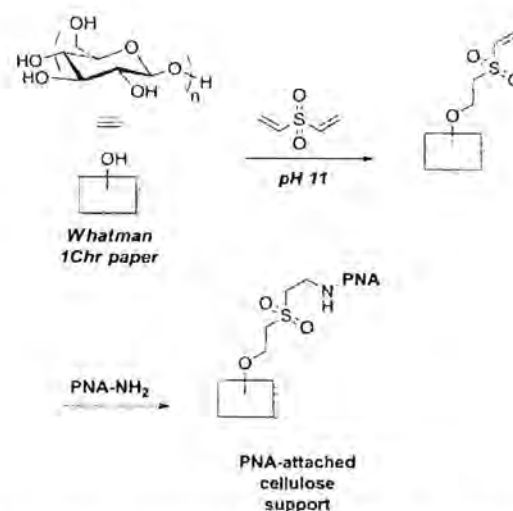
† Electronic supplementary information (ESI) available. See DOI: 10.1039/c4ra15287e

‡ Present address: Faculty of Liberal Arts, Rajamangala University of Technology Rattanakosin, Wang Klai Kangwon Campus, Huanhin, Prachuap Khiri Khan, Thailand, 77110.

PNA and DNA by electrostatic interaction between the dye and the bound negatively charged DNA (Fig. 2). By combining the relatively low cost of cellulose paper, and the performance of acpcPNA as a DNA probe, we envisioned that this new DNA sensor could have promise as an economical point-of-care DNA testing device.

The fabrication of the sensor commenced with selecting an appropriate chemistry for covalent immobilisation of acpcPNA via an appended lysine residue at the N- or C-termini. The hydroxyl group at C-6 position of the glucose monomer in cellulose is the most common site for functional group inter-conversion,²³ as it has been used as a "gateway" to attach various chemical scaffolds^{8,18,22,24-26} leading to diverse applications ranging from combinatorial synthesis (SPOT and macroarray synthesis)²⁷ to the immobilisation of biomolecules for sensor construction purposes.^{8,22,26} For the ultimate goal of naked-eye detection, we found that not all commonly used chemical reactions are equally suitable, as some attachment methods produced false-positive signal from PNA alone (without the presence of DNA – data not shown). Hence, we conducted a preliminary screening and found that divinyl sulfone (DVS) is a suitable attachment method and thus we decided to immobilise acpcPNA by this chemistry (Scheme 1).⁸

Thereafter, some experiments to prove that the PNA was really covalently attached on the cellulose support were needed. We confirmed the success of attachment by immobilising a fluorescein-labelled PNA onto cellulose (Fig. S1 – see ESI†). After thorough washing, it was found that the PNA with prior incubation of cellulose with DVS showed significantly higher fluorescence intensity than that without DVS incubation. This indirectly confirmed that the covalent attachment has occurred and is required for PNA retention on the paper. Also, we conducted another preliminary test by immobilising unlabelled PNA onto support, followed by incubation with fluorescently labelled DNA. We found that only the complementary DNA could be retained on support after extensive washing, confirming that the immobilised PNA is still capable of exerting Watson-Crick base pairing with the DNA (Fig. S2†). An



Scheme 1 The immobilisation of acpcPNA by DVS-mediated conjugate addition of acpcPNA onto support.

additional experiment where we varied the concentration (amount) of incubated DNA showed that the fluorescence signals, as quantified by the software ImageJ, had a logarithm relationship with the amount of bound DNA, roughly following the Langmuir isotherm (Fig. S3†).

Aiming to avoid labelling of the DNA samples,²² a third component that enables visualisation of the PNA-DNA binding event in a label-free and preferably instrument-free fashion is desired.^{12,26} Encouraged by the preliminary results, we screened for methods that allow detection of binding between unlabelled PNA and DNA. We envisaged that the difference of charges at physiological pH could provide a unique opportunity for detection – a method that would not be plausible with DNA or other DNA analogues as a probe. Indeed, this feature has been utilised before by Kim *et al.* where they used positively-charged gold nanoparticle with signal enhancement to allow naked-eye detection of aegPNA-DNA binding.¹² Unfortunately, this method did not work well in our condition, likely because of the drastic difference between the surfaces used in each study. We then focused on known, positively-charged, fluorescent dyes for DNA detection including ethidium bromide and SYBR gold, and found that none of them could give appreciable signal. Subtle molecular effects may influence this outcome and we are actively investigating this phenomenon with other cationic fluorescent dyes. Consequently, we turned our attention to optical cationic dyes that can be directly visualised by naked eyes. After some screening, thiazine dyes – a class of molecular biology staining agents including the commonly known methylene blue – was shown to be an appropriate visualising agent. Preliminary tests revealed that Azure A (structure shown in Fig. 2) showed the best staining profile among dyes tested (see details in ESI†). Hence, we selected this dye for the subsequent studies.

As a preliminary study of the new experimental setup, we studied the effect of the length of incubated DNAs and the

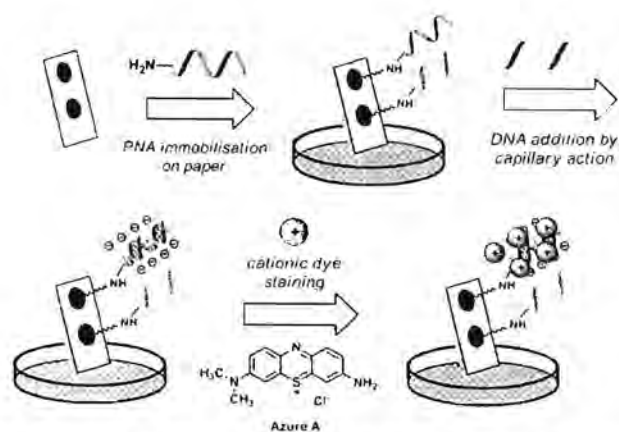


Fig. 2 The fabrication of the new DNA sensor by covalently attaching acpcPNA onto cellulose paper, followed by cationic dye staining.

orientation of the binding region to better understand the nature of this detection method. Fig. S4† showed the effect of the total length of DNA on signal intensity. It should be noted that longer DNA strands are expected to provide stronger signal since they gave more accessible sites for dye binding. In our case, the shortest DNA among the three in this study did give the lowest signal intensity. On the contrary, the longest DNA strand gave approximately the same signal intensity as the one with the second longest length, likely due to the saturation of signal. We decided to choose the DNA with the second longest length (41 nucleotides) for our subsequent experiments. Furthermore, we studied the effect of the expected binding orientation on the signal intensity, with the hypothesis that the "wrong" orientation where extra bases are forced to clash with the surface should lead to unfavourable interactions with both the probe and the dye, leading to reduced signal intensity. As shown in Fig. S5,† the wrong orientation (DNA "C") gave lowest signal intensity as anticipated.

After gaining some basic understanding of the system, we proceeded to showcase the utility of this sensor by applying it to detect DNA sequences that were derived from real biological settings. Extra hanging sequences were appended to either the 3' or 5' end of the synthetic DNA targets to mimic the detection of real DNA samples. It should be noted that phenothiazine dyes bind electrostatically to both duplex and single-stranded DNAs,²⁸ therefore the extra hanging bases should contribute to the dye adsorption.¹² First, we attempted to detect the binding of DNA sequences in human leukocyte antigen (HLA) alleles. HLA alleles such as HLA-B*5701 and HLA-B*5801 used in this study were found to have strong correlation with various forms of cutaneous adverse drug reactions.^{29,30} Therefore, the ability to screen patients for such genes would greatly reduce the risk associated with the prescription of relevant drugs. Another case was about the detection of a single-gene disorder thalassaemia. Codon 26 mutation (R06 G → A) is a cause of β -thalassaemia and the ability to detect this single-base mutation could be very useful for prenatal diagnosis and treatment.³¹ As shown in Fig. 3B, our detection system could unambiguously distinguish sequences with double mismatches (HLA-B*5701 vs. 5801). Notably, since sheets of paper can be scanned by a commercial scanner, images obtained could be used for further processing by imaging software (ImageJ) to produce some quantitative data. Fig. 3D showed a representative graph illustrating that our DNA sensing device could clearly differentiate related DNA sequences, as objectively confirmed by the Student's *t*-test of the obtained numerical data. In the case of single mismatched DNAs (R06C and T), the Student's *t*-test still suggested that values from the two DNA sequences differ with statistical significance. Nevertheless, it was more obvious by naked eyes that the mismatch DNA also gave significant false-positive signal. In order to solve this issue, we found that a more stringent washing (20% acetonitrile in PBS buffer) after the DNA incubation could efficiently remove this non-specific binding, albeit with a slight compromise of signal intensity (Fig. 3C and E). In addition, we also tested the performance of the sensing system in the presence of various interferences. First, the 5701/5801 DNA sensor was tested again with the

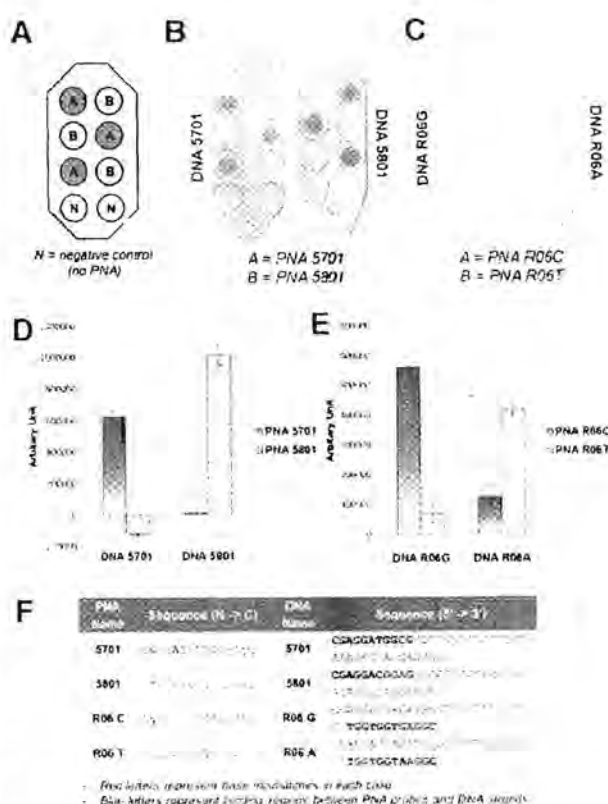


Fig. 3 (A) Layout of the paper-based DNA sensor; (B) and (C) the scanned images of DNA sensors for HLA-B*5701/5801, and R06 C/T, respectively. Each sheet was subject to DNA incubation of one sequence while each spot contained one PNA sequence as outlined in the figure; (D) and (E) signal intensities (HLA-B*5701/5801 and R06 C/T, respectively) derived from scanned images via the ImageJ image processing software; (F) The table showing all PNA and DNA sequences used in this study. All experiments were performed in triplicates of triplicates at the DNA concentration of 6 μ M (100 pmol per spot).

presence of two non-relevant DNA sequences (R06G and A9). As shown in Fig. S6,† nearly the same results as in Fig. 3B were obtained, confirming that the sensor is highly specific. Furthermore, we tested the performance of the 5801 system with the presence of nine other DNAs having varying lengths and sequences. The sensor again exhibited extremely good discrimination power by providing positive results only when the complementary sequence was present (Fig. S7†). Overall, the system could be applied with closely related DNA sequences with clear differentiation power, even with the presence of multiple DNA interferences. The ability to distinguish between complementary and single mismatch targets at ambient temperature highlights the benefits of the high specificity offered by pyrrolidinyl PNA probes.

Importantly, we also proved that an amino-linked DNA (aminohexyl group attached to 3' end) with the same sequence as the HLA-B*5801 PNA probe used in this work did not provide significantly discernible signal. This is most likely due to the much lower binding affinity of the DNA probe (Fig. S8†). In fact,

it is common practice to use at least 20-nucleotide DNA as probes. Therefore, the cost of PNA (at the required length and amount) is not considered a significant addition to the overall cost of the sensor although the cost of PNA is about 20–25 times higher than that of DNA oligonucleotides. This further underscores the power of acpPNA as a DNA probe. For the detection limit, we found the lowest detectable concentration of DNA to be about 200 nM or 3.3 pmol per spot (Fig. S9†). This value is comparable to the expected sensitivity of the DNA binding dye (~40 ng based on calculation vs. ~40–100 ng for Azure A and related dyes for gel-based detection of DNA)²² with the advantages of high specificity and being a simple disposable system that requires no complicated instruments for performing the hybridization, detection, and signal analysis. As a comparison to our previous work,¹⁸ the current sensor was found to exhibit greater resistance to signal interference when the sensor was incubated with a mixture of several DNA sequences (see above) with only one limitation of having lower sensitivity. This difference is attributed to the nature of the sensor chemical assembly, which aimed to provide a specific Watson–Crick interaction between PNA and DNA in the very first step, whereas the previous work¹⁸ relied on non-specific electrostatic interaction as the binding site. In addition, an enzymatically generated colorimetric reaction was used as a means for signal amplification,¹⁸ which should naturally lead to a lower detection limit. The results herein should therefore be considered as a promising system that can be further developed into a simple yet highly powerful DNA sensor.

Conclusions

We report herein the fabrication of a new DNA sensing device. This cellulose-based DNA sensor offers an economical way to detect DNA with great specificity. With low-cost fabrication and straightforward visual detection without requiring labelled samples nor strict temperature control, we envision that this new DNA sensor could become a robust tool for DNA detection in point-of-care testing. Further optimisation is being investigated in our laboratory to improve the sensitivity and allow label-free detection of double-stranded long DNA targets – this will be reported in due course.

Acknowledgements

This work is fully supported by the Thailand Research Fund (TRF - DBG5580007 and partially from DPG5780002) and the Ratchadapiseksompot Fund (Chulalongkorn University). The authors also acknowledge the Department of Chemistry, Faculty of Science, Chulalongkorn University for instruments funding.

Notes and references

- R. Pelton, *TrAC, Trends Anal. Chem.*, 2009, **28**, 925–942.
- A. W. Martinez, S. T. Phillips, M. J. Butte and G. M. Whitesides, *Angew. Chem., Int. Ed.*, 2007, **46**, 1318–1320.
- A. W. Martinez, S. T. Phillips, G. M. Whitesides and E. Carrilho, *Anal. Chem.*, 2010, **82**, 3–10.
- A. K. Yetisen, M. S. Akram and C. R. Lowe, *Lab Chip*, 2013, **13**, 2210–2251.
- A. Struss, P. Pasini, C. M. Ensor, N. Raut and S. Daunert, *Anal. Chem.*, 2010, **82**, 4457–4463.
- P. Rattanarat, W. Dungchai, D. M. Cate, W. Siangproh, J. Volckens, O. Chailapakul and C. S. Henry, *Anal. Chim. Acta*, 2013, **800**, 50–55.
- P. Rattanarat, W. Dungchai, D. M. Cate, J. Volckens, O. Chailapakul and C. S. Henry, *Anal. Chem.*, 2014, **86**, 3555–3562.
- A. Yu, J. Shang, F. Cheng, B. A. Paik, J. M. Kaplan, R. B. Andrade and D. M. Ratner, *Langmuir*, 2012, **28**, 11265–11273.
- A. Sassolas, B. D. Leca-Bouvier and L. J. Blum, *Chem. Rev.*, 2008, **108**, 109–139.
- P. Wittung, P. E. Nielsen, O. Buchardt, M. Egholm and B. Norden, *Nature*, 1994, **368**, 561–563.
- O. Brandt, J. Feldner, A. Stephan, M. Schröder, M. Schnölzer, H. F. Arlinghaus, J. D. Hoheisel and A. Jacob, *Nucleic Acids Res.*, 2003, **31**, e119.
- S. K. Kim, H. Cho, J. Jeong, J. N. Kwon, Y. Jung and B. H. Chung, *Chem. Commun.*, 2010, **46**, 3315–3317.
- O. Brandt and J. D. Hoheisel, *Trends Biotechnol.*, 2004, **22**, 617–622.
- N. Zhang and D. H. Appella, *J. Am. Chem. Soc.*, 2007, **129**, 8424–8425.
- C. Suparpprom, C. Srisuwannaket, P. Sangvanich and T. Vilaivan, *Tetrahedron Lett.*, 2005, **46**, 2833–2837.
- T. Vilaivan and C. Srisuwannaket, *Org. Lett.*, 2006, **8**, 1897–1900.
- B. Boontha, J. Nakkuntod, N. Hirankarn, P. Chaumpluk and T. Vilaivan, *Anal. Chem.*, 2008, **80**, 8178–8186.
- P. S. Laopa, T. Vilaivan and V. P. Hoven, *Analyst*, 2013, **138**, 269–277.
- S. Sankoh, S. Samanman, O. Thipmanee, A. Numnuam, W. Limbut, P. Kanatharana, T. Vilaivan and P. Thavarungkul, *Sens. Actuators, B*, 2013, **177**, 543–554.
- T. Theppaleak, M. Rutnakornpituk, U. Wichai, T. Vilaivan and B. Rutnakornpituk, *J. Nanopart. Res.*, 2013, **15**, 2106.
- S. Jampasa, W. Wonsawat, N. Rodthongkum, W. Siangproh, P. Yanatsaneejit, T. Vilaivan and O. Chailapakul, *Biosens. Bioelectron.*, 2014, **54**, 428–434.
- A. C. Araujo, Y. J. Song, J. Lundeberg, P. L. Stahl and H. Brumer, *Anal. Chem.*, 2012, **84**, 3311–3317.
- S. C. Fox, B. Li, D. Q. Xu and K. J. Edgar, *Biomacromolecules*, 2011, **12**, 1956–1972.
- D. Stollner, F. W. Scheller and A. Warsinke, *Anal. Biochem.*, 2002, **304**, 157–165.
- M. Y. He and Z. H. Liu, *Anal. Chem.*, 2013, **85**, 11691–11694.
- Y. J. Song, P. Gyarmati, A. C. Araujo, J. Lundeberg, H. Brumer and P. L. Stahl, *Anal. Chem.*, 2014, **86**, 1575–1582.
- H. E. Blackwell, *Curr. Opin. Chem. Biol.*, 2006, **10**, 203–212.
- M. Ortiz, A. Fragoso, P. J. Ortiz and C. K. O'Sullivan, *J. Photochem. Photobiol., A*, 2011, **218**, 26–32.

- 29 S. Mallal, D. Nolan, C. Witt, G. Masel, A. M. Martin, C. Moore, D. Sayer, A. Castley, C. Mamotte, D. Maxwell, I. James and F. T. Christiansen, *The Lancet*, 2002, **359**, 727–732.
- 30 S. I. Hung, W. H. Chung, L. B. Liou, C. C. Chu, M. Lin, H. P. Huang, Y. L. Lin, J. L. Lan, L. C. Yang, H. S. Hong, M. J. Chen, P. C. Lai, M. S. Wu, C. Y. Chu, K. H. Wang, C. H. Chen, C. S. J. Fann, J. Y. Wu and Y. T. Chen, *Proc. Natl. Acad. Sci. U. S. A.*, 2005, **102**, 4134–4139.
- 31 P. Winichagoon, V. Saechan, R. Sripanich, C. Nopparatana, S. Kanokpongsakdi, A. Maggio and S. Fucharoen, *Prenatal Diagn.*, 1999, **19**, 428–435.
- 32 M. R. Green and J. Sambrook, *Molecular Cloning: A Laboratory Manual*, 4th edn., Cold Spring Harbor Laboratory Press, 2012.

Bringing Macromolecules into Cells and Evading Endosomes by Oxidized Carbon Nanoparticles

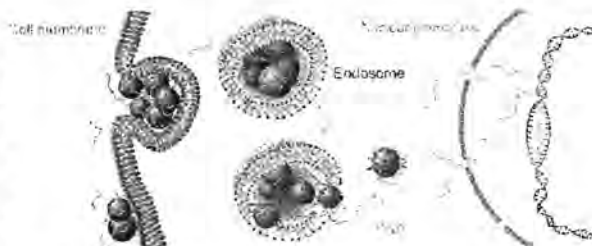
Sunatda Arayachukiat,^{†,○} Jiraporn Seemork,^{‡,○} Porntip Pan-In,[§] Kittima Amornwachirabodee,[§] Naunpun Sangphech,^{||} Titiporn Sansureerungsikul,[§] Kamonluck Sathornsantikun,[§] Chotima Vilaivan,[§] Kazuki Shigyou,[⊥] Prompong Pienpinijtham,[§] Tirayut Vilaivan,[§] Tanapat Palaga,^{||} Wijit Banlunara,^{||} Tsutomu Hamada,[⊥] and Supason Wanichwecharungruang^{*,§,▽}

[†]Macromolecular Science Program, Faculty of Science, Chulalongkorn University (CU), [‡]Program in Petrochemistry, Faculty of Science, CU, [§]Department of Chemistry, Faculty of Science, CU, ^{||}Department of Microbiology, Faculty of Science, and Interdisciplinary Program in Medical Microbiology, CU, [⊥]School of Materials Science, Japan Advanced Institute of Science and Technology (JAIST), [▽]Department of Pathology, Faculty of Veterinary Science, CU, [○]Nanotec-CU Center of Excellence on Food and Agriculture, Chulalongkorn University, Bangkok 10330, Thailand

Supporting Information

ABSTRACT: A great challenge exists in finding safe, simple, and effective delivery strategies to bring matters across cell membrane. Popular methods such as viral vectors, positively charged particles and cell penetrating peptides possess some of the following drawbacks: safety issues, lysosome trapping, limited loading capacity, and toxicity, whereas electroporation produces severe damages on both cargoes and cells. Here, we show that a serendipitously discovered, relatively nontoxic, water dispersible, stable, negatively charged, oxidized carbon nanoparticle, prepared from graphite, could deliver macromolecules into cells, without getting trapped in a lysosome. The ability of the particles to induce transient pores on lipid bilayer membranes of cell-sized liposomes was demonstrated. Delivering 12-base-long pyrrolidiny peptide nucleic acids with *D*-prolyl-(1*S*,2*S*)-2-aminocyclopentanecarboxylic acid backbone (acpCPNA) complementary to the antisense strand of the NF- κ B binding site in the promoter region of the *Il6* gene into the macrophage cell line, RAW 264.7, by our particles resulted in an obvious accumulation of the acpCPNAs in the nucleus and decreased *Il6* mRNA and IL-6 protein levels upon stimulation. We anticipate this work to be a starting point in a new drug delivery strategy, which involves the nanoparticle that can induce a transient pore on the lipid bilayer membrane.

KEYWORDS: cellular penetration, lipid bilayer membrane, transient pore, nanoparticle, antigene, PNA, oxidized carbon particle



Cell plasma membrane is the structure that not only separates the cell from its environment but also controls transports of all matters into and out of the cell. Various scientific investigations and therapeutic works require the transport of macromolecules such as antisense oligonucleotide, aptamer, siRNA, and peptides across the cell membrane.^{1,2} Current popular approaches include the use of positively charged particles (lipid vesicles^{3,4} and polymer particles^{5,6}) and cell penetrating peptides.^{7,8} Nevertheless, lysosome trapping, low transfection efficiency, toxicity, limited loading, and complicated preparation steps are drawbacks of these approaches.^{9,10} Transporting gene by viral vectors, although is highly effective, faces a limited size of DNA fragment to be delivered and safety issues,¹¹ whereas physical stimuli such as electroporation produce damages on the cargoes and cells.¹² Therefore, a great challenge still exists in finding inexpensive, easy to use and effective delivery strategies to bring molecules across a cell membrane without being trapped in a lysosome.

Here, we propose the use of the negatively charged, oxidized carbon nanoparticles, serendipitously isolated and discovered during our preparation of graphene oxide sheets to bring biologically active substances across cell membrane. Using graphite as a starting material, we could reproducibly prepare negatively charged oxidized carbon particles with outstanding ability to penetrate lipid bilayer membrane and have named the obtained particles "membrane penetrating oxidized carbon nanoparticles" (MPOCs). This paper reports the preparation and characterization of the MPOCs and shows that MPOCs can facilitate the penetration of peptide nucleic acids across a cell membrane without being trapped in a lysosome. The membrane penetration mechanism of MPOCs is proposed. To clearly show that the MPOCs can be used as a simple and effective delivery vehicle to bring macromolecules into cells for

Received: February 19, 2015

Revised: April 1, 2015

Published: April 7, 2015

biological applications, the paper demonstrates antigenic function of peptide nucleic acid (PNA) delivered into cells by MPOCs.

Among several PNAs, pyrrolidinyl PNA with D-prolyl-(1*S*,2*S*)-2-aminocyclopentanecarboxylic acid backbone (acpcPNA, called PNA in this paper) demonstrates greater binding affinity and specificity to complementary DNAs than to complementary RNAs¹⁵ and therefore is potentially useful in antigenic application. Nevertheless, successful cellular delivery of acpcPNAs has never been reported. Here, using MPOCs, we show successful cellular delivery of the challenging acpcPNA into RAW 264.7 macrophage cell line and 293T human embryonic kidney cell line. We evaluated, using RAW 264.7 cells, the antigenic property of acpcPNAs delivered into cells by MPOCs, focusing on the *Il6* gene expression. IL-6 is a multifaceted cytokine involved in both innate and adaptive immune responses. Dysregulation of IL-6 expression is linked to chronic inflammation and autoimmune diseases. Reports have shown that the promoter region of the *Il6* gene possesses a conserved binding site for the NF- κ B transcription factor¹⁴ and inhibition of NF- κ B binding can suppress transcription of *Il6*.^{15,16} Here, we selected the 12-bp DNA sequence, at the binding site of NF- κ B in the *Il6* promoter (between -74 and -63),¹⁷ as the target and synthesized the acpcPNAs complementary to this antisense sequence (here denoted as PNA_{NF κ B}). We then investigated the anti-*Il6* action of PNA_{NF κ B} through the monitoring of both *Il6*-mRNA and IL-6 protein levels.

Preparation and Characterization of MPOCs. When graphite powder (99.9999% purity from Alfa Aesar, Johnson Matthey Company, Lancashire, U.K., or 98.5% purity from Thai Carbon and Graphite Co., Ltd., Bangkok, Thailand) were vigorously oxidized under sonication, carbon materials of different sizes and shapes, for example, tubes, sheets, spheres, and irregular-shaped particulates, could be observed by scanning electron microscope (SEM). Multistep-centrifugation could successively pellet down other carbon allotropes and resulted in an aqueous suspension of mostly MPOCs. The MPOCs dispersed well in water and possessed an average hydrodynamic size around 37.7 ± 4.6 nm when freshly sonicated. The particle size then quickly increased to an average size of 225 ± 57 nm (Figure 1). The water dispersible aggregated particles could be easily redispersed back into smaller particles upon sonication. SEM and transmission electron microscopic (TEM) images of the freshly sonicated suspensions also showed semispherical morphology of ~ 40 nm particles, whereas analysis of the three-month-old-suspensions showed significant amounts of ~ 100 – 300 nm particles and the observed large particles were aggregates of smaller ones (Figure 1). Sonicating these three-month-old suspensions resulted in smaller numbers of large particles (Supporting Information, Figure S1). The aqueous suspension of MPOCs showed no precipitation after being kept still for more than 3 years at 23–35 °C (room temperature). Zeta potentials of MPOCs in water and phosphate buffer saline of pH 7.4 were -40.96 ± 5.25 and -30.97 ± 2.06 mV, respectively. The particles could also be dispersed well in methanol, ethanol, *N,N*-dimethylformamide, dimethyl sulfoxide, ethyl acetate, and Dulbecco's modified Eagle medium (Supporting Information, Figure S2).

Elemental analysis of different batches of MPOCs gave similar C:O:H mass ratio at (mean \pm SD) $47.35 \pm 5.41:42.56 \pm 2.52:2.62 \pm 0.26$, which corresponded to the C:O:H molar ratio around 1.0:0.68:0.66. SEM-energy dispersive X-ray

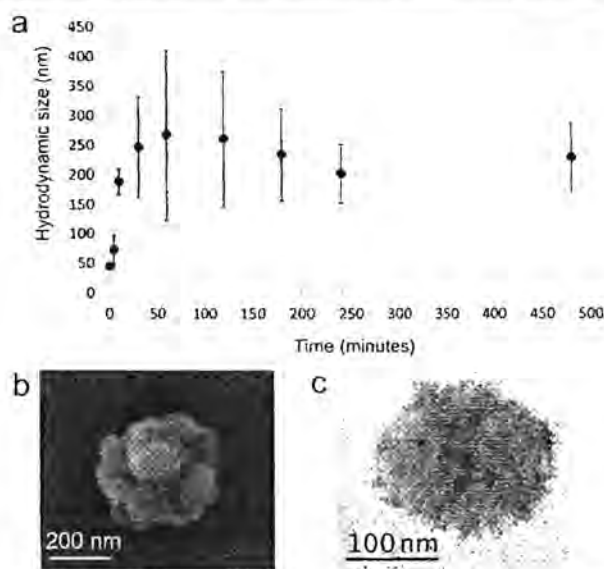


Figure 1. Size and morphology of MPOC. Hydrodynamic size distributions (shown as mean \pm SD) of MPOCs at various postsonication times (a). SEM (b) and high resolution TEM (c) images of MPOCs.

spectroscopic analysis could also detect C and O throughout the particles. ATR-FTIR and X-ray photoelectronic spectroscopic (XPS) analyses (Supporting Information, Figure S3) indicated a presence of C—O—C, C=C, C—C, C—OH and COOH functionalities in MPOCs. Raman spectrum of the particles revealed two strong broad absorption bands at 1360 cm^{-1} (D band, in-plane vibration of disordered planar (sp^2) bonded carbons, finite shape planar (sp^2) bonded carbons, tetrahedral (sp^3) carbons) and 1590 cm^{-1} (G band, vibration of in-plane planar (sp^2) bonded carbons), and weak broad absorption bands at 2500 – 3400 cm^{-1} with three maxima at 2720 , 2920 , and 3200 cm^{-1} (2D or G' band of disordered planar (sp^2) planes). The D band was always bigger than the G band. The broad D-band and G-band implied that the carbon networks in the MPOCs were in various orientations and possessed various bond strengths. The three broad 2D bands were likely a result of different interlayer interactions that occurred at different depths within the MPOCs. It should be noted here that the multiple 2D bands and the high intensity D band make the Raman spectrum of MPOCs different from those of graphene, graphite, nanocrystalline diamond, single-walled carbon nanotube, double-walled carbon nanotube and multiple-walled carbon nanotube, but quite similar to that of graphene oxide.^{18–20} The lack of 1462 cm^{-1} absorption indicated the absence of C₆₀ (buckyball) in the MPOCs.²¹

Thermo-gravimetric analysis of the MPOCs showed fast weight losses at 80–120 and 180–240 °C, corresponded to the loss of water followed with particle degradation. Although light scattering of the MPOCs suspension could not be subtracted out, UV-visible absorption spectrum of the suspension showed broad absorption with a maximum at 227 nm. X-ray diffraction pattern of MPOCs showed no sharp peak, indicating that the crystallinity of the graphite was not preserved in MPOCs (Supporting Information, Figure S3). We conclude that MPOCs are 40 nm oxidized carbon nanoparticles containing planar carbon planes, disordered planar carbon planes and tetrahedral carbons with C=C, C=O, COOH and OH

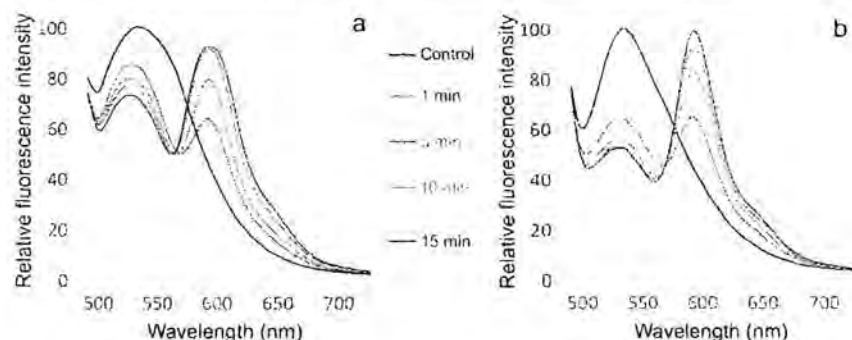


Figure 2. Monitoring the interaction between MPOCs and lipid bilayer membrane of the cell-sized liposome using FRET technique. Fluorescence emission of the aqueous suspensions of donor-containing liposomes after being incubated with free acceptor lipids (a) and acceptor lipid-loaded MPOCs (b) for 1, 5, 10, and 15 min. Aqueous suspensions of donor liposomes alone or that mixed with MPOCs were used as control in graphs a and b, respectively.

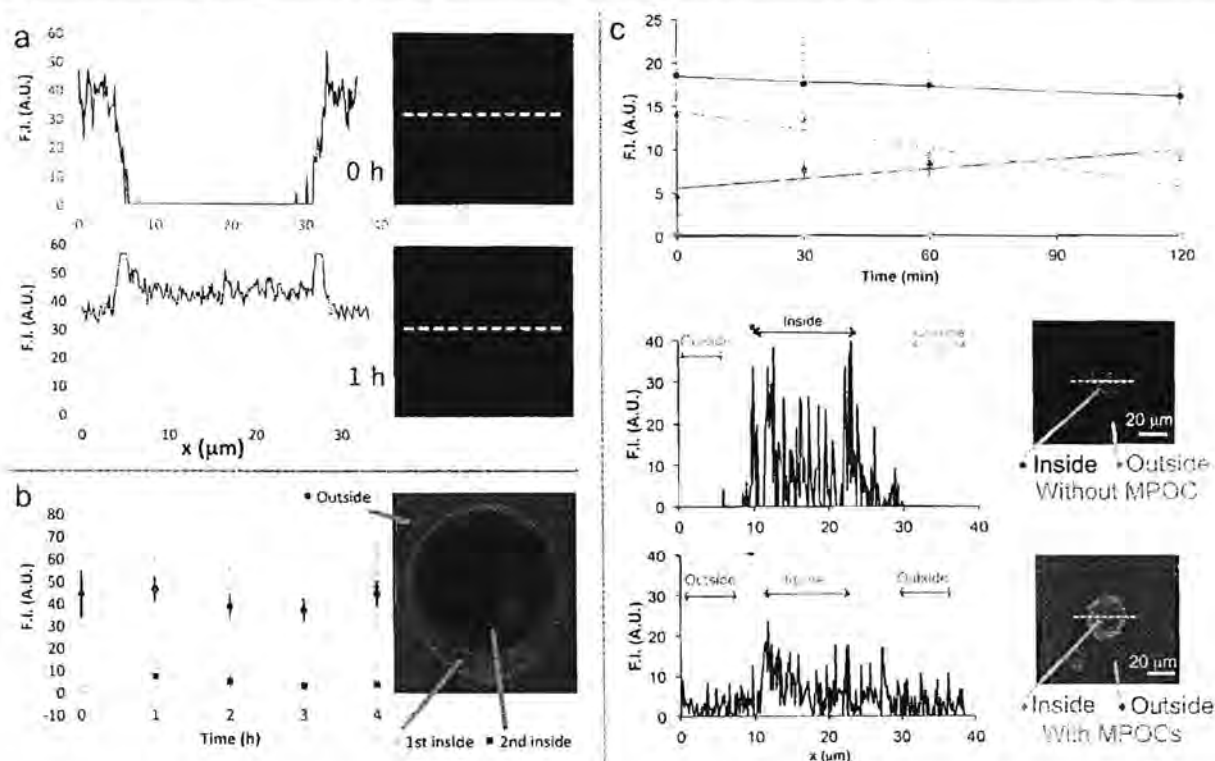


Figure 3. Liposome penetration. (A) Plots of fluorescence intensity (F.I.) of MPOC_{RhB} along the white dashed line of the corresponding liposome (on the right), at 0 and 1 h incubation of the liposome suspension with MPOC_{RhB}. (B) A plot of F.I. of MPOC_{RhB} at the outside, inside the first and the second layers, of the double layer liposomes (representative picture on the right) as a function of incubation time of liposomes and MPOC_{RhB} (shown as mean \pm SD, obtained from more than 20 liposomes). (C) A plot of anthocyanin F.I. at the inside and outside of the anthocyanin filled liposomes after water addition (without MPOC) or MPOC addition (with MPOCs), as a function of time (shown as mean \pm SD, obtained from more than 10 liposomes from independent experiments; representative intensities at 60 min time point of both conditions are shown at the bottom together with representative pictures of liposomes on the right).

functionalities. The particles can undergo reversible aggregation to give a broad size distribution of around 200–300 nm in water.

Cellular Uptake of MPOC. Incubation the MPOC_{TAMRA} the MPOCs covalently linked with 5(6)-carboxytetramethylrhodamine ($\lambda_{ex}/\lambda_{em}$ of 561/595 nm), with human epidermoid cervical carcinoma cell line (CaSki), mouse macrophage cell line (RAW 264.7) and AS49 human lung adenocarcinoma cells

(AS49) resulted in obvious cellular uptake of the MPOC_{TAMRA} (Supporting Information, Figure S4). In addition, the three cell lines showed complete survival when treated with 10 ppm MPOC_{TAMRA} (highest concentration tested). We conclude that MPOC_{TAMRA} can get into those cells and the particles are not toxic to the cells under the condition used.

Monitoring the Interaction between MPOCs and Lipid Bilayer Membrane by Förster Resonance Energy Trans-

fer (FRET) Using Cell-Sized Liposomes. We first prepared liposomes in which their lipid bilayer membranes contained a fluorescent donor (*N*-[6-[(7-nitro-2,1,3-benzoxadiazol-4-yl)-amino]hexanoyl]-phytosphingosine or C6NBD, $\lambda_{ex}/\lambda_{em} = 470/530$ nm). We next loaded a fluorescent acceptor (1,2-dimyristoyl-*sn*-glycero-3-phosphoethanolamine-*N*-(lissamine rhodamine B sulfonyl), $\lambda_{ex}/\lambda_{em} = 550/600$ nm) onto the MPOCs (weight ratio of MPOC: fluorescent acceptor of $1.0:3.84 \times 10^{-4}$). Complete adsorption of the acceptor on MPOCs was achieved. An ability of the acceptors on the MPOCs and that of the free acceptors to quench the emission of the donors in the liposomes was monitored through the decrease in donor emission accompanied by the increase in acceptor emission. It was clearly observed that the quenching was more quickly and more pronounced when the acceptors were loaded on MPOCs (Figure 2). Because the efficiency of this long-range dipole-dipole quenching is inversely proportional to the sixth power of the distance between donor and acceptor and usually can be detected when the distance does not exceed 10 nm, we conclude that MPOCs can facilitate a close association between the loaded acceptors and the donors in the liposome membrane.

Penetration of MPOCs into Cell-Sized Liposome. Next, we investigated the penetration of MPOCs across lipid bilayer membrane by incubating MPOC_{RhB}, the MPOCs covalently linked with Rhodamine B (RhB, $\lambda_{ex}/\lambda_{em}$ of 470–495/510–550 nm), with cell-sized liposomes. Through the fluorescence of RhB, we observed that MPOC_{RhB} moved toward the surface of the liposomes instantly after mixing (Figure 3a, 0 h). At the beginning the MPOC_{RhB} emission intensity at the inside of the liposome was undetectable. However, after 30 min incubation, MPOC_{RhB} emission intensity at the inside of the liposome was comparable to that at the outside (Figure 3a, 1 h). The result implied that MPOC_{RhB} interacted with the lipid bilayer membrane and penetrated into the interior of the liposomes. The fluorescence signals in the liposomes mostly appeared noncompartmentalized, indicating that the main penetration mechanism was not through an endocytic deformation of the membrane. We did observe some endocytic deformation of the liposomes and some compartmentalized fluorescence signals inside the liposomes, but very minor comparing to the diffusion of the noncompartmentalized fluorescence signals into the interior of the liposomes. In the case of double layer liposomes, signals of the MPOC_{RhB} was observed at the surface of the outer lipid bilayer membrane quickly after incubation, and later at first layer interior of the liposomes (Figure 3b). This indicated the penetration of MPOC_{RhB} across the first membrane layer. During the 4 h experiment, the second layer interior of the liposomes was never fully filled with MPOC_{RhB} emission. This indicated that after penetrating the first membrane layer, the MPOC_{RhB} could not effectively penetrate the second membrane layer.

We speculated that the penetration of MPOCs might occur through a transient pore formation at the lipid bilayer membrane. To prove this, we investigated an ability of MPOCs to leak anthocyanin (a water-soluble fluorescent dye) out of the liposomes. We first prepared liposomes filled with anthocyanin then monitored the fluorescence of the anthocyanin at the interior and exterior of the liposomes upon an addition of MPOCs into the liposome suspension. Anthocyanin signals at the exterior of the liposome could be detected only when MPOCs were added to the liposome suspension. More specifically, when MPOCs were added, the

signal of anthocyanin inside the liposomes decreased with incubation time while the signal of anthocyanin outside the liposomes increased with incubation time (Figure 3c). Adding water to the anthocyanin-filled liposome could not induce such leak. This indicated a continuous leakage of anthocyanin from the liposomes when MPOCs were added to the outside of the liposomes. The result agrees with our speculation that MPOCs can generate pores on lipid bilayer membrane of the liposomes. It is, therefore, concluded that anthocyanin molecules move out of the liposome through the transient pores generated on the lipid bilayer membrane by the MPOCs.

Lipid Adsorption on MPOCs. We speculated that the migration of phospholipid molecules from the bilayer membrane to the MPOC surface, was responsible for the pore formation on the membrane. Therefore, we evaluated an ability of MPOCs to adsorb phospholipids at pH 7.4 and 5.5. The result indicated that MPOCs could adsorb lipids at both pH conditions but adsorption at pH 5.5 was greater than at pH 7.4 (Supporting Information, Figure S5). It should be noted here that the zeta potential values of the MPOCs are -30.97 ± 2.06 mV and -33.31 ± 1.80 mV in pH 7.4 and 5.5 buffers, respectively. To further investigate the involvement of lipid adsorption on the pore generation, we tested an ability of phospholipid-loaded MPOCs to penetrate lipid bilayer membrane of the cell-sized liposomes. When the 2 to 1 (by weight) phospholipid/MPOC_{RhB} mixture was incubated with cell-sized liposomes, rhodamine fluorescence signals could be observed inside the liposomes. However, when the 10 to 1 (by weight) phospholipid/MPOC_{RhB} mixture was incubated with cell-sized liposomes, rhodamine fluorescence signals could not at all be observed inside the liposomes. The results imply that a high amount of phospholipid on the MPOC surface can suppress the lipid bilayer membrane penetration ability of the particles. This excellent ability of MPOCs to adsorb phospholipids also agreed well with the above FRET result and our observation that the MPOCs always instantly moved to the surface of the liposomes. All these results suggest that MPOC possesses high phospholipid affinity, and the particle's ability to induce leakage on lipid bilayer membrane may involve its phospholipid adsorption. It should be noted here that this is not the first report on the interaction between carbon-based materials and lipid bilayer membrane. An ability to situate themselves at the lipid bilayer membrane of carbon nanotubes (CNT) and oxidized CNT has been demonstrated earlier.^{22–24} Pore formation on lipid bilayer membrane by carbon based material, however, has been demonstrated only with carbon black particles in which the femto-second laser pulse was needed to assist their pore formation.²⁵

Using the obtained results, we explain the ability of MPOCs to penetrate only the first membrane layer, not the second membrane layer, of the double layer liposomes (Figure 3b) as follows: pore formation at the first membrane layer by MPOCs resulted in lipid-adsorbed MPOCs inside the first layer of the liposomes, and lipids on the MPOCs surface prevented the particles to significantly adsorb more lipids from the second membrane layer, thus inhibiting further pore induction.

Cellular Delivery of PNA by MPOC. Next, we used MPOCs to leak PNAs into cells to perform antigene function. The binding site of NF- κ B transcription factor is between -75 and -63 in the promoter of *Il6* gene¹⁷ and the sequence between -74 to -63 (GGGATTTTCCCA) was selected as the antigene target site. We synthesized two 12mer PNAs, one with the sequence specific to the antisense strand of the binding site

of NF- κ B transcription factor (PNA_{NF κ B}) and the other with a random sequence (PNA_{random}). Also we fluorescently labeled the two PNAs with fluorescein (Flu): PNA_{NF κ B-flu} and PNA_{random-flu}.

Cytotoxicity of PNA_{NF κ B}, MPOCs and the mixture of PNA_{NF κ B} and MPOCs, was investigated quantitatively by MTT assay in RAW 264.7 cells at up to 10.0 μ g/mL MPOCs and 100 nM PNA_{NF κ B}, and the result indicated no toxicity under our experimental conditions (Supporting Information, Figure S6).

Next we investigated the cellular uptake and localization of the PNA_{NF κ B-flu} in the presence and absence of MPOC_{TAMRA} by RAW 264.7 cells. CLFM images of the cells incubated with PNA_{NF κ B-flu} for 4 h (Figure 4 row 2) showed no signals of

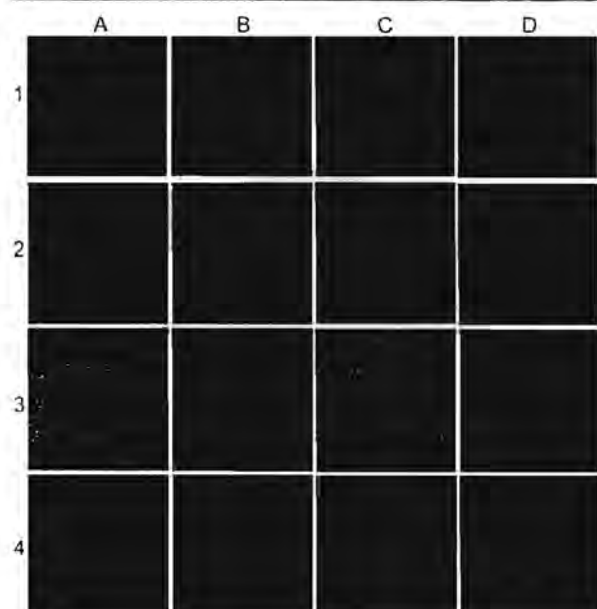


Figure 4. Cellular delivery of PNAs by MPOCs. Confocal fluorescence images of RAW 264.7 cells after being incubated with water (row 1), PNA_{NF κ B-flu} (row 2), PNA_{NF κ B-flu} plus MPOC_{TAMRA} (row 3), and MPOC_{TAMRA} (row 4). Images, as the original (column A) or separated (columns B–D), show the fluorescence signals indicating nucleus in blue (column B), PNAs in green (column C), and MPOCs in red (column D).

PNA_{NF κ B-flu} in the cells, indicating that without MPOC_{TAMRA} PNA_{NF κ B-flu} could not significantly penetrate into cells. Intense signals from PNA_{NF κ B-flu} inside the nuclei, intense signals from MPOC_{TAMRA} in the cytoplasm of the cells incubated with PNA_{NF κ B-flu} plus MPOC_{TAMRA} (Figure 4 row 3), implied effective delivery of PNA_{NF κ B-flu} into the cells by MPOC_{TAMRA} and accumulation of the PNA_{NF κ B-flu} and MPOC_{TAMRA} in the nuclei and cytoplasm, respectively. Noted that cells incubated with only MPOC_{TAMRA} (without PNAs) also showed the uptake of the particles (Figure 4 row 4). Similar results were observed for PNA_{random-flu} (Supporting Information, Figure S7). We further confirmed the ability of MPOCs to deliver the PNAs in another cell line. Comparing to the commercially available reagent, FuGENE-HD (positively charged liposome), using flow cytometry, MPOCs showed significantly higher efficiency in delivering PNAs into the 293T human embryonic kidney (HEK293T) cells (Supporting Information, Figure S8).

It should be noted that using MPOCs as carriers is simple and requires no organic solvent since MPOC is water dispersible (ethanol is needed for the lipid-based FuGENE-HD).

Endosome Evasion and Lysosome Avoidance. Next, we investigated the cellular trafficking by incubating the RAW 264.7 cells with PNA_{NF κ B-flu} mixed with coumarin-labeled MPOCs (MPOC_{Cou}) and monitoring the living cells under confocal laser fluorescence microscope (CLFM). Endosomes and lysosomes were tracked with early endosome and lysosome specific dyes. The same location of fluorescence signals from PNA_{NF κ B-flu}, MPOC_{Cou}, and endosome specific dye, was observed after 30 min postincubation, implying that the PNA_{NF κ B-flu} and MPOC_{Cou} were in the endosomes (Figure 5

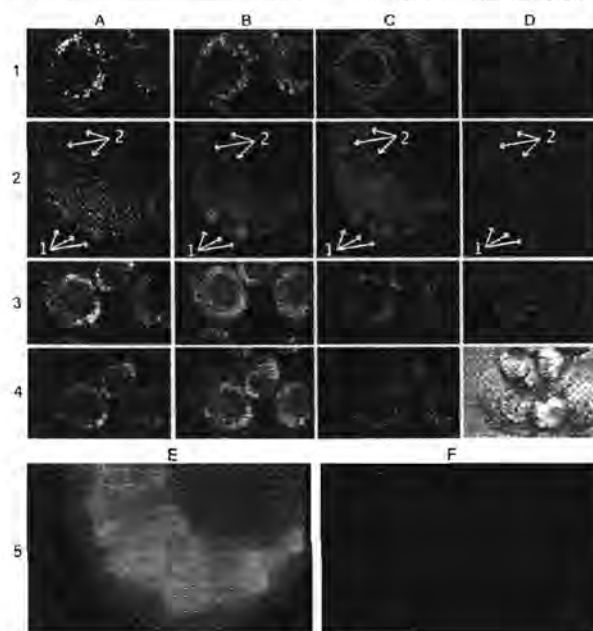


Figure 5. Endosome evasion of MPOCs. CLFM images of RAW 264.7 cells after being incubated with PNA_{NF κ B-flu} plus MPOC_{Cou} for 40 (row 1 and 2), 105 (row 3), and 210 (row 4 and 5) min. Signals from MPOC_{Cou} (column A), PNA_{NF κ B-flu} (column B), early endosome (column C) and lysosome (column D row 1, 2, and 3), are shown in white, green, red, and blue, respectively. Cell morphology at 210 min is shown in column D of row 4. Row 2 is an expansion of row 1; arrow 1 indicates colocalization of MPOC/PNA/endosome; arrow 2 indicates colocalization of endosomes/lysosomes. 5E and 5F are expansions of 4B and 4C, respectively.

and Supporting Information Video). Interestingly, signals from lysosomes did not colocalize with signals from the endosomes that contained PNA_{NF κ B-flu}/MPOC_{Cou} (arrow 1, Figure 5 row 2), indicating that the endosomes filled with PNA_{NF κ B-flu} and MPOC_{Cou} were not merging with lysosomes. Noted that a normal merging of lysosomes with the endosomes that contained no PNA_{NF κ B-flu}/MPOC_{Cou} could still be observed (arrow 2, Figure 5 row 2). Here the emission from the lysosome specific dye started to fade at \approx 150 min, and throughout the 150 min observation, no merging of lysosome and PNA_{NF κ B-flu}/MPOC_{Cou}-containing endosome was observed. After 90 min incubation, obvious fluorescence signals from PNA_{NF κ B-flu} and MPOC_{Cou} could be observed throughout the cytoplasm and nucleus. These late observed signals appeared noncompartmentalized and did not colocalize with the signals

from endosome/lysosome specific dyes, thus implying the leak of PNA_{NFκB-flu} and MPOC_{Cou} from some of the endosomes or the degradation of some of the endosomes. The leakage of the endosomes and the disruption of the endosomes together with the diffusion of PNA_{NFκB-flu} all over the cells were very obvious at 210 min postincubation (Figure 5 row 4). The result implies that a presence of MPOCs in the endosome not only can induce endosome leakage, but can also prevent the fusion between such endosome and a lysosome.

Although in the liposome experiments above, penetration of MPOCs via endocytic deformation of the membrane was quite minor comparing to the penetration via transient pores, the result in the cell culture clearly indicated that the majority of the PNA_{NFκB-flu} and MPOC_{Cou} were taken up into the cells via endocytosis. In the liposome experiment, we observed the instant binding of the MPOCs to the lipid bilayer membrane, whereas the penetration usually took at least 15–30 min longer. Therefore, it was likely that in the cell culture, MPOCs also quickly bound to the cell membrane, and the binding induced endocytic uptakes of the PNA_{NFκB-flu}/MPOC_{Cou} into the cells before the pores were formed. Therefore, we explain the results as follows: PNA_{NFκB-flu}-loaded MPOC_{Cou} bound the cell membrane and a majority of PNA_{NFκB-flu}-loaded MPOC_{Cou} entered the cells by endocytosis. The MPOC_{Cou} inside the endosomes continued the pore generation process and finally could successfully induce pores on the compartments, resulting the leakage of PNA_{NFκB-flu} and MPOC_{Cou} from the endosomes into the cytoplasm observable at approximately 90 min postincubation (Figure 5 rows 4 and 5, Supporting Information Video). Some PNA_{NFκB-flu} and MPOC_{Cou} might leak into the cells via transient pores on the cell membrane, but it is very minor compared to those that entered via the endosomes. The increase in acidity of the endosomes during their maturation should also increase the phospholipid adsorption capacity of MPOCs and might contribute to a more efficient induction of endosome leakage. It should be noted here that the time required for MPOCs to generate pores in the real cells was significantly longer than in the liposomes (endosome leakage was observed at approximately 90 min postincubation, whereas liposome penetration was observed at 15–30 min postincubation). The different lipid bilayer membrane composition between liposomes and cells is likely one of many factors contribute to this discrepancy.

Antigene Action. Next we investigated the gene silencing function of the PNA_{NFκB} delivered into the cells by MPOCs. We incubated RAW 264.7 cells with each tested sample (PNA_{andom} and PNA_{NFκB} either alone or with MPOCs), stimulated the cells with lipopolysaccharide (LPS) plus murine recombinant interferon gamma (rmIFN-γ), then monitored the amount of *Il6* mRNA by the quantitative-reverse transcription polymerase chain reaction (qRT-PCR) (Figure 6a) and amount of IL-6 protein by enzyme-linked immunosorbent assay (ELISA) (Figure 6b). The result showed that without MPOC, the presence of the two PNAs did not affect *Il6* mRNA level. Under the unstimulated condition, MPOCs (5.0 mg/L) caused a small increase in the level of *Il6* mRNA. It was possible that at the concentration used, MPOCs could mildly stimulate *Il6* mRNA expression. Elucidation on this point is, however, beyond the scope of this report. Comparing between the cells treated with PNA_{andom}/MPOCs and those treated with PNA_{NFκB}/MPOCs, the latter showed 70% less increase of *Il6* mRNA level upon LPS/rmIFN-γ stimulation (Figure 6a). Thus, when delivered into cells by MPOCs, only the PNA_{NFκB},

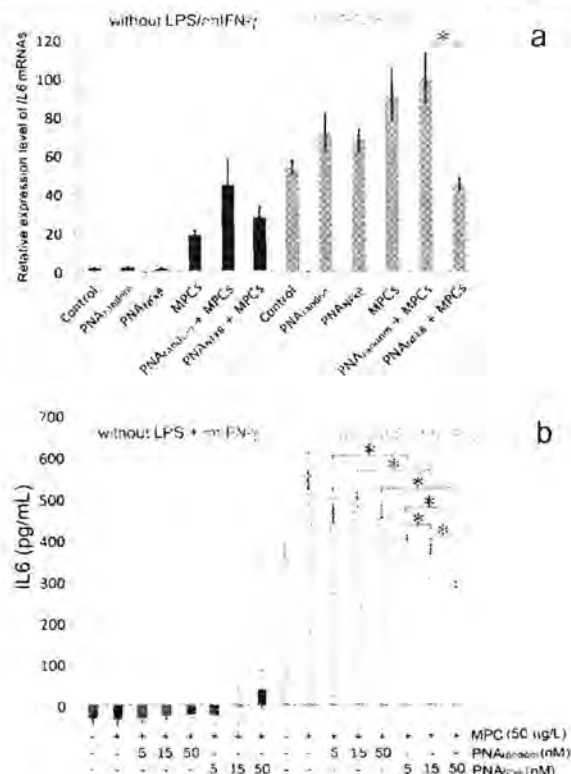


Figure 6. Interfering with *Il6* expression in vitro. A) Relative expression levels of *Il6* mRNA obtained when incubated RAW 264.7 cells (4×10^5 cells/mL) with various samples (control = water), under unstimulated (without LPS and rmIFN-γ) and stimulated (with LPS and rmIFN-γ) conditions, determined at the MPOC and PNA concentrations of 5 mg/L and 500 nM (2.1 μg/mL), respectively. B) Amounts of IL-6 proteins obtained when incubated RAW 264.7 cells with various samples under unstimulated (without LPS and rmIFN-γ) and stimulated (with LPS and rmIFN-γ) conditions. Data are shown as the mean ± 1 standard deviation and a star indicates the statistical significant difference between the two samples, as determined by one way ANOVA Duncan at $P < 0.05$.

and not the PNA_{andom} could suppress the transcription of *Il6* gene. This antigene action of PNA_{NFκB} was further confirmed at the translation level.

As shown in Figure 6b, a presence of 50 μg/L of MPOCs did not significantly affect the IL-6 protein level. It should be noted that the optimized MPOC concentration used here (50 μg/L) was lower than that used in the above transcription experiment. In the presence of MPOCs, only the PNA_{NFκB}, not the PNA_{andom}, could suppress IL-6 production upon LPS/rmIFN-γ stimulation in a dose dependent manner. The result agreed well with the decreased *Il6* mRNA level in the above experiment. We conclude that the PNA_{NFκB} delivered into cells by MPOCs can suppress the *Il6* gene transcription, resulting in the decreases in *Il6* mRNA and IL-6 protein levels. It is likely that the open-up of the actively transcribed *Il6* gene under LPS/rmIFN-γ stimulation should theoretically allow the access and binding of the PNA_{NFκB} to this targeted gene. In addition, the possibility of the 12 base long PNA_{NFκB} to bind to the open-up *Il6* gene, not to other genes in the chromatin, should also be increased under the stimulated condition.²⁶

In conclusion (Supporting Information, Figure S9), here we introduce the "particle-induced transient pore on lipid bilayer

membrane" strategy to deliver bioactive molecules into cells without getting trapped in a lysosome. Synthesis and characterization of oxidized carbon particles with membrane penetrating property (called membrane penetrating carbon oxide nanoparticles or MPOCs) are shown. The mechanism of pore formation and how the MPOCs evade endosome are included. Using this delivery strategy, we show an ability of the acpcPNA to block gene transcription under a stimulated condition. This work, thus, kindles the particle-induced transient pore strategy to deliver matters across lipid bilayer membranes. We also anticipate applications of (i) MPOC as a delivery vector with endosome evasion property and (ii) acpcPNA as a potential antigene agent.

■ ASSOCIATED CONTENT

Supporting Information

Figures S1–S9, Materials and methods, Cellular trafficking video. This material is available free of charge via the Internet at <http://pubs.acs.org>.

■ AUTHOR INFORMATION

Corresponding Author

*E-mail: psupason@chula.ac.th.

Author Contributions

These authors contributed equally.

The manuscript was written through contributions of all authors.

Notes

The authors declare no competing financial interest.

■ ACKNOWLEDGMENTS

We thank Dr. Tatsuya Murakami at Japan Advanced Institute of Science and Technology for XPS analysis, and the Olympus Bioimaging Center at Mahidol University for fluorescence recording of live-cells. This work was financially supported by the Grant for Chula Research Scholar from the Ratchadapiseksompot Fund from Chulalongkorn University (CU), the CU 90th anniversary fund, Advance material cluster (RES 560530097), Nanotec-CU Center of Excellence on Food and Agriculture, and the Thailand Research Fund (DPG5780002), Thailand; MEXT KAKENHI (Nos. 25104510 and 26103516) and the Kao Foundation for Arts and Sciences, Japan. J.S. is funded by CU Dutsadiphiphat Scholarship, and P.P.-I. is funded by postdoctoral fellowship from CU.

■ REFERENCES

- (1) De Rosa, G.; La Rotonda, M. I. *Molecules* 2009, 14, 2801–2823.
- (2) Devi, G. R. *Cancer Gene Ther.* 2006, 13, 819–829.
- (3) Akinc, A.; Zumbuehl, A.; Goldberg, M.; Leshchiner, E. S.; Busini, V.; Hossain, N.; Bacallado, S. A.; Nguyen, D. N.; Fuller, J.; Alvarez, R.; Borodovsky, A.; Borland, T.; Constien, R.; de Fougerolles, A.; Dorkin, J. R.; Narayanannair Jayaprakash, K.; Jayaraman, M.; John, M.; Kotliansky, V.; Manoharan, M.; Nechev, L.; Qin, J.; Racie, T.; Raitcheva, D.; Rajeev, K. G.; Sah, D. W. Y.; Soutschek, J.; Toudjarska, I.; Vornlocher, H.-P.; Zimmermann, T. S.; Langer, R.; Anderson, D. G. *Nat. Biotechnol.* 2008, 26, 561–569.
- (4) Falsini, S.; Ciani, L.; Ristori, S.; Fortunato, A.; Arcangeli, A. J. *Med. Chem.* 2014, 57, 1138–1146.
- (5) Boussif, O.; Lezoualc'h, F.; Zanta, M. A.; Mergny, M. D.; Scherman, D.; Demeneix, B.; Behr, J. P. *Proc. Natl. Acad. Sci. U.S.A.* 1995, 92, 7297–7301.
- (6) Islam, M. A.; Park, T. E.; Singh, B.; Maharjan, S.; Firdous, J.; Cho, M. H.; Kang, S. K.; Yun, C. H.; Choi, Y. J.; Cho, C. S. *J. Controlled Release* 2014, 193, 74–89.
- (7) Copolovici, D. M.; Langel, K.; Eriste, E.; Langel, U. *ACS Nano* 2014, 8, 1972–1994.
- (8) Jones, A. T.; Sayers, E. J. *J. Controlled Release* 2012, 161, 582–591.
- (9) Merkel, O. M.; Beyerle, A.; Beckmann, B. M.; Zheng, M.; Hartmann, R. K.; Stöger, T.; Kissel, T. H. *Biomaterials* 2011, 32, 2388–2398.
- (10) Shiraishi, T.; Nielsen, P. E. *Nat. Protoc.* 2006, 1, 633–636.
- (11) Somia, N.; Verma, I. M. *Nat. Rev. Genet.* 2000, 1, 91–99.
- (12) Lakshmanan, S.; Gupta, G. K.; Avci, P.; Chandran, R.; Sadasivam, M.; Jorge, A. E. S.; Hamblin, M. R. *Adv. Drug Delivery Rev.* 2014, 71, 98–114.
- (13) Vilaivan, T.; Srisuwannaket, C. *Org. Lett.* 2006, 8, 1897–1900.
- (14) Libermann, T. A.; Baltimore, D. *Mol. Cell. Biol.* 1990, 10, 2327–2334.
- (15) Grigoriev, M.; Praseuth, D.; Robin, P.; Hemar, A.; Saison-Behmoaras, T.; Dautry-Varsat, A.; Thuong, N. T.; Hélène, C.; Harel-Bellan, A. *J. Biol. Chem.* 1992, 267, 3389–3395.
- (16) Vickers, T. A.; Griffith, M. C.; Ramasamy, K.; Risen, L. M.; Freier, S. M. *Nucleic Acids Res.* 1995, 23, 3003–3008.
- (17) Ray, A.; Tatter, S. B.; May, L. T.; Sehgal, P. B. *Proc. Natl. Acad. Sci. U.S.A.* 1988, 85, 6701–6705.
- (18) Kim, H. J.; Lee, S. M.; Oh, Y. S.; Yang, Y. H.; Lim, Y. S.; Yoon, D. H.; Lee, C.; Kim, J. Y.; Ruoff, R. S. *Sci. Rep.* 2014, 4, 5176.
- (19) Dresselhaus, M. S.; Dresselhaus, G.; Saito, R.; Jorio, A. *Phys. Rep.* 2005, 409, 47–99.
- (20) Bandow, S.; Takizawa, M.; Hirahara, K.; Yudasaka, M.; Iijima, S. *Chem. Phys. Lett.* 2001, 337, 48–54.
- (21) Bethune, D. S.; Meijer, G.; Tang, W. C.; Rosen, H. J.; Golden, W. G.; Seki, H.; Brown, C. A.; de Vries, M. S. *Chem. Phys. Lett.* 1991, 179, 181–186.
- (22) Corredor, C.; Hou, W. C.; Klein, S. A.; Moghadam, B. Y.; Goryll, M.; Doudrick, K.; Westerhoff, P.; Posner, J. D. *Carbon* 2013, 60, 67–75.
- (23) Geng, J.; Kim, K.; Zhang, J.; Escalada, A.; Tunuguntla, R.; Comolli, L. R.; Allen, F. I.; Shnyrova, A. V.; Cho, K. R.; Munoz, D.; Wang, Y. M.; Grigoropoulos, C. P.; Ajo-Franklin, C. M.; Frolov, V. A.; Noy, A. *Nature* 2014, 514, 612–615.
- (24) Liu, L.; Yang, C.; Zhao, K.; Li, J.; Wu, H. C. *Nat. Commun.* 2013, 4, 2989.
- (25) Chakravarty, P.; Qian, W.; El-Sayed, M. A.; Prausnitz, M. R. *Nat. Nanotechnol.* 2010, 5, 607–611.
- (26) Janowski, B. A.; Kaihatsu, K.; Huffman, K. E.; Schwartz, J. C.; Ram, R.; Hardy, D.; Mendelson, C. R.; Corey, D. R. *Nat. Chem. Biol.* 2005, 1, 210–215.



Quaternized chitosan particles as ion exchange supports for label-free DNA detection using PNA probe and MALDI-TOF mass spectrometry

Jittima Meebungpraw^{a,b}, Oraphan Wiarachai^c, Tirayut Vilaivan^d,
Suda Kiatkamjornwong^e, Voravee P. Hoven^d

^a Program in Petrochemistry and Polymer Science, Faculty of Science, Chulalongkorn University, Phayathai Road, Pathumwan, Bangkok 10330, Thailand

^b Center of Excellence on Petrochemical and Materials Technology, Chulalongkorn University, Phayathai Road, Pathumwan, Bangkok 10330, Thailand

^c Program in Petrochemistry, Faculty of Science, Chulalongkorn University, Phayathai Road, Pathumwan, Bangkok 10330, Thailand

^d Organic Synthesis Research Unit, Department of Chemistry, Chulalongkorn University, Phayathai Road, Pathumwan, Bangkok 10330, Thailand

^e Department of Imaging and Printing Technology, Faculty of Science, Chulalongkorn University, Phayathai Road, Pathumwan, Bangkok 10330, Thailand

ARTICLE INFO

Article history:

Received 9 January 2015

Received in revised form 20 May 2015

Accepted 20 May 2015

Available online 29 May 2015

Keywords:

Chitosan

Pyrrrolidinyl peptide nucleic acid

Quaternary ammonium group

MALDI-TOF mass spectrometry

DNA sequence analysis

ABSTRACT

Quaternized chitosan particles are introduced as anion-exchanged captures to be used with a conformationally constrained pyrrolidinyl peptide nucleic acid (*acpcPNA*) and MALDI-TOF mass spectrometry for DNA sequence analysis. Methylated chitosan (MC) and methylated *N*-benzyl chitosan (MBzC) particles were obtained by heterogeneous chemical modification of ionically cross-linked chitosan particles via direct methylation and reductive benzylation/methylation, respectively. *N,N,N*-trimethylchitosan (TMC) and *N*-[(2-hydroxyl-3-trimethylammonium)propyl]chitosan chloride (HTACC) particles were prepared by ionic cross-linking of quaternized chitosan derivatives, homogeneously modified from chitosan, namely TMC and HTACC, respectively. The particles formed had a size in a sub-micrometer range and possessed positive charge. Investigation by MALDI-TOF mass spectrometry suggested that some quaternized particles in combination with *acpcPNA* were capable of detecting a single mismatched base out of 9–14 base DNA sequences. Potential application of this technique for the detection of wild-type and mutant *K-ras* DNA, a gene that mutation is associated with certain cancers, has also been demonstrated.

© 2015 Elsevier Ltd. All rights reserved.

1. Introduction

Chitosan is a natural polymer derived by partial deacetylation of chitin – a substance abundantly found in the exoskeletons of insects, the shells of crustaceans, and fungal cell walls. Due to the presence of ammonium groups in the structure, chitosan can form a stable complex with DNA in the solution having a pH range of 2–7 (Hayatsu, Kubo, Tanaka, & Negishi, 1997) and extract DNA with very high extraction efficiency (63–92%) even in complex DNA samples such as human genomic DNA from whole blood samples (Cao, Easley, Ferrance, & Sanders, 2006). The hydrophilic sugar-based structure of chitosan ensures low non-specific binding – mainly through hydrophobic interactions – with other non-DNA components such as proteins and other interfering samples. These, together with the fact that the ammonium groups of chitosan can be converted into various quaternary ammonium entities prompts

us to develop into an effective capture for negatively charged DNA that may be applicable for DNA sequence analysis.

Peptide nucleic acid (PNA), a neutral-peptide backbone DNA mimic firstly developed by Nielsen and co-workers (Egholm, Buchardt, Nielsen, & Berg, 1992; Nielsen, Egholm, Berg, & Buchardt, 1991), has a great potential to be used as a probe for DNA biosensor. The hybrid formed between PNA and its complementary DNA is more stable than the corresponding DNA-DNA hybrid due to the absence of electrostatic repulsion between negative charges along the phosphate backbone existing in the DNA structure (Sassolas, Toca-Bouvier, & Blum, 2007). Recently, a conformationally restricted pyrrolidinyl PNA based on *D*-prolyl-2-aminocyclopentane-carboxylic acid backbones (*acpcPNA*) was introduced by Vilaivan and co-workers. This PNA system possessed higher binding affinity and sequence specificity toward DNA than that of Nielsen's PNA, and with a much stronger preference for the antiparallel binding mode (Ananthanawat, Vilaivan, Hoven, & Su, 2010; Suparpprom, Srisuwannaket, Sangvanich, & Vilaivan, 2005; Vilaivan & Srisuwannaket, 2006). The powerful discrimination for single mismatched DNA makes *acpcPNA* a potential candidate for the development of highly effective DNA biosensors, which has

* Corresponding author. Tel.: +66 2218 7627; fax: +66 2218 7598.
E-mail address: vipasee.puthola@chul.ac.th (V.P. Hoven).

been continuously proven for both labeling (Boontha, Vilaivan, Wagenknecht, & Vilaivan, 2011; Maneelun & Vilaivan, 2013; Mansawat, Boontha, Sriwong, & Vilaivan, 2012; Rashatasakorn, Vongnam, Siripornnoppakun, Vilaivan, & Sukwattanasinitt, 2012; Reenabthue, Boontha, Vilaivan, Vilaivan, & Suparpprom, 2011) and non-labeling techniques (Ananthanawat, Hoven, Vilaivan, & Su, 2011; Ananthanawat, Vilaivan, & Hoven, 2009; Ananthanawat, Vilaivan, Mekboonsonglarp, & Hoven, 2009; Jampasa et al., 2014; Sankoh et al., 2013; Theppaleak, Rutnakornpituk, Wichai, Vilaivan, & Rutnakornpituk, 2013a, 2013b; Thipmanee et al., 2012).

Recently, a simple label-free DNA sensing platform which relied on distinct electrostatic properties of *acpc*PNA and DNA was developed for analysis of single nucleotide polymorphism and food adulteration detection (Boontha, Nakkuntod, Hirankarn, Chaumplok, & Vilaivan, 2008). Because PNA is an electrostatically neutral molecule, it cannot be captured by a positively charged anion-exchanger unless hybridized with its complementary DNA target. The captured PNA can then be detected by MALDI-TOF MS (Boontha et al., 2008; Theppaleak et al., 2013a, 2013b) or alternatively by enzyme-mediated colorimetric detection (Laopa, Vilaivan, & Hoven, 2013). In this assay, the crude DNA products obtained after PCR can be used directly without prior purification and the analysis can be performed at room temperature under non-stringent conditions. Besides the satisfactory binding properties and specificity of the PNA probe, the success of this approach should also depend upon the physical properties of the anion exchanger, especially the ability to prevent non-specific adsorption of the unhybridized PNA. Q-sepharose, a commercially crosslinked agarose particles bearing quaternary ammonium groups (Boontha et al., 2008), and quaternized poly(dimethylamino)ethyl methacrylate-grafted cellulose paper (Laopa et al., 2013) or magnetic nanoparticles (Theppaleak et al., 2013a, 2013b) were previously used as solid support for the DNA capture. From material science perspective, the issue related to chemical functionality and hydrophobicity/hydrophilicity of the anion exchanger on the DNA capturing is also worth to be explored and has not yet been addressed in previous investigations.

Here in this research, we synthesized and compared the efficiency of modified-chitosan particles as anion exchangers for PNA-based detection of DNA by MALDI-TOF mass spectrometry. Two routes for the preparation of quaternized chitosan particles were performed. The first route is based on heterogeneous chemical modification of ionically cross-linked chitosan particles via direct methylation and reductive benzylation/methylation that yielded methylated chitosan (MC), methylated *N*-benzyl chitosan (MBzC) particles, respectively. The second route is based on ionic cross-linking of quaternized chitosan derivatives, homogeneously modified from chitosan, namely *N,N,N*-trimethylchitosan (TMC) and *N*-[(2-hydroxy-3-trimethylammonium)propyl]chitosan chloride (HTACC) that gave TMC and HTACC particles, respectively. Synthetic methodology of both routes is outlined in Scheme 1. It is anticipated that this research should open up a new direction for chitosan applications in the area of biosensors in the format, to the best of our knowledge, that has never been reported.

2. Materials and methods

2.1. Materials

Chitosan flake ($M_v = 45,000$ Da) was purchased from Seafresh Chitosan (Lab) Co., Ltd (Thailand). Degree of deacetylation (%DD) of chitosan calculated based on ^1H NMR data (shown in Fig. S1 and Table S1 in Supplementary Data) was 96.8%. Acetaldehyde, methyl iodide (CH_3I), sodium borohydride (NaBH_4), sodium hydroxide (NaOH), sodium iodide (NaI), and sodium tripolyphosphate (TPP) were obtained from Fluka (Switzerland). Acetic acid,

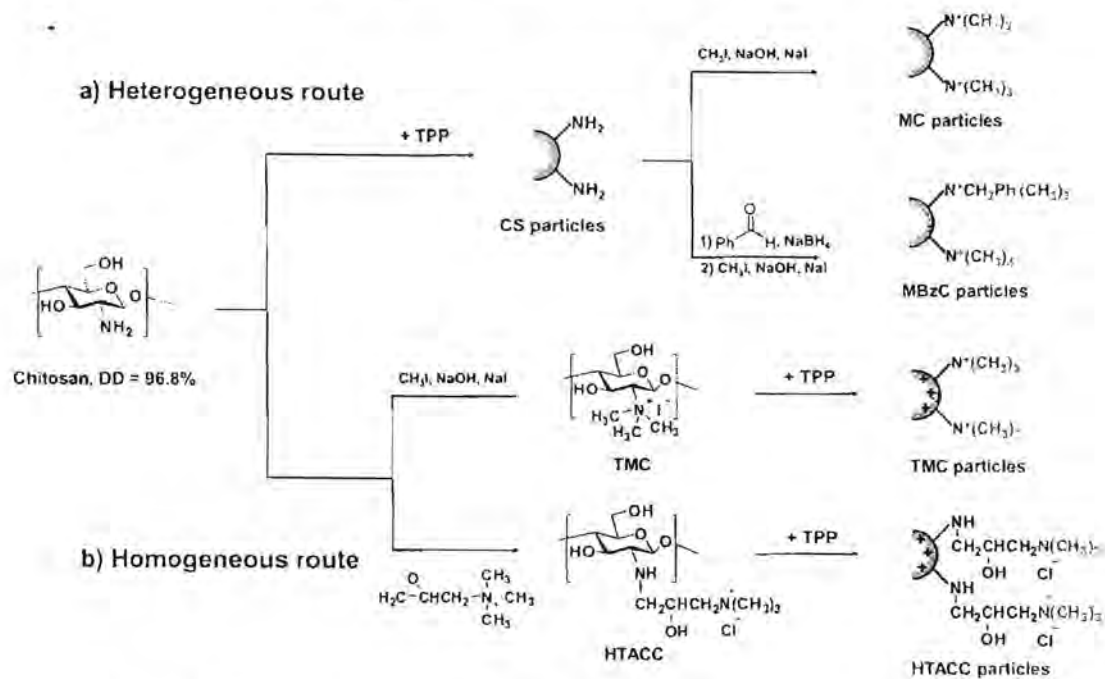
benzaldehyde, *N*-methylpyrrolidone (NMP), and methanol (MeOH) were purchased from Merck (Germany). Glycidyltrimethylammonium chloride (GTMAC) was obtained from Fluka (Switzerland). Genomic DNA from *Escherichia coli* strain B type VIII was obtained from Sigma (USA). PNAs were synthesized manually by solid phase peptide synthesis on TentaGel S RAM resin (Fluka) preloaded with Fmoc-L-Lys(Boc)-OPfp (Calbiochem Novabiochem Co., Ltd., USA) following the procedure described earlier (Vilaivan & Srisuwannaket, 2006). The identity of the PNAs was verified by MALDI-TOF mass spectrometry (Bruker Daltonik GmbH, Germany). Oligonucleotides were purchased from Bioservice Unit, National Science and Technology Development Agency (Thailand). All reagents and materials are analytical grade and used without further purification. Ultrapure distilled water was obtained after purification using a Millipore Milli-Q system (USA) that involves reverse osmosis, ion exchange, and a filtration step.

2.2. Preparation of quaternized chitosan particles by heterogeneous route

Chitosan (CS) particles were fabricated using TPP as a cross-linking agent according to the method reported by Qi, Xu, Jiang, Hu, and Zou (2004). Two types of quaternized chitosan particles, namely methylated *N*-benzyl chitosan (MBzC) and methylated chitosan (MC) particles were prepared following the method reported by Wiarachai, Thongchul, Kiatkanjornwong, and Hoven (2012). An anhydrous methanol solution of 1.0 M benzaldehyde (10 mL) was added into a flask containing the chitosan particles (0.03 g). After stirring for 4 h at room temperature, NaBH_4 (0.3 g, 8.0 mmol) was added into the reaction mixture and the solution was stirred for 24 h. The resulting *N*-benzyl chitosan particles were then isolated by centrifugation at 12,000 rpm for 30 min. The supernatant was discarded and the particles were centrifugally washed three times as above with methanol and then dried in vacuo. Methylation was then performed by an addition of anhydrous methanol solution (10 mL) of NaI (0.30 g, 2 mmol) and NaOH (0.13 g, 3.3 mmol) into the flask containing the *N*-benzyl chitosan particles (0.03 g) followed by CH_3I (2.0 M, 3.1 mL) via a syringe. The reaction mixture was stirred at 50 °C for 12 h and then the MBzC particles obtained were isolated and purified as above. MC particles, on the other hand, were prepared by direct methylation of the CS particles as follows. Anhydrous methanolic solution (10 mL) of NaOH (0.13 g, 3.3 mmol) and NaI (0.30 g, 2.0 mmol) was added into a flask containing chitosan particles (0.05 g), followed by an addition of CH_3I (0.4 mL, 6.4 mmol). The same portion of CH_3I was added after the mixture was stirred for 4 h at 50 °C. The reaction was allowed to proceed for another 4 h under the same condition. The synthesized MC particles were then isolated by the same procedure as described above.

2.3. Preparation of quaternized chitosan particles by homogeneous route

TMC was synthesized according to a modified method of Domard, Kinauchi, and Terrasch (1986). Chitosan (2.0 g) was dispersed in 80 mL of NMP followed by adding NaOH (0.81 g, 0.02 mol) and NaI (1.51 g, 0.01 mol). CH_3I (4.32 g, 0.03 mol) was added to the reaction mixture which was then stirred magnetically at 40 °C for 4 h. An additional portion of CH_3I was then added to the mixture and the reaction was allowed to proceed for another 4 h under the same condition. The final product was precipitated using acetone and isolated by centrifugation at 12,000 rpm for 30 min. The precipitate was dissolved in 15.0% (w/v) NaCl solution for 4 h in order to replace the iodide counterion with chloride. The suspension was dialyzed against deionized water in a dialysis bag (cut-off molecular weight of 14,000 g/mol) at ambient temperature for 5 days to



Scheme 1. Preparation of quaternized chitosan particles by (a) heterogeneous and (b) homogeneous routes.

remove residual small molecules. The final product was obtained after lyophilization.

To prepare TMC particles, TMC (0.2 g) was dissolved in deionized water (100 mL) to give a 0.2% (w/v) TMC solution. The particles were formed spontaneously upon an addition of an aqueous TPP solution (1.01 mM, 3 mL) to the TMC solution (3 mL) under magnetic stirring. The particles were isolated by centrifugation at 12,000 rpm for 30 min, centrifugally washed with deionized water three times and then dried by lyophilization before further use.

HTACC was synthesized according to a modified method of Seong, Whang, and Ko (2000). Chitosan (~5 g) was dissolved in 1% v/v acetic acid at ambient temperature. GTMAC (15.3 g, 4 equiv) was then added into the chitosan solution. The reaction was performed at 70 °C for 24 h. The product was dialyzed with deionized water for 3 days, followed by lyophilization to obtain a cotton-like material that was dissolved in deionized water overnight to obtain a stock solution with a concentration of 0.2% (w/v). HTACC particles were formed spontaneously upon an addition of an aqueous TPP solution (6.06 mM, 3 mL) to this HTACC aqueous solution (3 mL) under magnetic stirring. The obtained HTACC particles were isolated by centrifugation, washed and lyophilized as described above.

2.4. Characterization of quaternized chitosan particles

Chemical identity of the particles was confirmed by Fourier transform-infrared (FT-IR) spectroscopy (Nicolet Impact 410) and nuclear magnetic resonance spectroscopy (Varian Mercury 400, operating at 400 MHz). All samples for FT-IR analysis were prepared as KBr pellets. All ^1H NMR spectra were recorded in a 1% (v/v) solution of $\text{CF}_3\text{COOH}/\text{D}_2\text{O}$. Chemical shifts (δ) are reported in parts per million (ppm) relative to sodium 3-(trimethylsilyl)-1-propanesulfonate as internal standard using the residual protonated solvent signal as a reference. The size and the morphology of all particles were determined by transmission electron microscopy (TEM) on a JEOL Model JEM-2100 electron microscope. The average diameter calculated using Semafore

software and reported from the measurement of 100 randomly selected particles. The particle sizes as well as ζ -potential values of the particles were determined using a Nanosizer Nano-ZS (Malvern Instruments) at 25 °C with a scattering angle of 173°. All data are displayed as the mean \pm one standard deviation (SD) and are derived from at least three independent experiments.

2.5. Determination of adsorption efficiency of *E. coli* DNA on chitosan particles by UV-Vis spectroscopy

The genomic DNA from *E. coli* was dissolved in 10 mM sodium phosphate buffer solution (pH 7.4) to give a final DNA concentration of 0.07 mg/mL in a total volume of 800 μL . The absorbance of the mixture was measured by UV-Vis spectroscopy at 260 nm. Thereafter, the dried particles (1 mg) were added to this DNA solution. After the mixture was incubated at ambient temperature for 20 min, it was centrifuged in order to separate the particles from the solution. The absorbance of the DNA solution was measured again. The remaining DNA concentration as well as the absorption efficiency was calculated as shown in the Supplementary Data.

2.6. PNA-DNA hybridization and capture experiments

PNA-DNA hybridization and capture experiments were performed according to a previously reported procedure (Boonthea et al., 2008). Sequences of PNA and DNA used are shown in Table 1. The PNA probe (10 pmol) and DNA sample (10 pmol) were mixed in 30 μL of binding buffer (10 mM sodium phosphate, pH 7.4) and incubated at 25 °C for 20 min. The designated chitosan particles (1 mg) were then added to the solution of PNA-DNA hybrid, incubated for 20 min at ambient temperature, and then centrifugally washed with $3 \times 200 \mu\text{L}$ of Milli-Q water. Finally, the washed particles were analyzed for the adsorbed PNA by MALDI-TOF mass spectrometry. MALDI-TOF mass spectra were collected on Microflex MALDI-TOF mass spectrometry (Bruker Daltonics, Germany). The washed particles (1 μL) were mixed with 10 μL of saturated solution of α -cyano-4-hydroxycinnamic acid (CCA) in

Table 1
PNA and DNA sequences used in this study.

| PNA probe | | | DNA sample | | |
|--------------------|--|--------|--------------------|--------------------|--|
| Code | Sequence (N - C) | m/z | Code | Sequence (5' - 3') | Correlation with PNA |
| PNA ₁ | Ac-TTTTTTTT-LysNH ₂ | 3176.9 | DNA _{1c} | d{AAAAAAAAA} | Complementary to PNA ₁ |
| PNA ₂ | Ac-AAAAAAAA-LysNH ₂ | 3260.2 | DNA _{1v} | d{AAAACAAA} | Single mismatch to PNA ₁ |
| | | | DNA _{1n} | d{AGTGATCTAC} | Non-complementary to PNA ₁ |
| PNA _{mut} | Ac-Lys-O-CTACGCCAACAGCT-SerNH ₂ | 5071.9 | DNA _{mut} | d{AGCTGTTGGCCTAG} | Complementary to PNA _{mut} . Single mismatch to PNA _{wt} |
| PNA _{wt} | Ac-Lys-CTACGCCACCAGCT-SerNH ₂ | 4902.8 | DNA _{wt} | d{AGCTGTTGGCCTAG} | Complementary to PNA _{wt} . Single mismatch to PNA _{mut} |
| | | | DNA _{nc} | d{TAGTTGACTGACA} | Non-complementary to both PNA _{mut} and PNA _{wt} |

0.1% CF₃COOH in acetonitrile/water (1:1). This mixture (1 μL) was spotted onto the MALDI-TOF target, allowed to dry, and analyzed in positive ion linear time-of-flight mode with an accelerating voltage +20 kV. All spectra were processed by averaging between 20 and 30 individual laser shots.

3. Results and discussion

3.1. Chemical and physical characteristics of quaternized chitosan particles

Ionic cross-linking of chitosan solution with TPP was first performed to prepare chitosan (CS) particles. Heterogeneous quaternization was followed thereafter to generate methylated chitosan (MC) and methylated *N*-benzyl chitosan (MBzC) particles by the reactions schematically outlined in Scheme 1(a). MC particles were obtained by direct methylation of the CS particles with CH₃I whereas MBzC particles were prepared via reductive *N*-alkylation with benzaldehyde followed by methylation with CH₃I. The other two particles, namely TMC and HTACC, were prepared by ionic cross-linking of *N,N,N*-trimethylchitosan (TMC) and *N*-[(2-hydroxyl-3-trimethylammonium)propyl]chitosan chloride (HTACC) that were prepared from chitosan under homogeneous conditions as illustrated in Scheme 1(b).

It was found that all ionically crosslinked particles can partially dissolve in CF₃COOH/D₂O, the solvent used for NMR analysis as can be visually observed by the solution turning clearer from opaque upon dissolving in CF₃COOH/D₂O. Given that p*K*_a of CF₃COOH of 0.23 (Milne & Parker, 1981) is lower than p*K*_a of all acidic protons (p*K*_a = 1.0, 2.2, 2.3, 3.7, 8.5) (Wiberg, Holleman, & Wiberg, 2001) of tripolyphosphoric acid, the ionic crosslinking should be partially destroyed by protonation of the tripolyphosphate. Taking the benefit of partial solubility of the particles under acidic condition, we can semi-quantitatively determine the success of quaternization and to ensure that there are quaternary ammonium groups available for binding with DNA. This is very important, especially in the case of MC and MBzC particles of which quaternization was performed heterogeneously after particle formation by crosslinking. As presented in Fig. 1, ¹H NMR spectra of all quaternized chitosan particles show signals at 3.1–3.3 ppm (peak B for MC, MBzC, and TMC particles and peak E for HTACC particles), which belong to the methyl protons of the quaternary ammonium group. The signals at 3.0 (peak C) and 2.8 (peak D) ppm can be designated to the methyl protons of the disubstituted and monosubstituted amino groups, respectively for MC, MBzC, and TMC particles. The signal attributed to the acetyl group (peak A) of *N*-acetylglucosamine unit of chitosan appears at the chemical shift approximately 1.9–2.0 ppm for all particles. In the case of MBzC particles, a weak signal of aromatic protons at 7.5 ppm confirmed the presence of the benzyl group. Peak assignments of all quaternized chitosan derivatives agree very well with published data previously reported (Sajomsang, Tantayanon, Tangpasuthadol, & Daly, 2009; Seong et al., 2000; Sieval et al., 1998).

Degree of substitution of the quaternized chitosan particles can be deduced from ¹H NMR data. For the MC, TMC and HTACC

particles, the degree of quaternization (%DQ) or degree of tri-substitution of methyl groups (–N⁺(CH₃)₃) can be determined from the relative ratio between the integration of 9 protons from 3 methyl groups (–N⁺(CH₃)₃) having signal at δ ~3.1–3.3 ppm and the peak integration of 6 protons of chitosan signal at δ ~3.5–4.4 ppm, assigned to H_{2',3,4,5,6,6'} by using equation S1 (Supplementary Data). In the case of MBzC particles, the degree of substitution was estimated by assuming that the majority of quaternary ammonium groups existed in the form of N⁺(CH₃)₃ or presented in the form of –NR⁺(CH₃)₂, when substituted groups (R) were benzyl groups. This assumption is based on the fact that the remaining non-benzylated amino groups after the reductive alkylation step are less bulky, and should be more reactive than the benzylated amino group (–NHR) toward methylation by CH₃I. Such characteristic should favor the formation of –N⁺(CH₃)₃ as opposed to that of the –NR⁺(CH₃)₂. By using equation S1 for calculation, the degree of tri-substitution or quaternization (%DQ) of MC, MBzC, TMC, and HTACC were 6.3, 5.1, 1.9, and 60.8, respectively. For MC, MBzC, TMC particles, the degree of di-substitution and mono-substitution can also be estimated using equations S2 and S3, respectively (displayed in Supplementary Data). The data shown in Table S2 in Supplementary Data suggested that total degree of substitution (%DS_{total}) was in a range of ~36–73%. The degree of di-substitution possessed higher values than those of mono- and tri-substitution in the case of MC and MBzC particles. Among all particles, HTACC particles exhibited the highest degree of tri-substitution (quaternization). It should be emphasized, at this point, that the quaternized particles were not completely dissolved in the solvent used for ¹H NMR analysis (CF₃COOH/D₂O). Accordingly, the data obtained from ¹H NMR analysis may not reflect the actual degree of substitution, and should only be used as a semi-quantitative estimation of the extent of substitution.

The %DQ values of HTACC (60.8%) and TMC (1.9%) particles were lower than those of HTACC (84.9%) and TMC (11.8%), soluble precursors obtained from homogeneously modified chitosan. This can be explained by the fact that some positive charges of HTACC and TMC were ionically crosslinked with negatively charged TPP upon the particle formation. It is also interesting to note that TMC particles prepared by the homogeneous route possessed less %DQ (~1.9%) in comparison with the MC particles (%DQ ~6.3%) despite their similar functionalities. This may be described as a result of only a portion of the TMC perhaps at the surface TMC particles can dissolve in CF₃COOH/D₂O, the solvent used for ¹H NMR analysis because most of TMC ionically interacted with TPP. The TMC entangled and trapped inside the particles by crosslinking should not be able to dissolve out. The resulting TMC particles therefore possessed much less %DQ (1.9%). This value should be taken as a lower limit and does not necessarily mean that there are not quaternary ammonium groups available inside the particles. In the case of MC particles, on the other hand, the quaternization was performed after the particle formation. The quaternary ammonium entities formed from the uncrosslinked amino groups at the particle surface may be more freely dissolved in CF₃COOH/D₂O and can be more readily detected by ¹H NMR. This strongly suggested that the heterogeneous approach

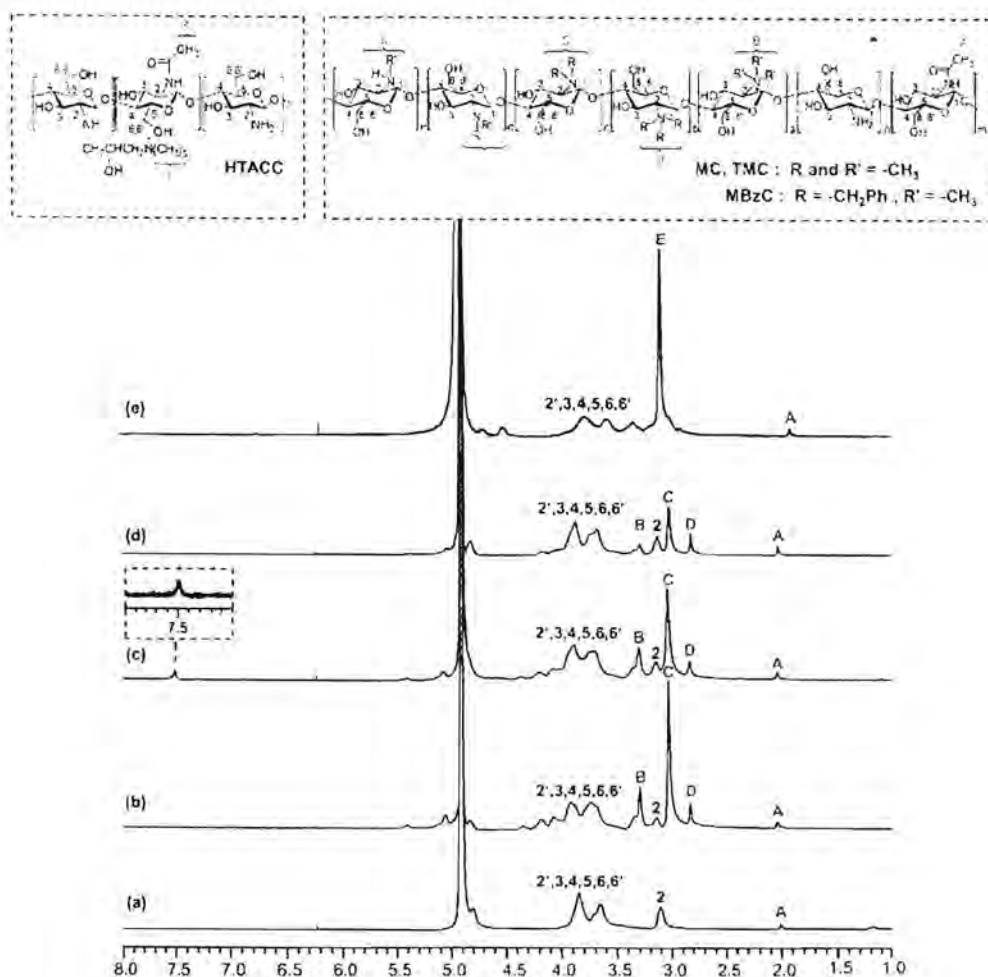


Fig. 1. ^1H NMR spectra of (a) CS, (b) MC, (c) MBzC, (d) TMC, and (e) HTACC particles.

is the more effective way to introduce the trimethylammonium groups to chitosan particles. This is highly advantageous considering that heterogeneous methylation is much more convenient to perform in comparison with the homogeneous methylation.

FT-IR analyses of all particles (Fig. S2, Supplementary Data) revealed two characteristic peaks at 1650 and 1543 cm^{-1} that can be assigned to C=O stretching (Amide I) and N–H bending (Amide II, Amine) of *N*-acetylglucosamine units. The decrement of the N–H bending signal at 1543 cm^{-1} and the appearance of C–H deformation signal in a range of 1460 – 1470 cm^{-1} demonstrated the successful quaternization by both homogeneous and heterogeneous routes. Peak characteristics are in good agreement with previously reported information (Jia, Shen, & Xu, 2001; Sajomsang et al., 2009; Seong et al., 2000).

As shown in Table S3, Supplementary Data, all particles were relatively spherical in shape, having diameters in a sub-micron range (~ 0.13 – $0.40\text{ }\mu\text{m}$) as determined by TEM. We have also measured the particle sizes by DLS technique (Table S4, Supplementary Data). Apparently, the sizes obtained from DLS analysis were much larger than those obtained from TEM analysis. This is mainly due to the fact that the sizes measured by DLS are hydrodynamic sizes at which the particles swell in the solution during the measurements. Whereas TEM analysis was done under reduced pressure atmosphere so the particles were in the dehydrated form. It is also worth noting that the size variations are most significant in the case of MC and TMC particles ($0.20 \pm 0.05\text{ }\mu\text{m}$ and $0.13 \pm 0.09\text{ }\mu\text{m}$ vs. $1.55 \pm 0.23\text{ }\mu\text{m}$ and $1.79 \pm 0.31\text{ }\mu\text{m}$ as determined by TEM and

DLS, respectively), implying their higher degree of swelling than other particles. As anticipated, the size variation ($0.16 \pm 0.05\text{ }\mu\text{m}$ vs. $0.26 \pm 0.01\text{ }\mu\text{m}$, as determined by TEM and DLS, respectively) is quite insignificant in the case of MBzC bearing relative hydrophobic benzyl groups indicating its lowest swellability.

As evaluated by DLS, all particles exhibited positive ζ -potential values confirming their positively charged characteristics. The magnitude of ζ -potential values beyond a range of $\pm 20\text{ mV}$ suggested that all particles were quite stable. It should be emphasized that the size and ζ -potential data were averaged values from three independent samples. Relatively small standard deviation of the size analyzed by TEM (Table S3, Supplementary Data) and those of both size and ζ -potential values reevaluated by DLS (Table S4, Supplementary Data) implied the reproducibility of the synthetic procedures. Due to the limited solubility of quaternized chitosan particles in the solvent used for NMR analysis, %DQ cannot be accurately determined by ^1H NMR analysis. For this reason, we feel that it would be intuitively incorrect to make a direct correlation between %DQ and ζ -potential of the particles.

3.2. DNA adsorption efficiency of quaternized chitosan particles

In this experiment, a commercially available *E. coli* genomic DNA was used as a DNA model to determine the adsorption of the negatively charged DNA on the positively charged quaternized chitosan particles by electrostatic interactions, the main attractive force that is believed to drive the adsorption. A calibration curve showing

a linear relationship between DNA concentration and absorbance was established as shown in Fig. S3, Supplementary Data. This was used as a basis for calculation of the DNA adsorption efficiency as demonstrated in Supplementary Data.

As illustrated in Fig. S4 (Supplementary Data), HTACC and TMC particles, prepared by the homogeneous quaternization can adsorb DNA of ~2.6% (wt/wt) whereas MBzC and MC particles, prepared by heterogeneous quaternization, can only adsorb DNA of ~0.4% and 1.5% (wt/wt). We explained the lowest DNA adsorptivity of the MBzC particles as a consequence of their inherent hydrophobicity preventing adsorption of negatively charged and hydrophilic DNA molecules despite their highest ζ -potential. Apparently, the quantity of adsorbed DNA does not correlate at all with %DQ previously estimated by ^1H NMR, especially in the case of TMC particles of which %DQ was as low as 1.9%. This warrants our previous assumption that such values may be under-estimated. And the particles synthesized by the homogeneous reaction should possess positive charges not only at the surface of but also inside the particles so that they can interact more effectively with the negatively charged *E. coli* DNA. On the other hand, the particles synthesized by the heterogeneous reaction may have positive charges only on their surface. Nevertheless, all quaternized chitosan particles can interact electrostatically with DNA molecules, suggesting their ability to be used for DNA sequence analysis in subsequent studies. We have found no specific correlation between the amount of adsorbed DNA and the size as well as ζ -potential of the particles from the data available.

Upon DNA adsorption experiments, ζ -potential values of all particles became less positive implying that the particles were covered with negatively charged DNA (Table S4, Supplementary Data). Two trends of the change in particle size were observed. The size became smaller in the case of CS, MC and TMC particles suggesting that the particles were less swollen upon electrostatically interacting with DNA. In the case of MBzC particles, the particles became more swollen once they were covered with the more hydrophilic DNA molecules as opposed to their inherently hydrophobic character prior to DNA adsorption.

3.3. Applications of quaternized chitosan particles as ion exchange supports for determination of PNA-DNA hybridization

The concept of using quaternized chitosan particles as anion exchange supports for capturing PNA-DNA hybrids is displayed in Scheme 2. The minimum quantity of PNA probe and DNA target that can be analyzed by MALDI-TOF mass spectrometry was first determined. PNA₁ having a T9 sequence and its complementary DNA, DNA₁ having an A9 sequence, were used for this investigation. As demonstrated in Fig. S5 (Supplementary Data), the minimum amount of PNA probe and DNA target that can be employed for detection of DNA sequence is 10 pmol. This finding is similar to the result previously reported by Boontha et al. (2008) in which Q-sepharose was used as the anion exchange support.

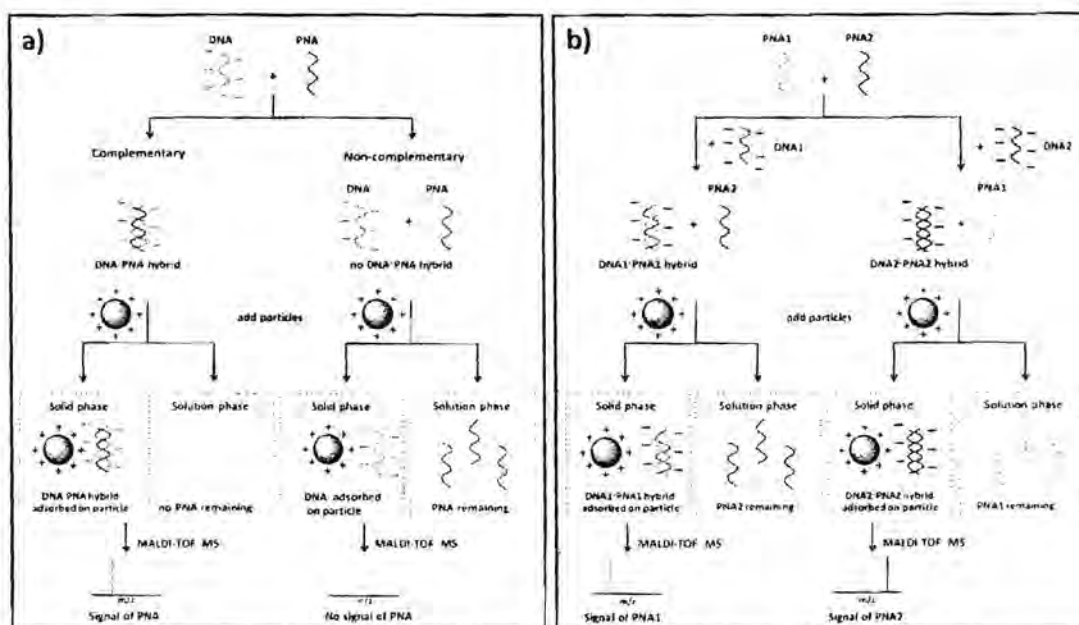
To test the ability of the particles for discrimination between complementary and mismatched DNA by the present anion-exchange capture technique, the PNA₁ was again chosen as the model. MALDI-TOF spectra of all particles after being washed by deionized water shown in Fig. 2 revealed the signal of PNA₁ probe only when the complementary DNA₁ (A9) was added. No signals were detected in the cases of both single-mismatched (DNA_{1s}) and non-complementary (DNA_{1n}) DNA, indicating the specificity of the detection. In the absence of the hybridized DNA, there was no appearance of PNA₁ signal, implying that there were no non-specific interactions between the particles and the PNA (with the exception of MBzC, vide infra). The mismatch discrimination cannot be realized in the case of the MBzC particles despite its high positive charge density (ζ -potential = 54.9 ± 1.0 eV). The PNA probe

signals were detected on the particles in the absence and presence of all DNA targets. This non-specific interaction is believed to stem from the presence of hydrophobic benzyl moieties introduced to the MBzC particles. The hydrophobic character of the quaternized particles may be indirectly expressed in term of water contact angle of the chitosan film being modified by the same chemistry. MBzC film possessed a water contact angle of $93.0 \pm 2.3^\circ$ (Vallapa et al., 2011) which was apparently greater than that of the MC film ($60.4 \pm 1.7^\circ$) (Hoven, Tangpasuthadol, Angkitpaiboon, Vallapa, & Kiatkanjornwong, 2007). It should also be noted that in MALDI-TOF MS detection, no DNA signal could be observed due to the much less effective ionization of DNA than PNA in the positive ion mode.

In order to investigate the applicability of the quaternized chitosan particles for the analysis of more complex DNA sequences, two mixed base 14mer PNA probes complementary to DNA sequences that mimic the wild-type *K-ras* DNA (DNA_{wt}) and mutant *K-ras* DNA (DNA_{mut}) (Table 1) were used. Human *K-ras* gene, a member of the Ras family GTPases, is one of the most useful genetic markers that can be used for cancer screening from body fluids and plasma DNA. (Bos, 1989). The data shown in Fig. 3, which were obtained from the particles that were washed with Milli-Q water alone, revealed that only HTACC particles exhibited satisfactory behavior by showing the signal of the PNA probe only when the complementary DNA (DNA_{mut}) was present. No signals were detected in the cases of single-mismatched (DNA_{wt}) and fully non-complementary (DNA_{nc}) DNA targets, suggesting the specificity of the detection. However, the detected signal was relatively low in the complementary case in comparison with other particles. The other three particles, TMC, MC, and MBzC, could discriminate the complementary DNA target (DNA_{mut}) from the unrelated DNA (DNA_{nc}) after washing with Mill-Q water, but not from the single-mismatched DNA (DNA_{wt}). Interestingly, the CS particles cannot at all distinguish the complementary DNA from the non-complementary targets, suggesting that a high degree of non-specific interactions between PNA and the particles. Having a pK_a of approximately 6.0 (Badawy, 2010), CS particles may not be effectively protonated and less likely to be fully charged at pH 7 where the analysis was done. This can explain the observed extensive non-specific adsorption and emphasizes the necessity of introducing the quaternary ammonium groups to provide pH-independent permanent positive charges that are essential to suppress the unwanted non-specific adsorption. Similar results were also observed when PNA_{wt} was used as a probe (Fig. S6, Supplementary Data).

To get rid of the non-specific interactions, formamide was added to the buffer that was used for rinsing the particles after capturing the DNA-PNA hybrid and washing with Milli-Q water. Formamide was previously reported to successfully reduce the hydrophobic interactions between PNA and solid support (streptavidin magnetic bead in that case) and destabilize the mismatched DNA-PNA hybrids (Ross, Lee, & Belgnader, 1997). MALDI-TOF mass spectra obtained from the particles after rinsing with 20% formamide in phosphate buffer are shown in Fig. 4. Gratifyingly, the non-specific absorption of PNA-single-mismatched DNA hybrid on all but the CS particles could be completely eliminated both when PNA_{mut} and PNA_{wt} were used as probes. Apparently, the complementary, but not the mismatched, PNA-DNA hybrids can survive the 20% formamide washing, allowing effective discrimination.

To allow simultaneous detection of both wild-type and mutant *K-ras* DNA, two different PNA probes (PNA_{mut} and PNA_{wt}) were combined in the same reaction and hybridized with the DNA target followed by an addition of designated particles. The concept of the selectivity test using dual PNA probes is outlined in Scheme 2(b). The m/z signals of PNA_{mut} and PNA_{wt} would appear at m/z 5070 and 4900, respectively. Only one signal should be observed for the specific binding to the DNA target. If both signals are observed on the solid support, they are likely to be due to non-specifically adsorbed



Scheme 2. A schematic diagram showing the concept of using quaternized chitosan particles as anion-exchange captures of PNA-DNA hybrid in combination with MALDI-TOF mass spectrometry for DNA sequence analysis: (a) single probe, (b) dual probes.

PNA. This provides an extra mechanism for validating the detection experiment. According to Fig. 5, only the CS particles showed significant non-specific adsorption of the PNA_{mut} or PNA_{wt}. Upon using 20% formamide as the rinsing reagent after hybridization, MC, TMC, and HTACC particles exhibited good selectivity by showing only the signal of PNA that was hybridized to the correct DNA target suggesting their equivalent ability to suppress non-specific adsorption. However, in term of sensitivity, the TMC particles seem to be better choices than the other two particles in that they gave the strongest PNA signals. This may be described as a result of adsorbed DNA and complementary PNA hybrid being at the surface of the MC particles where most of the quaternary ammonium groups are located because quaternization was done heterogeneously so that the PNA

ionization was most efficient and thus gave the highest signal. Although TMC and HTACC particles having quaternary ammonium entities both inside and outside so they exhibited higher DNA adsorption efficiency than the MC particles (see Fig.S4, Supplementary Data), PNA hybridized with complementary DNA absorbed inside the particles may not be effectively ionized therefore yielding lower signals. Overall, MC particles gave the best performance because it showed the strongest complementary PNA signal, and very low non-specific adsorption of the non-complementary probe. In addition, the heterogeneous method used to prepare the MC particles is less time-consuming and less complicated than that was used for the preparation of the TMC particles, which is based on the homogeneous method.

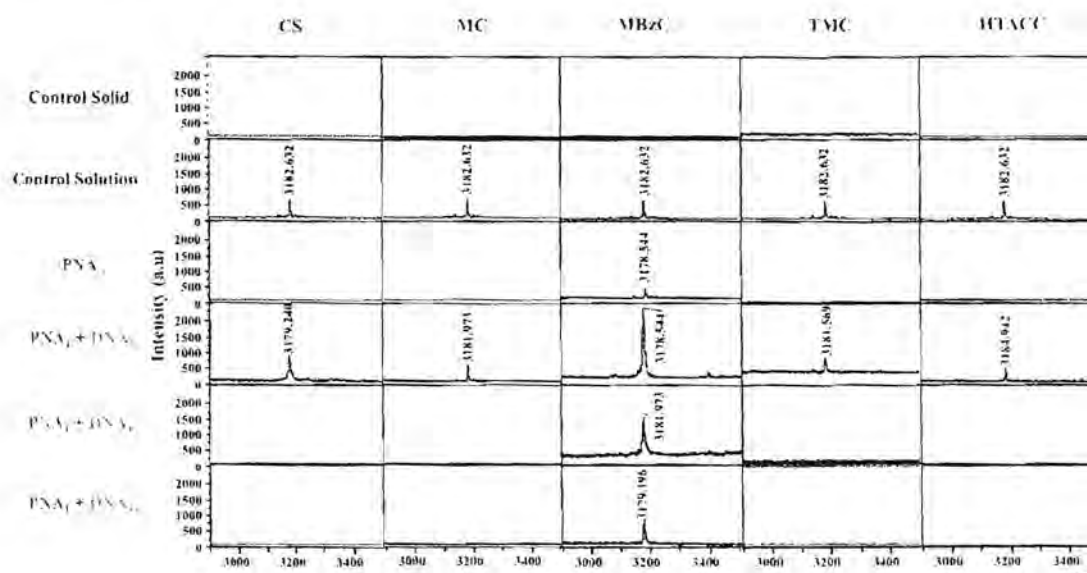


Fig. 2. MALDI-TOF mass spectra of control solid/solution and washed particles after capturing experiments with PNA₁ alone or in the presence of various DNA targets.

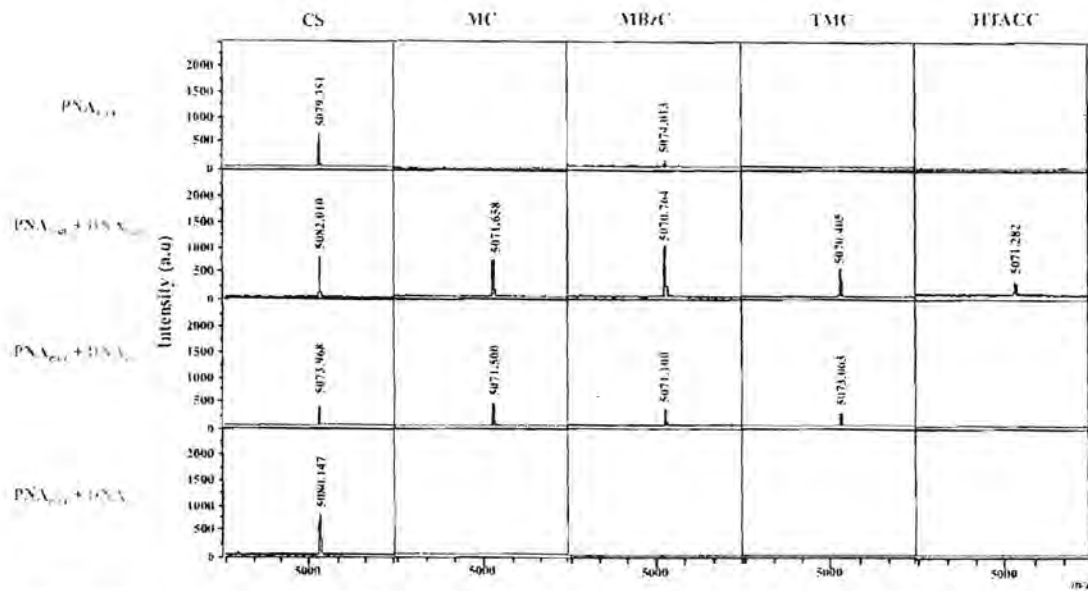


Fig. 3. MALDI-TOF mass spectra of particles after capturing experiments with PNA_{mur} alone or in the presence of various DNA targets.

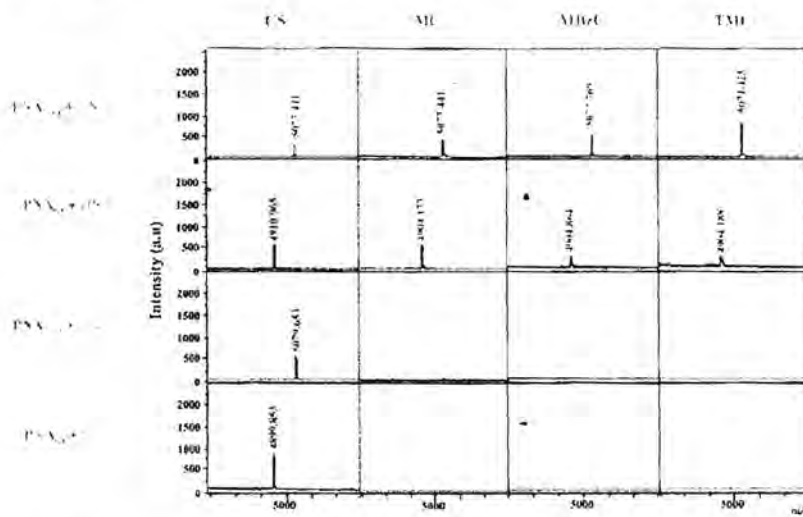


Fig. 4. MALDI-TOF mass spectra of particles after capturing the PNA-single-mismatched DNA hybrid and PNA-complementary DNA hybrid after washing with MilliQ water and 20% formamide in binding buffer using PNA_{mur} or PNA_{wt} as probes.

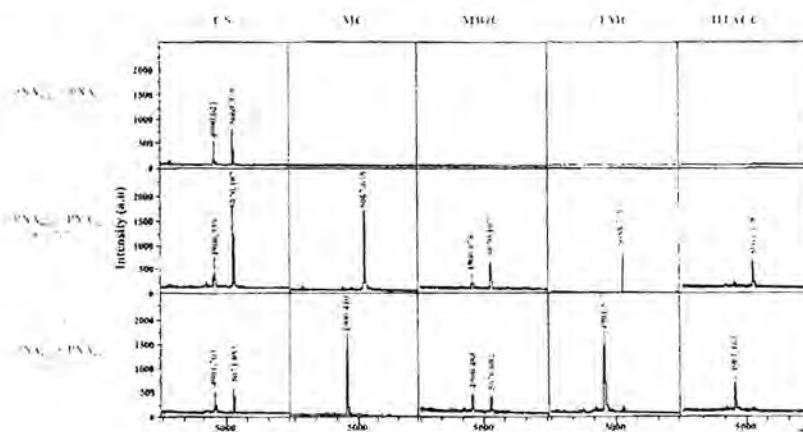


Fig. 5. MALDI-TOF mass spectra of particles after exposure to the mixture of PNA_{mur} and PNA_{wt} alone or the mixture of PNA_{mur} and PNA_{wt} that was previously hybridized with selected DNA target (DNA_{mur} or DNA_{wt}) after rinsing with 20% formamide.

4. Conclusions

Four quaternized chitosan particles having different alkyl substituents namely MC, MBzC, TMC, and HTACC particles were obtained by either heterogeneous or homogeneous quaternization. The success of particle formation was verified by ^1H NMR and FT-IR analyses. As determined by DLS, all particles carried positive charges with ζ -potential ranging from +30.2 to +49.4 mV. The results from TEM analysis indicated that all particles were relatively spherical and had diameters in a range of 0.16–0.40 μm . The concept of using quaternized chitosan particles as anion exchange captures in combination with *acpc*PNA and MALDI-TOF mass spectrometry for determination of DNA sequence has been proven practical for detection of synthetic 14-mer, mixed base DNAs of which sequence mimics mutant K-ras DNA. The specific detection of hybridization event can also be realized and is strongly affected by the variation of functionality introduced to the chitosan particles in the step of quaternization. Among all particles, MC particles gave the best performance with very low non-specific adsorption of PNA and a minimal detectable amount of DNA target of 10 pmol, which is comparable to that of the commercial anion exchanger Q-sepharose. Discrimination between complementary and single base mismatched DNA targets are readily achieved by rinsing with 20% formamide solution in PBS buffer. The fact that chitosan, especially in the form of quaternary-ammonium derivatives can effectively adsorb DNA strongly suggests their great potential in many advanced bio-related applications that relies on DNA capturing.

Acknowledgements

This research gratefully acknowledges the financial support provided by a Research Team Consolidation Grant from The Thailand Research Fund and the Office of Higher Education Commission (RTA5080004, RTA5280002), a Distinguished Research Professor Grant from the Thailand Research Fund and Chulalongkorn University (DPG5780002), the Ratchadaphiseksomphot Endowment Fund of Chulalongkorn University (RES560530126-AM), and the Thai Government Stimulus Package 2 (TKK2555), under the Project for Establishment of Comprehensive Center for Innovative Food, Health Products and Agriculture.

Appendix A. Supplementary data

Supplementary data associated with this article can be found, in the online version, at <http://dx.doi.org/10.1016/j.carbpol.2015.05.014>.

References

- Ananthanawat, C., Hoven, V. P., Vilaivan, T., & Su, X. (2011). Surface plasmon resonance study of PNA interactions with double stranded DNA. *Biosensors and Bioelectronics*, 26(3), 1918–1924.
- Ananthanawat, C., Vilaivan, T., & Hoven, V. P. (2009). Synthesis and immobilization of thiolated pyrrolidinyl peptide nucleic acids on gold-coated piezoelectric quartz crystals for the detection of DNA hybridization. *Sensors and Actuators B: Chemical*, 132(1), 215–221.
- Ananthanawat, C., Vilaivan, T., Hoven, V. P., & Su, X. (2010). Comparison of DNA-amineethylsilyl PNA and pyrrolidinyl PNA as probes for detection of DNA hybridization using surface plasmon resonance technique. *Biosensors and Bioelectronics*, 25(5), 1054–1059.
- Ananthanawat, C., Vilaivan, T., Mekboonsonglar, W., & Hoven, V. P. (2009). Thiolated pyrrolidinyl peptide nucleic acids for the detection of DNA hybridization using surface plasmon resonance. *Biosensors and Bioelectronics*, 24(12), 3531–3539.
- Badawy, M. E. I. (2010). Structure and antimicrobial activity relationship of quaternary N-alkyl chitosan derivatives against some plant pathogens. *Journal of Applied Polymer Science*, 117(2), 910–919.
- Boonlua, C., Vilaivan, C., Wagenknecht, H. A., & Vilaivan, T. (2011). 5-(pyren-1-yl)uracil as a base-discriminating fluorescent nucleobase in pyrrolidinyl peptide nucleic acids. *Chemistry – An Asian Journal*, 6(12), 3251–3259.
- Boontha, B., Nakkuntod, J., Hirankarn, N., Chaumpluk, P., & Vilaivan, T. (2008). Multiplex mass spectrometric genotyping of single nucleotide polymorphisms employing pyrrolidinyl peptide nucleic acid in combination with *in situ* carbon capture. *Analytical Chemistry*, 80(21), 8128–8135.
- Bos, J. L. (1989). Ras oncogenes in human cancer: A review. *Cancer Research*, 49(17), 4682–4689.
- Cao, W., Easley, C. J., Ferrance, J. P., & Landers, J. P. (2006). Chitosan as a polymer for pH-induced DNA capture in a totally aqueous system. *Analytical Chemistry*, 78(20), 7222–7228.
- Domard, A., Rinaudo, M., & Terrassin, C. (1986). New method for the quaternization of chitosan. *International Journal of Biological Macromolecules*, 8(2), 105–107.
- Egholm, M., Buchardt, O., Nielsen, P. E., & Berg, R. H. (1992). Peptide nucleic acids (PNA): Oligonucleotide analogs with an actual peptide backbone. *Journal of the American Chemical Society*, 114(5), 1695–1697.
- Hayatsu, H., Kubo, T., Tanaka, Y., & Negishi, K. (1997). Polynucleotide-oligonucleotide complex: an insoluble but reactive form of polynucleotide. *Chemical and Pharmaceutical Bulletin*, 45(5), 1363–1365.
- Hoven, V. P., Tangpasuthadol, V., Angkitpaiboon, Y., Vallapa, N., & Kiatkamjornwong, S. (2007). Surface-charged chitosan: Preparation and protein adsorption. *Carbohydrate Polymers*, 68(1), 44–52.
- Jampasa, S., Wonsawat, W., Rodthongkum, N., Siangproh, W., Yanatsanejit, P., Vilaivan, T., et al. (2014). Electrochemical detection of human papillomavirus DNA type 16 using a pyrrolidinyl peptide nucleic acid probe immobilized on screen-printed carbon electrodes. *Biosensors and Bioelectronics*, 54, 426–434.
- Jia, Z., Shen, D., & Xu, W. (2001). Synthesis and antibacterial activities of quaternary ammonium salt of chitosan. *Carbohydrate Research*, 333(1), 1–6.
- Laopa, P. S., Vilaivan, T., & Hoven, V. P. (2013). Positively charged polymer brush functionalized filter paper for DNA sequence determination following DNA blot hybridization employing a pyrrolidinyl peptide nucleic acid probe. *Analytical Chemistry*, 85(1), 269–277.
- Maneeelun, N., & Vilaivan, T. (2013). Dual pyrene-labeled pyrrolidinyl peptide nucleic acid as an excimer-to-monomer switching probe for DNA sequence detection. *Tetrahedron*, 69, 10805–10810.
- Mansawat, W., Boonlua, C., Siriwong, K., & Vilaivan, T. (2012). Chloro poly-cyclic aromatic hydrocarbon as a hybridization-responsive thiomercapto-aryl ether nucleobase in pyrrolidinyl peptide nucleic acids. *Tetrahedron*, 68(21), 3988–3995.
- Milne, J., & Parker, T. (1981). Dissociation constant of aqueous trifluoroacetic acid by cryoscopic and conductivity. *Journal of Solution Chemistry*, 10(7), 479–487.
- Nielsen, P., Egholm, M., Berg, R., & Buchardt, O. (1991). Sequence selective recognition of DNA by strand displacement with a thymine substituted polyamide. *Science*, 254(5037), 1497–1500.
- Qi, L., Xu, Z., Jiang, X., Hu, C., & Zou, X. (2004). Preparation and antibacterial activity of chitosan nanoparticles. *Carbohydrate Research*, 339(15), 2693–2700.
- Rashatasakhon, P., Vongnam, K., Siripornnoppakun, W., Vilaivan, T., & Sukwattanasinitt, M. (2012). FRET detection of DNA sequence via electrostatic interaction of polycationic phenyleneethynylene dendrimers with DNA/PNA hybrid. *Talanta*, 88, 593–598.
- Reenabthue, N., Boonlua, C., Vilaivan, C., Vilaivan, T., & Suparpprom, C. (2011). 3-Amino-pyrrolidine-4-carboxylic acid as versatile handle for intercalary labeling of pyrrolidinyl PNA. *Bioorganic and Medicinal Chemistry Letters*, 21(21), 6065–6069.
- Ross, P. L., Lee, K., & Belgrader, P. (1997). Discrimination of single nucleotide polymorphisms in human DNA using peptide nucleic acid probes detected by MALDI-TOF mass spectrometry. *Analytical Chemistry*, 69(20), 4107–4109.
- Sajomsang, W., Tantayanon, S., Tangpasuthadol, V., & Daly, W. H. (2009). Quaternization of N-aryl chitosan derivatives: synthesis, characterization, and antibacterial activity. *Carbohydrate Research*, 344(18), 2562–2573.
- Sankoh, S., Samanman, S., Thipmanee, O., Numnuam, A., Limbut, W., Kanatharana, P., et al. (2013). A comparative study of a label-free DNA sequence sensor using a pyrrolidinyl peptide nucleic acid probe immobilized through poly(phenylene-diamine) and poly(vinylidene fluoride) non-conducting polymers. *Sensors and Actuators B: Chemical*, 177(0), 543–554.
- Sassolas, A., Leca-Bouvier, B. D., & Blum, L. J. (2007). PNA-based microarray: *Chemical Reviews*, 107(1), 109–139.
- Seong, H. S., Whang, H. S., & Ko, S. W. (2000). Synthesis of a quaternary ammonium derivative of chito-oligosaccharide as antimicrobial agent for cellulose fibers. *Journal of Applied Polymer Science*, 76(14), 2009–2013.
- Sieval, A. B., Thanou, M., Kotze, A. F., Verhoef, J. C., Brussee, J., & Junginger, H. E. (1998). Preparation and NMR characterization of highly substituted N-trimethyl chitosan chloride. *Carbohydrate Polymers*, 36(2–3), 157–165.
- Suparpprom, C., Srisuwannaket, C., Sangvanich, P., & Vilaivan, T. (2005). Synthesis and oligodeoxynucleotide binding properties of pyrrolidinyl peptide nucleic acid bearing propyl 2-amino-cyclopentane-carboxylic acid (APC) backbone. *Tetrahedron Letters*, 46(16), 2833–2837.
- Theppaleak, T., Rutnakornpituk, B., Wichai, U., Vilaivan, T., & Rutnakornpituk, M. (2013). Magnetite nanoparticle with positively charged surface for immobilization of peptide nucleic acid and deoxyribonucleic acid. *Journal of Biomedical Nanotechnology*, 9(9), 1509–1520.
- Theppaleak, T., Rutnakornpituk, M., Wichai, U., Vilaivan, T., & Rutnakornpituk, B. (2013). Anion exchanged nanosolid support of magnetic nanoparticle in combination with PNA probes for DNA sequence analysis. *Journal of Nanoparticles Research*, 15(12), 1–12.

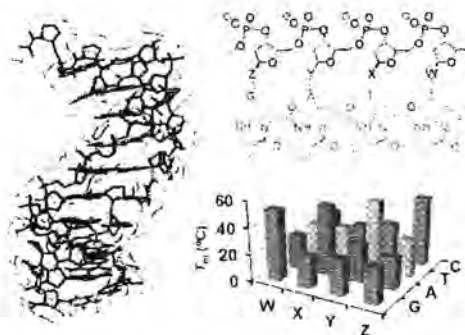
- Thipmanee, O., Samanman, S., Sankoh, S., Nurnnuam, A., Limbut, W., Kanatharana, P., et al. (2012). Label-free capacitive DNA sensor using immobilized pyrrolidinyI PNA probe. Effect of the length and terminating head group of the blocking oligo. *Biosensors and Bioelectronics*, 38(1), 430–435.
- Vallapa, N., Wiarachai, O., Thongchul, N., Pan, J., Tangpasuthadol, V., Kiatkamjornwong, S., et al. (2011). Enhancing antibacterial activity of chitosan surface by heterogeneous quaternization. *Carbohydrate Polymers*, 83(2), 865–873.
- Vilaivan, T., & Srisuwannaket, C. (2006). Hybridization of pyrrolidinyI peptide nucleic acids and DNA: Selectivity, base-pairing specificity, and direction of binding. *Organic Letters*, 8(9), 1897–1900.
- Wiarachai, O., Thongchul, N., Kiatkamjornwong, S., & Hoven, V. P. (2012). Surface-quaternized chitosan particles as an alternative and effective organic antibacterial material. *Colloids and Surfaces B: Biointerfaces*, 92, 121–129.
- Wiberg, N., Holleman, A. F., & Wiberg, E. (2001). *Inorganic chemistry*. San Diego: Academic Press.

Pyrrolidinyl PNA with α/β -Dipeptide Backbone: From Development to Applications

Tirayut Vilaivan*

Organic Synthesis Research Unit, Department of Chemistry, Faculty of Science, Chulalongkorn University, Phayathai Road, Patumwan, Bangkok 10330, Thailand

CONSPECTUS: The specific pairing between two complementary nucleobases (A·T, C·G) according to the Watson–Crick rules is by no means unique to natural nucleic acids. During the past few decades a number of nucleic acid analogues or mimics have been developed, and peptide nucleic acid (PNA) is one of the most intriguing examples. In addition to forming hybrids with natural DNA/RNA as well as itself with high affinity and specificity, the uncharged peptide-like backbone of PNA confers several unique properties not observed in other classes of nucleic acid analogues. PNA is therefore suited to applications currently performed by conventional oligonucleotides/analogues and others potentially beyond this. In addition, PNA is also interesting in its own right as a new class of oligonucleotide mimics. Unlimited opportunities exist to modify the PNA structure, stimulating the search for new systems with improved properties or additional functionality not present in the original PNA, driving future research and applications of these in nanotechnology and beyond. Although many structural variations of PNA exist, significant improvements to date have been limited to a few constrained derivatives of the privileged *N*-2-aminoethylglycine PNA scaffold. In this Account, we summarize our contributions in this field: the development of a new family of conformationally constrained pyrrolidinyl PNA having a nonchimeric α/β -dipeptide backbone derived from nucleobase-modified proline and cyclic β -amino acids. The conformational constraints dictated by the pyrrolidine ring and the β -amino acid are essential requirements determining the binding efficiency, as the structure and stereochemistry of the PNA backbone significantly affect its ability to interact with DNA, RNA, and in self-pairing. The modular nature of the dipeptide backbone simplifies the synthesis and allows for rapid structural optimization. Pyrrolidinyl PNA having a (2′*R*,4′*R*)-proline/(1*S*,2*S*)-2-aminocyclopentanecarboxylic backbone (acpcPNA) binds to DNA with outstanding affinity and sequence specificity. It also binds to RNA in a highly sequence-specific fashion, albeit with lower affinity than to DNA. Additional characteristics include exclusive antiparallel/parallel selectivity and a low tendency for self-hybridization. Modification of the nucleobase or backbone allowing site-specific incorporation of labels and other functions to acpcPNA via click and other conjugation chemistries is possible, generating functional PNAs that are suitable for various applications. DNA sensing and biological applications of acpcPNA have been demonstrated, but these are still in their infancy and the full potential of pyrrolidinyl PNA is yet to be realized. With properties competitive with, and in some aspects superior to, the best PNA technology available to date, pyrrolidinyl PNA offers great promise as a platform system for future elaboration for the fabrication of new functional materials, nanodevices, and next-generation analytical tools.



1 INTRODUCTION

Recognition between two complementary nucleic acids via highly specific Watson–Crick base pairing is the basis for the storage and transfer of genetic information. The high fidelity of the recognition event suggests potential uses of nucleic acids for regulation of genetic expression, as a probe for nucleic acid sequence detection, and many other purposes.¹ In addition, the Watson–Crick base pairing allows one to program nucleic acids to fold into complex architectures in a controllable fashion, making them particularly attractive as building blocks or scaffolds for the creation of novel structures or materials exhibiting unique functions.^{2–4} However, natural nucleic acids are not always ideal candidates for these “unnatural” purposes because of their limited stabilities and only modest binding affinities. Fortunately, the backbone of nucleic acids can tolerate structural modification to some extent without sacrificing the ability to form Watson–

Crick base pairs. Such modified nucleic acids are collectively known as “xeno-nucleic acids” or XNA, examples of which are shown in Figure 1.⁵ Some of these XNA can even be replicated, reversed-transcribed, and evolved with engineered polymerases.⁶

While the concept of redesigning nucleic acids by completely replacing the sugar–phosphate backbone with other polymeric backbones is not entirely new (see Figure 2 for examples), decent Watson–Crick base pairing in these synthetic systems has been demonstrated only relatively recently. In 1991, Nielsen et al.⁷ reported the first peptide nucleic acid (PNA) that could recognize double-stranded (ds) DNA through a novel triplex invasion mechanism. PNA also binds to single-stranded DNA/RNA with high affinity and specificity according to the Watson–

Received: February 16, 2015

Published: May 29, 2015

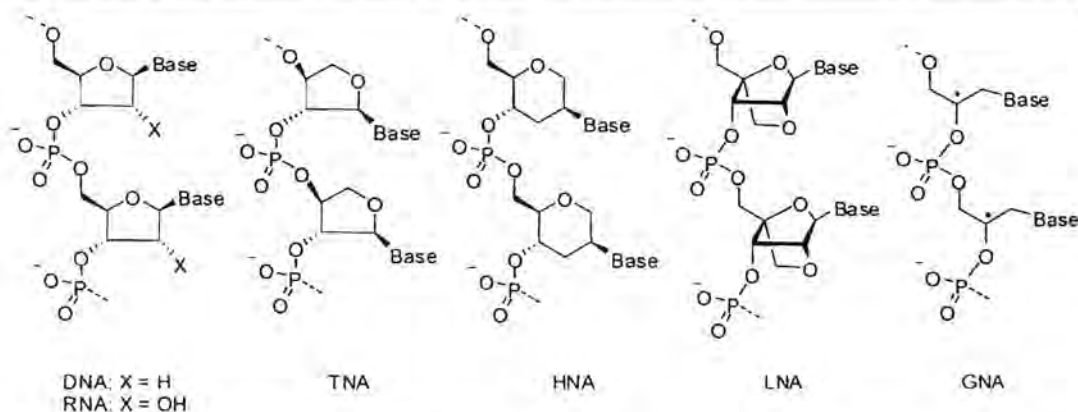


Figure 1. DNA/RNA and selected examples of xeno-nucleic acids.

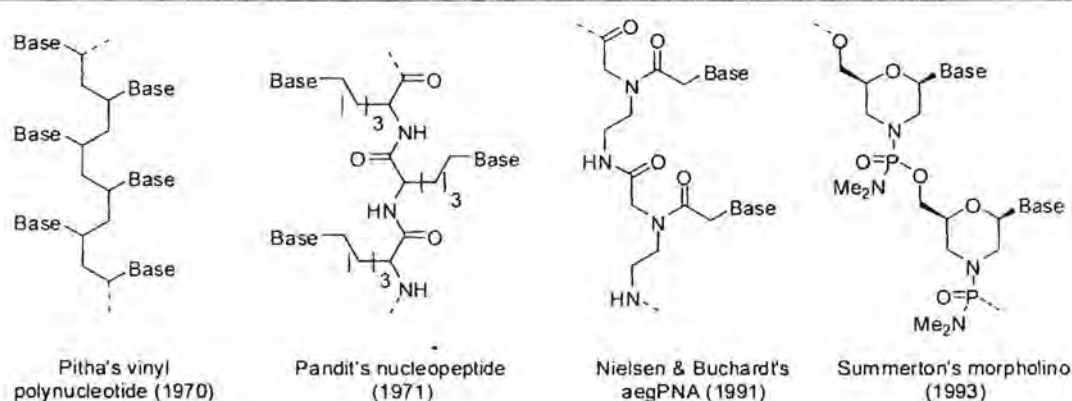


Figure 2. Examples of completely redesigned nucleic acid mimics.

Crick base-pairing rules. The electrostatically neutral backbone of PNA accounts for the unusually high stability as well as the relative insensitivity to ionic strength variations of PNA-containing duplexes.⁸ These properties, together with the excellent stability of PNA toward nucleases and proteases, open the door to its use in nucleic-acid-related applications and considerably broaden the potential scope of this field.⁹ In particular, the strong affinity of PNA is highly desirable for targeting of nucleic acids with secondary structures.¹⁰ In addition, PNA is also interesting as a model for studying molecular recognition events, in prebiotic chemistry, and in designing self-replicating systems.^{11,12} The virtually unlimited opportunities for structural modification should inspire the development of new PNAs having improved properties and functions.¹³ In this Account, we summarize our contribution to the PNA research landscape, which focuses on the development and utility of a series of conformationally constrained pyrrolidinyl PNAs consisting of a proline-derived dipeptide backbone.

2. CONFORMATIONALLY CONSTRAINED PNA

The X-ray and NMR structures of PNA-PNA, PNA-RNA, and PNA-DNA duplexes suggest that the *N*-2-aminoethylglycine backbone of the original PNA (now known as aegPNA) is flexible enough to adopt a range of conformations, including the A-, B-, and novel P-type helices.⁸ The concept of preorganizing the PNA structure to reduce the entropic penalty associated with the conformational change has been proposed to further enhance the

binding properties (Figure 3).¹⁴ Partial incorporation of the (*S,S*)-*trans*-cyclopentane ring into the aegPNA backbone improves its thermal stability and sequence specificity for DNA recognition.¹⁵ On the other hand, incorporation of the *cis*-cyclohexane ring results in an increase in RNA binding affinity,

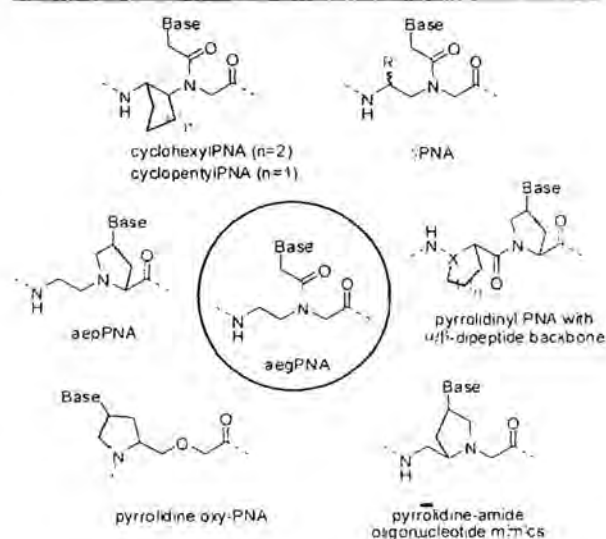


Figure 3. Examples of conformationally constrained PNA analogues.

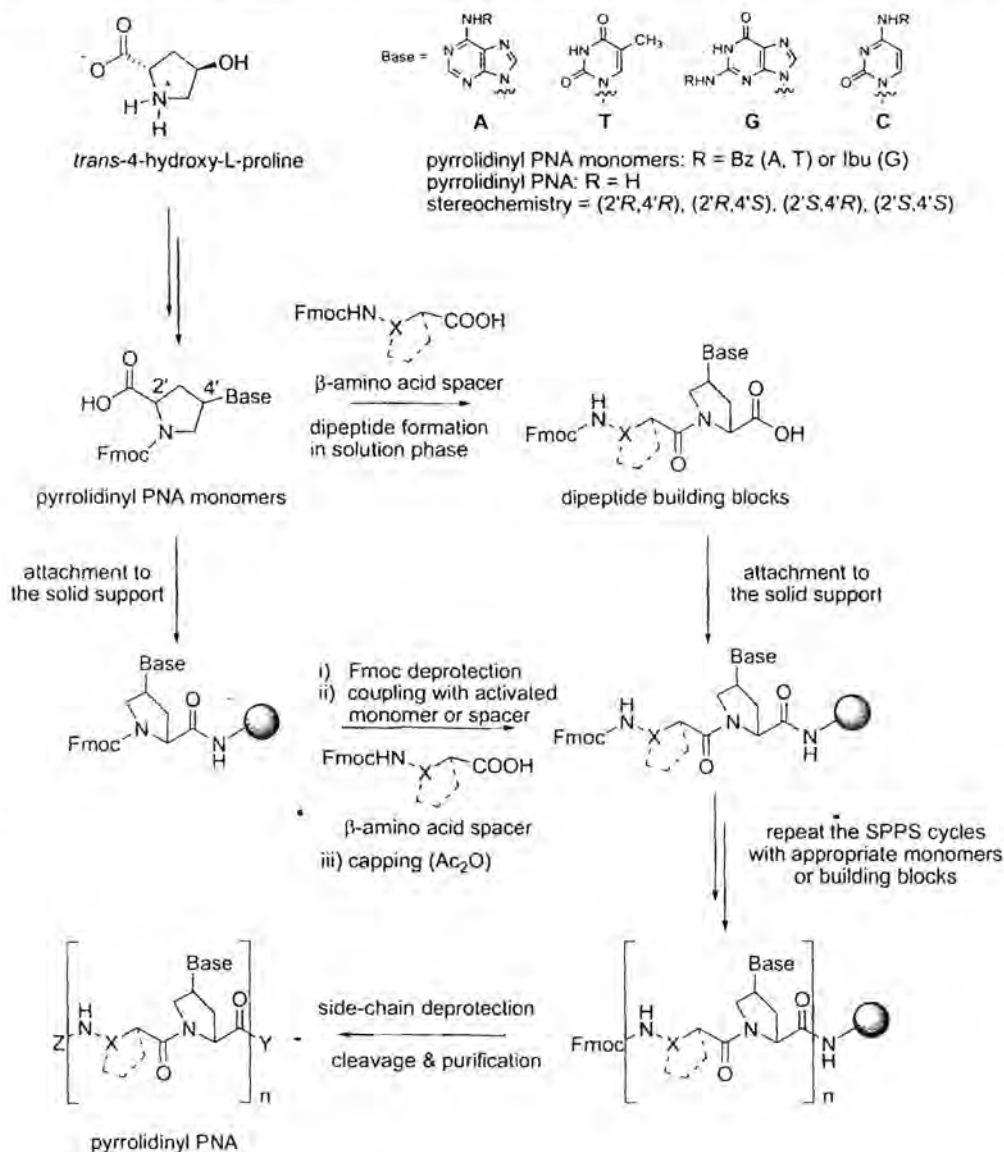


Figure 4. Synthesis of pyrrolidinyl PNA.

significantly more than for DNA.¹⁶ Also, preorganization resulting from a simple substitution at the γ -position in aegPNA significantly improves its binding properties.¹⁷ Various substituents can be placed at this position to improve water solubility¹⁸ or cell penetration^{19,20} or to incorporate other functions.^{21,22}

Because of its straightforward access via proline derivatives having well-defined stereochemistries, the pyrrolidine ring has been extensively used as a constraint element in the design of new PNA structures (Figure 3). However, few studies have fully evaluated the general base-pairing behaviors of nonchimeric mixed-sequence pyrrolidine-containing PNA,^{23,24} and none of these offer significant advantages over the well-established aegPNA. In 1996 we introduced a new pyrrolidinyl PNA having a modular dipeptide backbone consisting of nucleobase-modified prolines alternating with other amino acid "spacer" units.²⁵ However, it was not until 2001 that the active role of the cyclic β -amino acid spacer toward DNA binding was realized.²⁶ These

findings were coincident with the discovery that short β -peptides can fold into well-defined helices as a result of intramolecular hydrogen bonding and conformation constraints.²⁷

3. SYNTHESIS OF PYRROLIDINYL PNA

The structure of pyrrolidinyl PNA is divided into two parts: the pyrrolidine monomer and the β -amino acid spacer, which are equivalent to the nucleoside and phosphate groups in DNA, respectively. The four Fmoc-protected pyrrolidine monomers (A, T, C, G) were synthesized with full stereochemical control starting from *trans*-4-hydroxy-L-proline (Figure 4).^{28–30} The nucleobase protecting groups Bz (A, C) and Ibu (G) chosen here are compatible with the Fmoc solid-phase peptide synthesis (SPPS) strategy and can be removed by aqueous ammonia treatment as in standard DNA synthesis. In early studies, the pyrrolidine monomer and the spacer were first joined to form a "nucleotide" building block before being assembled into PNA oligomers using SPPS.³¹ The attractive feature of this approach is

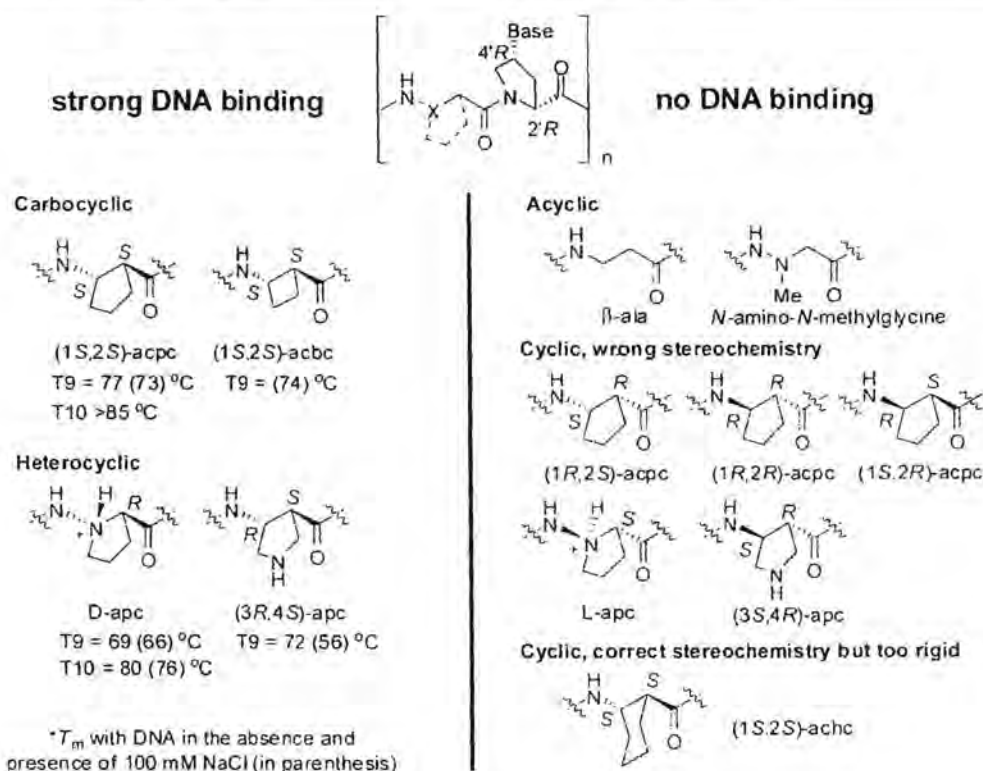


Figure 5. DNA binding properties of homothymine pyrrolidinyl PNAs having β-amino acid spacers.

that the number of solid-phase coupling steps is reduced by half. However, stepwise assembly of the monomer and spacer directly onto the solid phase is more convenient for building in structural variations, and this became the preferred method in later studies.^{26,29} L-Lysinamide is usually included at either the C- or N-terminus to impart aqueous solubility (to the mM range). Other labels such as fluorescent dyes, thiols, and biotin may also be incorporated at either the N- or C-terminus (via an orthogonally protected lysine side chain). After the desired sequence is obtained, the nucleobase protecting groups are removed prior to cleavage from the solid support. While aegPNA and pyrrolidinyl PNA consisting of α-amino acids in the backbone are readily degraded by intramolecular cyclization under basic conditions,²⁵ pyrrolidinyl PNA having an α/β-dipeptide backbone is completely stable. The crude PNA is purified by reversed-phase HPLC and characterized by MALDI-TOF mass spectrometry. Typical coupling yields are >95% per step, and the recovery of PNA with >90% purity is between 10–40%, depending on the sequence.

4. BASE-PAIRING PROPERTIES OF PYRROLIDINYL PNA

4.1. DNA Binding Properties

During the discovery phase, the most easily prepared oligothymine sequences (5–10 bases in length) were used as a model to preliminarily determine the DNA binding properties of pyrrolidinyl PNA. The configuration of the pyrrolidine monomer was initially fixed as (2R,4'R) to mimic that of natural nucleosides, and a limited set of β-amino acids were employed as spacers (Figure 5). A stable PNA-DNA hybrid ($T_m = 80$ °C for the T₁₀ sequence) was first observed in dapcPNA having the (2R)-1-aminopyrrolidine-2-carboxylic acid (D-apc) spacer.^{26,32}

UV and circular dichroism (CD) titrations clearly revealed a 1:1 stoichiometry, which is in sharp contrast to other PNA systems, wherein triplex formation was preferred for homopyrimidine sequences.³⁰ The CD spectra of the PNA-DNA duplexes exhibit features that are compatible with right-handed helices.³² As a hydrazino peptide, dapcPNA could potentially exist in its protonated form at physiological pH, which might provide additional attractive interactions with the negatively charged DNA backbone. The absence of DNA binding for pyrrolidinyl PNAs carrying either charged or uncharged open-chain spacers (β-alanine and N-amino-N-methylglycine) suggests the importance of structural constraints over electrostatic interactions to the DNA binding.³³ This hypothesis was further confirmed in subsequent studies of PNA with carbocyclic 2-aminocyclopentanecarboxylic acid (acpc) spacers. Out of the four possible diastereomers of acpc, only the pyrrolidinyl PNA having a (2'R,4'R)-pyrrolidine/(1S,2S)-acpc backbone (henceforth denoted as acpcPNA) formed a very stable hybrid with DNA ($T_m > 85$ °C for the T₁₀ sequence).^{30,34} The other two cyclic β-amino acids that promote DNA binding are (1S,2S)-2-aminocyclobutanecarboxylic acid [(1S,2S)-acbc]³⁵ and (3R)-aminopyrrolidine-(4S)-carboxylic acid [(3R,4S)-apc].³⁶ All of these have the same absolute stereochemistry as (1S,2S)-acpc and the protonated form of D-apc. Interestingly, although (1S,2S)-2-aminocyclohexanecarboxylic acid [(1S,2S)-achc] possesses the same configuration, achcPNA derived from this spacer cannot bind to DNA (vide infra). This underscores the importance of careful design and correct placements of conformational constraints in PNA systems.

After the key structural elements that are important for DNA binding had been established, more detailed studies directed to determining the DNA/RNA binding specificity and self-pairing

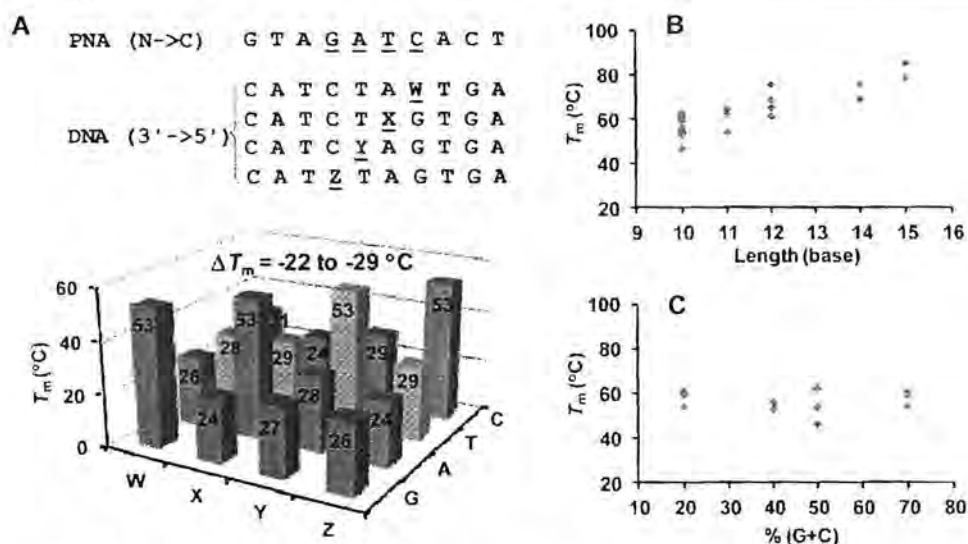


Figure 6. T_m of antiparallel acpcPNA-DNA duplexes. (A) Watson-Crick base-pairing specificity, (B) Relationships with number of base pairs ($n = 24$). (C) Relationships with base composition (10-mer, $n = 13$).

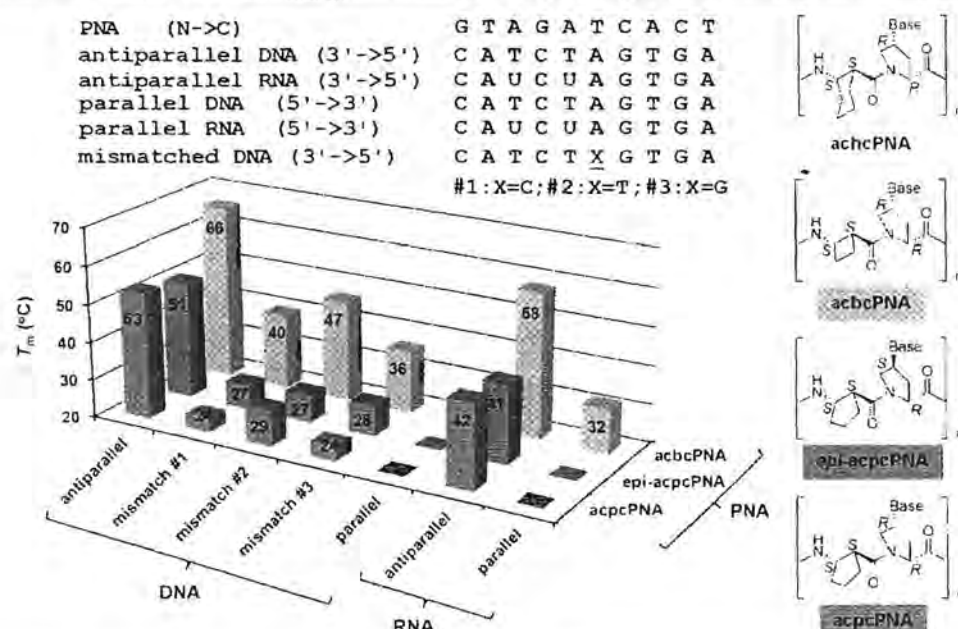


Figure 7. Comparison of T_m data of DNA and RNA hybrids of acpcPNA,³⁰ *epi*-acpcPNA,³⁸ and acbcPNA.³⁵ Values less than 20 °C are presented as 20 °C. acbcPNA showed no detectable binding to either DNA and RNA ($T_m < 20$ °C in all cases).

ability were performed with selected PNA systems having mixed-base nonchimeric sequences. While *aeg*PNA is known to form stable hybrids in both the antiparallel and parallel directions, acpcPNA exclusively forms antiparallel hybrids with DNA.²⁹ The pairing between acpcPNA and DNA exhibits excellent Watson-Crick specificity, as shown by an extremely large T_m decrease (22–29 °C) in the mismatched hybrids compared with the complementary hybrids (Figure 6A).³⁰ The T_m of acpcPNA-DNA hybrids increases with the number of base pairs (Figure 6B) but does not show obvious correlations with the base composition (G + C and purine/pyrimidine content) (Figure 6C). Whether this is a general phenomenon for the pyrrolidyl

PNA family remains to be confirmed, but preliminary studies with *epi*-acpcPNA and acbcPNA appear to suggest otherwise. An analysis of thermodynamic parameters suggests that the larger enthalpy gain due to G-C pairing relative to A-T pairing is counterbalanced by the more negative entropy term in the former case.³⁰ The different extents of puckering of the proline ring due to differences in electronegativity and steric bulkiness of the nucleobase substituents may partly explain such unusual sequence-dependent effects.³⁷

The effect of the pyrrolidine stereochemistry was next explored by employing (1*S*,2*S*)-acpc as the spacer.³⁰ Out of three remaining diastereomeric acpcPNAs, only the diaster-

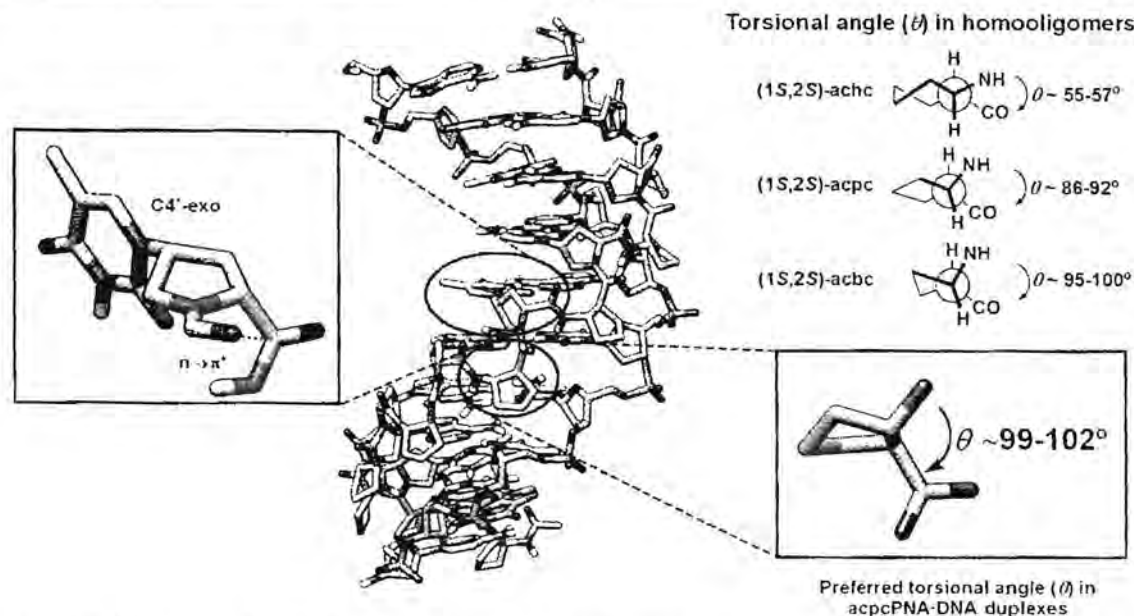


Figure 8. Model of the acpcPNA-DNA duplex showing the conformation of the pyrrolidine ring and torsional angles of the cyclic β -amino acids. Adapted from ref 35. Copyright 2012 American Chemical Society.

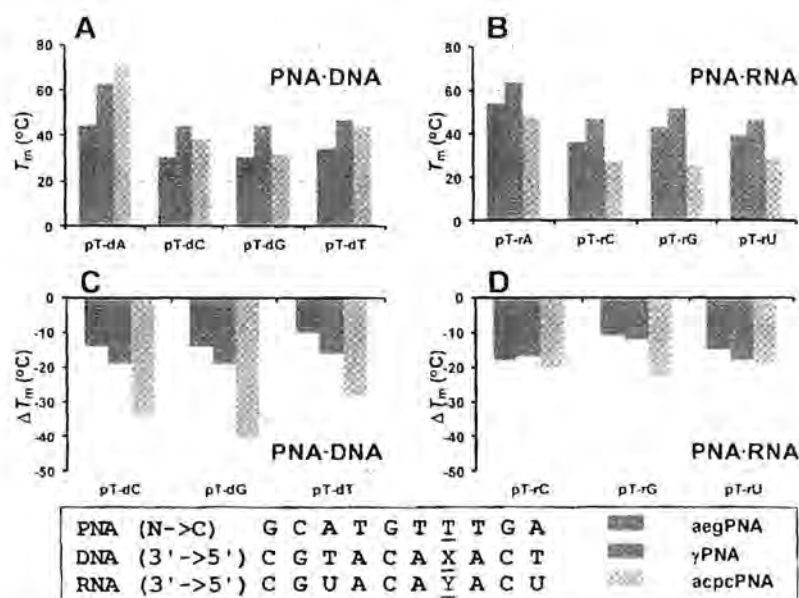


Figure 9. T_m and ΔT_m ($=T_m^{\text{mismatched}} - T_m^{\text{complementary}}$) data for (A, C) DNA hybrids and (B, D) RNA hybrids of aegPNA, γ PNA, and acpcPNA under comparable conditions. The L-serine-derived γ PNA was fully modified with hydroxymethyl side chains.¹⁷

eomer with the (2'*R*,4'*S*)-pyrrolidine/(1*S*,2*S*)-acpc backbone (henceforth denoted as *epi*-acpcPNA) shows appreciable DNA binding affinity, which is only slightly lower than that of the acpcPNA having the (2'*R*,4'*R*)-pyrrolidine/(1*S*,2*S*)-acpc backbone (Figure 7).^{30,38} This behavior is analogous to that of α -anomeric DNA, which can form Watson-Crick pairs with normal (β) DNA.³⁹

Importantly, decreasing the ring size of the cyclic β -amino acid spacer from five carbons in acpcPNA to four carbons in acbcPNA resulted in more stable PNA-DNA duplexes without compromising the base-pairing specificity, while achcPNA having a six-

membered-ring spacer showed no ability to bind DNA. This can be rationalized by considering the NH-C2-C1-CO torsional angle (θ) in the cyclic β -amino acid (Figure 8).³⁵ The native θ value of $95\text{--}100^\circ$, obtained from an X-ray structure of oligo(*trans*-acbc),⁴⁰ is closer to the values of $99\text{--}102^\circ$ obtained from molecular dynamics (MD) simulations of dacpcPNA-DNA⁴¹ and acpcPNA-DNA⁴² duplexes than those of *trans*-acpc ($86\text{--}92^\circ$), and *trans*-achc ($55\text{--}57^\circ$).⁴³ The rigid six-membered ring in *trans*-achc is likely to be far less flexible to adopt the desired optimal torsional angle for the DNA binding conformation compared with the five-membered ring in *trans*-

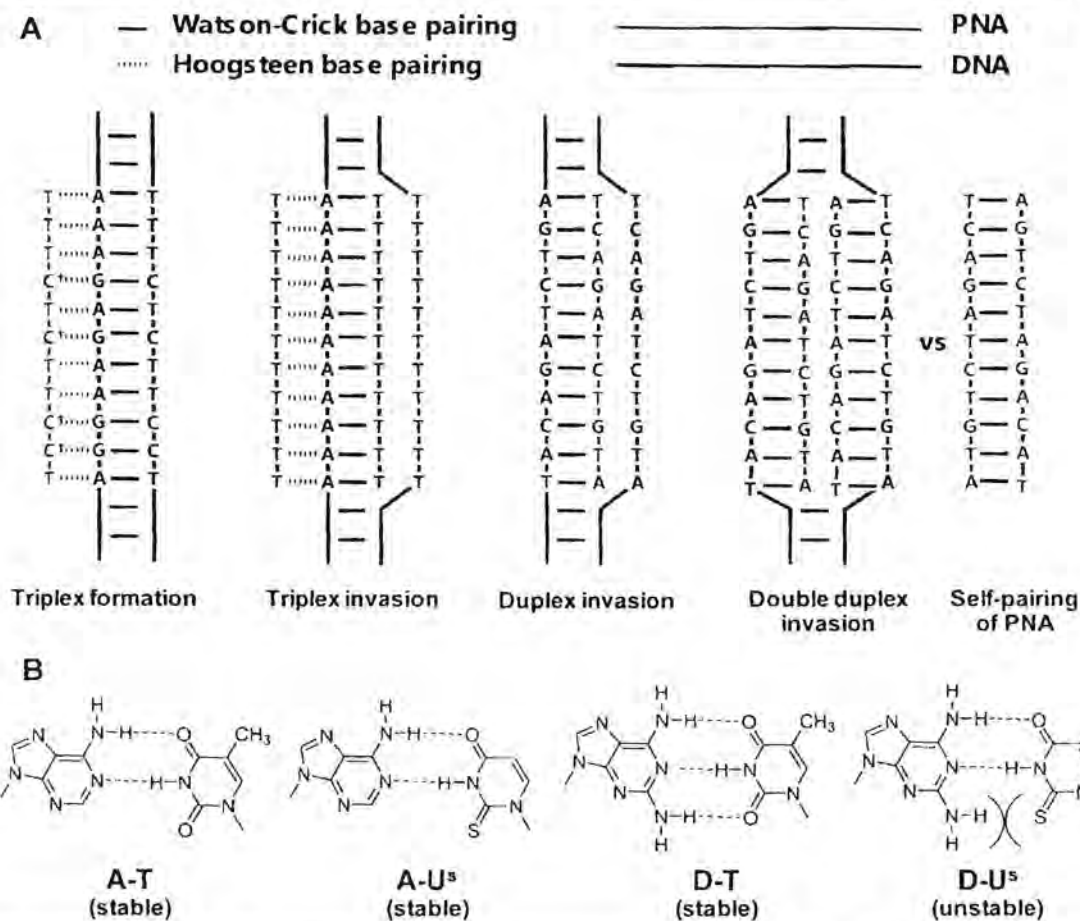


Figure 10. (A) Various modes of dsDNA recognition by PNA and (B) the concept of "pseudocomplementary" bases. Adapted with permission from ref 46. Copyright 1999 The National Academy of Sciences.

acpc. The MD simulations suggest that all of the amide bonds adopt a *trans* geometry, allowing $n \rightarrow \pi^*$ interactions between adjacent amide bonds in the $N \rightarrow C$ direction. In addition, they also suggest that the gas-phase enthalpy, calculated from a summation of bonded and nonbonded terms, is the major contributor to the high stability of pyrrolidiny PNA·DNA duplexes, which is consistent with the uncharged nature of the PNA backbone. This is in contrast to DNA·DNA duplexes, in which the gas-phase energy is high because of electrostatic repulsion, and thus solvation becomes the predominant stabilizing factor. A comparative simulation study of acpcPNA·DNA and *epi*-acpcPNA·DNA duplexes suggests that both the (2'*R*,4'*R*) and (2'*R*,4'*S*) pyrrolidine moieties can be well-accommodated in antiparallel B-DNA-like duplexes by adopting different ring-puckering modes.¹² The (2'*R*,4'*R*) acpcPNA showed C4'-*exo* puckering of the pyrrolidine ring while the (2'*R*,4'*S*) *epi*-acpcPNA showed C4'-*endo* puckering, placing the nucleobases in pseudoequatorial positions in both cases.

The availability of literature data for aegPNA and γ PNA^{17–19} allows a direct comparison of their DNA and RNA binding properties with those of acpcPNA (Figure 9). The T_m of the complementary acpcPNA·DNA hybrid (72 °C) was higher than those of aegPNA and γ PNA (44 and 63 °C, respectively). Moreover, mismatched DNA hybrids of acpcPNA showed larger T_m decreases (28–41 °C) than in aegPNA (10–14 °C), and

γ PNA (16–19 °C). The superior mismatch discrimination abilities of acpcPNA over aegPNA and DNA probes has also been clearly demonstrated by surface plasmon resonance (SPR)⁴⁴ and magnetic bead DNA capture experiments.⁴⁵

4.2. RNA Binding and Self-Pairing Properties

While most other PNAs bind more strongly to RNA over DNA, pyrrolidiny PNAs consistently show preferential DNA binding. The antiparallel binding mode is clearly preferred in pyrrolidiny PNA·RNA hybrids, although weak parallel hybrids are also occasionally observed.³⁰ The data in Figures 7 and 9 indicate that acpcPNA forms less stable RNA hybrids than aegPNA or γ PNA. Nevertheless, the T_m of 48 °C at 10 base pairs is still much higher than that of natural DNA/RNA pairs. Moreover, the larger T_m decrement for mismatched acpcPNA·RNA hybrids (19–23 °C) suggests a greater specificity compared with aegPNA (11–15 °C) and γ PNA (12–18 °C). Although the structural basis of the much higher thermal stability of acbcPNA·RNA hybrids relative to acpcPNA·RNA hybrids is not yet understood,³⁵ acbcPNA is clearly more useful for RNA-related applications.

Perhaps the most striking feature of pyrrolidiny PNA is the low propensity for self-pairing. While *epi*-acpcPNA forms only weakly stable self-hybrids,³⁸ no self-pairing has been observed in acpcPNA.³⁰ The order of pyrrolidiny PNA duplex stabilities (PNA·DNA > PNA·RNA > PNA·PNA) is therefore completely opposite to that of aegPNA (PNA·PNA > PNA·RNA > PNA·

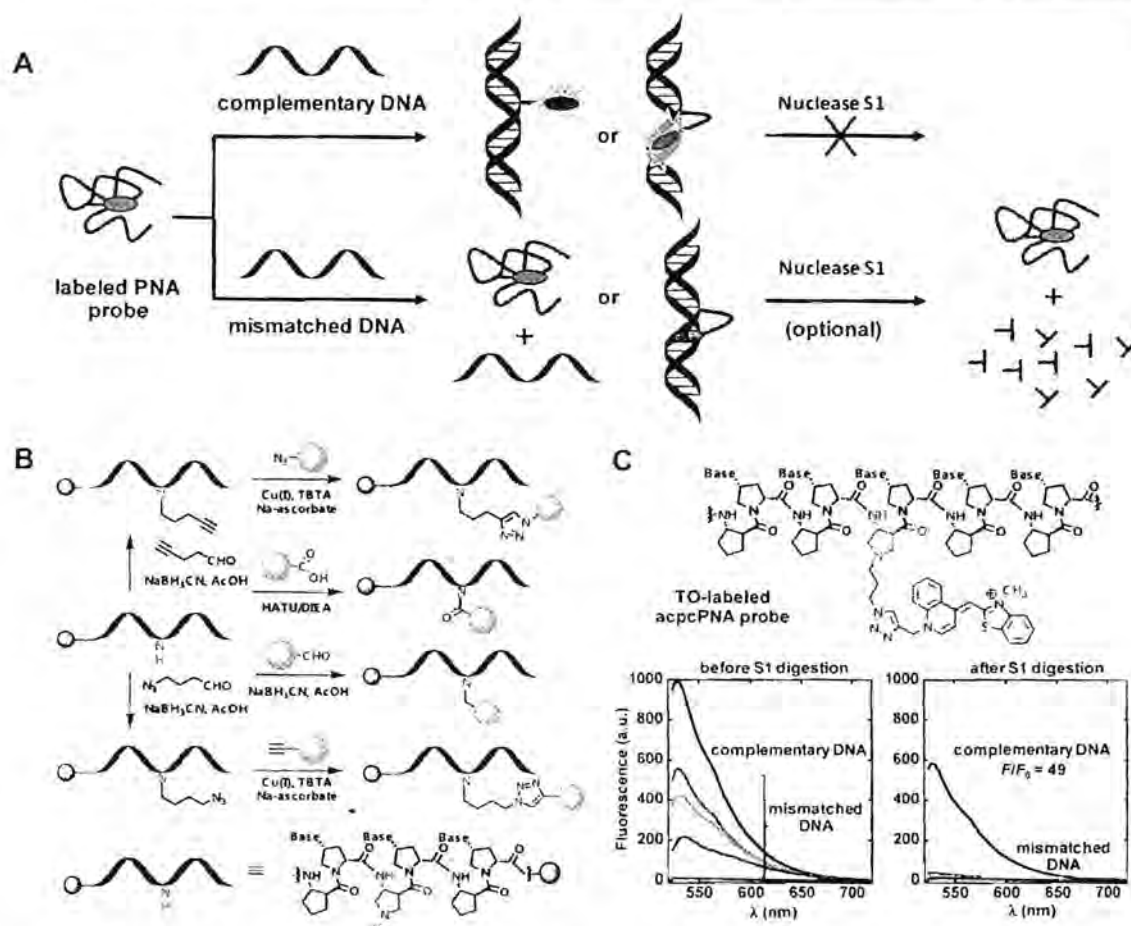


Figure 11. (A) Working principle of self-reporting PNA probes. (B) Strategies for backbone labeling of acpcPNA. Adapted from ref 58. Copyright 2013 American Chemical Society. (C) DNA-hybridization-responsive acpcPNA probes.

DNA). Destabilization of the acpcPNA self-hybrids was believed to be a consequence of the steric bulk of the acpcPNA strands. This hypothesis was experimentally supported by the observation that the less bulky acbcPNA formed considerably more stable self-hybrids than acpcPNA.³⁵ However, the greater stability of self-hybrids of *epi*-acpcPNA over acpcPNA also suggests the importance of stereochemistry to the self-pairing ability. NMR studies of three-dimensional structures as well as theoretical calculations are currently underway with the aim of further clarifying this issue. The obvious consequence of non-self-pairing PNA is that there is more flexibility in terms of sequence design without the concern of self-complementarity. On the other hand, such PNAs may not be suitable for applications that require self-pairing, such as in the construction of purely PNA-based nanomaterials, but they should still be useful when being used in combination with DNA such as in the development of DNA origami.^{3,4}

PNA is among the few synthetic molecules that can recognize structured nucleic acid targets, including dsDNA, in a sequence-specific fashion.¹⁰ In principle, double duplex invasion by PNA allows targeting of dsDNA without being limited to only purine rich regions as in triplex formation or triplex invasion (Figure 10A). However, the extremely high stability of aegPNA·aegPNA duplexes disfavors the double duplex invasion by two complementary strands of aegPNA designed to target the same

region of dsDNA. Replacement of the base A with diaminopurine (D) and the base T with 2-thiouracil (U^*) gave "pseudocomplementary" aegPNA having improved DNA invasion ability through destabilization of aegPNA·aegPNA duplexes and stabilization of aegPNA·DNA duplexes (Figure 10B).⁴⁶ Nevertheless, such pseudocomplementary base modification exists only for A·T pairs, and therefore, this may not completely suppress self-pairing in G·C-rich aegPNA sequences. In such cases, a combination of base modification and other strategies such as incorporation of positive charges into the aegPNA backbone is necessary.⁴⁷ Since acpcPNA is inherently pseudocomplementary, it should be a potential candidate for double duplex invasion of dsDNA without concerns over sequence-related limitations. Although a recent finding showed that unmodified γ PNA with sufficient length can directly invade into dsDNA without the need for the complementary PNA strand,⁴⁸ invasion by two strands of acpcPNA simultaneously should provide a much larger driving force. It also suggests the possibility of using single-stranded pyrrolidiny PNA to directly invade into dsDNA in a similar fashion.

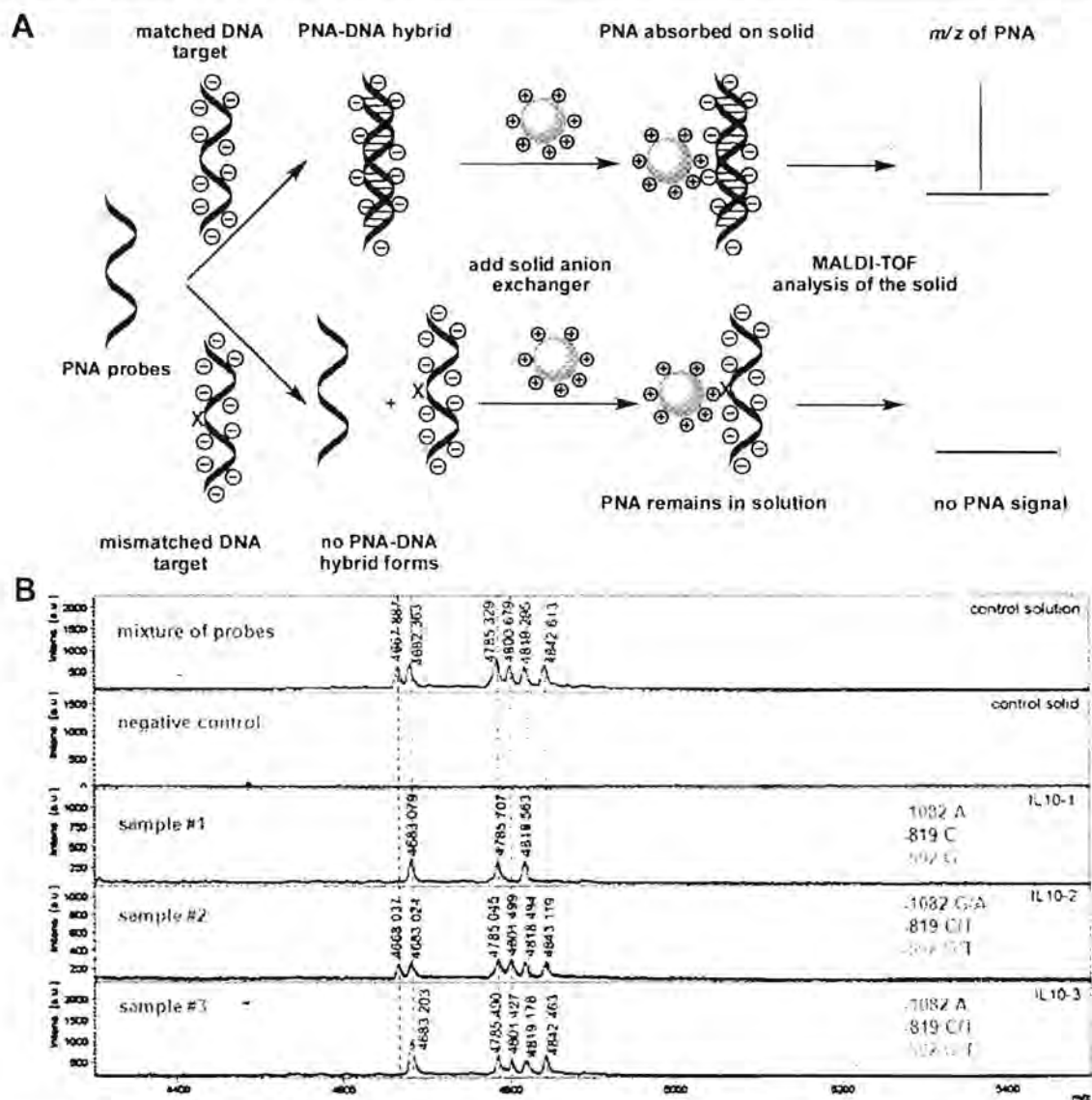


Figure 12. (A) Electrostatic capture of PNA-DNA hybrids. (B) SNP typing of human *IL-10* promoter region by MALDI-TOF analyses of the captured acpcPNA probes. Adapted from ref 63. Copyright 2008 American Chemical Society.

5. APPLICATIONS OF PYRROLIDINYL PNA

5.1. Sensor Probes

The excellent chemical and biological stability, the ability to form stable hybrids at low ionic strength, and the ability to recognize structured nucleic acid targets by strand invasion or triplex formation suggest the promising potential of PNA to improve the performance of nucleic acid biosensors.⁴⁹ Excellent mismatch discrimination has been demonstrated in various acpcPNA-based DNA detection platforms, including quartz crystal microbalance (QCM),⁵⁰ SPR,^{44,51} voltammetric,⁵² and capacitive detection.^{53,54}

5.2. Self-Reporting Fluorescence Probes

PNA generally adopts a compact structure in aqueous solution, thereby ensuring that dye-labeled single-stranded PNAs have distinctly different environments from duplexes without the requirement of a stem-loop structure as in classical beacons.⁵⁵

This, together with the potential for better mismatch discrimination, prompted us to develop self-reporting fluorescence acpcPNA probes (Figure 11A). The ability of PNA to protect DNA from digestion by S1 nuclease offers a unique opportunity to improve the discrimination further.⁵⁶

As an example, 5-pyren-1-yluracil (U^{Py}) incorporated into acpcPNA can specifically recognize dA in DNA and provides a strong fluorescence increase at 465 nm upon base pairing (3–42-fold, depending on the sequence).⁵⁷ This fluorescence enhancement was interpreted in terms of changes in the local environment and twisting between the pyrene and uracil moieties, which controls the degree of charge transfer.

To facilitate backbone labeling in acpcPNA, (3R,4S)-3-aminopyrrolidine-4-carboxylic acid (apc) was incorporated into the acpcPNA backbone to create a chimeric apc/acpcPNA. The (3R,4S)-apc spacer is structurally compatible with the acpcPNA backbone, as shown by the observation of very little

destabilization of the apc-containing PNA-DNA duplexes.⁵⁶ The inserted apc spacer provides a convenient handle for the introduction of various dyes or labels to the acpcPNA backbone via acylation, reductive alkylation, or click chemistry in a postsynthetic fashion (Figure 11B).⁵⁸ Pyrene appended to the acpcPNA backbone through a flexible linker is efficiently quenched by adjacent nucleobases ($T > C > G \gg A$) in the single-stranded acpcPNA. Hybridization with the DNA target restores the fluorescence (2.9–73-fold fluorescence increase). MD simulations suggest that the pyrene is located in the minor groove of the acpcPNA-DNA duplex and thus can no longer interact with the nucleobases.⁵⁹

The unsymmetrical cyanine dye thiazole orange (TO) has been extensively used in combination with aegPNA in light-up⁶⁰ and forced intercalation (FIT) probes.⁶¹ acpcPNA with a TO-labeled backbone shows an extremely large fluorescence increase upon hybridization to DNA. Nonspecific binding can be eliminated by S1 nuclease digestion, resulting in excellent mismatch discrimination (Figure 11C).⁵⁸ The solvatochromic benzophenoxazine dye Nile red attached to the acpcPNA backbone shows enhanced and blue-shifted fluorescence upon hybridization with DNA. This suggests that the Nile red in the PNA-DNA duplex is located in a more hydrophobic environment than in single-stranded PNA, and the effect may be used to probe local structures of the duplex such as bulge formation.⁶²

5.3. DNA Sensing Based on Differential Electrostatic Properties of PNA and DNA

The electrostatically neutral backbone of PNA provides a unique means for the development of novel DNA sensing methods. The different electrostatic properties of acpcPNA and acpcPNA-DNA hybrids allows selective capture of the hybridized PNA probe by a positively charged solid support such as Q-sepharose⁶³ or polymer-coated magnetite particles.⁶⁴ MALDI-TOF mass spectrometry can be used for sensitive detection of the captured PNA probe and hence identification of the DNA sequence in a label-free fashion (Figure 12). The high specificity of acpcPNA allows simultaneous multiplex discrimination of single nucleotide polymorphism (SNP), which can be difficult to achieve with conventional PNA probes.⁶⁵

A similar concept has been applied to the fabrication of a paper-based DNA sensor by functionalization of the cellulose paper with a positively charged polymer brush that can electrostatically capture the DNA sample together with its complementary biotinylated PNA probe. The presence or absence of captured PNA probes, which determines the identity of the DNA sequence, is revealed by an enzymatically amplified colorimetric reaction.⁶⁶

6. CONCLUSION AND OUTLOOK

This Account has highlighted our contribution to the development of conformationally constrained pyrrolidiny PNA having α/β -dipeptide backbones. The modular nature of the design enables the rapid synthesis and exploration of the base-pairing properties of these systems. AcpcPNA, a representative member of such pyrrolidiny PNA systems, binds to DNA with excellent affinity and specificity. In addition, acpcPNA possesses other unique and potentially useful characteristics: strong antiparallel selectivity, the preference for pairing to DNA over RNA, and the unprecedented inability to form self-hybrids. It is important to note that only minor changes in the pyrrolidiny PNA structure can lead to significantly different base-pairing behaviors, allowing one to fine-tune properties such as self-pairing or RNA binding

to suit the desired application. Although the structural contribution of the amino acid part to the binding characteristics of pyrrolidiny PNA is largely understood, little is known about the effect of the pyrrolidine part, and there are opportunities for improvement. Understanding factors contributing to these unusual behaviors through a combination of structural and theoretical studies will contribute to targeted, tailored "new generation" pyrrolidiny PNAs with improved/customizable properties. Finally, while diagnostic applications of pyrrolidiny PNA have been clearly demonstrated, its therapeutic/biological applications⁶⁷ and other areas such as functional materials⁶⁸ are only emerging. We invite others to join us as we continue to explore the full potential of utilizing acpcPNA and related pyrrolidiny PNAs in these cutting-edge research areas and beyond.

AUTHOR INFORMATION

Corresponding Author

*E-mail: vtirayut@chula.ac.th.

Notes

The author declares no competing financial interest.

Biography

Tirayut Vilaivan was born in Bangkok, Thailand, in 1971 and obtained his D.Phil. from Oxford in 1996. He is currently a professor of chemistry at Chulalongkorn University in Bangkok. His research interests involve organic synthesis and its applications to the areas of peptide nucleic acid and medicinal chemistry.

ACKNOWLEDGMENTS

The author acknowledges the inspiration provided by the late Prof. Gordon Lowe, FRS, and contributions from members of the research group and collaborators as well as financial support from The Thailand Research Fund and Chulalongkorn University (DPG5780002).

REFERENCES

- (1) Silverman, S. K. DNA as a Versatile Chemical Component for Catalysis, Encoding, and Stereocontrol. *Angew. Chem., Int. Ed.* **2010**, *49*, 7180–7201.
- (2) Zhang, F.; Nangreave, J.; Liu, Y.; Yan, H. Structural DNA Nanotechnology: State of the Art and Future Perspective. *J. Am. Chem. Soc.* **2014**, *136*, 11198–11211.
- (3) Rothmund, P. W. K. Folding DNA To Create Nanoscale Shapes and Patterns. *Nature* **2006**, *440*, 297–302.
- (4) Saccà, B.; Niemeyer, C. M. DNA Origami: The Art of Folding DNA. *Angew. Chem., Int. Ed.* **2012**, *51*, 58–66.
- (5) Schmidt, M. Xenobiology: A New Form of Life as the Ultimate Biosafety Tool. *Bioessays* **2010**, *32*, 322–331.
- (6) Pinheiro, V. B.; Taylor, A. I.; Cozens, C.; Abramov, M.; Renders, M.; Zhang, S.; Chaput, J. C.; Wengel, J.; Peak-Chew, S.-Y.; McLaughlin, S. H.; Herdewijn, P.; Holliger, P. Synthetic Genetic Polymers Capable of Heredity and Evolution. *Science* **2012**, *336*, 341–344.
- (7) Nielsen, P. E.; Egholm, M.; Berg, R. H.; Buchardt, O. Sequence-Selective Recognition of DNA by Strand Displacement with a Thymine-Substituted Polyamide. *Science* **1991**, *254*, 1497–1500.
- (8) Nielsen, P. E. Peptide Nucleic Acid. A Molecule with Two Identities. *Acc. Chem. Res.* **1999**, *32*, 624–630.
- (9) *Peptide Nucleic Acid: Protocols and Applications*; Nielsen, P. E., Ed.; Horizon Bioscience: Norfolk, U.K., 2004.
- (10) Armitage, B. A. The Impact of Nucleic Acid Secondary Structure on PNA Hybridization. *Drug Discovery Today* **2003**, *8*, 222–228.

- (11) Singhal, A.; Nielsen, P. E. Cross-Catalytic Peptide Nucleic Acid (PNA) Replication Based on Templated Ligation. *Org. Biomol. Chem.* 2014, 12, 6901–6907.
- (12) Plöger, T. A.; von Kiedrowski, G. A Self-Replicating Peptide Nucleic Acid. *Org. Biomol. Chem.* 2014, 12, 6908–6914.
- (13) Sugiyama, T.; Kittaka, A. Chiral Peptide Nucleic Acids with a Substituent in the *N*-(2-Aminoethyl)glycine Backbone. *Molecules* 2013, 18, 287–310.
- (14) Kumar, V. A.; Ganesh, K. N. Conformationally Constrained PNA Analogues: Structural Evolution toward DNA/RNA Binding Selectivity. *Acc. Chem. Res.* 2005, 38, 404–412.
- (15) Pokorski, J. K.; Witschi, M. A.; Purnell, B. L.; Appella, D. H. (*S,S*)-*trans*-Cyclopentane-Constrained Peptide Nucleic Acids. A General Backbone Modification That Improves Binding Affinity and Sequence Specificity. *J. Am. Chem. Soc.* 2004, 126, 15067–15073.
- (16) Govindaraju, T.; Kumar, V. A.; Ganesh, K. N. (*SR/RS*)-Cyclohexanyl PNAs: Conformationally Preorganized PNA Analogues with Unprecedented Preference for Duplex Formation with RNA. *J. Am. Chem. Soc.* 2005, 127, 4144–4145.
- (17) Dragulescu-Andrasi, A.; Rapireddy, S.; Frezza, B. M.; Gayathri, C.; Gil, R. R.; Ly, D. H. A Simple γ -Backbone Modification Preorganizes Peptide Nucleic Acid into a Helical Structure. *J. Am. Chem. Soc.* 2006, 128, 10258–10267.
- (18) Sahu, B.; Sacui, I.; Rapireddy, S.; Zanotti, K. J.; Bahal, R.; Armitage, B. A.; Ly, D. H. Synthesis and Characterization of Conformationally Preorganized, (*R*)-Diethylene Glycol-Containing γ -Peptide Nucleic Acids with Superior Hybridization Properties and Water Solubility. *J. Org. Chem.* 2011, 76, S614–S627.
- (19) Sahu, B.; Chenna, V.; Lathrop, K. L.; Thomas, S. M.; Zon, G.; Livak, K. J.; Ly, D. H. Synthesis of Conformationally Preorganized and Cell-Permeable Guanidine-Based γ -Peptide Nucleic Acids (γ GPNA). *J. Org. Chem.* 2009, 74, 1509–1516.
- (20) Jain, D. R.; Anandi V. L.; Lahiri, M.; Ganesh, K. N. Influence of Pendant Chiral *C'*-(Alkylideneamino/Guanidino) Cationic Side-Chains of PNA Backbone on Hybridization with Complementary DNA/RNA and Cell Permeability. *J. Org. Chem.* 2014, 79, 9567–9577.
- (21) Englund, E. A.; Appella, D. H. γ -Substituted Peptide Nucleic Acids Constructed from ϵ -Lysine are a Versatile Scaffold for Multifunctional Display. *Angew. Chem., Int. Ed.* 2007, 46, 1414–1418.
- (22) Jain, D. R.; Ganesh, K. N. Clickable *C'*-Azido(methylene/butylene) Peptide Nucleic Acids and Their Clicked Fluorescent Derivatives: Synthesis, DNA Hybridization Properties, and Cell Penetration Studies. *J. Org. Chem.* 2014, 79, 6708–6714.
- (23) Kitamatsu, M.; Takahashi, A.; Ohtsuki, T.; Sisido, M. Synthesis of Pyrrolidine-Based Oxy-Peptide Nucleic Acids Carrying Four Types of Nucleobases and Their Transport into Cytoplasm. *Tetrahedron* 2010, 66, 9659–9666.
- (24) Worthington, R. J.; Micklefield, J. Biophysical and Cellular-Uptake Properties of Mixed-Sequence Pyrrolidine–Amide Oligonucleotide Mimics. *Chem.—Eur. J.* 2011, 17, 14429–14441.
- (25) Lowe, G.; Vilaivan, T. Solid Phase Synthesis of Novel Peptide Nucleic Acids. *J. Chem. Soc., Perkin Trans. 1* 1997, 555–560.
- (26) Vilaivan, T.; Suparpprom, C.; Harnyuttanakorn, P.; Lowe, G. Synthesis and Properties of Novel Pyrrolidinyl PNA Carrying β -Amino Acid Spacers. *Tetrahedron Lett.* 2001, 42, 5533–5536.
- (27) Cheng, R. P.; Gellman, S. H.; DeGrado, W. F. β -Peptides: From Structure to Function. *Chem. Rev.* 2001, 101, 3219–3232.
- (28) Lowe, G.; Vilaivan, T. Amino Acids Bearing Nucleobases for the Synthesis of Novel Peptide Nucleic Acids. *J. Chem. Soc., Perkin Trans. 1* 1997, 539–546.
- (29) Vilaivan, T.; Srisuwannaket, C. Hybridization of Pyrrolidinyl Peptide Nucleic Acids and DNA: Selectivity, Base-Pairing Specificity, and Direction of Binding. *Org. Lett.* 2006, 8, 1897–1900.
- (30) Vilaivan, C.; Srisuwannaket, C.; Ananthanawat, C.; Suparpprom, C.; Kawakami, J.; Yamaguchi, Y.; Tanaka, Y.; Vilaivan, T. Pyrrolidinyl Peptide Nucleic Acid with α/β -Peptide Backbone: A Conformationally Constrained PNA with Unusual Hybridization Properties. *Artif. DNA: PNA XNA* 2011, 2, 50–59.
- (31) Lowe, G.; Vilaivan, T. Dipeptides Bearing Nucleobases for Synthesis of Novel Peptide Nucleic Acids. *J. Chem. Soc., Perkin Trans. 1* 1997, 547–554.
- (32) Vilaivan, T.; Lowe, G. A Novel Pyrrolidinyl PNA Showing High Sequence Specificity and Preferential Binding to DNA over RNA. *J. Am. Chem. Soc.* 2002, 124, 9326–9327.
- (33) Vilaivan, T.; Suparpprom, C.; Duanglaor, P.; Harnyuttanakorn, P.; Lowe, G. Synthesis and Nucleic Acid Binding Studies of Novel Pyrrolidinyl PNA Carrying an *N*-Amino-*N*-methylglycine Spacer. *Tetrahedron Lett.* 2003, 44, 1663–1666.
- (34) Suparpprom, C.; Srisuwannaket, C.; Sangvanich, P.; Vilaivan, T. Synthesis and Oligodeoxynucleotide Binding Properties of Pyrrolidinyl Peptide Nucleic Acids Bearing Prolyl-2-aminocyclopentanecarboxylic Acid (ACPC) Backbones. *Tetrahedron Lett.* 2005, 46, 2833–2837.
- (35) Mansawat, W.; Vilaivan, C.; Balázs, Á.; Aitken, D. J.; Vilaivan, T. Pyrrolidinyl Peptide Nucleic Acid Homologues: Effect of Ring Size on Hybridization Properties. *Org. Lett.* 2012, 14, 1440–1443.
- (36) Reenabthue, N.; Boonlua, C.; Vilaivan, C.; Vilaivan, T.; Suparpprom, C. 3-Aminopyrrolidine-4-carboxylic Acid as Versatile Handle for Internal Labeling of Pyrrolidinyl PNA. *Bioorg. Med. Chem. Lett.* 2011, 21, 6465–6469.
- (37) Shoulders, M. D.; Satyshur, K. A.; Forest, K. T.; Raines, R. T. Stereoelectronic and Steric Effects in Side Chains Preorganize a Protein Main Chain. *Proc. Natl. Acad. Sci. U.S.A.* 2010, 107, S59–S64.
- (38) Taechalerpaisarn, J.; Sriwarom, P.; Boonlua, C.; Yotapan, N.; Vilaivan, C.; Vilaivan, T. DNA-, RNA- and Self-Pairing Properties of a Pyrrolidinyl Peptide Nucleic Acid with a (2'*R*,4'*S*)-Prolyl-(1*S*,2*S*)-2-aminocyclopentanecarboxylic Acid Backbone. *Tetrahedron Lett.* 2010, 51, S822–S826.
- (39) Morvan, F.; Debart, F.; Vasseur, J.-J. From Anionic to Cationic α -Anomeric Oligodeoxynucleotides. *Chem. Biodiversity* 2010, 7, 494–535.
- (40) Fernandes, C.; Faure, S.; Pereira, E.; Théry, V.; Declercq, V.; Guillot, R.; Aitken, D. J. 1*Z*-Helix Folding of Cyclobutane β -Amino Acid Oligomers. *Org. Lett.* 2010, 12, 3606–3609.
- (41) Siri Wong, K.; Chuichay, P.; Saen-oon, S.; Suparpprom, C.; Vilaivan, T.; Hannongbua, S. Insight into Why Pyrrolidinyl Peptide Nucleic Acid Binding to DNA Is More Stable than the DNA-DNA Duplex. *Biochem. Biophys. Res. Commun.* 2008, 372, 765–771.
- (42) Poomsook, N.; Siri Wong, K. Structural Properties and Stability of PNA with (2'*R*,4'*R*)- and (2'*R*,4'*S*)-Prolyl-(1*S*,2*S*)-2-aminocyclopentanecarboxylic Acid Backbone Binding to DNA: A Molecular Dynamics Simulation Study. *Chem. Phys. Lett.* 2013, 588, 237–241.
- (43) Vasudev, P. G.; Chatterjee, S.; Shamala, N.; Balaran, P. Structural Chemistry of Peptides Containing Backbone Expanded Amino Acid Residues: Conformational Features of β , γ , and Hybrid Peptides. *Chem. Rev.* 2011, 111, 657–687.
- (44) Ananthanawat, C.; Vilaivan, T.; Hoven, V. P.; Su, X. Comparison of DNA, Aminoethylglycyl PNA and Pyrrolidinyl PNA as Probes for Detection of DNA Hybridization Using Surface Plasmon Resonance Technique. *Biosens. Bioelectron.* 2010, 25, 1064–1069.
- (45) Stubinitzky, C.; Vilaivan, T.; Wagenknecht, H.-A. The Base Discriminating Potential of Pyrrolidinyl PNA Demonstrated by Magnetic Fe₃O₄ Particles. *Org. Biomol. Chem.* 2014, 12, 3586–3589.
- (46) Lohse, J.; Dahl, O.; Nielsen, P. E. Double Duplex Invasion by Peptide Nucleic Acid: A General Principle for Sequence-Specific Targeting of Double-Stranded DNA. *Proc. Natl. Acad. Sci. U.S.A.* 1999, 96, 11804–11808.
- (47) Ishizuka, T.; Yoshida, J.; Yamamoto, Y.; Sumaoka, J.; Tedeschi, T.; Corradini, R.; Sforza, S.; Komiyama, M. Chiral Introduction of Positive Charges to PNA for Double-Duplex Invasion to Versatile Sequences. *Nucleic Acids Res.* 2008, 36, 1464–1471.
- (48) He, G.; Rapireddy, S.; Bahal, R.; Sahu, B.; Ly, D. H. Strand Invasion of Extended, Mixed-Sequence B-DNA by γ PNAs. *J. Am. Chem. Soc.* 2009, 131, 12088–12090.
- (49) Briones, C.; Moreno, M. Applications of Peptide Nucleic Acids (PNAs) and Locked Nucleic Acids (LNAs) in Biosensor Development. *Anal. Bioanal. Chem.* 2012, 402, 3071–3089.
- (50) Ananthanawat, C.; Vilaivan, T.; Hoven, V. P. Synthesis and Immobilization of Thiolated Pyrrolidinyl Peptide Nucleic Acids on

Gold-Coated Piezoelectric Quartz Crystals for the Detection of DNA Hybridization. *Sens. Actuators, B* 2009, 137, 215–221.

(51) Ananthanawat, C.; Vilaivan, T.; Mekboonsonglarp, W.; Hoven, V. P. Thiolated Pyrrolidinyl Peptide Nucleic Acids for the Detection of DNA Hybridization Using Surface Plasmon Resonance. *Biosens. Bioelectron.* 2009, 24, 3544–3549.

(52) Jampasa, S.; Wonsawat, W.; Rodthongkum, N.; Siangproh, W.; Yanatatsanejit, P.; Vilaivan, T.; Chailapakul, O. Electrochemical Detection of Human Papillomavirus DNA Type 16 Using a Pyrrolidinyl Peptide Nucleic Acid Probe Immobilized on Screen Printed Carbon Electrodes. *Biosens. Bioelectron.* 2014, 54, 428–434.

(53) Thipmanee, O.; Samanman, S.; Sankoh, S.; Numnuam, A.; Limbut, W.; Kanatharana, P.; Vilaivan, T.; Thavarungkul, P. Label-Free Capacitive DNA Sensor Using Immobilized Pyrrolidinyl PNA Probe: Effect of the Length and Terminating Head Group of the Blocking Thiols. *Biosens. Bioelectron.* 2012, 38, 430–435.

(54) Sankoh, S.; Samanman, S.; Thipmanee, O.; Numnuam, A.; Limbut, W.; Kanatharana, P.; Vilaivan, T.; Thavarungkul, P. A Comparative Study of a Label-Free DNA Capacitive Sensor Using a Pyrrolidinyl Peptide Nucleic Acid Probe Immobilized through Polyphenylenediamine and Polytyramine Non-conducting Polymers. *Sens. Actuators, B* 2013, 177, 543–554.

(55) Kuhn, H.; Demidov, V. V.; Coull, J. M.; Fiandaca, M. J.; Gildea, B. D.; Frank-Kamenetskii, M. D. Hybridization of DNA and PNA Molecular Beacons to Single-Stranded and Double-Stranded DNA Targets. *J. Am. Chem. Soc.* 2002, 124, 1097–1103.

(56) Komiyama, M.; Ye, S.; Liang, X.; Yamamoto, Y.; Tomita, T.; Zhou, J.-M.; Aburatani, H. PNA for One-Base Differentiating Protection of DNA from Nuclease and Its Use for SNPs Detection. *J. Am. Chem. Soc.* 2003, 125, 3758–3762.

(57) Boonlua, C.; Vilaivan, C.; Wagenknecht, H.-A.; Vilaivan, T. 5-(Pyren-1-yl)uracil as a Base-Discriminating Fluorescent Nucleobase in Pyrrolidinyl Peptide Nucleic Acids. *Chem.—Asian J.* 2011, 6, 3251–3259.

(58) Ditmangklo, B.; Boonlua, C.; Suparpprom, C.; Vilaivan, T. Reductive Alkylation and Sequential Reductive Alkylation—Click Chemistry for On-Solid-Support Modification of Pyrrolidinyl Peptide Nucleic Acid. *Bioconjugate Chem.* 2013, 24, 614–625.

(59) Boonlua, C.; Ditmangklo, B.; Reenabthue, N.; Suparpprom, C.; Poomsuk, N.; Siriwong, K.; Vilaivan, T. Pyrene-Labeled Pyrrolidinyl Peptide Nucleic Acid as a Hybridization-Responsive DNA Probe: Comparison between Internal and Terminal Labeling. *RSC Adv.* 2014, 4, 8817–8827.

(60) Svanvik, N.; Westman, G.; Wang, D.; Kubista, M. Light-Up Probes: Thiazole Orange-Conjugated Peptide Nucleic Acid for Detection of Target Nucleic Acid in Homogeneous Solution. *Anal. Biochem.* 2000, 281, 26–35.

(61) Köhler, O.; Jarikote, D. V.; Seitz, O. Forced Intercalation Probes (FIT Probes): Thiazole Orange as a Fluorescent Base in Peptide Nucleic Acids for Homogeneous Single-Nucleotide-Polymorphism Detection. *ChemBioChem* 2005, 6, 69–77.

(62) Yotapan, N.; Charoenpakdee, C.; Wathanathavorn, P.; Ditmangklo, B.; Wagenknecht, H.-A.; Vilaivan, T. Synthesis and Optical Properties of Pyrrolidinyl Peptide Nucleic Acid Carrying a Clicked Nile Red Label. *Beilstein J. Org. Chem.* 2014, 10, 2166–2174.

(63) Boontha, B.; Nakkuntod, J.; Hirankarn, N.; Chaumpluk, P.; Vilaivan, T. Multiplex Mass Spectrometric Genotyping of Single Nucleotide Polymorphisms Employing Pyrrolidinyl Peptide Nucleic Acid in Combination with Ion-Exchange Capture. *Anal. Chem.* 2008, 80, 8178–8186.

(64) Theppaleak, T.; Rutnakornpituk, B.; Wichai, U.; Vilaivan, T.; Rutnakornpituk, M. Magnetite Nanoparticle with Positively Charged Surface for Immobilization of Peptide Nucleic Acid and Deoxyribonucleic Acid. *J. Biomed. Nanotechnol.* 2013, 9, 1509–1520.

(65) Griffin, T. J.; Tang, W.; Smith, L. M. Genetic Analysis by Peptide Nucleic Acid Affinity MALDI-TOF Mass Spectrometry. *Nat. Biotechnol.* 1997, 15, 1368–1372.

(66) Laopa, P. S.; Vilaivan, T.; Hoven, V. P. Positively Charged Polymer Brush-Functionalized Filter Paper for DNA Sequence

Determination following Dot Blot Hybridization Employing a Pyrrolidinyl Peptide Nucleic Acid Probe. *Analyst* 2013, 138, 269–277.

(67) Arayachukiat, S.; Seemork, J.; Pan-In, P.; Amornwachirabodee, K.; Sangphech, N.; Sansureerungsikul, T.; Sathornsantikun, K.; Vilaivan, C.; Shigyou, K.; Pienpinijtham, P.; Vilaivan, T.; Palaga, T.; Banlunara, W.; Hamada, T.; Wanichwecharungruang, S. Bringing Macromolecules into Cells and Evading Endosomes by Oxidized Carbon Nanoparticles. *Nano Lett.* 2015, 15, 3370–3376.

(68) Sezi, S.; Varghese, R.; Vilaivan, T.; Wagenknecht, H.-A. Conformational Control of Dual Emission by Pyrrolidinyl PNA–DNA Hybrids. *ChemistryOpen* 2012, 1, 173–176.

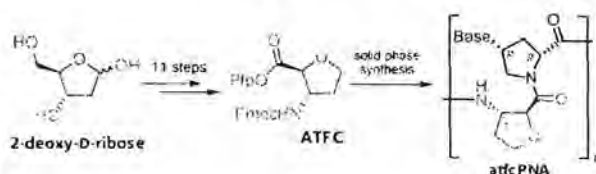
Synthesis and DNA/RNA Binding Properties of Conformationally Constrained Pyrrolidinyl PNA with a Tetrahydrofuran Backbone Deriving from Deoxyribose

Pitchanun Sriwarom, Panuwat Padungros, and Tirayut Vilaivan*

Organic Synthesis Research Unit, Department of Chemistry, Faculty of Science, Chulalongkorn University, Phayathai Road, Patumwan, Bangkok 10330, Thailand

Supporting Information

ABSTRACT: Sugar-derived cyclic β -amino acids are important building blocks for designing of foldamers and other biomimetic structures. We report herein the first synthesis of a C-activated *N*-Fmoc-protected *trans*-(2*S*,3*S*)-3-aminotetrahydrofuran-2-carboxylic acid as a building block for Fmoc solid phase peptide synthesis. Starting from 2-deoxy-D-ribose, the product is obtained in a 6.7% overall yield following an 11-step reaction sequence. The tetrahydrofuran amino acid is used as a building block for a new peptide nucleic acid (PNA), which exhibits excellent DNA binding affinity with high specificity. It also shows preference for binding to DNA over RNA and specifically in the antiparallel orientation. In addition, the presence of the hydrophilic tetrahydrofuran ring in the PNA structure reduces nonspecific interactions and self-aggregation, which is a common problem in PNA due to its hydrophobic nature.

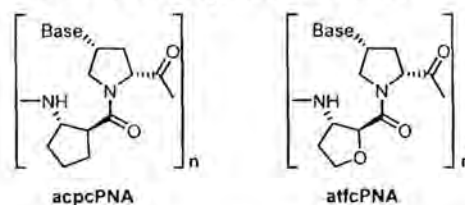


INTRODUCTION

Foldamers are synthetic oligomeric molecules that can mimic naturally occurring biological macromolecules by folding into well-defined secondary structures such as helices, turns, or sheets in solution states.¹ Amino acids, especially cyclic β -amino acids,² constitute an important class of building blocks for foldamers.³ A diverse range of secondary structures were obtained from simple cyclic β -amino acids building blocks with different ring size, stereochemistry, and substituents.⁴ The ability to precisely program the folding pattern is not only important from the molecular design aspect but also leads to desirable biological functions. Carbohydrate-derived amino acids⁵ have recently attracted much interest as potential building blocks for novel foldamers.⁶ It can be readily obtained from inexpensive sources in stereochemically defined configurations and possess a number of functional groups that can be fine-tuned as desired.

Deoxyribonucleoside-derived cyclic β -amino acids have been used in designing nucleobase-containing foldamers,⁷ some of which showed promising DNA and RNA binding properties.^{7d} These foldamers can therefore be regarded as a new class of peptide nucleic acid (PNA).^{8,9} Our research group had introduced a series of conformationally constrained pyrrolidinyl peptide nucleic acids derived from alternating nucleobase-modified *D*-proline and cyclic β -amino acids.^{10,11} A representative member of such pyrrolidinyl PNA is acpcPNA (Scheme 1) which carries *trans*-(1*S*,2*S*)-2-aminocyclopentanecarboxylic acid (ACPC) in the backbone.^{10b,d} This acpcPNA showed some distinct properties from DNA and commercial PNA that could be useful for many applications.¹² A recent study on ring homologues suggested that four- or five-membered ring cyclic β -amino acids with specific configurations are essential to provide

Scheme 1. Structures of acpcPNA and atfcPNA



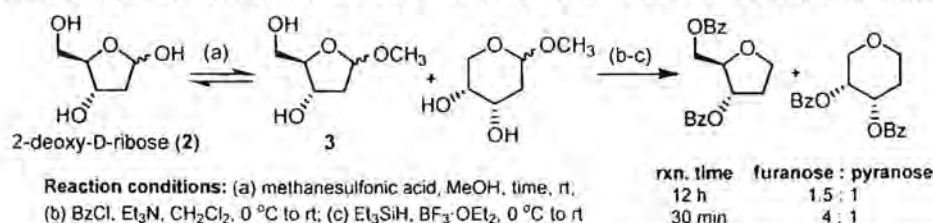
a balance between rigidity and flexibility that allows the PNA to adopt a DNA-binding conformation.^{10c} In addition to ACPC, other five-membered ring heterocyclic β -amino acids had been successfully incorporated into pyrrolidinyl PNA, including 1-aminopyrrolidine-2-carboxylic acid^{10a} and 3-aminopyrrolidine-4-carboxylic acid.^{10c}

In view of the structural similarity between 3-amino-tetrahydrofuran-2-carboxylic acid (ATFC) and ACPC, it is not surprising that oligomers of ATFC and its ring-substituted derivatives can also form well-defined helical foldamers.¹³ Oligomers of *trans*-ATFC formed a 12-helix similar to *trans*-ACPC. On the other hand, the *cis*-isomer adopted a 14-helix structure instead of the extended sheetlike structure of *cis*-ACPC, which was explained based on molecular modeling studies by a more favorable interaction between the less sterically hindered ring of ATFC and the backbone amide group.^{13a} We propose that replacement of ACPC in the acpcPNA backbone with *trans*-ATFC should provide a new pyrrolidinyl PNA that can still retain the excellent nucleic acid

Received: April 21, 2015

Published: June 17, 2015

Scheme 2. Structural Assignment of Methyl Glycoside Mixture by Conversion into Their 1-Deoxy Perbenzoylated Derivatives



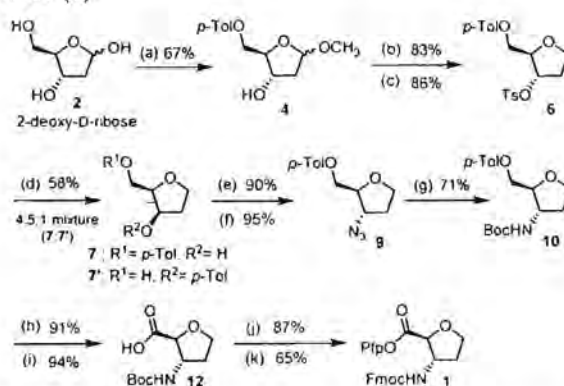
binding characteristics of acpcPNA. Moreover, it is expected that the more hydrophilic nature of tetrahydrofuran ring in ATFC as opposed to the cyclopentane ring in ACPC should be beneficial in reducing self-aggregation and nonspecific interactions occasionally observed in acpcPNA and other PNA systems due to their uncharged and hydrophobic peptide backbone.¹⁴ Herein, we report the synthesis of a new pyrrolidiny PNA with an ATFC backbone (will be named atfcPNA, Scheme 1) and a comparison with acpcPNA in terms of DNA/RNA binding properties and nonspecific binding behavior.

RESULTS AND DISCUSSION

Synthesis of Deoxyribose-Derived Cyclic β -Amino Acid (SS-ATFC). Our previous reports on the effects of stereochemistry of acpcPNA on DNA binding¹¹ suggests that the appropriately protected (2*S*,3*S*) enantiomer of the *trans*-ATFC (SS-ATFC) is required as a key building block. Interestingly, this particular configuration of ATFC is unknown in the literature despite some reports on the remaining stereoisomers.^{13a} We proposed that the required SS-ATFC monomer **1** should be readily synthesized starting from commercially available 2-deoxy-D-ribose (**2**). The key steps involved reductive removal of the anomeric hydroxyl group, stereospecific introduction of the amino group by a double inversion of configuration at C-3, and oxidation of the C-5 alcohol to the carboxylic acid.

With this synthetic strategy in mind, the anomeric hydroxyl group of 2-deoxy-D-ribose (**2**) was first converted to its methylglycoside derivative in the presence of an acid catalyst (Scheme 2).^{15,16} It should be noted that the reaction time played an important role for the outcome of the reaction.¹⁷ ¹H NMR analysis of the product mixture was simplified by perbenzoylation followed by reduction of the anomeric methyl ether with BF₃·Et₂O/Et₃SiH.¹⁸ Prolonged treatment of **2** with catalytic methanesulfonic acid in MeOH (12 h) provided a 1.5:1 mixture of furanoside **3** and the thermodynamically more stable pyranoside. However, immediate quenching of the reaction after consumption of the starting material (ca. 30 min) afforded the methylfuranoside **3** as the major product (>80% of the crude reaction mixture).

With the optimized conditions in hand, 2-deoxy-D-ribose (**2**) was smoothly converted to methylfuranoside **3** followed by selective protection¹⁹ of the C-5 primary hydroxyl group as the *p*-toluoyl ester to afford furanoside **4** in 67% yield over 2 steps (Scheme 3). Removal of the anomeric methoxy group by treatment with BF₃·Et₂O/Et₃SiH was previously reported on a fully protected 2-deoxyribose derivative,¹⁸ and thus it was uncertain if these conditions would be compatible with the unprotected C-3 hydroxyl group of furanoside **4**. It was envisioned that the C-3 hydroxyl group could be "protected" as a sulfonate ester prior to the anomeric reduction. Gratifyingly,

Scheme 3. Synthesis of SS-ATFC Starting from 2-Deoxy-D-ribose (**2**)

the furanoside **4** was tosylated to afford **5** in 83% yield, and the anomeric methoxy group was successfully reduced to provide intermediate **6** in 86% yield.

We next focused on the nucleophilic displacement of the tosylated furanoside **6**. The nitrite ion (NaNO₂) is relatively overlooked as an oxygen nucleophile for the stereochemical inversion of a hydroxyl group. It has been successfully employed in the inversion of various alcohols including carbohydrate derivatives.²⁰ The nucleophilic substitution of furanoside **6** with excess NaNO₂ at 120 °C for 5 h provided a 1:1 mixture of the expected inverted alcohol **7** and a side-product **7'** resulting from migration of the *p*-toluoyl group to the neighboring inverted C-3 hydroxyl group in moderate yield. Shortening the reaction time to 2 h gave a 4.5:1 regioisomeric mixture of 7:7' in 58% yield. The sterically hindered C-3 hydroxyl group of **7** is much less reactive than the free C-5 hydroxyl group of **7'**, and therefore, benzoylation of the mixture facilitated the chromatographic purification of unreacted **7** from benzoylated **7'** in 89% recovery yield.

The C-3 hydroxyl group of **7** was next converted to the mesylate **8** in 90% yield. It is worth noting that attempts to perform Mitsunobu reaction of furanoside **4** with MeOTf or methanesulfonic acid to yield the mesylate with inverted configuration at C-3 gave only complex mixtures.²¹ Reaction of **8** with excess NaN₃ at 90–100 °C for 2 h gave the expected azide **9** in 95% yield. Hydrogenation of **9** in the presence of Boc₂O gave the Boc-protected amine **10** in 71% yield as a white solid. Hydrolysis of *p*-toluoyl group in **10** followed by BAIB-TEMPO²² oxidation gave the Boc-protected amino acid **12** in high yield. Treatment with trifluoroacetic acid (TFA) liberated

Table 1. Sequence and Characterization Data of atfcPNA

| PNA | sequence (N→C) | N/C-terminal modification | t_R min ^a | m/z (calcd) ^b | m/z (found) ^c | yield % ^d |
|--------|----------------|---------------------------|------------------------|----------------------------|----------------------------|----------------------|
| T9 | TTTTTTTT | Ac/LysNH ₂ | 30.6 | 3198.2 | 3197.1 | 44 |
| M10 | GTAGATCACT | Ac/LysNH ₂ | 25.1 | 3578.6 | 3578.4 | 22 |
| M10Flu | GTAGATCACT | Flu/LysNH ₂ | 28.4, 29.2 | 3894.8 | 3893.3 | 15 |
| M10AT | TATGTACTAT | Bz/LysNH ₂ | 29.1 | 3630.6 | 3630.7 | 20 |
| M10CG | GCTACGTCGC | Bz/LysNH ₂ | 28.1 | 3617.6 | 3617.9 | 10 |

^aHPLC conditions: C18 column, 4.6 × 50 mm, 3 μ, gradient 0.1% TFA in H₂O:MeOH 90:10 for 5 min then linear gradient to 10:90 over 30 min, flow rate 0.5 mL/min, 260 nm. ^bAverage mass of M + H⁺. ^cMALDI-TOF. ^dIsolated yield after HPLC purification, spectrophotometrically determined.

Table 2. T_m of atfcPNA/acpcPNA and DNA/RNA

| PNA (N→C) | DNA or RNA (5'→3') | T_m atfcPNA (ΔT_m) ^a | T_m acpcPNA (ΔT_m) ^{a,b} | note |
|--------------------|----------------------|---|---|-------------------|
| GTAGATCACT (M10) | dAGTGATCTAC | 52.5 | 53.3 | complementary DNA |
| | dAGTG <u>C</u> TCTAC | 23.4 (-29.1) | 23.8 (-29.5) | mismatched DNA |
| | dAGTGGTCTAC | 23.4 (-29.1) | 23.9 (-29.4) | mismatched DNA |
| | dAGTG <u>T</u> TCTAC | 25.4 (-27.1) | 29.4 (-23.9) | mismatched DNA |
| | dCATCTAGTGA | <20 | <20 | parallel DNA |
| | rAGUGAUCUAC | 36.0 | 42.3 | complementary RNA |
| | rAGUG <u>C</u> UCUAC | <20 | 23.6 (-18.7) | mismatched RNA |
| | rAGUG <u>G</u> UCUAC | <20 | 24.8 (-17.5) | mismatched RNA |
| | rAGUG <u>U</u> UCUAC | <20 | <20 | mismatched RNA |
| | rCAUCUAGUGA | <20 | <20 | parallel RNA |
| TATGTACTAT (M10AT) | dATAGTACATA | 49.6 | 54.2 | complementary DNA |
| | dTAGA <u>C</u> ACATA | 25.4 (-24.2) | 23.4 (-30.8) | mismatched DNA |
| | dTAG <u>C</u> ACATA | 30.2 (-19.4) | 30.2 (-24.0) | mismatched DNA |
| | dATAG <u>G</u> ACATA | <20 | 24.4 (-29.8) | mismatched DNA |
| | dATACATGATA | <20 | <20 | parallel DNA |
| | rAUAGUACAUA | 29.2 | 32.6 | complementary RNA |
| | rAUACUAGUAU | <20 | <20 | parallel RNA |
| GCTACGTCGC (M10CG) | dGCGACGTAGC | 56.4 | 54.5 | complementary DNA |
| | dGCGA <u>A</u> GTAGC | 23.4 (-33.0) | <20 | mismatched DNA |
| | dGCGA <u>G</u> GTAGC | 31.2 (-25.2) | 30.2 (-24.3) | mismatched DNA |
| | dGCGA <u>T</u> GTAGC | 36.0 (-20.4) | 35.1 (-19.4) | mismatched DNA |
| | dCGATGCAGCG | <20 | <20 | parallel DNA |
| | rGCGACGUAGC | 41.8 | 48.0 | complementary RNA |
| | rCGAUGCAGCG | 24.4 (-17.4) | 39.2 (-8.8) | parallel RNA |

^aAll T_m were measured at PNA = 1 μM, 100 mM NaCl, 10 mM sodium phosphate buffer, pH 7.0, heating rate 1 °C/min; and $\Delta T_m = T_m - T_m^{\text{complementary hybrid}}$. ^bThe T_m data of acpcPNA are provided for comparison purposes. Except for the mismatched hybrids of M10AT and M10CG, T_m data of all acpcPNA hybrids were taken from ref 10d. Mismatch positions in DNA sequence are indicated by the underline.

the free amino acid which was further reacted with FmocOSu to give the desired Fmoc-protected amino acid 13 in 87% yield over 2 steps. Finally, the Fmoc-protected amino acid 13 was activated as its pentafluorophenyl (Pfp) ester 1 in 65% yield. The presence of the Pfp group was confirmed by ¹⁹F NMR analysis. In summary, the target cyclic β-amino acid spacer (SS-ATFC) 1 was successfully synthesized from commercially available 2-deoxy-D-ribose (2) in a straightforward fashion over 11 steps in 6.7% overall yield.

Synthesis of atfcPNA. Four different sequences of atfcPNA (T9, M10, M10AT, and M10CG) were synthesized from the activated SS-ATFC spacer 1 and the four Fmoc-protected pyrrolidinyl PNA monomers (A^{Bz}, T, C^{Bz}, and G^{Ibu}) following the stepwise coupling protocol for Fmoc solid phase synthesis of PNA previously developed in our laboratory (Table 1).^{10b} The atfcPNA sequences were end-capped at the N-termini by acetylation or benzylation. In addition, an atfcPNA sequence (M10) was also end-capped with 5(6)-carboxyfluorescein to yield a M10Flu sequence in order to study nonspecific interactions. All atfcPNAs were purified by reverse phase

HPLC and their identities were confirmed by MALDI-TOF mass spectrometry. In all cases, the PNAs were obtained with >90% purity, except for the M10Flu sequence which is split into two peaks on the HPLC chromatogram due to the presence of two carboxyfluorescein isomers. Isolated yields in the range of 10–44% were obtained, depending on the sequence. The poor isolated yields, which are typical for most solid phase syntheses, are attributed to the loss of product during HPLC purification due to separation issues rather than the synthetic efficiency. All PNAs are readily soluble in water (>1 mM). The sequences and characterization data of all atfcPNA are summarized in Table 1.

DNA and RNA Binding Properties of atfcPNA. Preliminary DNA binding studies were performed on the T9 sequence. Since homopyrimidine/homopurine PNA sequences are known to form triplex structures, it is important to first determine the stoichiometry of binding. This was accomplished by UV titration (Figure S22 of the Supporting Information), which clearly confirms a 1:1 stoichiometry of atfcPNA:DNA as shown by the inflection point at ca. 50 mol % DNA. This is in agreement with other pyrrolidinyl PNA, whereby no (PNA)₂

DNA triplex formation could be observed, presumably due to the bulkiness of the pyrrolidinyl PNA backbone.

Melting temperature measurements by UV spectrophotometry suggest that the T9 atfcPNA binds cooperatively to its complementary DNA (dA₉), giving well-defined melting curves with melting temperatures (T_m) of 60.3 and 64.1 °C (in the presence and absence of 100 mM NaCl, respectively). These T_m figures are somewhat lower than the corresponding T9 acpcPNA ($T_m = 72.5$ and >76.8 °C, in the presence and absence of 100 mM NaCl, respectively).^{10d,e} Nevertheless, it is clear that T9 atfcPNA can form a stable hybrid with its complementary DNA. In the presence of a mismatched base in the DNA strand, the T_m was dramatically decreased (-21.6 , -21.9 , and -31.8 °C for pT-dC, pT-dT, and pT-dG mismatches, respectively). The large decrease of T_m suggests that the atfcPNA binds to DNA with high specificity similar to that of acpcPNA.

Next, the DNA and RNA binding properties of mixed base atfcPNA were investigated and compared with the corresponding acpcPNA sequences (Table 2). Three sequences with different G+C content were compared (%G+C content: M10AT = 20; M10 = 40; and M10CG = 70). As shown in Table 2, all atfcPNA sequences showed a strong DNA binding affinity, and specifically in antiparallel orientation similar to acpcPNA. They also exhibit very high sequence specificity as shown by a large decrease in T_m values of mismatched compared to the complementary hybrids ($\Delta T_m \sim 19$ – 33 °C), which are in the same range as acpcPNA ($\Delta T_m \sim 19$ – 31 °C) and are much more discriminating than acgPNA.¹¹ It is interesting to note that while acpcPNA-DNA hybrids did not show a definite relationship between T_m and the base composition,^{10d} the T_m of atfcPNA showed a normal correlation with base composition (i.e., the T_m is increased with %G+C content). Further studies are clearly required in order to understand the basis of different behaviors between the two PNA systems, but it is beyond the scope of the present study.

In addition to DNA, atfcPNA can also bind to RNA in an antiparallel fashion, albeit with much lower affinity compared to the corresponding antiparallel DNA. Parallel hybrids with RNA were observed in G+C-rich sequences for both atfcPNA and acpcPNA, but the parallel hybrid was much less stable than the antiparallel hybrid, especially in the case of atfcPNA. Moreover, the RNA binding was highly sequence-specific as shown by a large decrease of T_m value in the presence of mismatched RNA targets. The normal correlation between T_m and base composition was again observed in atfcPNA-RNA hybrids. In addition, atfcPNA exhibits a greater selectivity for binding to DNA over RNA than acpcPNA as shown by the larger T_m difference between atfcPNA-RNA and atfcPNA-DNA hybrids (-20.4 , -16.5 , and -14.6 °C for M10AT, M10, and M10CG, respectively) compared to acpcPNA-RNA and acpcPNA-DNA hybrids (-21.6 , -11.0 , and -6.5 °C for M10AT, M10, and M10CG, respectively). Smaller differences were observed at higher G+C content in both PNA systems. The results suggest that atfcPNA and acpcPNA cannot effectively adjust themselves to the more limited conformational space of RNA duplexes exerted by the 2'-hydroxyl group in RNA, and that there are subtle differences between structures of A+T-rich and G+C-rich sequences.

Circular dichroism (CD) spectroscopy was also used to study the binding between the T9 atfcPNA and DNA (Figure 1a). The T9 atfcPNA exhibited weak CD signals in single-stranded form. The only prominent features were the positive band at 210

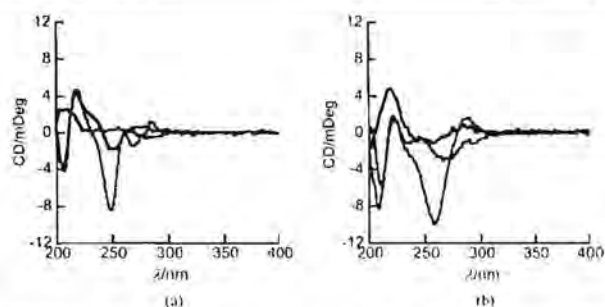


Figure 1. CD spectra of (a) T9 atfcPNA (blue), dA₉ (black), and their 1:1 hybrid (green) and (b) M10CG atfcPNA (blue) and its hybrids with antiparallel DNA (green) or antiparallel RNA (red). Conditions: PNA = DNA = 2.5 μ M in 10 mM sodium phosphate buffer (pH 7.0) and 100 mM NaCl at 20 °C.

nm and a very small negative band at 280 nm. The single-stranded dA₉ DNA showed two minima at 206 and 250 nm and maxima at 220, 232 (shoulder), and 275 nm. Upon hybrid formation, the negative band at 250 nm was markedly intensified and shifted to a slightly shorter wavelength (248 nm). Moreover, significant changes were observed in the nucleobase absorption region (260–300 nm) as shown by the appearance of a new negative band at 268 nm and a positive band at 285 nm. These probably reflect a change in the orientation of the nucleobase, most likely as a result of base–base pairing and stacking in the atfcPNA-DNA duplex. The overall shape of the CD spectrum of atfcPNA-DNA hybrid is quite similar to the corresponding acpcPNA-DNA and DNA-DNA hybrid.^{10b,d} It is therefore reasonable to assume that these hybrids adopt similar right-handed helical conformations. Heating caused the CD signal to return to the sum of the single-stranded components (Figure S23 of the Supporting Information). A plot of the CD signal at 248 nm as a function of temperature gave a sigmoidal curve (Figure S23 of the Supporting Information, inset). From this CD melting curve, a CD T_m of around 60 °C was obtained which is in good agreement to the T_m obtained by UV–vis spectrophotometry.

In contrast to the homothymine sequence, CD spectra of single-stranded mixed base atfcPNA suggested pronounced intrastrand base stacking (Figure 1b, see also Figures S28–S30 of the Supporting Information). The CD spectra are remarkably similar to single-stranded DNA as shown by a negative band at 205 nm, a strong positive band at 220 nm, a negative band at 256–260 nm, and a positive band around 280 nm with a crossover point around 267–273 nm.²³ Hybridization with antiparallel DNA did not change the overall shape of the CD spectra. However, the negative band at 260 nm became more intense and slightly shifted toward a longer wavelength. These are in agreement with tightening of the helical pitch after duplex formation.¹⁴ The effect is most clearly observed in the G+C-rich sequence M10CG. The overall shape of the CD spectra of atfcPNA-DNA hybrids corresponds to the B-form of DNA-DNA duplexes.²⁴ On the other hand, CD spectra of atfcPNA-RNA hybrids exhibited distinct features in the 250–300 nm region (Figure 1b, see also Figures S28–S30 of the Supporting Information). A positive band was observed between 245–256 nm together with a negative band with minima around 265 nm. This suggests that the atfcPNA-DNA and atfcPNA-RNA hybrids adopt different conformations, which could contribute to their different stabilities.

resolution mass spectra (HRMS) were recorded in electrospray ionization-time-of-flight (ESI-TOF) mode. MALDI-TOF mass spectra of all atcPNAs were obtained in linear positive ion mode using α -cyano-4-hydroxy cinnamic acid (CCA) as a matrix.

Methyl 2-Deoxy-D-ribofuranoside (3) (Mixture of α and β Anomers). Methyl 2-deoxy-D-ribofuranoside 3 was synthesized according to the literature procedure with a slight modification on the catalyst quantity and reaction time.^{16,17} 2-Deoxy-D-ribose (11.4 g, 85.0 mmol) was dissolved in anhydrous methanol (55 mL) under a nitrogen atmosphere, and then methanesulfonic acid (0.27 mL, 4.16 mmol) was added at room temperature. The reaction reached completion after stirring for 30 min at room temperature as confirmed by TLC analysis (CH_2Cl_2 :MeOH 9:1, *p*-anisaldehyde stain; $R_f = 0.42$). The reaction was then quenched by portionwise addition of 4-(*N,N*-dimethylamino)pyridine (DMAP) (1.02 g, 8.35 mmol). The reaction mixture was concentrated under reduced pressure by azeotropic distillation with toluene to afford a brown syrup (14.15 g, >90% purity by TLC), which was used for the next steps without further purification.

Methyl 5-O-*p*-toluoyl-2-deoxy-D-ribofuranoside (4) (Mixture of α and β Anomers). *p*-Toluoyl chloride (13 mL, 98.3 mmol) dissolved in anhydrous CH_2Cl_2 (20 mL) was added dropwise to a solution of crude 3 (prepared from 85.0 mmol of 2) in 1:3 anhydrous pyridine/ CH_2Cl_2 (80 mL) at 0 °C and stirred for 5 h. The reaction mixture was then diluted with CH_2Cl_2 (20 mL) and washed with cold H_2O (2×50 mL) and 5% aqueous CuSO_4 . The combined organic extracts were washed with saturated NaHCO_3 (2×50 mL), followed by 2 M HCl (2×50 mL), and then dried over Na_2SO_4 and concentrated under reduced pressure to afford a brown syrup (21.64 g). The crude product was purified by column chromatography on silica gel to yield compound 4 as a colorless oil (15.1 g, 56.8 mmol, 67% yield from 2). TLC analysis (hexanes:EtOAc 3:2; *p*-anisaldehyde stain; $R_f = 0.27$). $[\alpha]_D^{24} +67^\circ$ (c 0.5, CHCl_3). IR (thin film): 3467.5, 2949.5, 2917.7, 2828.0, 1716.7, 1609.7, 1447.6, 1268.2, 1181.4, 1077.2, 842.8, 758.8 cm^{-1} . ^1H NMR (400 MHz, CDCl_3) (major isomer): δ 7.92 (d, $J = 8.2$ Hz, 2H), 7.25 (d, $J = 8.1$ Hz, 4H), 5.16 (m, 1H), 4.32–4.41 (m, 3H), 4.26 (m, 1H), 3.42 (s, 3H), 3.01 (m, 1H), 2.43 (s, 3H), 2.20 (m, 1H), 2.08 (m, 1H). ^{13}C NMR (100 MHz, CDCl_3) (major isomer): δ 166.4, 143.9, 129.7, 129.1, 127.0, 105.5, 85.1, 73.1, 64.4, 54.9, 40.9, 21.6. HRMS (ESI+): m/z calcd for $\text{C}_{14}\text{H}_{18}\text{O}_5\text{Na}$ [$M + \text{Na}^+$], 289.1052; found, 289.1061.

Methyl 5-O-*p*-toluoyl-3-O-tosyl-2-deoxy-D-ribofuranoside (5). A solution of 4 (4.26 g, 16.0 mmol) and DMAP (183 mg, 1.5 mmol) in anhydrous CH_2Cl_2 (10 mL) was cooled to 0 °C under a N_2 atmosphere and then treated with Et_3N (5.00 mL, 35.8 mmol) and a solution of TsCl (4.011 g, 21.0 mmol) in CH_2Cl_2 (5 mL). The reaction mixture was allowed to warm to room temperature and monitored by TLC (hexanes:EtOAc 3:2; *p*-anisaldehyde stain; $R_f = 0.42$). After completion, the reaction mixture was quenched at 0 °C with 2 M HCl, neutralized with saturated aqueous NaHCO_3 and extracted with EtOAc. The combined organic extracts were washed with water (40 mL), brine (40 mL), dried over Na_2SO_4 , and evaporated. The crude product (6.40 g) was purified by column chromatography on silica gel to afford compound 5 (5.59 g, 13.3 mmol, 83%). $[\alpha]_D^{24} +75^\circ$ (c 0.5, CHCl_3). IR (thin film): 3027.6, 2949.5, 2929.3, 2836.7, 1922.2, 1716.7, 1606.8, 1450.5, 1363.7, 1276.8, 1172.7, 1106.1, 1056.9, 984.6, 920.9, 848.5, 810.9, 753.0, 666.2, 567.8, 550.5 cm^{-1} . ^1H NMR (400 MHz, CDCl_3): δ 7.85 (d, $J = 8.0$ Hz, 2H), 7.77 (d, $J = 8.3$ Hz, 2H), 7.27 (d, $J = 8.3$ Hz, 2H), 7.24 (d, $J = 8.0$ Hz, 2H), 5.06 (m, 1H), 4.93 (m, 1H), 4.38–4.44 (m, 2H), 4.20 (m, 1H), 3.36 (s, 3H), 2.42 (s, 3H), 2.39 (s, 3H), 2.34 (m, 1H), 2.13 (m, 1H). ^{13}C NMR (100 MHz, CDCl_3): δ 166.0, 145.1, 144.0, 133.4, 129.9, 129.7, 129.1, 127.9, 126.9, 104.5, 80.1, 79.4, 63.0, 55.1, 39.2, 21.7, 21.6. HRMS (ESI+): m/z calcd for $\text{C}_{21}\text{H}_{24}\text{O}_8\text{SNa}$ [$M + \text{Na}^+$], 443.1135; found, 443.1137.

5-O-*p*-toluoyl-3-O-tosyl-1,2-dideoxy-D-ribose (6). A solution of compound 5 (2.41 g, 5.73 mmol) in anhydrous CH_2Cl_2 (2 mL) was cooled to 0 °C and treated with Et_3SiH (2.90 mL, 18.2 mmol), followed by dropwise addition of $\text{BF}_3 \cdot \text{OEt}_2$ (2.00 mL, 16.2 mmol). The progress of the reaction was monitored by TLC (Hexanes:EtOAc 1:1; negative *p*-anisaldehyde stain; $R_f = 0.58$). After completion, the reaction mixture was neutralized with saturated aqueous NaHCO_3 (30 mL) and extracted with CH_2Cl_2 (3×10 mL). The combined organic extracts

were dried over Na_2SO_4 and evaporated. The crude product (2.31 g) was purified by column chromatography to afford compound 6 as a colorless oil (1.92 g, 4.92 mmol, 86%). $[\alpha]_D^{23} +30^\circ$ (c 1.0, CH_2Cl_2). IR (thin film): 2958.2, 2880.1, 1716.8, 1606.8, 1447.6, 1363.7, 1268.2, 1172.7, 1091.6, 1016.4, 955.6, 906.4, 816.7, 753.0, 669.1, 553.4 cm^{-1} . ^1H NMR (400 MHz, CDCl_3): δ 7.87 (d, $J = 8.3$ Hz, 2H), 7.77 (d, $J = 8.1$ Hz, 2H), 7.28 (d, $J = 8.2$ Hz, 2H), 7.24 (d, $J = 8.1$ Hz, 2H), 5.00 (m, 1H), 4.15–4.25 (m, 3H), 4.05 (m, 1H), 3.94 (m, 1H), 2.42 (s, 3H), 2.40 (s, 3H), 2.15–2.20 (m, 2H). ^{13}C NMR (100 MHz, CDCl_3): δ 166.1, 145.1, 144.0, 133.6, 130.0, 129.7, 129.2, 127.8, 126.9, 82.2, 81.6, 67.4, 63.6, 33.1, 21.7, 21.6. HRMS (ESI+): m/z calcd for $\text{C}_{20}\text{H}_{22}\text{O}_6\text{SNa}$ [$M + \text{Na}^+$], 413.1029; found, 413.1026.

[(2*R*,3*R*)-3-Hydroxytetrahydrofuran-2-yl]methyl-4-methylbenzoate (7). A mixture of compound 6 (1.08 g, 2.77 mmol) and NaNO_2 (0.96 g, 13.9 mmol) in DMSO (10 mL) was heated to 120 °C for 5 h. After completion as monitored by TLC analysis (hexanes:EtOAc 1:1; $R_f = 0.27$), the reaction was diluted with water. The aqueous layer was then extracted with CH_2Cl_2 (3×10 mL) and the combined organic extracts were washed with brine, dried over Na_2SO_4 , and evaporated. The crude product was purified by column chromatography to afford a mixture of 7 and the toluoyl migrate product 7' in a 1:1 ratio as determined by NMR analysis (0.41 g, 1.75 mmol, combined yield 63%). When the reaction time was reduced to 2 h at 120 °C, the product was obtained as 4.5:1 regioisomeric mixture of product 7:7' in 58% combined yield.

For characterization purposes, the 1:1 regioisomeric mixture from the experiment above (0.41 g, 1.75 mmol) was dissolved in anhydrous CH_2Cl_2 (3 mL), cooled to 0 °C, and then treated with Et_3N (1.25 mL, 8.96 mmol) and Bz_2O (0.3370 g, 1.49 mmol). The reaction mixture was concentrated to dryness and purified by column chromatography to yield 7 as colorless oil (0.18 g, 0.76 mmol, 28% overall yield from 6). This corresponds to a 89% recovery from the mixture. Mp: 65–67 °C; $[\alpha]_D^{23} -4^\circ$ (c 1, CH_2Cl_2). IR (ATR) 3420.7, 2986.2, 2950.6, 2923.3, 2896.0, 2868.7, 1704.4, 1611.5, 1444.7, 1269.8, 1174.2, 1100.4, 1021.1, 969.2, 834.5, 750.6, 693.2 cm^{-1} . ^1H NMR (400 MHz, CDCl_3): δ 7.94 (d, $J = 8.2$ Hz, 2H), 7.24 (d, $J = 8.0$ Hz, 2H), 4.77 (dd, $J = 7.1, 11.6$ Hz, 1H), 4.34–4.39 (m, 2H), 4.11 (m, 1H), 3.96 (ddd, $J = 3.3, 5.4, 7.1$ Hz, 1H), 3.89 (dt, $J = 3.8, 8.6$ Hz, 1H), 2.41 (s, 3H), 2.18 (m, 1H), 2.05 (m, 1H). ^{13}C NMR (100 MHz, CDCl_3): δ 167.2, 144.1, 129.8, 129.2, 126.9, 80.6, 71.5, 66.5, 62.6, 35.1, 21.7. HRMS (ESI+): m/z calcd for $\text{C}_{13}\text{H}_{16}\text{O}_4\text{Na}$ [$M + \text{Na}^+$], 259.0946; found, 259.0941.

[(2*R*,3*R*)-3-(Methylsulfonyloxy)tetrahydrofuran-2-yl]methyl-4-methylbenzoate (8). A solution of 7 (0.49 g, 2.07 mmol) in anhydrous CH_2Cl_2 (4 mL) was cooled to 0 °C and treated with DMAP (50 mg, 0.41 mmol), Et_3N (1.15 mL, 8.25 mmol), and MsCl (0.48 mL, 6.20 mmol). After 1 h, the reaction was complete as indicated by TLC (CH_2Cl_2 :acetone 4:1; $R_f = 0.76$) and was diluted with H_2O (10 mL) and EtOAc (10 mL). The aqueous layer was extracted with EtOAc (3×10 mL), and the combined organic extracts were washed with brine, dried over Na_2SO_4 , and concentrated under reduced pressure. The crude product (0.62 g) was purified by column chromatography to afford 8 as a white solid (0.58 g, 1.85 mmol, 90%). Mp: 102–104 °C. $[\alpha]_D^{23} -44^\circ$ (c 1.0, CH_2Cl_2). IR (KBr): 3424.1, 3024.8, 2964.0, 2940.8, 2891.6, 2862.7, 1722.5, 1609.6, 1349.2, 1271.1, 1178.5, 1109.0, 1010.6, 967.2, 897.7, 750.2, 524.4 cm^{-1} . ^1H NMR (400 MHz, CDCl_3): 7.94 (d, $J = 7.8$ Hz, 2H), 7.24 (d, $J = 8.1$ Hz, 2H), 5.38 (m, 1H), 4.53 (m, 2H), 4.25 (dt, $J = 4.0, 6.1$ Hz, 1H), 4.15 (m, 1H), 3.96 (dt, $J = 2.7, 8.5$ Hz, 1H), 3.01 (s, 3H), 2.41 (s, 3H), 2.39 (m, 2H). ^{13}C NMR (100 MHz, CDCl_3): δ 166.2, 144.0, 129.8, 129.2, 127.0, 79.9, 78.8, 66.5, 62.2, 38.5, 34.0, 21.7; HRMS (ESI+): m/z calcd for $\text{C}_{14}\text{H}_{18}\text{O}_6\text{SNa}$ [$M + \text{Na}^+$], 337.0722; found, 337.0716.

[(2*S*,3*S*)-3-Azidotetrahydrofuran-2-yl]methyl-4-methylbenzoate (9). A solution of 8 (0.14 g, 0.46 mmol) in DMSO (2 mL) was treated with NaN_3 (0.21 g, 3.15 mmol) and then heated at 90 °C for 2 h. After the reaction reached completion as monitored by TLC analysis (hexanes:EtOAc 3:2; $R_f = 0.62$), it was diluted with water (15 mL) and extracted with EtOAc (3×15 mL). The combined organic extracts were dried over Na_2SO_4 and concentrated to dryness to afford compound 9 as a colorless oil (113 mg, 0.43 mmol, 95%), which was subjected to the next step without further purification. $[\alpha]_D^{23} +64^\circ$ (c

The shorter C–O bond as well as the presence of lone pair electrons in atfcPNA resulted in reduced steric effects compared to acpcPNA. It may also provide an additional potential hydrogen-bonding site and repulsion with the negatively charged phosphate group in the DNA/RNA strand. These factors could potentially contribute to the subtle difference in nucleic acid binding properties of atfcPNA and acpcPNA. An NMR study of oligomers of the opposite enantiomer (2*R*,3*R*) of *trans*-atfc suggested torsional angle (θ) values in the range of 52–64° based on coupling constant ($^3J_{\text{H-H}}$) analyses.^{13a} These values are much smaller than the optimal values obtained from MD simulations of acpcPNA-DNA hybrids (99–102°).¹¹ The fact that atfcPNA can still form stable hybrids with DNA suggests that the tetrahydrofuran ring should be sufficiently flexible to adopt the required torsional angle. On the basis of NMR experiments, no evidence of intramolecular hydrogen bonding between the amide bonds and the oxygen atom of the atfc ring was observed in *trans*-atfc oligomers.^{13a} However, this does not rule out the possibilities of interstrand hydrogen bonding and/or additional interactions such as repulsion with the phosphate group of DNA or RNA. The absence of detailed three-dimensional structures of atfcPNA and its DNA/RNA hybrids precludes us from drawing a more definite conclusion.

Solubility and Nonspecific Binding Properties of atfcPNA versus acpcPNA. It was expected that the replacement of the cyclopentane ring in acpcPNA with the hydrophilic tetrahydrofuran ring in atfcPNA should result in a less hydrophobic PNA backbone. The more polar nature of atfcPNA is evidenced in the decreased retention time from reverse-phase HPLC analyses (T9: atfcPNA 30.6 min, acpcPNA 33.3 min; M10: atfcPNA 25.1 min, acpcPNA 30.0 min) (Figures S14, S19, S15, and S20 of the Supporting Information). Due to the small synthesis scale, it was not possible to directly compare the solubility because all lysine-modified PNA sequences are readily soluble in water and saturation could not be achieved. Acetylation of the C-terminal lysine modifier allowed the comparison of solubility between T9 acpcPNA and atfcPNA. Unfortunately, the solubility of T9 atfcPNA was only marginally improved ($425 \pm 21 \mu\text{M}$ or ca. 1.4 mg/mL) over T9 acpcPNA ($348 \pm 10 \mu\text{M}$ or ca. 1.1 mg/mL). This unexpected solubility behavior might be interpreted in terms of a combination between stable packing of the PNA molecules in the solid state and unfavorable entropy of dissolution as proposed to explaining the low aqueous solubility of cellulose²⁵ and cyclodextrins.²⁶

Similar to conventional PNA,¹⁴ nonspecific binding with hydrophobic materials was occasionally observed with acpcPNA. This becomes a serious problem when the PNA is modified with one or more hydrophobic dyes. To compare the nonspecific binding behaviors of atfcPNA and acpcPNA, *N*-terminal fluorescein-labeled atfcPNA and acpcPNA M10Flu were synthesized and compared. Both fluorescein-labeled PNAs form stable hybrids with their complementary DNA target with T_m of 45.7 and 46.7 °C, respectively. The nonspecific adsorption of the fluorescein-labeled PNAs by two different brands of polypropylene plastic tubes were investigated (Figure 2a). Fluorescence measurements of PNA solutions (50 nM) were recorded before and after repeated transfer between the plastic tube and the cuvette until there was no further change in the fluorescence intensity. It was observed that the acpcPNA signal decreased quite significantly (80.1 ± 3.6 and $53.3 \pm 2.3\%$ of the original value for brands 1 and 2, respectively), while the

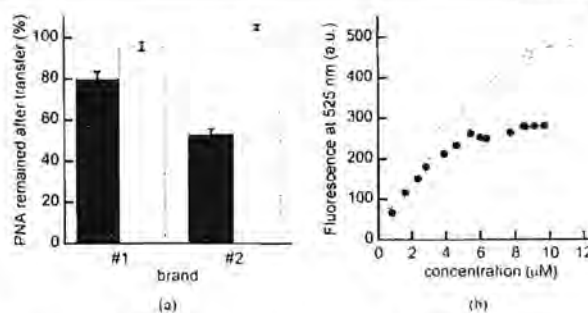


Figure 2. Comparison of fluorescein-labeled acpcPNA (gray) and atfcPNA (white) (M10Flu) for (a) nonspecific adsorption onto polypropylene microcentrifuge tube and (b) self-aggregation as demonstrated by fluorescence spectrophotometry.

atfcPNA signal does not change as much (95.8 ± 3.6 and $105.8 \pm 1.4\%$ of the original value for brands 1 and 2, respectively).

Reduction of the nonspecific self-aggregation of M10Flu atfcPNA was further demonstrated by fluorescence spectroscopy (Figure 2b). At low concentrations ($\leq 1 \mu\text{M}$), both PNAs showed comparable fluorescence. However, at higher concentrations, the fluorescence of M10Flu acpcPNA was significantly lower and reached a plateau at concentrations above $5 \mu\text{M}$ due to self-aggregation of the PNA, resulting in self-quenching of the fluorescein label. The same leveling effect was also observed in M10Flu atfcPNA but at twice as high a concentration. Accordingly, at $10 \mu\text{M}$, the fluorescence of M10Flu atfcPNA is 70% brighter than acpcPNA at the same concentration. Addition of complementary DNA to M10Flu acpcPNA and to atfcPNA restored the fluorescence of both PNAs to the same level due to repulsion between the negatively charged PNA-DNA hybrids, which separated the fluorescein dyes from each other. These results support the beneficial effects of the hydrophilic ATFC spacer in reducing nonspecific interactions of pyrrolidiny PNA, which should further expand the applications of these PNAs.

CONCLUSION

In conclusion, we report an efficient synthesis of Fmoc-protected tetrahydrofuran cyclic- β -amino acid from 2-deoxy-D-ribose. The cyclic amino acid was successfully incorporated as a building block for synthesizing a new tetrahydrofuran-containing pyrrolidiny PNA (atfcPNA). This novel atfcPNA retained the excellent DNA binding affinity and specificity of pyrrolidiny PNA, with improved selectivity toward hybridization to DNA over RNA, a fact that is interesting in its own right and should deserve further investigation in the context of development of a selective DNA binding agent. In addition, the hydrophilic tetrahydrofuran backbone provided beneficial effects in reducing nonspecific interactions and self-aggregation generally observed in acpcPNA and most other PNA systems.

EXPERIMENTAL SECTION

General Methods. All chemicals were purchased from commercial sources and were used as received without further purification. Solvents were dried over CaH_2 or 4 Å molecular sieves and then freshly distilled under argon prior to use. IR spectra were acquired on a FT-IR spectrometer using either attenuated total reflection (ATR) or transmission module. Optical rotations ($[\alpha]_D$) were measured at the specified temperature using sodium light (D line, 589.3 nm); concentrations (c) are reported as g/100 mL. ^1H and ^{13}C NMR spectra were recorded at 400 and 100 MHz, respectively. High-

1.6, CH₂Cl₂). IR (thin film): 2952.4, 2872.4, 2098.7, 1716.7, 1606.7, 1271.1, 1172.7, 1103.2, 750.2 cm⁻¹. ¹H NMR (400 MHz, CDCl₃): δ 7.93 (d, *J* = 8.0 Hz, 2H), 7.25 (d, *J* = 8.0 Hz, 2H), 4.38 (m, 2H), 4.03–4.12 (m, 3H), 3.95 (m, 1H), 2.42 (s, 3H), 2.29 (m, 1H), 2.08 (m, 1H). ¹³C NMR (100 MHz, CDCl₃): δ 166.3, 144.0, 129.7, 129.2, 127.0, 81.5, 67.4, 64.4, 62.9, 32.2, 21.7. HRMS (ESI⁺): *m/z* calcd for C₁₁H₁₃N₃O₃Na [M + Na⁺], 284.1006; found, 284.1003.

(2S,3S)-3-(tert-Butoxycarbonylamino)tetrahydrofuran-2-yl-methyl 4-methylbenzoate (10). A solution of 9 (0.47 g, 1.8 mmol) in MeOH (5 mL) was treated with Boc₂O (1.03 g, 4.72 mmol) and Pd/C (20% w/w, 74.2 mg). The reaction flask was flushed with H₂ gas and a H₂ balloon was attached through a rubber septum. The reaction was monitored by TLC analysis (hexanes:EtOAc 3:2; ninhydrin stain; R_f = 0.46) until it reached completion. It was then filtered through Celite, concentrated to dryness, and the residue was washed with hexanes to afford 10 as a white solid (0.43 g, 1.28 mmol, 71%). Mp: 108–110 °C. [α]_D²³ +28° (c 1.0, CH₂Cl₂). IR (KBr): 3348.9, 2975.6, 2937.9, 2868.5, 1724.8, 1682.0, 1609.0, 1528.6, 1432.5, 1369.5, 1271.1, 1172.7, 1108.3, 1077.2, 1021.5, 1001.2, 882.6, 884.9, 753.1, 607.6 cm⁻¹. ¹H NMR (400 MHz, CDCl₃): δ 7.93 (d, *J* = 8.2 Hz, 2H), 7.22 (d, *J* = 8.1 Hz, 2H), 4.71 (br s, 1H), 4.49 (dd, *J* = 3.5, 11.7 Hz, 1H), 4.34 (dd, *J* = 5.9, 11.8 Hz, 1H), 4.16 (m, 1H), 3.92–4.06 (m, 3H), 2.40 (s, 3H), 2.34 (m, 1H), 1.83 (dt, *J* = 5.7, 12.8 Hz, 1H), 1.44 (s, 9H). ¹³C NMR (100 MHz, CDCl₃): δ 166.5, 155.5, 143.7, 129.8, 129.1, 127.2, 82.9, 79.9, 67.2, 65.1, 53.2, 33.3, 28.4, 21.6. HRMS (ESI⁺): *m/z* calcd for C₁₈H₂₅NO₅Na [M + Na⁺], 358.1625; found, 358.1635.

tert-Butyl (2S,3S)-2-(Hydroxymethyl)tetrahydrofuran-3-ylcarbamate (11). A mixture of 10 (0.39 g, 1.16 mmol) and LiOH·H₂O (0.13 g, 3.1 mmol) was dissolved in 1:1 THF:H₂O (4 mL) and stirred at room temperature overnight. The completion of the reaction was confirmed by TLC analysis (EtOAc:hexanes 4:1; ninhydrin stain; R_f = 0.33), and then the organic solvent was removed by rotary evaporation, and the aqueous residue was extracted with CH₂Cl₂ (3 × 10 mL). The combined organic phases were dried over anhydrous Na₂SO₄ and evaporated to give compound 11 as a white solid (0.23 g, 1.06 mmol, 91%). Mp: 85–87 °C. [α]_D²³ –11° (c 1.0, CH₂Cl₂). ¹H NMR (400 MHz, CDCl₃): δ 4.47 (s, 1H), 3.85–4.00 (m, 3H), 3.65–3.69 (m, 3H), 2.87 (s, 1H), 2.29 (m, 1H), 1.79 (m, 1H), 1.44 (s, 9H). ¹³C NMR (100 MHz, CDCl₃): δ 155.9, 85.1, 80.2, 66.7, 63.1, 52.9, 33.1, 28.3. IR (ATR): 3346.8, 2987.4, 2964.1, 2908.1, 2849.5, 1676.0, 1522.0, 1363.3, 1300.3, 1239.6, 1160.3, 1097.3, 1073.9, 1015.6, 866.3, 621.2 cm⁻¹. HRMS (ESI⁺): *m/z* calcd for C₁₀H₁₉NO₄Na [M + Na⁺], 240.1206; found, 240.1207.

(2S,3S)-3-(tert-Butoxycarbonylamino)tetrahydrofuran-2-carboxylic acid (12). To a solution of 11 (0.27 g, 1.24 mmol) in 1:1 acetonitrile:H₂O was added TEMPO (95 mg, 0.61 mmol) and bis(acetoxy)iodobenzene (BAIB) (1.13 g, 3.5 mmol). The reaction mixture was stirred overnight at room temperature. The completion of the reaction was monitored by TLC analysis (EtOAc; ninhydrin stain; R_f = 0.17). The pH of the resulting solution was adjusted 8–9 by addition of solid NaHCO₃ and extracted with EtOAc. The collected aqueous phase was acidified to pH 2 with solid NaHSO₄ followed by extraction with EtOAc. The combined organic phases were evaporated to dryness to give 12 as a colorless oil (0.27 g, 1.2 mmol, 94%). [α]_D²² +49° (c 1.5, DMSO). IR (thin film): 3328.6, 2972.7, 1710.9, 1528.6, 1363.7, 1279.7, 1161.1, 1100.3, 1016.4 cm⁻¹. ¹H NMR (400 MHz, DMSO-*d*₆): δ 12.60 (br s, 1H), 7.27 (d, *J* = 6.9 Hz, 1H), 4.10 (m, 1H), 4.04 (m, 1H), 3.83–3.92 (m, 2H), 2.06 (m, 1H), 1.76 (dt, *J* = 6.3, 12.0 Hz, 1H), 1.38 (s, 9H). ¹³C NMR (100 MHz, DMSO-*d*₆): δ 172.7, 154.9, 81.0, 77.9, 67.1, 54.9, 31.6, 28.1. HRMS (ESI⁺): *m/z* calcd for C₁₀H₁₇NO₅Na [M + Na⁺], 254.0999; found, 254.0992.

(2S,3S)-3-[[[9H-Fluoren-9-yl)methoxy]carbonylamino]tetrahydrofuran-2-carboxylic acid (13). Compound 12 (0.21 g, 0.91 mmol) was dissolved in 1:1 TFA:CH₂Cl₂ (6 mL) and stirred at room temperature for 30 min. The solvent was removed by flushing with N₂. The crude amino acid was dissolved in H₂O (4 mL), and the pH of the solution was adjusted to 8–9 by the addition of solid NaHCO₃. Next, FmocOSu (0.31 g, 0.92 mmol) dissolved in 0.5 mL of DMSO was added in small portions along with more NaHCO₃ to maintain the pH around 8–9. To this mixture, MeCN was added to make a

homogeneous solution. After stirring overnight, the solution was diluted with water and extracted with diethyl ether. The aqueous phase was acidified to pH 2 with concentrated HCl to give a white suspension. After filtration, the precipitate was air-dried to afford compound 13 as a white solid (0.28 g, 0.79 mmol, 87%). Mp: 166–168 °C. [α]_D²³ +42° (c 1.0, DMSO). IR (KBr): 3308.4, 3062.4, 2946.6, 2362.1, 2341.8, 1722.5, 1690.7, 1540.2, 1447.6, 1259.6, 1099.4, 732.8 cm⁻¹. ¹H NMR (400 MHz, DMSO-*d*₆): δ 12.75 (br s, 1H), 7.89 (d, *J* = 7.4 Hz, 2H), 7.74 (d, *J* = 7.5 Hz, 1H), 7.69 (m, 2H), 7.42 (t, *J* = 7.0 Hz, 2H), 7.34 (t, *J* = 7.0 Hz, 2H), 4.33 (d, *J* = 6.4 Hz, 2H), 4.22 (t, *J* = 6.9 Hz, 1H), 4.17 (m, 1H), 4.09 (m, 1H), 3.90 (t, *J* = 6.8 Hz, 2H), 2.09 (m, 1H), 1.79 (m, 1H). ¹³C NMR (100 MHz, DMSO-*d*₆): δ 172.8, 155.5, 143.7, 140.6, 127.5, 127.0, 125.0, 120.0, 81.1, 67.0, 65.3, 55.3, 46.6, 31.8. HRMS (ESI⁺): *m/z* calcd for C₂₀H₁₉NO₅Na [M + Na⁺], 376.1155; found, 376.1180.

Pentafluorophenyl (2S,3S)-3-[[[9H-fluoren-9-yl)methoxy]carbonylamino]tetrahydrofuran-2-carboxylate (1). A suspension of compound 13 (0.22 g, 0.62 mmol) in CH₂Cl₂ (2 mL) was treated with DIEA (600 μL, 3.45 mmol) and PfpOTf (600 μL, 3.39 mmol) in three portions. The completion of the reaction was monitored by TLC analysis (hexanes:EtOAc 1:1; R_f = 0.50). The reaction mixture was diluted with CH₂Cl₂ (10 mL), washed with 1 M HCl and saturated aqueous NaHCO₃ and dried over anhydrous Na₂SO₄. After removal of the solvent, the resulting pink oil was sonicated with hexanes to give a white suspension which was collected by filtration to give 1 as a white solid (0.207 g, 0.40 mmol, 65%). Mp: 123–125 °C. [α]_D²³ +57° (c 1.0, CH₂Cl₂). IR (ATR): 3309.4, 1799.7, 1687.6, 1550.0, 1519.6, 1291.0, 1234.9, 1066.9, 1031.9, 994.6, 761.2, 735.6, 665.6. ¹H NMR (400 MHz, CDCl₃): δ 7.77 (d, *J* = 7.4 Hz, 2H), 7.58 (d, *J* = 7.2 Hz, 2H), 7.41 (t, *J* = 6.9 Hz, 2H), 7.31 (t, *J* = 7.1 Hz, 2H), 5.06 (d, *J* = 5.3, 1H), 4.70 (m, 1H), 4.62 (m, 1H), 4.50 (m, 2H), 4.19 (m, 2H), 4.12 (m, 1H), 2.36 (m, 1H), 1.98 (m, 1H). ¹³C NMR (100 MHz, CDCl₃): δ 167.3, 155.5, 143.7, 141.4, 127.8, 127.0, 124.9, 120.0, 81.7, 68.3, 66.9, 56.2, 47.3, 31.9. ¹⁹F NMR (376 MHz, CDCl₃): δ –161.8 (t, *J* = 20.2 Hz), –157.1 (t, *J* = 19.9 Hz), –152.4 (d, *J* = 18.0 Hz). HRMS (ESI⁺) *m/z* calcd for C₂₆H₁₈F₅NO₄K [M + K⁺], 542.0788; found, 542.0795.

Synthesis of atfcPNA. All atfcPNA were manually synthesized at 1.5 μmol scale on a Tentagel S-RAM resin (0.24 mmol/g loading) from the four Fmoc-protected pyrrolidiny PNA monomers (A^{Bt}, T, C^{Bt}, and G^{Bt}) and pentafluorophenyl-activated ATFC spacer 1 following the previously published protocol for acpcPNA synthesis.^{10b,d} The nucleobase protecting groups (Bz, Ibu) were removed by treating the resin with 1:1 aqueous ammonia:dioxane at 60 °C overnight. The crude PNA was obtained by TFA cleavage and purified by reverse-phase HPLC (C18 column, 0.1% TFA in water–methanol gradient).

Fluorescence Spectroscopy to Compare Nonspecific Interactions and Self-Aggregation of acpcPNA and atfcPNA. (a) Nonspecific adsorption of fluorescein-modified acpcPNA and atfcPNA M10Flu were compared by fluorescence measurements. The PNA samples were prepared at 0.05 μM in 10 mM sodium phosphate buffer pH 7.0 (1000 μL) at 25 °C. The solution was transferred back and forth between the cuvette and a 1.5 mL polypropylene microcentrifuge tube, and the fluorescence spectra were recorded after each transfer until no further change was observed. The average fluorescence at 520 nm and standard deviation were calculated from the last three measurements after the signal was constant. The excitation wavelength was 480 nm, slit widths 5 nm, and the PMT voltage was set to high. (b) Self-aggregation of fluorescein-modified acpcPNA and atfcPNA M10Flu were compared by fluorescence measurements. The fluorescence data was plotted against concentration in the range of 1 to 10 μM or until a plateau was reached. The excitation wavelength was 480 nm, slit widths 5 nm, and the PMT voltage was set to 500.

■ ASSOCIATED CONTENT

Supporting Information

¹H and ¹³C NMR spectra for numbered compounds, HPLC chromatogram, and MALDI-TOF mass spectra of PNA, as well as additional spectroscopic data. The Supporting Information is

available free of charge on the ACS Publications website at DOI: 10.1021/acs.joc.5b00890.

AUTHOR INFORMATION

Corresponding Author

*E-mail: vtirayut@chula.ac.th.

Notes

The authors declare no competing financial interest.

ACKNOWLEDGMENTS

Financial support of this work provided by the Thailand Research Fund (DPGS780002) and the Thai government stimulus package 2 (TKK2555, SP2) under the Project for Establishment of Comprehensive Center for Innovative Food, Health Products and Agriculture is gratefully acknowledged. We thank Haruthai Pansuwan and Nattawut Yotapan for partial data collection.

REFERENCES

- (1) (a) Gellman, S. H. *Acc. Chem. Res.* 1998, 31, 173–180. (b) Hill, D. J.; Mio, M. J.; Prince, R. B.; Hughes, T. S.; Moore, J. S. *Chem. Rev.* 2001, 101, 3893–4011.
- (2) (a) Fülöp, F. *Chem. Rev.* 2001, 101, 2181–2204. (b) Fülöp, F.; Martinek, T. A.; Tóth, G. K. *Chem. Soc. Rev.* 2006, 35, 323–334.
- (3) (a) Cheng, R. P.; Gellman, S. H.; DeGrado, W. F. *Chem. Rev.* 2001, 101, 3219–3232. (b) Vasudev, P. G.; Chatterjee, S.; Shamala, N.; Balaram, P. *Chem. Rev.* 2011, 111, 657–687.
- (4) (a) Appella, D. H.; Christianson, L. A.; Klein, D. A.; Powell, D. R.; Huang, X.; Barchi, J. J., Jr; Gellman, S. H. *Nature* 1997, 387, 381–384. (b) Appella, D. H.; Christianson, L. A.; Karle, I. L.; Powell, D. R.; Gellman, S. H. *J. Am. Chem. Soc.* 1999, 121, 6206–6212. (c) Appella, D. H.; Christianson, L. A.; Klein, D. A.; Richards, M. R.; Powell, D. R.; Gellman, S. H. *J. Am. Chem. Soc.* 1999, 121, 7574–7581. (d) Wang, X.; Espinosa, J. F.; Gellman, S. H. *J. Am. Chem. Soc.* 2000, 122, 4821–4822. (e) LePlac, P. R.; Fisk, J. D.; Porter, E. A.; Weisblum, B.; Gellman, S. H. *J. Am. Chem. Soc.* 2002, 124, 6820–6821. (f) Izquierdo, S.; Rúa, F.; Sbai, A.; Parella, T.; Álvarez-Larena, Á.; Branchadell, V.; Ortuño, R. M. *J. Org. Chem.* 2005, 70, 7963–7971. (g) Fernandes, C.; Faure, S.; Pereira, E.; Théry, V.; Declercq, V.; Guillot, R.; Aitken, D. J. *Org. Lett.* 2010, 12, 3606–3609.
- (5) (a) Chakraborty, T. K.; Srinivasu, P.; Tapadar, S.; Mohan, B. K. *Glycoconjugate J.* 2005, 22, 83–93. (b) Risseuw, M. D. P.; Overhand, M.; Fleet, G. W. J.; Simone, M. I. *Tetrahedron: Asymmetry* 2007, 18, 2001–2010. (c) Risseuw, M. D. P.; Overhand, M.; Fleet, G. W. J.; Simone, M. I. *Amino Acids* 2013, 45, 613–689. (d) Rjabovs, V.; Turks, M. *Tetrahedron* 2013, 69, 10693–10710.
- (6) (a) Clandige, T. D. W.; Goodman, J. M.; Moreno, A.; Angus, D.; Barker, S. F.; Taillefumier, C.; Watterson, M. P.; Fleet, G. W. J. *Tetrahedron Lett.* 2001, 42, 4251–4255. (b) Chandrasekhar, S.; Reddy, M. S.; Jagadeesh, B.; Prabhakar, A.; Rao, M. H. V. R.; Jagannadh, B. *J. Am. Chem. Soc.* 2004, 126, 13586–13587. (c) Sirwardena, A.; Pulkuri, K. K.; Kandiyal, P. S.; Roy, S.; Bande, O.; Ghosh, S.; Fernández, J. M. G.; Martin, F. A.; Ghigo, J.-M.; Beloin, C.; Ito, K.; Woods, R. J.; Ampapathi, R. S.; Chakraborty, T. K. *Angew. Chem., Int. Ed.* 2013, 52, 10221–10226.
- (7) (a) Threlfall, R.; Davies, A.; Howarth, N.; Cosstick, R. *Nucleosides, Nucleotides Nucleic Acids* 2006, 26, 611–614. (b) Threlfall, R.; Davies, A.; Howarth, N. M.; Fisher, J.; Cosstick, R. *Chem. Commun.* 2008, 585–587. (c) Chandrasekhar, S.; Reddy, G. P. K.; Kiran, M. U.; Nagesh, Ch.; Jagadeesh, B. *Tetrahedron Lett.* 2008, 49, 2969–2973. (d) Gogoi, K.; Kumar, V. A. *Chem. Commun.* 2008, 706–708. (e) Bagmare, S.; D'Costa, M.; Kumar, V. A. *Chem. Commun.* 2009, 6646–6648. (f) Bagmare, S.; Varada, M.; Banerjee, A.; Kumar, V. A. *Tetrahedron* 2013, 69, 1210–1216.
- (8) Merino, P.; Matute, R. Chemical Synthesis of Conformational Constrained PNA Monomers. In *Chemical Synthesis of Nucleoside Analogues*; Merino, P., Ed.; Wiley-VCH: New Jersey, 2013; pp 847–880.
- (9) (a) Egholm, M.; Buchardt, O.; Christensen, L.; Behrens, C.; Freier, S. M.; Driver, D. A.; Berg, R. H.; Kim, S. K.; Norden, B.; Nielsen, P. E. *Nature* 1993, 365, 566–568. (b) Nielsen, P. E. *Chem. Biodiversity* 2010, 7, 786–804.
- (10) (a) Vilaivan, T.; Lowe, G. J. *Am. Chem. Soc.* 2002, 124, 9326–9327. (b) Vilaivan, T.; Srisuwannaket, C. *Org. Lett.* 2006, 8, 1897–1900. (c) Reenabthue, N.; Boonlua, C.; Vilaivan, C.; Vilaivan, T.; Suparpprom, C. *Bioorg. Med. Chem. Lett.* 2011, 21, 6465–6469. (d) Vilaivan, C.; Srisuwannaket, C.; Ananthanawat, C.; Suparpprom, C.; Kawakami, J.; Yamaguchi, Y.; Tanaka, Y.; Vilaivan, T. *Artif. DNA: PNA & XNA* 2011, 2, 50–59. (e) Mansawat, W.; Vilaivan, C.; Balázs, Á.; Aitken, D. J.; Vilaivan, T. *Org. Lett.* 2012, 14, 1440–1443.
- (11) Vilaivan, T. *Acc. Chem. Res.* 2015, 48, 1645–1656.
- (12) (a) Boontha, B.; Nakkuntod, J.; Hirankarn, N.; Chaumpluk, P.; Vilaivan, T. *Anal. Chem.* 2008, 80, 8178–8186. (b) Boonlua, C.; Vilaivan, C.; Wagenknecht, H.-A.; Vilaivan, T. *Chem.—Asian J.* 2011, 6, 3251–3259. (c) Laopa, P. S.; Vilaivan, T.; Hoven, V. P. *Analyst* 2013, 138, 269–277. (d) Jampasa, S.; Wonsawat, W.; Rodthongkum, N.; Siangproh, W.; Yanatsanejit, P.; Vilaivan, T.; Chailapakul, O. *Biosens. Bioelectron.* 2014, 54, 428–434.
- (13) (a) Pandey, S. K.; Jogdand, G. F.; Oliveira, J. C. A.; Mata, R. A.; Rajamohanam, P. R.; Ramana, C. V. *Chem.—Eur. J.* 2011, 17, 12946–12954. (b) Giri, A. G.; Jogdand, G. F.; Rajamohanam, P. R.; Pandey, S. K.; Ramana, C. V. *Eur. J. Org. Chem.* 2012, 2656–2663.
- (14) Sahu, B.; Sacui, I.; Rapireddy, S.; Zanotti, K. J.; Bahal, R.; Armitage, B. A.; Ly, D. H. *J. Org. Chem.* 2011, 76, 5614–5627.
- (15) Larsen, C. H.; Ridgway, B. H.; Shaw, J. T.; Woerpel, K. A. *J. Am. Chem. Soc.* 1999, 121, 12208–12209.
- (16) Rabi, J. A. U.S. patent application 2004/0266996 A1, 2004.
- (17) (a) Pedersen, C.; Diehl, H. W.; Fletcher, H. G., Jr. *J. Am. Chem. Soc.* 1960, 82, 3425–3428. (b) Chenault, H. K.; Mandes, R. F. *Tetrahedron* 1997, 53, 11033–11038. (c) Adamo, M. F. A.; Adlington, R. M.; Baldwin, J. E.; Day, A. L. *Tetrahedron* 2004, 60, 841–849.
- (18) Takeshita, M.; Chang, C. N.; Johnson, F.; Will, S.; Grollman, A. P. *J. Biol. Chem.* 1987, 262, 10171–10179.
- (19) Chong, Y.; Gumina, G.; Mathew, J. S.; Schinazi, R. F.; Chu, C. K. *J. Med. Chem.* 2003, 46, 3245–3256.
- (20) (a) Dong, H.; Pei, Z.; Ramström, O. *J. Org. Chem.* 2006, 71, 3306–3309. (b) Kornblum, N.; Blackwood, R. K.; Mooberry, D. D. *J. Am. Chem. Soc.* 1956, 78, 1501–1504. (c) Albert, R.; Dax, K.; Link, R. W.; Stütz, A. E. *Carbohydr. Res.* 1983, 118, C5–C6. (d) McGeary, R. P.; Amini, S. R.; Tang, V. W. S.; Toth, I. *J. Org. Chem.* 2004, 69, 2727–2730. (e) Dong, H.; Rahm, M.; Thota, N.; Deng, L.; Brinck, T.; Ramström, O. *Org. Biomol. Chem.* 2013, 11, 648–653. (f) Ren, B.; Dong, H.; Ramström, O. *Chem.—Asian J.* 2014, 9, 1298–1304.
- (21) (a) Guo, X.; Liu, C.; Zheng, L.; Jiang, S.; Shen, J. *Synlett* 2010, 1959–1962. (b) Swamy, K. C. K.; Kumar, N. N. B.; Balaraman, E.; Kumar, K. V. P. *Chem. Rev.* 2009, 109, 2551–2651.
- (22) (a) Tojo, G.; Fernandez, M. TEMPO-mediated Oxidations. In *Oxidation of Primary Alcohols to Carboxylic Acids: A Guide to Current Common Practices*; Tojo, G., Ed.; Springer: New York, 2007; pp 79–103. (b) Dettwiler, J. E.; Lubell, W. D. *J. Org. Chem.* 2003, 68, 177–179. (c) Epp, J. B.; Widlanski, T. S. *J. Org. Chem.* 1999, 64, 293–295.
- (23) (a) Johnson, W. C. CD of Nucleic Acids. In *Circular Dichroism: Principles and Applications*; Berova, N.; Nakanishi, K.; Woody, R. W., Eds.; Wiley-VCH: New York, 2000; pp 703–718. (b) Kang, H.; Chou, P.-J.; Johnson, W. C., Jr; Weller, D.; Huang, S.-B.; Summerton, J. E. *Biopolymers* 1992, 32, 1351–1363.
- (24) Vorlíčková, M.; Kejniovská, I.; Bednářová, K.; Renčíuk, D.; Kypr, J. *Chirality* 2012, 24, 691–698.
- (25) Bergensträhle, M.; Wohler, J.; Himmel, M. E.; Brady, J. W. *Carbohydr. Res.* 2010, 345, 2060–2066.
- (26) Jozwiakowski, M. J.; Connors, K. A. *Carbohydr. Res.* 1985, 143, 51–59.



Cite this: *Org. Biomol. Chem.*, 2015, **13**, 9223

Strand displacement and duplex invasion into double-stranded DNA by pyrrolidinyl peptide nucleic acids†

Peggy R. Bohländer,^a Tirayut Vitaivan^{a,b} and Hans-Achim Wagenknecht^{a*}

The so-called acpcPNA system bears a peptide backbone consisting of 4'-substituted proline units with (2'R,4'R) configuration in an alternating combination with (2S)-amino-cyclopentane-(1S)-carboxylic acids. acpcPNA forms exceptionally stable hybrids with complementary DNA. We demonstrate herein (i) strand displacements by single-stranded DNA from acpcPNA-DNA hybrids, and by acpcPNA strands from DNA duplexes, and (ii) strand invasions by acpcPNA into double-stranded DNA. These processes were studied *in vitro* using synthetic oligonucleotides and by means of our concept of wavelength-shifting fluorescent nucleic acid probes, including fluorescence lifetime measurements that allow quantifying energy transfer efficiencies. The strand displacements of preannealed 14mer acpcPNA-7mer DNA hybrids consecutively by 10mer and 14mer DNA strands occur with rather slow kinetics but yield high fluorescence color ratios (blue : yellow or blue : red), fluorescence intensity enhancements, and energy transfer efficiencies. Furthermore, 11mer acpcPNA strands are able to invade into 30mer double-stranded DNA, remarkably with quantitative efficiency in all studied cases. These processes can also be quantified by means of fluorescence. This remarkable behavior corroborates the extraordinary versatile properties of acpcPNA. In contrast to conventional PNA systems which require 3 or more equivalents PNA, only 1.5 equivalents acpcPNA are sufficient to get efficient double duplex invasion. Invasions also take place even in the presence of 250 mM NaCl which represents an ionic strength nearly twice as high as the physiological ion concentration. These remarkable results corroborate the extraordinary properties of acpcPNA, and thus acpcPNA represents an eligible tool for biological analytics and antigene applications.

Received 22nd June 2015

Accepted 21st July 2015

DOI: 10.1039/c5ob01273b

www.rsc.org/obc

Introduction

Peptide nucleic acid (PNA) represents a very important nucleic acid analog and chemical-biological tool based on its important features like affinity, sequence selectivity and stability against degradation by nucleases and proteases.¹ Especially the uncharged pseudopeptide backbone makes PNA an attractive scaffold for diagnostic applications. PNA with *N*-(2-aminoethyl)glycine backbone (aegPNA) is able to form complexes with double-stranded DNA either by binding from outside forming triplexes, or by duplex, double-duplex or triplex invasion.¹⁻⁴ The attempt to increase affinity and, more importantly, sequence selectivity of PNA by incorporation of cyclic

derivatives in the peptide backbone failed in many cases since the nucleic acid hybridization properties are deteriorated.^{3,6} Among several of those PNA architectures reported to date, and especially among those with cyclic structures as part of the backbone,⁷⁻⁹ the so-called acpcPNA system (Fig. 1) exhibits significant features. The peptide backbone consists of 4'-substituted proline units with (2'R,4'R) configuration in an alternating combination with (2S)-amino-cyclopentane-(1S)-carboxylic acids. As a result of this structural design, acpcPNA forms stable hybrids with complementary DNA but significantly less stable hybrids with complementary RNA.¹⁰⁻¹³ The

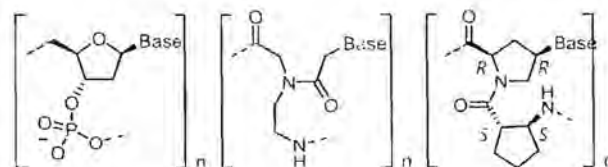


Fig. 1 Monomeric unit of DNA (left), aegPNA (middle) and acpcPNA (right) in comparison.

^aInstitute of Organic Chemistry, Karlsruhe Institute of Technology (KIT), Fritz-Haber-Weg 6, 76131 Karlsruhe, Germany. E-mail: Wagenknecht@kit.edu; Fax: +49-721-608-44825; Tel: +49-721-608-47486

^bOrganic Synthesis Research Unit, Department of Chemistry, Faculty of Science, Chulalongkorn University Phayathai Road, Patumwan, Bangkok 10330, Thailand. E-mail: vitayut@chula.ac.th; Fax: +66-2-2187598; Tel: +66-2-2187627

† Electronic supplementary information (ESI) available. See DOI: 10.1039/c5ob01273b

recognition and binding to DNA shows high sequence selectivity and does not tolerate single base mismatches. The sequence selectivity can be visualized by fluorescent dyes such as pyrene,^{14,15} thiazole orange¹⁶ and Nile red,¹⁷ that were synthetically incorporated into acpcPNA. Most importantly, self-paired hybrids are not formed by acpcPNA.¹¹ This feature stands in contrast to many other PNA scaffolds that bind to themselves equally or even better than to naturally occurring nucleic acids.⁴

Base and/or PNA backbone modifications are traditionally required to destabilize PNA–PNA duplexes in order to allow efficient double duplex invasion of DNA.^{18,19} Alternatively, PNA modifications like carcinogenic acridine moieties or nucleobase substitutions of cytosine (G-clamp) also promote invasion into mixed sequence B-DNA.^{20–23} To prevent extensive or biologically harmful modifications, a chiral derivative of PNA called γ PNA that exhibits even higher DNA affinity than normal PNA with extended strand length was employed. However, 20 equivalents of γ PNA and incubating times of 8 hours are necessary to accomplish quantitative invasion and complex formation with double-stranded DNA.²⁴ Moreover, limitations for applications *in vivo* still remain due to the high affinity of γ PNA to both DNA and RNA. In order to demonstrate the advantages of acpcPNA in this regard we report herein (i) strand displacements by single-stranded DNA from acpcPNA–DNA hybrids, and by acpcPNA strands from DNA duplexes, and (ii) strand invasions by acpcPNA strands into double-stranded DNA with high efficiency. These processes have high biological significance; however, we studied them *in vitro* with model PNA strands by means of fluorescence color changes as well as fluorescent intensity enhancements using our concept of wavelength-shifting nucleic acid probes (“DNA traffic lights”).²⁵

Results and discussion

Strand displacements

DNA strand displacements are biologically relevant and enzymatically driven processes inside living cells.^{26–29} Furthermore, these processes play a crucial role in DNA nanotechnology.³⁰ Consecutive annealing and strand displacement steps represent the methodological basis to dynamically control the formation of highly ordered and self-assembled DNA nanoarchitectures, such as DNA switches, DNA tweezers,^{31–34} DNA-based logic gates,^{34–38} DNA walkers^{39–42} and others. In order to readout the strand displacement dynamics with acpcPNA not only by conventional fluorescence intensity changes at a single emission wavelength, we followed our concept of wavelength-shifting nucleic acid probes.²⁵ Five years ago, we introduced this concept that is based on energy transfer between thiazole orange and thiazole red as fluorescent DNA base substitutions and applied it for molecular beacons.^{25,13} Moreover, we showed that this concept works also for pairs of fluorescent dyes attached to the 2'-positions in

two different DNA strands and yields even better emission color contrasts as readout.⁴⁴

In order to apply such fluorescence color changes to directly report the dynamics of strand displacements *in vitro* we synthesized the 14mers PNA1 and PNA2 that carry the blue emitting dye 1 in the middle of the sequence (Fig. 2). These acpcPNA modifications were introduced by post-synthetic copper(i)-catalyzed cycloaddition between the precursor of dye 1 bearing an azide group and the synthesized precursors of PNA1 and PNA2 that carry an alkyne functionality. The only difference between the two PNA strands is the position of dye 1 as modification of the aminopyrrolidinecarboxylic acid spacers either on the carboxy or on the amino side of the central thymine unit in the sequence. All synthesized PNA strands bear five lysine residues at the C-terminus to enhance solubility. Five DNA counterparts of different lengths were synthesized. The shortest one, 7mer DNA1, was not labelled. The 10mers DNA2 and DNA4 were labelled by the yellow emitting dye 2 attached to the 2'-position of uridine next to the central adenosine unit (either on the 5' or 3' side). The longest

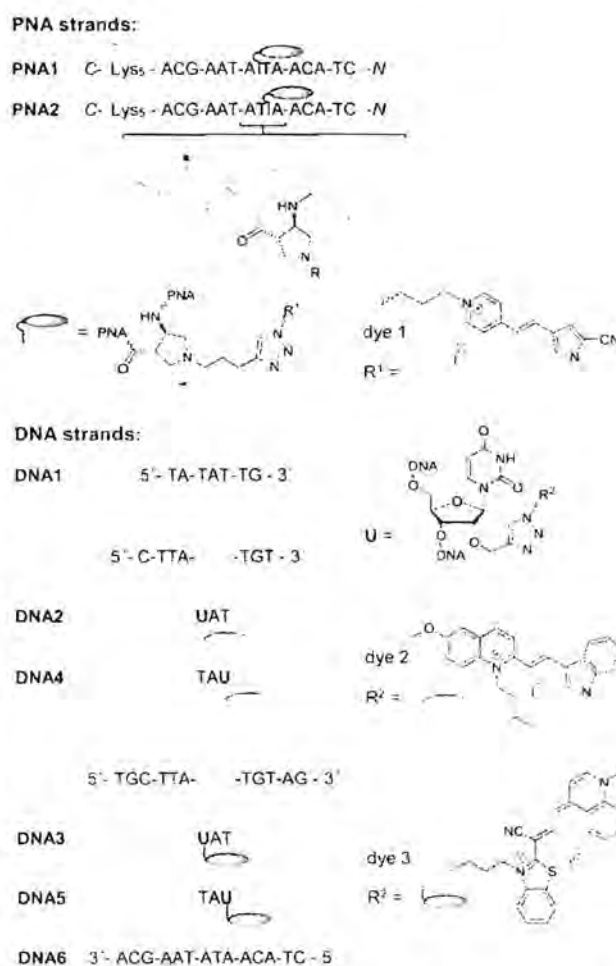


Fig. 2 Sequences of PNA1, PNA2, DNA1–DNA6 and structures of acpcPNA and of dyes 1–3 as PNA or DNA labels, respectively.

counterparts, 14mers DNA3 and DNA5, were modified at corresponding positions by the red emitting dye 3 (for the syntheses of dyes 1–3 and PNA/DNA labelling procedures see ESI†).

The dye 1-labeled PNA1 and PNA2 were separately annealed with the unmodified 7mer oligonucleotide counterstrand DNA1 to obtain the starting duplexes for strand displacement experiments. Both samples were consecutively titrated with 1.0 equivalent of DNA2 or DNA4, followed by DNA3 or DNA5, respectively (Fig. 3). The first titrations with DNA2 or DNA4

place the energy acceptor dye 2 into proximity to donor dye 1. If the excitation wavelength is kept constant at 389 nm, the efficient (*vide infra*) energy transfer between these two dyes causes significant fluorescence color changes from blue to yellow which were observed in all four cases (PNA1-DNA1 and PNA2-DNA1, each with DNA2 or DNA4). The second titrations with DNA3 or DNA5, respectively, remove dye 2 from the hybrids and place the energy acceptor dye 3 into close proximity to dye 1. As a result the fluorescence color changes from yellow to red; again at the same excitation wavelength (389 nm).

From these titrations the following two observations have been made and further investigated. (i) The first strand displacements of 7mer DNA1 by 10mer DNA2 or DNA4 take place relatively fast (within 5 minutes). The second strand displacements of 10mer DNA2 or DNA4 as part of the intermediate acpcPNA hybrids by 14mer DNA3 or DNA5 occur significantly slower than the first displacement processes (approximately 1 h). This can be explained by the increasing affinity of acpcPNA to longer DNA pieces during the strand displacements and the exceptionally high stability of acpcPNA-DNA hybrids in general. Melting temperatures of the starting, intermediate and final acpcPNA-DNA hybrids were determined (Table 1). The representative titration of hybrid PNA2-DNA1 with DNA2 and DNA3 is shown in Fig. 3 and exhibits a T_m increase from 71.5 °C over 77.2 °C to >90 °C. As expected all PNA-DNA hybrids possess far higher T_m than comparable DNA-DNA duplexes (see ESI†). Both PNA strands, PNA1 and PNA2, form especially stable hybrids with unmodified DNA counterstrands as shown by T_m of >90 °C (see ESI†), whereas singly and doubly modified acpcPNA-DNA hybrids exhibit lower T_m values. The singly modified duplex DNA6-DNA3 exhibits a T_m which is around 50 °C lower in comparison to the corresponding acpcPNA-14mer DNA hybrid (see ESI†) and hence, affirms strong binding between acpcPNA and DNA even

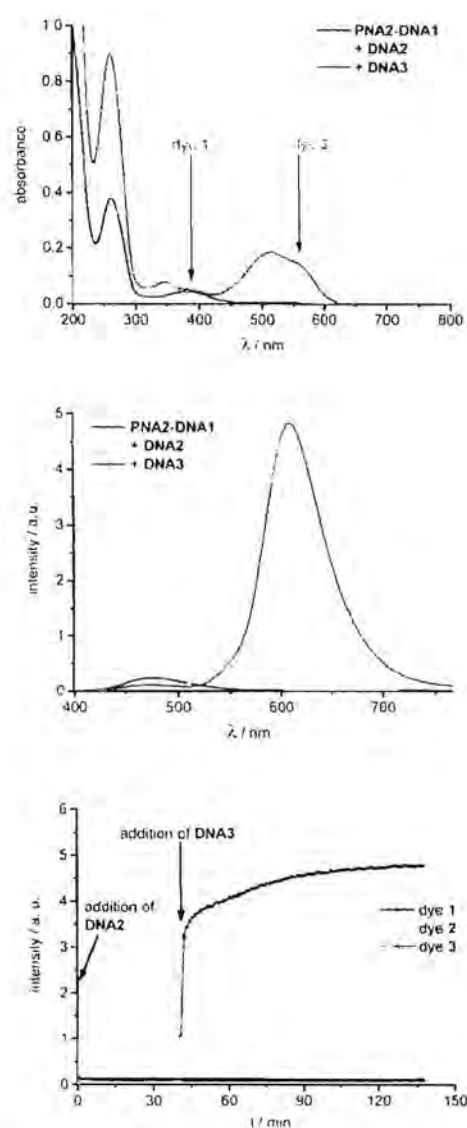


Fig. 3 Optical spectra of the representative strand displacement experiment with PNA2-DNA1 (2.5 μ M in 10 mM Na-P_i buffer, pH 7) by consecutive addition of DNA2 (1.0 equiv.) and DNA3 (1.0 equiv.): UV/Vis absorption (top), fluorescence (middle, λ_{exc} = 389 nm) and time-dependent fluorescence intensity changes (dye 1: λ_{em} = 478 nm, dye 2: λ_{em} = 560 nm, dye 3: λ_{em} = 606 nm) after addition of DNA2 (0–41 min, and DNA3 (41–138 min).

Table 1 Color contrasts, fluorescence intensity increase factors, energy transfer efficiencies and melting temperatures T_m of PNA/DNA hybrids

| Duplex | Color contrast | Fluorescence intensity increase factor ^a | Energy transfer efficiency ^b | T_m ^c [°C] |
|-----------|---------------------|---|---|-------------------------|
| PNA1-DNA1 | — | — | — | 71.0 |
| PNA1-DNA2 | 1:3.4 ^d | 16.6 | 0.82 ± 0.13 | 78.2 |
| PNA1-DNA3 | 1:1.41 ^e | 21.1 | 0.99 ± 0.13 | >90 |
| PNA1-DNA4 | 1:3.8 ^f | 15.0 | 0.79 ± 0.12 | >90 |
| PNA1-DNA5 | 1:1.73 ^g | 8.9 | 0.98 ± 0.16 | >90 |
| PNA2-DNA1 | — | — | — | 71.5 |
| PNA2-DNA2 | 1:2.0 ^d | 10.8 | 0.78 ± 0.11 | 77.2 |
| PNA2-DNA3 | 1:4.7 ^e | 20.1 | 0.98 ± 0.05 | >90 |
| PNA2-DNA4 | 1:4.9 ^f | 9.8 | 0.75 ± 0.10 | 82.7 |
| PNA2-DNA5 | 1:2.23 ^g | 19.8 | 0.98 ± 0.07 | >90 |
| DNA6-DNA3 | — | — | — | 32.7 |

^a See definition in text. ^b Calculated by fluorescence lifetimes (see ESI). ^c λ = 260 nm, 5–95 °C, interval: 0.5 °C min⁻¹, 2.5 μ M duplex in 10 mM Na-P_i pH 7. ^d 1.478 nm/1.561 nm; ^e 1.478 nm/1.608 nm; ^f 1.478 nm/1.524 nm; ^g 1.478 nm/1.699 nm.

in the presence of an attached dye. In case of the majority of acpcPNA-10mer DNA hybrids, e.g. PNA1-DNA2, the T_m values show that the fluorescent dye labels are destabilizing and require carefully chosen placements in complementary hybrids.¹⁷ Especially the dye attachment in the hybrid PNA1-DNA4 causes less destabilizing effects and gives a T_m of >90 °C. (ii) Large fluorescence color ratios blue:yellow/blue:red and fluorescence intensity enhancements were accomplished by an efficient energy transfer (*vide infra*) from donor dye 1 to both acceptor dyes 2 and 3, respectively (Table 1). The highest blue:red contrast ($I_{478\text{ nm}}/I_{600\text{ nm}}$) of 1:223 is obtained during displacement of 10mer DNA4 by 14mer DNA5 yielding hybrid PNA2-DNA5. The enhancements of the yellow and red fluorescence signals were quantified by the fluorescence intensity increase factors (Table 1) that were determined for both acceptor dyes 2 or 3, respectively, at their corresponding emission maximum. The factors represent the ratios of the fluorescence intensities of the acceptor dyes after excitation at the absorption maximum of donor dye 1 to the fluorescence intensities of the acceptor dyes upon excitation at the same wavelength but in the absence of the donor dye 1. The latter fluorescence intensities were obtained with single-stranded DNA1 to DNA5. The largest fluorescence enhancement factor of 21.1 was obtained during the strand displacement of PNA1-DNA2 by DNA3.

In order to calculate energy transfer efficiencies, fluorescence lifetimes of dye 1 ($\lambda_{\text{exc}} = 389$ nm, $\lambda_{\text{em}} = 478$ nm) were determined for all modified PNA-DNA hybrids (see ESI†). In the absence of energy acceptor, dye 1 in hybrids of PNA1 and PNA2 with full length DNA counterstrands (see ESI†) exhibits lifetimes of approximately 1.6 ns and 1.5 ns, respectively. Due to the presence of acceptor dyes 2, or 3, respectively, these lifetimes are significantly shortened to the sub-ns range in all doubly labeled acpcPNA-DNA hybrids yielding excellent energy transfer efficiencies between 75% and 99%.

The following strand displacement experiment representatively shows the ability of acpcPNA to displace one DNA strand out of the 14mer duplex DNA6-DNA3. The recorded fluorescence of dye 3 shows a significant intensity increase due to the fact that the unmodified DNA6 is replaced by PNA1 bearing the energy donor which is dye 1 (Fig. 4). This clearly demonstrates that strand displacement of DNA6 by PNA1 occurs efficiently within several minutes due to the large increase in stability from 32.7 °C (DNA6-DNA3) to >90 °C (PNA1-DNA3). This kind of strand displacement is an important prerequisite for the *in vitro* strand invasion experiments described in the second part below.

Strand invasions

Antigene targeting of double stranded (ds) DNA by PNA is an important goal for biological applications inside living cells. It was shown^{10,11} that the conformationally restricted acpcPNA is not able to form triplex structures like conventional PNA that binds to dsDNA in several different binding modes, including

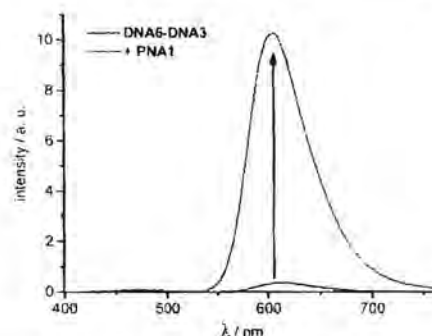
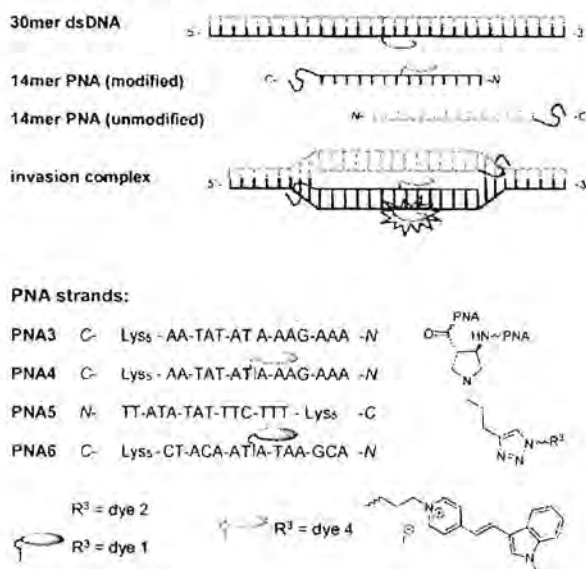


Fig. 4 Fluorescence intensity change during the strand displacement of DNA6-DNA3 (2.5 μ M in 10 mM Na-P, buffer, pH 7) by PNA1 (1.0 equiv.). $\lambda_{\text{exc}} = 389$ nm, for UV/Vis absorption spectra and time-dependent fluorescence intensity changes see ESI.†

triplex formation, triplex invasion, duplex invasion and double duplex invasion.^{1,18} In order to confirm that acpcPNA is able to undergo double duplex invasion and to follow this process by fluorescence spectroscopy, dsDNA7 to dsDNA10 were synthesized (Fig. 5). They were labeled by the blue emitting dye 1 or the red emitting dye 3, respectively, at the central A (dsDNA7, dsDNA9) or at the U on the 3'-side (dsDNA8, dsDNA10). PNA3 to PNA5 contain 14mer sequences that are complementary to the central part of the sequences of dsDNA7 to dsDNA10, and again 5 lysine residues to get enough solubility. Based on studies in other PNA systems^{17,19} it can be assumed that the lysine residues facilitate the strand invasion process by stabilizing the PNA-DNA duplex and destabilizing the PNA-PNA self duplex, although whether their presence is essential for the invasion is difficult to confirm due to the poor solubility of dye-labeled PNA without lysine. The stability of these double strands is only slightly diminished, if at all, by the attached dyes: the T_m difference is only between -1.7 °C and $+0.1$ °C, if compared to a 30mer, completely unmodified DNA double strand (DNA16-DNA15, $T_m = 70.4$ °C, see Table S5 in ESI†). PNA3 was modified with the yellow emitting dye 2 that serves as energy acceptor for dye 1 in dsDNA7 and dsDNA8, whereas PNA4 is modified with the green emitting dye 4 that represents the energy donor for dye 3 in dsDNA9 and dsDNA10 (for synthesis of dye 4, see ESI†). With respect to the biological context, PNA3 and PNA4 are complementary to the TIAM1 sequence that is regulated by miRNA-21 and miRNA-31 in colon carcinoma cells.¹⁶ The unmodified PNA5 serves as the fourth strand that was originally thought to be essential for the double duplex invasions. PNA6 bears a non-sense sequence for control experiments. Invasions were detected by blue:yellow or green:red fluorescence color contrasts (e.g. $I_{478\text{ nm}}/I_{585\text{ nm}}$) and by fluorescence intensity increase factors (Table 2) that were determined similarly as described above, for both acceptor dyes 2 or 3, respectively, at their corresponding emission maximum. The factors represent

Double duplex invasion:



dsDNA strands:

dsDNA 3'-GCC-TCC-TT-AA-TAT-ATA-AAG-AAA-TT-CCT-CGG-5'
5'-CCG-AGG-AA-TT-ATA- -TTC-TTT-AA-GGA-GCC-3'

dsDNA7 TAT R³ = dye 1

dsDNA8 TAU R⁴ = dye 1

dsDNA9 TAT R³ = dye 3

dsDNA10 TAU R⁴ = dye 3

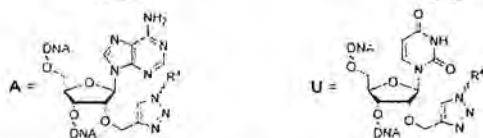


Fig. 5 Schematic drawing of double duplex invasion, sequences of PNA3–PNA6, structure of dye 4 and sequences of dsDNA7–dsDNA10 (from top to bottom).

the ratios of the fluorescence intensities of the acceptor dyes after excitation at the absorption maxima of donor dyes 1 or 4, respectively, to the fluorescence intensities of the acceptor dyes upon excitation at the same wavelength but in the absence of the donor dyes 1 or 4. The latter fluorescence intensities were obtained with the non-invaded dsDNA7 to dsDNA10.

Energy transfer efficiencies (Table 2) of all invasion complexes were calculated from the corresponding fluorescence lifetimes of donor dyes 1 ($\lambda_{\text{exc}} = 370$ nm, $\lambda_{\text{em}} = 475$ nm) and 4 ($\lambda_{\text{exc}} = 435$ nm, $\lambda_{\text{em}} = 528$ nm). All strand invasion experiments were performed in presence and absence of 250 mM NaCl since we assumed that duplex invasions by acpcPNA might be salt-dependent processes. At first, we studied kinetics of strand invasion into dsDNA7 and dsDNA8 by 1.0 equiv. of PNA3 together with 1.0 equiv. of PNA5. Constant fluorescence intensities are reached within 60 minutes with NaCl and

Table 2 Color contrasts, fluorescence intensity increase factors and energy transfer efficiencies of acpcPNA strand invasion into dsDNA

| Invasion complex | NaCl ^a | Color contrast | Fluo-rescence intensity increase factor ^b | Energy transfer efficiency ^c |
|------------------|-------------------|-----------------------|--|---|
| dsDNA7- | + | 1 : 2.1 ^d | 18.1 | 0.67 ± 0.09 |
| PNA3-PNA5 | - | 1 : 7.5 ^e | 19.6 | 0.74 ± 0.12 |
| dsDNA8- | + | 1 : 1.4 ^f | 14.6 | 0.66 ± 0.15 |
| PNA3-PNA5 | - | 1 : 4.8 ^g | 20.8 | 0.76 ± 0.12 |
| dsDNA9- | + | 1 : 43.0 ^h | 16.6 | 0.97 ± 0.04 |
| PNA4-PNA5 | - | 1 : 87.0 ⁱ | 23.2 | 0.99 ± 0.01 |
| dsDNA9- | + | 1 : 23.7 ^j | 14.4 | 0.94 ± 0.03 |
| PNA4 | - | 1 : 23.0 ^k | 17.4 | 0.94 ± 0.13 |
| dsDNA9- | + | 1 : 2.2 ^l | 1.8 | — |
| PNA6 | - | — | — | — |
| dsDNA10- | + | 1 : 28.6 ^m | 10.0 | 0.93 ± 0.06 |
| PNA4-PNA5 | - | 1 : 61.1 ⁿ | 13.3 | 0.97 ± 0.02 |

^a 250 mM. ^b $I_{\text{dsDNA}/\text{PNA}}/I_{\text{dsDNA}}$ (definition see text). ^c Calculated by fluorescence lifetimes (see ESI†). ^d $I_{475 \text{ nm}}/I_{585 \text{ nm}}$. ^e $I_{475 \text{ nm}}/I_{585 \text{ nm}}$. ^f $I_{475 \text{ nm}}/I_{585 \text{ nm}}$. ^g $I_{528 \text{ nm}}/I_{661 \text{ nm}}$. ^h $I_{528 \text{ nm}}/I_{661 \text{ nm}}$. ⁱ $I_{528 \text{ nm}}/I_{661 \text{ nm}}$. ^j $I_{475 \text{ nm}}/I_{613 \text{ nm}}$. ^k $I_{529 \text{ nm}}/I_{611 \text{ nm}}$. ^l $I_{528 \text{ nm}}/I_{608 \text{ nm}}$.

90 minutes without NaCl (see ESI†). Although NaCl-free conditions show comparable kinetics, they yield stronger increase of emission intensities and considerably higher color contrasts blue:yellow. Obviously the dye interactions with DNA in the hybrids with DNA are salt dependent and alter the fluorescence intensities. Further titrations revealed that the fluorescence color change is maximized upon addition of 3.0 equiv. of acpcPNA (see ESI†). Hence, full double-duplex invasions into dsDNA7 and dsDNA8, respectively, were carried out by addition of 3.0 equiv. of PNA3 together with PNA5. In absence of acceptor dyes, the blue emitting dye 1 exhibit lifetimes of approximately 2.4–2.6 ns in dsDNA7 and dsDNA8. The lifetimes are shortened down to 0.6–0.9 ns in the invasion complexes with PNA3 and PNA5, which yields energy transfer efficiencies in the range from 66% to 76% (see ESI†). Moreover, strand invasion efficiencies could be determined based on these energy transfer efficiencies. As fluorescence reference for complete invasion, reference hybrids of PNA3 with full-length complementary DNA strands bearing dye 1 at the central A were annealed. The energy transfer efficiencies of these hybrids were measured and represent 100% reference values. Remarkably, invasion efficiencies of approximately 99% could be accomplished in all cases (see ESI†). Best results with this dye combination were accomplished e.g. with dsDNA7 in absence of NaCl (Fig. 6). The invasion by PNA3 together with PNA5 exhibits an intensity increase of the yellow emission by a factor of 19.6, a color contrast blue:yellow ($I_{475 \text{ nm}}/I_{585 \text{ nm}}$) of 1 : 7.5 and an energy transfer efficiency of 74%.

Similarly, double-duplex invasion kinetics of dsDNA9 and dsDNA10 after adding 1.0 equivalent PNA4 together with PNA5 were recorded. It is important to note that titrations revealed that 1.5 equiv. PNA4 and PNA5 were sufficient for this type of strand invasions to obtain maximal fluorescence change (see ESI†). Hence, quantification of energy transfer efficiencies,

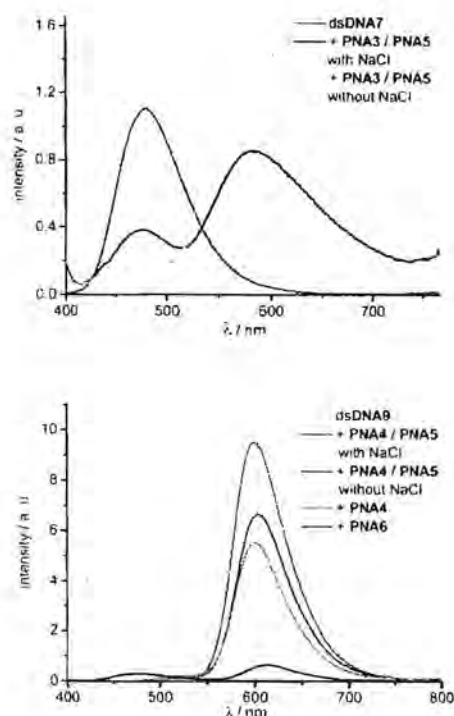


Fig. 6 Representative fluorescence spectra before and after double duplex invasion; dsDNA7 (2.5 μ M in 10 mM Na-P, buffer, pH 7) invaded by 3.0 equiv. PNA3 together with PNA5, in absence and presence of NaCl (250 mM), λ_{exc} = 391 nm (top); dsDNA9 (2.5 μ M in 10 mM Na-P, buffer, pH 7) invaded by 1.5 equiv. PNA4 together with PNA5 in absence and presence of NaCl (250 mM), by 1.5 equiv. PNA4 without PNA5, and by 1.5 equiv. non-sense PNA6, λ_{exc} = 391 nm (bottom).

fluorescence intensity increase factors and color contrasts green : red were carried out under these conditions, in absence and presence of NaCl, respectively (Table 2).

Remarkably, energy transfer from donor dye 4 to acceptor dye 3 occurs with 97–99% efficiency which yields very large increase factors and color contrasts. Here again, invasion efficiencies of 99% were achieved in all cases (see ESI[†]). Especially the modification at the central adenosine by dye 3 (dsDNA9) and invasion in the absence of NaCl turned out to be the optimal condition for double duplex invasion (Fig. 6). After addition of 1.5 equiv. of PNA3 together with PNA5 an increase factor of 23.3 and a color contrast green : red ($I_{528\text{ nm}}/I_{600\text{ nm}}$) of 1 : 87 could be accomplished. The observed variation of intensity enhancements and color contrasts could be assigned to the different anchor point of the post-synthetic DNA labeling by dye 3. Reference measurements with corresponding DNA duplexes bearing the dye 3 modification at an adenosine (dsDNA9) vs. uridine (dsDNA10) clearly show approximately 20% stronger fluorescence intensities (see ESI[†]). Importantly, the possibility of strand invasion of dsDNA9 by using only one PNA strand (PNA4) yields a D-loop and could be evidenced by energy transfer efficiency of 94% and invasion efficiency of 96% (see ESI[†]) which is only slightly lower compared to 99% invasion efficiencies obtained for

double duplex invasions. Hence, the latter result demonstrates that single stranded acpcPNA may be sufficient to open double stranded DNA without requiring the other acpcPNA strand.

The duplex of the 14-mer PNA with DNA containing a single mismatch base was still quite stable under the experimental conditions, therefore the invasion also proceeded with dsDNA target containing a mismatch at the invasion site (data not shown). In order to rule out that unspecific PNA aggregation to dsDNA occurs instead of the expected invasion, a random sequence and non-sense PNA6 was synthesized and modified with the blue donor dye 1 (Fig. 5). A rather small fluorescence enhancement after addition of 1.5 equiv. non-sense PNA6 to dsDNA9 was observed (Fig. 6, Table 2). As proven in strand displacement experiments above, an efficient energy transfer is only possible between dye 1 and dye 3 if they get in close proximity to each other. Thus, the very small intensity increase factor of 1.8 in case of PNA6 clearly excludes non-specific PNA-DNA aggregation.

In order to support the duplex invasions by PNA3 and PNA4, melting temperatures of dsDNAs, acpcPNA-DNA-hybrids, their DNA-DNA-analogs and of complexes invaded by 1.0 equiv. acpcPNA were determined, in the absence or presence of NaCl, respectively (see ESI[†]). Fig. 7 representatively displays the normalized absorption changes during T_m determination of the complex dsDNA8 invaded by only 1.0 equiv. PNA3 together with PNA5 without NaCl. It should be noted here that strand invasion with 1.0 equiv. of PNA3 is not complete. Accordingly, discrete melting temperature regions for each part of the invading complex are explicitly visible: (i) Comparison 8mer dsDNA13 (overhang on both ends of dsDNA8) that invasion takes place without dissociation of the remaining duplex regions on both sides of invasion, and with a locally displaced complementary strand. (ii) The melting transition of dsDNA8 which corresponds to the non-invaded

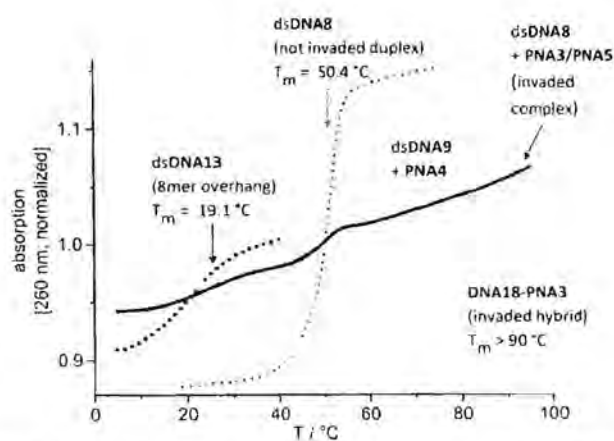


Fig. 7 Representative, normalized melting temperature determination of dsDNA8 invaded by 1.0 equiv. PNA3 and PNA5 (blue line), and dsDNA9 invaded by PNA4 only (gray line), and those of references dsDNA8 (green dotted), 8mer dsDNA13 (black dotted) and DNA18-PNA3-hybrid (light blue dotted), in absence of NaCl.

duplex vanishes with more equivalents of PNA3:PNA5. (iii) The T_m of the DNA18–PNA3 hybrid is >90 °C represents the T_m and the exceptionally stability of the invaded duplex (for sequences of dsDNA13 and DNA18 see ESI†).

Experimental

All experimental details, syntheses and spectroscopic data are described in the ESI†.

Conclusions

In conclusion to the first part of experiments, it became clear that displacements of DNA strands from acpcPNA–DNA hybrids can be followed by fluorescence color changes using our concept of wavelength probes ("DNA traffic lights") and are possible with longer oligonucleotides than the preannealed ones. The kinetics of these strand displacements are rather slow due to the high stability of the acpcPNA–DNA hybrids. Moreover, acpcPNA is able to displace a DNA strand from double stranded DNA of the same length. There is important significance of these *in vitro* experiments for cell biological applications. The intracellular transport could potentially be facilitated by annealing acpcPNA to a short DNA counter-strand. In combination with attached positively charged lysine residues on the termini of acpcPNA strands, such acpcPNA/DNA hybrids may potentially be easier delivered into the cells.

In the second part, we demonstrated that acpcPNA is able not only to displace one of the strands in double-stranded DNA of the same length, but also to invade into long double-stranded A–T rich DNA, remarkably with quantitative efficiency. Again, these processes can be followed by means of fluorescence color changes. Compared to conventional PNA systems which require 3 or more equiv. PNA, only 1.5 equiv. acpcPNA are sufficient to get efficient invasion. Although initial DNA duplex invasion experiments were performed with two non-self-pairing acpcPNA strands, single stranded acpcPNA was also able to invade into DNA duplex without requiring the other PNA strand, at least in the A–T rich sequence context being studied. Beyond that, our findings clearly confirm that the invasion takes place even at high ionic strength, a condition that is known to decrease the PNA duplex invasion efficiency. Therefore, acpcPNA exhibits sophisticated properties which are highly desirable in the field of biological analytics and antigene applications.

Acknowledgements

Financial support by the DFG (grant WA1387/17-1, GRK 2039), KIT and the Thailand Research Fund (DPG5780002) is gratefully acknowledged. P. Bohländer thanks the Karlsruhe House of Young Scientists (KHYS) for a fellowship to support a research stay in Bangkok.

Notes and references

- P. E. Nielsen, M. Egholm, R. H. Berg and O. Buchardt, *Science*, 1991, **254**, 1497–1500.
- M. Egholm, O. Buchardt, L. Christensen, C. Behrens, S. M. Freier, D. A. Driver, R. H. Berg, S. K. Kim, B. Norden and P. E. Nielsen, *Nature*, 1993, 566–568.
- P. E. Nielsen, *Acc. Chem. Res.*, 1999, **32**, 624–630.
- P. E. Nielsen, *Chem. Biodiversity*, 2010, **7**, 786–804.
- K. N. Ganesh and P. E. Nielsen, *Curr. Org. Chem.*, 2000, **4**, 931–943.
- V. Kumar and K. N. Ganesh, *Acc. Chem. Res.*, 2005, **38**, 494–412.
- K. Matsumoto, E. Nakata, T. Tamura, I. Saito, Y. Aizawa and T. Morii, *Chem. – Eur. J.*, 2013, **19**, 5034–5040.
- J. K. Pokorski, M. A. Witschi, B. L. Purnell and D. H. Appella, *J. Am. Chem. Soc.*, 2004, **126**, 15067–15073.
- C. M. Micklitsch, B. Y. Oqu岸, C. Zhao and D. H. Appella, *Anal. Chem.*, 2012, **85**, 251–257.
- T. Vilaivan and C. Srisuwannaket, *Org. Lett.*, 2006, **8**, 1897–1900.
- C. Vilaivan, C. Srisuwannaket, C. Ananthanawat, C. Suparpprom, J. Kawakami, Y. Yamaguchi, Y. Tanaka and T. Vilaivan, *Artificial DNA: PNA & XNA*, 2011, **2**, 50–59.
- J. Taechalerpaisarn, P. Sriwarom, C. Boonlua, N. Yotapan, C. Vilaivan and T. Vilaivan, *Tetrahedron Lett.*, 2010, **51**, 5822–5826.
- T. Vilaivan, *Acc. Chem. Res.*, 2015, **48**, 1645–1656.
- C. Boonlua, C. Vilaivan, H. A. Wagenknecht and T. Vilaivan, *Chem. – Asian J.*, 2011, **6**, 3251.
- C. Boonlua, B. Ditmangklo, N. Reenabthue, C. Suparpprom, N. Poomsuk, K. Siritwong and T. Vilaivan, *RSC Adv.*, 2014, **4**, 8817–8827.
- B. Ditmangklo, C. Boonlua, C. Suparpprom and T. Vilaivan, *Bioconjugate Chem.*, 2013, **24**, 614–625.
- N. Yotapan, C. Charoenpakdee, P. Wathanathavorn, B. Ditmangklo, H.-A. Wagenknecht and T. Vilaivan, *Beilstein J. Org. Chem.*, 2014, **10**, 2166–2174.
- J. Lohse, O. Dahl and P. E. Nielsen, *Proc. Natl. Acad. Sci. U. S. A.*, 1999, **96**, 11804–11808.
- T. Ishizuka, J. Yoshida, Y. Yamamoto, J. Sumaoka, T. Tedeschi, R. Corradini, S. Sforza and M. Komiyama, *Nucleic Acids Res.*, 2008, **36**, 1464–1471.
- T. Bentin and P. E. Nielsen, *J. Am. Chem. Soc.*, 2003, **125**, 6378–6379.
- S. Rapireddy, G. He, S. Roy, B. A. Armitage and D. H. Ly, *J. Am. Chem. Soc.*, 2007, **129**, 15596–15600.
- V. Chenna, S. Rapireddy, B. Sahu, C. Ausin, E. Pedroso and D. H. Ly, *ChemBioChem*, 2008, **9**, 2388–2391.
- M. E. Hansen, T. Bentin and P. E. Nielsen, *Nucleic Acids Res.*, 2009, 4498–4507.
- G. He, S. Rapireddy, R. Bahal, B. Sahu and D. H. Ly, *J. Am. Chem. Soc.*, 2009, **131**, 12088–12090.
- C. Holzhauser and H.-A. Wagenknecht, *J. Org. Chem.*, 2013, **78**, 7373–7379.

- 26 Q. Zheng, M. F. Juette, S. Jockusch, M. R. Wasserman, Z. Zhou, R. B. Altman and S. C. Blanchard, *Chem. Soc. Rev.*, 2014, **43**, 1044-1056.
- 27 P. V. Chang and C. R. Bertozzi, *Chem. Commun.*, 2012, **18**, 8864-8879.
- 28 B. A. Armitage, *Curr. Opin. Chem. Biol.*, 2011, **15**, S06-S12.
- 29 R. W. Sinkeldam, N. J. Greco and Y. Tor, *Chem. Rev.*, 2010, **110**, 2579-2619.
- 30 D. Y. Zhang and G. Seelig, *Nat. Chem.*, 2011, **3**, 103-113.
- 31 B. Yurke, A. J. Turberfield, A. P. Mills, F. C. Simmel and J. L. Neumann, *Nature*, 2000, **406**, 605-608.
- 32 H. Yan, X. Zhang, Z. Shen and N. C. Seeman, *Nature*, 2002, **415**, 62-65.
- 33 B. Chakraborty, R. Sha and N. C. Seeman, *Proc. Natl. Acad. Sci. U. S. A.*, 2008, **105**, 17245-17249.
- 34 K. Takahashi, S. Yaegashi, A. Kameda and M. Hagiya, in *DNA computing*, Springer, 2006, pp. 347-358.
- 35 G. Seelig, D. Soloveichik, D. Y. Zhang and E. Winfree, *Science*, 2006, **314**, 1585-1588.
- 36 B. M. Frezza, S. L. Cockroft and M. R. Ghadiri, *J. Am. Chem. Soc.*, 2007, **129**, 14875-14879.
- 37 J. M. Picuri, B. M. Frezza and M. R. Ghadiri, *J. Am. Chem. Soc.*, 2009, **131**, 9368-9377.
- 38 L. Qian, D. Soloveichik and E. Winfree, in *DNA computing and molecular programming*, Springer, 2011, pp. 123-140.
- 39 W. B. Sherman and N. C. Seeman, *Nano Lett.*, 2004, **4**, 1203-1207.
- 40 J.-S. Shin and N. A. Pierce, *J. Am. Chem. Soc.*, 2004, **126**, 10834-10835.
- 41 H. Gu, J. Chao, S.-J. Xiao and N. C. Seeman, *Nature*, 2010, **465**, 202-205.
- 42 I. K. Astakhova, K. Pasternak, M. A. Campbell, P. Gupta and J. Wengel, *J. Am. Chem. Soc.*, 2013, **135**, 2423-2426.
- 43 C. Holzhauser, R. Liebl, A. Goepferich, H.-A. Wagenknecht and M. Breunig, *ACS Chem. Biol.*, 2013, **8**, 890-894.
- 44 P. R. Bohländer and H. A. Wagenknecht, *Eur. J. Org. Chem.*, 2014, 7547-7551.
- 45 P. R. Bohländer and H.-A. Wagenknecht, *Org. Biomol. Chem.*, 2013, **11**, 7458-7462.
- 46 T. Bentin, H. J. Larsen and P. E. Nielsen, *Biochemistry*, 2003, **42**, 13987-13995.
- 47 A. Abibi, E. Protozanove, V. V. Demidov and M. D. Frank-Kamenetskii, *Biophys. J.*, 2004, **86**, 3070-3078.



Immobilization-free electrochemical DNA detection with anthraquinone-labeled pyrrolidinyl peptide nucleic acid probe

Jutatip Kongpeth^a, Sakda Jampasa^b, Piyasak Chaumpluk^c, Orawon Chailapakul^d,
Tirayut Vilaivan^{a,*}

^a Organic Synthesis Research Unit, Department of Chemistry, Faculty of Science, Chulalongkorn University, Phayathai Road, Patumwan, Bangkok 10330, Thailand

^b Program in Petrochemistry, Faculty of Science, Chulalongkorn University, Phayathai Road, Patumwan, Bangkok 10330, Thailand

^c Laboratory of Plant Transgenic Technology and Biosensor, Department of Botany, Faculty of Science, Chulalongkorn University, Phayathai Road, Patumwan, Bangkok 10330, Thailand

^d Electrochemistry and Optical Spectroscopy Research Unit, Department of Chemistry, Faculty of Science, Chulalongkorn University, Phayathai Road, Patumwan, Bangkok 10330, Thailand

ARTICLE INFO

Article history:

Received 15 June 2015

Received in revised form

25 August 2015

Accepted 26 August 2015

Available online 28 August 2015

Keywords:

Redox active label

Peptide nucleic acid

Electrochemical detection

DNA biosensor

Screen-printed carbon electrode

ABSTRACT

Electrochemical detection provides a simple, rapid, sensitive and inexpensive method for DNA detection. In traditional electrochemical DNA biosensors, the probe is immobilized onto the electrode. Hybridization with the DNA target causes a change in electrochemical signal, either from the intrinsic signal of the probe/target or through a label or a redox indicator. The major drawback of this approach is the requirement for probe immobilization in a controlled fashion. In this research, we take the advantage of different electrostatic properties between PNA and DNA to develop an immobilization-free approach for highly sequence-specific electrochemical DNA sensing on a screen-printed carbon electrode (SPCE) using a square-wave voltammetric (SWV) technique. Anthraquinone-labeled pyrrolidinyl peptide nucleic acid (AQ-PNA) was employed as a probe together with an SPCE that was modified with a positively-charged polymer (poly quaternized-(dimethylamino-ethyl)methacrylate, PQDMAEMA). The electrostatic attraction between the negatively-charged PNA-DNA duplex and the positively-charged modified SPCE attributes to the higher signal of PNA-DNA duplex than that of the electrostatically neutral PNA probe, resulting in a signal change. The calibration curve of this proposed method exhibited a linear range between 0.35 and 50 nM of DNA target with a limit of detection of 0.13 nM ($3SD_{blank}/Slope$). The sub-nanomolar detection limit together with a small sample volume required (20 μ L) allowed detection of < 10 fmol (< 1 ng) of DNA. With the high specificity of the pyrrolidinyl PNA probe used, excellent discrimination between complementary and various single-mismatched DNA targets was obtained. An application of this new platform for a sensitive and specific detection of isothermally-amplified shrimp's white spot syndrome virus (WSSV) DNA was successfully demonstrated.

© 2015 Elsevier B.V. All rights reserved.

1. Introduction

The ability to precisely and sensitively identify specific DNA sequence has found widespread applications in many areas e.g. medical diagnostics, agricultural and food sciences [1], and environmental monitoring [2]. In addition to the direct sequencing that require expensive instrument and gel-based approaches that are labor intensive and time-consuming, various DNA sensing platforms that are more suitable for point-of-care diagnostics have been developed over the past decades [3–5]. Among these,

electrochemical DNA biosensors offer several advantages including the operational simplicity, high sensitivity, miniaturization and low cost of instrument [6,7]. In general, a probe that can specifically recognize the nucleic acid target is first immobilized onto the electrode. Binding to the target results in a measurable signal change either directly or through a redox-active indicator or labels [8–14]. The most frequently employed immobilization methods include gold–thiol interaction [15–17] and amide bond formation [18,19]. The immobilization step is time-consuming, requires large excess of the probe, and needs careful optimization. Attempts were made to avoid this by using biotin–streptavidin [20,21], host–guest interaction [22], or by electrostatic adsorption [23]. Alternatively, an intercalating redox indicator [24] or a redox-active probe [25–27] had been used in combination with PCR or other

* Corresponding author. Fax: +66 22187598.

E-mail address: vilaiv@post.chula.ac.th (T. Vilaivan).

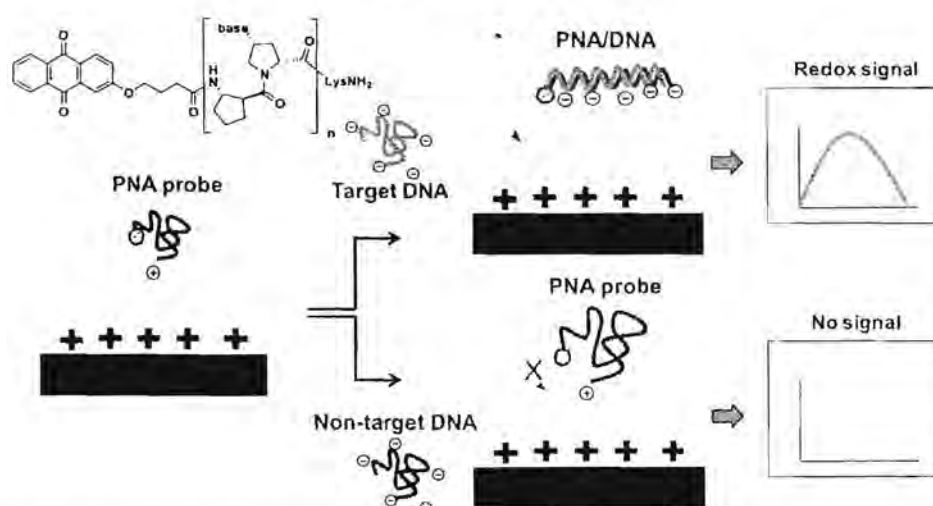


Fig. 1. The principle of immobilization-free electrochemical DNA biosensor employing AQ-PNA probe (structure of AQ-PNA shown in the inset).

enzymatic reactions for immobilization-free DNA detection.

Although DNA had been the most frequently employed probe, several new DNA analogs such as locked nucleic acid (LNA), morpholino and peptide nucleic acid (PNA) are becoming more popular alternatives because they can offer additional advantages including higher sensitivity, specificity and stability [28]. We recently reported a new conformationally constrained pyrrolidinyll peptide nucleic acid that showed excellent DNA hybridization properties [29–31] and demonstrated its applications as a probe for DNA sensing [32,33], including electrochemical detection [34–36].

The electrostatically neutral backbone of PNA allows designing of novel immobilization/detection concepts [37,38]. Luo et al. had recently developed an immobilization-free DNA sensing platform employing ferrocene-labeled PNA probes and indium-tin oxide (ITO) electrodes [39–41]. They observed that the signal detection can be switched from on-off to off-on mode by modifying the surface charge of the electrode [39]. Here we propose an immobilization-free electrochemical DNA sensing platform employing PNA and a polymer-modified screen-printed carbon electrode (SPCE), which can be easily and inexpensively prepared in one step. The electrostatic properties of the electrode can be readily controlled by adding the polymer modifier into the carbon ink without the need to form a monolayer or coating as usually the cases with other electrodes. A practical application was demonstrated in a highly specific detection of WSSV—a shrimp viral pathogen that causes large economic losses to shrimp aquaculture [42].

2. Material and methods

2.1. General materials and methods

Graphite powder (mesh size < 100) was purchased from Sigma-Aldrich. Carbon ink and silver/silver chloride were purchased from Acheson (California, USA). Other reagents and solvents were obtained from commercial suppliers and used without further purification. Poly quaternized-(dimethylamino)ethyl methacrylate (PQDMAEMA, $M_n = 1.38 \times 10^4$ Da) was synthesized and supplied by Dr. Voravee Hoven and Miss Pornpen Sae-ung (Chulalongkorn University). NMR spectra were recorded on a Bruker Avance 400 instrument operating at 400 MHz for ^1H and 100 MHz for ^{13}C . Chemical shifts were referenced to the residual protonated solvent peaks. MALDI-TOF MS spectra were measured on a Microflex

MALDI-TOF mass spectrometer (Bruker Daltonik GmbH, Bremen, Germany) in linear positive mode using α -cyano-4-hydroxycinnamic acid (CCA) matrix. Synthetic oligodeoxynucleotides were purchased from Pacific Science (Bangkok, Thailand) and were used as received. The sequences of PNA and DNA oligonucleotides used in this study, which correspond to a partial sequence of WSSV, are as follows:

AQ-labeled WSSV PNA probe (AQ-PNA): 2AQ-CTAAATTCAGALysNH₂

Target DNA (Dcomp): 5'-TCTGAATTTAG-3'

Single base mismatched DNA (DsmC): 5'-TCTGACTTTAG-3'

Long single stranded complementary DNA (ssDcomp19):

5'-CTAAGTCTGAATTTAGGGG-3'

Long single stranded mismatched DNA (ssDsmC19):

5'-CTAAGTCTGACTTTAGGGG-3'

Long double stranded complementary DNA (dsDcomp19):

5'-CTAAGTCTGAATTTAGGGG-3'

3'-GATTCAGACTTAAATCCCC-5'

Long double stranded mismatched DNA (dsDsmC19):

5'-CTAAGTCTGACTTTAGGGG-3'

3'-GATTCAGACTGAAATCCCC-5'

Other oligonucleotides used in the specificity test include (mismatch positions underlined):

DsmC6: 5'-TCTGACTTTAG-3' DsmA4: 5'-TCTAAATTTAG-3'

DsmG6: 5'-TCTGAGTTTAG-3' DsmT4: 5'-TCTTAATTTAG-3'

DsmT6: 5'-TCTGATTTTAG-3' DsmA7: 5'-TCTGAAATTTAG-3'

DsmC5: 5'-TCTGCAATTTAG-3' DsmC7: 5'-TCTGAATTTAG-3'

DsmG5: 5'-TCTGGATTTAG-3' DsmG7: 5'-TCTGAAGTTAG-3'

DsmT5: 5'-TCTGATTTTAG-3' DsmA11: 5'-TCTGAATTTAA-3'

2.2. General procedure for synthesis and labeling of the PNA probe

The WSSV PNA probe (AQ-PNA) used in this study is a pyrrolidinyll PNA with prolyl-2-aminocyclopentanecarboxylic acid backbone (acpcPNA) with a sequence of 2AQ-CTAAATTCAGALysNH₂ (Fig. 1). The unlabeled PNA probe was synthesized by Fmoc solid-phase peptide synthesis on a TentaGel resin with a Rink amide linker following a previously described protocol [30]. The Fmoc group at the N-terminus of the PNA on the solid support was next removed by treatment with 2% 1,8-diazabicycloundec-7-ene (DBU) and 20% piperidine in dimethylformamide (DMF) (100 μL) for 5 min. The free PNA (0.5 μmol) was next reacted with 4-(anthraquinone-2-oxy)butyric acid (pre-activated as a pentafluorophenyl ester, 7.5 μmol) and diisopropylethylamine (DIEA) (20 μL) in DMF (100 μL). After completion of the reaction

(monitored by MALDI-TOF MS), the AQ-PNA was heated with 1:1 (v/v) aqueous ammonia:dioxane in a sealed tube at 60 °C overnight to remove the nucleobase protecting groups. Following a cleavage from the solid support with trifluoroacetic acid (TFA), the crude AQ-PNA was purified by reverse phase HPLC (C18 column, 0.1% v/v TFA in H₂O–MeOH gradient).

2.3. Preparation of the PQDMAEMA-modified screen-printed carbon electrode (PQDMAEMA-SPCE)

The SPCE used in this study consisted of a three-electrode system prepared as described previously [36,43] (Fig. S1, S1). The only difference is that the carbon ink mixture was prepared by mixing PQDMAEMA solution (1% w/v), graphite powder and carbon ink together at a ratio of 0.35:0.2:1 (0.26% w/v PQDMAEMA in the ink mixture) followed by the binder solution (1 mL/g carbon ink) and sonicated to give a homogenous mixture.

2.4. DNA extraction and amplification by Loop-Mediated Isothermal Amplification (LAMP)

DNA of total genomic and associated WSSV viral DNA was extracted via a commercialized Genomic DNA Extraction Mini Kit (RBC, USA) using 50 mg broodstock specimen. The extracted DNA specimen was amplified by LAMP [41] with a set of primers consisting of WSSV F3, WSSV B3, WSSV FIP, and WSSV BIP (Table S1). The reaction mixture consisted of 40 mM Tris pH 8.8, 20 mM KCl, 16 mM MgSO₄, 0.2% Tween 20, 1.6 M betaine, 2.8 mM dNTP, and 8 U *Bst* DNA polymerase. After the incubation at 63 °C for 30 min, the LAMP products were examined by electrophoresis on 3% agarose gel and visualized under a UV transilluminator after staining with ethidium bromide.

For the specificity test, four strains of shrimp virus including WSSV, Infectious Hypodermal and Hematopoietic Necrosis Virus (IHHNV), Yellow Head Virus (YHV), and Taura Syndrome Virus (TSV) were included in the specificity test (Fig. S2, S1). The WSSV and IHHNV DNA samples were extracted and amplified by LAMP as described above. For RNA viruses (YHV and TSV), total RNA was extracted based on the Nucleospin RNA kit (RBC, USA) as recommend in the manufacturer's protocol. The YHV and TSV RNA were amplified by RT-LAMP [44]. The first two viral-infected specimens were kindly provided by Chachoengsao Coastal Fisheries Research and Development Center, Chachoengsao, Thailand, and the latter two specimens were from a private hatchery in Phang Nga, Thailand.

The sensitivity of the assay was determined using equivalent copy numbers of control plasmid nucleic acid at 10-fold dilutions [45]. These samples having copy number covering from 10⁷ to 10 copies were then amplified by LAMP at 63 °C for 30 min. The sensitivity of assay was analyzed and compared with standard PCR [46] via gel electrophoresis (Fig. S3, S1). To construct plasmid DNA for standard control, the DNA products corresponding to the transmembrane signal peptide gene were cloned into the TA vector as described by manufacturer (Invitrogen, Madison USA). This vector was transformed to *Escherichia coli* [47] and the nucleotide sequence was confirmed via direct nucleotide sequencing prior to use as control DNA. These plasmid DNAs were also used as a standard template of known copy number DNA.

2.5. Sample preparation and electrochemical measurement

2.5.1. Sample preparation

The concentrated stock solutions of AQ-PNA and DNA were mixed to give the desired concentration in an appropriate buffer. Twenty microliters of the AQ-PNA or AQ-PNA + DNA sample was dropped onto the PQDMAEMA-modified electrode. For double-

stranded synthetic DNA and appropriately diluted LAMP samples, the AQ-PNA + DNA mixture was heated at 90 °C for 10 min and was cooled to room temperature before the measurement.

2.5.2. Electrochemical measurement

Electrochemical measurements were carried out on the PQDMAEMA-modified SPCE (surface area of the working electrode = 0.16 cm²) by using PGSTAT 30 potentiostat (Metrohm Siam Company Ltd., Switzerland) and controlled with the General Purpose Electrochemical System (GPES) software version 4.9 (Eco Chemie B.V., Utrecht, The Netherlands). Unless otherwise specified, all measurements were conducted using a square-wave voltammetric method at room temperature (25 °C) in 10 mM Tris-HCl buffer pH 8.0. The redox signal was measured by SWV, with baseline subtraction. The measured signals are shown as average of three independent measurements ± standard deviations.

2.5.3. Optimization of parameters

For optimization of SWV parameters (amplitude, step potential and frequency), the SPCE prepared from 0.26% PQDMAEMA-modified carbon ink was used. The initial concentration of the AQ-PNA probe and DNA targets was 50 μM and was decreased to 50 nM during the optimization steps.

2.5.4. Specificity test and effects of excess non-target DNA

Specificity test was performed by measurement of the SWV signals of various mismatched DNA (see the sequence in Section 2.1) (50 nM) after hybridized with the AQ-PNA probe (50 nM) in 10 mM Tris-HCl buffer (pH 8.0) under the optimized conditions. Effects of excess non-target DNA to the signal of PNA and complementary PNA-DNA hybrid were studied with AQ-PNA (50 nM) and complementary DNA (Dcomp) (50 nM or 0 nM), in the presence of non-target DNA (DsmC) (0, 50, 500 and 5000 nM) in 10 mM Tris-HCl buffer (pH 8.0) under the optimized conditions.

2.5.5. Reproducibility test

Six PQDMAEMA-modified electrodes were prepared with the same process, and the signal was measured in the presence of AQ-PNA and complementary DNA (50 nM each) under the optimized conditions. Percent relative standard deviations (%RSD) were calculated according to Eq. (1), where SD is the standard deviation of current signal.

$$\%RSD = (SD/\text{mean}) \times 100 \quad (1)$$

3. Results and discussion

3.1. Synthesis and characterization of the AQ-PNA probe

Anthraquinone [48,49] was chosen as the redox active reporter group in this study because of its simple structure and excellent chemical stability. The carboxy-containing anthraquinone label 4-(anthraquinone-2-oxy)butyric acid was synthesized from commercially available 2-hydroxyanthraquinone (see details in Supporting information) and was characterized spectroscopically (Fig. S4-S6). It was next coupled to the PNA at the N-terminus to install the anthraquinone label. The *m/z* value of unlabeled PNA probe was 3844.2 (calcd *m/z* = 3842.2) and that of the AQ-PNA was 4134.5 (calcd *m/z* = 4134.3) (Fig. S7, S1). The mass increase of 290 Da corresponds to the AQ label, thus it can be concluded that the redox-active reporter AQ was successfully incorporated into the PNA probe. The purity of the AQ-PNA was confirmed to be > 90% by reverse phase HPLC (Fig. S8, S1).

Melting temperature (*T_m*) of the hybrid between the AQ-

Table 1
Thermal stability data of AQ-PNA: 2AQ-CTAAATTCAGA-LysNH₂ after hybridized with various DNA.

| DNA | Sequence (5'–3') | T_m (°C) ^a | ΔT_m ^b |
|---------|---------------------|-------------------------|---------------------------|
| Dcomp | TCTGAATTGA | 82.7 | 22.2 |
| DsmC | TCTGACTTTGA | 60.5 | |
| Dcomp19 | CTAAGTCTGAATTAGGGC | > 90 (83.7) | ~ 20 (22.7) |
| DsmC19 | CTAAGTCTGACTTTAGGGC | 70.5 (61.0) | |

^a T_m was measured in 10 mM sodium phosphate buffer pH 7.0, [PNA]=[DNA] = 1.0 μ M.

^b T_m (complementary hybrid) – T_m (single base mismatched hybrid).

^c Values in parenthesis were obtained in the presence of 100 mM NaCl.

labeled probe and its complementary DNA was 82.7 °C, which was higher than the corresponding DNA hybrid with the unlabeled probe (80.0 °C). Furthermore, the T_m value of the AQ-PNA decreased by more than 20 °C when hybridized with single base mismatched DNA (60.5 °C). These results (Table 1) indicate that the AQ-PNA probe binds to DNA with high affinity and specificity.

3.2. Preliminary electrochemical characterization of AQ-PNA probe

To test the possibility of using the labeled PNA as a probe for immobilization-free electrochemical detection of DNA sequence, the single stranded AQ-PNA was subjected to a SWV measurement on an unmodified SPCE that was pre-conditioned in 0.5 M aqueous NaOH at 1.3 V for 30 s [50]. A redox peak was observed at –0.71 V which corresponds well to that of the free AQ label (Fig. S9, S1). After hybridization with the complementary DNA target (Dcomp), the signal was completely suppressed. Hybridization with the single base mismatched DNA (DsmC) resulted in less signal suppression. It was hypothesized that the unmodified electrode possesses a negatively-charged surface after conditioning due to partial oxidation of the electrode surface to form carboxylate groups [50]. This can electrostatically interact with the AQ-PNA (carrying a positively-charged lysine residue) but not the corresponding PNA–DNA hybrid (negatively-charged due to the phosphate groups), resulting in the observed signal change.

3.3. Preparation and characterization of PQDMAEMA-modified electrode

It was proposed that if the electrode was first modified to provide a positively-charged surface, an electrochemical detection should be possible according to the principle shown in Fig. 1.

According to Fig. 1, no signal of the labeled PNA probe should be observed due to the unfavorable electrostatic interaction between the free AQ-PNA probe and the positively-charged electrode. Upon binding to the complementary DNA, the negatively-charged PNA–DNA hybrid should electrostatically attract to the electrode surface, allowing efficient electron transfer, resulting in a detectable electrochemical signal. A related concept for signal on PNA-based electrochemical DNA detection had been previously performed on a poly(allylamine hydrochloride) (PAH)-coated indium tin oxide (ITO) electrode [39].

In this work, a much simpler approach was proposed whereby the positively-charged polymer was mixed into the carbon ink mixture to be used for screening of the electrode [51]. Chitosan was previously incorporated into the SPCE to provide a handle for immobilization of the PNA probe [36]. Since chitosan contains positively-charged amino groups, we proposed that chitosan could be employed to provide positive charges on the electrode. Although a preliminary experiment confirmed that the immobilization-free electrochemical DNA detection was possible with the chitosan-modified SPCE, the limited solubility and

operating pH range of chitosan [52] prompted us to find a more suitable candidate. The positively-charged quaternized polymer PQDMAEMA was found to be the most suitable polymer and was selected as the modifier in all subsequent studies. In a control experiment (Fig. S10, S1), the SWV signal at –0.78 V corresponding to the anthraquinone label in AQ-PNA was observed only when the complementary DNA was present and not in bare electrode, AQ-PNA or DNA alone, thus validating the concept proposed in Fig. 1.

3.4. Optimization of parameters and calibration curve

First, the buffer was optimized by comparing the SWV signals between free and hybridized probes (with complementary and mismatched DNA) and Tris–HCl buffer pH 8.0 was chosen (Fig. S11, S1). To determine the optimal amount of the polymer modifier, the percentage of the polymer in the carbon ink mixture to be used for the electrode screening was varied from 0.13% to 5.2% w/v and the electrochemical signal of the PNA probe was measured in the absence and presence of the complementary DNA target (Fig. S12, S1). Increasing the polymer amount resulted in higher signals, but also higher backgrounds. The carbon ink containing 0.26% PQDMAEMA was chosen for the next studies because it gave the best compromise between the signal and background. The performances of unmodified and PQDMAEMA-modified SPCE were also evaluated by cyclic voltammetry. At identical scan rate, the signal of [Fe(CN)₆]^{3–/4–} was stronger in the PQDMAEMA-modified electrode, which is to be expected based on its positively-charged nature. The signal of [Fe(CN)₆]^{3–/4–} increased as a linear function of square root of scan rate, providing linearity in the range of 0.2–0.6 V s^{–1} with $R^2=0.9974$ and 0.9986 for oxidation and reduction processes, respectively (Fig. S13, S1). The results imply that the oxidation and reduction of the redox active reporter on these modified electrodes is diffusion controlled. However, when the target DNA or PNA–DNA duplex are present, they may strongly adsorb onto the electrode surface, which makes the conclusion based on the response to [Fe(CN)₆]^{3–/4–} not applicable.

By employing 50 nM AQ-PNA–DNA hybrids on 0.26% PQDMAEMA-modified SPCE, the optimal SWV parameters including frequency 40 Hz, step potential 0.0075 V and amplitude 100 mV were identified (Fig. S14, S1). At 50 nM AQ-PNA probe concentration, the measured SWV signal showed a logarithmic relationship with the concentration of complementary DNA (Dcomp) (Fig. 2A). The calibration curve exhibited a linear range between 0.35 and 50 nM of DNA (log scale) with $R^2=0.9757$ (Fig. 2B). At high concentrations of DNA, the signal decreased (at 350 nM, the signal was approximately 50% of the maximum signal at 50 nM) which can be explained by a competitive adsorption of the excess unhybridized DNA (vide infra, Section 3.6). The limit of detection (LOD), as calculated from 3 times the ratio between the standard deviation of the blank signal and slope of the calibration graph was 0.13 nM (130 pM). The single mismatched DNA target (DsmC) yielded signals that are indistinguishable from the background at all concentrations tested. The sub-nanomolar LOD are comparable to other non-amplified electrochemical DNA detection platforms that employ covalently-labeled redox-active probes [11,53], see also Table 2. The small sample volume required (20 μ L) means that the total amount of detectable DNA sample is small (LOD < 10 fmol or < 1 ng for 300nt ssDNA). This is considerably better than the detection limit obtained from the PAH-modified ITO electrode by Luo et al. (40 fmol) [39]. Although not the best by electrochemical detection standard, this level of sensitivity is better than what can be achieved by optical dyes commonly used in gel staining (1–50 ng of DNA), and is more than sufficient for detection of real DNA samples obtained from PCR or other suitable amplification methods. Moreover, the quantity of the probe required for each measurement (50 nM, 20 μ L or 1 pmol) was also

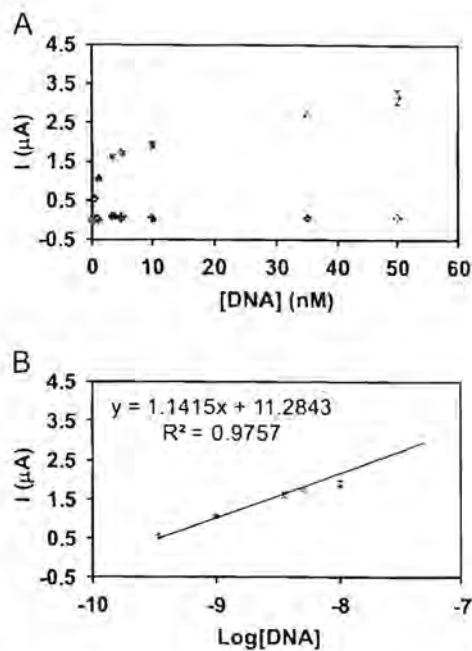


Fig. 2. (A) Scan of linear range of AQ-PNA (50 nM) after addition of complementary DNA (blue) and non-complementary DNA (red) at 0.1, 0.35, 1, 3.5, 5, 10, 35 and 50 nM (total volume = 20 μ l in 10 mM Tris-HCl buffer pH 8.0) on PQDMAEMA-modified SPCE (polymer content 0.26% in the carbon ink composition before screening) under optimized conditions (frequency 40 Hz, step potential 0.075 V, amplitude 0.100 V) (B) same as (A), but the concentrations were expressed in log scale. For interpretation of the references to color in this figure legend, the reader is referred to the web version of this article.

much smaller than the typical concentration required for probe immobilization (μ M range), and the hybridization and the measurement take only a few minutes to complete.

It should be noted that the sensor exhibits satisfactory reproducibility. Since the screen-printed carbon electrodes employed are disposable type, only the electrode-to-electrode reproducibility was calculated at 50 nM AQ-PNA probe and two concentrations of DNA at low and high ends of the linearity range (3.5 nM and 35 nM). The percent relative standard deviations (RSD) of 9.06% and 8.50% were obtained at 3.5 and 35 nM DNA, respectively.

3.5. Specificity of AQ-PNA probe

Specificity is one of the most important aspects in DNA sequence detection. The specificity of this new immobilization-free PNA-based platform was investigated with several DNA targets containing a single base mismatch in the sequence at various positions. From Fig. 3, it is clear that the developed DNA sensing platform exhibits excellent specificity without the requirement for elevated temperature [39], addition of organic co-solvents [56], or more elaborated design [57]. The signal was observed only with complementary DNA and the mismatched DNA DsmA11 carrying a single base mismatched at the 3'-end of the strand. This is not unexpected considering the small difference in stabilities of complementary and terminal mismatched hybrids [58]. All other single base mismatched DNA targets gave virtually no detectable signal, hence it is important to design the probe that include the hotspot towards the middle of the sequence for single mismatch discrimination purposes. The high specificity of the sensor can be attributed to the high specificity of the pyrrolidiny PNA probe (acpcPNA) used. The large difference in stability ($\Delta T_m = 22$ °C, see Table 1) means that the mismatched PNA-DNA hybrid is much less stable than the complementary hybrid, and therefore cannot

Table 2
Comparison of performance of the present work with previous works.

| Electrode ^a | Probe ^b | Detection | Linear range | Detection limit | References |
|-----------------------------|--|---|--|--------------------------|------------|
| ITO | 19nt Fe-labeled PNA (non-immobilized) | DIV | 0.25×10^{-6} – 2×10^{-6} M | 0.25×10^{-6} M | [10] |
| PAH/ITO | 19nt Fe-labeled PNA (non-immobilized) | DIV | 20×10^{-9} – 100×10^{-9} M | 20×10^{-9} M | [8] |
| ITO | 11nt Fe-labeled PNA and 47nt hairpin-forming oligonucleotide (non-immobilized) | DIV (with DNA polymerase-assisted target recycling) | 0.1×10^{-9} – 20×10^{-9} M | 0.1×10^{-9} M | [27] |
| ITO | 28nt MB-labeled hairpin DNA oligonucleotide (non-immobilized) | DIV (with Exonuclease III-assisted target recycling) | 20×10^{-12} – 0.3×10^{-9} M | 20×10^{-12} M | [6] |
| ITO | 37nt Fe-labeled hairpin DNA oligonucleotide (non-immobilized) | DIV (with Exonuclease III-assisted autocatalytic target recycling) | 0.1×10^{-12} – 0.1×10^{-9} M | 0.1×10^{-11} M | [9] |
| AuF | 77nt Fe-labeled hairpin DNA oligonucleotide with streptavidin aptamer region (non-immobilized) | SWV (with polymerase/melting-induced isothermal signal amplification) | 5×10^{-12} – 10^{-4} M | 2.56×10^{-10} M | [5] |
| ITO/p-phenylenediamine)-AuF | 9–12nt unlabeled acpcPNA (immobilized) | Capacitive | 1×10^{-12} – 1×10^{-8} M | 0.2×10^{-12} M | [6] |
| Chitosan-modified SPCE | 14nt AQ-labeled acpcPNA (immobilized) | SWV | 0.02×10^{-12} – 12×10^{-6} M | 4×10^{-9} M | [36] |
| PQDMAEMA-modified SPCE | 11nt AQ-labeled acpcPNA (non-immobilized) | SWV | 0.35×10^{-7} – 35×10^{-8} M | 0.13×10^{-6} M | this work |

^a AuF = gold electrode; ITO = indium tin oxide; SPCE = screen print carbon electrode.

^b Fe = ferrocene; MB = methylene blue; AQ = anthraquinone.

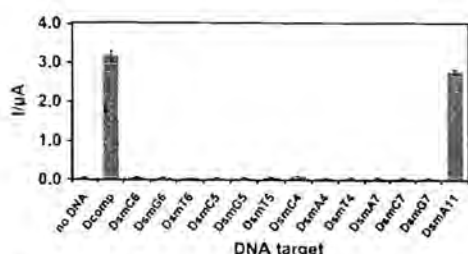


Fig. 3. Specificity test of AQ-PNA (50 nM) with various mismatched DNA (50 nM) in 10 mM Tris-HCl buffer (pH 8.0) under optimized conditions.

efficiently form and be adsorbed by the positively charged electrode. The excellent mismatch discrimination of acpCPNA had been repeatedly demonstrated in prior publications [31–36,38].

3.6. Effects of excess target and non-target DNA

Since both unhybridized and hybridized DNA are negatively charged and can be electrostatically adsorbed by the electrode, any DNA detection platforms that rely on the differential adsorption DNA and PNA–DNA hybrids onto the electrode are subjected to interference by competitive adsorption of free DNA that may result in decreased signal [39]. In the case of complementary DNA target, the signal does decrease when the concentration of the DNA exceeds that of the probe (Section 3.4). In principle, one could solve this problem by increasing the probe concentration in order to avoid the situation of having excess of target DNA over the probe. Next, the effect of non-complementary DNA target was investigated. When non-complementary DNA was added into the solution in 1, 10 and 100 folds relative to the complementary DNA, it competes with the PNA–DNA hybrids in adsorption to the electrode as shown by the decreased electrochemical signals. Nevertheless, a clear signal could still be observed at the amount of non-complementary DNA as high as 100 times to that of the complementary DNA. It should be noted that in all cases, the non-complementary DNA does not contribute to the electrochemical signal even at high concentrations (Fig. 4). The negative effect due to high concentration of unhybridized DNA was also observed in Luo's work [39], which was so pronounced that the signal decreased to <20% in the presence of 10 equiv. of non-complementary DNA, and almost completely disappeared at 15 equiv. Our sensor is less sensitive to the interference by the non-target DNA, about 50% and 20% of the signal relative to the maximum was retained at 10 and 100 equiv., respectively (Fig. 4). In addition, the possible interferences by proteins were studied using bovine serum albumin (BSA) as a model protein. It was observed that more than 90% of the PNA–DNA signal was retained at BSA concentrations of 0.7% or less. However, at high concentrations of BSA, the signal was suppressed considerably (Fig. S15, S1). Nevertheless, these potential interferences by excess of DNA and proteins should

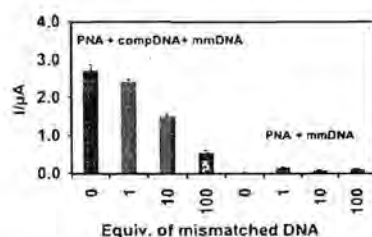


Fig. 4. Effects of non-target DNA to the signal of PNA and complementary PNA–DNA hybrid; concentrations: PNA=50 nM, complementary DNA (Dcomp)=50 or 0 nM and non-target DNA (Dsmc)=0, 50, 500 and 5000 nM (0, 1, 10 and 100 equiv.) in 10 mM Tris-HCl buffer (pH 8.0) under optimized conditions.

not negatively affect the analysis of amplified DNA samples, which contain predominantly the DNA target of interest in nanomolar concentration ranges (see Section 3.5).

3.7. Effects of long and duplex target DNA

The situation for detection of real DNA samples will be significantly different from the proof-of-principle experiments above because real DNA samples are usually much longer than the probe and exist as a duplex. The ability of this platform to detect long and duplex DNA targets was therefore investigated. A single stranded 19bp DNA target (ssDcomp19) having a central region that is complementary to the AQ-PNA probe gave comparable signal to the short DNA target, suggesting that the extra hanging part in the DNA strand does not interfere with the detection (Fig. S16A and B, S1). The electrochemical signal was still observed with the duplex DNA target (dsDcomp19) formed by annealing ssDcomp19 and its complementary DNA strand. However, longer times are required for the signal to reach maximum (10 and 20 min in the absence and presence of 100 mM NaCl, respectively). To improve the PNA–DNA binding kinetics, the DNA duplex and PNA was mixed and heated to 90 °C and cooled down, after which the maximum signal was reached immediately. No signals were observed in the analogous experiment carried out with single and double stranded DNA target containing a mismatched base (dsDsmc19), thus confirming the high specificity of the PNA probe (Fig. S16C, S1).

3.8. Detection of real DNA samples

In detection of real DNA samples, the DNA extracted from the shrimp was first amplified by LAMP [44]. This technique was chosen because it offers several advantages over PCR including high specificity, larger amplification factor and the ability to operate at a constant temperature (no need for thermal cycling). The LAMP samples were mixed with the probe before denaturation by heating to 90 °C before cooling down. As shown in Fig. 5A and B, a clear signal was observed with the WSSV-positive sample and not

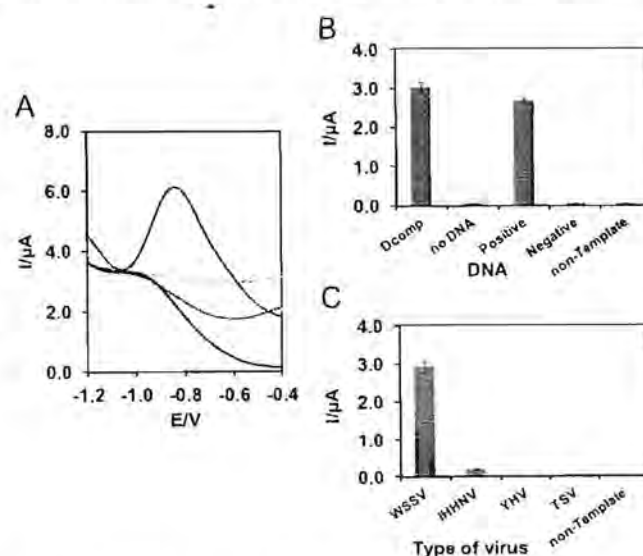


Fig. 5. Comparison of SWV signals [(A) raw data, (B) bar graph] obtained from detection of various LAMP-amplified WSSV samples: positive (orange), negative (pink), non-template control (green), synthetic complementary DNA (Dcomp, red), no DNA (blue) and (C) specificity test for WSSV among other samples including non-template control, IHNV, YHV and TSV. (For interpretation of the references to color in this figure legend, the reader is referred to the web version of this article.)

Table 3
Comparison of detection limit of this work with other WSSV detection methods.

| DNA amplification | Detection | Detection limit | References |
|--|-------------------------------------|-----------------|------------|
| PCR | Gel electrophoresis (EtBr staining) | 100 pg | [94] |
| Nested PCR | Gel electrophoresis (EtBr staining) | 100 fg | [95] |
| LAMP | Gel electrophoresis (EtBr staining) | 1 fg | [96] |
| Real-time LAMP | Turbidity | 100 copies | [97] |
| LAMP | Fluorescence (FRET probes) | 100 copies | [98] |
| LAMP | Colorimetric (gold nanoparticles) | 200 copies | [92] |
| Real time, isothermal recombinase polymerase amplification | Fluorescence (SYBR green) | 5 copies | [99] |
| Insulated isothermal PCR | Fluorescence (TaqMan probe) | 10 copies | [100] |
| LAMP | Electrochemical (PNA probe/SPCE) | 10 copies | This work |

with the negative samples and non-template DNA control.

The specificity of the DNA detection was further studied by comparison of the signals of LAMP samples obtained from various types of shrimp virus including IHNV, YHV, and TSV. The results suggested that this PNA-based sensor is highly specific and can unambiguously differentiate WSSV from other types of virus (Fig. 5C). Finally, the sensitivity test suggested that in combination with LAMP technique as low as 10 copies of WSSV DNA in the sample could be readily detected (Fig. S17, S1). This level of sensitivity is competitive with other PCR and LAMP-based WSSV DNA assays with optical detection (Table 3). Therefore, the new technique shows a great promise in high throughput analysis of DNA samples.

4. Conclusions

An immobilization-free miniaturized electrochemical platform for DNA sequence detection based on anthraquinone-labeled pyrrolidiny peptide nucleic acid (AQ-PNA) probe was successfully developed. The working principle involves a differential electrostatic adsorption between PNA and PNA-DNA hybrids onto a screen-printed carbon electrode modified with a positively-charged polymer (PDMAEMA) that result in a positive signal only when the AQ-PNA is hybridized with the complementary DNA target. Although the same basic principle has been reported and implemented in previous works, the combination of pyrrolidiny PNA probe and PDMAEMA-modified screen print carbon electrode for DNA detection in an immobilization-free format is previously unreported. Hence, the ability of the developed DNA sensing platform to exhibit an excellent specificity in discriminating of complementary DNA from various non-complementary, including single-mismatched, DNA targets with a sub-nanomolar detection limit, and its applications in sensitive detection of real DNA samples should be considered as a significant achievement. The immobilization-free procedure means that there is no extra probe immobilization step that is time-consuming (several hours) and requires large excess of probes (usually in the μM range) [15,34]. The amount of probe required for each measurement in this immobilization-free system is very small (1 pmol or less), which compensates for its disposable nature. In addition to the performance, this DNA sensing platform offers significant advantages when compared to other related DNA sensing platforms in terms of operational simplicity, costs and portability. However, one limitation that requires further improvement is the inability to reuse the electrode due to potential loss of the water-soluble linear polymers upon washing, which could be solved by using more highly cross-linked polymers. Another additional limitation is the signal suppression by competitive adsorption of DNA and proteins at high concentrations which could complicate the DNA analysis in the presence of large excess of such interferences. Even with such limitations, the developed sensor was successfully used in

combination with LAMP for a rapid and specific detection of WSSV from shrimp DNA with a higher sensitivity than gel- or fluorescence-based detection.

Acknowledgments

The authors would like to acknowledge financial supports from the Thailand Research Fund (DPC5780002) and Center of Innovative Nanotechnology (CIN). We also gratefully acknowledge Dr. Voravee Hoven and Miss Pornpen Sae-ung for kindly providing the PDMAEMA samples.

Appendix A. Supplementary material

Supplementary data associated with this article can be found in the online version at <http://dx.doi.org/10.1016/j.talanta.2015.08.059>.

References

- [1] P.S. Elena, J.P. Kalojanov, E. Glynova, P.C. Ioannou, I.S. Christopoulos, *Anal. Bioanal. Chem.* 292 (2005) 347–355.
- [2] A. Palchetti, M. Mascini, *Analyst* 134 (2005) 846–851.
- [3] K. Glynova, P.C. Ioannou, I.S. Christopoulos, *J. Electroanal. Chem.* 75 (2003) 4155–4160.
- [4] V. Gubala, J.F. Harris, A.J. Kintz, M.X. Tan, G.L. Williams, *Sens. Actuators B* 2014, 467–475.
- [5] X. Mao, Y. Ma, A. Zhang, J. Zhang, *J. Phys. Chem. Anal. Chem.* 81 (2009) 1660–1668.
- [6] S. Luo, M. Hsing, *Analyst* 134 (2009) 1957–1964.
- [7] K.C. Frongia, J. Canciani, V. Scudorotto, *J. Nanosci. Nanotechnol.* 14 (2014) 378–385.
- [8] M.I. Pividori, A. Merino, S. Alegret, *Sensory Bioelectron.* 15 (2002) 209–302.
- [9] J.C. Drummond, M.C. Hill, J.K. Butler, *Anal. Biochem.* 10 (2003) 1192–1195.
- [10] J. Lucarelli, G. Marrazza, S.P. Tomas, M. Mascini, *Sensory Bioelectron.* 15 (2004) 519–530.
- [11] B. de Boer, A. Alegria, M. J. Lopez, E. Garcia, A.J. Miranda-Olivares, P. Gomez-Blanco, *Anal. Bioanal. Chem.* 378 (2004) 102–110.
- [12] P. Shi, Y. Xu, *J. Electroanal. Chem.* 600 (2006) 200–207.
- [13] R.Y. Liu, E.J. Logoff, S.H. Lee, P.J. Yeh, *SSV sensor for detection and detection of SSV*, *Accel. Sci. USA* 102 (2006) 0607–0621.
- [14] J. Tabuda, A.M.O. Brett, G. Ferragone, M. Eça, M. Marques, A. Costa, J. B. Soares, J. Pawlak, J. Wang, *Prog. Appl. Chem.* 52 (2010) 1167–1183.
- [15] Y. Zhou, X. Guo, K.Y. Park, M.J. Frerking, *J. Am. Chem. Soc.* 129 (2007) 11866–11877.
- [16] A. Ali, F.I. Petropoulos, *J. Am. Chem. Soc.* 134 (2012) 14589–14597.
- [17] K. Fujami, J. Chino, K. Kodell, E.S. Perapomata, *Anal. Chem.* 82 (2010) 1594–1602.
- [18] H. Cai, X. Guo, Y. Jiang, P. Li, Y. Long, *Anal. Bioanal. Chem.* 278 (2005) 187–192.
- [19] N. Zhu, Z. Chang, P. He, Y. Peng, *Anal. Chem.* 81 (2009) 21–24.
- [20] A. Fredoni, F. Papakonstantinou, H. Sauerbrey, M. Molinari, H. Grosse, *Electrochim. Acta* 52 (2007) 511–517.
- [21] G. Liu, Y. Wang, Y. Guo, J. Zhang, J. Wang, S. Wang, C. Han, *J. Appl. Chem. Sci.* 30 (2008) 6820–6825.
- [22] H. Fan, Y. Xu, Z. Chang, B. King, G. Yuan, P. He, Y. Long, *Sensory Bioelectron.* 26 (2011) 2655–2659.
- [23] C. Xu, H. Guo, P.G. Ho, Y.Z. Tang, *Analyst* 136 (2011) 97–105.
- [24] M. Yoneyama, J. Furukawa, M. Ueda, T. Ando, H. Shimizu, S. Wakayama, *J. Electroanal. Chem.* 537 (2002) 103–110.

- [25] S. Hasan, E. Tamaya, *Electrochem. Commun.* 6 (2004) 527–543.
- [26] X. Luo, I.M. Hung, *Electrochem. Commun.* 13 (2011) 742–745.
- [27] F. Xian, X. Luo, I.M. Hung, *Anal. Chem.* 84 (2012) 5216–5220.
- [28] F.X. Xian, I.M. Hung, *Biosens. Bioelectron.* 35 (2012) 230–234.
- [29] C. Boinnes, M. Moreno, *Anal. Bioanal. Chem.* 402 (2012) 3071–3069.
- [30] C. Vilavon, C. Srisuwanakiet, C. Anandhanawat, C. Suparpprom, J. Kawakami, Y. Toraguchi, Y. Tanaka, T. Vilavon, *Artif. DNA: PNA XNA 2* (2011) 50–59.
- [31] T. Vilavon, *C. Srisuwanakiet, Org. Lett.* 9 (2006) 1897–1899.
- [32] T. Vilavon, *Act. Chem. Res.* 48 (2015) 1645–1656.
- [33] C. Anandhanawat, T. Vilavon, V.P. Hoven, K. Su, *Biosens. Bioelectron.* 25 (2010) 1064–1069.
- [34] W. Jitrongrakul, I. Vilavon, C. Vilavon, S. Watchasi, C. Sukjai, W. Ngendee, W. Anungmatrepporn, T. Tuntulan, *Talanta* 105 (2013) 1–7.
- [35] S. Sankoh, S. Samanman, O. Thipmanee, A. Numnuam, W. Limbui, P. Kanatharana, I. Vilavon, P. Thavarungkul, *Sens. Actuators B* 177 (2013) 543–550.
- [36] O. Thipmanee, S. Samanman, S. Sankoh, A. Numnuam, W. Limbui, P. Kanatharana, I. Vilavon, P. Thavarungkul, *Biosens. Bioelectron.* 38 (2012) 435–438.
- [37] S. Sompas, W. Monsawa, N. Redhngkam, W. Sangproh, P. Yimatsaneerit, T. Vilavon, D. Chailapakul, *Biosens. Bioelectron.* 54 (2014) 128–134.
- [38] K. Kermar, M. Vestergaard, N. Nagatani, Y. Takamura, E. Tamaya, *Anal. Chem.* 78 (2006) 2182–2189.
- [39] B. Boontha, J. Nakkamud, N. Hirankarn, P. Champluk, T. Vilavon, *Anal. Chem.* 80 (2008) 5178–5189.
- [40] X. Luo, T.H. Lee, I.M. Hung, *Anal. Chem.* 80 (2008) 7341–7346.
- [41] X. Luo, I.M. Hung, *Electroanalysis* 21 (2009) 1557–1561.
- [42] X. Luo, I.M. Hung, *Biosens. Bioelectron.* 25 (2009) 803–808.
- [43] C.M. Pineda-Sorolla, V. Alday-Sanz, M. Wille, P. Sorgeloms, M.S. Priovett, H. J. Sawynck, *J. Fish Dis.* 31 (2009) 1–18.
- [44] E. Khaled, H.N.A. Hassan, A. Girgis, R. Metelka, *Talanta* 77 (2008) 737–743.
- [45] T. Notomi, H. Okayama, H. Masubuchi, T. Yonekawa, K. Watanabe, N. Arino, T. Hori, *Nucleic Acids Res.* 28 (2000) e63.
- [46] http://www6.appliedbiosystems.com/support/tutorials/pdf/jpjpant_low.pdf, accessed 27.07.14.
- [47] I.M. Nunn, D.V. Lightner, *J. Virol. Methods* 171 (2011) 316–321.
- [48] E.F. Fritsch, E. Manias, *Molecular Cloning, A Laboratory Manual* 2nd ed., Cold Spring Harbor Laboratory Press, Plainview, New York, 1989.
- [49] S. Rujmota, M. Watanabe, N. Kawakami, M. Nakamura, K. Yamada, *Bioconjugate Chem.* 19 (2008) 65–69.
- [50] M.T. Tiemeij, M.W. Grinstaff, *J. Org. Chem.* 65 (2000) 5255–5257.
- [51] J. Wang, M. Pedersen, H. Sakstad, O. Hammerich, *J. Purification Analyt.* 121 (1996) 345–350.
- [52] E. Khaled, H.N.A. Hassan, H.H. Habib, R. Metelka, *Int. J. Electrochem. Sci.* 5 (2010) 158–167.
- [53] W. Cao, C. Easley, J.B. Ferrience, J.P. Landers, *Anal. Chem.* 78 (2006) 7222–7228.
- [54] M. Lavezzi, S. Bedout, *Anal. Bioanal. Chem.* 405 (2013) 3705–3716.
- [55] S. Liu, Y. Liu, J. Wang, J. Liu, C. Cheng, W. Wei, B. Tang, *Anal. Chem.* 86 (2014) 4004–4015.
- [56] J. Zhuang, D. Tang, W. Lai, G. Chen, H. Yang, *Anal. Chem.* 86 (2014) 8600–8607.
- [57] A.K. Lau, X. Su, K.M.M. Au, *Biosens. Bioelectron.* 24 (2009) 1717–1722.
- [58] M. Inoue, R. Suda, M. Takase, T. Tsuji, *J. Clin. Proc. Natl. Acad. Sci. USA* 102 (2005) 11606–11610.
- [59] G.J. Igler, *Proc. Natl. Acad. Sci. USA* 89 (1992) 8562–8567.
- [60] T. Kono, R. Sawai, M. Sakai, T. Itano, *J. Virol. Methods* 115 (2004) 39–45.
- [61] T. Mekata, R. Sudhakara, T. Kono, K. Supamattaya, M. I. Lim, M. Sakai, T. Itano, *Int. Appl. Microbiol.* 48 (2009) 25–32.
- [62] P.H. Chou, Y.C. Lin, P.H. Teng, C.L. Chen, F.Y. Lee, *J. Virol. Methods* 77 (2011) 67–74.
- [63] S. Seetang-Nua, W. Jareonvan, S. Sittaratana, K. Suebnog, W. Kitpathonchai, *Mol. Cell. Probes* 27 (2013) 71–79.
- [64] X. Xia, Y. Yu, M. Weidmann, Y. Pan, S. Yan, Y. Wang, *PLoS One* 9 (2014) e104667.
- [65] Y.-L. Tsai, H.-J. Wang, H.-C.G. Chang, C.-H. Tsai, K.-K. Lin, B.-H. Jeng, C.-S. C. Jeng, P.-Y. Lee, *PLoS One* 7 (2012) e45278.

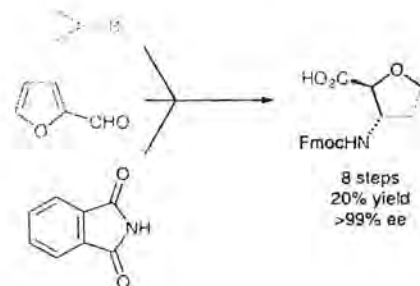
Synthesis of a Tetrahydrofuranyl β -Amino Acid for Peptide Nucleic Acid Construction

Roderick W. Bates^{a*}
Tirayut Vilalvan^b
Suryavanshi Padmakar Apparao^a
Tu Thanh Ho^a

^a Division of Chemistry and Biological Chemistry, School of Physical and Mathematical Sciences, Nanyang Technological University, 21 Nanyang Link, 637371, Singapore
roderick@ntu.edu.sg

^b Organic Synthesis Research Unit, Department of Chemistry, Faculty of Science, Chulalongkorn University, Phayathai Road, Patumwan, Bangkok 10330, Thailand

Dedicated to Professor Steven Ley on the occasion of his 70th birthday



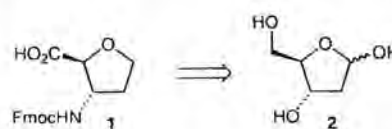
Received: 21.08.2015
Accepted after revision: 13.09.2015
Published online: 13.10.2015
DOI: 10.1055/s-0035-1560649; Art ID: st-2015-d0655-1

Abstract A tetrahydrofuranyl β -amino acid has been prepared by using the asymmetric dihydroxylation of a furyl alkene to establish the stereochemistry. The furan moiety was employed as a carboxylic acid surrogate.

Key words amino acid, tetrahydrofuran, dihydroxylation, oxidation, furan

β -Amino acids have gained in importance as building blocks in bio-organic chemistry over the last few decades with the realisation that they offer advantages over the traditional α -amino acids.¹ The peptides resulting from such novel amino acids have been studied for diverse reasons. These include the effect on peptide structure, such as folding properties,² and on function, as well as their use in peptide nucleic acids (PNA).³ Indeed, certain PNAs, especially those using unnatural amino acids, can bind more strongly to the complementary strand of DNA than DNA itself. Studies on such systems, and their applications are, naturally, constrained by the availability of such amino acids. Recently, one of our laboratories reported the use of a PNA containing the novel tetrahydrofuranyl β -amino acid **1**.^{3b,4} This compound, in an N-protected/C-activated form, was synthesised in 11 steps from, appropriately, 2-deoxyribose **2** (Scheme 1). The use of carbohydrates as chiral starting materials (the 'chiron approach') can be enormously effective;⁵ on the other hand, the synthetic scheme may become encumbered with multiple functional group transformations. In this instance, we speculated that a synthesis from achiral, noncarbohydrate starting materials, taking advantage of asymmetric dihydroxylation (AD),⁶ might prove advantageous. The core of the strategy was to employ dihydroxylation of a furyl alkene,⁷ bearing a homoallylic leaving group,

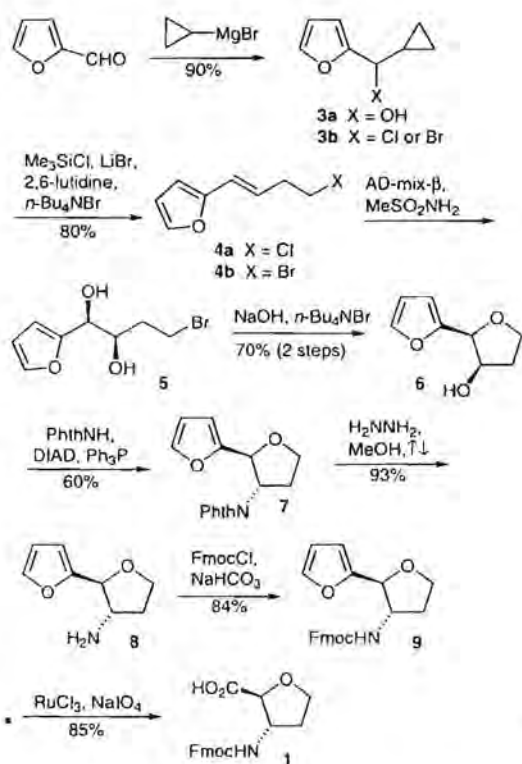
to form the tetrahydrofuran, with the furyl group acting as a carboxylic acid surrogate. We anticipated that the presence of the furyl group would be advantageous for the dihydroxylation.



Scheme 1 THF β -amino acid **1** from deoxyribose **2**

Alkene **4** was prepared by nucleophilic ring opening of cyclopropyl alcohol **3a**, a reaction originally developed by Julia et al.⁸ Alcohol **3a** is readily available by the addition of cyclopropyl magnesium bromide to 2-furaldehyde (Scheme 2).

Ring-opening substitution with hydrochloric acid in a variety of solvents gave modest yields of the desired chloride **4a** (Table 1, entries 1–3). Use of magnesium bromide⁹ also gave modest yields of the corresponding bromide **4b** but, in most cases, the product was contaminated with the direct substitution product **3b** (entries 4 and 5). The use of either lithium bromide or lithium chloride in diethyl ether at reflux resulted in no reaction. The use of zinc chloride gave predominantly the direct substitution product, with only a trace of ring opening (entry 6). Ultimately, the use of a combination of trimethylsilyl chloride and lithium bromide was found to be effective, giving bromide **4b** in 80% yield.^{10,11} Running this reaction in the presence of 2,6-lutidine as a Brønsted acid scavenger, and tetra-*n*-butylammonium bromide (TBAB) as a phase-transfer catalyst gave the cleanest product. Notably, even though chloride is present, the product was exclusively obtained as the bromide **4b**.

Scheme 2 Synthesis of THF β -amino acid 1

Dihydroxylation of bromide **4b** was achieved by using AD-mix- β , with the addition of methane sulfonamide¹² and an extra amount of potassium osmate. Interestingly, the product bromodiol **5**, did not cyclise in situ despite the basicity of the AD conditions. Further exposure to hydroxide under phase-transfer conditions was required to ensure cyclisation. The enantiomeric excess of the resulting tetrahydrofuran **6** was determined at a later stage. To introduce the nitrogen atom of the amino group, we initially tried to form the corresponding mesylate, but without success. Applica-

tion of the Rollin modification of the Mitsunobu reaction using the bis-pyridine complex of zinc azide gave none of the desired product and returned the starting alcohol **6**.¹³ The Mitsunobu reaction with phthalimide, however, proceeded smoothly to give the desired phthalimide **7**.¹⁴ We speculate that the zinc-activated diisopropyl azodicarboxylate (DIAD)-triphenylphosphine adduct was too bulky to react with the relatively hindered secondary alcohol. The proton-activated adduct is, in contrast, sufficiently reactive. At this point, the enantiomeric excess of the material could be determined by chiral HPLC analysis, and was found to be >99%. The structure of phthalimide **7** was also confirmed by X-ray crystallographic analysis (Figure 1),¹⁵ demonstrating the clean inversion during the Mitsunobu reaction.¹⁶ The phthaloyl group could then be removed by hydrazinolysis in the traditional way and amine **8** was reprotected as its Fmoc derivative **9**. Finally, oxidative destruction of the furyl moiety using ruthenium(VIII) oxide generated in situ^{17,18} gave carboxylic acid **1**, which was suitable for use in PNA synthesis or other synthetic applications.

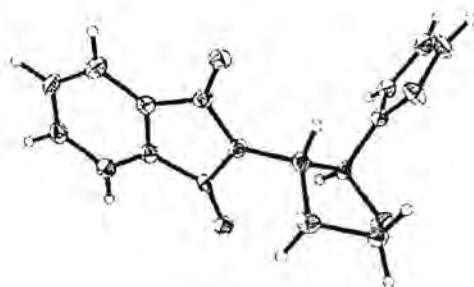


Figure 1 ORTEP structure of phthalimide 7

In conclusion, vinyl furan dihydroxylation has provided a more efficient access to the title compound, and the approach should be applicable to related β -amino acids. The overall sequence from furfuraldehyde consists of eight steps and has an overall yield of 20%.

Table 1 Ring-Opening-Substitution of Cyclopropyl Alcohol **3a**

| Entry | Reagent | Conditions | Product | Yield (%) |
|-------|--|--|-----------|--------------------|
| 1 | aq HCl | Et ₂ O, r.t. | 4a | 45 ^a |
| 2 | aq HCl | dioxane, r.t. | 4a | 19 ^a |
| 3 | aq HCl | CH ₃ CN, r.t. | 4a | 50 |
| 4 | MgBr ₂ | Et ₂ O, reflux | 4b | 34 ^b |
| 5 | MgBr ₂ | Et ₂ O, 0 °C | 4b | 30 ^a |
| 6 | ZnCl ₂ | CH ₂ Cl ₂ , reflux | 4a | trace ^c |
| 7 | Me ₃ SiCl, LiBr, 2,6-lutidine, TBAB | CH ₂ Cl ₂ , r.t. | 4b | 80 |

^a The direct substitution product **3b** was also obtained.

^b Addition of MgO as a Bronsted acid scavenger had no effect on the yield.

^c The direct substitution product **3b** was formed predominantly (67%).

Acknowledgment

R.W.B., S.P.A. and T.T.H. thank NTU for financial support of this work. T.V. acknowledges financial support from the Thailand Research Fund (DPGS780002).

Supporting Information

Supporting information for this article is available online at <http://dx.doi.org/10.1055/s-0035-1560649>.

References and Notes

- (1) (a) Seebach, D.; Beck, A. K.; Capone, S.; Deniau, G.; Grosej, U.; Zass, E. *Synthesis* **2009**, 1. (b) Seebach, D.; Matthews, J. L. *Chem. Commun.* **1997**, 2015.
- (2) (a) Cheng, R. P.; Gellman, S. H.; DeGrado, W. F. *Chem. Rev.* **2001**, *101*, 3219. (b) Vasudev, P. G.; Chatterjee, S.; Shamala, N.; Balaram, P. *Chem. Rev.* **2011**, *111*, 657. (c) Pandey, S. K.; Jogdand, G. F.; Oliveira, J. C. A.; Mata, R. A.; Rajamohanan, P. R.; Ramana, C. V. *Chem. Eur. J.* **2011**, *17*, 12946.
- (3) (a) Vilaivan, T. *Acc. Chem. Res.* **2015**, *48*, 1645. (b) Sriwarom, P.; Padungros, P.; Vilaivan, T. *J. Org. Chem.* **2015**, *80*, 7058; see also ref. 2c.
- (4) Rjabovs, V.; Turks, M. *Tetrahedron* **2013**, *69*, 10693.
- (5) Hanessian, S. *Total Synthesis of Natural Products: The 'Chiron' Approach*; Pergamon: Oxford, **1983**.
- (6) Kolb, H. C.; VanNieuwenhze, M. S.; Sharpless, K. B. *Chem. Rev.* **1994**, *94*, 2483.
- (7) (a) Harris, J. M.; Keränen, M. D.; Nguyen, H.; Young, V. G.; O'Doherty, G. A. *Carbohydr. Res.* **2000**, *328*, 17. (b) Takeuchi, M.; Taniguchi, T.; Ogasawara, K. *Synthesis* **1999**, 341. (c) Harris, J. M.; Keränen, M. D.; O'Doherty, G. A. *J. Org. Chem.* **1999**, *64*, 2982. (d) Kobayashi, Y.; Nakano, M.; Biju Kuamr, G.; Kishihara, K. *J. Org. Chem.* **1998**, *63*, 7505. (e) For the aminohydroxylation of vinylfurans, see: Bushey, M. L.; Haukaas, M. H.; O'Doherty, G. A. *J. Org. Chem.* **1999**, *64*, 2984.
- (8) (a) Julia, M.; Julia, S.; Guegan, R. *Bull. Soc. Chim. Fr.* **1960**, 1072. (b) A one-pot Grignard addition and ring-opening substitution has been reported, see: Qi, W.; Wang, P.; Fan, L.; Zhang, S. *J. Org. Chem.* **2013**, *78*, 5918.
- (9) McCormick, J. P.; Barton, D. L. *J. Org. Chem.* **1980**, *45*, 2566.
- (10) Balme, G.; Fournet, G.; Gore, J. *Tetrahedron Lett.* **1986**, *27*, 1907.
- (11) Cheskis, B. A.; Ivanova, N. M.; Moiseenkov, A. M.; Nefedov, O. M. *Bull. Acad. Sci. USSR, Div. Chem. Sci. (Engl. Transl.)* **1990**, *39*, 1839; *Izv. Akad. Nauk SSSR, Ser. Khim.* **1990**, 2025.
- (12) Sharpless, K. B.; Amberg, W.; Youssef, L. B.; Crispino, G. A.; Hartung, J.; Jeong, K.-S.; Morikawa, K.; Wang, Z.-M.; Xu, D.; Zhang, X.-L. *J. Org. Chem.* **1992**, *57*, 2768.
- (13) Viaud, M. C.; Rollin, P. *Synthesis* **1990**, 130.
- (14) (a) Mitsunobu, O. *Synthesis* **1981**, 1. (b) Hughes, D. L. *Org. Prep. Proced. Int.* **1996**, *28*, 129. (c) Simon, C.; Hosztafi, S.; Makleit, S. *J. Heterocycl. Chem.* **1997**, *34*, 349.
- (15) Details of the X-ray structure determination for compound **7** have been deposited with the Cambridge Crystallographic Database, CCDC-1408970. Copies of the data may be obtained, free of charge, on application to CCDC, 12 Union Road, Cambridge, CB2 1EZ, UK (fax: +44 1223 336033 or e-mail: deposit@ccdc.cam.ac.uk).
- (16) Inversion is also shown by the change of $J_{2,3}$ in the ^1H NMR spectrum from 4 Hz in **6** to 8.4 Hz in **7**.
- (17) (a) Carlsen, P. H. J.; Katsuki, T.; Martin, V. S.; Sharpless, K. B. *J. Org. Chem.* **1981**, *46*, 3936. (b) Plietker, B. *Synthesis* **2005**, 2453. (c) Begliomini, S.; Sernissi, L.; Scarpi, D.; Occhiato, E. G. *Eur. J. Org. Chem.* **2014**, 5448.
- (18) (+)-(2S,3S)-3-[(9H-Fluoren-9-yl)(methoxy)(carbonyl)amino]-tetrahydrofuran-2-carboxylic Acid (**1**): Ruthenium trichloride hydrate (55 mg, 0.026 mmol) was added to a solution of sodium periodate (1.98 g, 9.33 mmol) in a mixture of EtOAc (1.5 mL), CH_2CN (2 mL) and H_2O (1 mL) at 0 °C. The mixture was stirred for 15 min, then carbamate **9** (0.5 g, 1.33 mmol) in the minimum of EtOAc was slowly added. The mixture was stirred for an additional 10 min, H_2O (10 mL) was added and the mixture was extracted with EtOAc (2 × 15 mL). The combined organic layers were washed with NaHCO_3 (20 mL) and acidified with 2 M HCl then extract with EtOAc (3 × 15 mL). The combined organic phase was dried over anhydrous Na_2SO_4 and concentrated under reduced pressure to give amino acid derivative **1** (85%, 400 mg) as a colourless solid. Mp 90–92 °C; $[\alpha]_D^{25} +40$ (c 1.0, DMSO). IR (neat): 3332, 2924, 2854, 1720, 1535, 1450, 1095, 1049 cm^{-1} . ^1H NMR (500 MHz, $\text{DMSO}-d_6$): δ = 1.80–1.81 (m, 1 H), 2.07–2.11 (m, 1 H), 3.89–3.91 (m, 2 H), 4.10 (d, J = 4.0 Hz, 1 H), 4.18–4.24 (m, 2 H), 4.34 (d, J = 6.5 Hz, 2 H), 7.32–7.35 (m, 2 H), 7.41–7.44 (m, 2 H), 7.70–7.77 (m, 3 H), 7.89 (d, J = 7.5 Hz, 2 H), 12.7 (br. s, 1 H). ^{13}C NMR (100 MHz, $\text{DMSO}-d_6$): δ = 32.2, 47.1, 55.8, 65.8, 67.7, 81.4, 120.6, 125.6, 127.5, 128.1, 141.2, 144.3, 156.0, 173.2. MS (ESI $^+$): m/z = 354.3 [M + H] $^+$. HRMS: m/z [M + H] $^+$ calcd. for $\text{C}_{20}\text{H}_{20}\text{NO}_5$: 354.1318; found: 354.1341.

Clickable and Antifouling Platform of Poly[(propargyl methacrylate)-*ran*-(2-methacryloyloxyethyl phosphorylcholine)] for Biosensing Applications

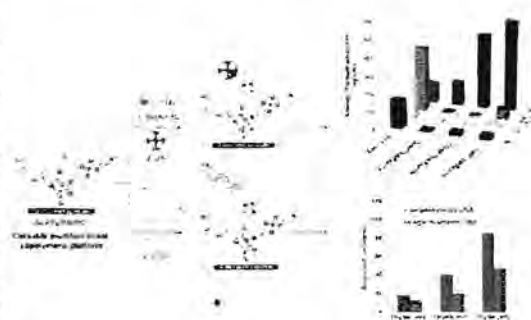
Oraphan Wiarachai,[†] Tirayut Vilaivan,[‡] Yasuhiko Iwasaki,[§] and Voravee P. Hoven^{*†}

[†]Program in Petrochemistry, Faculty of Science, and [‡]Organic Synthesis Research Unit, Department of Chemistry, Faculty of Science, Chulalongkorn University, Phayathai Road, Pathumwan, Bangkok 10330, Thailand

[§]Faculty of Chemistry, Materials and Bioengineering, Kansai University, 3-3-35 Yamate-cho, Suita-shi, Osaka 564-8680, Japan

Supporting Information

ABSTRACT: A functional copolymer platform, namely, poly-[(propargyl methacrylate)-*ran*-(2-methacryloyloxyethyl phosphorylcholine)] (PPgMAMPC), was synthesized by reversible addition-fragmentation chain-transfer polymerization. In principle, the alkyne moiety of propargyl methacrylate (PgMA) should serve as an active site for binding azide-containing molecules via a click reaction, i.e., Cu-catalyzed azide/alkyne cycloaddition (CuAAC), and 2-methacryloyloxyethyl phosphorylcholine (MPC), the hydrophilic monomeric unit, should enable the copolymer to suppress nonspecific adsorption. The copolymers were characterized using Fourier transform infrared (FTIR) and ¹H NMR spectroscopies. Thiol-terminated, PPgMAMPC-SH, obtained by aminolysis of PPgMAMPC, was immobilized on a gold-coated substrate using a "grafting to" approach via self-assembly. Azide-containing species, namely, biotin and peptide nucleic acid (PNA), were then immobilized on the alkyne-containing copolymeric platform via CuAAC. The potential use of surface-attached PPgMAMPC in biosensing applications was shown by detection of specific target molecules, i.e., streptavidin (SA) and DNA, by the developed sensing platform using a surface plasmon resonance technique. The copolymer composition strongly influenced the performance of the developed sensing platform in terms of signal-to-noise ratio in the case of the biotin-SA system and hybridization efficiency and mismatch discrimination for the PNA-DNA system.



INTRODUCTION

Effective functionalization with biomolecules is important in the development of materials for biotechnology-related applications such as biosensors, protein/cell microarrays, microfluidic devices, and tissue engineering. Polymeric platforms are becoming increasingly attractive for biomolecule immobilization because a variety of functional groups can be conveniently incorporated and proportionally customized using combinations of specific monomers in the polymerization step. The superiority of this approach, which provides a three-dimensional platform and therefore offers a higher functional group density for biomolecular probe binding per surface area than in the case of a conventional two-dimensional platform based on self-assembled monolayers (SAMs)^{1–4} of end-functionalized alkanethiols, for biosensing applications has been shown by our group^{4,5} and other researchers.^{6–9}

Most biomolecules (e.g., proteins, antibodies, enzymes, and DNA) carry carboxyl and/or amino groups. Polymers with versatile functionalities that can accommodate covalent bond formation, particularly via hydrolytically stable amide linkages, including poly[oligo(ethylene glycol) methacrylate],^{8,10,11} poly(2-hydroxyethyl methacrylate),^{12,13} and poly(acrylic acid)

(PAA),^{4,5,14–16} are therefore commonly used as platforms for biomolecule conjugation. However, an additional activation step using an appropriate coupling reagent is required for biomolecule conjugation to such polymers. PAA, in particular, suffers from nonspecific adsorption of positively charged components such as lysozyme (LYZ) because its carboxylic groups (–COOH) can be ionized to negatively charged carboxylate ions (–COO[–]).⁷ This is problematic in the analyses of complex samples. Precursor polymers have recently emerged as alternative and ready-to-use functional materials that can directly bind with designated nucleophilic modifiers such as amino-containing biomolecules, without having to undergo activation. Well-known precursor polymeric systems include polymers bearing succinimidyl ester^{17–22} or pentafluorophenyl ester groups,^{23,24} poly[propargyl (me)thacrylate] [PPg(M)A],^{25,26} and poly(glycidyl methacrylate) (PGMA).^{27,28} From the perspective of chemical robustness, PPg(M)A is a good choice because the alkynyl side group in

Received: July 23, 2015

Revised: December 8, 2015

Published: December 22, 2015

each repeat unit specifically undergoes a Huisgen 1,3-dipolar azide-alkyne cycloaddition with azide-containing molecules, or thiol-yne reactions with thiol-containing molecules; the reaction yields under mild conditions are high, and no byproducts are generated. Socaci and co-workers²⁵ prepared core-shell nanoparticles consisting of magnetite cores and poly(*O*-propargyl acrylate) shells. They showed that acryloyl-containing phosphonates or methacryloyl phosphates anchored to the magnetic nanoparticle (MNP) surfaces acted as initiating sites for polymerization of a series of alkyne-terminated acrylate monomers with different spacers between the carboxyl oxygen atom and the alkyne moiety. The ability of the alkyne moieties on MNPs to form triazole linkages via azide-alkyne cycloaddition was tested using azide-terminated biotin fluorescently labeled with dansyl groups. Wang and co-workers²⁶ successfully developed an alkyne-functionalized microporous polypropylene membrane via a combination of plasma treatment and UV-induced graft polymerization of 3-(trimethylsilyl)propargyl methacrylate. The PPgMA-modified membrane obtained after trimethylsilyl removal can directly bind with a thiol-containing carbohydrate ligand, 2,3,4,6-tetra-*O*-acetyl- β -*D*-glucopyranoside thiol, and yields a glycosylated membrane via a thiol-yne click reaction. The glycosyl density of the glycosylated membrane can be tuned based on the polymer graft density, and the membrane showed specific adsorption of lectin concanavalin A over peanut agglutinin.

Specific detection of target molecules rather than the nontargeted components or the ability to resist nonspecific adsorption, known as antifouling, is another key element in biosensor development, especially for the analysis of real biologically relevant samples in which numerous types of interference exist concurrently. A number of copolymeric platforms have therefore been designed to incorporate biocompatible and highly hydrophilic polymers along with precursor polymers. Among the developed hydrophilic polymers, zwitterionic polymers, which contain positively and negatively charged moieties within the same structure, such as poly(2-methacryloyloxyethyl phosphorylcholine) (PMPC), poly(carboxybetaine methacrylate) (PCBMA), and poly(sulfobetaine methacrylate) (PSBMA) have received growing attention for use in new-generation antifouling materials.²⁷⁻²⁹ Emmenegger and co-workers³⁰ reported that plasma protein adsorption completely suppressed on surface-immobilized PCBMA, whereas PMPC and PSBMA prevented adsorption of the main plasma proteins (human serum albumin, IgG, Fbg, and LYZ) from single-protein solutions, but could not prevent plasma deposition. In this study, based on our previous work using MPC-containing copolymer brushes between PMPC and poly(methacrylic acid) (PMA) as precursor layers for biosensor applications,¹⁴ we used PMPC as an antifouling zwitterionic polymer to prevent nonspecific adsorption. It has been proven that PMPC helps to suppress undesirable nonspecific adsorption of proteins and cells,³¹⁻³⁶ and also provides a suitable environment for preserving the stability and activity of immobilized biomolecular probes.³⁷⁻⁵⁹ Ishihara and co-workers³⁷ used monitoring with a quartz crystal balance to show that poly[2-methacryloyloxyethyl phosphorylcholine (MPC)-*co*-*n*-butyl methacrylate (BMA)-*co*-*p*-nitrophenyloxycarbonyl poly(ethylene glycol) methacrylate (MEONP)] (PMBN), adsorbed on a gold-coated substrate and conjugated with anti-C-reactive protein antibodies via nitrophenyloxycarbonyl active ester binding sites in the MEONP unit can specifically bind with the respective antigens. The developed platform simultaneously

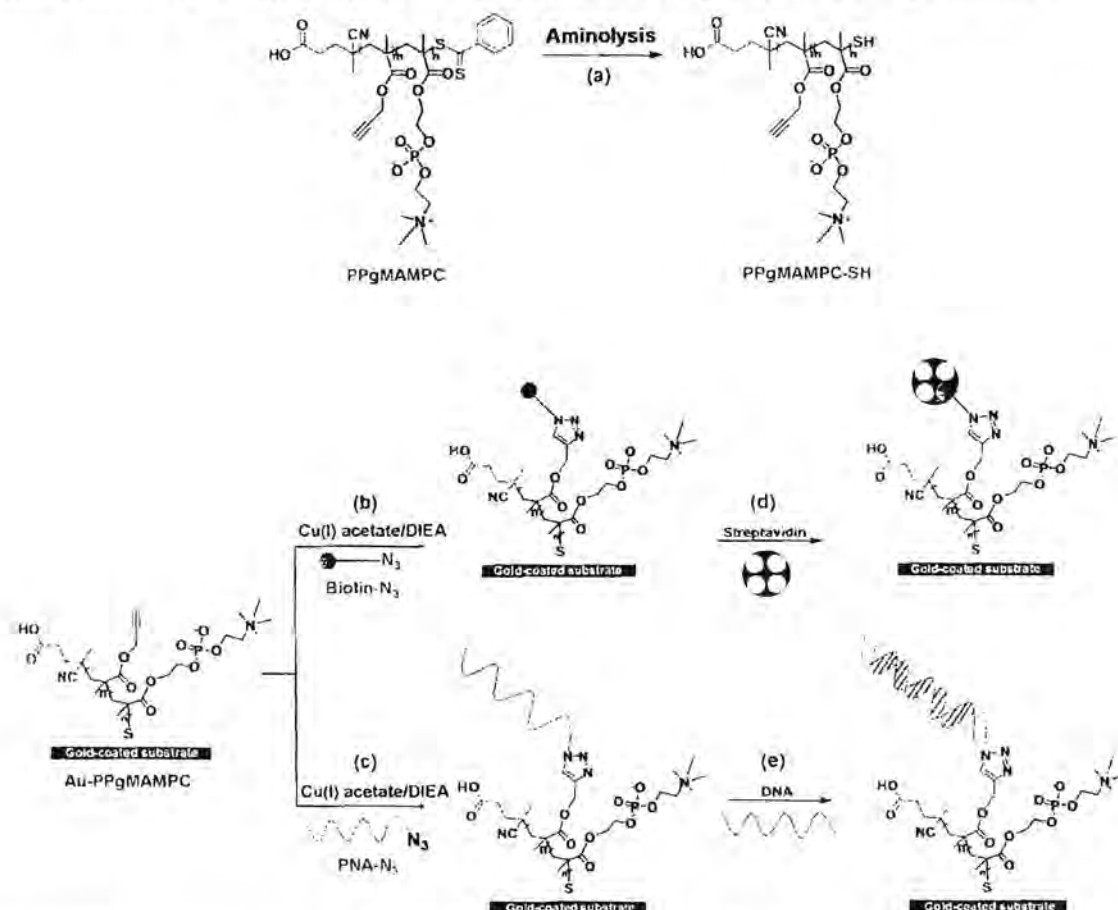
prevented adsorption of bovine serum albumin and γ -globulin. PMBN physically adsorbed on poly(methyl methacrylate) microchips and polystyrene well plates has also been used for antigen detection via ELISA-based assays, and for affinity-based protein separation when deposited on poly(L-lactic acid) nanoparticles.⁴⁰⁻⁴³ Iwata et al.⁴⁴ generated block copolymer brushes of PGMA, another precursor polymer, and PMPC via surface-initiated atom-transfer radical polymerization. An antibody fragment was conjugated to the surface-grafted copolymer brushes via a thiol-disulfide interchange reaction with pyridyl disulfide linkages, previously introduced by epoxide ring opening of GMA repeat units in the copolymer. The activity of the conjugated antibody fragment in antigen detection was better for the PMPC copolymer platform than those for platforms based on PGMA alone or epoxysilane.

Inspired by the research described above, the aim of this study was to develop a multifunctional copolymer platform based on clickable PPgMA and antifouling PMPC, a combination that, to the best of our knowledge, has never been explored. The alkyne moiety of the PgMA unit should serve as an active site for binding of azide-containing molecules via a Cu-catalyzed azide/alkyne cycloaddition (CuAAC) click reaction, without the need for activation. The hydrophilic monomeric unit, MPC, should enable the copolymer to suppress nonspecific adsorption. The copolymer poly-[(propargyl methacrylate)-*ran*-(2-methacryloyloxyethyl phosphorylcholine)] (PPgMAMPC) was first synthesized by reversible addition-fragmentation chain-transfer (RAFT) polymerization. Thiol-terminated PPgMAMPC (PPgMAMPC-SH), obtained by aminolysis of PPgMAMPC, was immobilized on a gold-coated substrate using a "grafting to" method via Au-S bond formation between the thiol end groups of the copolymer and the gold surface. Azide-containing biotin and peptide nucleic acid (PNA) were used as model probes to demonstrate the potential of the surface-attached PPgMAMPC for probe immobilization and subsequent detection of target molecules, namely, streptavidin (SA) and deoxyribonucleic acid (DNA), using a surface plasmon resonance (SPR) technique. The parameters that may affect the sensitivity and specificity, in terms of the signal-to-noise (*S/N*) ratio, in detecting SA in a complex sample using a biotin-based sensor were also investigated. The hybridization efficiency (%HE) and mismatch discrimination (%MD) for DNA detection were evaluated for the PNA-based sensor.

EXPERIMENTAL SECTION

Materials. MPC was purchased from the NOF Corp. (Japan). Methacrylic acid (MA), 4,4'-azobis(4-cyanovaleric acid) (ACVA), 4-cyano-4-(phenylcarbonothioylthio)pentanoic acid (CPADB), azide-PEG₃-biotin conjugate (biotin-N₃), copper(I) acetate, bovine serum albumin (BSA), and LYZ were purchased from Aldrich. MA was distilled under reduced pressure to remove hydroquinone monomethyl ether, a polymerization inhibitor, prior to use. Phosphate-buffered saline (PBS; pH 7.4) was purchased from Sigma. Hydrazine monohydrate and *N,N'*-diisopropylethylamine (DIEA) were purchased from Sigma-Aldrich. SA was purchased from Thermo Fisher Scientific Inc. PgMA was synthesized using the method reported by He et al.⁴⁵ DNA was purchased from the Pacific Science Co., Ltd. PNA was synthesized by solid-phase peptide synthesis on Tentagel S RAM resin (Fluka) preloaded with 9-fluorenylmethoxycarbonyl-L-lysine(*tert*-butoxycarbonyl)-pentafluorophenyl ester (Fmoc-L-lys-(Boc)-oPfp) (Calbiochem/Novabiochem Co., Ltd.) using a previously reported procedure.¹⁰ The PNA was modified at the N-terminus by reductive alkylation with N₃(CH₂)₃CHO to prepare azide-terminated PNA (PNA-N₃).¹⁷ After cleavage of PNA-N₃ from the solid support

Scheme 1. Schematic Diagram of (a) Preparation of PPgMAMPC-SH, (b,c) Immobilization of Biotin-N₃ and PNA-N₃ on PPgMAMPC-Modified SPR Chip, and (d,e) Specific Binding between Conjugated Probe and Target Molecule



using trifluoroacetic acid, the crude PNA-N₃ was purified using reverse-phase high performance liquid chromatography (HPLC) and analyzed by matrix-assisted laser desorption/ionization-time-of-flight (MALDI-TOF) mass spectrometry (Bruker Daltonik GmbH, Germany) (see Figure S1 in the supporting information for chromatogram and mass spectra). Ethylenediaminetetraacetic acid (EDTA) was purchased from Fluka. Human platelet-poor plasma was donated by a healthy volunteer. Milli-Q water was purified using an ultrapure water system with a Millipak-40 filter unit (0.22 μm , Millipore) and a Millipore Milli-Q system that involved reverse osmosis followed by ion exchange and filtration steps (18.2 M Ω). All reagents and materials were analytical grade and used without further purification unless specified.

Synthesis of Thiol-Terminated Poly[(propargyl methacrylate)-*ran*-(2-methacryloyloxyethyl phosphorylcholine)] (PPgMAMPC-SH). MPC monomer (0.59 g, 2.0 mmol), ACVA (0.7 mg, 2.5 μmol), and CPADB (5.6 mg, 20 μmol) were dissolved in 2 mL of an ethanol/tetrahydrofuran (EtOH:THF) (1:1 v/v) mixture. PgMA (0.25 mL, 2.0 mmol) was added to the solution under magnetic stirring. The clear pink solution was purged with nitrogen gas for 30 min and then immersed in an oil bath at 70 $^{\circ}\text{C}$, and polymerization was performed for a set reaction time. The reaction was terminated in an ice bath. The resulting PPgMAMPC was purified, using a dialysis membrane (molecular weight cutoff = 3500 g/mol), against EtOH for 2 d, and then against deionized water for 2 d. An orange cotton-like material was obtained after lyophilization. The copolymer composition was varied by varying the molar ratio of PgMA to MPC in the feed. PPgMAMPC was characterized using ¹H NMR and Fourier transform

infrared (FTIR) spectroscopies. The molar percentage contents of PgMA and MPC units in the copolymer (PPgMA_{*m*}MPC_{*n*}) were denoted by *m* and *n*, respectively.

¹H NMR (400 MHz, CD₃OD) δ (ppm): characteristic peaks of PgMA unit (-C \equiv CH 3.10, -O-CH₂-C \equiv CH 4.55–4.80), MPC unit [(-N(CH₃)₃ 3.25, -N-CH₂CH₂-O- 3.75, -POCH₂CH₂N-, -COOCH₃, -CH₂OP 4.0–4.4], and aromatic protons (-C₆H₅ 7.40–7.95).

PPgMAMPC-SH was prepared by aminolysis of the dithioester groups at the chain ends of the copolymer with hydrazine monohydrate (Scheme 1a).⁴⁵ PPgMAMPC (0.2 g) was dissolved in EtOH (3 mL) for PPgMA₃₈MPC₆₂-SH and PPgMA₄₄MPC₅₆-SH, or a mixture of EtOH and THF (7:3 v/v) for PPgMA₆₃MPC₃₇-SH, until the solution was clear. Hydrazine monohydrate (30 mol equiv with respect to dithioester groups) was added to the copolymer solution under magnetic stirring. When addition was complete, the solution was stirred for 2 h at ambient temperature and then added dropwise to aqueous 1.0 M HCl (10 mL) and stirred for 1 h. The obtained PPgMAMPC-SH was purified using a dialysis membrane (molecular weight cutoff = 3500 g/mol) against aqueous HCl, pH 3–4, for 2 d, and then against deionized water for 2 d. A white cotton-like product was obtained after lyophilization. The copolymer was characterized using ¹H NMR, FTIR, and UV-vis spectroscopies.

Immobilization of PPgMAMPC-SH on Gold-Coated SPR Chip. A gold-coated SPR chip was cleaned with air plasma in a plasma cleaner (Harrick Plasma PDC-32G, Power 18 W) for 5 min, washed with Milli-Q water for 5 min, and dried under a nitrogen stream. The cleaned SPR sensor chip was immersed in 3 mL of a 0.1

mM copolymer solution [PPgMA₃₄MPC₆₂-SH and PPgMA₃₅MPC₅₅-SH in EtOH, PPgMA₆₅MPC₃₅-SH in EtOH/THF (7:3 v/v)] at ambient temperature for 48 h. The modified SPR chip was removed from the solution and rinsed five times by constant agitation, for 5 min each time, in EtOH for Au-PPgMA₃₄MPC₆₂ and Au-PPgMA₃₅MPC₅₅, and in EtOH/THF (7:3 v/v) for Au-PPgMA₆₅MPC₃₅. The SPR sensor chip with the immobilized copolymer was dried under a nitrogen stream and characterized using contact angle and SPR measurements and attenuated total reflection (ATR)-FTIR spectroscopy.

Characterization. Dynamic advancing (θ_A) water contact angles were measured using a contact angle goniometer equipped with a Gilmont syringe and a 24-gauge flat-tipped needle (Ramé-Hart, model 200-F1). All measurements were performed in air at ambient temperature. Data for each sample were collected from five different areas of the substrate and analyzed using DROPimage standard 2.0 software. The characteristic functional groups of the copolymer brushes on the SPR sensor chip were characterized using ATR-FTIR spectroscopy (Nicolet 6700 FTIR spectrometer). Spectra were recorded in the IR region (4000–650 cm^{-1}) based on 32 scans, at a spectral resolution of 4 cm^{-1} . ^1H NMR spectra were recorded in CD_3OD using a Varian NMR spectrometer (Mercury-400; USA) operated at 400 MHz. The disappearance of the dithioester groups of the copolymer was monitored using UV-vis spectroscopy (CARY 100Bio UV-visible spectrophotometer, Varian Inc., Palo Alto, CA, USA). Gel permeation chromatography (GPC) was performed using a refractive index detector equipped with a Shodex Asahipak GF-1G guard column and a 7.0 μm bead GF-7 M HQ column (exclusion limit $\sim 10^7$) at 40 $^\circ\text{C}$ and a flow rate of 0.6 mL/min. A phosphate buffer (pH 9) containing 10 vol % acetonitrile was used as the eluent. The M_n and M_w/M_n values were calibrated with standard sodium poly(styrenesulfonate) samples. The elemental composition on a selected SPR chip with an immobilized copolymer was determined by X-ray photoelectron spectroscopy (XPS; AXIS Ultra DLD, Kratos Analytical Ltd., Manchester, UK) using an Al K α X-ray source. All XPS data were collected at a takeoff angle of 90 $^\circ$. Atomic force microscopy (AFM) images were obtained using a scanning probe microscope (NanoScopeIV, Veeco, Plainview, NY, USA). Measurements were performed in air in tapping mode with a silicon nitride tip at a resonance frequency of 267–295 kHz and a spring constant of 20–80 N/m. The thickness of the polymer brushes was measured using a spectroscopic ellipsometer (J. A. Woollam Co., Lincoln, NE, USA) at an incident angle of 70–80 $^\circ$ in steps of 5 $^\circ$. The calculation was performed based on a Cauchy layer model with assumed refractive index of 1.34 ± 0.09 for gold-coated substrate at 632.8 nm.

SPR Measurements. SPR measurements were performed using a double-channel AutoLab ESPR instrument (Eco Chemie, Utrecht, The Netherlands) at 25 $^\circ\text{C}$, with the plane face of the prism coupled to the gold-coated glass via an index-matching fluid. The instrument uses a laser diode at a wavelength of 670 nm and a vibrating mirror to modulate the angle of incidence of the p-polarized light beam on the SPR substrate. An autosampler was used to inject the test solution, and the SPR angle shift measurements were performed under nonflow liquid conditions. The SPR angle shift at the end-point of each step and after baseline subtraction (angle shift) was used to calculate the density of molecules bound to the surface or the target density, using a sensitivity factor of 120 mdeg, equal to 100 ng/cm^2 . This sensitivity factor is specifically calibrated for the AutoLab ESPR, which uses an N-BK 7 prism refractive index of 1.518, and incident light wavelength of 670 nm. Each gold-coated SPR chip bearing PPgMAMPC was first seated in an SPR cell before being stabilized with a running solution of 10 mM PBS (pH 7.4). When the equilibrium SPR angle frequency in the buffer solution was obtained, the substrate was ready to be used.

Probe Conjugation on Copolymer-Modified SPR Chip by CuAAC Reaction. For conjugation of biotin- N_3 (Scheme 1b), Cu(I) acetate (1.23 mg, 0.01 mmol) and biotin- N_3 (0.5 M, 4.0 μL , 2.0 μmol) were dissolved in 10 mM PBS (pH 7.4, 2 mL) for 10 min to obtain a final biotin- N_3 concentration of 1.0 mM. The PPgMAMPC-modified SPR chip was immersed in the mixture, with constant agitation for 5 min. DIEA (1.71 μL , 0.01 mmol) was added to the reaction mixture,

and the SPR chip was immersed in the mixture for 24 h under constant agitation at ambient temperature. The modified SPR chip was removed from the solution and then rinsed by constant agitation in 10 mM EDTA for 1 min and 10 mM PBS (pH 7.4) five times for 5 min each. The azide-containing PNA (PNA- N_3) probe was immobilized on the PPgMAMPC-modified SPR chip (Scheme 1c) by dissolving Cu(I) acetate (0.1 mg, 8.2 μmol) and PNA- N_3 (10 nmol) in methanol (2 mL) for 10 min to obtain a final PNA- N_3 concentration of 5.0 μM . The modified SPR chip was immersed in the solution with constant agitation for 5 min. A solution of DIEA (50 μM , 1.0 mL) was added to the reaction mixture, and then the SPR chip was immersed in this mixture for 24 h under constant agitation at ambient temperature. The modified SPR chip was removed from the solution and rinsed by constant agitation in 10 mM EDTA for 1 min and in methanol five times for 5 min each. The SPR sensor chip was dried under a nitrogen stream and characterized using contact angle and SPR measurements and ATR-FTIR spectroscopy.

Specific Interactions between Conjugated Probes and Target Molecules. A PPgMAMPC-modified SPR chip conjugated with the desired probe was seated in an SPR cell and then rinsed with a running solution of 10 mM PBS buffer (pH 7.4). Once the baseline SPR response was stable, the target molecule was applied to the chip. In the case of the PPgMAMPC-modified SPR chip conjugated with biotin- N_3 (Scheme 1d), SA (0.1 mg/mL, equivalent to 1.9 μM) in blood plasma solution (0.1 mg/mL, 0.14% in PBS buffer) was applied to the surface and left for 15 min. Unbound SA was removed by washing with 10 mM PBS buffer (pH 7.4) for 5 min. The specific binding of SA was quantified from the shift in the SPR response angle at the end-point of the washing step and after baseline subtraction. Nonspecific binding (binding in the absence of SA in blood plasma solution) was also determined to quantify the specific binding of SA in blood plasma in terms of the S/N ratio; this ratio was calculated using the following equation:

$$S/N = \frac{\text{SPR angle shift after exposure to blood plasma with streptavidin}}{\text{SPR angle shift after exposure to blood plasma without streptavidin}} \quad (1)$$

For the PPgMAMPC-modified SPR chip conjugated with a PNA- N_3 probe (Scheme 1e), DNA (50 μM) in 10 mM PBS (pH 7.4) containing 100 mM NaCl was applied to the surface and left for 15 min. Unbound DNA was removed by washing with PBS for 5 min. The specific binding of DNA was quantified from the shift in the SPR response angle at the end-point of the washing step and after baseline subtraction. The sensor was regenerated by washing with 50 mM NaOH for 5 min. The %HE and %MD were calculated using the following equations:

$$\%HE = \frac{\text{target density}}{\text{probe density}} \times 100 \quad (2)$$

$$\%MD = \frac{\%HE \text{ of complementary DNA} - \%HE \text{ of mismatched DNA}}{\%HE \text{ of complementary DNA}} \times 100 \quad (3)$$

RESULTS AND DISCUSSION

Synthesis and Characterization of Thiol-Terminated Poly[(propargyl methacrylate)-*ran*-(2-methacryloyloxyethyl phosphorylcholine)] (PPgMAMPC-SH). A PPgMAMPC copolymer was synthesized via RAFT polymerization using CPADB and ACVA as the chain transfer agent (CTA) and radical initiator (In), respectively. The molar percentage contents of P_gMA and MPC units in the copolymer (PPgMA_{*m*}MPC_{*n*}) are denoted by *m* and *n*, respectively. Our survey suggested that the optimum [CTA]/[In] ratio for obtaining a copolymer with a well-controlled molecular weight was 8; the data are shown in Table S1 in the Supporting Information. The control over the copolymerization process

was also demonstrated for a targeted degree of polymerization (DP) of 200 based on the linear first-order relationship between $\ln[M]_0/[M]$ and the polymerization time (Figure S2, Supporting Information), suggesting that the polymeric radical concentration remained unaltered throughout the polymerization. ^1H NMR spectroscopy (Figure S3 and explanation in the Supporting Information) showed that the copolymer composition varied as a function of the monomer ratio in the feed (Table 1). The molecular weight of the copolymer was

Table 1. Copolymer Compositions and Molecular Weights of PPgMAMPC (Target DP 200) Synthesized by RAFT Polymerization

| monomer composition in feed (mol %) | | monomer composition in copolymer (mol %) ^a | | \bar{M}_n ^a (kDa) | DP ^a | copolymer abbreviation |
|-------------------------------------|-----|---|-----|--------------------------------|-----------------|---------------------------------------|
| PgMA | MPC | PgMA | MPC | | | |
| 70 | 30 | 65 | 35 | 38.4 | 208 | PPgMA ₆₅ MPC ₃₅ |
| 50 | 50 | 45 | 55 | 46.7 | 213 | PPgMA ₄₅ MPC ₅₅ |
| 30 | 70 | 38 | 62 | 40.0 | 173 | PPgMA ₃₈ MPC ₆₂ |

^aCalculated from ^1H NMR data.

close to the target (35 375–46 327 kDa). We also attempted to determine the molecular weight and polydispersity indices (PDIs) of the copolymers using GPC. The data are shown in Figure S4 (Supporting Information). It should be emphasized that it is not possible to dissolve the copolymers in a common polar protic solvent (such as methanol) generally used for GPC analysis of MPC-based copolymers. And it was rather difficult to dissolve them in the mobile phase used for GPC analysis, phosphate buffer (pH 9) containing 10 vol % acetonitrile, especially the copolymer having high PgMA composition, PPgMA₆₅MPC₃₅, of which molecular weight information cannot be obtained. The fact that the \bar{M}_n determined by

GPC analysis are underestimated and proportionally decreased as a function of PgMA content suggested that the molecular weight information obtained via GPC analysis is somewhat not reliable. Additionally, PDI values were high, which may be ascribed to possible copolymer self-assembly in the phosphate buffer solution. This is why ^1H NMR spectroscopy was used as the main tool for determining the molecular weight of the copolymer. Despite the relatively high PDI, the unimodal distribution evidenced from GPC chromatograms (also shown in Figure S4) is reasonable evidence of copolymer formation. The functional groups in the synthesized copolymer were identified using FTIR spectroscopy (Figure 1). The characteristic peaks for C=O (ester) stretching, at 1725 cm^{-1} , asymmetric O=P–O– stretching, at 1240 cm^{-1} , symmetric O=P–O– stretching, at 1087 cm^{-1} , and $-\text{N}^+(\text{CH}_3)_3$, at 960 cm^{-1} for the MPC units were observed; a $-\text{C}\equiv\text{C}-$ stretching peak was observed at 2127 cm^{-1} , and its intensity increased proportionally with the PgMA content. These results confirm copolymer formation.

Aminolysis with hydrazine transformed the dithiobenzoate groups at the chain ends of the PPgMAMPC copolymer into thiol groups, yielding PPgMAMPC-SH,⁴⁸ as shown by the disappearance after aminolysis of the aromatic proton signals at 7.40–7.95 ppm in the ^1H NMR spectrum and the UV–vis absorption peak at 305 nm (Figure S5, Supporting Information).

Immobilization of PPgMAMPC-SH on Gold-Coated SPR Chip. Unlike PPgMA₃₈MPC₆₂-SH and PPgMA₄₅MPC₅₅-SH, PPgMA₆₅MPC₃₅-SH, which has a higher content of the more hydrophobic PgMA unit, is not soluble in EtOH but dissolves in a mixture of EtOH and THF (7:3 v/v). Au–S bond formation between the gold layer of the SPR chip and the thiol-terminated copolymer (PPgMAMPC-SH) via a “grafting to” approach was performed at ambient temperature for 48 h. The presence of PPgMAMPC brushes on the SPR chip was confirmed using water contact angle

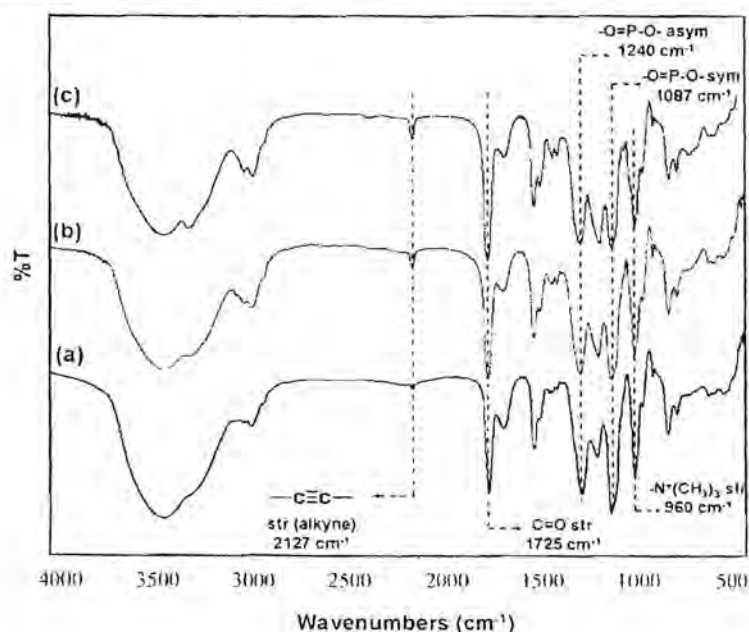


Figure 1. FTIR spectra of (a) PPgMA₃₈MPC₆₂ (40.0 kDa), (b) PPgMA₄₅MPC₅₅ (46.7 kDa), and (c) PPgMA₆₅MPC₃₅ (38.4 kDa).

measurements, and SPR, ATR-FTIR, and XPS analyses. The data in Table 2 show that the advancing (θ_A) water contact

Table 2. Water Contact Angle and SPR Data for Gold-Coated SPR Chips after PPgMAMPC-SH Immobilization and Subsequent Conjugation with Biotin- N_3

| sample | advancing water contact angle (deg) | SPR data | |
|--|-------------------------------------|-----------------------|--|
| | | angle shift (mDegree) | amount adsorbed for each modification step (ng/cm ²) |
| Au | 71.9 ± 1.3 | - | - |
| Au-PPgMA ₃₈ MPC ₆₂ | 44.6 ± 0.9 | 1024.8 ± 81.8 | 854.0 ± 68.1 |
| Au-PPgMA ₄₅ MPC ₅₅ | 46.6 ± 3.5 | 882.1 ± 166.6 | 735.0 ± 138.9 |
| Au-PPgMA ₆₅ MPC ₃₅ | 87.9 ± 4.2 | 1323.1 ± 56.1 | 1102.0 ± 46.8 |
| Au-PPgMA ₃₈ MPC ₆₂ -biotin | 32.7 ± 2.7 | 15.2 ± 7.4 | 12.7 ± 6.1 |
| Au-PPgMA ₄₅ MPC ₅₅ -biotin | 41.6 ± 1.3 | 229.5 ± 50.4 | 191.2 ± 42.0 |
| Au-PPgMA ₆₅ MPC ₃₅ -biotin | 62.2 ± 1.7 | 209.5 ± 6.7 | 174.5 ± 5.6 |

angle of the SPR chip decreased from 71.9 ± 1.3° to 44.6 ± 0.9° and 46.6 ± 3.5° upon immobilization of PPgMA₃₈MPC₆₂-SH and PPgMA₄₅MPC₅₅-SH, respectively, indicating their highly hydrophilic characters. The copolymer with the highest content of hydrophobic PgMA, i.e., PPgMA₆₅MPC₃₅-SH, yielded a gold surface with a contact angle (87.9 ± 4.2°) higher than that of the pristine gold surface. Chemisorption of the copolymer brushes on the gold-coated SPR chip was monitored using an SPR technique. The SPR angle shift upon PPgMAMPC-SH immobilization was used to calculate the amount of copolymer bound to the surface, using a sensitivity factor of 120 mDegree, which is equivalent to 100 ng/cm² (Table 2).^{19,50}

Figure S6 (Supporting Information) shows the XPS atomic spectra of the gold-coated substrate with immobilized PPgMA₄₅MPC₅₅-SH and the substrate before immobilization (bare gold). At a takeoff angle of 90°, phosphorus (P_{2p}) and nitrogen (N_{1s}) signals attributed to the phosphorylcholine group of the MPC units were observed on the substrate, indicating that the copolymer is bound to the gold-coated substrate. The S_{2p} signal of the bound thiol, at a binding energy of 163 eV, was also detected, implying that the copolymer was strongly adsorbed on the substrate by interactions between the thiol groups of the copolymer and the gold surface. The characteristic absorption peaks of the MPC unit, i.e., C=O stretching (ester) at 1725 cm⁻¹, O=P-O_{asym} stretching at 1264 cm⁻¹, O=P-O_{sym} stretching at 1091 cm⁻¹, and -N⁺(CH₃)₃ stretching at 968 cm⁻¹, were observed in the ATR-FTIR spectra (Figure S7, Supporting Information), but the characteristic absorption peak of the PgMA unit, i.e., -C≡C- stretching at 2127 cm⁻¹, was not clearly observed because of overlap with the characteristic peak of diamond (in the region 1500–2650 cm⁻¹), which is the reflectance material used for ATR-FTIR measurements. This signal from diamond dominates the other signals, particularly when the adsorbed material to be characterized is very thin, 1.89–3.12 nm in our case (estimated by ellipsometry).

Surface grafting of PPgMAMPC brushes on the gold-coated substrate was confirmed using AFM. The surface roughness before and after grafting with PPgMAMPC brushes were similar (1.5 vs 1.3 nm), suggesting that the gold surface was smooth and homogeneously covered with the copolymer. The thicknesses (t), measured using ellipsometry, of PPgMA₃₈MPC₆₂, PPgMA₄₅MPC₅₅, and PPgMA₆₅MPC₃₅ were 1.89 ± 0.12, 2.66 ± 0.26, and 3.12 ± 0.19 nm, respectively. The thickness can be used to calculate the graft density (σ) as follows:

$$\sigma = \frac{t\rho N_A}{M_n} \quad (4)$$

where ρ is the mass density (1.1 g/cm³ for PPgMA₆₅MPC₃₅ and 1.2 g/cm³ for PPgMA₄₅MPC₅₅ and PPgMA₃₈MPC₆₂), M_n is the molecular weight of the free polymer, and N_A is Avogadro's number. The copolymer mass densities were estimated proportionally using $\rho_{\text{PMPC}} = 1.3 \text{ g/cm}^3$ and $\rho_{\text{PPgMA}} = 1.085 \text{ g/cm}^3$, on the assumption that they are equal to that of poly(propyl methacrylate),⁵¹ which has the same number of carbon atoms. For the copolymer synthesized with M_n in the range 38.4–46.7 kDa (DP 173–213), the calculated graft densities of surface-grafted PPgMA₃₈MPC₆₂, PPgMA₄₅MPC₅₅, and PPgMA₆₅MPC₃₅ were 0.04, 0.04, and 0.05 chain/nm², respectively. These values are below 0.08 chains/nm²,⁵² which suggests that the PPgMAMPC brushes can be categorized as being in the "mushroom regime."

Biotin Conjugation on Copolymer-Modified SPR Chip by CuAAC Reaction and Subsequent Binding with Streptavidin. Biotin was used as the first sensing probe model. It has a high binding affinity with SA (dissociation constant $K_D \approx 10^{-14} \text{ M}$).¹³ Biotin- N_3 was immobilized on the PPgMAMPC-modified SPR chip using the SPR instrument by CuAAC.^{14,55} The data in Table 2 show that the water contact angles of the PPgMAMPC-modified SPR chip decreased after biotin attachment, indicating that the hydrophobic alkyne moieties from the PgMA repeat units were consumed and bound with biotin with three repeat units of the hydrophilic PEG spacer. The amounts of immobilized biotin increased significantly, from 12.7 ± 6.1 to 191.2 ± 42.0 ng/cm², when the PgMA content of the copolymer was increased from 38% to 45%. However, further increasing the PgMA composition to 65% reduced the quantity of bound probe, implying that biotin may have limited access to the alkyne moieties of copolymers with high PgMA contents, in which the swellability would be suppressed because of the inherent hydrophobicity. This is confirmed by the water contact angle (87.9 ± 4.2°) being much higher than those of the PPgMAMPC-modified SPR chips with PgMA contents of 38% and 45% (44.6 ± 0.9° and 46.6 ± 3.5°, respectively). As shown in Figure S6 in the Supporting Information, similar characteristic atomic spectra of the PPgMAMPC-modified SPR chips were observed after biotin and PNA immobilization but with much better signal, especially for N_{1s} , S_{2p} , P_{2p} peaks in comparison with those before probe immobilization. A Cu peak appears in the Au-PPgMAMPC spectra after probe immobilization (both biotin and PNA), suggesting that Cu remained after the click reaction, although the surface was thoroughly rinsed with 10 mM EDTA and 10 mM PBS (pH 7.4). However, we believe that the Cu contamination should not affect the target molecule detection efficiency.

Nonspecific adsorption of the biotin-modified PPgMAMPC copolymer platform with different copolymer compositions on gold-coated SPR chips was investigated by comparison of adsorption of nontargeted proteins, bovine serum albumin (BSA; 69 kDa, $pI = 4.8$), LYZ (14 kDa, $pI = 12$), and 0.14% blood plasma (equivalent to 0.1 mg/mL of protein in PBS buffer, pH 7.4) with that of a targeted analyte, SA (60 kDa, $pI = 5$). BSA and LYZ were selected as model proteins with negative and positive charges, respectively, at pH 7.4 in PBS. Blood plasma is a complex biological-mimic medium comprising about 7% (70 mg of proteins per milliliter of plasma) of different proteins, e.g., fibrinogen, albumin, and globulin, and other components such as water, inorganic ions, and organic compounds.⁵⁶ As anticipated, the biotin-conjugated PPgMAMPC platform was specifically bound to the targeted SA (Figure 2). The bound content of SA increased with

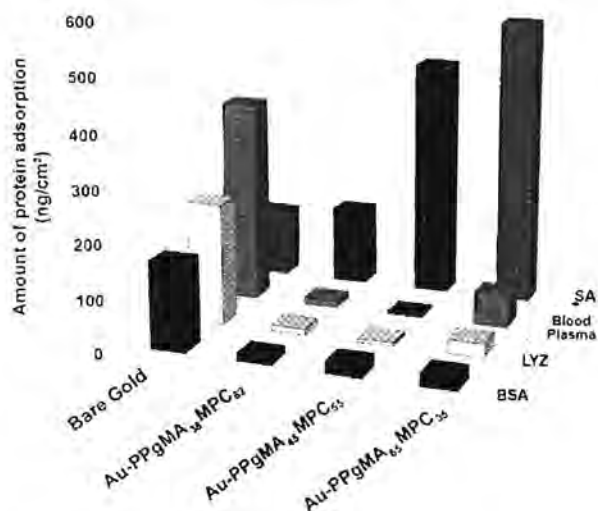


Figure 2. Protein adsorption on biotin-conjugated PPgMAMPC platforms with various copolymer compositions.

increasing PgMA content in the copolymer and increasing biotin content (Table 2). Nonspecific adsorption of the nontargeted proteins (BSA, LYZ, 0.14% blood plasma) was greatly suppressed on the biotin-conjugated PPgMAMPC platform compared with that on the bare gold surface. These results indicate that the MPC units in the PPgMAMPC copolymer are of paramount importance in suppressing nonspecific protein adsorption. This agrees well with reported studies of other MPC-containing (co)polymers.^{14,34,35,57} Although the copolymer platform with the highest PgMA content, i.e., 65%, had the greatest bound SA content, it also gave the highest nonspecific adsorption of blood plasma.

In principle, the biotin/SA binding ratio should be 4 if all biotin molecules can be bound to SA. However, the biotin/SA binding ratios, listed in Figure 3, were much higher than the theoretical value, indicating that not all of the conjugated biotin molecules were bound to SA. The biotin/SA binding ratios were extremely high for the Au-PPgMAMPC platforms with high contents of hydrophobic PPgMA (45% and 65%). This may be because of the limited accessibility of SA, which is a large protein (MW = 60 kDa), to the immobilized biotin embedded inside the inner layer of the polymer brushes. Au-

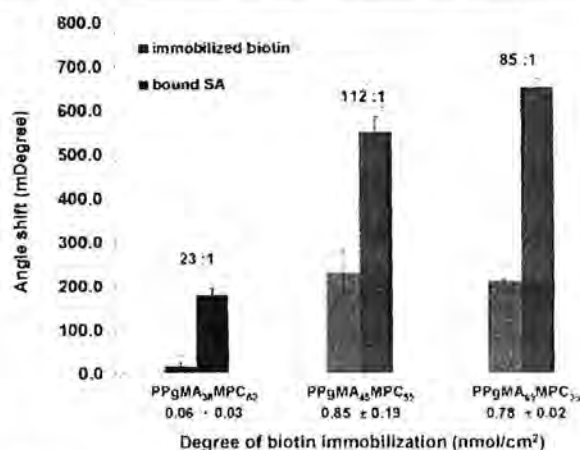


Figure 3. SPR angle shifts corresponding to the amounts of immobilized biotin, and subsequent SA (0.1 mg/mL) binding in PBS solution (10 mM, pH 7.4) on SPR chip modified with PPgMAMPC copolymers of various compositions. Biotin/SA binding ratio is shown on each set of bar charts.

PPgMA₃₈MPC₆₂ had the lowest immobilized biotin content, because it had the lowest content of PgMA, which provides active binding sites for biotin immobilization, and because its assembled layer on the gold-coated SPR chip was very thin (1.89 ± 0.12 nm). Although the amount of biotin bound on the Au-PPgMA₆₅MPC₃₅ platform (0.78 ± 0.02 nmol/cm²) was lower than that on the PPgMA₄₅MPC₅₅ platform (0.85 ± 0.19 nmol/cm²), it had a higher content of bound SA. To verify this contradictory outcome, we performed additional experiments to determine the nonspecific adsorption of SA (0.1 mg/mL SA in 10 mM PBS) on Au-PPgMA₄₅MPC₅₅ and Au-PPgMA₆₅MPC₃₅ before biotin immobilization, using an SPR technique. The data shown in Figure S8 in the Supporting Information indicate that nonspecific adsorption of SA on the Au-PPgMA₆₅MPC₃₅ platform was approximately 3 times higher than that on the PPgMA₄₅MPC₅₅ brushes. This helps to explain why the Au-PPgMA₆₅MPC₃₅ platform (with the highest PgMA content) bound the most SA, although it bound slightly less biotin than did the Au-PPgMA₄₅MPC₅₅ platform. SA can bind to the biotin-conjugated Au-PPgMAMPC platform not only by specific interactions with biotin probes but also by nonspecific interactions with the PgMA units of the copolymers.

The amount of SA adsorbed on the biotin-modified PPgMAMPC was low, particularly on the Au-PPgMA₃₈MPC₆₂-biotin platform. The adsorbed quantity of SA, 149.8 ± 12.3 ng/cm², was less than that in the SA monolayer adsorbed on a mixed monolayer containing 10% thiol-terminated biotin and 90% thiol-terminated ethylene glycol (379.7 ng/cm²), as reported by Su et al.⁵¹ This seems reasonable because the amount of biotin immobilized on the Au-PPgMA₃₈MPC₆₂ platform was lower than the amounts adsorbed on the platforms based on PPgMA₄₅MPC₅₅ and PPgMA₆₅MPC₃₅. Nevertheless, the amounts of SA adsorbed on Au-PPgMA₄₅MPC₅₅-biotin and Au-PPgMA₆₅MPC₃₅-biotin, i.e., 457.8 ± 28.6 and 549.5 ± 14.8 ng/cm², respectively, were well above that in the monolayer, suggesting three-dimensional character of the deposited copolymer in binding with the biotin probes.

The biotin-modified PPgMAMPC platforms with different copolymer compositions were further investigated to determine the lowest SA concentration detectable in a complex protein sample (blood plasma). The SA concentration was varied in the range 0.19–190 nM (equivalent to 0.01 to 0.1 mg/mL) in 0.14% blood plasma (0.1 mg/mL). Nonspecific binding with 0.14% blood plasma (in the absence of SA) was also measured to evaluate the sensor efficiency in terms of the *S/N* ratio, as shown in Figure 4. The *S/N* ratio can be calculated from eq

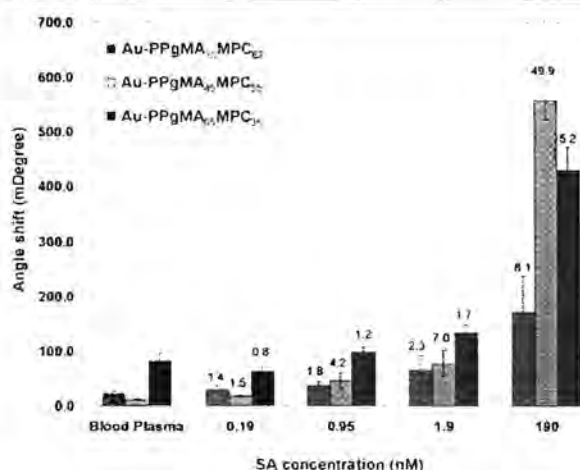


Figure 4. SPR angle shifts corresponding to SA binding on Au-PPgMAMPC–biotin platforms from SA solutions of various concentrations in 0.14% blood plasma. *S/N* ratios are shown as the number above each bar graph.

1.^{9,14} The SPR angle shift obtained for the complex sample containing SA is considered to be the signal, whereas that obtained from the sample without SA, i.e., the target molecules, is considered to be background or noise. The results shown in Figure 4 indicate that the SPR chip modified with a copolymer platform containing 65% PgMA (PPgMA₆₅MPC₃₅-SH) showed the highest nonspecific binding with blood plasma in a control experiment (absence of SA in 0.14% blood plasma). This may be the result of nonspecific adsorption between the remaining alkyne moieties on the copolymer platform and nontargeted proteins in the blood plasma. The limits of detection (LODs) of the sensor platforms that can discriminate between target and nontargeted binding signals (*S/N* ≥ 3) were 190, 0.95, and 190 nM for PMA₃₈MPC₆₂-SH, PMA₄₅MPC₅₅-SH, and PMA₆₅MPC₃₅-SH, respectively. These results suggest that the platform based on a copolymer containing 45% PgMA was the most efficient for detecting SA in blood plasma solution. The LOD of this PPgMA₄₅MPC₅₅ platform (0.95 nM) was even lower than that (1.5 nM) obtained for a platform based on poly[(methacrylic acid)-*ran*-(2-methacryloyloxyethyl phosphorylcholine)] (PMAMPC), previously developed by our group, and approximately 158 times lower than that of a platform based on a SAM of mercaptoundecanoic acid.¹⁴ The fact that the PPgMAMPC sensor platform can directly immobilize an azide-containing biotin probe via a click reaction, without a functional group activation step, as required for the PMAMPC platform, makes it an attractive copolymer platform for probe binding in biosensing applications.

The developed PPgMAMPC platforms with clickable PgMA units for probe binding and MPC antifouling units were also used to immobilize a PNA-N₃ probe to explore its applicability as a DNA sensor. PNA is a DNA mimic with a peptide-like backbone, first introduced by Nielsen and co-workers in 1991.⁵⁸ Because it is uncharged, PNA-DNA hybrids are more stable than DNA-DNA hybrids, because electrostatic repulsion between negatively charged phosphate groups in the DNA backbone are absent. This, together with its greater specificity for complementary DNA than mismatched DNA, makes PNA an attractive nucleotide probe with potential applications as a DNA sensor. In this study, a conformationally restricted pyrrolidinyl PNA with *D*-prolyl-2-aminocyclopentanecarboxylic acid backbones (*acpc*PNA), developed by Vilaivan and co-workers, was selected as a model nucleic acid probe. It has been reported that its binding affinity and sequence specificity toward DNA are higher than those of Nielsen's PNA.^{16,59,60} We previously showed that *acpc*PNA can act as an effective probe for DNA detection when immobilized on a gold-coated SPR chip either by Au-S bond formation between thiolated PNA (PNA-SH) and the gold surface⁶¹ or by biotin-SA-biotin linkage between biotinylated PNA (PNA-biotin) and an SA layer assembled on a biotin-functionalized gold substrate.⁵⁹ Besides blocking, which is a necessary step in most SAM-based sensors, the longer and greater hydrophilicity of the spacer between the PNA part and the thiol end of the thiolated PNA has a positive impact on the %HE of the platform developed by direct immobilization of thiolated PNA. Both %HE and %MD were significantly improved for the platform later developed by indirect PNA conjugation via biotin-SA-biotin linkage, which yielded PNA with a reasonably well-controlled density and orientation (see Table 3 for comparison). The results of these

Table 3. Values of %HE_{com} and %MD for DNA Detection by Surface-Modified Gold-Coated SPR Chips Conjugated with PNA

| sample | %HE _{com} | %MD |
|---|--------------------|------|
| Au-PPgMA ₁₈ MPC ₆₂ -PNA | 20 | 32 |
| Au-PPgMA ₄₅ MPC ₅₅ -PNA | 61 | 52 |
| Au-PPgMA ₆₅ MPC ₃₅ -PNA | 71 | 58 |
| Au-S-PNA ⁶¹ | 20 | > 54 |
| Au-biotin-SA-biotin-PNA ⁵⁹ | 58 | > 90 |

two studies suggest that the clickable and antifouling PPgMAMPC platforms developed in the current study should meet all the above-mentioned criteria for developing an effective PNA-based sensor for DNA detection. Anchoring the copolymer to the gold surface prior to PNA binding should provide a reasonable distance between the immobilized PNA probes and the gold substrate, and allow the PNA molecules to interact freely with the incoming DNA targets. PMPC provides a hydrophilic environment for the platform so that nonspecific adsorption of nontargeted DNA can be suppressed. It is anticipated that good control of the content of clickable PgMA units in the copolymer will enable the density of immobilized PNA to be tailored using efficient CuAAC-based reactions.

In this work, azide-terminated PNA with a T₉ sequence (PNA-N₃), selected as a PNA probe model, was immobilized by the alkyne moieties of sensing platforms with various copolymer compositions, i.e., PPgMA₁₈MPC₆₂-SH, PPgMA₄₅MPC₅₅-SH, and PPgMA₆₅MPC₃₅-SH, via CuAAC reactions. Specific binding of 50 μM DNA in 10 mM PBS was

monitored using an SPR technique. The %HE and %MD were calculated using eqs 2 and 3, respectively, to evaluate the efficiency of the sensor. As shown in Figure 5, the sensing

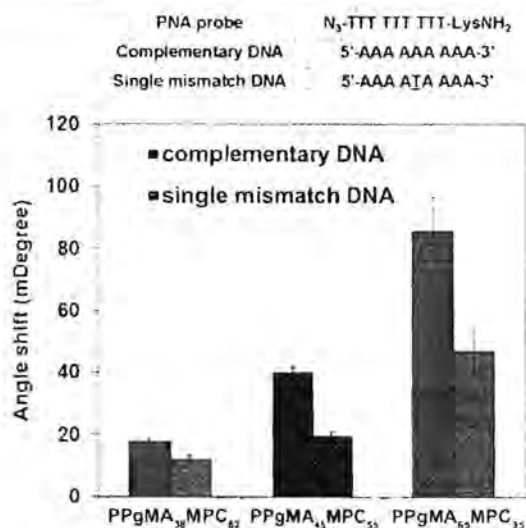


Figure 5. SPR angle shifts corresponding to DNA binding to Au-PPgMAMPC-PNA platforms in 10 mM PBS.

platform based on Au-PPgMA₆₅MPC₃₅-PNA, which had the highest amount of PgMA units, gave the greatest detectable signal, corresponding to binding of the complementary DNA sequence, A₉ (85.5 ± 10.9 mdeg), with a %HE of 71%, which is higher than those for sensing platforms based on Au-S-PNA⁵¹ and Au-biotin-PNA,⁵⁹ as shown in Table 3. However, this copolymer platform still showed high nonspecific interactions toward a single mismatched DNA sequence (AAAATAAAA), therefore its %MD was not satisfactorily high compared with that for a platform based on Au-biotin-SA-biotin-PNA. Despite this limitation, a %HE as high as 71% may be suitable for other DNA-based applications, such as affinity-based DNA separation, in which the mismatch discrimination efficiency is not a critical issue. There is also room for improvement in terms of %MD. For example, possible nonspecific interactions between the remaining unreacted alkyne moieties of PgMA and mismatched DNA may be decreased by blocking the unreacted PgMA with hydrophilic molecules, enabling %HE of mismatched DNA to be minimized. Stable triazole linkages between the PNA probe and the sensing platform should have the additional advantage of being more robust to the regeneration conditions than Au-S or Au-biotin-SA-biotin linkages. This should enable probe recycling, making the process economically viable.

CONCLUSIONS

Clickable and antifouling PPgMAMPC copolymer platforms were successfully synthesized by RAFT polymerization. The dithioester end groups of the copolymer were converted to thiol groups before surface immobilization on a gold-coated SPR chip via a "grafting to" approach. The alkyne moieties of PgMA bound azide-containing molecules (biotin-N₃ and PNA-N₃) via a CuAAC reaction, and the hydrophilic monomeric MPC unit suppressed nonspecific adsorption of nontargeted analytes, namely BSA, LYZ, and blood plasma. Specific detection of SA by biotin probes conjugated with the

PPgMAMPC platforms in 0.14% blood plasma was investigated using an SPR technique. Among all the platforms investigated, copolymer brushes of PPgMA₄₅MPC₅₅ performed best, giving the lowest detection limit, i.e., 0.95 nM. The potential of the surface-attached PPgMAMPC as a sensing layer for DNA detection was investigated by conjugating a PNA-N₃ probe with PPgMAMPC platforms with various copolymer compositions. The sensor platform based on Au-PPgMA₆₅MPC₃₅-PNA detected the highest amount of complementary DNA sequence, with 71%HE, and a reasonable degree of mismatch discrimination (58%MD) between the fully complementary DNA and single-mismatched DNA. These results suggest that substrate-modified PPgMAMPC brushes are potential copolymer platforms for azide-containing probe immobilization for detecting target molecules in diagnostic and related applications. Both types of probe functioned effectively, which shows the versatility of the developed platform, and suggests that it can be used for both antibody-based and DNA-based biosensors.

ASSOCIATED CONTENT

Supporting Information

The Supporting Information is available free of charge on the ACS Publications website at DOI: 10.1021/acs.langmuir.5b02727.

HPLC chromatogram and MALDI-TOF MS spectrum of PNA, data and calculations related to RAFT polymerization (% conversion, MW, PDIs, GPC chromatograms, and copolymer composition), ¹H NMR and UV-vis spectra of copolymer, XPS and ATR-FTIR for copolymer brushes grafted on gold-coated SPR chips, and amounts of SA adsorbed on PPgMAMPC platforms (PDF)

AUTHOR INFORMATION

Corresponding Author

* Tel.: +66-2218-7627; fax: +66-2218-7598; E-mail address: vipavee.p@chula.ac.th.

Notes

The authors declare no competing financial interest.

ACKNOWLEDGMENTS

This work was financially supported by a Directed Basic Research Grant by the Thailand Research Fund (DBG5580003), a Distinguished Research Professor Grant by the Thailand Research Fund and Chulalongkorn University (DPG5780002), the Ratchadaphiseksomphot Endowment Fund of Chulalongkorn University (RES560530126-AM), and the Thai Government Stimulus Package 2 (TKK2555), under the Project for Establishment of a Comprehensive Center for Innovative Food, Health Products, and Agriculture. O.W. acknowledges receipt of an academic scholarship from Chulalongkorn University Dutsadiphiphat Scholarship for her Ph.D. study. The authors are grateful to Professor Shin-ichi Yusa and Mr. Keita Nakai from the Graduate School of Engineering, University of Hyogo, Japan, for their assistance in GPC analysis.

REFERENCES

- (1) Nakamura, F.; Ito, E.; Hayashi, T.; Hara, M. Fabrication of COOH-Terminated Self-Assembled Monolayers for DNA Sensors. *Colloids Surf., A* 2006, 284–285, 495–498.

- (2) Senaratne, W.; Andruzzi, L.; Ober, C. K. Self-Assembled Monolayers and Polymer Brushes in Biotechnology: Current Applications and Future Perspectives. *Biomacromolecules* 2005, 6 (5), 2427–48.
- (3) Su, X. L.; Li, Y. A Self-Assembled Monolayer-Based Piezoelectric Immunosensor for Rapid Detection of *Escherichia coli* O157:H7. *Biosens. Bioelectron.* 2004, 19 (6), 563–574.
- (4) Akkhat, P.; Hoven, V. P. Introducing Surface-Tethered Poly(acrylic acid) Brushes as 3D Functional Thin Film for Biosensing Applications. *Colloids Surf., B* 2011, 86 (1), 198–205.
- (5) Akkhat, P.; Mekboonsonglarp, W.; Kiatkamjornwong, S.; Hoven, V. P. Surface-Grafted Poly(acrylic acid) Brushes as a Precursor Layer for Biosensing Applications: Effect of Graft Density and Swellability on the Detection Efficiency. *Langmuir* 2012, 28 (11), 5302–5311.
- (6) Henry, O. Y.; Mehdi, A. D.; Kirwan, S.; Sanchez, J. L.; O'Sullivan, C. K. Three-Dimensional Arrangement of Short DNA Oligonucleotides at Surfaces via the Synthesis of DNA-Branched Polyacrylamide Brushes by SI-ATRP. *Macromol. Rapid Commun.* 2011, 32 (18), 1405–1410.
- (7) Kurosawa, S.; Aizawa, H.; Talib, Z. A.; Athoff, B.; Hilborn, J. Synthesis of Tethered-Polymer Brush by Atom Transfer Radical Polymerization from a Plasma-Polymerized-Film-Coated Quartz Crystal Microbalance and Its Application for Immunosensors. *Biosens. Bioelectron.* 2004, 20 (6), 1165–1176.
- (8) Lee, B. S.; Chi, Y. S.; Lee, K.-B.; Kim, Y.-G.; Choi, I. S. Functionalization of Poly(oligo(ethylene glycol) methacrylate) Films on Gold and Si/SiO₂ for Immobilization of Proteins and Cells: SPR and QCM Studies. *Biomacromolecules* 2007, 8 (12), 3922–3929.
- (9) Yang, N.; Su, X.; Tjong, V.; Knoll, W. Evaluation of Two- and Three-Dimensional Streptavidin Binding Platforms for Surface Plasmon Resonance Spectroscopy Studies of DNA Hybridization and Protein-DNA Binding. *Biosens. Bioelectron.* 2007, 22 (11), 2700–2706.
- (10) Jeong, S. P.; Lee, B. S.; Kang, S. M.; Ko, S.; Choi, I. S.; Lee, J. K. Binding Behaviors of Protein on Spatially Controlled Poly[oligo(ethylene glycol) methacrylate] Brushes Grafted from Mixed Self-Assembled Monolayers on Gold. *Chem. Commun.* 2014, 50 (40), 5291–5293.
- (11) Trmcic-Cvitas, J.; Hasan, E.; Ramstedt, M.; Li, X.; Cooper, M. A.; Abell, C.; Huck, W. T. S.; Gautrot, J. E. Biofunctionalized Protein Resistant Oligo(ethylene glycol)-Derived Polymer Brushes as Selective Immobilization and Sensing Platforms. *Biomacromolecules* 2009, 10 (10), 2885–2894.
- (12) Gam-Derouich, S.; Lamouri, A.; Redeuilh, C.; Decorse, P.; Maurel, F.; Carbonnier, B.; Beyazit, S.; Yilmaz, G.; Yagci, Y.; Chehimi, M. M. Diazonium Salt-Derived 4-(Dimethylamino)phenyl Groups as Hydrogen Donors in Surface-Confining Radical Photopolymerization for Bioactive Poly(2-hydroxyethyl methacrylate) Grafts. *Langmuir* 2012, 28 (21), 8035–8045.
- (13) Vaisocherova, H.; Sevcu, V.; Adam, P.; Spac kova, B.; Hegnerova, K.; de los Santos Pereira, A.; Rodriguez-Emmenegger, C.; Riedel, T.; Houska, M.; Brynda, E.; Homola, J. Functionalized Ultra-Low Fouling Carboxy- and Hydroxy-Functional Surface Platforms: Functionalization Capacity, Biorecognition Capability and Resistance to Fouling from Undiluted Biological Media. *Biosens. Bioelectron.* 2014, 51, 150–157.
- (14) Akkhat, P.; Kiatkamjornwong, S.; Yusa, S.-i.; Hoven, V. P.; Iwasaki, Y. Development of a Novel Antifouling Platform for Biosensing Probe Immobilization from Methacryloyloxyethyl Phosphorylcholine-Containing Copolymer Brushes. *Langmuir* 2012, 28 (13), 5872–5881.
- (15) Audouin, F.; Larragy, R.; Fox, M.; O'Connor, B.; Heise, A. Protein Immobilization onto Poly(acrylic acid) Functional Macroporous PolyHIPE Obtained by Surface-Initiated ARGET ATRP. *Biomacromolecules* 2012, 13 (11), 3787–3794.
- (16) Cullen, S. P.; Liu, X.; Mandel, I. C.; Himpel, F. J.; Gopalan, P. Polymeric Brushes as Functional Templates for Immobilizing Ribonuclease A: Study of Binding Kinetics and Activity. *Langmuir* 2008, 24 (3), 913–920.
- (17) Dai, J. H.; Bao, Z. Y.; Sun, L.; Hong, S. U.; Baker, G. L.; Bruening, M. L. High-Capacity Binding of Proteins by Poly(acrylic acid) Brushes and Their Derivatives. *Langmuir* 2006, 22 (9), 4274–4281.
- (18) Qu, Z.; Chen, K.; Gu, H.; Xu, H. Covalent Immobilization of Proteins on 3D Poly(acrylic acid) Brushes: Mechanism Study and a More Effective and Controllable Process. *Bioconjugate Chem.* 2014, 25 (2), 370–378.
- (19) Thilakarathne, V.; Briand, V. A.; Zhou, Y.; Kasi, R. M.; Kumar, C. V. Protein Polymer Conjugates: Improving the Stability of Hemoglobin with Poly(acrylic acid). *Langmuir* 2011, 27 (12), 7663–7671.
- (20) Baek, M.-G.; Roy, R. Relative Lectin Binding Properties of T-Antigen-Containing Glycopolymers: Copolymerization of *N*-Acryloylated T-Antigen Monomer vs. Graft Conjugation of Aminated T-Antigen Ligands onto Poly(*N*-acryloxysuccinimide). *Macromol. Biosci.* 2001, 1 (7), 305–311.
- (21) Chen, J.-P.; Chiu, S.-H. A Poly(*N*-isopropylacrylamide-*co*-*N*-acryloxysuccinimide-*co*-2-hydroxyethyl methacrylate) Composite Hydrogel Membrane for Urease Immobilization to Enhance Urea Hydrolysis Rate by Temperature Swing. *Enzyme Microb. Technol.* 2000, 26 (56), 359–367.
- (22) Minard-Basquin, C.; Chaix, C.; D'Agosto, F.; Charreyre, M.-T.; Pichot, C. Oligonucleotide Synthesis onto Poly(*N*-acryloylmorpholine-*co*-*N*-acryloxysuccinimide): Assessment of The Resulting Conjugates in a DNA Sandwich Hybridization Test. *J. Appl. Polym. Sci.* 2004, 92 (6), 3784–3795.
- (23) Duque, L.; Menges, B.; Borros, S.; Forch, R. Immobilization of Biomolecules to Plasma Polymerized Pentafluorophenyl Methacrylate. *Biomacromolecules* 2010, 11 (10), 2818–2823.
- (24) McRae, S.; Chen, X.; Kratz, K.; Samanta, D.; Henchey, E.; Schneider, S.; Emrick, T. Pentafluorophenyl Ester-Functionalized Phosphorylcholine Polymers: Preparation of Linear, Two-Arm, and Grafted Polymer-Protein Conjugates. *Biomacromolecules* 2012, 13 (7), 2099–2109.
- (25) Socaci, C.; Rybka, M.; Magerusan, L.; Nan, A.; Turcu, R.; Liebscher, J. Magnetite Nanoparticles Coated with Alkyne-Containing Polyacrylates for Click Chemistry. *J. Nanopart. Res.* 2013, 15 (6), 1747.
- (26) Wang, C.; Fan, Y.; Hu, M. X.; Xu, W.; Wu, J.; Ren, P. F.; Xu, Z. K. Glycosylation of the Polypropylene Membrane Surface via Thiol-Yne Click Chemistry for Lectin Adsorption. *Colloids Surf., B* 2013, 110, 105–112.
- (27) Liu, Y.; Li, C. M.; Hu, W.; Lu, Z. High Performance Protein Microarrays Based on Glycidyl Methacrylate-Modified Polyethylene Terephthalate Plastic Substrate. *Talanta* 2009, 77 (3), 1165–1171.
- (28) Xiu, K. M.; Cai, Q.; Li, J. S.; Yang, X. P.; Yang, W. T.; Xu, F. J. Anti-Fouling Surfaces by Combined Molecular Self-Assembly and Surface-Initiated ATRP for Micropatterning Active Proteins. *Colloids Surf., B* 2012, 90, 177–183.
- (29) Chang, Y.; Shu, S.-H.; Shih, Y.-J.; Chu, C.-W.; Ruan, R.-C.; Chen, W.-Y. Hemocompatible Mixed-Charge Copolymer Brushes of Pseudozwitterionic Surfaces Resistant to Nonspecific Plasma Protein Fouling. *Langmuir* 2010, 26 (5), 3522–3530.
- (30) Rodriguez Emmenegger, C.; Brynda, E.; Riedel, T.; Sedlakova, Z.; Houska, M.; Alles, A. B. Interaction of Blood Plasma with Antifouling Surfaces. *Langmuir* 2009, 25 (11), 6328–6333.
- (31) Zhang, Z.; Zhang, M.; Chen, S.; Horbett, T. A.; Ratner, B. D.; Jiang, S. Blood Compatibility of Surfaces with Superlow Protein Adsorption. *Biomaterials* 2008, 29 (32), 4285–4291.
- (32) Fuchs, A. V.; Ritz, S.; Putz, S.; Mailander, V.; Landfester, K.; Ziener, U. Bioinspired Phosphorylcholine Containing Polymer Films with Silver Nanoparticles Combining Antifouling and Antibacterial Properties. *Biomater. Sci.* 2013, 1 (5), 470–477.
- (33) Fuchs, A. V.; Walter, C.; Landfester, K.; Ziener, U. Biomimetic Silver-Containing Colloids of Poly(2-methacryloyloxyethyl phosphorylcholine) and Their Film-Formation Properties. *Langmuir* 2012, 28 (11), 4974–4983.

- (34) Ishihara, K.; Nomura, H.; Mihara, T.; Kurita, K.; Iwasaki, Y.; Nakabayashi, N. Why do Phospholipid Polymers Reduce Protein Adsorption? *J. Biomed. Mater. Res.* 1998, 39 (2), 323–330.
- (35) Ishihara, K.; Ueda, T.; Nakabayashi, N. Preparation of Phospholipid Polymers and Their Properties as Polymer Hydrogel Membranes. *Polym. J.* 1990, 22 (5), 355–360.
- (36) Iwasaki, Y.; Fujke, A.; Kurita, K.; Ishihara, K.; Nakabayashi, N. Protein Adsorption and Platelet Adhesion on Polymer Surfaces Having Phospholipid Polar Group Connected with Oxyethylene Chain. *J. Biomater. Sci., Polym. Ed.* 1997, 8 (2), 91–102.
- (37) Ishihara, K.; Oshida, H.; Endo, Y.; Ueda, T.; Watanabe, A.; Nakabayashi, N. Hemocompatibility of Human Whole Blood on Polymers with a Phospholipid Polar Group and Its Mechanism. *J. Biomed. Mater. Res.* 1992, 26 (12), 1543–1552.
- (38) Iwata, R.; Suk-In, P.; Hoven, V. P.; Takahara, A.; Akiyoshi, K.; Iwasaki, Y. Control of Nanobiointerfaces Generated from Well-Defined Biomimetic Polymer Brushes for Protein and Cell Manipulations. *Biomacromolecules* 2004, 5 (6), 2308–2314.
- (39) Park, J.; Kurosawa, S.; Takai, M.; Ishihara, K. Antibody Immobilization of Phospholipid Polymer Layer on Gold Substrate of Quartz Crystal Microbalance Immunosensor. *Colloids Surf., B* 2007, 55 (2), 164–172.
- (40) Goto, Y.; Matsuno, R.; Konno, T.; Takai, M.; Ishihara, K. Polymer Nanoparticles Covered with Phosphorylcholine Groups and Immobilized with Antibody for High-Affinity Separation of Proteins. *Biomacromolecules* 2008, 9 (3), 828–833.
- (41) Mark, S. S.; Nishizawa, K.; Takai, M.; Ishihara, K. A Bioconjugated Phospholipid Polymer Biointerface with Nanometer-Scaled Structure for Highly Sensitive Immunoassays. In *Bioconjugation Protocols*; Mark, S. S., Ed. Humana Press: New York, 2011; Vol. 751, pp 491–502.
- (42) Nishizawa, K.; Konno, T.; Takai, M.; Ishihara, K. Bioconjugated Phospholipid Polymer Biointerface for Enzyme-Linked Immunosorbent Assay. *Biomacromolecules* 2008, 9 (1), 403–407.
- (43) Sakai-Kato, K.; Kato, M.; Ishihara, K.; Toyo'oka, T. An Enzyme-Immobilization Method for Integration of Biofunctions on a Microchip Using a Water-Soluble Amphiphilic Phospholipid Polymer Having a Reacting Group. *Lab Chip* 2004, 4 (1), 4–6.
- (44) Iwata, R.; Satoh, R.; Iwasaki, Y.; Akiyoshi, K. Covalent Immobilization of Antibody Fragments on Well-Defined Polymer Brushes via Site-Directed Method. *Colloids Surf., B* 2008, 62 (2), 288–298.
- (45) He, H.; Zhang, Y.; Gao, C.; Wu, J. 'Clicked' Magnetic Nanohybrids with a Soft Polymer Interlayer. *Chem. Commun.* 2009, 13, 1655–1657.
- (46) Vilaivan, T.; Srisuwannaket, C. Hybridization of Pyrrolidinyl Peptide Nucleic Acids and DNA: Selectivity, Base-Pairing Specificity, and Direction of Binding. *Org. Lett.* 2006, 8 (9), 1897–1900.
- (47) Dittmangklo, B.; Boonlua, C.; Suparpprom, C.; Vilaivan, T. Reductive Alkylation and Sequential Reductive Alkylation-Click Chemistry for On-Solid-Support Modification of Pyrrolidinyl Peptide Nucleic Acid. *Bioconjugate Chem.* 2013, 24 (4), 614–625.
- (48) Shen, W.; Qiu, Q.; Wang, Y.; Miao, M.; Li, B.; Zhang, T.; Cao, A.; An, Z. Hydrazine as a Nucleophile and Antioxidant for Fast Aminolysis of RAFT Polymers in Air. *Macromol. Rapid Commun.* 2010, 31 (16), 1444–1448.
- (49) Metallo, S. J.; Kane, R. S.; Holmlin, R. E.; Whitesides, G. M. Using Bifunctional Polymers Presenting Vancomycin and Fluorescein Groups to Direct Anti-Fluorescein Antibodies to Self-Assembled Monolayers Presenting *D*-Alanine-*D*-Alanine Groups. *J. Am. Chem. Soc.* 2003, 125 (15), 4534–4540.
- (50) Su, X.; Wu, Y.-J.; Knoll, W. Comparison of Surface Plasmon Resonance Spectroscopy and Quartz Crystal Microbalance Techniques for Studying DNA Assembly and Hybridization. *Biosens. Bioelectron.* 2005, 21 (5), 719–726.
- (51) Ellis, B.; Smith, R. *Polymers: A Property Database*, 2nd ed.; Taylor & Francis Group: Boca Raton, FL, 2008.
- (52) Wu, T.; Gong, P.; Szeifer, I.; Vlcek, P.; Subr, V.; Genzer, J. Behavior of Surface-Anchored Poly(acrylic acid) Brushes with Grafting Density Gradients on Solid Substrates: I. Experiment. *Macromolecules* 2007, 40 (24), 8756–8764.
- (53) Green, N. M. Avidin. *Adv. Protein Chem.* 1975, 29, 85–133.
- (54) Huisgen, R. 1,3-Dipolar cycloadditions: Past and future. *Angew. Chem., Int. Ed. Engl.* 1963, 2 (10), 565–598.
- (55) Tornøe, C. W.; Christensen, C.; Meldal, M. Peptidotriazoles on Solid Phase: [1,2,3]-Triazoles by Regiospecific Copper(I)-Catalyzed 1,3-Dipolar Cycloadditions of Terminal Alkynes to Azides. *J. Org. Chem.* 2002, 67 (9), 3057–3064.
- (56) Hansen, J. T. *Netter's Clinical Anatomy*, 3rd ed.; Elsevier, Inc: Philadelphia, PA, 2014.
- (57) Kim, G.; Park, S.; Jung, J.; Heo, K.; Yoon, J.; Kim, H.; Kim, I. J.; Kim, J. R.; Lee, J. I.; Ree, M. Novel Brush Polymers with Phosphorylcholine Bristle Ends: Synthesis, Structure, Properties, and Biocompatibility. *Adv. Funct. Mater.* 2009, 19 (10), 1631–1644.
- (58) Nielsen, P.; Egholm, M.; Berg, R.; Buchardt, O. Sequence-Selective Recognition of DNA by Strand Displacement with a Thymine-Substituted Polyamide. *Science* 1991, 254 (5037), 1497–1500.
- (59) Ananthanawat, C.; Vilaivan, T.; Hoven, V. P.; Su, X. Comparison of DNA, Aminoethylglycyl PNA and Pyrrolidinyl PNA as Probes for Detection of DNA Hybridization Using Surface Plasmon Resonance Technique. *Biosens. Bioelectron.* 2010, 25 (5), 1064–1069.
- (60) Suparpprom, C.; Srisuwannaket, C.; Sangvanich, P.; Vilaivan, T. Synthesis and Oligodeoxynucleotide Binding Properties of Pyrrolidinyl Peptide Nucleic Acids Bearing Propyl-2-Aminocyclopentanecarboxylic Acid (ACPC) Backbones. *Tetrahedron Lett.* 2005, 46 (16), 2833–2837.
- (61) Ananthanawat, C.; Vilaivan, T.; Mekboonsonglarp, W.; Hoven, V. P. Thiolated Pyrrolidinyl Peptide Nucleic Acids for the Detection of DNA Hybridization Using Surface Plasmon Resonance. *Biosens. Bioelectron.* 2009, 24 (12), 3544–3549.



Contents lists available at ScienceDirect

Biosensors and Bioelectronics

journal homepage: www.elsevier.com/locate/bios

Enhancing capacitive DNA biosensor performance by target overhang with application on screening test of HLA-B*58:01 and HLA-B*57:01 genes



Orawan Thipmanee^{a,b,c}, Apon Numnuam^{a,b,c}, Warakorn Limbut^{a,b,d},
Chittanon Buranachai^{a,e}, Proespichaya Kanatharana^{a,f,g}, Tirayut Vilaivan^f,
Nattiya Hirankarn^{g,h,*}, Panote Thavarungkul^{a,h,g,*}

^a Trace Analysis and Biosensor Research Center, Prince of Songkla University, Hat Yai, Songkhla 90112, Thailand

^b Center of Excellence for Innovation in Chemistry, Faculty of Science, Prince of Songkla University, Hat Yai, Songkhla 90112, Thailand

^c Department of Chemistry, Faculty of Science, Prince of Songkla University, Hat Yai, Songkhla 90112, Thailand

^d Department of Applied Science, Faculty of Science, Prince of Songkla University, Hat Yai, Songkhla 90112, Thailand

^e Department of Physics, Faculty of Science, Prince of Songkla University, Hat Yai, Songkhla 90112, Thailand

^f Organic Synthesis Research Unit, Department of Chemistry, Faculty of Science, Chulalongkorn University, Bangkok 10330, Thailand

^g Department of Microbiology, Faculty of Medicine, Chulalongkorn University, Bangkok 10330, Thailand

^h Center of Excellence in Immunology and Immune-Mediated Diseases, Chulalongkorn University, Bangkok 10330, Thailand

ARTICLE INFO

Article history:

Received 18 December 2015

Received in revised form

12 March 2016

Accepted 24 March 2016

Available online 28 March 2016

Keywords:

Label-free capacitive DNA biosensor

acpcPNA probe

Target DNA overhang

HLA-B*58:01

HLA-B*57:01

ABSTRACT

A highly sensitive label-free DNA biosensor based on PNA probes immobilized on a gold electrode was used to detect a hybridization event. The effect of a target DNA overhang on the hybridization efficiency was shown to enhance the detected signal and allowed detection at a very low concentration. The sensors performances were investigated with a complementary target that had the same length as the probe, and the signal was compared to the target DNAs with different lengths and overhangs. A longer target DNA overhang was found to provide a better response. When the overhang was on the electrode side the signal enhancement was greater than when the overhang was on the solution side due to the increased thickness of the sensing surface, hence produced a larger capacitance change. Using conformationally constrained acpcPNA probes, double stranded DNA was detected sensitively and specifically without any denaturing step. When two acpcPNA probes were applied for the screening test for the double stranded HLA-B*58:01 and HLA-B*57:01 genes that are highly similar, the method differentiated the two genes in all samples. Both purified and unpurified PCR products gave comparable results. This method would be potentially useful as a rapid screening test without the need for purification and denaturation of the PCR products.

© 2016 Elsevier B.V. All rights reserved.

1. Introduction

Specific-sequence detection of DNA has potential applications in many areas such as clinical diagnostics (O'Connor and Glynn, 2010), detection of genetically modified organisms (Manzanares-Palenzuela et al., 2015) and environmental monitoring (Paniel et al., 2013). DNA biosensors are generally composed of single stranded DNA (ssDNA) or peptide nucleic acid (PNA) probes immobilized on a transducer surface that are able to form a duplex with the target DNAs

(Odenthal and Gooding, 2007). We have recently reported the formation of label-free DNA biosensors based on the sensitive capacitive detection using pyrrolidiny PNA with a conformationally rigid *o*-propyl-2-aminocyclopentanecarboxylic acid (ACPC) backbone (acpcPNA) (Sankoh et al., 2013; Thipmanee et al., 2012; Vilaivan, 2015). When tested with target DNAs of the same length as the PNA probe, they provided excellent performance. However, real DNA samples are usually much longer than the probe, and exist in double-stranded forms. It was therefore of interest to investigate the performance of a biosensor with a long and double stranded DNA target, as this was a more realistic situation when testing real samples.

The influence of target length, or more accurately the overhang, on the hybridization response in a label-free biosensor has been reported using cantilevers (Mukhopadhyay et al., 2005) and mostly by detection using electrochemical impedance spectrometry (EIS)

* Corresponding author at: Department of Physics, Faculty of Science, Prince of Songkla University, Hat Yai, Songkhla 90112, Thailand.

** Corresponding author at: Department of Microbiology, Faculty of Medicine, Chulalongkorn University, Bangkok 10330, Thailand.

E-mail addresses: nattiya.hirankarn@psu.ac.th (N. Hirankarn),
panote.t@psu.ac.th (P. Thavarungkul).

(Booth et al., 2011; Corrigan et al., 2014; Riedel et al., 2014; Shamsi and Kraatz, 2011). It was expected that the response would increase with the length of the overhang. However, using the EIS response (charge transfer resistance – R_{ct}), the results seemed to vary, from an increased response with the length of the overhang (on the solution side) (Booth et al., 2011) to the existence of an optimal overhang length for the highest response (Corrigan et al., 2014) and to a decrease in the response with the length of overhang despite the increased mass on the sensing surface (Riedel et al., 2014). In all cases the explanation for these behaviors was attributed to the increased negative charges from the overhang target DNA but with different principles on its effect on the electrode/electrolyte charge transfer, hence, the different outcomes. The position of the overhang in the DNA target was also of interest (Riedel et al., 2014; Shamsi and Kraatz, 2011), however, the results were inconclusive, possibly due to the different experimental conditions. Since a capacitive system relies on the ability of an electrode to store a charge without any charge transfer, it was important to see how the target DNAs with different overhangs contributed to the capacitive detection. Capacitance determination is generally performed via EIS or by a potentiostatic step method (Berggren et al., 2001). In this case when a potential was given to an electrode, with the insulating sensing layer on the surface, the electrode will possess the same amount of charge as the solution but with an opposite sign. It was expected that the overhang, with its increased mass on the electrode surface changed the thickness of the insulating sensing layer, hence, increased the change in the capacitance.

In this work the effect of the target DNA overhang on the hybridization efficiency of a potentiostatic step capacitive DNA sensor based on an acpcPNA probe was, for the first time, studied with the objective that this effect may help to enhance the detected signal and that the system could be readily applied to a real sample. The detection of the single stranded target DNAs with different lengths and overhangs was first explored. The advantage of using the acpcPNA probe for binding with the double stranded target DNAs was also reported. As a proof of the application we investigated the performance of the developed DNA biosensor on the screening test for the PCR products of two interesting genes HLA-B*58:01 and HLA-B*57:01 in which the targeted sequences have only two nucleotides different (Robinson et al., 2015), and both had long non-hybridizing segments. HLA-B*58:01 is strongly associated with hypersensitivity to allopurinol that is used to treat hyperuricemia and recurrent gout, as for HLA-B*57:01, it strongly predicts hypersensitivity to the anti-retroviral drug abacavir (Yoon et al., 2012). A detection system that can differentiate and detect the PCR product rapidly with high accuracy is needed, to screen for patients with HLA-B*57:01 or HLA-B*58:01 in the clinic to identify those who should avoid the prescription of potentially harmful drugs. The standard method to detect a specific HLA type in the laboratory is usually conducted by the polymerase chain reaction (PCR) that employs several sets of primers (Horn et al., 1995) or by using nested PCR (Martin et al., 2005) followed by the time consuming detection of the PCR products by gel electrophoresis. The ability of this capacitive DNA biosensor to achieve a rapid, sensitive and selective differentiation between HLA-B*57:01 and HLA-B*58:01 genes was demonstrated.

2. Experimental

2.1. Materials

The 11-mer lysine-modified acpcPNA probes were synthesized by Mrs. Chotima Vilaivan at Chulalongkorn University, Thailand according to the published protocol (Vilaivan and Srisuwannaket, 2006). The acpcPNA probes were purified by reverse phase HPLC (to 90% purity) and their identities were verified by MALDI-TOF

mass spectrometry. The sequence of the lysine-modified acpcPNA probes for both the HLA-B*58:01 (P1 and P2) and the HLA-B*57:01 (P3) genes are shown in Table 1.

The synthetic target DNAs used in this work were synthesized and purified by the Bioservice Unit, National Science and Technology Development Agency and BioDesign Co., Ltd., Thailand, and their sequences are shown in Table 1. The HLA-B*58:01 and HLA-B*57:01 PCR-amplified DNA samples were 200 bases in length, with only a 2-nucleotide difference (Table 1). These genes were amplified from the genomic DNA, extracted from white blood cells (see Supplementary material for the PCR protocol) and their concentrations were determined from the optical density at 260 nm using a Nanodrop spectrophotometer (Wilmington, USA).

The blocking thiol, 11-mercapto-1-undecanol (11-MUL) was from Aldrich (Steinheim, Germany), para-phenylenediamine (p-PD) was from UNILAB reagent (Sydney-Melbourne, Australia). Glutaraldehyde was from Sigma-Aldrich (Steinheim, Germany). All buffers were prepared with deionized water treated with a reverse osmosis-deionizing system (Pentair, Inc., USA). Before use, buffers were filtered through a nylon membrane (0.2 μm pore size, 47 mm diameter, Vertical[®], Spain) before being degassed. Other chemicals were analytical reagent grade and were used as received.

2.2. Immobilization of acpcPNA probe

Gold rod electrodes (99.99% purity) with a diameter of 3.0 mm were cleaned by dipping in piranha solution (3:1%v/v of conc. H_2SO_4 : 30% H_2O_2) for 20 min followed by rinsing with distilled water. Then, they were polished using an alumina slurry (5, 1, and 0.3 μm), on a polishing cloth until a mirror-like surface was obtained and subsequently washed with distilled water. The electrodes were placed inside a plasma cleaner (Model PDC-32G, Harrick, New York, USA) to remove organic and inorganic molecules adsorbed on the surface of the electrodes.

The P1, P2 and P3 PNA probes were immobilized on separate electrodes via a polymer layer of pPD (PpPD) following an earlier reported protocol (Sankoh et al., 2013) (Supplementary material Fig. S1). The pPD monomer of 5.0 mM was first prepared in 1.0 mM sodium acetate buffer pH 5.18. Electropolymerization was carried out by cyclic voltammetry at 15 scans using the potential range from 0.0 to 0.8 V vs. Ag/AgCl with a scan rate of 50 mVs^{-1} . The PpPD coated electrode was cleaned by rinsing with distilled water and treated with 5.0% (v/v) glutaraldehyde in 10 mM phosphate buffer pH 7.00 at room temperature for 20 min to activate the aldehyde group. Then 20 μL of 5.0 μM of acpcPNA probe was placed on the PpPD coated electrode and left for 24 h at 4 °C. The electrode was then treated with 1.0 mM ethanalamine pH 8.00 for 7 min to deactivate all the remaining aldehyde groups not coupled to the immobilized acpcPNA probe. Finally, 1.0 mM 11-MUL solution was applied for 1 h to block the remaining pinholes, hence, preventing any non-specific binding on the electrode surface.

2.3. Capacitance measurement

The measurements were performed in a flow-injection system. The modified gold electrode was used as the working electrode together with an Ag/AgCl reference electrode and a Pt wire counter electrode connected to a potentiostat (Model EA161, EDAQ, New South Wales, Australia). The conditions were, carrier buffer: 10 mM phosphate buffer pH 7.00, flow rate: 50 $\mu\text{L min}^{-1}$, sample volume: 300 μL and the regeneration solution: 50 mM NaOH, 300 μL .

The capacitance was obtained based on a potential step method (Berggren et al., 2001) as previously described (Sankoh et al., 2013) (Supplementary material Fig. S1). In brief, the transient current response of an applied potential step (50 mV, 1 pulse/min) was used to obtain the linear least-square fitting of $\ln(i(t))$ versus t . The

Table 1
Sequence of PNA probes and target DNAs. The italic and underlining alphabets indicate the mismatched and non-hybridizing segment, respectively.

| Name | Type | Sequence | Number of base |
|-------------|---|--|----------------|
| P1 | acpcPNA probe for HLA-B*58:01 gene | Ac-GCTCCGTCCTC-LysNH ₂ (N-C) | 11 |
| P2 | acpcPNA probe for HLA-B*58:01 gene (one base shift from P1) | Ac-CTCCGTCCTCG-LysNH ₂ (N-C) | 11 |
| P3 | acpcPNA probe for HLA-B*57:01 gene | Ac-CGCCATCCTCG-LysNH ₂ (N-C) | 11 |
| T1 | Single stranded complementary to P1 | 5'- GAGGACGGAGC -3' | 11 |
| T2 | Single stranded complementary to P1 Overhang, 15 bases on each side | 5'-CGACGCCCGGAGTCC GAGGACGGAGC CCCC GGCGCC ATGGA-3' | 41 |
| T2mis1 | Single stranded, single mismatched to P1 Overhang, 15 bases on each side | 5'-CGACGCCCGGAGTCC GAGGATGGAG CCCC GGCGCC ATGGA-3' | 41 |
| T2mis2 | Single stranded, double mismatched to P1 Overhang, 15 bases on each side | 5'-CGACGCCCGGAGTCC GAGGTCGAGC CCCC GGCGCC ATGGA-3' | 41 |
| T3 | Single stranded complementary to P1 Overhang, 25 bases on each side | 5'-GGTTCGAGAGCGAGCCCGGAGTCC GAGGACGGAG CCCCGGCGCCATGGATAGAGCAGGA-3' | 61 |
| T4 | Single stranded complementary to P1 Overhang, 54 bases on solution side | 5'- GAGGACGGAG CCCCGGCGCC ATGGATAGAGCAGGAGGGGCCCGA GTATTGGGACGGGACACAC-3' | 65 |
| T5 | Single stranded complementary to P1 Overhang, 54 bases on electrode side | 5'-GGGTACTGTGGACGACCCAGTT CGTGAGGTTGACAGCGAGC CCGGAGTCC GAGGACGGAGC -3' | 65 |
| HLA-B*58:01 | Double stranded PCR product Overhang, 107 bases on electrode side, 82 bases on solution side Bold alphabets show the sequence complementary to P2, the sequence complementary to P1 is one base shift to the left | 5'-TTTCTACACCCGATGTC CCGGCCCGCGGGGAGC CCGCTTCATCGCAGTGGGC TACGTGGACGA-CACCCAGTT CGTGAGGTTGACAGCGAGC CCGCGAGTCC GAGGACGGAG CCCC GGCGCCATGGATAGAGCAGGAGGGCCCGGAGTATT GGGACGGGAGACCGGAAC ATGAAGGCCTCCCGCAGACTI-3' | 200 |
| HLA-B*57:01 | Double stranded PCR product, 2-nucleotide difference from the HLA-B* 5801 Overhang, 107 bases on electrode side, 82 bases on solution side Bold alphabets show the sequence complementary to P3 | 5'-TTTCTACACCCGATGTC CCGGCCCGCGGGGAGC CCGCTTCATCGCAGTGGGC TACGTGGACGA-CACCCAGTT CGTGAGGTTGACAGCGAGC CCGCGAGTCC GAGGATGGG CCCC GGCGCCATGGATAGAGCAGGAGGGCCCGGAGTATT GGGACGGGAGACCGGAAC ATGAAGGCCTCCCGCAGACTI-3' | 200 |

value of the capacitance of the electrode surface, C_{total} was then obtained from the slope of the linear regression equation. The measuring flow cell had a dead volume of approximately 10 μ L. The flow of the carrier buffer through the measuring cell was maintained by a peristaltic pump (Miniplus3, Gilson, France) that provided a baseline capacitance. Then, the synthetic target DNA or the gene sample with a volume of 300 μ L was injected into the flow system and the hybridization between the PNA probes on the electrode surface and the target DNAs in the flow through sample was performed at room temperature. The decrease in the total capacitance upon hybridization due to the increase of the dielectric layer thickness can be described by Eq. (1):

$$\frac{1}{C_{total}} = \frac{1}{C_{PpPD}} + \frac{1}{C_{acpcPNA}} + \frac{1}{C_{DNA}} \quad (1)$$

where C_{total} is the total double layer capacitance measured at the electrode-solution interface, C_{PpPD} is the capacitance of the PpPD modified layer, $C_{acpcPNA}$ is the capacitance of the acpcPNA layer,

and C_{DNA} is the capacitance of the DNA layer. The measure C_{total} was plotted as a function of time. The capacitance change (ΔC) is the difference between the capacitance obtained before and after the binding of the PNA probe and the target DNA (Supplementary material Fig. S1). The regeneration solution (50 mM NaOH, 300 μ L) was then injected and flowed through the electrode surface to break the binding between the probe and the target and the capacitance returned to its baseline, ready for a new analytical cycle.

3. Results and discussion

3.1. Effect of target DNA overhang

The hybridization between the PNA probe and target DNA of unequal lengths results in non-hybridized segments. The target DNA overhang was first investigated, with an immobilized P1 probe, using different lengths of synthetic ssDNAs with overhangs

on either side between 1.0×10^{-14} and 1.0×10^{-6} M. Linear relationship between ΔC and the logarithm of the concentration of all targets were between 1.0×10^{-12} and 1.0×10^{-8} M. The limit of detection (LOD) of the capacitive biosensor for the complementary target DNA (T1) was 1.0 pM (Buck and Lindner, 1991). For the 41 and 61 bases target DNAs (T2 and T3) with a 15 and 25 nt overhang on each side, the limit of detection improved slightly with the length of the overhang, i.e., 0.8 pM and 0.5 pM for the target with a 15 and 25 nt overhang, respectively. For the sensitivity (expressed by the slope of the calibration plot), the results in Fig. 1a indicated that the targets T2 and T3 had higher sensitivities (18.0 ± 1.0 and 23.2 ± 1.1 $\text{nF cm}^{-2} (\log M)^{-1}$, respectively) than the 11 bases DNA without the overhang (11.1 ± 0.2 $\text{nF cm}^{-2} (\log M)^{-1}$). As anticipated a longer overhang (25 bases of the 61 bases T3), which added more mass to the surface, gave a higher sensitivity (and a better LOD). This was in contrast to some earlier reports based on EIS in which the highest R_{ct} was obtained from the hybridization between the DNA probe and the complementary target DNA that has no overhang. The lower response was said to be due to the lower charge transfer resistance caused by the lower hybridization efficiency of a target with an overhang on the electrode side (Shamsi and Kraatz, 2011) or to the direct increase of the negative charges (of the target DNA) near the electrode, which disturbed the permeation of ferri-/ferrocyanide on the electrode (Küedel et al., 2014). These effects were probably overcome by the use of the PNA probe, which has proven to be very efficient for hybridization with target DNA (Vilavain, 2015; Vilavain and Srisuwannaker, 2006) and for the detection of the change in capacitance as it does not depend on the charge transfer.

Further experiments were carried out to see the effect of the position of the overhanging part. This was investigated using two 65 bases as target DNAs with a 54 base overhang on either side (T4 and T5). As shown in Fig. 1b, a much higher sensitivity was obtained

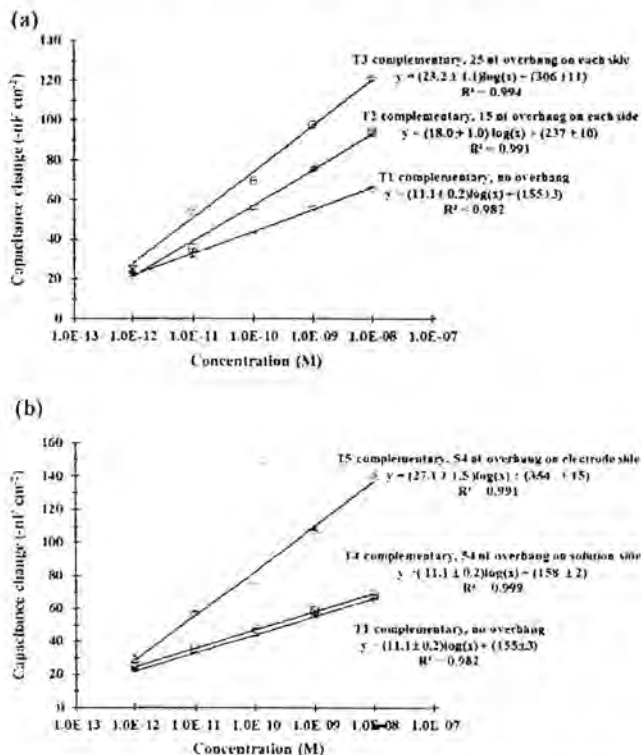


Fig. 1. Capacitance change from the hybridization of probe P1 with the same length target DNA (T1) and (a) target DNAs with different lengths of overhang on both sides, T2 and T3 (b) target DNAs with the same length of overhang (54 bases) but on opposite side (T4 and T5) ($n = 3$).

from the target DNA with the overhanging part on the electrode surface (27.1 ± 1.5 $\text{nF cm}^{-2} (\log M)^{-1}$) compared to the one with the overhang in the solution (11.1 ± 0.2 $\text{nF cm}^{-2} (\log M)^{-1}$). This is most likely because the overhang on the electrode surface pushed the electrolyte further away from the electrode surface, i.e., making the interface thicker resulted in a decreased capacitance (Berggren et al., 2001; Gebbert et al., 1992), and thus increased the ΔC . On the other hand the target DNA with the overhang in the solution gave the same sensitivity as the fully complementary DNA (11 bases) but with a slightly higher signal. It was therefore likely that an overhang of the target DNA on the electrode surface was more effective for displacing water and electrolyte molecules away from the surface, and provided for a more enhanced sensitivity. This is in contrast to the results of Shamsi and Kraatz (2011). Using DNA probes they found that the same length of an overhang on the electrode side, compared to the solution side, decreased the response (ΔR_{ct}). They reasoned that this was most likely due to the decrease in hybridization efficiency caused by steric congestions at the electrode surface. This again confirmed the advantage of this newly reporting system, i.e., the use of a neutral PNA probe can reduce such a steric effect from the DNA-DNA hybridization.

3.2. Detection of double stranded target DNA

As most DNA targets are in duplex forms (dsDNA), almost all previous DNA sensors require denaturation of the target dsDNA prior to detection. One advantage of using PNA is that it can also bind directly to dsDNA or other structured DNA targets in various configurations depending on the base sequence (Armitage, 2003; Wang and Xu, 2004). For the first time, a direct capacitive detection with immobilized PNA probes was investigated for its binding capability to dsDNA targets, with and without denaturation. Two dsDNAs were tested with the P1 probe, i.e., the PCR products of the target HLA-B*58:01 gene and the HLA-B*57:01 gene that had only two nucleotides different. The denaturation was carried out by heating at 90 °C in a water bath for 15 min and rapidly cooled down on ice for 10 min. The responses from the DNAs with and without denaturation are shown in Fig. 2. The slightly higher response of the denatured DNA was most likely due to the better accessibility of the PNA probe to the hybridization segment. However, the responses of the DNA without denaturation were only about 10% lower than those from non-denatured DNA. As expected the responses to the HLA-B*57:01 gene were much lower than those to the HLA-B*58:01, but a similar behavior was obtained, i.e., the denatured DNA gave a higher response than the dsDNA. From the results, this system could be applied to

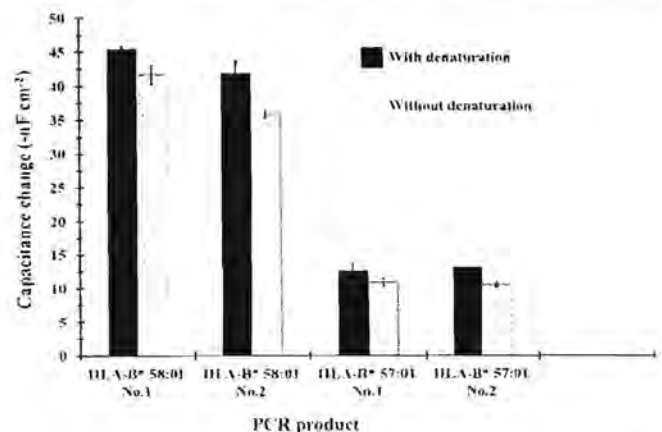


Fig. 2. Capacitance change from the hybridization of probe P1 with 1.0×10^{-11} M PCR product of the HLA-B*58:01 and HLA-B*57:01 genes, with and without denaturation ($n = 3$).

detect target dsDNA without the need for denaturation, and therefore reduced the time taken and simplified the method.

3.3. Analysis of the purified HLA-B*58:01 and HLA-B*57:01 genes

Using the electrode with the immobilized P1 probes, the purified HLA-B*58:01 and HLA-B*57:01 genes were first tested in the concentration range from 1.0×10^{-14} and 1.0×10^{-7} M. The linear range of both targets were from 1.0×10^{-12} to 1.0×10^{-8} M, with the same LOD of 0.4 pM. However, the %signal suppression values (%SS = $100 \times$ (complementary response – mismatched response)/complementary response) within the linear range were only 15–30%. This led to the investigation of using a hybridization suppressor (additive) that helped to control the hybridization behavior of the perfect matched and mismatched target DNA (Lao et al., 2009). Two additives were tested, using the carrier buffer of 100 mM phosphate buffer, pH 7.00. Acetamide (0.10, 0.25, 0.50, 0.80, 0.90 and 1.0 M) and formamide (0.25 M) were investigated with the P1 probe to detect a 41 base target DNA (T2) at 1.0×10^{-10} M.

The additives did lower the responses for both the complementary (T2) and mismatched DNAs (T2mis1 and T2mis2). However, the presence of the additive considerably improved the %SS values (Supplementary material Table S1). Comparing the presence of formamide and acetamide at the same concentration (0.25 M) the latter provided a better %SS. This is because acetamide has a lower dielectric constant (D) than formamide ($D=4.7$ and 109.5 at 25°C , respectively) (Covington and Dickinson, 1973), so gave a lower baseline that resulted in a larger ΔC response. The optimum concentration for acetamide was studied and found to be 0.25 M. This provided the highest %SS for both a single (75%) and double (81%) mismatched DNAs. The HLA-B*58:01 and HLA-B*57:01 genes within the same concentration range were then tested again by adding 0.25 M acetamide in the buffer. The %SS improved by 50–70%, compared to when there was no additive, and therefore the acetamide additive was included for the remaining experiments.

The use of the P2 probe with a slightly different sequence to P1

(one base shift towards the C-terminus: Table 1) for the detection of HLA-B*58:01 was also tested. A calibration curve was established from a purified PCR product of HLA-B*58:01. The linearity between the capacitance change ($-\text{nF cm}^{-2}$) and the logarithm of the HLA-B*58:01 concentration ($\log M$) was observed between 1.0×10^{-12} and 1.0×10^{-8} M (Fig. 3a). The very low concentration of the linear range would allow for detecting a sample with a very small amount of DNA. For samples with high concentration, dilution can be easily performed, hence only a small sample volume is required. The dilution will also reduce any interfering effect from the sample matrix. The performance of the P2 probe was comparable to P1 (data not shown), P2 was then used for further experiments. It should also be noted that the dsDNA of the HLA-B*58:01 gene with a 107-base non-hybridizing segment on the electrode side provided a much higher sensitivity ($36.0 \pm 1.3 \text{ -nF cm}^{-2} (\log M)^{-1}$) (Fig. 3a) than the ssDNA target with a 54 base overhang ($27.1 \pm 1.5 \text{ -nF cm}^{-2} (\log M)^{-1}$) (Fig. 1b). This also confirmed that a longer non-hybridizing segment provided a better sensitivity.

The detection for the HLA-B*57:01 genes yielded a sensitivity of $8.1 \pm 0.2 \text{ -nF cm}^{-2} (\log M)^{-1}$ (Fig. 3a). Although the sensitivity from the purified HLA-B*58:01 was 4.4 times more than the one from the HLA-B*57:01 genes, an incorrect quantitative result may still be obtained. For example, a sample with a large amount of the HLA-B*57:01 genes might give the same response as a sample with a lower amount of the HLA-B*58:01 genes. Therefore, the same samples were detected twice using two probes, and the signals were compared to eliminate the effect of concentration. In this set up, the same sample was tested with two modified electrodes, one with the P2 probes and the other with the P3 probes. Using the P3 probes, the sensitivity to the complementary HLA-B*57:01 was 4.6 times higher than that for the highly similar HLA-B*58:01 (Fig. 3b).

By following this protocol of using two PNA probes, a total of 21 blind purified PCR gene samples (SP1–SP21) from human white blood cells were analyzed. Samples were sequentially diluted from the initial concentration to be approximately 10^{-10} M. This was done to eliminate any interferences from the PCR matrix as well as to adjust the concentration of the sample to be within the linear range

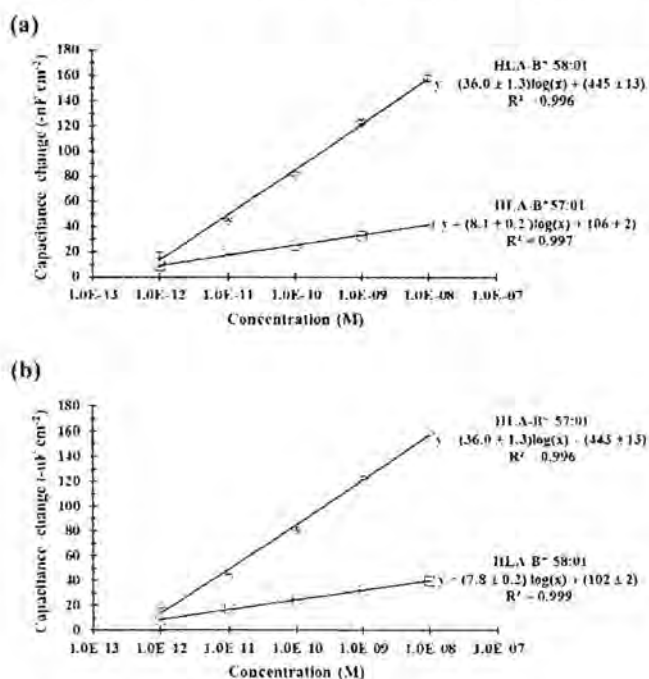


Fig. 3. Calibration plots of purified HLA-B*58:01 and HLA-B*57:01 using modified electrodes with (a) P2 probe (for HLA-B*58:01) and (b) P3 probe (for HLA-B*57:01) with 0.25 M acetamide in phosphate buffer ($n=3$).

Table 2

The results of the blind purified PCR gene samples obtained from the white blood cell using a direct capacitive system (this work, $n=3$) and the Sanger sequencing technique.

| Sample | Concentration (M) | Capacitive DNA biosensor | | Sanger sequencing | |
|--------|-----------------------|---|-----------------|-------------------|------|
| | | Capacitance change ($-\text{nF cm}^{-2}$) | | Gene | |
| | | Probe P2 | Probe P3 | Gene | Gene |
| SP1 | 2.3×10^{-10} | 34 ± 1 | 105 ± 2 | 5701 | 5701 |
| SP2 | 2.2×10^{-10} | 95 ± 2 | 23 ± 1 | 5801 | 5801 |
| SP3 | 1.7×10^{-10} | 29 ± 1 | 99 ± 2 | 5701 | 5701 |
| SP4 | 2.3×10^{-10} | 99 ± 3 | 25 ± 1 | 5801 | 5801 |
| SP5 | 1.3×10^{-10} | 88 ± 2 | 23 ± 2 | 5801 | 5801 |
| SP6 | 2.1×10^{-10} | 97 ± 3 | 28.0 ± 0.2 | 5801 | 5801 |
| SP7 | 2.9×10^{-10} | 35 ± 1 | 103 ± 3 | 5701 | 5701 |
| SP8 | 2.1×10^{-10} | 98 ± 1 | 27 ± 2 | 5801 | 5801 |
| SP9 | 3.3×10^{-10} | 102 ± 3 | 25.0 ± 0.2 | 5801 | 5801 |
| SP10 | 4.1×10^{-10} | 34 ± 2 | 112 ± 1 | 5701 | 5701 |
| SP11 | 4.1×10^{-10} | 33 ± 1 | 113 ± 1 | 5701 | 5701 |
| SP12 | 4.3×10^{-10} | 103 ± 2 | 28 ± 1 | 5801 | 5801 |
| SP13 | 4.1×10^{-10} | 33 ± 1 | 111.0 ± 0.3 | 5701 | 5701 |
| SP14 | 4.2×10^{-10} | 106 ± 1 | 27 ± 1 | 5801 | 5801 |
| SP15 | 4.1×10^{-10} | 108 ± 4 | 27 ± 1 | 5801 | 5801 |
| SP16 | 4.1×10^{-10} | 34 ± 2 | 112 ± 1 | 5701 | 5701 |
| SP17 | 4.1×10^{-10} | 34 ± 2 | 110.0 ± 0.2 | 5701 | 5701 |
| SP18 | 1.8×10^{-10} | 32 ± 1 | 100 ± 1 | 5701 | 5701 |
| SP19 | 1.6×10^{-10} | 93 ± 1 | 25 ± 1 | 5801 | 5801 |
| SP20 | 1.7×10^{-10} | 31 ± 1 | 99 ± 1 | 5701 | 5701 |
| SP21 | 1.8×10^{-10} | 97 ± 1 | 28 ± 1 | 5801 | 5801 |

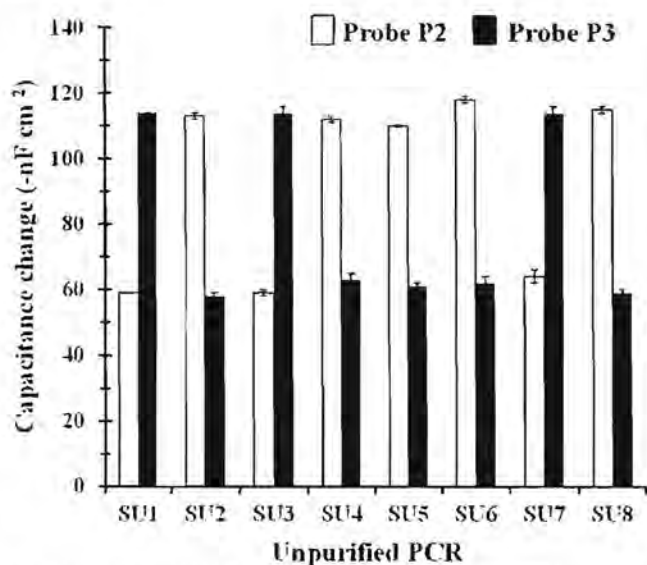


Fig. 4. Capacitance change of the blind unpurified HLA-B*58:01 and HLA-B*57:01 gene samples with 0.25 M acetamide in phosphate buffer ($n=3$).

of the sensor. The results in Table 2 clearly showed that the responses of each sample based on the two probes differed by at least 3 fold. A higher response from the P2 probe indicated a HLA-B*58:01 gene and vice versa. That is, this method had a distinct ability to distinguish between the HLA-B*58:01 and the HLA-B*57:01 genes.

To verify the results, the blind samples were independently tested by the Sanger sequencing technique (Ward Medic Ltd., PART, Malaysia) using the forward primer (5'-TTT CTA CAC CGC CAT GTC C-3') and the reverse primer (5'-AAG TCT GCG CGG AGG C-3'). The results of the capacitive system and the Sanger sequencing technique were in complete agreement (Table 2). Therefore, a direct capacitive DNA biosensor can be used to differentiate between the purified PCR products of HLA-B*58:01 and HLA-B*57:01 with a high specificity. In addition, it required a very small sample volume, of only 1–2 μL of the original PCR product for each measurement.

3.4. Analysis of unpurified PCR samples

Although there was an exceptionally good discrimination between the two genes, the experiments above were carried out with purified PCR products. If a similar discrimination could be achieved with an unpurified product much process time and cost could be reduced. Eight unpurified DNA samples (SU1-SU8, unpurified versions of blind samples SP1-SP8; diluted to be approximately 10^{-10}M) were then tested. A good differentiation between the two genes was obtained (Fig. 4). The results provided a high %SS and the type of genes were in complete agreement with the purified samples SP1-SP8 (Supplementary material Table S2). It is clear that the two genes can be easily distinguished without the need for purification of the PCR sample.

4. Conclusions

This research has shown that enhancement of the capacitive signal can be achieved by using the overhanging part of the target DNA. The longer the overhanging part on the electrode surface the better the signal, i.e., more capacitance change. This would be useful for the detection of samples that have a small amount of DNA. Another advantage is that dsDNA targets can be detected by the immobilized PNA probe without an additional denaturation

step so the method for detection becomes much simpler. This work also demonstrated the successful use of a direct capacitive system based on two acpcPNA probes that could discriminate between the HLA-B*58:01 and HLA-B*57:01 genes from both purified and unpurified PCR samples. Adding acetamide to the carrier buffer improved the discrimination. This method provided for a rapid screening test, with a high sensitivity and specificity, and required only a small sample volume (1–2 μL from the original PCR product). In addition, the unpurified PCR products can be tested directly, without the need for a denaturing step.

Acknowledgements

The authors are grateful to Grants from the Thailand Research Fund (TRF, DPG5780002), The Office of the Higher Education Commission (CHE-SSR-Ph.D-THA); the Center of Excellence for Innovation in Chemistry (PERCH-CIC), the Office of the Higher Education Commission; the Higher Education Research Promotion and National Research University Project of Thailand, Office of the Higher Education Commission; the Trace Analysis and Biosensor Research Center (TAB-RC), and Graduate School, Prince of Songkla University, Hat Yai, Thailand are all gratefully acknowledged. NH would like to acknowledge the Grant for International Research Integration, Chula Research Scholar, Ratchadaphiseksomphot Endowment Fund. The authors thank Dr. Brian Hodgson, Prince of Songkla University, Hat Yai, Songkhla, Thailand for assistance with English.

Appendix A. Supplementary material

Supplementary data associated with this article can be found in the online version at <http://dx.doi.org/10.1016/j.bios.2016.03.065>.

References

- Amisage, B.A., 2003. *Drug Discov Today* 8, 222–228.
- Berggren, C., Björnström, E., Johansson, C., 2001. *Electroanalysis* 13, 1–6 (66).
- Bonth, M.A., Harrison, S., Tavan, S., 2011. *Biosens Bioelectron* 26, 309–311.
- Buck, R.P., Lindner, E., 1994. *Pure Appl Chem* 66, 2527–2528.
- Corrigan, D.K., Schulze, H., McDermott, R.A., Schmitter, J., Henlon, C., Henry, J.F., Bachmann, J.T., Mount, A.K., 2014. *J Electroanal Chem* 771, 25–35.
- Covington, C.K., Dickinson, E., 1973. Introduction and solvent properties of vinyl-4-aminobenzene. In: *Physical Chemistry of Organic Solvents*, Wiley-Interscience, New York, pp. 1–24.
- Gebhart, P., Akawa, T., Sato, M., Saito, W., Saito, R., 1993. *Anal Chim Acta* 266, 997–1003.
- Horn, J., Borchert, W., Grundmann, R., Rüdiger, H., Beil, G., 1993. *J Electroanal Chem* 347, 35.
- Yao, A.J.K., Shi, K., Tang, K.M.M., 2009. *Biosens Bioelectron* 24, 1870–1874.
- Martinez, P., Val, D.M., C.J., Martín-Fernández, F., Sánchez, P., 2012. *J Electroanal Chem* 266, 17–21.
- Martin, A.M., Sauer, D., Marz, E., 2005. *Trends Biotechnol* 23, 374–376.
- Mekhrizadeh, B., Fardipour, M., Khatami, J., Ghanbari, J., 2005. *Sens Actuators B* 112, 536–540.
- O'Connell, L., Glynn, B., 2010. *Expert Rev Med Devices* 7, 129–139.
- Okamoto, K.T., 2002. *Analyst* 131, 603–608.
- Sanfel, G., Barrios, J., López, A., Barrios, J., 2003. *Sens Actuators B* 100, 299–304.
- Recht, M., Lichtenhan, J., Schoning, M., 2001. *J Electroanal Chem* 50, 7867–7874.
- Johnson, J., Havelle, T.A., Holmes, D.R., Miles, P., Patten, J., Mann, S., 2005. *Nature Rev* 43, 1425–1431.
- Sankh, S., Srinivasan, S., Thipmanee, O., Nimmannit, A., Limbut, W., Wanchaisri, P., Viladon, T., Thavarakul, T., 2015. *Sens Actuators B* 205, 1–7 (13).
- Shams, M.H., Khatami, J., 2011. *Analyst* 136, 2107–2111.
- Thipmanee, O., Srinivasan, S., Sankh, S., Nimmannit, A., Limbut, W., Wanchaisri, P., Viladon, T., Thavarakul, T., 2012. *Biosens Bioelectron* 36, 620–625.
- Wang, J., 2013. *Acc Chem Res* 46, 10–16.
- Witkowiak, T., Srinivasan, S., 2006. *Org Lett* 8, 1997–1999.
- Wang, C., Xu, S., 2009. *Electrochim Acta* 54, 111–116.
- Yan, J., An, J., 2009. *J Electroanal Chem* 661, 101–105.





Recyclable magnetite nanoparticle coated with cationic polymers for adsorption of DNA

B. Rutnakornpituk, T. Theppaleak, M. Rutnakornpituk & T. Vilaivan

To cite this article: B. Rutnakornpituk, T. Theppaleak, M. Rutnakornpituk & T. Vilaivan (2016) Recyclable magnetite nanoparticle coated with cationic polymers for adsorption of DNA, Journal of Biomaterials Science, Polymer Edition, 27:11, 1200-1210, DOI: 10.1080/09205063.2016.1189378


To link to this article: <http://dx.doi.org/10.1080/09205063.2016.1189378>


 View supplementary material [↗](#)

 Accepted author version posted online: 20 May 2016.
Published online: 02 Jun 2016.

 Submit your article to this journal [↗](#)

 Article views: 14

 View related articles [↗](#)

 View Crossmark data [↗](#)

Full Terms & Conditions of access and use can be found at
<http://www.tandfonline.com/action/journalInformation?journalCode=tbsp20>

Recyclable magnetite nanoparticle coated with cationic polymers for adsorption of DNA

B. Rutnakornpituk^{a,b}, T. Theppaleak^a, M. Rutnakornpituk^{a,b} and T. Vilaivan^c

^aFaculty of Science, Department of Chemistry and Center of Excellence in Biomaterials, Naresuan University, Phitsanulok, Thailand; ^bFaculty of Science, The Center of Excellence for Innovation in Chemistry, Naresuan University, Phitsanulok, Thailand; ^cOrganic Synthesis Research Unit, Faculty of Science, Department of Chemistry, Chulalongkorn University, Bangkok Thailand

ABSTRACT

Magnetite nanoparticle (MNP) grafted with a cationic copolymer between poly(2-(*N,N*-diethylamino) ethyl methacrylate) and poly(poly(ethylene glycol) methyl ether methacrylate)) for efficient and recyclable adsorption of 5'-fluorescein-tagged DNA (FAM-dT₉) was prepared. MNP having highest degree of positive charge (+32.1 ± 1.9 mV) retained 100% adsorption of FAM-dT₉ during eight adsorption–separation–desorption cycles. The MNP having lower degree of positive charge showed a slight decrease in adsorption percentages (94–98% adsorption) after multiple recycling processes. This biocompatible hybrid material with charged surface and magnetic-responsive properties might be applicable for use as a nanosolid support for efficient and facile separation of various bioentities.

ARTICLE HISTORY

Received 3 February 2016
 Accepted 10 May 2016


KEYWORDS


Magnetite; nanoparticle;
 ionic adsorption; recyclable;
 DNA

1. Introduction

During the last decade, surface modification of magnetite nanoparticle (MNP) has become a rapidly developed strategy for a wide range of applications, especially in biomedical areas such as site-specific drug transfer system,[1] diagnostics,[2] hyperthermia treatment of tumors,[3] and contrast enhancement agents in magnetic resonance imaging.[4] Because of the large surface area-to-volume ratio of MNP, it tends to form macroscopic aggregation due to attractive forces, e.g. dipole–dipole interaction and magnetic force. In an attempt to prevent them from proximity to each other, steric and/or electrostatic stabilization mechanisms were usually employed by coating the particles surface with long-chain polymers and/or charged molecules. In addition, the grafted polymers on the MNP surface can also serve as a platform for designing and tailoring to have specific interactions with various bioentities such as protein,[5] amino acid [6], and DNA.[7]

Recently, two efficient approaches for surface modification of MNP, 'grafting to' and 'grafting from' strategies, have been developed. The 'grafting to' approach involves the anchoring of the pre-synthesized polymers having suitable functional groups to the particle surface,

CONTACT B. Rutnakornpituk  boonjirab@nu.ac.th

 Supplemental data for this article can be accessed <http://dx.doi.org/10.1080/09205063.2016.1189378>

© 2016 Informa UK Limited, trading as Taylor & Francis Group

while the 'grafting from' approach involves the polymerization initiated directly from its surface.[8–10] The latter approach seemed to be an effective synthetic strategy to functionalize MNP surface with high polymer density. The grafted polymer composition and structure on the MNP surface were well controllable particularly when the controlled radical polymerization techniques, such as reversible addition fragmentation chain transfer [11] and atom transfer radical polymerization (ATRP) were employed.[12–14]

In particular, surface modification of MNP with stimuli-responsive polymers has gained much attention because it can produce 'smart' hybrid materials that can sense environmental changes, e.g. temperature, pH, and ionic strength. These materials possessed both magnetically guidable properties of MNP and stimuli-responsive properties of the polymers. These multifunctional materials have been reported for use in many biomedical fields, such as controlled release and immobilization of bioentities. pH-responsive polymers such as poly(2-(N,N-diethylamino) ethyl methacrylate) (PDEAEMA) and/or its derivatives,[15–17] chitosan [18], and poly(ethylenimine), have been grafted from or grafted to the MNP surface. [19,20] These charged polymers-grafted MNP can electrostatically adsorb to charged bioentities such as phosphate groups of DNA [21–23] and amino groups of protein or peptide to applied as hydrophobic affinity for conveniently, efficiently, and quickly concentrating low-concentration peptides.[24,25] Hao and co-workers have reported the use of a magnetic-responsive polycationic poly(2-(dimethylamino) ethyl methacrylate) in the applications for gene vector.[26] In addition, other bio-applications of polycation-grafted MNP such as gene delivery,[27] cell separation [28], and biosensor,[29] have also been reported.

Adsorption of bioentities on MNP surface could be advantageous for practical applications because magnetic MNP can facilitate the separation process with an assistance of an external magnet. In addition, the adsorption percentages of the nanoparticle should be greatly enhanced due to its high surface area-to-volume ratio. Taking advantages of the facile magnetic separation, poly(quaternary ammonium)-coated MNP was synthesized and repeatedly used for an antibacterial purpose.[30] The MNP retained 100% biocidal efficiency against *Escherichia coli* at least eight exposure/collect/recycle procedures without washing with any solvents or water. Recyclable MNP for other applications such as protein separation [31,32] has been reported. Mesoporous silica nanoparticle comprising of magnetite inner core and mesoporous silica shell was reported for use for DNA adsorption/desorption.[33] The use of recyclable cationic MNP for DNA adsorption was previously reported from our group.[34] However, the effect of degree of positive charges of the grafted polymer on the efficiency in DNA adsorption and recycling has never been investigated.

Therefore, the novelty of the current work is that we herein demonstrated the use of MNP grafted with the polymer having various degrees of positive charge for efficient and recyclable adsorption of DNA. The positively charged polymer-grafted MNP was prepared via a surface-initiated ATRP copolymerization of diethylamino ethyl methacrylate (DEAEMA) and/or poly(ethylene glycol) methyl ether methacrylate (PEGMA) in an attempt to tune the degree of positive charge on the MNP surface after quaternization. Effect of the degree of positive charge on the MNP surface on adsorption percentages of a model DNA (T_9) tagged with fluorescein at 5'-position (FAM-d T_9) was investigated. Adsorption percentages of FAM-d T_9 on the MNP were determined by fluorescence spectroscopy and the recycling efficiency of the copolymer-grafted MNP in the adsorption of FAM-d T_9 was also discussed (Figure 1).

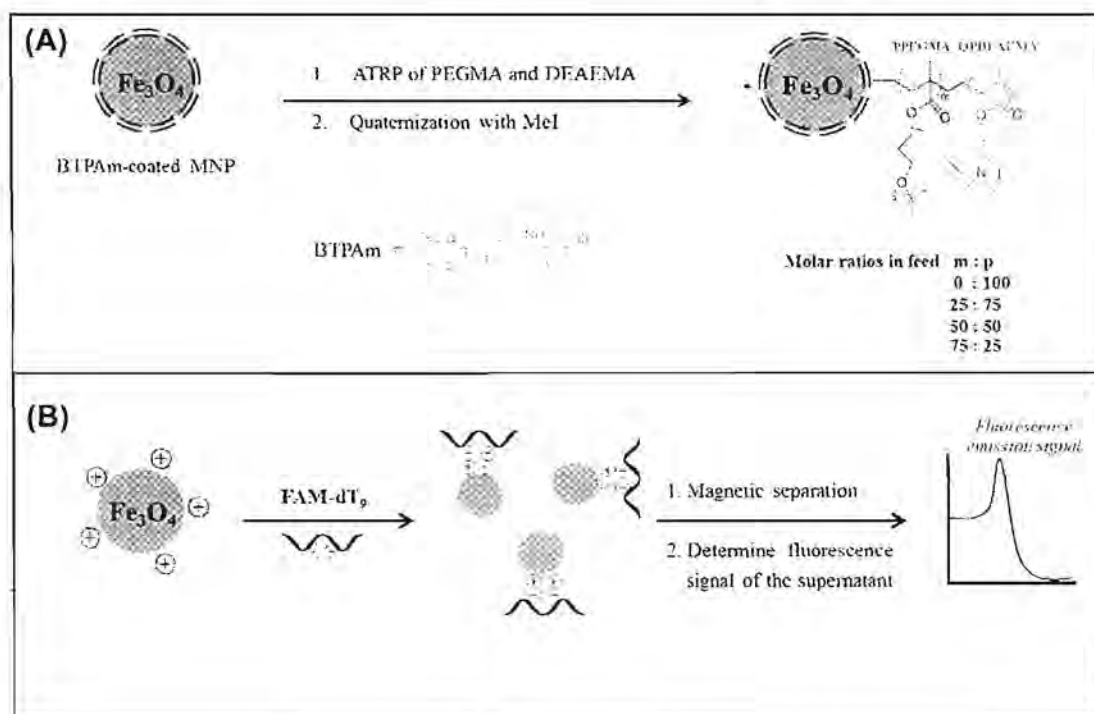


Figure 1. (A) Synthesis of positively charged polymer-grafted MNP and (B) the concept and detection of DNA adsorption on the particle surface. (Please see the online article for the color version of this figure: <http://dx.doi.org/10.1080/09205063.2016.1189378>.)

2. Experimental

2.1. Materials

DEAEMA (99%, Acros) and PEGMA ($\overline{M}_n \sim 300$ g/mol) were passed through a basic alumina column and stored at 4 °C until used. Triethylamine (97%, Carlo Erba) and toluene were purified by distillation over CaH₂. Iron (III) acetylacetonate (99%, Acros), 3-amino-propyl triethoxysilane (APS, 99%, Acros), 2-bromoisobutyryl bromide (BIBB, 98%, Acros), *N,N,N',N',N'*-pentamethyl diethylenetriamine (PMDETA, 99%, Aldrich) and CuBr (98%, Acros) were used as received, DNA T₉ tagged with fluorescein at 5'-position (FAM-dT₉) were purchased from BioDesign (Thailand) and used as received, TE buffer was prepared by the mixing of tris(hydroxymethyl) aminomethane pH 7.5 (99%, Labscan) and diaminoethane tetraacetic acid pH 8 (99%, Carlo Erba) in water, CaCl₂·2H₂O (99.5%, Merck), NaCl (99.5%, Labscan) and other organic solvents were used as received.

2.2. Synthesis of positively charged poly(PEGMA-co-DEAEMA)-grafted MNP

The details of the synthesis of the cationic copolymer-grafted MNP have been described in our previously reported paper.[35] Briefly, oleic acid-coated MNP was first synthesized by the thermal decomposition of Fe(acac)₃ (5 g) in benzyl alcohol (90 ml) at 175 °C for 48 h under N₂ gas. After washing the resultant mixture with ethanol and CH₂Cl₂, oleic acid (4 ml) was then added to the MNP-toluene dispersion, followed by sonication for 3 h under N₂ to obtain oleic acid-coated MNP. BTPAm, an ATRP initiator and synthesized according to the previously reported procedure,[36] was then immobilized onto the oleic acid-coated MNP through the combination of a ligand exchange reaction and silanization.

To prepare the copolymers via a surface-initiated ATRP from the BTPAm-coated MNP, the reaction having 50:50:1:1 molar ratio of PEGMA:DEAEMA:CuBr:PMDETA, respectively, is herein explained in details as an example. Other reactions were performed in a similar manner with an appropriate PEGMA-to-DEAEMA molar ratio. PEGMA (2.4 ml, 8.4 mmol), DEAEMA (1.7 ml, 8.4 mmol), CuBr (0.024 g, 0.17 mmol) and BTPAm-coated MNP (0.1 g, 8.89 $\mu\text{mol Br}$) were dissolved in toluene (2.4 ml) in a Schenk tube. After applying three freeze-pump-thaw cycles to the mixture, PMDETA (0.035 ml, 0.17 mmol) was added to the mixture and the ATRP was performed at 50 °C for 3 h to obtain about 50% monomer conversion. After centrifugation, the MNP was thoroughly washed with ethanol and dried *in vacuo*. To quaternize the copolymer-grafted MNP, methyl iodide (5 ml) was added dropwise to the MNP (0.1 g) suspended in THF (tetrahydrofuran) (5 ml). After sonication for 3 h in dark, the MNP was separated by an external magnet and washed with THF. The particles were dried *in vacuo* to give a fine black powder of quaternized poly(PEGMA-co-DEAEMA)-grafted MNP.

2.3. Determination of FAM-dT₉ adsorption percentages on the positively charged copolymer-grafted MNP

After sonication of MNP dispersion (1.5 mg in 2 ml of TE buffer) for 30 min, 100 μl of the dispersion was then mixed with 3 μl of 10 μM FAM-dT₉ solution (30 pmol of FAM-dT₉ used) by stirring. After applying a permanent magnet, the adsorption percentages of the copolymer-grafted MNP to FAM-dT₉ were determined from the fluorescence signal intensity of the non-adsorbed FAM-dT₉ remaining in the supernatant. The fluorescence emission signal at $\lambda_{\text{max}} = 520 \text{ nm}$ was used to determine the adsorption percentages of FAM-dT₉ on the MNP according to Equation (1),

$$\text{Adsorption percentage} = [(A - B)/A] \times 100 \quad (1)$$

where A is the initial concentration of FAM-dT₉ before adsorption and B is the concentration of FAM-dT₉ in the supernatant after adsorption.

2.4. Determination of the recycling efficiency of the copolymer-grafted MNP in adsorption of FAM-dT₉

To recycle the copolymer-grafted MNP for adsorption of FAM-dT₉, the precipitated MNP was thoroughly washed with $3 \times 100 \mu\text{l}$ of an optimal salt solution (NaCl or CaCl₂) to wash off the FAM-dT₉ adsorbed on the MNP surface. The fluorescence emission signal at $\lambda_{\text{max}} = 520 \text{ nm}$ was used to investigate of the salt solutions after washing the FAM-dT₉ adsorbed on the MNP. After complete desorption of FAM-dT₉ from the MNP, 100 μl of dispersion particles were then suspended in 3 μl of fresh 10 μM FAM-dT₉ solutions (30 pmol of FAM-dT₉ used) with stirring. After precipitation of the MNP, the FAM-dT₉ in the supernatant (non-adsorbed portion) was again quantified by fluorescence spectroscopy. The fluorescence emission signal at $\lambda_{\text{max}} = 520 \text{ nm}$ was used to determine desorption percentages of FAM-dT₉ from the MNP according to Equation (2),

$$\text{Desorption percentage} = [(C)/D] \times 100 \quad (2)$$

where C is the concentration of FAM-dT₉ in the supernatant after washing process and D is the concentration of FAM-dT₉ adsorbed of the MNP. The adsorption–separation–desorption process was performed repeatedly to evaluate the recycling efficiency of the copolymer-grafted MNP in adsorption with FAM-dT₉ using Equation (3),

$$\text{Recycling efficiency (\%)} = [(E)/F] \times 100 \quad (3)$$

where E is the adsorption percentage of the MNP after recycling and F is the adsorption percentage of the MNP at initial.

2.5. Characterization

Zeta potential of the particles was measured by photocorrelation spectroscopy using NanoZS4700 nanoseries Malvern instrument. The sample dispersions were sonicated for 30 min before the measurement at 25 °C without filtration. The DNA-binding capability of the MNP was determined by fluorescence spectrometer on a Perkin-Elmer instrument model LS 55 using a DNA T₉ tagged with fluorescein at the 5'-position (FAM-dT₉) with $\lambda_{\text{excited}}/\lambda_{\text{emission}} = 495/520$ nm.

3. Results and discussion

This work presents the use of the magnetically guidable and recyclable MNP having positively charged surface for recyclable adsorption of DNA. The degree of positive charge on the MNP surface can be fine-tuned by systematically varying molar ratio of PEGMA to DEAEMA on the particle surface. The preparation and characterization of the polymer-grafted MNP has been previously reported from our group; [35] the main objective of the current work is to demonstrate the applications of such particles for DNA adsorption and recovery. The effect of degree of positive charge of the particles on its recycling efficiency in adsorption of DNA was investigated using FAM-dT₉ as a representative negatively charged bioentity because it can be quantitatively determined via fluorescence spectroscopy.

To investigate the composition of the copolymer-grafted MNPs, the relative amount of the copolymer that can be grafted on the particle surface was investigated via TGA (thermogravimetric analysis). Using the hypothesis that char yield was the weight of magnetite core remaining at 600 °C, the weight loss of the samples was the decomposed organic components including BTPAm and the copolymers that grafted to the particle surface. From the TGA results shown in the supporting information (Figure 1S), BTPAm content in BTPAm-coated MNP was about 10% and those of the copolymers in each sample were not significantly different from each other (ranging between 10% and 17%).

To validate the concept of adsorption of FAM-dT₉ on the MNP, FAM-dT₉ was loaded in the MNP dispersed in buffer solutions (Figure 2) and the adsorption percentages at equilibrium of FAM-dT₉ to the particle was then determined. After the magnetic separation of the FAM-dT₉-adsorbed MNP, the fluorescence emission signals of the supernatant were determined at 5-min interval and compared to a calibration curve (Figure 2S in the supporting information). The decrease in the fluorescence signal reflected the FAM-dT₉ adsorbed on the MNP surface and this can be calculated according to Equation (1).

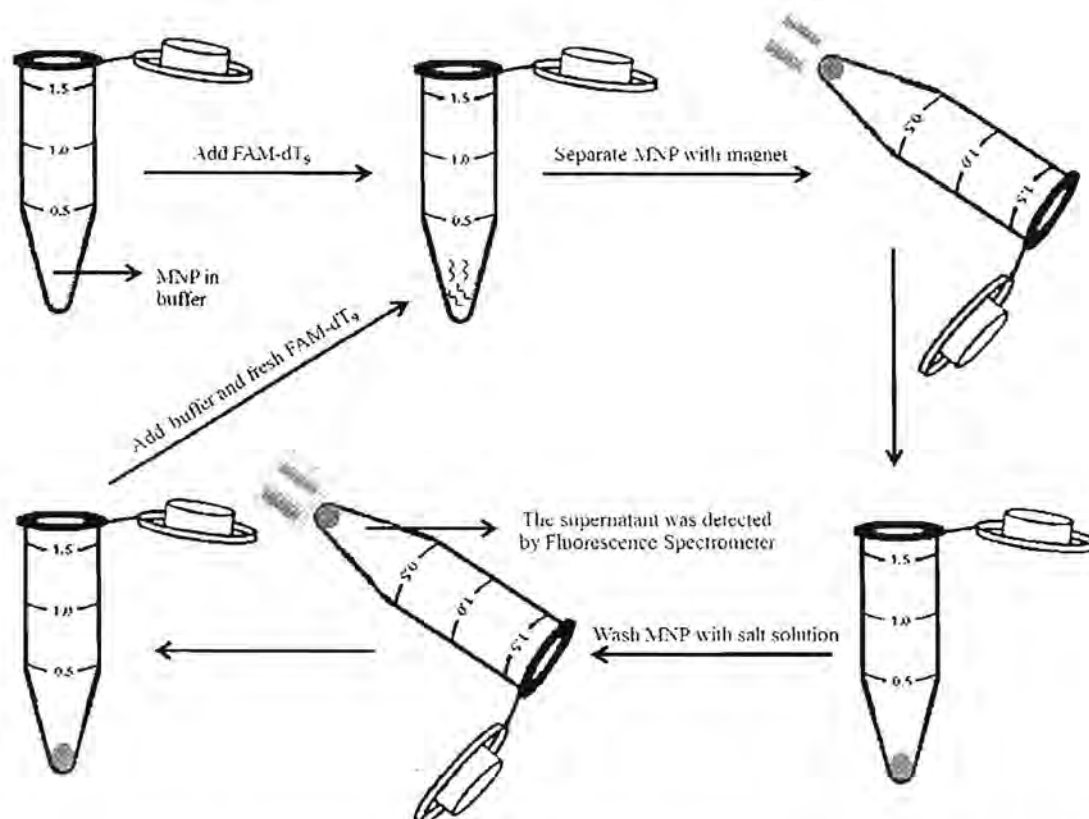


Figure 2. A schematic illustration of the adsorption–separation–desorption cycles of the recyclable PDEAEMA-grafted MNP in adsorption of FAM-dT₉. (Please see the online article for the color version of this figure: <http://dx.doi.org/10.1080/09205063.2016.1189378>.)

Figure 3 shows the adsorption percentages of FAM-dT₉ on the particles having different molar ratios of PEGMA to DEAEMA on their surface. In all cases, the adsorption percentages of FAM-dT₉ rapidly increased during the first 5 min and then reached their equilibrium within 60 min. The adsorption percentages at equilibrium consistently increased with increasing DEAEMA moiety in the copolymers. The results are in good agreement with the increase in zeta potential values of the MNP with increasing DEAEMA moiety in the copolymer (Figure 4). It was hypothesized that the negatively charged FAM-dT₉ can bind to the positively charged MNP via ionic interaction; the high degree of positive charge of the MNP resulted in high FAM-dT₉ adsorption percentages to its surface (Figure 4).

To prove the recycling concept of the particles, an appropriate washing solution for desorption of the FAM-dT₉ from the MNP surface was then investigated. After 60-min adsorption, the particles were removed from the dispersions with the assistance of a permanent magnet. The solutions of CaCl₂ or NaCl at 0.1, 0.5, 1.0, and 2.5 M were used for desorption of FAM-dT₉ from the MNP by washing. The fluorescence emission signals of the salt solutions after washing FAM-dT₉ adsorbed on the MNP were investigated and their desorption percentages were calculated (Figure 3S in the supporting information). Figure 5(A) illustrates the percentage of FAM-dT₉ desorption of washed solutions in the case of 0:100 PEGMA:DEAEMA copolymer-grafted MNP. It was apparent that 2.5 M CaCl₂ salt solutions showed the most promising washing solution for removal of the adsorbed FAM-dT₉ from the MNP surface (95.00% FAM-dT₉ desorbed). The time course of FAM-dT₉ desorption

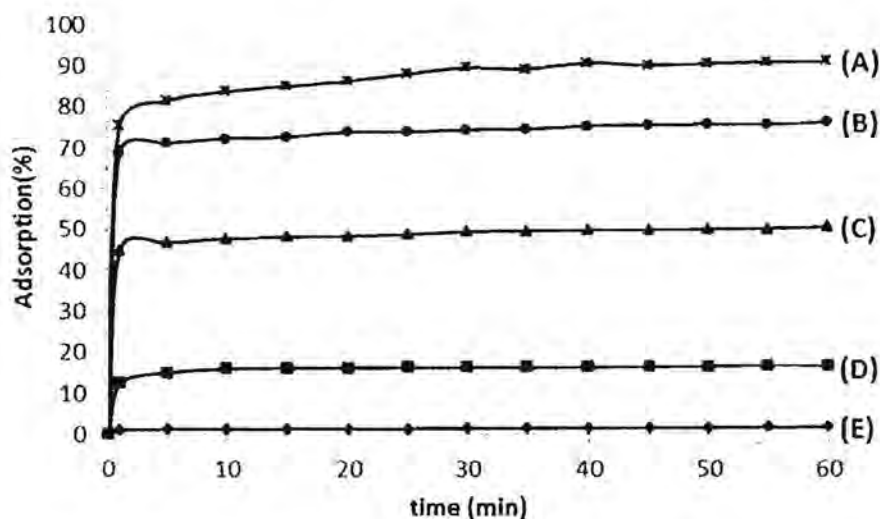


Figure 3. Adsorption percentages of DNA to the copolymer-grafted MNP, where PEGMA:DEAEMA molar ratios are (A) 0:100, (B) 25:75, (C) 50:50, (D) 75:25, and (E) 100:0, respectively. The concentrations of FAM-dT₉ DNA used in these experiments were equivalent (0.3 μ M of FAM-dT₉ used).

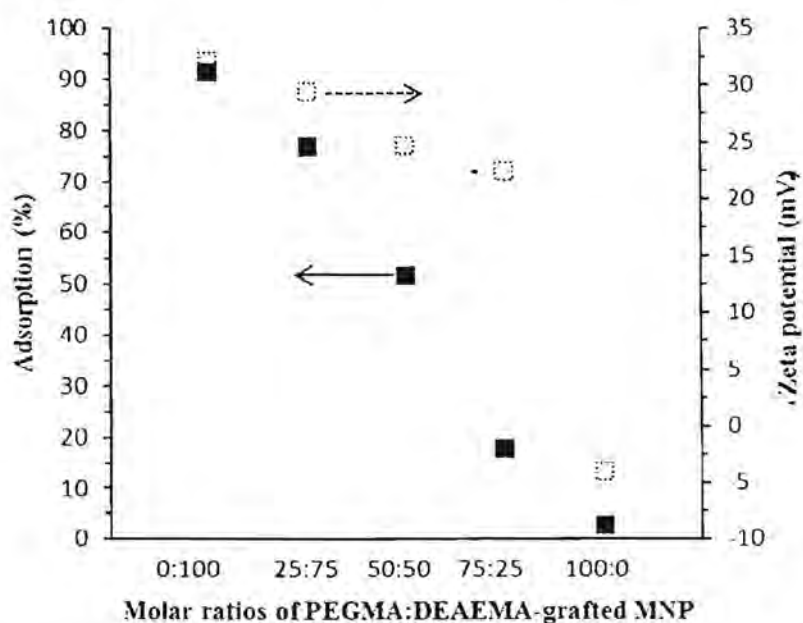


Figure 4. Zeta potential (\square) and DNA adsorption percentage (\blacksquare) of the copolymer-grafted MNP having various molar ratios of PEGMA to DEAEMA after 60-min adsorption.

from the MNP surface after washing with 2.5 M CaCl₂ solution was about 25–30 min (Figure 5(B)). Emission fluorescence signals of the desorption kinetics are provided in the supporting information (Figure 4S). The washing process was repeated until the fluorescence signals of the washed solutions were no longer observed (Figure 5S in supporting information). In the MNP grafted with other copolymers, similar washing process of the particles using 2.5 M CaCl₂ solution was applied.

Because these particles possess magnetically guidable properties, which thus facilitate the recycling process, the investigation of the recycling efficiency of the copolymer-grafted

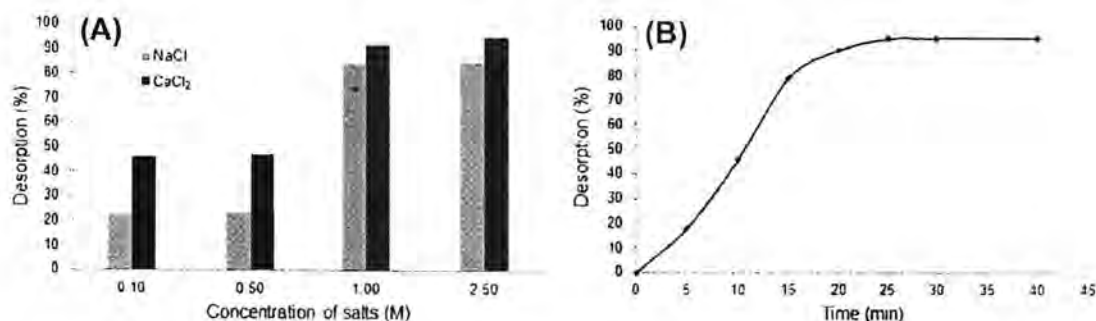


Figure 5. (A) Desorption percentages of FAM-dT₉ after washing the FAM-dT₉ adsorbed on the copolymer-grafted MNP with various NaCl and CaCl₂ concentrations and (B) the time course of FAM-dT₉ desorption from the MNP surface after washing with 2.5 M CaCl₂ solution. The MNP having 0:100 molar ratio of PEGMA:DEAEMA was used in this experiment. The concentration of FAM-dT₉ in this experiment was 0.3 μM.

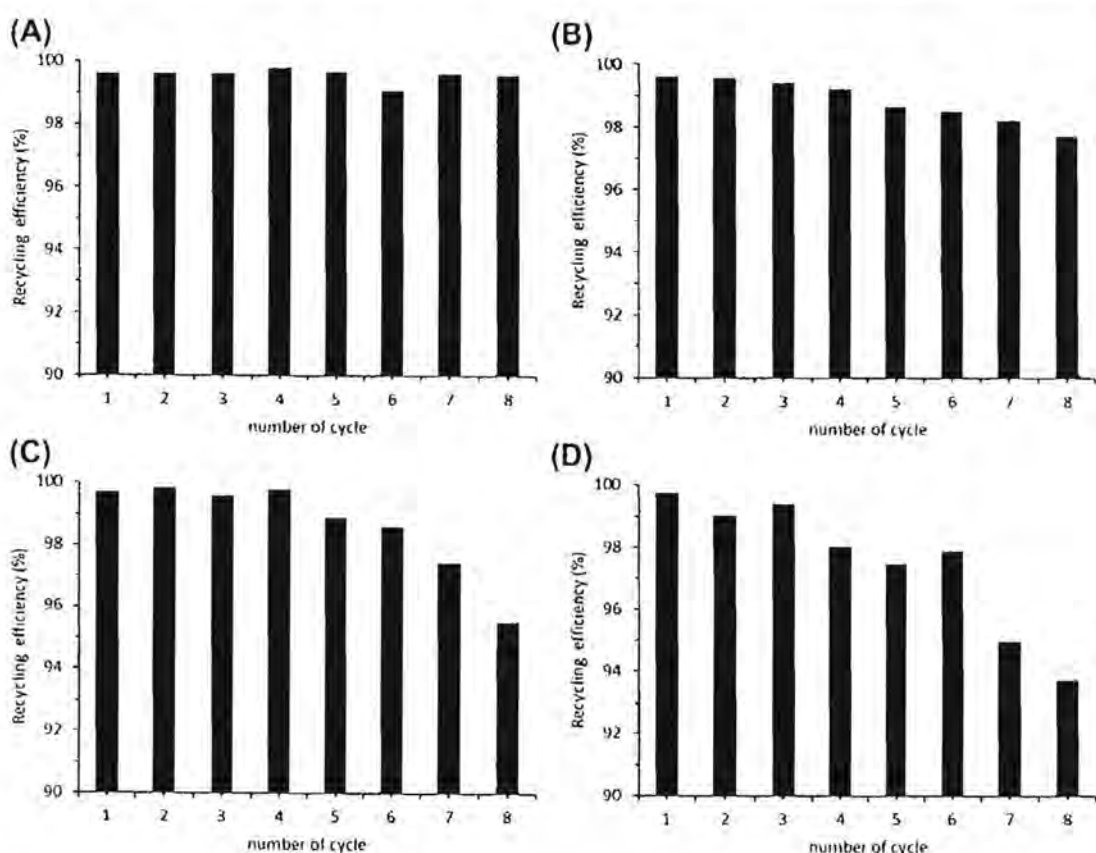


Figure 6. The recycling efficiency of the copolymer-grafted MNP in adsorption with FAM-dT₉, where PEGMA:DEAEMA molar ratios are (A) 0:100, (B) 25:75, (C) 50:50, and (D) 75:25, respectively.

MNP was of our interest. This concept is greatly beneficial to magnetic separation applications, especially in biomedical fields, in which the MNP for the biomolecule separation is usually costly. The MNP having consistent adsorption percentages after multiple recycling processes is greatly desirable.

Figure 6 illustrates FAM-dT₉ adsorption percentages of the MNP grafted with the copolymers having PEGMA:DEAEMA molar ratio of 0:100, 25:75, 50:50, and 75:25, respectively. The MNP grafted with 100:0 PEGMA:DEAEMA molar ratio was not used in this experiment because, according to Figure 4, the amounts of FAM-dT₉ adsorbed by the particle

was insignificant (2% adsorption) which is consistent with its negatively charged surface. After the adsorption–separation process, the fluorescence signals of the washed solutions (2.5 M CaCl₂ solution) from each cycle were then determined. The decrease in the signal corresponded to the FAM-dT₉ adsorbed on the MNP surface; the percent adsorption can be determined using Equation (1). In Figure 6, the recycling efficiency of the MNP in adsorption with FAM-dT₉ was calculated according to Equation (3). The increase in the fluorescence intensity of the supernatants corresponded to the depletion of these values after multiple adsorption–separation–desorption cycles (Figure 6S in the supporting information). In the case of the MNP grafted with PEGMA:DEAEMA copolymer (0:100 molar ratio), the recycling efficiency retained at 100% after 8-recycling process. The MNP having other copolymer ratios showed a slight decrease in the recycling efficiency (94–98%) after eight-recycling process. The recycling efficiency after multiple cycles seemed to correspond to the degree of positive charge on the MNP; the recycling efficiency decreased from 100 to 94% when the degree of positive charge decreased from 32 to 22 mV (Figures 4 and 6).

4. Conclusions

The recyclable MNP grafted with cationic copolymers having various degrees of positive charge for adsorption of DNA was prepared. The copolymer-grafted MNP was first synthesized via a surface-initiated ATRP copolymerization of DEAEMA and PEGMA with various loading ratios of each monomer to obtain different degrees of positive charges on its surface. Adsorption/desorption percentages and recycling efficiency of the cationic MNP using FAM-dT₉ as a model compound was investigated by fluorescence spectroscopy. The adsorption percentages of FAM-dT₉ on the particle surface highly depended on the degree of positive charge; increasing degree of positive charge of the particles seemed to enhance the DNA adsorption percentages. Likewise, in the recycling efficiency study, the particles grafted with poly(DEAEMA) homopolymer (the highest degree of positive charge in the series) retained their good adsorption percentages (100% DNA adsorbed) even after eight-recycling process, while the recycling efficiency seemed to be decreased after eight-recycling process (94–98%) when degree of positive charge decreased. This hybrid material with positively charged surface and magnetic properties might be applicable for use as a nanosolid support for efficient and facile separation/pre-concentration of various bioentities.

Acknowledgment

The Thailand Research Fund (TRG5780124)(DPG5780002). The Center of Excellence for Innovation in Chemistry (PERCH-CIC), Commission on Higher Education, Ministry of Education are gratefully acknowledged for financial support

Disclosure statement

No potential conflict of interest was reported by the authors.

Funding

This work was supported by the Royal Golden Jubilee for the scholarship [grant number PHD/0325/2550]; Thailand Research Fund [grant number TRG5780124], [grant number DPG5780002]

References

- [1] Verma NK, Crosbie-Staunton K, Satti A, et al. Magnetic core-shell nanoparticles for drug delivery by nebulization. *J. Nanobiotechnol.* 2013;11:1-12.
- [2] Hergt R, Hiergeist R, Zeisberger M, et al. Magnetic properties of bacterial magnetosomes as potential diagnostic and therapeutic tools. *J. Magn. Magn. Mater.* 2005;293:80-86.
- [3] Akbarzadeh A, Samiei M, Joo SW, et al. Synthesis, characterization and in vitro studies of doxorubicin-loaded magnetic nanoparticles grafted to smart copolymers on A549 lung cancer cell line. *J. Nanobiotechnol.* 2012;10:46-58.
- [4] Hoskins C, Min Y, Gueorguieva M, et al. Hybrid gold-iron oxide nanoparticles as a multifunctional platform for biomedical application. *J. Nanobiotechnol.* 2012;10:27-38.
- [5] Arakaki A, Masuda F, Amemiya Y, et al. Control of the morphology and size of magnetite particles with peptides mimicking the Mms6 protein from magnetotactic bacteria. *J. Colloid Interface Sci.* 2010;343:65-70.
- [6] Lee HJ, Jang KS, Jang S, et al. Poly(amino acid)s micelle-mediated assembly of magnetite nanoparticles for ultra-sensitive long-term MR imaging of tumors. *Chem. Commun.* 2010;46:3559-3561.
- [7] Chiang CL, Sung CS, Chen CY. Application of silica-magnetite nanocomposites to the isolation of ultrapure plasmid DNA from bacterial cells. *J. Magn. Magn. Mater.* 2006;305:483-490.
- [8] Mu B, Wang T, Wu Z, et al. Fabrication of functional block copolymer grafted superparamagnetic nanoparticles for targeted and controlled drug delivery. *Colloids Surf., A.* 2011;375:163-168.
- [9] Cheng G, Böker A, Zhang M, et al. Amphiphilic cylindrical core-shell brushes via a 'grafting from' process using ATRP. *Macromolecules.* 2001;34:6883-6888.
- [10] Garcia I, Zafeiropoulos NE, Janke A, et al. Functionalization of iron oxide magnetic nanoparticles with poly(methyl methacrylate) brushes via grafting-from atom transfer radical polymerization. *J. Polym. Sci., Part A: Polym. Chem.* 2007;45:925-932.
- [11] Saoud FM, Tonge MP, Weber WG, et al. Magnetite nanoparticles for the preparation of ultrapure RAFT polymers. *Macromolecules.* 2008;41:1598-1600.
- [12] Braunecker WA, Matyjaszewski K. Controlled/living radical polymerization: features, developments, and perspectives. *Prog. Polym. Sci.* 2007;32:93-146.
- [13] Matyjaszewski K, Xia J. Atom transfer radical polymerization. *Chem. Rev.* 2001;101:2921-2990.
- [14] Sun Y, Ding X, Zheng Z, et al. Surface-initiated ATRP in the synthesis of iron oxide/polystyrene core/shell nanoparticles. *Eur. Polymer J.* 2007;43:762-772.
- [15] Zhou L, Yuan J, Yuan W, et al. Synthesis, characterization, and controllable drug release of pH-sensitive hybrid magnetic nanoparticles. *J. Magn. Magn. Mater.* 2009;321:2799-2804.
- [16] Papaphilippou P, Christodoulou M, Marinica OM, et al. Multiresponsive polymer conetworks capable of responding to changes in pH, temperature, and magnetic field: synthesis, characterization, and evaluation of their ability for controlled uptake and release of solutes. *ACS Appl. Mater. Interfaces.* 2012;4:2139-2147.
- [17] Yuan L, Tang Q, Yang D, et al. Preparation of pH-responsive mesoporous silica nanoparticles and their application in controlled drug delivery. *J. Phys. Chem. B.* 2011;115:9926-9932.
- [18] Salehizadeh H, Hekmatian E, Sadeghi M, et al. Synthesis and characterization of core-shell Fe₃O₄-gold-chitosan nanostructure. *J. Nanobiotechnol.* 2012;10:3-9.
- [19] Wang X, Zhou L, Ma Y, et al. Control of aggregate size of polyethyleneimine-coated magnetic nanoparticles for magnetofection. *Nano Res.* 2009;2:365-372.
- [20] Goon IY, Lai LMH, Lim M, et al. Fabrication and dispersion of gold-shell-protected magnetite nanoparticles: systematic control using polyethyleneimine. *Chem. Mater.* 2009;21:673-681.
- [21] Zhang J, Sun W, Bergman L, et al. Magnetic mesoporous silica nanospheres as DNA/drug carrier. *Mater. Lett.* 2012;67:379-382.
- [22] Lellouche JP, Senthil G, Joseph A, et al. Magnetically responsive carboxylated magnetite-polydipyrrole/polydicarbazole nanocomposites of core-shell morphology. Preparation, characterization, and use in DNA hybridization. *J. Am. Chem. Soc.* 2012;127:11998-12006.
- [23] Sen T, Sebastianelli A, Bruce IJ. Mesoporous silica magnetite nanocomposite: fabrication and applications in magnetic bioseparations. *J. Am. Chem. Soc.* 2006;128:7130-7131.

- [24] Shinkai M. Functional magnetic particles for medical application. *J. Biosci. Bioeng.* 2002;94:606–613.
- [25] Chen H, Liu S, Li Y, et al. Development of oleic acid-functionalized magnetite nanoparticles as hydrophobic probes for concentrating peptides with MALDI-TOF-MS analysis. *Proteomics.* 2011;11:890–897.
- [26] Hao Y, Zhang M, He J, et al. Magnetic DNA vector constructed from PDMAEMA polycation and PEGylated brush-type polyanion with cross-linkable shell. *Langmuir.* 2012;28:6448–6460.
- [27] Lee K, Bae KH, Lee Y, et al. Pluronic/polyethylenimine shell crosslinked nanocapsules with embedded magnetite nanocrystals for magnetically triggered delivery of siRNA. *Macromol Biosci.* 2010;10:239–245.
- [28] Jiang C, Xu S, Zhang S, et al. Chitosan functionalized magnetic particle-assisted detection of genetically modified soybeans based on polymerase chain reaction and capillary electrophoresis. *Anal. Biochem.* 2012;420:20–25.
- [29] Hsing IM, Xu Y, Zhao W. Micro- and nano- magnetic particles for applications in biosensing. *Electroanalysis.* 2007;19:755–768.
- [30] Dong H, Huang J, Koepsel RR, et al. Recyclable antibacterial magnetic nanoparticles grafted with quaternized poly(2-(dimethylamino)ethyl methacrylate) brushes. *Biomacromolecules.* 2011;12:1305–1311.
- [31] Liu Z, Li M, Yang X, et al. The use of multifunctional magnetic mesoporous core/shell heteronanostructures in a biomolecule separation system. *Biomaterials.* 2011;32:4683–4690.
- [32] Liao Y, Cheng Y, Li Q. Preparation of nitrilotriacetic acid/Co²⁺-linked, silica/boron-coated magnetite nanoparticles for purification of 6 × histidine-tagged proteins. *J. Chromatogr. A.* 2007;1143:65–71.
- [33] Li X, Zhang J, Gu H. Adsorption and desorption behaviors of DNA with magnetic mesoporous silica nanoparticles. *Langmuir.* 2011;27:6099–6106.
- [34] Theamdee P, Rutnakornpituk B, Wichai U, et al. Recyclable magnetic nanoparticle grafted with pH-responsive polymer for adsorption with DNA. *J. Nanopart. Res.* 2014;16:2494–2506.
- [35] Theppaleak T, Rutnakornpituk B, Wichai U, et al. Magnetite nanoparticle with positively charged surface for immobilization of peptide nucleic acid and deoxyribonucleic acid. *J. Biomed. Nanotechnol.* 2013;9:1509–1520.
- [36] Rutnakornpituk M, Puangsin N, Theamdee P, et al. Poly(acrylic acid)-grafted magnetic nanoparticle for conjugation with folic acid. *Polymer.* 2011;52:987–995.



RESEARCH PAPER

Anionic magnetite nanoparticle conjugated with pyrrolidiny peptide nucleic acid for DNA base discrimination

Sudarat Khadsai · Boonjira Rutnakornpituk · Tirayut Vilaivan · Maliwan Nakkuntod · Metha Rutnakornpituk

Received: 9 May 2016 / Accepted: 20 August 2016
© Springer Science+Business Media Dordrecht 2016

Abstract Magnetite nanoparticles (MNPs) were surface modified with anionic poly(*N*-acryloyl glycine) (PNAG) and streptavidin for specific interaction with biotin-conjugated pyrrolidiny peptide nucleic acid (PNA). Hydrodynamic size (D_h) of PNAG-grafted MNPs varied from 334 to 496 nm depending on the loading ratio of the MNP to NAG in the reaction. UV-visible and fluorescence spectrophotometries were used to confirm the successful immobilization of streptavidin and PNA on the MNPs. About 291 pmol of the PNA/mg MNP was immobilized on the particle surface. The PNA-functionalized MNPs were effectively used as solid supports to differentiate between fully complementary and non-complementary/single-base mismatch DNA using the

PNA probe. These novel anionic MNPs can be efficiently applicable for use as a magnetically guidable support for DNA base discrimination.

Keywords Magnetite · Nanoparticle · PNA probe · DNA · Base discrimination

Introduction

Magnetite nanoparticles (MNPs) (Fe_3O_4) modified with polymers have recently shown a great potential in biomedical applications, including magnetic resonance imaging (MRI) enhancement (Mornet et al. 2006; Li et al. 2005; Xu et al. 2012), magnetic hyperthermia (Maity et al. 2010), drug delivery (Sahoo et al. 2013; Wang et al. 2013a, b), magnetic separation and diagnosis of biomolecules such as deoxyribonucleic acid (DNA) and antibodies (Prai-in et al. 2012; Pita et al. 2008; Anirudhan and Rejeena 2013; Cui et al. 2011; Bayrakci et al. 2013). Apart from that, the use of ultrananocrystalline Fe_3O_4 (UNCFO) as catalyst for comprehensive quantitative analysis of biocrudes was reported (Rojas-Pérez et al. 2015). They have been of particular interest in scientific and technological aspects because of their good magnetic responsiveness and good biocompatibility (Srivastava et al. 2012). However, without nanoparticle stabilization, they tend to aggregate to each other when dispersed in water/organic solvents, resulting in the loss in their nanoscale-related

Electronic supplementary material The online version of this article (doi:10.1007/s11051-016-3574-z) contains supplementary material, which is available to authorized users.

S. Khadsai · B. Rutnakornpituk · M. Rutnakornpituk (✉)
Department of Chemistry and Center of Excellence in Biomaterials, Faculty of Science, Naresuan University, Phitsanulok 65000, Thailand
e-mail: methar@nu.ac.th

T. Vilaivan
Department of Chemistry, Organic Synthesis Research Unit, Faculty of Science, Chulalongkorn University, Patumwan, Bangkok 10330, Thailand

M. Nakkuntod
Department of Biology, Faculty of Science, Naresuan University, Phitsanulok 65000, Thailand

Published online: 31 August 2016

Springer

properties. Coating MNPs with long-chain polymers is a promising approach to improving their stability because it provides steric stabilization, dispersibility in the media and biocompatibility to the particles. In addition, the polymers grafted on the MNP surface can also serve as a platform for desirable conjugation with various biological functional molecules (Theamdee et al. 2015). Surface grafting of charged polymers is one of the most effective approaches for stabilization of MNPs because they can provide electrostatic repulsion to the particles in addition to the steric repulsion mechanism and can be used for ionic adsorption of other bioentities having opposite charges (Theppaleak et al. 2013a, b).

DNA separation using magnetic particles has attracted much attention in the recent years (Stubnitzky et al. 2014). Particularly for DNA pre-concentration purpose, magnetic particles can be a great advantage because they simplified the purification process by the use of an external magnetic field. The so-called FluMag-Systematic Evolution of Ligands by Exponential Enrichment (FluMag-SELEX) method was previously reported for DNA aptamer selection involved the use of magnetic beads as immobilizing matrix for the target molecules and utilizing a fluorescence label for quantification of the DNA (Stoltenburg et al. 2005; Sun et al. 2014). Amino-functionalized silica-coated MNPs have been demonstrated for use as solid supports for DNA separation process (Park and Chang 2007). In addition, previous works also reported the use of streptavidin-immobilized magnetic particles/beads and biotinylated target DNA for DNA enrichment applications (Stoltenburg et al. 2005; Horák et al. 2011; Erdem et al. 2007; Ashtari et al. 2005; Holmberg et al. 2005; Deng et al. 2003; Liu et al. 2008; Xia and O'Connor 2001).

Recently, much attention has been paid on the use of peptide nucleic acid (PNA) as a probe for enrichment of DNA targets (Ahour et al. 2013; Yaroslavsky and Smolina 2013; Choi et al. 2014; Thipmanee et al. 2012; Ananthanawat et al. 2010; Meebungpraw et al. 2015; Bertucci et al. 2015; Liu et al. 2010). PNA was of great interest in this application because it has strong binding affinity, high specificity toward complementary DNA and high Watson-Crick specificity in recognition of DNA and enables the formation of PNA/DNA or PNA/RNA duplex with excellent thermal stability and unique ionic strength effect (Shi et al. 2015). Moreover, the binding of PNA/DNA strand is

stronger than DNA/DNA strand due to the lack of electrostatic repulsion (Vilaivan and Srisuwannaket 2006). However, reports about the utilization of MNP immobilized with PNA as a probe for specific adsorption with DNA target are quite limited (Theppaleak et al. 2013a, b). The concept was to use this MNP to immobilize PNA ("anchoring strand") permanently on the surface and used it to capture its complementary DNA ("working strand") (Stubnitzky et al. 2014; Kerman et al. 2004).

In this research, MNPs were coated with anionic poly(*N*-acryloyl glycine) (PNAG) which functioned as particle stabilizer as well as provided a handle for immobilization of positively charged biological entities. PNAG has attracted our attention in the present work because it shows pH-responsive properties and possesses high degree of negative charges (Deng et al. 2011; Barbucci et al. 1991; Moon et al. 2010). The PNAG-grafted MNPs were further covalently functionalized with streptavidin and then with biotin-conjugated pyrrolidinyl PNA (Vilaivan 2015) via the specific biotin-streptavidin interaction. These pyrrolidinyl PNA-functionalized MNPs were then used to differentiate between fully complementary and non-complementary/single-base mismatch DNA sequences.

In this report, ^1H NMR spectroscopy was used to confirm the chemical structures of synthesized NAG monomer. The particle size and its distribution in each step of modification on MNPs were investigated via transmission electron microscopy (TEM). Hydrodynamic size (D_h) and zeta potential values of PNAG-grafted MNPs were measured via photon correlation spectroscopy (PCS). Vibrating sample magnetometer (VSM) was used to study the magnetic properties of MNPs, indicating the presence of the polymers in the surface-modified MNP. The PNA immobilization and DNA base discrimination were detected by UV-visible and fluorescence spectrophotometries, respectively. In addition, gel electrophoresis was used to confirm that the DNA was adsorbed with PNA probe on the MNPs (Fig. 1).

Experimental

Materials

Unless otherwise stated, all reagents were used without further purification: glycine (AR grade),

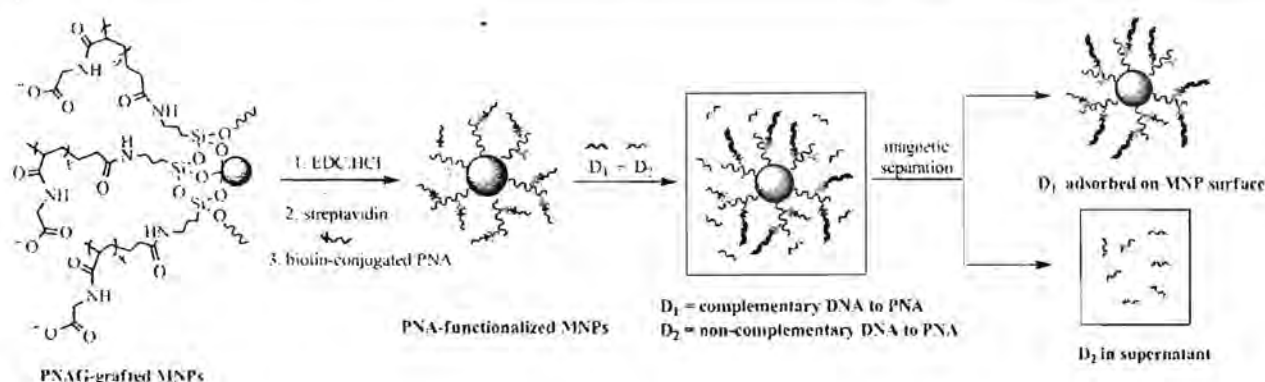


Fig. 1 Overall view of the bioconjugation of PNAG-grafted MNPs with streptavidin and biotinylated PNA for DNA base discrimination

iron(III) chloride anhydrous (FeCl_3 , 98 %, Acros), iron(II) chloride tetrahydrate ($\text{FeCl}_2 \cdot 4\text{H}_2\text{O}$, 99 %, Acros organic), ammonium hydroxide (NH_4OH , 28–30 %, J.T. Baker), sodium hydroxide (NaOH , 98 %, Aldrich), oleic acid (Carlo Erba), 3-aminopropyltriethoxysilane (APTES, 99 %, Acros), triethylamine (TEA, 97 %, Carlo Erba) and ammonium persulfate (APS, 98 %, Carlo Erba) were used as received. Acryloyl chloride was freshly prepared via a chloride exchange reaction between acrylic acid (98 %, Acros) and benzoyl chloride (99 %, Acros) at 75 °C to give a colorless liquid: 60 % yield. 1-Ethyl-3-(3-dimethylaminopropyl) carbodiimide hydrochloride (EDC.HCl, GL Biochem (Shanghai) Ltd.) and 2-(*N*-morpholino)ethanesulfonic acid (MES, 99 %, Acros) were used as received. Fluorophore-tagged DNAs and streptavidin (95 %, Pacific Science) were used as received. Biotin-conjugated pyrrolidiny peptide nucleic acid (biotin-acpcPNA) were synthesized via a manual Fmoc solid-phase peptide synthesis and purified by reverse-phase HPLC as described earlier (Vilaivan and Srisuwannaket 2006).

Syntheses

Synthesis of *N*-acryloyl glycine (NAG) monomer (Deng et al. 2011)

A solution of acryloyl chloride (10 mL, 123.6 mmol) in tetrahydrofuran was slowly added to a solution of glycine (9.28 g, 123.6 mmol) in NaOH solution (9.89 g NaOH, 247.25 mmol, in 30 mL DI water) at 0 °C, and the mixture was vigorously stirred for 3 h. The solution was extracted with diethyl ether, and the

aqueous layer was acidified with conc. HCl to pH 2, followed by extraction with ethyl acetate. The combined organic extracts were dried with anhydrous Na_2SO_4 , filtered and evaporated under reduced pressure: 66 % yield (10.50 g of NAG obtained). $^1\text{H NMR}$ (400 MHz, D_2O) δ_{H} : 4.08 [s, 2H, $-\text{NH}-\text{CH}_2-\text{C}=\text{O}$], 5.84 [m, 1H, $\text{CH}_2=\text{CH}-\text{CO}-$] and 6.27–6.35 [m, 2H, $\text{CH}_2=\text{CH}-\text{CO}-$].

Synthesis of MNPs via a co-precipitation method and their stabilization with oleic acid

FeCl_3 (1.66 g, 10.23 mmol, in 10 mL deionized water) and $\text{FeCl}_2 \cdot 4\text{H}_2\text{O}$ (1.00 g, 5.03 mmol, in 10 mL deionized water) were mixed together with rigorous stirring. After addition of 30 % NH_4OH solution (10 mL), a black precipitate was observed, signifying the formation of MNPs. After stirring for another 30 min to complete the reaction, the dispersion was centrifuged at 5000 rpm for 20 min and the aqueous supernatant was discarded. To stabilize the particles in the dispersion, an oleic acid solution (2 mL in 10 mL hexane) was slowly added into the MNPs with stirring for 30 min. The oleic acid-coated MNPs were re-precipitated in acetone (three times) and dried *in vacuo*.

Synthesis of acrylamide-grafted MNPs (Fig. 2)

TEA (2 mL) was added into the oleic acid-coated MNP-toluene dispersion (200 mg of the MNP in 30 mL toluene), followed by the addition with APTES (5 mL). The mixture was stirred at room temperature under N_2 atmosphere for 24 h. The particles were

separated using an external magnet and washed with ethanol and DI water to obtain amino-grafted MNPs. After drying, 200 mg of the amino-grafted MNPs was re-dispersed in a NaOH solution (3.96 g NaOH in 15 mL DI water), followed by an addition of acryloyl chloride (8 mL, 98.9 mmol) at 0 °C. The mixture was stirred at room temperature under nitrogen atmosphere for 24 h to obtain acrylamide-grafted MNPs. They were magnetically separated and repeatedly washed with DI water. The particles were re-dispersed in DI water to obtain the dispersion of 0.2 g MNPs in 20 mL water.

Synthesis of PNAG-grafted MNPs (Fig. 2)

The aqueous dispersion of acrylamide-grafted MNPs (25 mg MNPs in 2.5 mL water) was added to a NAG solution (0.5 g, 3.88 mmol, in 20 mL water). Ninety microliters of aqueous ammonium persulfate (APS) (10 % in water) was added to the solution to initiate the polymerization. It should be noted that 1:100 molar ratio of the initiator to monomer was used in this reaction. The mixture was incubated at 70 °C for 3 h under nitrogen gas flow. After the polymerization, the PNAG-grafted MNPs were repeatedly washed with DI water with an assistance of a permanent magnet to

remove unreacted monomers and ungrafted polymers from the particles and then dried under *vacuo*. The PNAG-grafted MNPs will be characterized by FTIR, TEM, TGA, VSM and PCS techniques.

Bioconjugation of PNAG-grafted MNPs with PNA for DNA base discrimination

Specific interaction of streptavidin with biotin-conjugated PNA onto the MNP surface EDC-HCl (16 mg, 0.0835 mmol) was added to a PNAG-grafted MNP dispersion (5 mg MNPs in 5 mL of 10 mM MES buffer, pH 5.2) with stirring to activate the carboxylate groups on the particle surface, followed by addition of a streptavidin solution (0.1 mg streptavidin in 200 μ L of MES buffer). After stirring for 24 h, the streptavidin-grafted MNPs were separated by a magnet, repeatedly washed with 10 mM MES buffer and dried *in vacuo*. The supernatant was analyzed via UV-visible spectrophotometry to confirm the decrease in streptavidin concentration in the solution due to its grafting on the MNPs surface (Fig. 3a).

Next, the streptavidin-grafted MNPs (2 mg) were stirred with 30 μ L of biotin-acpcPNA solution (30.16 μ M in pH 7 phosphate buffer) for 45 min to immobilize the PNA onto the MNPs surface via a

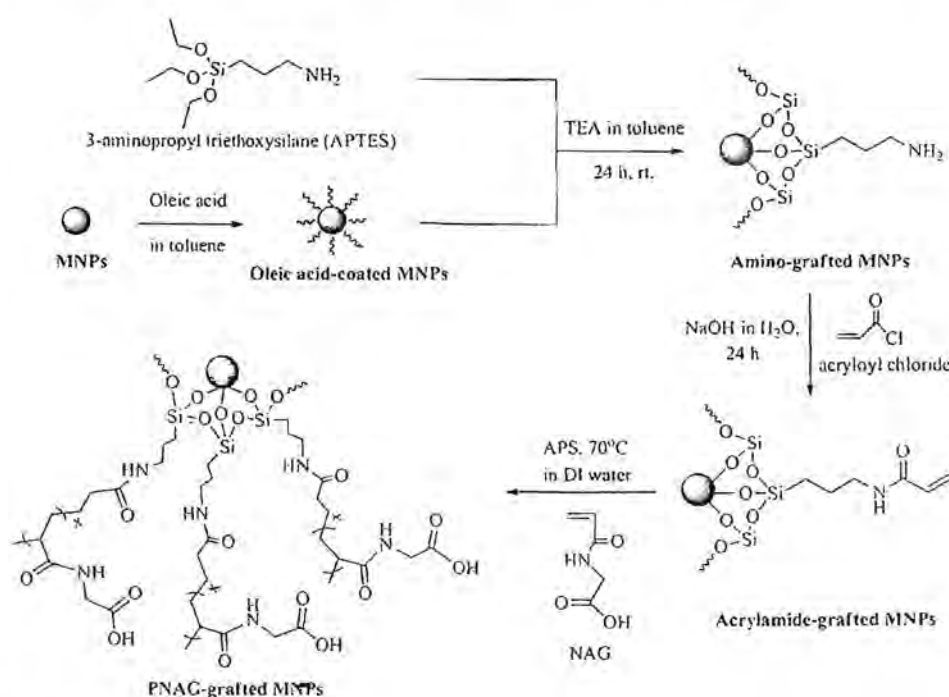


Fig. 2 Synthetic scheme of PNAG-grafted MNPs

specific biotin–streptavidin interaction. The supernatant was then analyzed via UV–Vis spectrophotometry to quantify the decrease in the PNA in the solution, corresponding to the amounts of the PNA functionalized on the MNP surface (Fig. 3b). The calibration curve of biotin-conjugated PNA was constructed as shown in supporting information (Figure S1).

DNA base discrimination using PNA-functionalized MNPs Two milligrams of the PNA-functionalized MNPs was stirred for 45 min with 2 mL of fluorophore-tagged DNA solution (0.8 μ M in pH 7 phosphate buffer) and separated with a magnet (Fig. 3c). The supernatant was analyzed via fluorescence spectrophotometry and gel electrophoresis. It was hypothesized that the PNA-functionalized MNPs can specifically interact with only the complementary DNA, leaving the mismatched DNA (non-complementary and single-base mismatch) in the supernatant.

In addition, the possibilities of non-specific adsorption between the MNP surface and DNA were also investigated using the streptavidin-grafted MNPs (without PNA immobilization).

Characterization

^1H NMR spectroscopy was performed on a 400-MHz Bruker NMR spectrometer using D_2O as a solvent. FTIR spectrophotometry was performed on a Perkin-Elmer Model 1600 Series FTIR Spectrophotometer. The particles size and size distribution were observed from TEM. The TEM images were taken using a Philips Tecnai 12 operated at 120 kV equipped with Gatan model 782 CCD camera. The particles were re-suspended in water with sonication before deposition on a TEM grid. The hydrodynamic diameter (D_h) of the particles was measured by PCS using NanoZS4700 nanoseries Malvern instrument. The sample dispersions were sonicated for 30 min before the

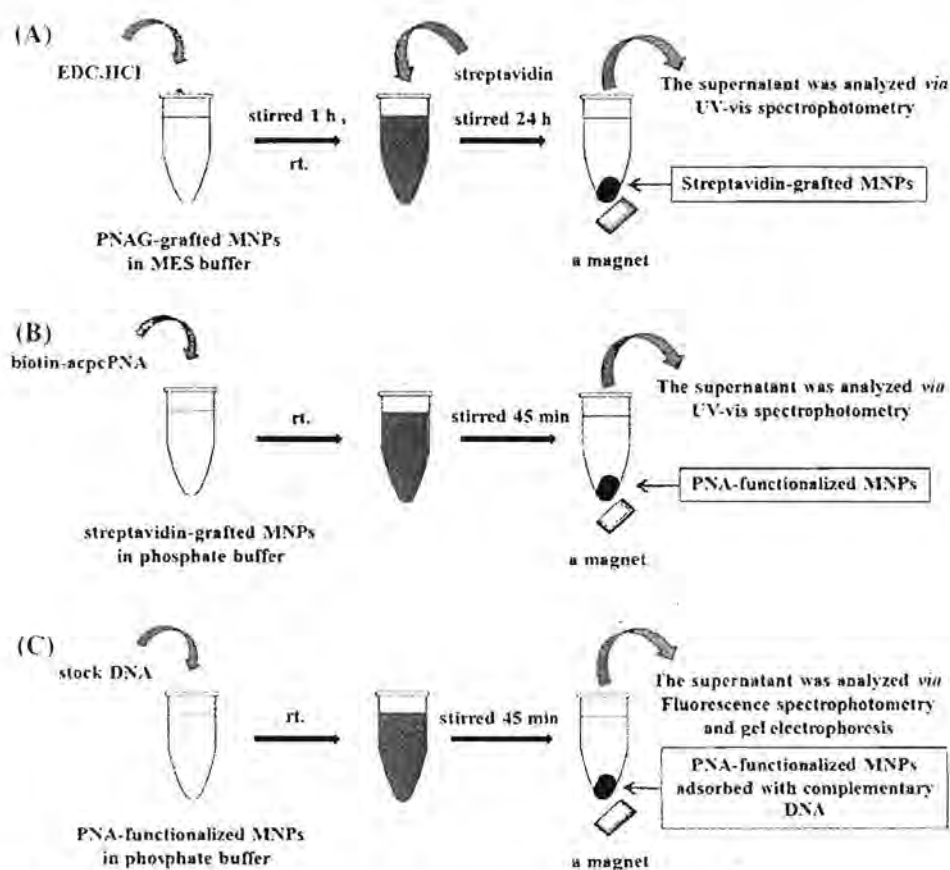


Fig. 3 Preparations of **a** streptavidin-grafted MNPs, **b** PNA-functionalized MNPs and **c** the DNA base discrimination using the PNA-functionalized MNPs

measurement at 25 °C without filtration. Magnetic properties of the particles were measured at room temperature using a Standard 7403 Series, Lakeshore vibrating sample magnetometer (VSM). Magnetic moment of each sample was investigated over a range of $\pm 15,000$ G of applied magnetic fields. TGA was performed on Mettler–Toledo's SDTA 851 at the temperature ranging between 25 and 600 °C and a heating rate of 20 °C/min under oxygen atmosphere.

UV–visible spectrophotometry was performed on Thermo Scientific NanoDrop 2000 UV–Vis Spectrophotometer at $\lambda = 260$ nm. Fluorescence spectrophotometry was conducted on a Varian Eclipse Fluorescence Spectrophotometer using 12-mer DNA sequences tagged with a fluorophore at the 5'-position. The fluorophores used in the work included 6-carboxyfluorescein (FAM) and 6-carboxytetramethylrhodamine (TAMRA) where their $\lambda_{\text{excited}}/\lambda_{\text{emission}}$ ratios are 494/521 nm and 552/584 nm, respectively. The gels in the gel electrophoresis experiments were prepared using 2 % agarose in 1× Tris–acetate (TAE) buffer.

Results and Discussion

In this work, anionic PNAG-grafted MNPs were synthesized via a radical polymerization of NAG in the presence of acrylamide-grafted MNPs, followed by the immobilization of PNA on their surface via streptavidin–biotin interaction. The PNA-functionalized MNPs were then used as magnetic solid supports for DNA base discrimination. To use these MNPs for DNA base discrimination using a PNA probe specific for the DNA sequence, high negatively charged surface was desirable in order to minimize the non-specific adsorption between non-complementary DNA sequences and the MNP surface. In our previous works, MNPs coated with positively charged poly((2-diethylamino)ethyl methacrylate) (PDEAEMA) were synthesized for ionic adsorption with negatively charged DNA for use in various applications such as detection of DNA sequences and magnetic separation of DNA (Theppaleak et al. 2013, b, 2014; Rutnakompituk et al. 2016). However, the colloidal stability of these particles was rather dependent on the change in the dispersion pH. Therefore, in the current report, the carboxylic acid groups of PNAG on the MNP surface were chemically coupled with streptavidin via an

amide bond formation to obtain streptavidin-grafted MNPs. These MNPs with streptavidin on their surface should specifically interact with biotinylated PNA probe to form PNA-functionalized MNPs. It is well known that these biotin–streptavidin interactions are highly specific and rather stable in various pHs, temperatures, organic solvents and denaturing agents (Liu et al. 2010).

Synthesis and characterization of PNAG-grafted MNPs

FTIR spectra of the products from each step of the reactions are shown in Fig. 4. The FTIR spectrum of MNP cores showed the signal at 585 cm^{-1} of Fe–O bonds, and this signal was observed in all FTIR spectra of the MNPs (Fig. 4a, c–e). After the reaction of the MNPs with APTES, N–H stretching (3360 cm^{-1}), N–H bending (1551 cm^{-1}) and Si–O stretching (1011 cm^{-1}) were observed, indicating the formation of amino-grafted MNPs (Fig. 4b, c). After the reaction of the MNPs with acryloyl chloride, C=C stretching signals ($1535\text{--}1430\text{ cm}^{-1}$) and amide bond signals (1619 and 1538 cm^{-1}) were observed, indicating the existence of acryloyl groups on the particle surface (Fig. 4d). After the polymerization of NAG monomers in the presence of acrylamide-grafted MNPs, the FTIR spectrum shows the characteristic adsorption signals of C=O stretching (1740 cm^{-1}), C–O stretching (1261 cm^{-1}) of carboxyl groups and C–C stretching (800 cm^{-1}) of PNAG (Fig. 4e; Deng et al. 2011). In addition, the FTIR spectrum of bare PNAG is shown in supporting information (Fig. S2). It should be noted that the MNPs in each step of the reactions were repeatedly washed with ethanol/water to completely remove unreacted species from the particles before the FTIR analyses.

To determine the composition of the PNAG-grafted on MNPs, TGA was used to investigate their weight loss at 600 °C (Fig. 5). It was hypothesized that the residue weight was the weight of iron oxide from oxidized MNP cores remaining at 600 °C, while the weight loss was attributed to the organic contents including the acrylamide linker and PNAG on the MNP surface. The observed residual weights in each step of the reaction consistently decreased, indicating more organic contents in the composites. According to the TGA thermograms in thermograms c and d in Fig. 5a, there was about 14 % weight of PNAG coated

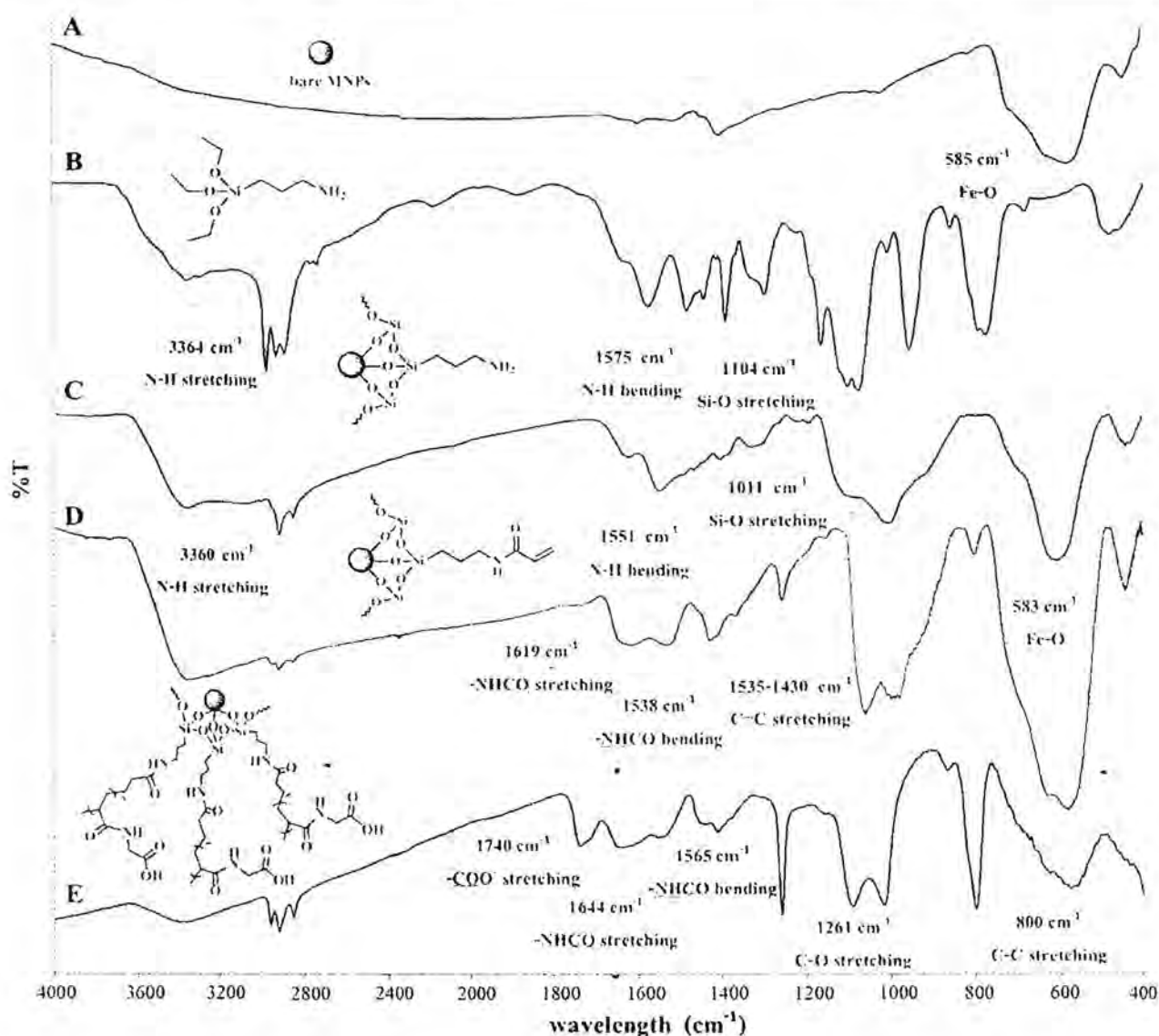


Fig. 4 FTIR spectra of a bare MNPs, b 3-aminopropyltriethoxysilane (APTES), c amino-grafted MNPs, d acrylamide-grafted MNPs and e PNAG-grafted MNPs

on the MNP surface. This result corresponded well with their improved water dispersibility as opposed to those without PNAG coating. PNAG-grafted MNPs were well dispersible in aqueous dispersion without noticeable aggregation after standing for 3 h, and some slight aggregation was observed after 6 h (Fig. 5b), signifying that coating with PNAG provided an improved colloidal stability to the particles due to steric and/or electrostatic repulsion mechanisms. The stability of the dispersions after longer aging time (48 h) is shown in supporting information (Fig. S3). On the other hand, bare MNPs showed large particle

aggregation only a few minutes after dispersing in water (Fig. 5b).

Magnetic properties of bare MNPs and PNAG-grafted MNPs were investigated via VSM technique (Fig. 6). PNAG-grafted MNPs showed superparamagnetic behavior at room temperature as indicated by the absence of magnetic remanence (M_r) and coercivity (H_c) (the top inset in Fig. 6). The saturation magnetization (M_s) values of PNAG-grafted MNPs (31 emu/g) were lower than those of bare MNPs (55 emu/g). This was attributed to the decrease in the magnetite content (% of MNP) in the nanocomposite

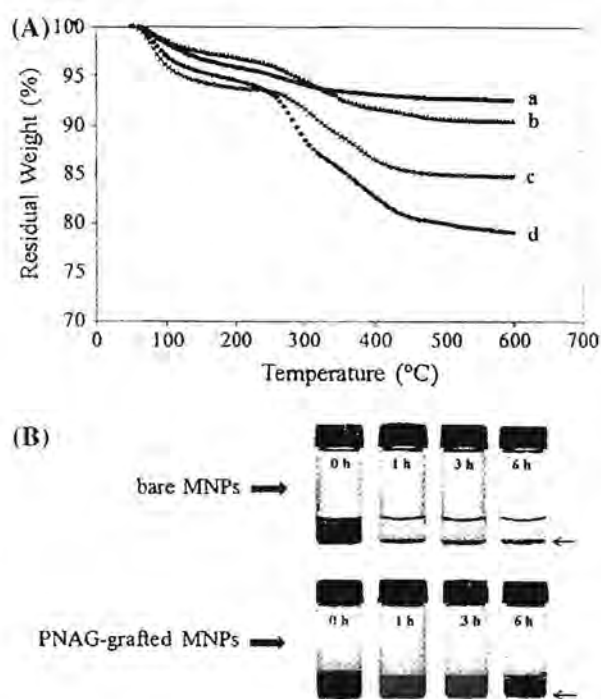


Fig. 5 **A** TGA curves of *a* bare MNPs, *b* amino-grafted MNPs, *c* acrylamide-grafted MNPs and *d* PNAG-grafted MNPs. **B** apparent dispersibilities of MNPs in water with and without PNAG coatings (arrows indicate the formation of particle aggregation)

due to the surface coating with diamagnetic PNAG. These results were in good agreement with those observed in TGA experiments (the decrease in the residual weights). Despite some decrease in the M_s values due to the presence of PNAG in the

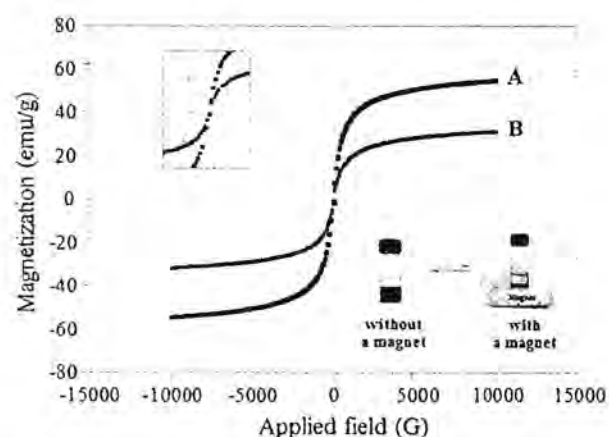


Fig. 6 *M-H* curves of *a* bare MNPs and *b* PNAG-grafted MNPs. The *top inset* shows an expansion of the ± 2000 G region and the *bottom inset* shows the magnetic separation of the particles after 5 min upon applying a permanent magnet

nanocomposite, these particles are still well responsive to a permanent magnet. PNAG-grafted MNPs can be completely separated from the dispersion within 5 min upon applying a permanent magnet as shown in the bottom inset in Fig. 6. The complete removal of the MNPs from the dispersion was necessary for the analysis of adsorbed moiety on the particle surface in this work, and this would be discussed in details in the later section.

Zeta potential values of PNAG-grafted MNPs as a function of dispersion pH are shown in Fig. 7. The presence of ionizable carboxylic acid groups of PNAG in the structure should make them a polyelectrolyte in aqueous dispersion. In addition to serving as steric and electrostatic stabilizers, the PNAG polyelectrolyte should also advantageously provide pH-responsive properties to the particles due to their large electrostatic potentials. The results in Fig. 7 suggest that these particles were indeed pH responsive. Zeta potential values of these particles in water continuously decreased with increasing pH of the dispersion and became highly negatively charged in basic pH. This was attributed to the formation of various degrees of deprotonated carboxylates ($-\text{COO}^-$) depending on the dispersion pH. It is worth to mention that the surface charge of these particles was highly negative at pH 7 (-55 mV), which is important in terms of decreasing non-specific interaction between PNAG-grafted MNPs and DNA in the base discrimination experiments.

Hydrodynamic diameter (D_h) of PNAG-grafted MNPs was found to be in the range of 334–494 nm, regardless of the pH. The observed sizes of D_h were rather high, which could be attributed to the formation

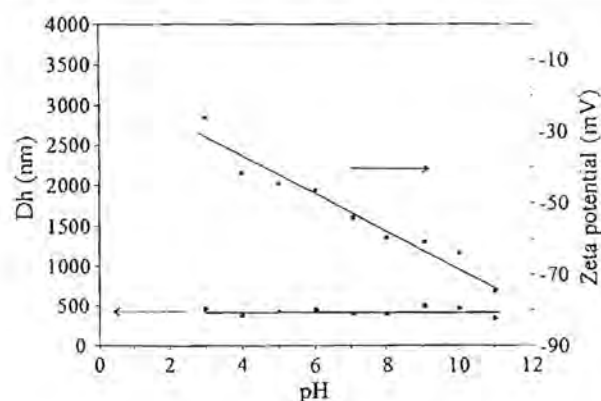


Fig. 7 Hydrodynamic size (D_h) and zeta potential values of PNAG-grafted MNPs at pH 3–11

of nanoclusters of multiple particles in the dispersion. The acrylamide-grafted MNPs can copolymerize with PNAG in the radical polymerization due to the presence of polymerizable acrylamide groups on their surface and eventually formed anionic magnetic nanoclusters. It should be noted that some degree of MNP nanoclustering might be necessary for use in magnetic separation applications (Meerod et al. 2015).

Bioconjugation of PNAG-grafted MNPs with PNA for DNA base discrimination

Representative TEM images of the MNPs from each step of the reactions are shown in Fig. 8. TEM samples of acrylamide-grafted MNPs were prepared from toluene dispersions, while those of PNAG-grafted MNPs, streptavidin-grafted MNPs and PNA-functionalized MNPs were prepared from pH 7 aqueous dispersions. Acrylamide-grafted MNPs were spherical in shape with the size of 6–10 nm in diameter without any aggregation visually observed (Fig. 8a). After the polymerization of PNAG in the presence of MNPs, formation of particle nanoclusters was observed (Fig. 8b), which was in good agreement with the rather high D_h of PNAG-grafted MNPs observed in PCS experiments (Fig. 7). This was attributed to the presence of polymerizable acrylamide on the particle surface, allowing for the inter-particle polymerization reactions (Fig. 9). It should be noted that PNAG homopolymers might also be formed in the solutions during the polymerization, but these were magnetically separated from the MNP nanoclusters.

The size of PNAG-grafted MNPs ranged between 200 and 400 nm in diameter, which correspond to approximately 50 nanoparticles/cluster (Fig. 8b). As opposed to well-dispersible single nanoparticles, these nanoclusters would be great advantageous for use as supports for magnetically assisted separation of DNA discussed in this work. Although these particles showed a sign of nanoclustering, they still well dispersed in aqueous dispersions for more than 6 h without macroscopic aggregation (Fig. 5b).

Streptavidin-grafted MNPs and PNA-functionalized MNPs (Fig. 8c, d) also showed the MNP nanoclustering with slightly larger sizes (400–600 nm in diameter) than those of PNAG-grafted MNPs (Fig. 8b). This was attributed to the large molecular structures of streptavidin and PNA, resulting in higher degrees of aggregation of the particles.

The increase in D_h of the particles after the conjugations with streptavidin and then PNA (from ≈ 500 nm to ≈ 700 nm) also supported those observed in TEM experiments. In addition, the UV spectrophotometry was also used to confirm that the streptavidin was successfully grafted on the MNP surface as indicated by the decrease in the UV spectrum intensity (shown in supporting information, Table S1 and Fig. S4). Interestingly, due to the good solubilities of streptavidin and PNA in buffers, the water dispersibilities of both streptavidin-grafted MNPs and PNA-functionalized MNPs were apparently improved (shown in supporting information, Figure S5).

To determine the amount of PNA adsorbed on the MNP surface, the MNP nanoclusters were magnetically separated from the dispersion and repeatedly washed with phosphate buffer solutions (Fig. 3b). The supernatant was then analyzed via UV–visible spectrophotometry at 15-min interval to quantify the decrease in the PNA in the solution, corresponding to the amount of PNA immobilized on the MNPs surface. It was found that the maximum amount of PNA adsorbed on the particle surface was 291 pmol/mg MNP after 45 min of mixing. The adsorption kinetics and the calculation of the PNA adsorbed on the particles are shown in supporting information (Fig. S6). These MNPs were then used as magnetic nanosolid supports with PNA as a probe for selective adsorption with targeted DNA.

To proof the concept for use of these MNPs for selective adsorption with targeted DNA, one biotin-conjugated PNA probe (P1) and three DNA sequences (D1–D3) were selected as a model in this study (Table 1). These three DNA sequences were tagged with 6-carboxytetramethylrhodamine (TAMRA) or 6-carboxyfluorescein (FAM). Two different fluorophores having different emission wavelengths were employed in order to differentiate complementary and non-complementary DNA targets by the PNA probe. The level of non-specific background adsorption between DNA and the MNPs was first investigated. This non-specific interaction might arise from physical adsorption between hydrophobic moiety of DNA and that of streptavidin on MNP surface. This non-specific adsorption is not desirable because the principle for DNA base discrimination here relies on the specific hybridization between DNA and the PNA immobilized on the particle surface. Due to the negatively charged repulsion of carboxylate groups

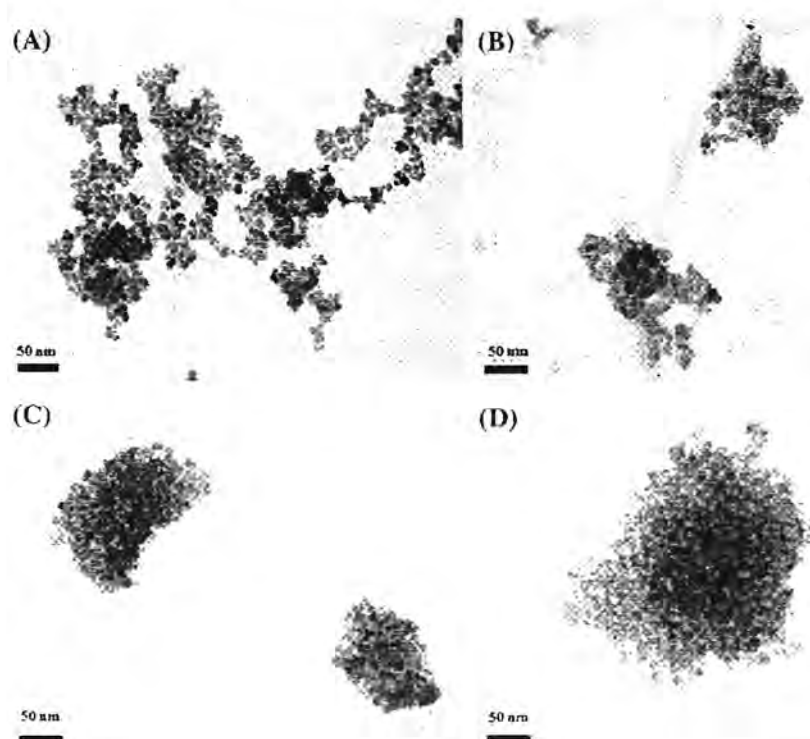


Fig. 8 TEM images of **a** acrylamide-grafted MNPs, **b** PNAG-grafted MNPs, **c** streptavidin-grafted MNPs and **d** PNA-functionalized MNPs

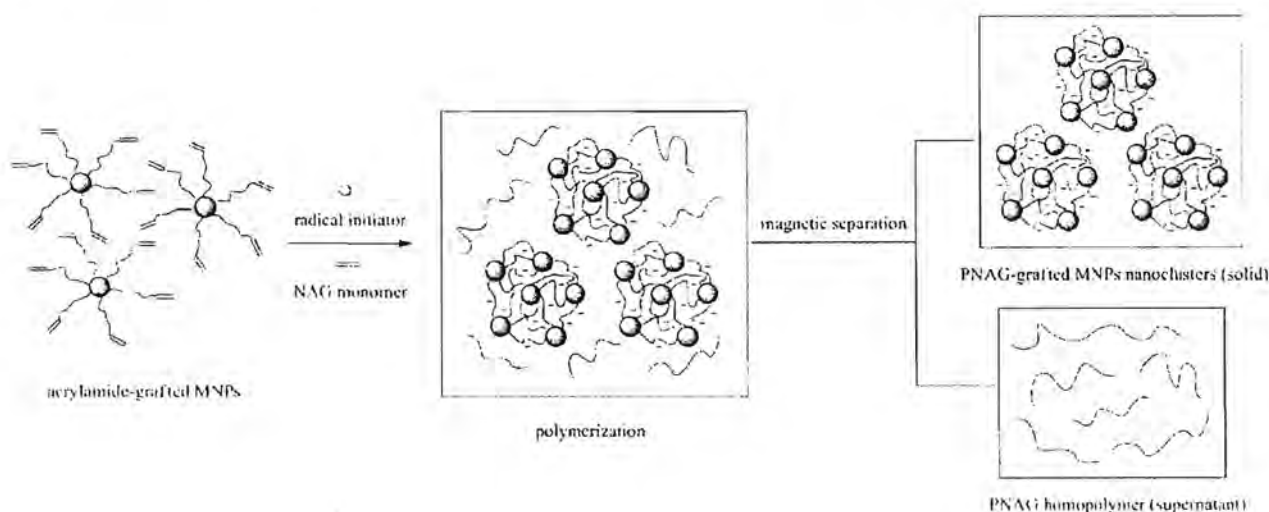


Fig. 9 Proposed mechanism of the formation of PNAG-MNPs nanoclusters

of PNAG and deoxyribose phosphate groups of DNA. coating the particle surface with anionic PNAG should minimize this undesired non-specific adsorption of DNA.

To study the non-specific interaction, streptavidin-grafted MNPs (without PNA) were dispersed in phosphate buffer solutions, followed by addition of the DNA

(D1, D2 or D3). After magnetic separation of the particles, the fluorescence spectra of the supernatant showed no change in their intensities, indicating that there was no non-specific adsorption of the DNA on the particle surface in all DNA samples (Fig. 10a–c).

PNA-functionalized MNPs were then tested in the differentiation between complementary and non-

Table 1 Sequences of biotin-conjugated PNA and fluorophore-tagged DNAs used in this work

| Biotin-conjugated PNA | Sequence of DNAs used | Excitation wavelength (nm) | Emission wavelength (nm) |
|--|--|----------------------------|--------------------------|
| P1: Biotin-CTACA AGCATAT-lys-NH ₂ | D1: 5'-ATATGCTTGTAG-3' (FAM) (fully complementary) | 494 | 521 |
| | D2: 5'-CACGTICCCAGGA-3' (TAMRA) (non-complementary) | 552 | 584 |
| | D3: 5'-ATATGCATGTAG-3' (TAMRA) (single-base mismatch) | 552 | 584 |

complementary, including completely mismatch and single-base mismatch DNA targets. The DNA targets (D1, D2 or D3; 2 mL of 0.8 μ M DNA, 1600 pmol each) were added to the dispersions of PNA-functionalized MNPs (P1, 582 pmol/2 mg MNP) in phosphate buffer solutions (Fig. 3c). The amount of PNA used in this experiment was equivalent to the calculated amounts of PNA adsorbed on the particles discussed in the previous section (291 pmol/mg MNP). It was found that the fluorescence spectrum in the complementary case showed a significant decrease in its intensity (Fig. 10a), corresponding to about 33 % of D1 adsorbed on the particles (Fig. 11a). One might question that the adsorption of D1 on the particles was probably due to the physical adsorption of FAM molecules tagged at the terminal of D1 because different types of fluorophores were used in this experiment. Additional studies were performed with the use of fully complementary DNA (D1) and non-complementary DNA (D1': 5'-CACgTTCCAGGA-3') both tagged with FAM (shown in supporting information Table S2 and Figure S7). It was found that the case of D1' exhibited no change in the fluorescence intensity, indicating that the depletion of fluorescence intensity in Fig. 10a was due to the hybridization of P1 and D1.

On the other hand, the non-complementary DNAs exhibited no change in the fluorescence intensity (Fig. 10b, c). These results indicated that the PNA (P1) probe immobilized on the MNPs can clearly differentiate between the complementary (D1) and non-complementary (D2) as well as single-base mismatch (D3) DNAs. The comparative plot of the percent DNA (D1–D3) adsorbed by the PNA-functionalized MNP nanoclusters is shown in Fig. 11a. The fluorescence spectra and calibration curve of DNA (D1) (fully complementary), DNA (D2) (non-

complementary) and DNA (D3) (single-base mismatch) are provided in Fig. S8.

Gel electrophoresis was also used to confirm that PNA-functionalized MNPs can differentiate between the complementary DNA (D1) and non-complementary DNA (D2 and D3) (Fig. 11b). In good agreement with the fluorescence spectrophotometry results discussed above, the supernatant after removing PNA-functionalized MNPs (number 2) only in the case of fully complementary DNA showed the obvious decrease in the band intensity as compared to the band of the initial DNA (number 1) at the same DNA concentration (1600 pmol or 2 mL of 0.8 μ M). Interestingly, those of the MNPs without PNA (number 3) showed no decrease in the band intensity, indicating that there was no non-specific interaction between DNA and the particle surface, as well as PNA and streptavidin.

The specific hybridization between DNA and PNA immobilized on the particle surface was further investigated using the mixture of two DNA sequences. An equimolar mixture of the fully complementary DNA (D1) and non-complementary DNA (D2) in phosphate buffer was mixed with the PNA-functionalized MNPs (582 pmol/2 mg MNPs). After mixing for 45 min and magnetic separation, the supernatant was then analyzed by fluorescence spectrophotometry. It was found that only the fluorescence spectrum in the complementary case showed a significant decrease in its intensity (Fig. 12a), corresponding to about 42.42 % of DNA (D1) adsorbed on the particles (Fig. 12c). Similar results were obtained with the equimolar mixture of fully complementary DNA (D1) and single-base mismatch DNA (D3). In the presence of PNA-functionalized MNPs, only the fluorescence intensity of the complementary case decreased

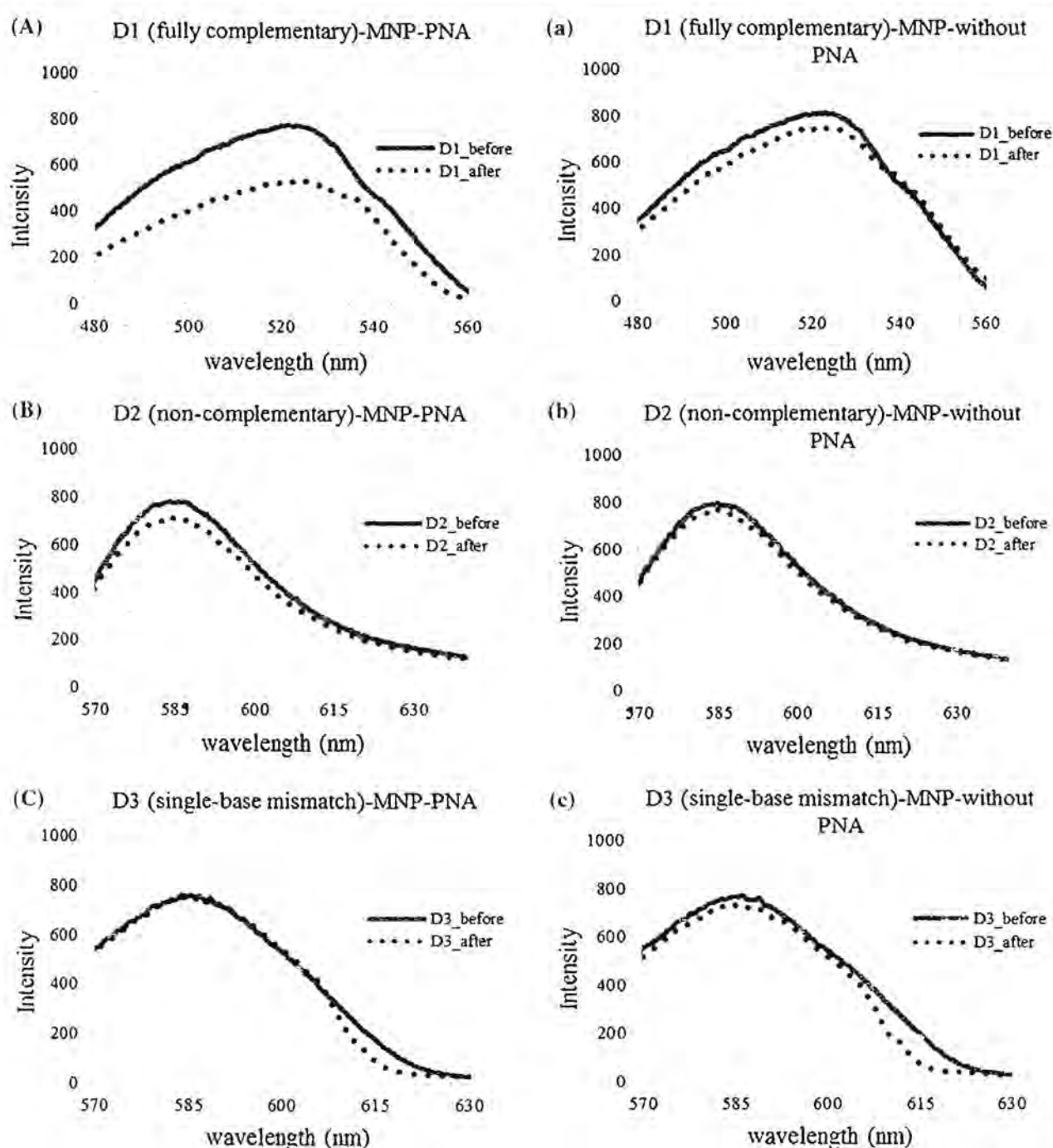


Fig. 10 Fluorescence spectra of a–c the dispersions before and after magnetic separations, and a–c the studies in non-specific adsorptions (without PNA functionalized)

(Fig. 12b) (about 35.66 % of DNA (D1) adsorbed) (Fig. 12c). These results confirmed that PNA-functionalized MNPs can be effectively used for selective adsorption of targeted DNA.

Due to the high stability and high specificity between PNA and DNA hybrids, these novel anionic

MNPs might be potentially great advantage for use as magnetic nanosupports for various future technologies, such as diagnostics of genetic diseases and enrichment of DNA mixture. The applications of these MNPs in real DNA samples are underway and will be reported in the future studies.

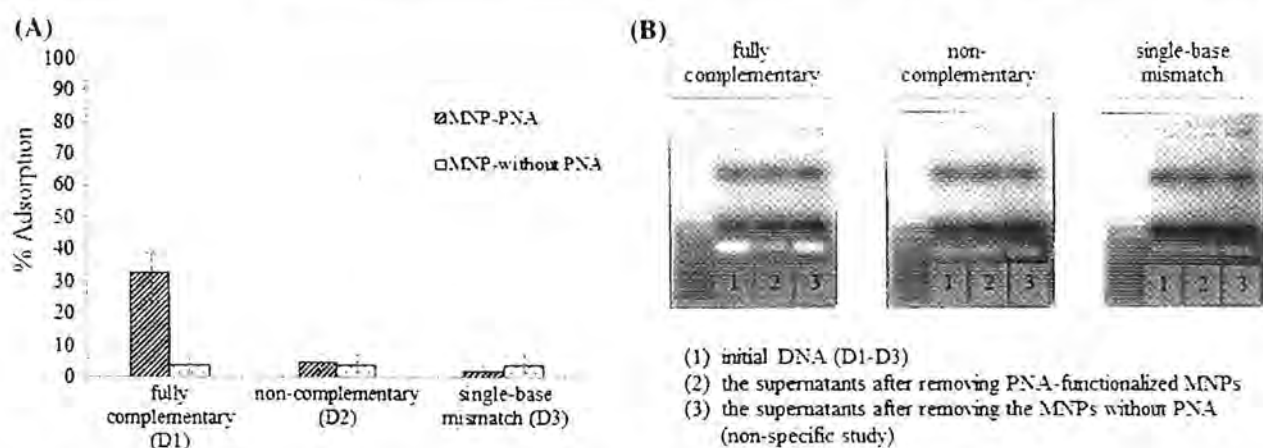


Fig. 11 a % Adsorption of DNA (D1–D3) on MNP nanoclusters and b gel electrophoresis (agarose gel) showing the decrease in band intensity in the complementary case (fully complementary)

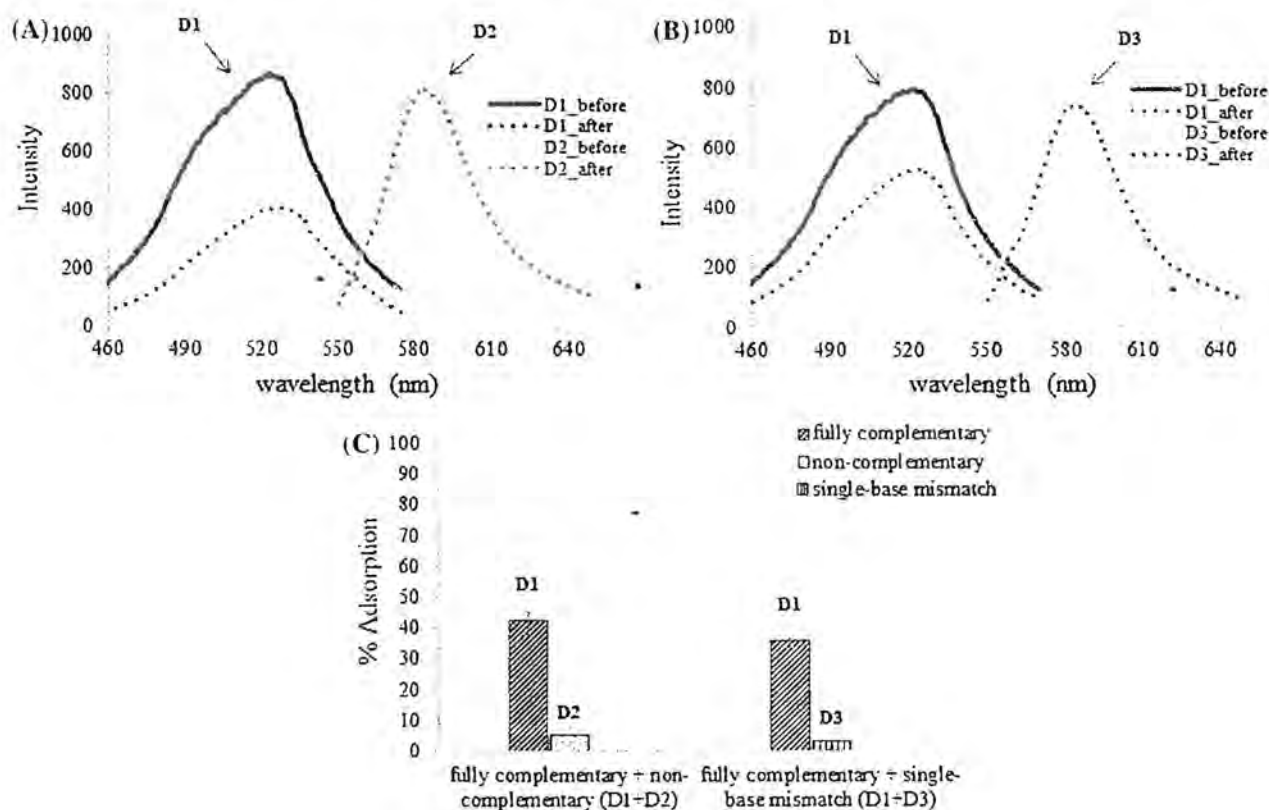


Fig. 12 Fluorescence spectra of the dispersions before and after magnetic separations of DNA mixture a DNA (D1) + DNA (D2), b DNA (D1) + DNA (D3) and c % Adsorption of DNA (D1–D3) on MNP nanoclusters

Conclusions

The MNPs surface was successfully modified with PNAG via a one-step free radical polymerization to obtain the magnetic nanoclusters with negatively charged surface, high magnetic responsiveness, good

dispersibility and good stability in water. PNA was efficiently functionalized onto the particle surface through the streptavidin–biotin interaction. The PNA-functionalized MNP nanoclusters were then used as solid supports to differentiate between fully complementary and single-base mismatch/non-comple

mentary DNA sequences using the PNA probe. These novel anionic MNP nanoclusters can be potentially applicable for use as a magnetically guidable tool for pre-concentration of DNA mixtures.

Acknowledgments The authors thank the Thailand Research Fund (TRF) (DPG5780002) for financial support. SK especially acknowledges the Royal Golden Jubilee PhD program for the scholarship (PHD/0250/2553).

References

- Ahour F, Pourmaghi-Azar MH, Alipour E, Hejazi MS (2013) Detection and discrimination of recombinant plasmid encoding hepatitis C virus core/E1 gene based on PNA and double-stranded DNA hybridization. *Biosens Bioelectron* 45:287–291
- Ananthanawat C, Vilaivan T, Hoven VP, Su X (2010) Comparison of DNA, aminoethylglycyl PNA and pyrrolidinyl PNA as probes for detection of DNA hybridization using surface plasmon resonance technique. *Biosens Bioelectron* 25:1064–1069
- Anirudhan TS, Rejeena SR (2013) Poly(methacrylic acid-co-vinyl sulfonic acid)-grafted-magnetite/nanocellulose superabsorbent composite for the selective recovery and separation of immunoglobulin from aqueous solutions. *Sep Purif Technol* 119:82–93
- Ashtari P, He X, Wang K, Gong P (2005) An efficient method for recovery of target ssDNA based on amino-modified silica-coated magnetic nanoparticles. *Talanta* 67:548–554
- Barbucci R, Casolaro M, Magnani A (1991) The role of poly-electrolytes in the permeability control of insulin: behavior of poly(*N*-acryloyl glycine) grafted on porous cellulose membrane. *J Control Release* 17:79–88
- Bayrakci M, Maltas E, Yigiter S, Özmen M (2013) Synthesis and application of novel magnetite nanoparticle based azacrown ether for protein recognition. *Macromol Res* 21:1029–1035
- Bertucci A, Manicardi A, Candiani A, Giannetti S, Cucinotta A, Spoto G, Konstantaki M, Pissadakis S, Selli S, Corradini R (2015) Detection of unamplified genomic DNA by a PNA-based microstructured optical fiber (MOF) bragg-grating optofluidic system. *Biosens Bioelectron* 63:248–254
- Choi Y, Metcalf G, Sleiman MH, Vair-Turnbull D, Ladame S (2014) Oligonucleotide-templated reactions based on Peptide Nucleic Acid (PNA) probes: concept and biomedical applications. *Bioorgan Med Chem* 22:4395–4398
- Cui YR, Hong C, Zhou YL, Li Y, Gao XM, Zhang XX (2011) Synthesis of orientedly bioconjugated core/shell Fe₃O₄@Au magnetic nanoparticles for cell separation. *Talanta* 85:1246–1252
- Deng WG, Zhu Y, Montero A, Wu KK (2003) Quantitative analysis of binding of transcription factor complex to biotinylated DNA probe by a streptavidin-agarose pull-down assay. *Anal Biochem* 323:12–18
- Deng K, Li Q, Bai Y, Gou Y, Dong L, Huang C, Wang S, Gao T (2011) A pH/Thermo-responsive injectable hydrogel system based on poly(*N*-acryloyl glycine) as a drug carrier. *Iran Polym J* 20(3):185–194
- Erdem A, Sayar F, Karadeniz H, Guven G, Ozsoz M, Piskin E (2007) Development of streptavidin carrying magnetic nanoparticles and their applications in electrochemical nucleic acid sensor systems. *Electroanal* 19:798–804
- Holmberg A, Blomstergren A, Nord O, Lukacs M, Lundberg J, Uhlén M (2005) The biotin-streptavidin interaction can be reversibly broken using water at elevated temperatures. *Electrophoresis* 26:501–510
- Horák D, Španová A, Tvrđíková J, Rittich B (2011) Streptavidin-modified magnetic poly(2-hydroxyethyl methacrylate-co-glycidyl methacrylate) microspheres for selective isolation of bacterial DNA. *Eur Polym J* 47:1090–1096
- Kerman K, Matsubara Y, Morita Y, Takamura Y, Tamiya E (2004) Peptide nucleic acid modified magnetic beads for intercalator based electrochemical detection of DNA hybridization. *Sci Technol Adv Mater* 5:351–357
- Li Z, Wei L, Gao MY, Lei H (2005) One-pot reaction to synthesize biocompatible magnetite nanoparticles. *Adv Mater* 17(8):1001–1005
- Liu YJ, Yao DJ, Chang HY, Liu CM, Chen C (2008) Magnetic bead-based DNA detection with multi-layers quantum dots labeling for rapid detection of *Escherichia coli* O157:H7. *Biosens Bioelectron* 24:558–565
- Liu X, Qu X, Fan H, Ai S, Han R (2010a) Electrochemical detection of DNA hybridization using a water-soluble branched polyethyleneimine-cobalt(III)-phenanthroline indicator and PNA probe on Au electrodes. *Electrochim Acta* 55:6491–6495
- Liu Z, Galli F, Janssen KGH, Jiang L, van der Linden HJ, de Geus DC, Voskamp P, Kuil ME, Olsthoorn RCL, Oosterkamp TH, Hankemeier T, Abrahams JP (2010b) Stable single-walled carbon nanotube-streptavidin complex for biorecognition. *J Phys Chem C* 114:4345–4352
- Maitly D, Chandrasekharan P, Yang CT, Chuang KH, Shuter B, Xue JM, Ding J, Feng SS (2010) Facile synthesis of water-stable magnetite nanoparticles for clinical MRI and magnetic hyperthermia applications. *Nanomedicine* 5:1571–1584
- Meebungpraw J, Wiarachai O, Vilaivan T, Kiatkamjornwong S, Hoven VP (2015) Quaternized chitosan particles as ion exchange supports for label-free DNA detection using PNA probe and MALDI-TOF mass spectrometry. *Carbohydr Polym* 131:80–89
- Meerod S, Rutnakornpituk B, Wichai U, Rutnakornpituk M (2015) Hydrophilic magnetic nanoclusters with thermo-responsive properties and their drug controlled release. *J Magn Magn Mater* 392:83–90
- Moon JM, Kim BS, Choi YS, Lee JO, Nakahara T, Yoshinaga K (2010) Preparation of polymer-coated magnetite fine particles for immunoassay magnetic marker. *Macromol Res* 8:793–799
- Mornet S, Vasseur S, Grasset F, Verveka P, Goglio G, Demourgues A, Portier J, Pollert E, Duguet E (2006) Magnetic nanoparticle design for medical applications. *Prog Solid State Chem* 34:237–247
- Park ME, Chang JH (2007) High throughput human DNA purification with aminosilanes tailored silica-coated magnetic nanoparticles. *Mater Sci Eng* 27:1232–1235

- Pita M, Abad JM, Vaz-Dominguez C, Briones C, Mateo-Martí E, Martín-Gago JA, Morales MP, Fernández VM (2008) Synthesis of cobalt ferrite core/metallic shell nanoparticles for the development of a specific PNA/DNA biosensor. *J Colloid Interface Sci* 321:484–492
- Prai-in Y, Tankanya K, Rutnakornpituk B, Wichai U, Montembault V, Pascual S, Fontaine L, Rutnakornpituk M (2012) Azlactone functionalization of magnetic nanoparticles using ATRP and their bioconjugation. *Polymer* 53:113–120
- Rojas-Pérez A, Diaz-Diestra D, Frias-Flores CB, Beltrán-Huarc J, Das KC, Weiner BR, Morell G, Díaz-Vázquez LM (2015) Catalytic effect of ultrananocrystalline Fe₃O₄ on algal bio-crude production via HTL process. *Nanoscale* 7:17664–17671
- Rutnakornpituk B, Theppaleak T, Rutnakornpituk M, Vilaivan T (2016) Recyclable magnetite nanoparticle coated with cationic polymers for adsorption of DNA. *J Biomater Sci Polym E* 27:1200–1210
- Sahoo B, Devi KSP, Banerjee R, Maiti TK, Pramanik P, Dhara D (2013) Thermal and pH responsive polymer-tethered multifunctional magnetic nanoparticles for targeted delivery of anticancer drug. *ACS Appl Mater Interfaces* 5:3884–3893
- Shi H, Yang F, Li W, Zhao W, Nie K, Dong B, Liu Z (2015) A review: fabrications, detections and applications of peptide nucleic acids (PNAs) microarray. *Biosens Bioelectron* 66:481–489
- Srivastava M, Singh J, Yashpal M, Gupta DK, Mishra RK, Tripathi S, Ojha AK (2012) Synthesis of superparamagnetic bare Fe₃O₄ nanostructures and core/shell (Fe₃O₄/alginate) nanocomposites. *Carbohydr Polym* 89:821–829
- Stoltenburg R, Reinemann C, Strehlitz B (2005) FluMag-SELEX as an advantageous method for DNA aptamer selection. *Anal Bioanal Chem* 383:83–91
- Stubinitzky C, Vilaivan T, Wagenknecht HA (2014) The base discriminating potential of pyrrolidiny PNA demonstrated by magnetic Fe_xO_y particles. *Org Biomol Chem* 12:3586–3589
- Sun MQ, Cao FQ, Hu XL, Zhang YR, Lu XW, Zeng LB (2014) DNA aptamer selection in vitro for determining ketamine by FluMag-SELEX. *J Forensic Med* 30(5):346–349
- Theamdee P, Rutnakornpituk B, Wichai U, Rutnakornpituk M (2014) Recyclable magnetic nanoparticle grafted with pH-responsive polymer for adsorption with DNA. *J Nanopart Res* 16:2494–2506
- Theamdee P, Rutnakornpituk B, Wichai U, Nakkuntod M, Rutnakornpituk M (2015) Recyclable silver-magnetite nanocomposite for antibacterial application. *J Ind Eng Chem* 29:63–70
- Theppaleak T, Rutnakornpituk M, Wichai U, Vilaivan T, Rutnakornpituk B (2013a) Anion-exchanged nanosolid support of magnetic nanoparticle in combination with PNA probes for DNA sequence analysis. *J Nanopart Res* 15:2106–2117
- Theppaleak T, Rutnakornpituk B, Wichai U, Vilaivan T, Rutnakornpituk M (2013b) Magnetite nanoparticle with positively charged surface for immobilization of peptide nucleic acid and deoxyribonucleic acid. *J Biomed Nanotechnol* 9:1509–1520
- Thipmanee O, Samanman S, Sankoh S, Numnuam A, Limbut W, Kanatharana P, Vilaivan T, Thavarungkul P (2012) Label-free capacitive DNA sensor using immobilized pyrrolidiny PNA probe: effect of the length and terminating head group of the blocking thiols. *Biosens Bioelectron* 38:430–435
- Vilaivan T (2015) Pyrrolidiny PNA with α/β -dipeptide backbone: from development to applications. *Acc Chem Res* 48:1645–1656
- Vilaivan T, Srisuwannaket C (2006) Hybridization of pyrrolidiny peptide nucleic acids and DNA: selectivity, base-pairing specificity and direction of binding. *Org Lett* 8(9):1897–1900
- Wang Y, Ibrahim NL, Jiang J, Gao S, Erathodiyil N, Ying JY (2013a) Construction of block copolymers for the coordinated delivery of doxorubicin and magnetite nanocubes. *J Control Release* 169:211–219
- Wang N, Guan Y, Yang L, Jia L, Wei X, Liu H, Guo C (2013b) Magnetic nanoparticles (MNPs) covalently coated by PEO-PPO-PEO block copolymer for drug delivery. *J Colloid Interface Sci* 395:50–57
- Xia L, O'Connor TR (2001) DNA glycosylase activity assay based on streptavidin paramagnetic bead substrate capture. *Anal Biochem* 298:322–326
- Xu B, Lu R, Dou H, Tao K, Sun K, Qiu Y, Ding J, Zhang D, Li J, Shi W, Sun K (2012) Exploring the structure-property relationships of ultrasonic/MRI dual imaging magnetite/PLA microbubbles: magnetite@cavity versus magnetite@shell systems. *Colloid Polym Sci* 290:1617–1626
- Yaroslavsky AI, Smolina IV (2013) Fluorescence imaging of single-copy DNA sequences within the human genome using PNA-directed padlock probe assembly. *Chem Biol* 20:445–453

Cite this: *RSC Adv.* 2016, 6, 74314

Synthesis and fluorescence properties of 3,6-diaminocarbazole-modified pyrrolidinyl peptide nucleic acid†

Aukkrapon Dangsopon,^a Nattawee Poomsuk,^b Khatcharin Siriwong,^b Tirayut Vilaivan^c and Chaturong Suparpprom^{*a}

This work aims to explore a new clickable carbazole-based fluorescent label, its incorporation into pyrrolidinyl peptide nucleic acid (acpcPNA), and the interactions between the labeled PNA probe and DNA by fluorescence spectrophotometry and molecular dynamics simulation. A carbazole derivative, namely 3,6-diaminocarbazole (DAC), was synthesized and incorporated into the internal and terminal positions of azide-modified acpcPNA via a sequential reductive alkylation and click reaction previously developed by our group. The DAC-modified acpcPNA can form a stable hybrid with complementary DNA with somewhat lower stability compared to unmodified acpcPNA. Most importantly, the DAC-modified acpcPNA exhibits a remarkable fluorescence increase in the presence of DNA (up to 35.5 fold with complementary DNA). Non-complementary as well as single mismatched DNA targets gave a smaller fluorescence increase (1.1 to 18.6 fold), and the discrimination could be further improved by increasing the temperature to dissociate the mismatched hybrids. Molecular dynamic simulations revealed that the DAC interacts with adjacent nucleobases in single stranded PNA, resulting in quenching of the fluorescence signal. When the PNA formed a hybrid with DNA, the DAC was pushed away from the duplex, resulting in a fluorescence increase. Thus, the DAC-labeled acpcPNA is a potential candidate as a self-reporting probe for determination of DNA sequences.

Received 30th June 2016
Accepted 26th July 2016

DOI: 10.1039/c6ra15861g

www.rsc.org/advances

Introduction

Self-reporting fluorescence oligonucleotides have been extensively used as a probe for the determination of DNA sequences. Several approaches have been explored in order to introduce a mechanism for fluorescence changes upon hybridization of the probe with the correct DNA target. Classically, two labels that can interact by static quenching,¹ Fluorescence Resonance Energy Transfer (FRET)^{2–4} or excimer/excimer formation⁵ are used in combination. More recently, there are attempts to develop singly labeled self-reporting probes by attachment of an intercalative or environment sensitive dye to the oligonucleotide.⁶ However, the performance of these singly-labeled probes is generally variable, depending on the sequence and therefore still leaves room for improvements.

Carbazole is an electron rich aromatic molecule that showed many interesting properties such as high thermal stability, excellent photophysical and electroconductive properties and the ease of synthesis and chemical modification at 3-, 6- and 9-positions. Carbazole derivatives, both in monomeric and oligomeric forms, have found widespread applications as photoconductivity polymers,^{7–10} polymeric light emitting devices,^{11,12} high temperature thermostable polymers,¹³ electrochromic materials,^{14–16} dye-sensitized solar cell and dendrimeric electro phosphorescent devices.^{17–19} In addition, carbazole derivatives have been used as fluorophores in sensor applications, including DNA detection.²⁰ Carbazole derivatives with cationic groups at 3,6-positions have been reported to bind in the DNA groove of AT-rich sequences.^{21–24} However, the use of carbazole derivatives in combination with an oligonucleotide or analogues for sequence-specific detection of DNA sequences is unknown.

Peptide nucleic acid or PNA is a DNA mimic consisting of nucleobases attached onto a peptide-like backbone.^{25,26} PNA can hybridize with DNA according to Watson-Crick base pairing rules with high affinity and sequence specificity. The absence of phosphate group in the PNA backbone results in decreasing of the electrostatic repulsion with DNA, and therefore PNA can form a more stable duplex with DNA than DNA itself. In addition, the binding of PNA and DNA is highly sequence specific

^aDepartment of Chemistry and Center of Excellence for Innovation in Chemistry, Faculty of Science, Naresuan University, Muang, Phitsanulok 65000, Thailand. E-mail: chaturong@nu.ac.th

^bMaterials Chemistry Research Center, Department of Chemistry and Center of Excellence for Innovation in Chemistry, Faculty of Science, Khon Kaen University, Khon Kaen 40002, Thailand

^cOrganic Synthesis Research Unit, Department of Chemistry, Faculty of Science, Chulalongkorn University, Phayathai Road, Patumwan, Bangkok 10330, Thailand

† Electronic supplementary information (ESI) available. See DOI: 10.1039/c6ra15861g

and is not sensitive to ionic strength. These properties, together with the excellent chemical and biological stabilities, make PNA a promising tool for several applications in medical and biotechnology fields. Recently, we reported a series of new PNA system with restricted conformation flexibility as a result of incorporation of cyclic structures into the PNA backbone.^{27–30} Pyrrolidiny PNA probes labeled with environment sensitive dyes such as pyrene,^{31,32} Nile red,^{32,33} or other DNA binding dyes such as thiazole orange³⁴ have been successfully applied as self-reporting fluorescence probes for DNA sequence detection.

From the remarkable photophysical properties and DNA binding ability mentioned above, carbazole has a potential to be developed into a probe for DNA detection by fluorescence spectroscopy. In the present work, an electron rich carbazole derivative, namely 3,6-diaminocarbazole (DAC), was incorporated at an internal position of acpcPNA in order to develop a new self-reporting fluorescence hybridization probe. Here we report the synthesis, thermal stabilities and fluorescence properties of DAC-modified acpcPNA probes, as well as their ability to discriminate between complementary and single-mismatched DNA targets. Moreover, molecular dynamics simulation was performed to explain the behavior of DAC-labeled acpcPNA probes.

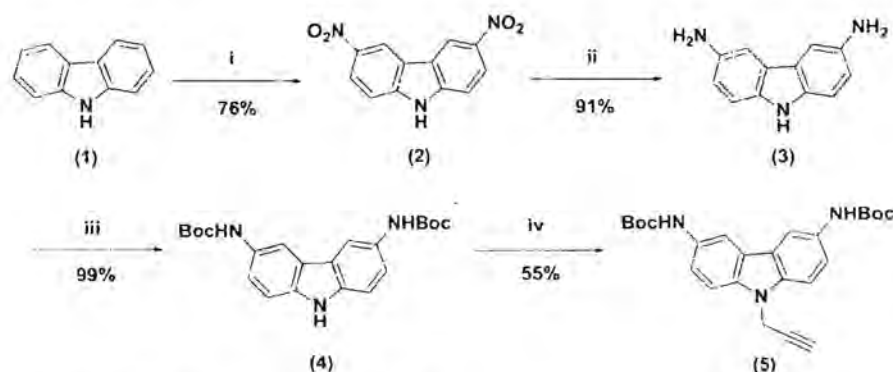
Results and discussion

Synthesis of diaminocarbazole (DAC)-labeled PNA

A novel clickable 3,6-diaminocarbazole for labeling of the acpcPNA was first prepared. *N*⁹-Propargylated, Boc-protected-3,6-diaminocarbazole (5) was prepared in 4 steps with 37% overall yield starting from carbazole (Scheme 1). Controlled nitration of the carbazole (1) with fuming nitric acid in 1,2-dichloroethane at 45 °C afforded the dinitration product 2 in good yield. Subsequent reduction of the dinitro-compound 2 with tin(II) chloride in a mixture of acetic acid and concentrated hydrochloric acid provided the desired diaminocarbazole 3 in

excellent yield after simple precipitation. The amino groups in 3 were protected to avoid undesired side reactions at this position during subsequent steps. Boc group was chosen as it could be easily introduced and subsequently cleaved under acidic conditions required for the cleavage of the modified PNA from the solid support. The Boc-protected DAC (4) was next alkylated with propargyl bromide in the presence of K₂CO₃/KI to get the desired clickable diaminocarbazole derivative (5).

AcpcPNA sequences were synthesized manually by Fmoc solid phase peptide synthesis as described previously.^{27,35} In order to provide a handle for attachment of the DAC *via* the previously reported reductive alkylation-Click chemistry strategy,³¹ one of the 2-amino cyclopentanecarboxylic acid (ACPC) spacer in the middle of the acpcPNA strand was replaced with 3-aminopyrrolidine-4-carboxylic acid (APC) for internal labeling.³⁵ For terminal labeling, no modification with APC was required, but the last ACPC residue was omitted from the PNA sequence. After end-capping by acetylation (this step was skipped for the terminal modification) and removal of all protecting groups from the nucleobase and the APC spacer, the azide group was introduced by reductive alkylation with 4-azidobutanol. Finally, the clickable DAC label (5) was attached to the azide-modified acpcPNA on the solid support by Cu-catalyzed click chemistry. Four DAC-modified acpcPNA sequences were designed to investigate the DNA binding and fluorescent properties under different sequence context. These include an internally-labeled homothymine (T9^{DAC}), two internally-labeled mix sequences with different flanking bases (A/T and C/G pairs) (M10AT^{DAC} and M10GC^{DAC}) and a terminally-labeled mix sequence (DAC-M10). All modified PNAs were purified by reverse phase HPLC (to >90% purity). The identities of the obtained PNA sequences were confirmed by MALDI-TOF mass spectrometry, which showed the mass signals that are in a good agreement with the expected values. The sequences and characterization data of all PNA involved in this studies are shown in Table 1.



- i) 90% HNO₃, 1,2-dichloroethane, 45 °C, 4h
 ii) SnCl₂/HOAc/HCl, reflux
 iii) Boc₂O, Et₃N, MeOH, rt
 iv) Propargyl bromide, K₂CO₃, KI, DMF, rt

Scheme 1 Synthesis of clickable 3,6-diaminocarbazole label (5).

Table 1 Sequence and characterization data of DAC-labeled acpcPNA

| PNA | Sequence (N → C) | t_R^a (min) | Yield ^b (%) | m/z (calcd) | m/z (found) |
|----------------------|---|---------------|------------------------|---------------|---------------|
| T9 ^{DAC} | Ac-TTTT ^(DAC) TTTT-LysNH ₂ | 32.0 | 5.8 | 3513.6 | 3512.4 |
| M10AT ^{DAC} | Ac-GTAGA ^(DAC) TCACT-Lys NH ₂ | 29.5 | 5.2 | 3892.8 | 3894.1 |
| M10GC ^{DAC} | Ac-GTAGC ^(DAC) GCACT-Lys NH ₂ | 27.7 | 4.4 | 3893.8 | 3893.2 |
| DAC-M10 | DAC-GTAGATCACT-Lys NH ₂ | 29.0 | 5.4 | 3738.8 | 3738.3 |

^a HPLC condition: C18 column 4.6 × 50 mm, particle size 3 μm, gradient 0.1% TFA in H₂O : MeOH 90 : 10 for 5 min then linear gradient to 10 : 90 over 30 min, flow rate 0.5 mL min⁻¹. ^b Isolated yield after HPLC.

Thermal stability and fluorescent properties of DAC-labeled acpcPNA

To investigate the binding properties with DNA, the stabilities of complementary and mismatched DAC-modified PNA-DNA hybrids were determined by thermal denaturation experiments. Thermal stability (T_m) and fluorescent properties of DAC-labeled acpcPNA are summarized in Table 2. The complementary DNA hybrid of T9^{DAC} sequence showed a T_m of 65.2 °C, which was considerably lower than the corresponding DNA hybrid of unmodified T9 acpcPNA (>80 °C). The T_m of the DNA hybrid of the M10AT^{DAC} sequence of 53.4 °C was also reduced compared to the unmodified PNA (57.0 °C). This suggests that the internal modification with the DAC dye destabilizes the acpcPNA-DNA duplex, probably due to steric effect. This behavior was also observed in our previous studies with the same acpcPNA system with different labels.^{34,35} The mix-base sequences PNA M10GC^{DAC} and DAC-M10 showed T_m values of 59.0 and 58.2 °C, respectively. The T_m value of the terminally DAC-modified DAC-M10 duplex was in fact larger than that of the unmodified duplex ($\Delta T_m = +1.2$ °C). This can be explained by the additional stabilization from the end stacking of the DAC at the terminal base pair of the PNA-DNA duplex as observed in the case of pyrene label.³¹ All single mismatched

PNA-DNA hybrids exhibited considerably lower T_m than complementary hybrids ($\Delta T_m = -27.0$ to -41.6 °C for T9^{DAC} and -18.4 to -28.9 °C for M10GC^{DAC}/M10AT^{DAC} and less than -38.2 °C for DAC-M10). The ΔT_m values are comparable to those of unmodified PNA, which indicated that the base pairing specificity of the DAC-labeled acpcPNA remained high.

Next, fluorescence experiments were performed with all PNA sequences and their DNA hybrids. The responsiveness of the PNA probe was reported in terms of fluorescence intensity ratio (F/F_0 ; where F = fluorescence intensity of PNA-DNA hybrid, F_0 = fluorescence intensity of single stranded PNA; λ_{ex} 315 nm; λ_{em} 450 nm). While free 3,6-diaminocarbazole showed a high Φ_F of 0.489, all internally-labeled single stranded PNA probes exhibited very low Φ_F values of 0.01 or less, regardless of the identity of the neighboring nucleobase (Table 2, entries 1, 6, 11). This suggests that the DAC label is quenched upon incorporation into the PNA, probably by interactions with the nucleobases similar to pyrene.³¹ The sequences M10AT^{DAC} and T9^{DAC} showed lower quantum yields than M10GC^{DAC}, which means that A/T are better quenchers than C/G bases for DAC label. Nevertheless, judging from the uniformly low quantum yields of all PNA probes, the difference in quenching efficiency by different nucleobases is much less than pyrene, which emphasizes the important feature of the DAC label.³¹

Table 2 Thermal stability (T_m) and fluorescence properties of DAC-labeled acpcPNA^a

| Entry | PNA | DNA (3' → 5') | T_m (°C) | F/F_0 | Φ_F | Φ_F (ds)/ Φ_F (ss) ^b | Notes ^c |
|-------|----------------------|---------------|------------|---------|----------|---|--------------------|
| 1 | T9 ^{DAC} | None | — | — | 0.009 | — | ss |
| 2 | | AAAAAAAA | 65.2 | 35.5 | 0.242 | 26.7 | comp |
| 3 | | AAAACAAAA | 33.7 | 18.6 | 0.139 | 15.3 | smC |
| 4 | | AAAAGAAAA | 23.6 | 6.0 | 0.041 | 4.5 | smG |
| 5 | | AAAATAAAA | 38.2 | 15.7 | 0.160 | 17.6 | smT |
| 6 | M10AT ^{DAC} | None | — | — | 0.007 | — | ss |
| 7 | | AGTGATCTAC | 53.4 | 13.2 | 0.083 | 11.9 | comp |
| 8 | | AGTGCTCTAC | 29.0 | 2.7 | 0.012 | 1.7 | smC |
| 9 | | AGTGGTCTAC | 24.5 | 1.7 | 0.014 | 2.0 | smG |
| 10 | M10GC ^{DAC} | AGTGTTCTAC | 35.0 | 6.5 | 0.034 | 4.8 | smT |
| 11 | | None | — | — | 0.011 | — | ss |
| 12 | | AGTGCGCTAC | 59.0 | 10.2 | 0.117 | 11.1 | comp |
| 13 | | AGTGATCTAC | 30.8 | 4.9 | 0.099 | 9.4 | smA |
| 14 | | AGTGGTCTAC | 33.4 | 7.0 | 0.085 | 8.0 | smG |
| 15 | | AGTGTTCTAC | 39.2 | 9.1 | 0.104 | 9.9 | smT |

^a All measurements were performed in 10 mM sodium phosphate buffer (pH 7.0), [PNA] = 1.0 μM, [DNA] = 1.2 μM, λ_{ex} 315 nm, λ_{em} 450 nm.

^b Quantum yields were measured in phosphate buffer using quinine sulfate (0.540) as a reference. ^c ss = single stranded PNA, comp = complementary, sm = single mismatched.

A remarkable increase in fluorescence signal was observed upon hybridization with complementary DNA, as shown by the fluorescence intensity ratio (F/F_0) between 10.2 and 35.5 (Table 2, entries 2, 7, 12). The quantum yield of the DAC-labeled PNA·DNA duplexes was also consistently increased by >10-fold to around 0.08–0.24, which is still considerably lower than the free DAC (3). This indicates that the interaction between the DAC and the neighboring nucleobases is reduced in PNA·DNA duplexes due to the formation of base pairs. This behavior is similar to pyrene label and a similar mechanism of fluorescence increase is proposed.³¹ It should be noted that free DAC also interact with single stranded DNA, resulting in fluorescence quenching, which is consistent with the proposed mechanism (see ESI Fig. S22†). CD spectra of M10GC^{DAC} and its complementary DNA hybrid (see ESI Fig. S23†) also clearly confirms the formation of PNA·DNA hybrids as shown by the change in CD signals at 210 and 260 nm. No CD signal was observed in the UV absorption region of DAC, suggesting that the DAC label was not well-oriented and thus did not appreciably interact with the PNA·DNA duplex.

Single mismatched PNA·DNA hybrids generally showed smaller fluorescence increase, but some variations in the sequence context were observed (Fig. 1). The M10AT^{DAC} showed a better mismatch discrimination than the T9^{DAC} and

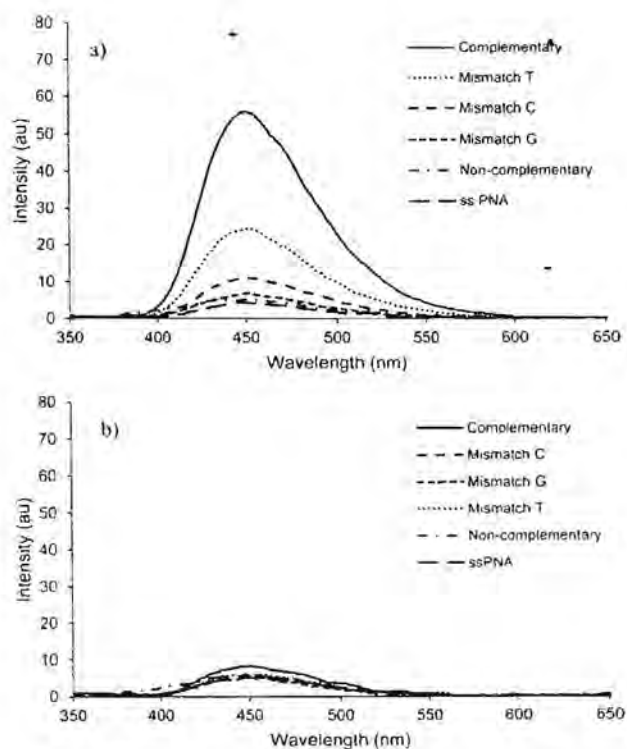


Fig. 1 Fluorescence spectra of DAC-labeled acpcPNA with complementary, single mismatch, non-complementary and single strand form of (a) M10AT^{DAC} (b) DAC-M10. Conditions: 10 mM sodium phosphate buffer, pH 7.0 at 25 °C, [PNA] = 1.0 μ M and [DNA] = 1.2 μ M, excitation wavelength = 315 nm. Complementary DNA = AGT-GATCTAC, mismatch C DNA = AGTGCTCTAC, mismatch G DNA = AGTGGTCTAC and mismatch T DNA = AGTGTCTAC

M10GC^{DAC} probes. Possible explanation is that certain mismatched PNA·DNA hybrids (Table 2, entries 3, 5, 10, 13–15) are still sufficiently stable at 20 °C – the temperature at which the fluorescent experiments were carried out. Completely unrelated DNA target provided a signal that was indistinguishable from the single stranded probes in all cases. For terminal labeled PNA probe DAC-M10, no fluorescence change could be observed for both complementary and mismatched DNA targets (Fig. 1b). Since the single stranded PNA probe exhibited low fluorescence similar to internally labeled PNA probes, it can be concluded that the quenching by neighboring nucleobases still operates. T_m measurement confirms the strong binding between the DAC-M10 probe and DNA in a sequence specific fashion (58 °C for complementary duplexes and <20 °C for mismatched

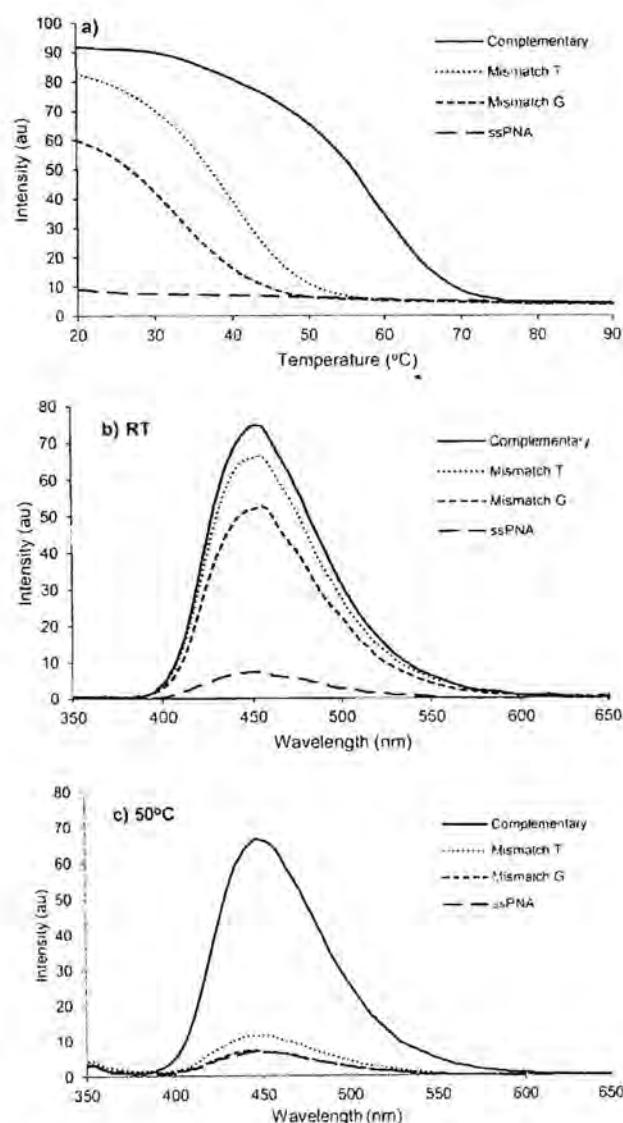


Fig. 2 (a) Fluorescence melting curves of M10GC^{DAC} (b) fluorescence spectra of M10GC^{DAC} at RT (c) fluorescence spectra of M10GC^{DAC} at 50 °C. All experiments were performed in 10 mM phosphate-buffered pH 7.0, [PNA] = 1.0 μ M, [DNA] = 1.2 μ M, λ_{ex} 315 nm, PMT voltage = medium.

duplexes). The absence of fluorescence increase upon duplex formation was therefore explained by the interaction between the DAC and the terminal GC base pair of the PNA·DNA duplex similar to the pyrene label.³¹

These results clearly demonstrate that the fluorescence of internally DAC-labeled acpcPNA is low in single stranded PNA probes due to quenching by neighboring nucleobases, especially T and A bases. This interaction diminished - resulting in a large fluorescence increase - when the PNA·DNA duplexes are formed, provided that the DAC label does not locate at the end of the duplex which allows interactions with the terminal base pairs.

Improving single mismatch discrimination of the DAC-labeled acpcPNA probes

Although the T_m measurement indicated the high specificity as shown by a large decrease in the T_m values between complementary and single mismatch PNA·DNA duplexes (ΔT_m ranging from -18.4 to -31.5 °C), but the fluorescence spectra of certain mismatch duplexes still showed relatively high fluorescence signal. Based on a hypothesis that the high fluorescence was due to the high stability of some mismatched duplexes at room temperature, the temperature was increased to improve the single mismatch discrimination by fluorescence spectrophotometry. Single mismatch hybrids should dissociate more easily than complementary hybrids, and therefore the temperature increase should be able to enhance the mismatch discrimination ability of DAC-labeled acpcPNA. The experiment was carried out only with the complementary hybrids and mismatched hybrids that does not show satisfactory discrimination in Table 2. The fluorescence spectra were measured at different temperature from 20 °C to 90 °C (see ESI†). Upon heating, the duplex dissociated with concomitant decrease in the fluorescence intensity. The plots between the fluorescence signal at 450 nm and temperature appeared in the form of reverse S-curves (Fig. 2a).

Since the maximal difference will be obtained at the temperature whereby the mismatched duplexes were dissociated as much as possible and the complementary duplexes are still stable, it is important to vary the temperature to find the optimal value case by case. The specific temperature that provided maximum differentiation in the case of $T9^{DAC}$, $M10AT^{DAC}$ and $M10GC^{DAC}$ was 55, 45 and 50 °C, respectively. The mismatched hybrids of $T9^{DAC}$ and $M10GC^{DAC}$ were more stable than those of $M10AT^{DAC}$ and therefore required a higher temperature to complete the separation. At the aforementioned optimal temperature, the fluorescence ratio between complementary and single mismatch hybrids improved from 1.0-2.5 folds to 6.0-21.1 folds (Fig. 2b and c and Table 3). The results confirm that the specificity of DAC-labeled acpcPNA in distinguishing between complementary and single-mismatched DNA by DAC-labeled PNA probes can be improved by simply increasing the temperature without requiring more complex operations such as enzymatic digestion.

Next, to support the proposed mechanism of fluorescence change of the DAC-labeled PNA probe, molecular dynamics simulation and energy calculation were performed on both single stranded and duplex PNA probe.

Molecular modeling

MD structures. For both simulated systems (ssPNA and PNA·DNA duplex), the structure of DAC started by pointing to bulk solvent was rolled and close to PNA strand after 0.5 ns and then fluctuated in such position along 10 ns of simulation time, as displayed in Fig. 3. The root mean squared deviations (RMSDs) of the MD structures with respect to their starting structures were 4.42 ± 0.67 Å and 4.02 ± 0.40 Å for ssPNA and PNA·DNA systems, respectively, averaged over the last 2000 structures, see Fig. S25† for the RMSD profiles. Clearly, single stranded PNA provides larger fluctuation because of a less restriction of its structure. The average structure revealed that the DAC is closer to the nucleobases in the single stranded PNA than that in the PNA·DNA

Table 3 Comparison of F/F_0 of DAC-labeled acpcPNA at room temperature and high temperature^a

| Entry | PNA | DNA (3' → 5') | F/F_0 (25 °C) | F_{comp}/F_{mm} (25 °C) | F/F_0 (high temp) ^b | F_{comp}/F_{mm} (high temp) ^b |
|-------|---------------|---------------|-----------------|---------------------------|----------------------------------|--|
| 1 | $T9^{DAC}$ | AAAAAAAA | 35.4 | — | 35.7 | — |
| 2 | | AAAACAAAA | 18.6 | 1.9 | 2.5 | 14.2 |
| 3 | | AAAAGAAAA | 6.0 | 5.9 | — | — |
| 4 | | AAAATAAAA | 15.7 | 2.3 | 1.7 | 21.1 |
| 5 | | TTTTTTTTT | 1.1 | 32.4 | — | — |
| 6 | $M10AT^{DAC}$ | AGTGATCTAC | 13.2 | — | 12.9 | — |
| 7 | | AGTGCTCTAC | 2.6 | 5.2 | 1.3 | 10.0 |
| 8 | | AGTGGTCTAC | 1.6 | 8.2 | — | — |
| 9 | | AGTGTTCTAC | 5.7 | 2.3 | 1.2 | 10.6 |
| 10 | | GGGGGGGGG | 1.2 | 10.9 | — | — |
| 11 | $M10GC^{DAC}$ | AGTGCCTAC | 10.1 | — | 10.2 | — |
| 12 | | AGTGATCTAC | 5.3 | 1.9 | — | — |
| 13 | | AGTGGTCTAC | 7.1 | 1.4 | 1.0 | 10.3 |
| 14 | | AGTGTTCTAC | 9.0 | 1.1 | 1.7 | 6.0 |
| 15 | | GGGGGGGGG | 0.9 | 11.1 | — | — |

^a All measurements were performed in 10 mM sodium phosphate buffer (pH 7.0), [PNA] = 1.0 μM, [DNA] = 1.2 μM, λ_{ex} 315 nm, λ_{em} 450 nm. ^b High temperature: $T9^{DAC}$ = 55 °C; $M10AT^{DAC}$ = 45 °C; $M10GC^{DAC}$ = 50 °C.

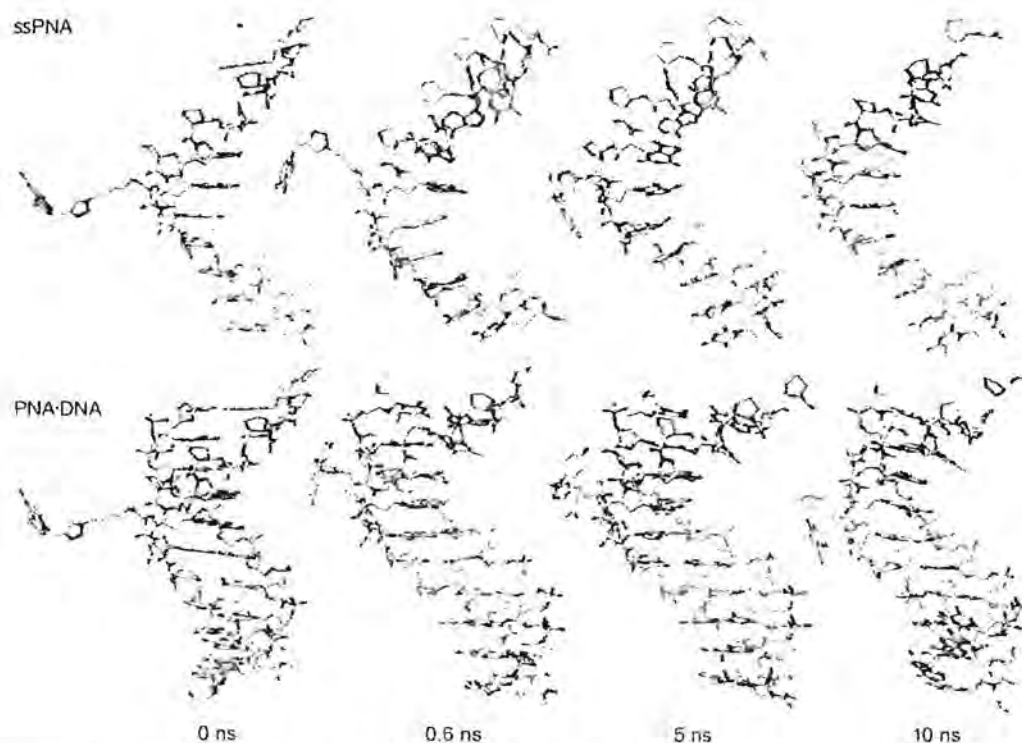


Fig. 3 MD snapshots of a single stranded PNA and the corresponding PNA·DNA duplex.

duplex (Fig. 4), which should lead to a larger interaction between DAC and PNA for the single stranded PNA system.

Energy calculation. In order to investigate the DAC–PNA interactions between DAC and nucleobases in single stranded PNA as well as PNA·DNA duplexes in more details, we have calculated the binding energy between the DAC and three closest PNA nucleobases, whereas other fragments were omitted. The calculations were performed using Gaussian 09

Table 4 The binding energy ($\Delta E_{\text{binding}}$) between DAC and three closest PNA nucleobases^a

| System | $\Delta E_{\text{binding}}$ (kcal mol ⁻¹) |
|---------|---|
| ssPNA | 11.40 |
| PNA·DNA | -3.86 |

^a The calculation is expressed as $\Delta E_{\text{binding}} = E_{\text{DAC-PNA}} - E_{\text{DAC}} - E_{\text{PNA}}$ where $E_{\text{DAC-PNA}}$, E_{DAC} and E_{PNA} are the total energy of DAC and three PNA nucleotides, DAC moiety and three PNA nucleotides, respectively.

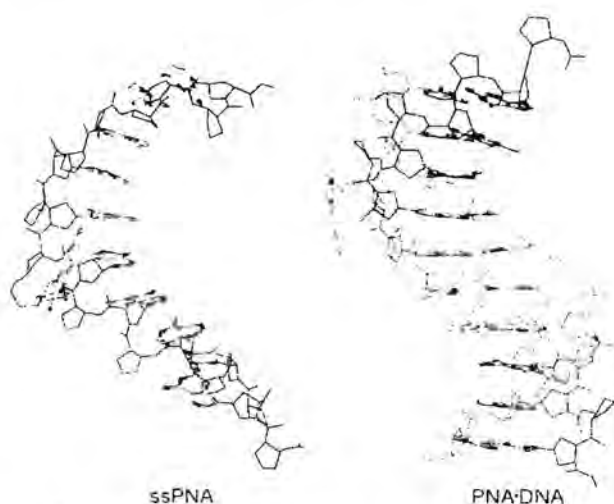


Fig. 4 Average MD structures of single stranded PNA and PNA·DNA duplex

program with the density functional theory B3LYP/6-31G* level based on the average MD structures for ssPNA and PNA·DNA systems. As shown in Table 4, the binding energy of single stranded PNA system is significantly higher than that of PNA·DNA duplex. This confirms that there are stronger interactions between DAC and nucleobases in single stranded PNA than in PNA·DNA duplex, and further supports the mechanism of fluorescence change proposed above.

Experimental section

General procedures

Carbazole (reagent grade for synthesis) was purchased from Merck. All reagent grade chemicals and solvents were purchased from standard suppliers and were used without further purification. ¹H and ¹³C NMR spectra were recorded on Bruker Avance 400 NMR spectrometer operating at 400 MHz for ¹H and 100 MHz

for ^{13}C . RP-HPLC experiments were performed on a Waters Delta 600 HPLC system. Oligonucleotides were obtained from Pacific Science (Thailand) or BioDesign (Thailand).

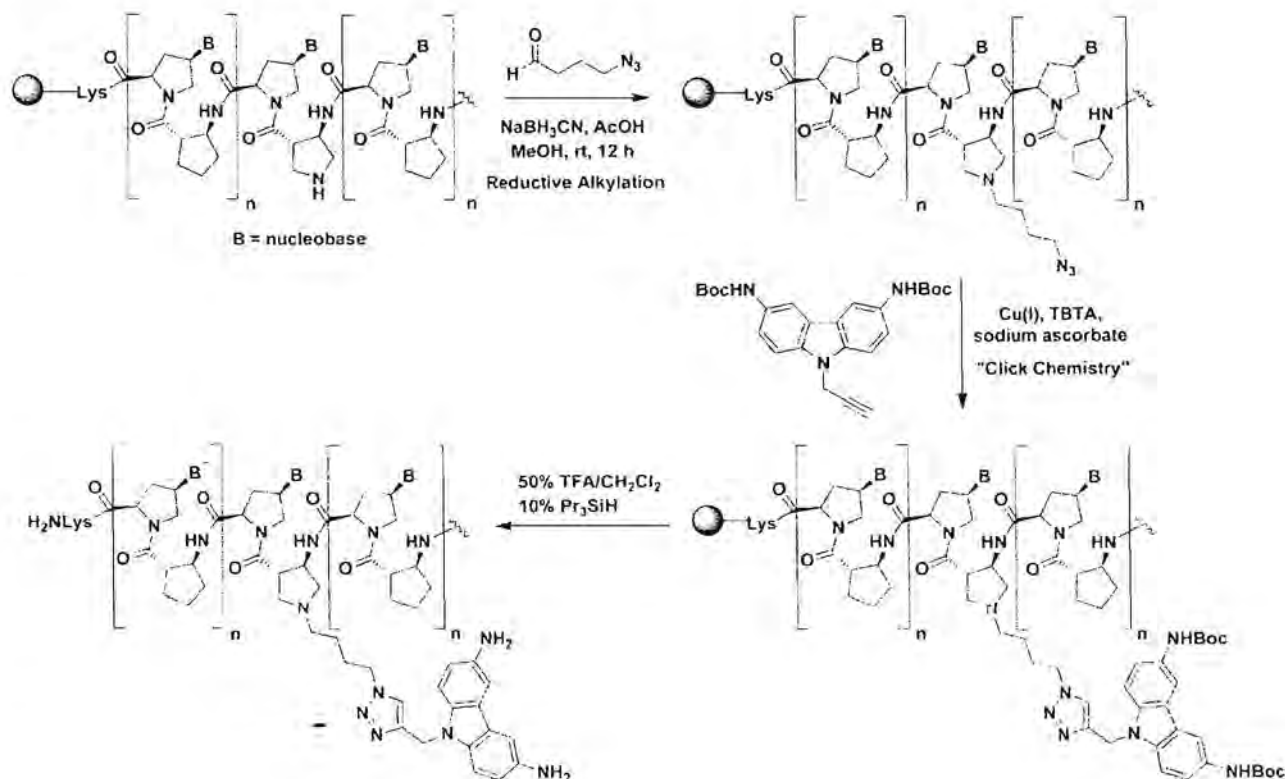
N^9 -Propargyl-3,6-bis(*tert*-butoxycarbonylamino)carbazole (5)

A reaction mixture containing 3,6-bis(*tert*-butoxycarbonylamino)carbazole (4) (0.80 g, 2.00 mmol) (see ESI[†]), propargyl bromide (0.28 mL, 3.00 mmol), KI (0.33 g, 2.00 mmol) and K_2CO_3 (2.77 g, 20.0 mmol) in dry DMF (5 mL) was stirred under N_2 atmosphere at room temperature overnight. The reaction mixture was diluted with water and extracted with CH_2Cl_2 . The combined organic extracts were washed with water and brine, dried over anhydrous Na_2SO_4 and evaporated to dryness. The crude product was purified by column chromatography on silica gel to obtain the pure compound as a yellow solid. ^1H NMR (400 MHz, $\text{DMSO}-d_6$): δ 1.49 (s, 18H), 3.20 (t, $J = 2.2$ Hz, 1H), 5.18 (s, 2H), 7.41 (d, $J = 8.7$ Hz, 2H), 7.49 (d, $J = 8.7$ Hz, 2H), 8.21 (s, 2H), 9.30 (s, 2H). ^{13}C NMR (100 MHz, $\text{DMSO}-d_6$): δ 153.2, 136.2, 131.9, 122.3, 118.2, 109.5, 79.2, 78.7, 74.3, 31.9, 28.2, 27.9; IR: 3397, 3254, 2974, 2112 ($\text{C}\equiv\text{C}$), 1720, 1702 ($\text{C}=\text{O}$), 1524, 1490, 1048, 1023, 864, 792, 578 cm^{-1} ; HRMS (ESI⁺): m/z calcd for $\text{C}_{25}\text{H}_{29}\text{N}_3\text{O}_4\text{Na}^+$: 458.2056 [M + Na]⁺ found: 458.2092, m/z calcd for $\text{C}_{25}\text{H}_{29}\text{N}_3\text{O}_4\text{K}^+$: [M + K]⁺ 474.1795 found: 474.1826.

Synthesis, purification and characterization of DAC-modified acpcPNA

The apc-modified acpcPNA was synthesized *via* solid phase peptide synthesis using the four Fmoc-protected pyrrolidine

monomers [Fmoc-A^{Bz}-OPfp, Fmoc-T-OPfp, Fmoc-C^{Bz}-OPfp, and Fmoc-G^{Ibu}-OPfp] and spacers [Fmoc-(1*S*,2*S*)-ACPC-OPfp, Fmoc-(3*R*,4*S*)-APC(Tfa)-OPfp] at 1.5 μmol scale on Tentagel S-RAM resin according to the previously published protocol.^{27,28,35} Lysine was included at the C-terminus in the form of Fmoc-Lys(Boc)-OPfp to improve the water solubility of the PNA. After completion of the PNA synthesis, the N-terminal Fmoc group was removed and the free amino group was capped by acetylation. The apc-modified acpcPNA was split to 0.5 μmol portions for further labeling experiments. The nucleobase protecting groups (Bz, Ibu) and APC spacer protection (Tfa) were removed by heating with 1 : 1 aqueous ammonia/dioxane at 60 $^\circ\text{C}$ overnight. The apc-modified acpcPNA (0.5 μmol) was alkylated at the pyrrolidine ring nitrogen of the APC spacer with 4-azidobutanol (15 μmol , 30 equiv.) in the presence of sodium cyanoborohydride (30 μmol , 60 equiv.) and acetic acid (30 μmol , 60 equiv.) in methanol (100 μL) at room temperature overnight.³⁴ The azide-modified acpcPNA was further reacted with N^9 -propargyl-3,6-bis(Boc-amino)carbazole (5) (7.5 μmol , 15 equiv.) while still attached to the solid support in the presence of tris[(1-benzyl-1*H*-1,2,3-triazol-4*yl*)methyl]amine (TBTA, 30 μmol , 60 equiv.), tetrakis(acetonitrile)copper(i) hexafluorophosphate (15 μmol , 30 equiv.) and (+)-sodium-*L*-ascorbate (60 μmol , 120 equiv.) in 3 : 1 (v/v) DMSO : *t*-BuOH at room temperature overnight.³⁴ After the reaction was completed as monitored by MALDI-TOF analyses (12 h), the diaminocarbazole-modified acpcPNA was cleaved from the resin with 50% trifluoroacetic acid (TFA) in dichloromethane



Scheme 2 Synthesis of DAC-modified acpcPNA.

and 10% triisopropylsilane (TIS) (500 $\mu\text{L} \times 30 \text{ min} \times 3$). The combined cleavage solution was dried under a stream of nitrogen gas and the crude PNA was precipitated by addition of diethyl ether (Scheme 2). The crude PNA was purified by reverse-phase HPLC with using mobile phase A : B (A: 0.1% TFA in H_2O ; B: 0.1% TFA in MeOH) 9 : 1 for 5 min followed by a linear gradient to A : B 1 : 9 over 55 min. The purified PNA was characterized by MALDI-TOF mass spectrometry (Microflex, Bruker Daltonics) by using α -cyano-4-hydroxy-cinnamic acid (CCA) as a matrix.

Spectroscopic experiments

All samples were prepared at PNA concentration = 1.0 μM and DNA concentration = 1.2 μM in 10 mM phosphate buffer pH 7.0. UV-visible spectra and thermal stabilities (T_m) were measured on a CARY 100 Bio UV-vis spectrophotometer at 260 nm from 20–90 $^\circ\text{C}$ at a rate of 1 $^\circ\text{C min}^{-1}$. The melting temperatures were determined from first derivative plots. Fluorescence spectra were measured on Cary Eclips Fluorescence Spectrophotometer at excitation wavelength of 315 nm. Both excitation and emission slits were set to 5 nm and PMT voltage = medium.

Fluorescence quantum yield (Φ_F) measurement

The fluorescence quantum yield (Φ_F) of 3,6-diaminocarbazole (3), single stranded-PNA and PNA-DNA duplexes [T9^{DAC} , $\text{M10AT}^{\text{DAC}}$ and $\text{M10GC}^{\text{DAC}}$] were calculated using quinine sulfate ($\Phi_F = 0.540$) as a ref. 36 Absorption and fluorescence spectra were measured on CARY 100 Bio UV-vis spectrophotometer (Varian) and CARY Eclipse Fluorescence spectrophotometer (Varian/Agilent Technologies), respectively. Seven concentrations (1.0, 2.0, 2.5, 5.0, 7.5, 10.0, 12.0 μM) of quinine sulfate samples in phosphate buffer were prepared from a stock solution (1.0 mM quinine sulfate in 0.1 M H_2SO_4). The absorbance at 315 nm was less than 0.1 for all concentrations. The magnitudes of integrated fluorescence intensity were plotted against the absorbance of the solution absorbance. The quantum yield of sample was then calculated according to eqn (1).³¹

$$\Phi_F(\text{sample}) = \Phi_F(\text{standard})[m(\text{sample})/m(\text{standard})][\eta(\text{sample})^2/\eta(\text{standard})^2] \quad (1)$$

where m is the slope from the plot of integrated fluorescence intensity vs. absorbance and η is the refractive index of the solvent.

Molecular dynamics (MD) simulation. MD simulations were performed on single stranded acpcPNA with a sequence of GTAGATCACT whereby the DAC was linked to the apc spacer at the underlined position, and the corresponding acpcPNA-DNA duplex. Because the three-dimensional structures of ssPNA and PNA-DNA duplex were not available, the starting structure of PNA-DNA duplex was built up based on the corresponding sequence of DNA-DNA duplex (dGTA-GATCACT-dAGTGATCTAC) which was generated using the NAB module of the AMBER 12 package.³⁷ The first strand of the

duplex was replaced with PNA strand in an antiparallel direction yielding the PNA-DNA duplex.³⁸ The structure of diaminocarbazole (DAC) linked to backbone of PNA was first optimized with B3LYP/6-31G* calculation using Gaussian 09 (ref. 39) before adding to the PNA strand. The initial structure of single stranded acpcPNA was obtained in a similar manner. The force field parameters of the PNA and DAC were generated using the standard procedure.³⁸ To setup the simulations, the starting structure of each system was immersed in a rectangular water box with TIP3P water molecules⁴⁰ extended by 10 \AA in each direction from the solute and then neutralized by adding Na^+ counterions (for PNA-DNA system). The MD simulations were carried out using AMBER 12 suite of program with parm10 force field complemented with the prepared parameters of PNA and DAC, SHAKE algorithm⁴¹ employed for all hydrogen atoms, a 9 \AA cutoff applied to the non-bonding Lennard-Jones interactions, the particle mesh Ewald method used to account for long-range interactions,⁴² time step of 1 fs and NPT ensemble ($P = 1 \text{ atm}$ and $T = 300 \text{ K}$). The simulation protocol consists of heating, equilibration and production steps, and was described in details elsewhere.³⁸ The MD trajectories were generated for 10 ns and the coordinates were stored every 1 ps, totally 10 000 structures.

Conclusion

In conclusion, we successfully synthesized novel internally and terminally 3,6-diamino-carbazole-labeled acpcPNA and evaluated their binding and fluorescence properties. Thermal denaturation experiments revealed the high stability (T_m 53.4–65.2 $^\circ\text{C}$) and high specificity ($\Delta T_m > 20 \text{ }^\circ\text{C}$) of PNA-DNA hybrid similar to unmodified acpcPNA. Single stranded DAC-labeled acpcPNA showed low fluorescence signals due to quenching of the DAC label with neighboring nucleobases. After hybridization with DNA, the internally DAC-labeled acpcPNA showed moderate to large fluorescence increase (10.1–35.5 folds) compared to the single stranded PNA. The specificity was further improved to allow discrimination between complementary and single mismatched DNA targets by increasing the temperature. Terminally DAC-labeled acpcPNA showed no significant fluorescence change after hybridization with DNA. A model was proposed to explain the mechanism of fluorescence change, which was further supported by MD simulations and energy calculation. These results demonstrate the potential of DAC as a fluorescence label to be used in combination with oligonucleotide probes for detection of specific DNA sequences.

Acknowledgements

We acknowledge Naresuan University (NU grant No. P2558C371 to CS) and The Thailand Research Fund (DPG5780002, to TV and KS) for financial supports and National e-Science Infrastructure Consortium (URL: <http://www.e-science.in.th>) for computing resources. Partial technical supports by Ms Boonsong Ditmangklo (Chulalongkorn University) are also gratefully acknowledged.

References

- 1 M. K. Johansson, H. Fidler, D. Dick and R. M. Cook, *J. Am. Chem. Soc.*, 2002, **124**, 6950–6956.
- 2 L. Giestas, G. N. M. Ferreira, P. V. Baptista and J. C. Lima, *Sens. Actuators, B*, 2008, **134**, 146–157.
- 3 E. G. Matveeva, Z. Gryczynski, D. R. Stewart and I. Gryczynski, *J. Lumin.*, 2010, **130**, 698–702.
- 4 P. Rashatasakhon, K. Vongnam, W. Siripornnoppakhun, T. Vilaivan and M. Sukwattanasinitt, *Talanta*, 2012, **88**, 593–598.
- 5 N. Maneelun and T. Vilaivan, *Tetrahedron*, 2013, **69**, 10805–10810.
- 6 B. S. Gaylord, A. J. Heeger and G. C. Bazan, *J. Am. Chem. Soc.*, 2003, **125**, 896–900.
- 7 Z.-K. Xu, B.-K. Zhu and Y.-Y. Xu, *Chem. Mater.*, 1998, **10**, 1350–1354.
- 8 D. Li-yun, J. De-sheng, H. Jun, D. Lei, L. Cheng, W. Jun-tao and L. Bin, *Trans. Nonferrous Met. Soc. China*, 2006, **16**, s191–s194.
- 9 D. W. Kim, H. Moon, S. Y. Park and S. I. Hong, *React. Funct. Polym.*, 1999, **42**, 73–86.
- 10 I. F. Perepichka, D. D. Mysyk and N. I. Sokolov, *Synth. Met.*, 1999, **101**, 9–10.
- 11 X. Pan, S. Liu, H. S. O. Chan and S. C. Ng, *Macromolecules*, 2005, **38**, 7629–7635.
- 12 J. Sun, H.-J. Jiang, J.-L. Zhang, Y. Tao and R.-F. Chen, *New J. Chem.*, 2013, **37**, 977–985.
- 13 J. P. Chen and A. Natansohn, *Macromolecules*, 1999, **32**, 3171–3177.
- 14 A. Oral, S. Koyuncu and I. Kaya, *Synth. Met.*, 2009, **159**, 1620–1627.
- 15 S. Koyuncu, I. Kaya, F. B. Koyuncu and E. Ozdemir, *Synth. Met.*, 2009, **159**, 1034–1042.
- 16 F. B. Koyuncu, S. Koyuncu and E. Ozdemir, *Electrochim. Acta*, 2010, **55**, 4935–4941.
- 17 C.-H. Tao, N. Zhu and V. W.-W. Yam, *J. Photochem. Photobiol., A*, 2009, **207**, 94–101.
- 18 P. Thongkasee, A. Thangthong, N. Janthasing, T. Sudyoadsuk, S. Namuangruk, T. Keawin, S. Jungstittiwong and V. Promarak, *ACS Appl. Mater. Interfaces*, 2014, **6**, 8212–8222.
- 19 G. Sathiyam, E. K. T. Sivakumar, R. Ganesamoorthy, R. Thangamuthu and P. Sakthivel, *Tetrahedron Lett.*, 2016, **57**, 243–252.
- 20 B. Dumat, G. Bordeau, E. Faurel-Paul, F. Mahuteau-Betzer, N. Saettel, M. Bombled, G. Metgé, F. Charra, C. Fiorini-Debuisschert and M.-P. Teulade-Fichou, *Biochimie*, 2011, **93**, 1209–1218.
- 21 F. A. Taniou, D. Y. Ding, D. A. Patrick, R. R. Tidwell and W. D. Wilson, *Biochemistry*, 1997, **36**, 15315–15325.
- 22 F. A. Taniou, D. Y. Ding, D. A. Patrick, C. Bailly, R. R. Tidwell and W. D. Wilson, *Biochemistry*, 2000, **39**, 12091–12101.
- 23 F. A. Taniou, W. D. Wilson, D. A. Patrick, R. R. Tidwell, P. Colson, C. Houssier, C. Tardy and C. Bailly, *Eur. J. Biochem.*, 2001, **268**, 3455–3464.
- 24 T. Jia, J. Xiang, J. Wang, P. Guoa and J. Yu, *Org. Biomol. Chem.*, 2013, **11**, 5512–5520.
- 25 P. E. Nielsen, M. Egholm, R. H. Berg and O. Buchardt, *Science*, 1991, **254**, 1497–1500.
- 26 M. Egholm, O. Buchardt, L. Christensen, C. Behrens, S. M. Freier, D. A. Driver, D. A. R. H. Berg, S. K. Kim, B. Norden and P. E. Nielsen, *Nature*, 1993, **365**, 566–568.
- 27 T. Vilaivan and C. Srisuwannaket, *Org. Lett.*, 2006, **8**, 1897–1900.
- 28 C. Vilaivan, C. Srisuwannaket, C. Anantthanawat, C. Suparpprom, J. Kawakami, Y. Yamaguchi, Y. Tanaka and T. Vilaivan, *Artif. DNA*, 2011, **2**, 50–59.
- 29 W. Mansawat, C. Vilaivan, A. Balazs, D. J. Aitken and T. Vilaivan, *Org. Lett.*, 2012, **14**, 1440–1443.
- 30 T. Vilaivan, *Acc. Chem. Res.*, 2015, **48**, 1645–1656.
- 31 C. Boonlua, B. Ditmangklo, N. Reenabthue, C. Suparpprom, N. Poomsuk, K. Siriwong and T. Vilaivan, *RSC Adv.*, 2014, **4**, 8817–8827.
- 32 S. Sezi, R. Varghese, T. Vilaivan and H.-A. Wagenknecht, *ChemistryOpen*, 2012, **1**, 173–176.
- 33 N. Yotapan, C. Charoenpakdee, P. Wathanathavorn, B. Ditmangklo, H.-A. Wagenknecht and T. Vilaivan, *Beilstein J. Org. Chem.*, 2014, **10**, 2166–2174.
- 34 B. Ditmangklo, C. Boonlua, C. Suparpprom and T. Vilaivan, *Bioconjugate Chem.*, 2013, **24**, 614–625.
- 35 N. Reenabthue, C. Boonlua, C. Vilaivan, T. Vilaivan and C. Suparpprom, *Bioorg. Med. Chem. Lett.*, 2011, **21**, 6465–6469.
- 36 W. H. Melhuish, *J. Phys. Chem.*, 1961, **65**, 229–235.
- 37 AMBER 12, University of California, San Francisco, 2012.
- 38 N. Poomsuk and K. Siriwong, *Chem. Phys. Lett.*, 2012, **588**, 237–241.
- 39 GAUSSIAN 09 (Revision B.01), Gaussian, Inc., Wallingford, Connecticut, 2009.
- 40 W. L. Jorgensen, *J. Am. Chem. Soc.*, 1981, **103**, 335–340.
- 41 J. P. Ryckaert, G. Cicotti and J. C. Berendsen, *J. Comput. Phys.*, 1997, **23**, 327–341.
- 42 T. Darden, D. York and L. Pedersen, *J. Chem. Phys.*, 1993, **98**, 10089–10092.

Biological Chemistry & Chemical Biology

Preparation and Performance Evaluation of a Pyrrolidinylyl Peptide Nucleic-Acid-Based Displacement Probe as a DNA Sensor

Chalothorn Boonlua, Chayan Charoenpakdee, Tirayut Vilaivan, and Thanit Praneenararat^{*(a)}

A new displacement probe based on pyrrolidinylyl peptide nucleic acid was designed and evaluated for DNA sequence recognition. The probe was prepared by combining an *N*-terminally fluorophore-modified pyrrolidinylyl peptide nucleic acid (Flu- or TMR-acpcPNA) and a 3'-Dabcyl-modified DNA as a quencher. Fluorescence studies showed that the fluorophore in the acpcPNA strand was efficiently quenched by the quencher strand. After some optimisation, the fluorescence was significantly restored upon the addition of the complementary DNA

target, while the fluorescence stayed at a low level with the addition of mismatched DNA. Even with double-stranded DNA analytes, the high specificity of the PNA-based displacement probes allowed unambiguous discrimination between complementary and single mismatched DNA targets. Furthermore, immobilisation of the probes onto agarose resin could also recognise only the complementary DNA, thereby demonstrating its potential as a practical DNA sensor.

Introduction

Synthetic analogues of nucleic acids have been extensively studied as their utilities can have profound impact on a variety of scientific disciplines. Among these, peptide nucleic acid (PNA) remains as a prominent class of analogues that exhibits several promising properties such as great stability and high affinity towards nucleic acids (even higher than duplexes from nucleic acids themselves due to reduced electrostatic repulsion).^[1] Of much interest to chemists is the development of novel types of PNAs with the aim to improve the binding affinity and specificity even further.^[2] The conformational flexibility of the original aminoethylglycyl (aeg) backbone suggests considerable entropic penalty from conformation change to accommodate the duplex formation. Pyrrolidinylyl PNA with a conformationally restricted PNA dipeptide backbone deriving from prolyl-aminocyclopentanecarboxylic acid (acpcPNA) was proposed by Vilaivan et al. to overcome this problem.^[3] Owing to several by-design advantages over the original PNA such as higher affinity towards DNA, greater mismatch discrimination and exclusive binding in antiparallel fashion, this PNA system has been utilised in a number of applications, especially in the field of DNA sensor.^[4]

Fluorescence resonance energy transfer (FRET) is a spectroscopic phenomenon that has been extensively studied and applied in several molecular systems including nucleic acids.^[5] This process is known to provide a reliable means to gauge the

distance between the donor and the acceptor due to its extremely sensitive nature to distance. Therefore, several forms of nucleic acids studies involving FRET have been demonstrated. For example, molecular beacons are a class of hybridisation probe that can report the presence of specific nucleic acid sequences by providing hybridisation-dependent conformational changes, which led to a change of the distance between the fluorescence reporter and the quencher, and thus the fluorescence.^[6] Another important class of probes is nucleic acids displacement probes, whose designs can vary to serve diverse applications.^[7] This type of probes is usually constructed by forming a double-stranded oligonucleotide - each strand would carry either a fluorescence reporter or a quencher (Figure 1). Initially, these molecular scaffolds arrange the dyes in

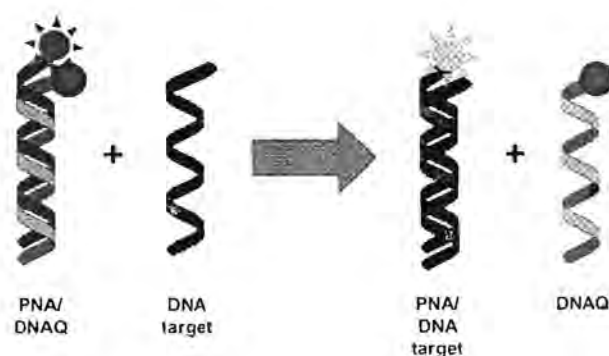


Figure 1. A typical construction of a displacement probe. A DNA target with higher duplex stability can displace a quencher-bound oligonucleotide to release the quencher and restore the fluorescence signal.

[a] Dr. C. Boonlua, C. Charoenpakdee, Prof. T. Vilaivan, Prof. T. Praneenararat
Organic Synthesis Research Unit, Department of Chemistry
Faculty of Science, Chulalongkorn University
Phayathai Rd., Pathumwan, Bangkok 10330, Thailand
E-mail: Thanit.P@chula.ac.th

Supporting information for this article is available on the WWW under
<http://dx.doi.org/10.1002/slct.201601075>

close proximity and quenching is effective. When the system is allowed to interact with another nucleic acid strand possessing higher affinity to any of the strands in the initial duplex, strand exchange will occur and a new duplex is eventually formed, thus restoring fluorescence as a result of the separation between the fluorophore and the quencher. The key to the success of displacement probes lies in the subtle difference in stabilities of probe-quencher duplex and probe-target DNA duplex. The quencher is usually designed to have slightly less affinity towards the probe than the DNA analyte so that it could be displaced later by the complementary DNA analyte. This could be achieved by two methods: 1) using quenchers with shorter length than the fluorophore probe; 2) using quenchers with some mismatches in the strand.^[7a] After extensive investigations, this concept has been demonstrated in a number of studies, and paved the way to real applications such as the use of displacement probes in quantitative polymerase chain reaction (qPCR).^[8]

Nevertheless, conventional probes based on natural oligonucleotides still have some limitations. For example, molecular beacons, despite being carefully designed, can occasionally suffer from complication from other unwanted intramolecular interactions. Sometimes this is found only after testing the probe in real experiments, thus leading to the process of re-tuning the probe with inevitably additional costs. In the case of DNA-based displacement probes, the minimum required length for reliable hybridisation is usually long enough to promote the formation of secondary structures. Thus, it can sometimes be tedious for the whole designing process to get suitable probes for certain DNA sequences. In this study, we aimed to investigate the possibility of adopting acpcPNA as a displacement probe. Since acpcPNA has greater affinity to DNA than DNA itself, the minimum length to obtain reliable hybridisation is much lower, i.e., a PNA strand with 10 nucleotides could serve as a probe. This, in addition to the low tendency of acpcPNA to form self-pairing duplexes, automatically simplifies the designing process. Regarding with the probe construction, this can be achieved by forming a duplex between a strand of acpcPNA containing a fluorophore, and another DNA strand containing a quencher. Thereafter, a DNA target can be recognised by allowing it to form a more stable duplex with the PNA strand, thereby releasing the quencher from the fluorophore and resulting in the increase of fluorescence (Figure 1). As anticipated, the new type of displacement probes was shown to provide reliable recognition power without complicated design or fine-tuning.^[9] The design, construction, and performance evaluation of the acpcPNA displacement probes are described as follows.

Results and Discussion

Design, synthesis and characterisation of acpcPNAs and DNAs

We designed the displacement probes by appending acpcPNAs with a fluorophore (fluorescein or tetramethylrhodamine) at the *N*-terminus via the activated ester coupling (see experimen-

tal section). We chose to add the fluorophores on this end due to the ease of synthesis based on our previously established chemistry.^[10] After the deprotection of the side-chain protecting groups and the cleavage of the PNA from the resin, fluorophore-labelled PNAs (Figure 2) were obtained. HPLC

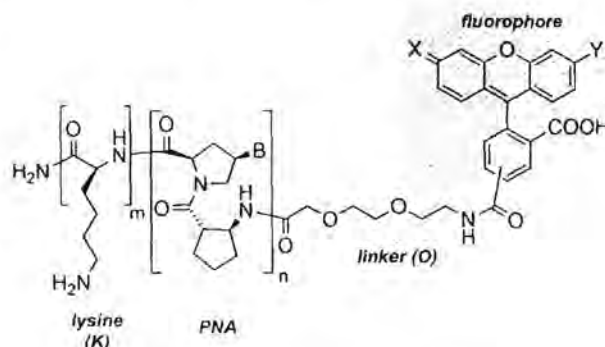


Figure 2. A general structure of fluorophore-appended acpcPNAs used in this study (B is a standard nucleobase (A, T, C, and G). X = O; Y = OH for fluorescein; X = NMe₂; Y = NMe₂ for tetramethylrhodamine).

analysis indicated that all synthesised PNAs were > 95% purity, while MALDI-TOF mass spectrometry confirmed the identity of all synthesised PNA used in this work (Figure S1-S7 in the Supporting Information). Since it is known that acpcPNA binds to DNA only in anti-parallel arrangement (where the *N*- and *C*-termini correspond to the 5' and 3' ends, respectively),^[10b] the DNA quenchers were thus modified with the dabcyI group on the 3' end so that both counterparts are in close proximity for effective quenching upon duplex formation (Figure 1).

The sequences of PNAs and DNAs used in this study are shown in Table 1 and 2. There were mainly four PNA sequences in this study, with some variations of fluorophores and *C*-terminus extensions on the PNAs. DNA quenchers (DNAQ) were also varied to probe a variety of effects. In addition, melting temperatures (*T_m*) of selected duplexes were measured (Table S1) to gain some insight in the strand exchange process as discussed below.

Construction and evaluation of the displacement probes

To test the utility of the displacement probes, a series of fluorescence experiments was conducted with a model sequence corresponding to a shrimp white spot syndrome virus (WSSV) DNA.^[11] In a preliminary experiment, K1Flu1, after mixing with the quencher carrying a mismatched base d5mQ1, exhibited significantly reduced fluorescence, which can be fully restored within 100 minutes (see Figure S8 in the Supporting Information for full spectra containing fluorescence signals at 10-min interval along with a kinetics plot at the wavelength of emission maximum) to the original level after the addition of the complementary single-stranded DNA, DNA1a (the 3'-terminal base was changed to adenine instead of guanine due to known quenching effect).^[12] On the other hand, the

Table 1. The sequences of fluorophore-modified acpcPNAs, DNA quenchers (DNAQ), and DNA oligos used in this study.

| Type | Name | Séquence | Name | Sequence |
|------|-----------------|---|--------|--|
| PNA | K1Flu1 | Flu-O-CTAAATTCAGA-KNH ₂ | K1Flu2 | Flu-O-AGTTATCCCTGC-KNH ₂ |
| | K4Flu1 | Flu-O-CTAAATTCAGA-KKKKNH ₂ | K5Flu3 | Flu-O-GCGCCGACTGTCCGGC-KKKKNH ₂ |
| | K4TMR1 | TMR-O-CTAAATTCAGA-KKKKNH ₂ | | |
| DNAQ | dSmQ1 | <u>GGGG</u> 1-GATTTACGCT-5' | d8Q1 | <u>GGGG</u> 1-GATTTAAG-5' |
| | dSmQ2 | <u>GGGG</u> 1-TCAATGGGACG-5' | d9Q2 | <u>GGGG</u> 1-TCAATAGGG-5' |
| | dCmQ3 | <u>GGGG</u> 1-CGCGGCTGACA-5' | d8Q2 | <u>GGGG</u> 1-TCAATAGG-5' |
| DNA | DNA1a | 3'- <u>AATTTA</u> AGTCT-5' | DNA2a | 3'-TCAATAGGGACG-5' |
| | DNA1b | 3'- <u>AATTTA</u> CGTCT-5' | DNA2b | 3'-TCAATGGGACG-5' |
| | DNA1c | 3'- <u>AATTTA</u> AGACT-5' | DNA2c | 3'-TCAATCGGGACG-5' |
| | DNA1d | 3'- <u>AATTTT</u> AGTCT-5' | DNA2d | 3'-TCAATGGGACG-5' |
| | DNA1e | 3'- <u>AATTGA</u> AGTCT-5' | DNA2e | 3'-TCAAAGGGACG-5' |
| | DNA1f | 3'- <u>AACTTA</u> AGTCT-5' | DNA2f | 3'-TCAATAGCGACG-5' |
| | comp- dsDNA1 | 3'- <u>ATAC</u> AATTTAAGTCTGAATC-5' + 5'-TATGTTAAATTCAGACTTAA-3' | DNA3a | 3'-CGCGGCTGACAGCCGC-5' |
| | sm-dsDNA1 | 3'- <u>AGAC</u> AATTTAAGTCTGAATC-5' + 5'-TATGTTAAATTCAGACTTAA-3' | DNA3b | 3'-CGCGGCTTACAGCCGC-5' |

A, T, C and G are the abbreviations of the standard nucleobases, whereas K is lysine. The 2-aminoethoxyethoxyacetyl linker, used to join the N-terminal base and the fluorophore is abbreviated as O. Flu = fluorescein. TMR = tetramethylrhodamine. PNAs are written from N to C termini, while the orientations of DNAs are clearly noted. Red underlined bases are mismatches compared to the original sequences, while blue bases are extra hanging bases. Purple underlined bases are purposely placed mismatches due to a known quenching effect of the G base (see text).

fluorescence signal of K1Flu1/dSmQ1 probe stayed at the quenching level after the addition of a single mismatched DNA1b, thereby demonstrating the discrimination power of this type of probes (Figure 3).

Next, the effect of the lysine linker at the C-terminus was studied. It was found that K4Flu1, having four units of lysine at the C-terminus, did not show significant difference when combined with the same quencher, dSmQ1 (Figure S9 in the Supporting Information). We then investigated the scope of fluorophores in this probe setting by replacing fluorescein with tetramethylrhodamine. The probe K4TMR1, when combined with the quencher dSmQ1, could also effectively differentiate between the two DNA sequences described before (DNA1a vs DNA1b), indicating some flexibility in terms of fluorophores variety (Figure 4).

The difference in the level of fluorescence restoration between complementary and mismatched DNA targets, which may be defined as discrimination factor $[(F/F_0)_{comp}/(F/F_0)_{mismatch}]$, is most likely determined by the difference in stabilities between probe-quencher and probe-target duplexes. It is therefore important to choose a quencher probe that can form a sufficiently stable duplex with the PNA probe to exert effective quenching, and still allow strand exchange with complementary DNA target, but not with the mismatched DNA target. As shown in Table S1, the T_m values of the duplexes K1Flu1/dSmQ1, K1Flu1/DNA1a and K1Flu1/DNA1b are 53.5,

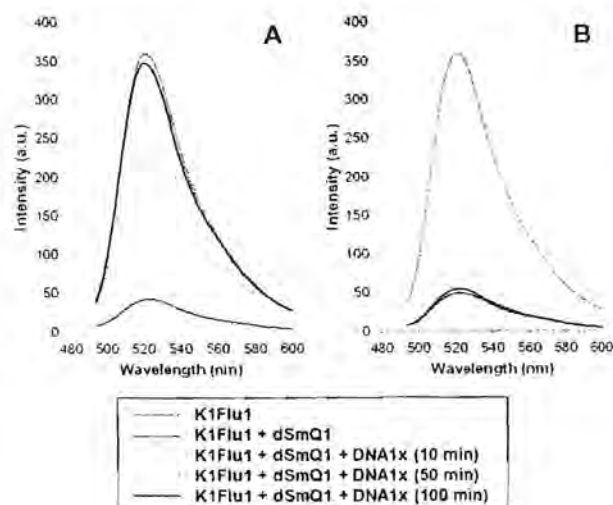


Figure 3. Fluorescence profiles of K1Flu1/dSmQ1 in discriminating between A) complementary DNA (DNA1x = DNA1a), and B) single mismatched DNA (DNA1x = DNA1b) [K1Flu1] = 0.05 μ M, [dSmQ1] = [DNA1x] = 0.50 μ M, excitation wavelength = 480 nm. All experiments were performed at 20 $^{\circ}$ C.

63.1 and 33.1 $^{\circ}$ C, respectively. It can be clearly seen that only DNA1a could displace the dSmQ1 from the K1Flu1/dSmQ1 to form a more stable K1Flu1/DNA1a duplex. The analogous

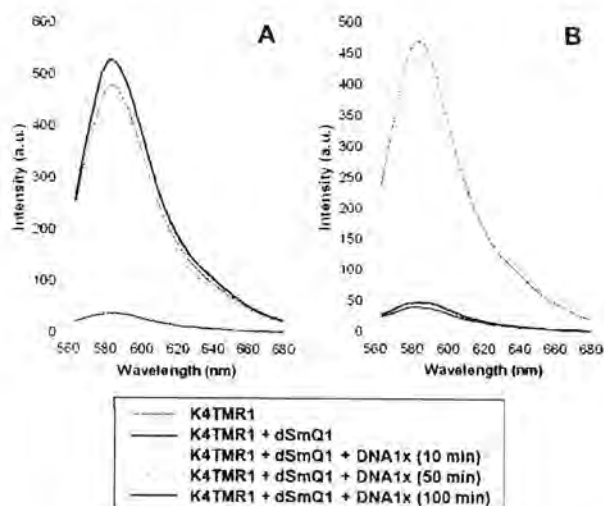


Figure 4. Fluorescence profiles of K4TMR1/dSmQ1 in discriminating between A) complementary DNA (DNA1x = DNA1a), and B) single mismatched DNA (DNA1x = DNA1b). [K4TMR1] = 0.05 μ M, [dSmQ1] = [DNA1x] = 0.50 μ M, excitation wavelength = 550 nm. All experiments were performed at 20 $^{\circ}$ C.

exchange with DNA1b would be energetically unfavourable, resulting in a large discrimination factor of 7.5 between DNA1a and DNA1b. While the stability of the probe-target hybrid is fixed by their base sequence, the stability of the probe-quencher hybrid is tunable. The effect of different quencher sequences (shorter strand vs extra mismatches) was thus also investigated. In this regard, fluorescence profiles of another PNA probe, K1Flu2, with three DNA quenchers (d8Q2, d9Q2, and dSmQ2), were obtained. As expected, the longer quencher probe d9Q2 reduced the fluorescence of K1Flu2 to a greater degree (94% reduction, Figure S10) than did d8Q2 (76% reduction, Figure S11) due to increased duplex stability from an extra base pair. On the other hand, the mismatched quencher probe dSmQ2 exhibited 90% reduction (Figure S12), which is comparable to d9Q2. Based on quenching power, it could be concluded that both d9Q2 and dSmQ2 are suitable as a quencher for our displacement probe system. Nevertheless, the fluorescence restoration must also be taken into account. In this regard, although K1Flu2/d8Q2 showed restoration that was significantly higher than the other two systems (Figure S13), we surmised that there is still room for improvement in terms of kinetics and discrimination power on all of these systems. Fortunately, heating the solution briefly seemed to promote the strand exchange,^[13] and the fluorescence signals of K1Flu2/dSmQ2 and K1Flu2/d9Q2 were thus found to significantly increase (nearly instantly in almost all cases), albeit to different degrees which may reflect the different extent of the strand displacement reactions. Specifically, dSmQ2 showed a greater extent of fluorescence restoration (Figure 5) than did d9Q2 (Figure S14). Nevertheless, the discrimination factors suggested that K1Flu2/d9Q2 gave higher factors to all mismatched targets compared to K1Flu2/dSmQ2 and certainly K1Flu2/d8Q2 (Table S5). Thus, although nearly complete

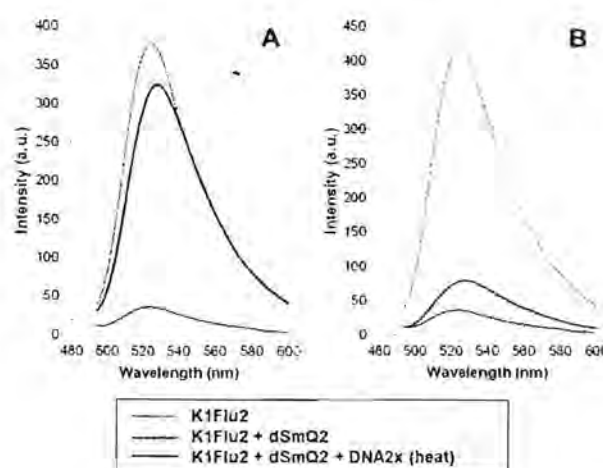


Figure 5. Fluorescence profiles of K1Flu2/dSmQ2 in discriminating between A) complementary DNA (DNA2x = DNA2a), and B) single mismatched DNA (DNA2x = DNA2b). Heating was included at 95 $^{\circ}$ C for 5 min. [K1Flu2] = 0.05 μ M, [dSmQ2] = [DNA2x] = 0.50 μ M, excitation wavelength = 480 nm.

fluorescence restoration may be generally desired, discrimination factors should rather be used to determine probe efficiency. In this particular case, d9Q2 was likely a better quencher.

Encouraged by the results, we expanded the scope of the sensing system by testing all aforementioned probes with more DNA sequences (DNA1c–DNA1f to be tested with K1Flu1/dSmQ1, K4Flu1/dSmQ1, and K4TMR1/dSmQ1; DNA2c–DNA2f to be tested with K1Flu2/d8Q2, K1Flu2/d9Q2, and K1Flu2/dSmQ2). As shown in Tables S2–S5, the complementary sequence gave fluorescence signals that were about 3.5–13 folds higher than those of mismatches (obtained by comparing fluorescence signals of the final time points with those before the addition of each DNA target). It is worth noting that this was found to be true for all systems tested (with an exception of only two cases where lower than 3.5-fold fluorescence change was observed), thereby showcasing the versatile nature of the PNA displacement probes. Although the absolute fluorescence values may vary from one experiment to another due to minor variation in concentrations and other parameters, the range of complementary/mismatched fluorescence ratios held pretty well, indicating that this system is robust enough for use with various probes and targets.

In addition, an extra-long PNA probe (K5Flu3) was also tested for its performance as a displacement probe, together with a complementary, but shorter-in-length quencher (dCmQ3). This 16-nt PNA represented a long PNA system that offers more flexibility in generating unique sequences for broader applications. As illustrated in Figure 6, the displacement probe could provide sufficient discrimination power (over 2 folds) although the mismatched case resulted in visible fluorescence restoration. Notably, this behaviour could be predicted from T_m data (Table S1), which showed lower T_m for PNA/DNAQ than PNA/mismatched target. Also, this issue is specific to certain sequences; therefore, the whole principle

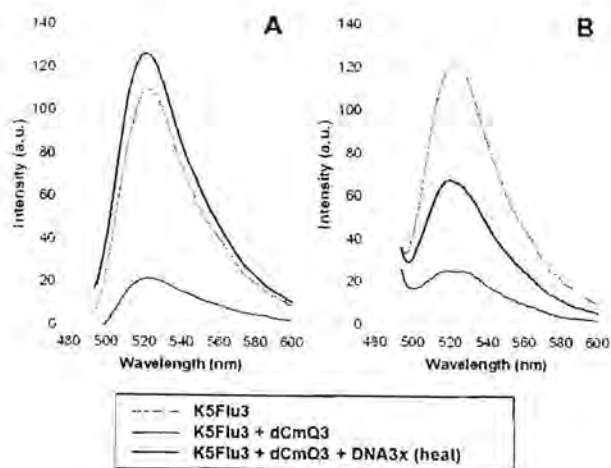


Figure 6. Fluorescence profiles of K5Flu3/dCmQ3 in discriminating between A) complementary DNA (DNA3 x = DNA3 a), and B) single mismatched DNA (DNA3 x = DNA3 b). Heating was included at 95 °C for 5 min. [K5Flu3] = 0.05 μM, [dCmQ3] = [DNA3 x] = 0.50 μM, excitation wavelength = 480 nm.

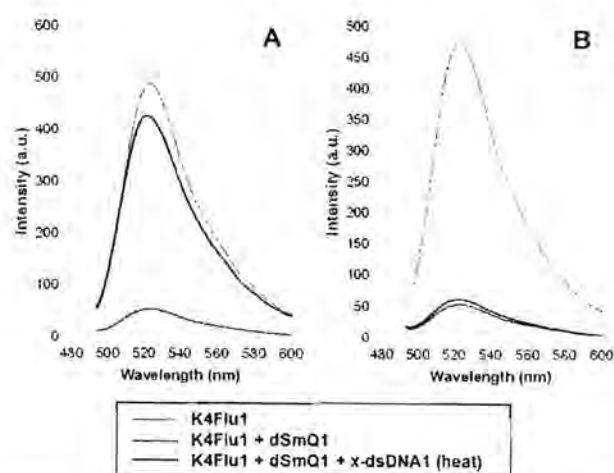


Figure 7. Fluorescence profiles of K4Flu1/dSmQ1 in discriminating between A) complementary double-stranded DNA (x = comp), and B) single mismatched double-stranded DNA (x = sm). Heating was included at 95 °C for 5 min. [K4Flu1] = 0.05 μM, [dSmQ1] = [x-dsDNA1] = 0.50 μM, excitation wavelength = 480 nm.

should work fine in many more applications using different base sequences.

Investigation of the performance of the displacement probes with double-stranded DNAs

Since DNA exists as a stable duplex, the ability to efficiently recognise the DNA analyte without sample pre-treatment, i.e., to separate DNA strands, is highly desirable. Therefore, the PNA displacement probes were also tested for the in-situ recognition of different double-stranded DNAs. Using K4Flu1/dSmQ1 as a model, the results (Figure S15) showed that fluorescence restoration of a double-stranded DNA target (comp-dsDNA1) was much slower at ambient temperature compared to the single-stranded version (DNA1a), although the high specificity was still retained. To resolve the slow kinetics issue, brief heating was again applied and found to expectedly promote efficient strand exchange, leading to almost complete fluorescence restoration and successful discrimination between the complementary DNA (comp-dsDNA1) and a single mismatched DNA (sm-dsDNA1) (Figure 7 for K4Flu1/dSmQ1, and Figure S16 and S17 for K1Flu1/dSmQ1 and K4TMR1/dSmQ1, respectively). These results, along with our recently published study,^[14] corroborated the power of acpPNA in undergoing duplex invasion, thus suggesting that the displacement probe should be well applicable to double stranded DNA targets.

To further demonstrate the utility of our PNA displacement probe, the possibility of detecting different DNA sequences in multiplex manner was also investigated. In this regard, we selected DNA sequences derived from single nucleotide polymorphisms (SNP) in the human *IL10* promoter gene that are found to be associated with systemic lupus erythematosus (SLE) disease (Table 2).^[15] Two acpPNAs differing by one nucleobase were synthesised and these were appended with

Table 2. Sequences of PNA, DNAQ, and DNA analytes used for the multiplex detection experiments.

| Type | Name | Sequence |
|--------------|-----------------------|------------------------------------|
| PNA | Flu-SLE(T) | 5'-O-ATGTAATATCTC-KNH ₂ |
| | TMR-SLE(C) | 5'-O-ATGTAACATCTC-KNH ₂ |
| DNAQ | dSm-SLE(T) | 3'-TACATTTAGAG-5' |
| | | 3'-TACATTGATAGAG-5' |
| DNA | DNA4a | 3'-TACATTTAGAG-5' |
| | DNA4b | 3'-TACATTGATAGAG-5' |
| | SLE(A)-dsDNA | 3'-TACATTTAGAG-5' + |
| | | 5'-ATGTAATATCTC-3' |
| SLE(G)-dsDNA | 3'-TACATTGATAGAG-5' + | |
| | 5'-ATGTAACATCTC-3' | |

different fluorophores, namely fluorescein (Flu-SLE(T)) and tetramethylrhodamine (TMR-SLE(C)). In the same solution, a DNA quencher with one mismatch to both sequences, dSm-SLE(T), was used to quench both PNAs, and the DNA analyte would be added. The presence of the complementary DNAs to each PNA would result in the fluorescence increase specific to the emission wavelengths of each fluorophore. Hence, both signals can be independently but simultaneously monitored in the spectrophotometer.

In a preliminary experiment, each probe system (Flu-SLE(T)/dSm-SLE(T) and TMR-SLE(C)/dSm-SLE(T)) was first tested individually for its ability to detect single DNA sequence in the solution. As expected, although these duplexes especially with TMR-SLE(C) showed incomplete fluorescence restoration (which, in turn, was supported by the T_m difference between probe-quencher and probe-target duplexes), each SLE probe could successfully distinguish its complementary sequence

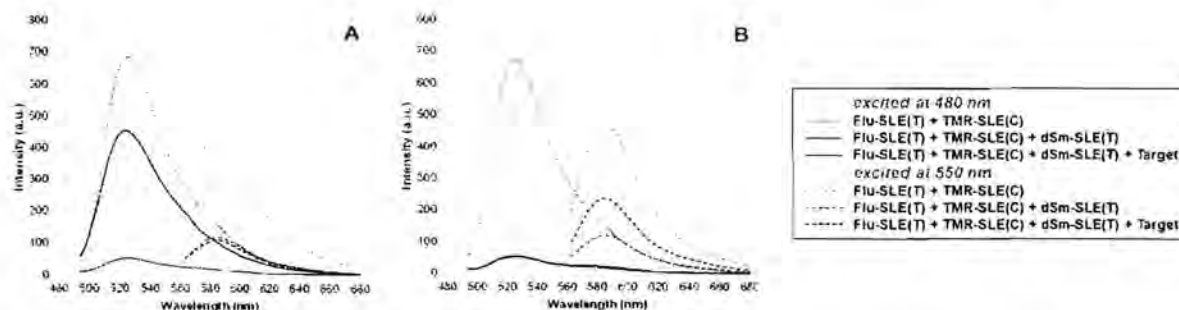


Figure 8. A multiplex experiment showing the ability of the SLE PNA probe system (consisting of Flu-SLE(T)/TMR-SLE(C)/dSm-SLE(T)) in discriminating double-stranded DNAs. Each experiment consists of two sets of spectra, which were obtained from excitations at 480 nm (fluorescein) and 550 nm (tetramethylrhodamine). A) Target = SLE(A)-dsDNA. B) Target = SLE(G)-dsDNA. The data in solid lines were obtained from the excitation at 480 nm. The data in dashed lines were obtained from the excitation at 550 nm. Heating was included at 95 °C for 5 min. [Flu-SLE(T)] = [TMR-SLE(C)] = 0.05 μ M, [dSm-SLE(T)] = [Target] = 0.50 μ M.

(DNA4a or DNA4b) from single mismatches, with both single-stranded and double-stranded systems (after heating; Figure S18 for Flu-SLE(T)/dSm-SLE(T), and Figure S19 for TMR-SLE(C)/dSm-SLE(T)). Encouraged by these results, we proceeded to test the system in the multiplex mode. In each experiment, both PNA probes and the DNA quencher were added into a solution, followed by the addition of one double-stranded DNA analyte. Thereafter, spectra were obtained by exciting the solution with either 480-nm, or 550-nm light. As shown in Figure 8, our PNA displacement probe could clearly distinguish between two DNA sequences differing only by single base. For instance, the 530-nm fluorescence signal of fluorescein increased significantly after the addition of SLE(A)-dsDNA (Figure 8 A), while the same signal (at the same excitation wavelength) remained low and unchanged after the addition of SLE(G)-dsDNA (Figure 8B). This obviously suggested an existence of significant duplex formation between Flu-SLE(T) and SLE(A)-dsDNA, thus inferring that both are complementary sequences. Even though the signal restoration may not be as high as previous experiments, it proved to be ample for unambiguous DNA sequence determination.

acpcPNA-immobilised agarose resin as a solid-phase displacement probe

Solid-phase platforms have recently been exploited in a variety of chemical research due to their unique advantages, e.g., the ease of purification in combinatorial chemistry on polystyrene resin. Therefore, we sought to study the feasibility of constructing the displacement probe on resin and applying such system as a DNA sensor. The experiments were set up in a similar manner as in solution-phase experiments with some modifications. Since the agarose resin contains an *N*-hydroxysuccinimide (NHS) ester, a side-chain amino group on lysine residues of the PNA is expected to react and covalently immobilise the PNA (and the DNAQ) onto the resin. A DNA analyte was then incubated and the fluorescence signal was observed under the 365-nm UV lamp. Preliminary results showed that, with the solid-phase condition, the single mismatched probe (dSmQ1)

could not quench the fluorophore PNA to a satisfactory level - this is likely due to the increased difficulty of duplex formation in the resin matrix. Therefore, another probe, d8Q1, was tested and, to our surprise, was found to give a more satisfactory quenching - this outcome was opposite to the trend of duplex stability found in aforementioned experiments. We surmised that the resin matrix may contribute to this complication. Consequently, we proceeded to prepare the K1Flu1/d8Q1 displacement probe and found that this system could restore the fluorescence signal only with the addition of the complementary sequence (DNA1a - tube 3, Figure 9), while a single



Figure 9. Fluorescence of NHS-agarose resins under 365-nm light. 1) agarose + K1Flu1; 2) agarose + K1Flu1 + d8Q1; 3) agarose + K1Flu1 + d8Q1 + DNA1a; 4) agarose + K1Flu1 + d8Q1 + DNA1b. All experiments started simultaneously, and the photo was taken after the last condition was finished, which is an incubation step of 1 hour after DNA1a and DNA1b were added to 3) and 4), respectively.

mismatched sequence (DNA1b - tube 4, Figure 9) could not appreciably increase the fluorescence signal. These results confirmed that the acpcPNA displacement probe can also work on a solid phase system. Further development and elucidation of the dynamics of this resin probe will be investigated and reported elsewhere.

Conclusions

We reported herein a construction of displacement probes based on acpcPNA, which has been shown to provide several attractive features as a DNA probe. The results showed that the systems could unambiguously recognise the complementary sequence by giving significant fluorescence increase only after the complementary DNA was added (but not with any type of mismatched DNA targets). In most cases, brief heating was found to improve fluorescence restoration and is thus recommended if no other concern exists. On the other hand, temperature-sensitive samples may be incubated at ambient temperature. Although this resulted in incomplete fluorescence restoration and long reaction time, it should be emphasised that, in many cases, the signal from the complementary sequence was far higher than that of mismatches since early time points. Therefore, maximum restoration may not be required, thereby resulting in significantly reduced incubation time. Also, the displacement probes worked well even with double-stranded DNA analytes, indicating that the probe is applicable with real DNA samples. Combined with a possibility to couple the probe with a solid phase system, this new type of displacement probes could become another practical tool for DNA detection.

Acknowledgements

This research is financially supported by the Thailand Research Fund (DPG5780002), the Development and Promotion of Science and Technology Talents Project (DPST) (Ph.D. scholarship to CB) and the 100th Anniversary Chulalongkorn University for Doctoral Scholarship (to CC).

Keywords: peptide · nucleic acid · biosensors · DNA recognition · fluorescence probes

- [1] a) P. Wittung, P. E. Nielsen, O. Buchardt, M. Egholm, B. Norden, *Nature* **1994**, *368*, 561–563; b) Y. Choi, G. Metcalf, M. H. Sleiman, D. Vair-Turnbull, S. Ladame, *Bioorg. Med. Chem.* **2014**, *22*, 4395–4398; c) R. Gambari, *Expert Opin. Ther. Pat.* **2014**, *24*, 267–294; d) H. Shi, F. Yang, W. Li, W. Zhao, K. Nie, B. Dong, Z. Liu, *Biosens. Bioelectron.* **2015**, *66*, 481–489.
- [2] a) V. A. Kumar, K. N. Ganesh, *Acc. Chem. Res.* **2005**, *38*, 404–412; b) T. Sugiyama, A. Kittaka, *Molecules* **2013**, *18*, 287–310.
- [3] T. Vilaivan, *Acc. Chem. Res.* **2015**, *48*, 1645–1656.
- [4] a) T. Theppaleak, M. Rutnakornpituk, U. Wichai, T. Vilaivan, B. Rutnakornpituk, *J. Nanopart. Res.* **2013**, *15*, 2106; b) C. Stubinitzky, T. Vilaivan, H.-A. Wagenknecht, *Org. Biomol. Chem.* **2014**, *12*, 3586–3589; c) N. Jirakittiwut, N. Panyain, T. Nuanyai, T. Vilaivan, T. Praneenararat, *RSC Adv.* **2015**, *5*, 24110–24114.
- [5] a) S. Preus, L. M. Wilhelmsson, *ChemBioChem* **2012**, *13*, 1990–2001; b) G. Chen, F. Song, X. Xiong, X. Peng, *Ind. Eng. Chem. Res.* **2013**, *52*, 11228–11245.
- [6] a) J. Guo, J. Ju, N. J. Turro, *Anal. Bioanal. Chem.* **2012**, *402*, 3115–3125; b) K. Huang, A. A. Marti, *Anal. Bioanal. Chem.* **2012**, *402*, 3091–3102.
- [7] a) Q. Q. Li, G. Y. Luan, Q. P. Guo, J. X. Liang, *Nucleic Acids Res.* **2002**, *30*, e5; b) J. P. Cheng, Y. Y. Zhang, Q. G. Li, *Nucleic Acids Res.* **2004**, *32*, e61; c) Z. H. Mo, X. C. Yang, K. P. Guo, Z. Y. Wen, *Anal. Bioanal. Chem.* **2007**, *389*, 493–497.
- [8] W. Shengqi, W. Xiaohong, C. Suhong, G. Wei, *Anal. Biochem.* **2002**, *309*, 206–211.
- [9] D. Y. Zhang, S. X. Chen, P. Yin, *Nat. Chem.* **2012**, *4*, 208–214.
- [10] a) C. Suparpprom, C. Srisuwannaket, P. Sangvanich, T. Vilaivan, *Tetrahedron Lett.* **2005**, *46*, 2833–2837; b) T. Vilaivan, C. Srisuwannaket, *Org. Lett.* **2006**, *8*, 1897–1900.
- [11] C. M. Escobedo-Bonilla, V. Alday-Sanz, M. Wille, P. Sorgeloos, M. B. Pensaert, H. J. Nauwynck, *J. Fish Dis.* **2008**, *31*, 1–18.
- [12] a) W. Wang, C. Chen, M. X. Qian, X. S. Zhao, *Sens. Actuators, B* **2008**, *129*, 211–217; b) J. N. Wilson, Y. Cho, S. Tan, A. Cuppoletti, E. T. Kool, *ChemBioChem* **2008**, *9*, 279–285; c) D. S. Xiang, K. Zhai, L. Z. Wang, *Analyst* **2013**, *138*, 5318–5324.
- [13] T. N. Grossmann, S. Sasaki, M. Ritzfeld, S. W. Choi, A. Maruyama, O. Seitz, *Biorg. Med. Chem.* **2008**, *16*, 34–39.
- [14] P. R. Bohlender, T. Vilaivan, H.-A. Wagenknecht, *Org. Biomol. Chem.* **2015**, *13*, 9223–9230.
- [15] N. Hiranakarn, J. Wongpiyabovorn, O. Hanvivatvong, J. Netsawang, S. Akkasilpa, J. Wongchinsri, P. Hanvivadhanakul, W. Korkit, Y. Avihingsanon, *Tissue Antigens* **2006**, *68*, 399–406.

Submitted: August 5, 2016

Accepted: October 21, 2016



Pyrrolidinyl peptide nucleic acid terminally labeled with fluorophore and end-stacking quencher as a probe for highly specific DNA sequence discrimination[☆]



Nattawut Yotapan, Duangrat Nim-anussornkul, Tirayut Vilaivan^{*}

Organic Synthesis Research Unit, Department of Chemistry, Faculty of Science, Chulalongkorn University, Phayathai Road, Patumwan, Bangkok 10330, Thailand

ARTICLE INFO

Article history:

Received 19 June 2016

Received in revised form 3 October 2016

Accepted 14 October 2016

Available online 17 October 2016

Keywords:

Molecular beacons

Fluorescence

Hybridization probes

DNA

PNA

ABSTRACT

Peptide nucleic acid (PNA) labeled with a dye/quencher pair is useful as a high-performance fluorescence probe for DNA sequence determination. Previous work has mainly focused on placing the dye/quencher at different ends of the PNA strand. In this work, we propose a new pyrrolidinyl PNA probe bearing a fluorescent dye and an anthraquinone quencher at the same end of the PNA molecule. The single-stranded PNA probe exhibits a weak fluorescence as a result of close contact between the dye and the quencher. End-stacking of the anthraquinone to the terminal base pair of the PNA-DNA duplex disrupts the fluorophore-quencher interaction, resulting in a large fluorescence increase in the presence of complementary DNA. The high specificity of the present PNA probe allows multicolor, multiplex detection of single mismatched DNA targets. In addition, direct detection of double stranded DNA target by double duplex invasion was demonstrated.

© 2016 Elsevier Ltd. All rights reserved.

1. Introduction

Fluorescence oligonucleotides are useful as probes for molecular diagnostic applications such as the determination of DNA or RNA sequences¹ as well as other targets such as proteins^{2,4} and small molecules.^{3–7} To enable the detection of these targets in homogeneous format which does not require immobilization or washing and thus applicable for *in vivo* detection, a mechanism that can modulate the fluorescence properties of the probe in response to the target binding must be introduced. A classic example of such probes is molecular beacon⁸—an oligonucleotide carrying two labels at the opposite end with a partial self-complementary sequence so that it can form a stem-loop structure in the free state. Binding with the correct target DNA at the loop region leads to a conformational change that result in different interactions between the two labels when compared to the free probes,⁹ leading to a fluorescence change. Limitations of this probe design are the requirement of a rather long sequence to form the stem-loop structure which is expensive to make, slow reaction kinetics and further functionalization being difficult since both ends are occupied. Several alternative designs to overcome one or more these

limitations have been proposed such as in-stem molecular beacons,^{10,11} strand displacement probes,¹² binary probes,¹³ and quencher-free molecular beacons.^{14,15} The performance of these probes could be improved further by the use of oligonucleotide analogues that offer stronger binding affinity/specificity such as locked nucleic acid (LNA) or peptide nucleic acid (PNA).¹⁶ The latter is particularly promising because the design of PNA beacons does not generally require the stem-loop structure.^{17,18} The potential problem of non-specific binding in unstructured probes¹⁹ is compensated by the high specificity of PNA probes, and thus several impressive examples of linear PNA beacons have been reported.^{20–22} Most of these PNA beacons carry either an environment sensitive label or two labels placed at different positions in the PNA strand.

Linear oligonucleotide probes bearing two labels attached to the same end or adjacent positions have been reported as early as 1994.²³ Instead of relying on conformational change as in classical molecular beacons, the mechanisms of fluorescence change in these linear probes upon hybridization with the target was due to the change in the interactions between the two labels as a result of end stacking, intercalation,^{24–25} or uncoupling of excitons.^{26–27} This probe design tends to give a lower background signal than linear DNA probes in general due to the more efficient quenching as a results of a better contact between the dye and the quencher. Inspired by this promising probe design and our long interest in the development of self-reporting PNA probes,^{28–30} we proposed to

[☆] In remembrance of His Majesty King Bhumibol Adulyadej (1927–2016), for his life-time dedication to Thailand.

^{*} Corresponding author. E-mail address: tirayut@chem.chula.ac.th (T. Vilaivan).

combine the concept of a doubly-end-labeled linear probe with our new conformationally constrained acpcPNA.³¹ In this report, we synthesize and evaluate the performance for DNA detection of some doubly-end-labeled linear PNA probes bearing a fluorophore (FAM or TMR) and a quencher with end-stacking ability (anthraquinone) at the same end of the molecule. The anthraquinone is expected to stack on top of terminal base pairs of the PNA-DNA duplexes. As a result, hybridization with the correct DNA target is expected to produce a signal by fluorescence change.

2. Results and discussion

2.1. Design and synthesis of doubly-end-labeled acpcPNA probes

The present doubly-end-labeled PNA probe design consists of a fluorophore and a quencher (denoted X and Y). Both of which are attached to a diamine linker (lysine or APC) at the *N*-termini of the acpcPNA probes (Fig. 1). One or more lysine residues were incorporated at the *C*-termini to improve water solubility and stability of the PNA-DNA hybrids. Anthraquinone (AQ) was chosen as

the quencher because of its known ability to intercalate and/or end-stack with DNA duplexes.³⁸ The previously observed increased in T_m of duplexes with terminally anthraquinone-labeled acpcPNA suggests that the end stacking should also be possible in acpcPNA-DNA duplexes.³⁷

The strategy for end-labeling of acpcPNA with the fluorophore-quencher pair involves attachment of the orthogonally protected (Fmoc/Tfa) diamine linker (lysine or 3-amino-4-pyrrolidine carboxylic acid, APC) at the *N*-terminus of the PNA. The amino groups were selectively deprotected and modified with the label (FAM or TMR) or the quencher (AQ or Dab). The crude PNA was purified by reversed phase HPLC (to >90% purity) and characterized by MALDI-TOF mass spectrometry. Characterization data of all PNA probes, as well as selected thermal stability data of their DNA hybrids are shown in Table 1.

2.2. Fluorescence properties of acpcPNA probes bearing various end-labeling groups and linker chemistry

The performance of several end-labeled acpcPNA probe designs was first evaluated by measuring fluorescence spectra of the probes

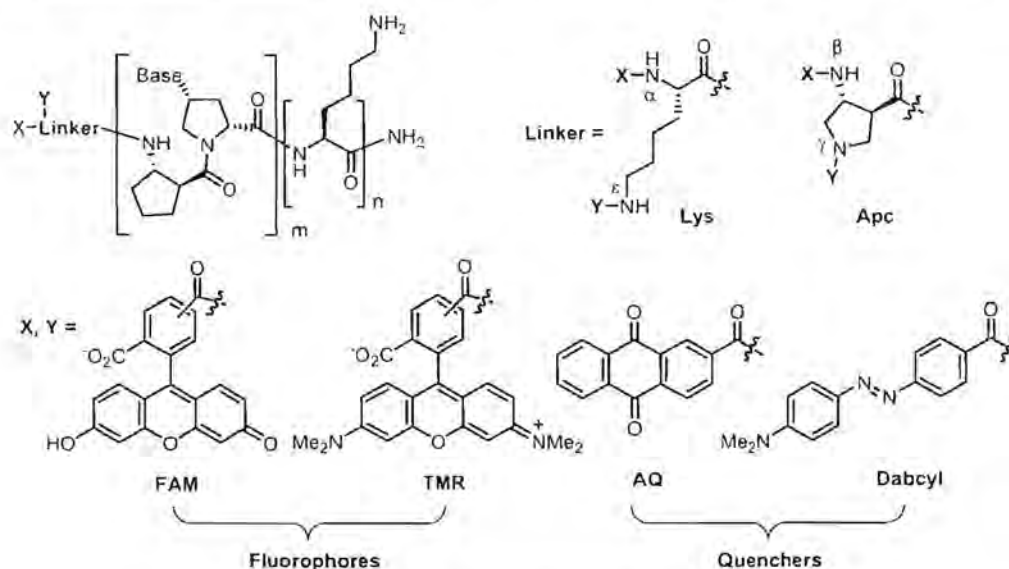


Fig. 1. Chemical structure of doubly-end-labeled acpcPNA probes described in this study.

Table 1
Sequence and characterization data of end-labeled acpcPNA probes synthesized in this study

| PNA | Sequence (N–C) | t_R (min) ^a | Yield (%) ^b | m/z (calcd) | m/z (found) | T_m (°C) |
|---------------------|--|--------------------------|------------------------|---------------|---------------|------------|
| (AQ/FAM)Lys-P1 | N ^{AQ} N ^{FAM} Lys-GTAGATCACT-LysNH ₂ | 31.2 | 3.0 | 4239.5 | 4237.6 | 58 |
| (AQ/TMR)Lys-P1 | N ^{AQ} N ^{TMR} Lys-GTAGATCACT-LysNH ₂ | 33.8, 34.3 | 8.3 | 4293.6 | 4294.6 | 55 |
| (AQ/FAM)Apc-P1 | N ^{AQ} N ^{FAM} Apc-GTAGATCACT-LysNH ₂ | 30.5 | 6.9 | 4111.3 | 4111.1 | N.D. |
| (FAM/AQ)Lys-P1 | N ^{FAM} N ^{AQ} Lys-GTAGATCACT-LysNH ₂ | 30.8 | 6.8 | 4239.5 | 4237.6 | N.D. |
| (FAM)Lys-P1 | N ^{FAM} Lys-GTAGATCACT-LysNH ₂ | 31.2, 31.5 | 12.0 | 4004.2 | 4002.5 | 65 |
| (Dab/FAM)Lys-P1 | N ^{Dab} N ^{FAM} Lys-GTAGATCACT-LysNH ₂ | 31.2 | 5.5 | 4256.5 | 4253.6 | N.D. |
| (AQ/TMR)Lys-P2 | N ^{AQ} N ^{TMR} Lys-GTAGATCACT-LysNH ₂ | 34.0 | 8.2 | 4253.6 | 4250.5 | N.D. |
| (AQ/FAM)Lys-P3 | N ^{AQ} N ^{FAM} Lys-TACAGACATC-LysNH ₂ | 34.1, 34.3 | 9.1 | 4208.5 | 4205.9 | 50 |
| (AQ/FAM)Lys-P4 | N ^{AQ} N ^{FAM} Lys-CTAATTCAGA-LysNH ₂ | 34.4, 34.5 | 3.8 | 4564.9 | 4564.1 | 74 |
| (AQ/FAM)Lys-P5 | N ^{AQ} N ^{FAM} Lys-AGTTATCCCTGC-LysNH ₂ | 34.5, 34.8 | 4.1 | 4865.2 | 4863.6 | 71 |
| (AQ/FAM)Lys-P6 | N ^{AQ} N ^{FAM} Lys-GAACAAGCTCGAA-LysNH ₂ | 33.1, 33.4 | 2.0 | 5671.0 | 5673.0 | 84 |
| (AQ/FAM)Lys-P1-Lys5 | N ^{AQ} N ^{FAM} Lys-GTAGATCACT-Lys ₅ NH ₂ | 33.1, 33.5 | 5.4 | 4752.2 | 4752.7 | 66 |

^a HPLC conditions: flow rate 0.5 mL/min. The gradient consists of two solvent systems: A (0.1% TFA in MilliQ water) and B (0.1% TFA in methanol). The elution started with 90:10 A:B for 5 min, followed by a linear gradient to 10:90 A:B over 35 min. Some peaks are doubled due to the presence of two fluorescein isomers from the commercially available 5(6)-carboxyfluorescein used.

^b Isolated yield after HPLC

^c Average mass (M–H⁺).

^d MALDI-TOF.

^e T_m with complementary DNA as determined by fluorescence spectrophotometry; conditions: 10 mM phosphate buffer pH 7.0, [PNA] = 1.0 μM, [DNA] = 1.2 μM, λ_{ex} = 490 nm, λ_{em} = 520 nm.

Table 2
Fluorescence properties of selected doubly-end-labeled PNA probes in the absence and presence of DNA

| Entry | PNA | F_{55} | F_{ds}/F_{ss} | | |
|-------|-----------------|-------------|-----------------|----------|-----------|
| | | | DNA (comp) | DNA (sm) | DNA (non) |
| 1 | (FAM)Lys-P1 | 383.2 (100) | 0.6 (60) | 0.7 (65) | 1.0 (100) |
| 2 | (Dab/FAM)Lys-P1 | 2.7 (1) | 4.7 (3) | 2.3 (2) | 1.1 (0.8) |
| 3 | (AQ/FAM)Lys-P1 | 19.0 (5) | 18.9 (95) | 6.0 (5) | 1.1 (5) |
| 4 | (FAM/AQ)Lys-P1 | 31.5 (8) | 6.4 (53) | 4.7 (39) | 2.5 (21) |
| 5 | (AQ/FAM)Apc-P1 | 92.4 (24) | 2.4 (54) | 1.2 (28) | 1.1 (28) |

^a Fluorescence of single stranded PNA; %fluorescence relative to the control sequence (FAM)Lys-P1 are shown in parentheses.

^b DNA sequence (5'→3'): DNA(comp) AGTGATCTAC; DNA(sm) AGTGCTCTAC; DNA(non) TCTGCATTAG; %fluorescence relative to the control sequence (FAM)Lys-P1 is shown in parentheses; conditions: 10 mM phosphate buffer pH 7.0; [PNA] 1.0 μM, [DNA]=1.2 μM, λ_{ex} =490 nm, λ_{em} =520 nm.

bearing the same 10-mer sequence before and after the addition of complementary DNA. The fluorescence emissions were compared with a control apcPNA probe (FAM)Lys-P1 carrying only the fluorescein label without the quencher. The results are summarized in Table 2.

All single stranded doubly-labeled apcPNA probes exhibited significantly weaker fluorescence at 520 nm than the control apcPNA probe (FAM)Lys-P1 ($\Phi=0.154$). The most efficient quenching effects were observed in (Dab/FAM)Lys-P1 (>99%; $\Phi=0.002$), as well as (AQ/FAM)Lys-P1 (ca. 95%; $\Phi=0.019$) (Table 2, entries 2 and 3; see also Table S1 for fluorescence quantum yields Φ). The smallest quenching (i.e., highest fluorescence) was observed in (AQ/FAM)Apc-P1 when the fluorophore and quenchers were attached via a rigid APC (Table 2, entry 5). In this particular situation, the two labels cannot directly interact due to the rigid nature of the linker. This suggests that contact quenching is the major mechanism for quenching in these doubly-labeled probes. The proposal is supported by the UV spectra of the quenched probe, which clearly show the reduction in magnitude and red-shifting of the absorption spectra compared to the singly-labeled probe (Fig. S14).^{2,3} However, since the (AQ/FAM)Apc-P1 probe with a rigid linker also exhibited quite significant quenching effects (ca. 76%), additional quenching mechanisms such as FRET cannot be ruled out.

In the presence of the complementary DNA strand, the fluorescence emissions of all AQ/FAM-labeled PNA probes were increased relative to the single stranded probes. The most pronounced change was observed in the (AQ/FAM)Lys-P1 probe, whereby the signal was increased by 18.9 fold (Fig. 2A, Table 2 entry 3; see also Table S1 for fluorescence quantum yields Φ). This value is almost the same as that of single stranded (FAM)Lys-P1 probe

without the quencher (i.e., maximum possible fluorescence). The observed un-quenching upon binding to DNA is explained by end-stacking of the anthraquinone on the terminal base pairs of the PNA-DNA duplexes, resulting in separation of the quencher from the fluorophore and thus the fluorescence increase. The decreased interaction between the fluorescein label and the anthraquinone quencher was supported by the change in UV absorption spectra in the presence of DNA as shown by the increase in the intensity and blue-shifting (Fig. 2A). The UV spectra of the duplex became similar to the singly labeled PNA probe (Fig. S14). Reversing the position of the two dyes as in (FAM/AQ)Lys-P1 probe resulted in a smaller fluorescence increase after adding the DNA, which could be explained by the poor stacking ability of the anthraquinone attached to a shorter/more rigid N_x of the lysine linker. The singly labeled (FAM)Lys-P1 probe exhibited a slight decrease of fluorescence upon hybridization with complementary target DNA, presumably due to interactions of the fluorescein label and the terminal G-C base pair of the PNA-DNA duplex as previously observed in the case of DNA.³¹ Other probes showed a considerably smaller fluorescence increase, especially (Dab/FAM)Lys-P1. This is not totally unexpected considering the poor stacking ability of the dabcyI group compared to the planar fused ring system of anthraquinone. This further emphasizes the unique ability of anthraquinone used as a quencher in this particular doubly-end-labeled beacon design. Importantly, the contact quenching mechanism suggests that anthraquinone can act as a quencher for a broad range of fluorescence labels.^{45,56} This is demonstrated by the quenching of the TMR label in single stranded PNA probe (AQ/TMR)Lys-P1 as well as the 18-fold enhancement of the fluorescence upon addition of complementary DNA (Fig. 2B).

The specificity of the PNA probes was evaluated by comparison of fluorescence properties of the PNA probes in the presence of complementary DNA target and unrelated DNA (Table 2). In all cases, the presence of non-complementary DNA does not significantly change the fluorescence of the probe, indicating the requirement of a specific interaction between the probe and the DNA target to the unquenching of the probe. The fluorescence intensity ratios (F_{ds}/F_{ss}) of the single mismatched and complementary duplexes are also quite different. In the case of (AQ/FAM)Lys-P1 probe, the F_{ds}/F_{ss} ratios of internal mismatched and non-complementary DNA hybrids were 6.0 and 1.1, respectively. Although the fluorescence increase in the case of single mismatched DNA target was still relatively high compared to single stranded probe, the value is still much smaller than the complementary DNA (18.9) (Table 2, entry 3). A similar level of mismatch discrimination (F_{ds}/F_{ss} 18.1 for complementary vs 4.9 for single mismatched DNA) was observed in

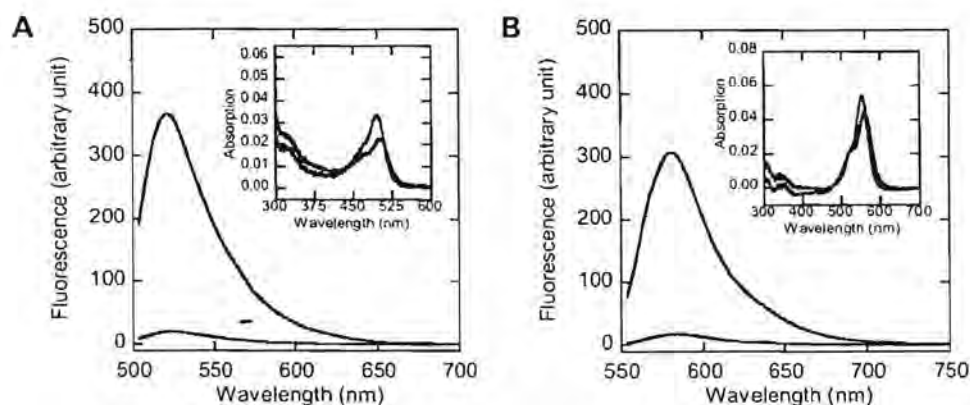


Fig. 2. Fluorescence and UV absorption spectra (inset) of (A) (AQ/FAM)Lys-P1 (blue) and its hybrid with complementary DNA (red) (B) (AQ/TMR)Lys-P1 (blue) and its hybrid with complementary DNA (red). Conditions: 10 mM phosphate buffer pH 7.0; [PNA] 1.0 μM, [DNA]=1.2 μM, λ_{ex} =490 nm (FAM) or 540 nm (TMR).

(AQ/TMR)Lys-P1 probe. Poorer selectivities in terms of single mismatch discrimination were observed with other PNA probes. From the results, it can be concluded that the fluorescence of the (AQ/FAM)Lys-P1 probe is highly sensitive to its hybridization state and is specific to the DNA hybridization event.

2.3. Effects of terminal nucleobase in the doubly-end-labeled acpcPNA probes

Since the fluorescence change event relies on the end stacking ability of the anthraquinone quencher to the terminal base pair, the nature of terminal nucleobase that may directly interact with the anthraquinone should exert significant effects on the performance of the probe. To investigate the effects of different terminal nucleobases, fluorescence experiments were performed with (AQ/FAM)PNA probes bearing different terminal nucleobases [(AQ/FAM)Lys-P1 (G), (AQ/FAM)Lys-P3 (T), (AQ/FAM)Lys-P4 (C), (AQ/FAM)Lys-P5 (A)] and their DNA hybrids. The results are summarized in Fig. 3 and Fig. S15.

The single stranded (AQ/FAM)Lys-P4 and (AQ/FAM)Lys-P5 probes showed comparable fluorescence to (AQ/FAM)Lys-P1 (F_{55} 19–24 a.u.), but (AQ/FAM)Lys-P3 was significantly brighter than the others. This may be interpreted as the combined quenching effects of the anthraquinone and neighboring nucleobases,¹⁶ but other factors such as different secondary structures of the probes may also involve. In all cases, hybridization with complementary DNA resulted in fluorescence increases relative to single stranded probes. Larger fluorescence increases were observed with (AQ/FAM)Lys-P1 and (AQ/FAM)Lys-P5 (19.3 and 14.4-fold) than (AQ/FAM)Lys-P4 and (AQ/FAM)Lys-P3 (8.1 and 5.8-fold). Although larger fluorescence increases were observed with a purine as the terminal nucleobase in the PNA strand, the results clearly demonstrate that the principle of using anthraquinone as an end-stacking quencher is quite general. In all cases, no significant fluorescence increase was observed in the presence of non-complementary DNA targets.

In another experiment to probe the effect of terminal nucleobases in the DNA strand, fluorescence of the (AQ/FAM)Lys-P1 and (AQ/TMR)Lys-P1 probes and various DNA bearing different terminal nucleobases were measured (Table 3). Hybridization with DNA bearing 3'-terminal base extension resulted in an even larger fluorescence increase than the perfectly complementary hybrid (Table 3, entries 1 and 2). In this case, the end-stacking of the anthraquinone is still possible, and may even be further stabilized by the adjacent nucleobase in the hanging DNA segment. DNA with 3'-terminal base deletion showed very little fluorescence change from the single stranded probe. A much lower fluorescence increase was

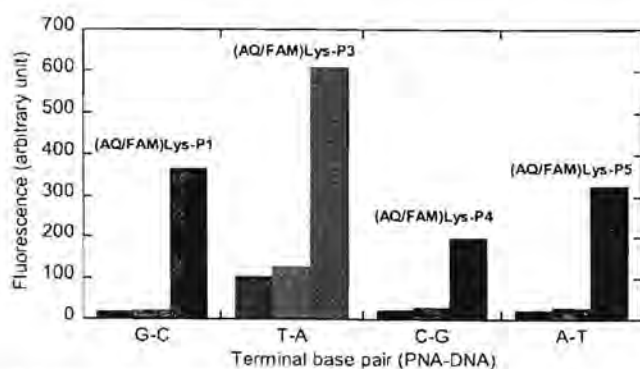


Fig. 3. Effects of terminal base pairs to the fluorescence of (AQ/FAM)PNA probes before (blue) and after addition of non-complementary DNA (gray) or complementary DNA (red); sequences of DNA involved are listed in Fig. S15; conditions: 10 mM phosphate buffer pH 7.0; [PNA]=1.0 μ M, [DNA]=1.2 μ M, λ_{ex} =490 nm, λ_{em} =520 nm.

Table 3
 F_{ds}/F_{ss} of AQ/FAM-acpcPNA beacons

| Entry | PNA ^a | DNA (5' → 3') ^c | Remarks | F_{ds}/F_{ss} |
|-------|------------------|----------------------------|-----------------------|-----------------|
| 1 | (AQ/FAM)Lys-P1 | AGTCATCTAC | complementary | 18.9 |
| 2 | (AQ/FAM)Lys-P1 | AGTCATCTAC <u>TAC</u> | 3'-terminal extension | 22.4 |
| 3 | (AQ/FAM)Lys-P1 | AGTCCTCT <u>—</u> | 3'-terminal deletion | 2.4 |
| 4 | (AQ/FAM)Lys-P1 | AGTCATCTAA | 3'-terminal mismatch | 7.0 |
| 5 | (AQ/TMR)Lys-P1 | AGTCATCTAC | complementary | 18.1 |
| 6 | (AQ/TMR)Lys-P1 | AGTCATCTAA | 3'-terminal mismatch | 3.0 |

^a PNA sequence: N-GTAGATCACT-C.

^b mismatch base and base extension are indicated by underlined and italicized letters, base deletion is indicated by underscore; conditions: 10 mM phosphate buffer pH 7.0; [PNA]=1.0 μ M, [DNA]=1.2 μ M, λ_{ex} =490 nm (FAM) or 540 nm (TMR), λ_{em} =520 nm (FAM) or 580 nm (TMR).

also observed in DNA with mismatched base at 3'-terminus. All of these observations are consistent with the expectation based on the proposed working principle of the doubly-end-labeled PNA beacon described herein. It is also important to note that terminal mismatches, which are generally difficult to detect due to the similar stabilities of the complementary and terminal mismatched duplexes, can be readily distinguished from complementary DNA by this probe.¹⁷

2.4. Improving the mismatch discrimination of the PNA probe

While the threefold difference in the fluorescence of the complementary and single mismatched DNA hybrids of the PNA probe (AQ/FAM)Lys-P1 is quite acceptable compared to other reports,^{23–26} it would be highly advantageous to improve the discrimination even further. In principle, increasing the temperature should improve the discrimination between complementary and single mismatched hybrids if one can find a temperature at which the mismatch hybrid is completely dissociated, while the complementary hybrid is still stable. The large difference in the stabilities of complementary and single mismatched PNA-DNA hybrids facilitate this process as it offers a large window for temperature adjustment. The T_m curves of the DNA hybrids of (AQ/FAM)Lys-P1 are shown in Fig. 4A. The fluorescence T_m values of 58 and 27 °C were obtained for complementary and internal single-mismatched hybrids, respectively. Beyond 40 °C, the fluorescence of the single mismatched hybrid was almost the same as that of single stranded (AQ/FAM)Lys-P1 PNA probe. However, the fluorescence of single stranded PNA probe was also increased, presumably due to the heat-induced dissociation of the two interacting dyes. The maximum discrimination, as expressed by discrimination factor [$F_{ds(comp)}/F_{ds(mm)}$], of 5.5-fold was observed around 40 °C. This is considerably better than the selectivity observed at 20 °C. Beyond 70 °C, no discrimination was observed because both the complementary and mismatched duplexes were completely dissociated. Similar results were obtained with other PNA probes, but the maximum discrimination in each case was observed at different temperature. The benefit of increasing temperature was more pronounced in longer PNA probe sequences such as in (AQ/FAM)Lys-P6 (14 bases), whereby a decent discrimination factor of 3.3 was observed at 80 °C—a temperature at which the mismatched hybrid was completely dissociated. Almost no discrimination was observed at 20 °C in this case (Fig. 4B).

In an alternative strategy for improving mismatch discrimination without increasing temperature, the concept of displacement probe¹⁸ was employed, taking advantage of the low fluorescence increase of the probe upon hybridization with a short DNA with 3'-base deletion (see Table 3, entry 3). In contrast to the single stranded probe which binds readily to either complementary or mismatched DNA target as long as the resulting hybrids are sufficiently stable

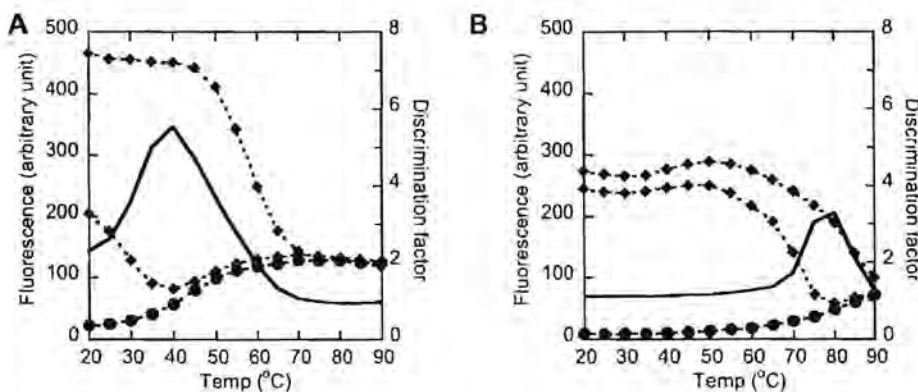


Fig. 4. Fluorescence T_m curves of single stranded PNA probes (blue) and their hybrids with complementary (red) and single mismatched DNA (green) together with the discrimination factor at different temperature (black) (A) (AQ/FAM)Lys-P1 (B) (AQ/FAM)Lys-P6; conditions: 10 mM phosphate buffer pH 7.0; [PNA]–1.0 μ M, [DNA]–1.2 μ M, λ_{ex} –490 nm, λ_{em} –520 nm.

under the experimental condition, the displacement probe requires displacement of the short DNA strand by a new DNA strand. This will be energetically feasible only if the new PNA–DNA hybrid is more stable than the original displacement probe complex. Since the mismatched duplex is generally much less stable than a short complementary duplex, this strategy should help improve the specificity for mismatch discrimination.

The concept was demonstrated by first forming a duplex between (AQ/FAM)Lys-P1 and a short complementary DNA with 3'-terminal base deletion. The fluorescence of this displacement probe complex (F_0) is only slightly higher than the single stranded probe. Addition of complementary DNA resulted in a rapid increase of the fluorescence (F). The F/F_0 ratio reach a high value of ~ 11 after 60 min. Much less fluorescence increase was observed with the mismatched DNA. The discrimination factor [$F_{(comp)}/F_{(mm)}$] improved from ~ 3 (without strand displacement) to ~ 5 (with strand displacement) (Fig. 5). This experiment showed the specificity of the dual end-labeled PNA probe can be further improved by the strand displacement concept.

2.5. Multicolor detection of two DNA targets

The possibilities of using two PNA probes to simultaneously detect two DNA targets differing by only one base was evaluated. One of the PNA probes was the fluorescein-labeled (AQ/FAM)Lys-P1 ('AQ/FAM probe') and another probe (AQ/TMR)Lys-P2 having a similar sequence but with one mismatch base was labeled with TAMRA ('AQ/TMR probe'). The mixture of the two probes exhibited very low fluorescence (Fig. 6) in the absence of DNA. Addition of a DNA target complementary to the AQ/FAM probe resulted in a large fluorescence increase at the emission wavelength of FAM upon excitation at 490 nm. No fluorescence change at the emission wavelength of TMR was observed upon excitation at either 490 or 540 nm. This sample exhibited green fluorescence when observed under a UV lamp. Likewise, addition of the DNA target complementary to the AQ/TMR probe to the probe mixture similarly resulted in an increased fluorescence of TMR but not FAM. The sample gave orange fluorescence under UV light. When both DNAs are present, the sample exhibited yellow fluorescence (a combination of red and

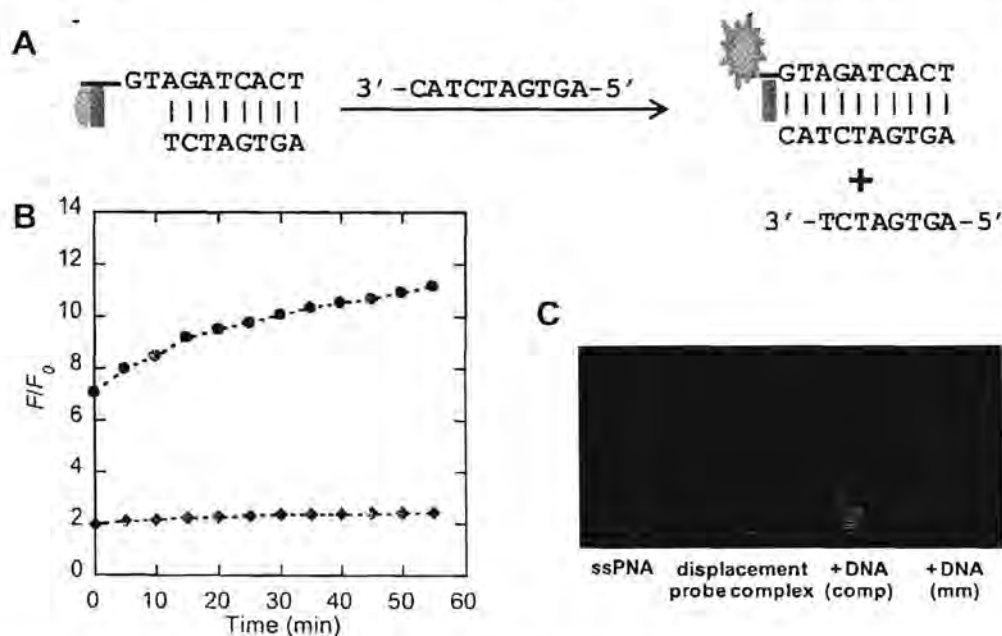


Fig. 5. (A) The working principle of strand displacement probe (B) fluorescence ratios of the displacement probe (AQ/FAM)Lys-P1–dAGTCACTAC after addition of complementary DNA (dAGTCACTAC, green) and mismatched DNA (dAGTCTCTAC, red) as a function of time; conditions: 10 mM sodium phosphate buffer pH 7.0, [PNA]–1.0 μ M and [DNA]–1.2 μ M, λ_{ex} –490 nm, λ_{em} –520 nm (C) photograph of the strand displacement experiment under UV lamp (365 nm); conditions: 10 mM sodium phosphate buffer pH 7.0, [PNA]–10 μ M and [DNA]–12 μ M.

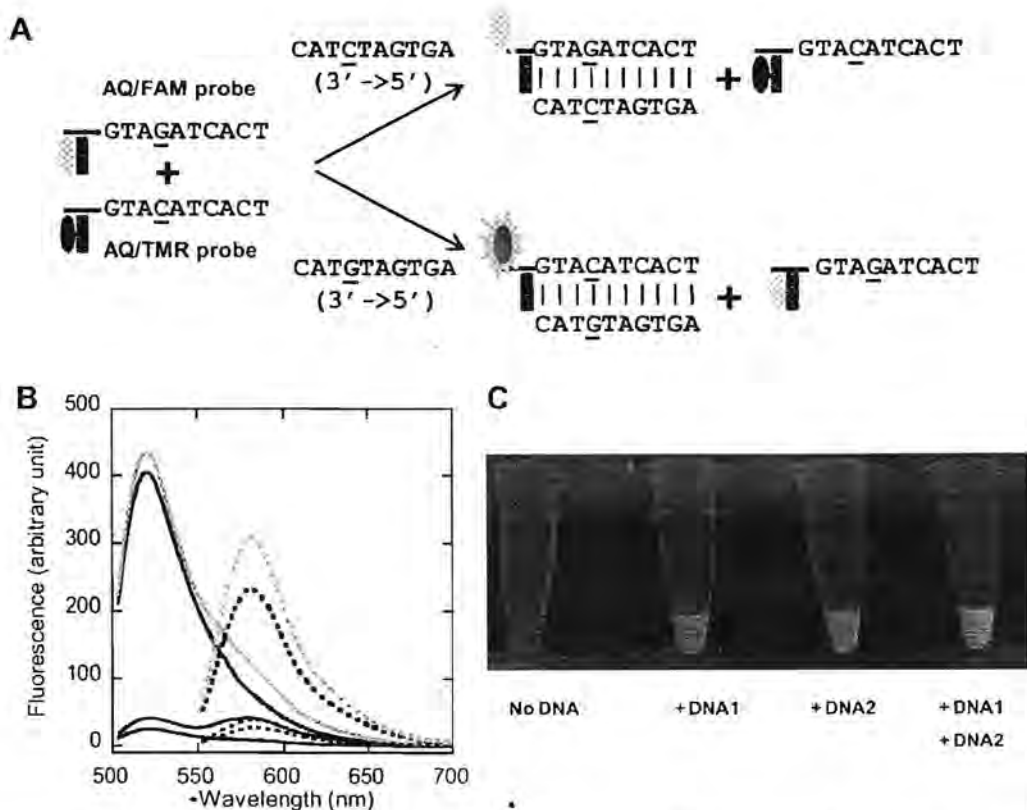


Fig. 6. (A) The concept of multiplex detection by two PNA probes (B) fluorescence spectra of the mixture of AQ/FAM and AQ/TMR probes before (blue) and after addition of DNA complementary to the AQ/FAM probe (green), DNA complementary to the AQ/TMR probe (red) and both (orange) at λ_{exc} 490 nm (solid lines) and 540 nm (dashed lines); conditions: 10 mM sodium phosphate buffer pH 7.0, [PNA]=1.0 μM and [DNA]=1.2 μM (C) photograph of the multiplex DNA detection experiment under UV lamp (365 nm); conditions: 10 mM sodium phosphate buffer pH 7.0, [PNA]=10 μM and [DNA]=12 μM .

green). The results are fully consistent with the expected high discrimination ability of the PNA probes.

2.6. DNA double duplex invasion by doubly-end-labeled acpcPNA probes

Finally, the possibilities of directly detecting dsDNA targets by the doubly-end-labeled PNA probe were evaluated (Fig. 7). The

inability of two complementary strands of acpcPNA to form self-hybrids³¹ suggests the possibility of targeting dsDNA by the so-called double duplex invasion mechanism.^{25,30} The (AQ/FAM)Lys-P1 probe could not efficiently invade into a 30-mer DNA duplex carrying a 10-base region corresponding to the PNA probe sequence as shown by the rather weak fluorescence increase relative to the single stranded probe (estimated to be less than 10% invasion efficiency). Addition of another unlabeled acpcPNA probe designed to

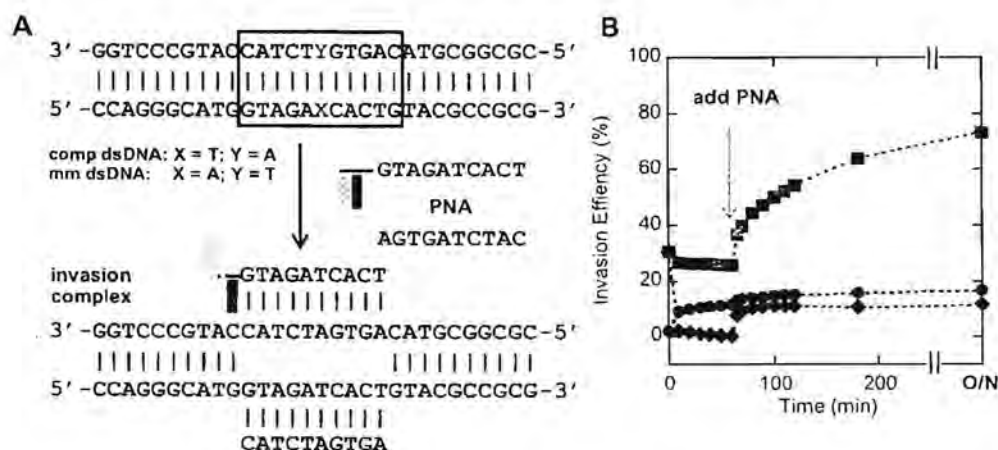


Fig. 7. (A) Double duplex invasion experiment (B) %invasion as calculated from fluorescence change at 520 nm of the labeled PNA probe [(AQ/FAM)Lys-P1+comp dsDNA (blue), (AQ/FAM)Lys-P1-Lys5+comp dsDNA (red); (AQ/FAM)Lys-P1-Lys5-mismatched dsDNA (green)] before and after addition of the second unlabeled complementary PNA strand (shown by arrow at 60 min); conditions: 10 mM sodium phosphate buffer pH 7.0, [labeled PNA] = [DNA] = 1.0 μM ; [unlabeled PNA] = 1.2 μM ; λ_{exc} = 490 nm.

bind to the opposite strand of DNA in the same region only slightly improved the invasion efficiency to around 15% after leaving overnight. A control experiment by mixing the two acpcPNA strands did not give any fluorescence increase due to the inability of acpcPNA to form self-hybrids therefore the fluorescence increase must be due to the formation of the PNA–DNA invasion complex (Fig. S19). Increasing the number of positive charge by adding a polylysine tail as in the (AQ/FAM)Lys-P1-Lys5 probe improves the duplex invasion efficiency further to more than 70%.³¹ A control double duplex invasion experiment with a dsDNA target carrying a mismatched invasion site showed a negligible fluorescence increase and the extent of the invasion was estimated to be less than 10%. In addition, polyacrylamide gel electrophoresis also clearly demonstrated the invasion only in the case of complementary PNA/DNA duplexes (Fig. S20), thus confirming the specificity of the duplex invasion process. It should be noted that accurate quantification of the extent of duplex invasion is difficult by this fluorescence approach due to the variable degree of quenching of the probe upon contact with the dsDNA, most likely by non-specific interaction between the polylysine and the phosphate backbone of DNA. Nevertheless, it is clear that the PNA probe can be used for direct sequence-specific detection of dsDNA target by double duplex invasion.

3. Conclusion

We have successfully synthesized doubly-end-labeled fluorescence conformationally constrained acpcPNA probes and demonstrate their potential for specific detection of single and double stranded DNA sequences in homogeneous format. The presently described PNA probes gave a low background and good response with DNA ($F_{ds}/F_{ss} \sim 6$ to 20) which outperforms other linear DNA probes with similar design,^{21–25} and compares favorably with conventional stem-loop DNA beacons^{17,20} or linear PNA probes bearing the fluorophore and the quencher at the opposite ends of the molecule ($F_{ds}/F_{ss} \sim 10$).¹⁷ The large difference between the stabilities of the complementary and mismatched acpcPNA–DNA duplexes allows effective discrimination between complementary and single mismatched DNA targets at room temperature, and could be further improved by increasing the temperature or by using the strand displacement concept ($F_{comp}/F_{mismatch} \sim 3–5$). The specificity was further demonstrated in a multicolor, multiplex detection of DNA targets that are different by just one base. As the mechanism of un-quenching relies on the end stacking of the quencher and the terminal base pairs of the PNA–DNA duplexes, DNA with terminal base mismatches and short DNA with terminal deletion could also be readily distinguished from complementary DNA. Finally, the inherently pseudocomplementary acpcPNA which could not form self-duplexes allowed direct detection of double stranded DNA targets via DNA double duplex invasion.

4. Experimental

4.1. Synthesis of doubly-end-labeled acpcPNA

The acpcPNA probes were synthesized by Fmoc solid phase peptide synthesis on TentagelS–RAM resin (0.24 mmol/g). The resin was first loaded with one or five lysine residues via Fmoc-Lys(Boc)-OPfp. The four Fmoc-protected acpcPNA monomers (A^{Bz}, T, C^{Bz}, C^{Ibu}) and ACPC spacers were next incorporated until the desired PNA sequence was obtained. Finally, the N-terminus was capped with Fmoc-Lys(Tfa)-OH or Fmoc-Apc(Tfa)-OH via HATU activation. The Fmoc protecting group was removed and the free amino group was modified with the fluorophore (FAM or TMR) via the corresponding succinimidyl esters. Next, the Tfa protecting group was removed by treatment with aqueous ammonia:dioxane (1:1) at 65 °C overnight. This procedure also simultaneously removed the

nucleobase side chain protection. This was followed by attachment of the quencher (AQ or Dab) via the corresponding HATU-activated carboxylic acids. The reaction progress was monitored by MALDI-TOF mass spectrometry. After completion of the reaction, the labeled PNA probes were cleaved from the resin by treatment with TFA followed by reversed phase HPLC purification. The isolated yield of PNA with 90% purity or more were in the range of 3–12%.

4.2. Fluorescence experiments

Fluorescence experiments were performed on Cary Eclipse fluorescence spectrophotometer (Varian/Agilent Technologies). All fluorescence experiments were carried out at the specified concentrations of PNA and DNA in 10 mM sodium phosphate buffer (pH 7.0) (1000 μ L) in a 10 mm quartz cell with a Teflon stopper. The excitation and emission slits were set to 5 nm, and the photomultiplier tube (PMT) voltage set to an appropriate value (to give the fluorescence read-out not exceeding 1000 a.u.). Fluorescence melting experiments were carried out by preparing the sample as in normal fluorescence experiments. The fluorescence emission was recorded from 20 to 90 °C at 5 °C intervals with temperature ramp of 1 °C/min. The temperature recorded was the block temperature and was uncorrected. T_m values were estimated from first derivative plots of the fluorescence melting curves.

4.3. UV–vis experiments

UV–vis experiments were performed on Cary 100 UV–vis spectrophotometer (Varian/Agilent Technologies) at 20 °C under similar conditions to the fluorescence experiments.

Acknowledgements

This work was supported by the Thailand Research Fund (DPG5780002), Chulalongkorn University (postdoctoral fellowship to NY), the Royal Golden Jubilee Ph.D. Program (RGJ) PhD Grant No. PHD/0316/2550, to NY and TV), and Science Achievement Scholarship of Thailand (SAST, to DN).

Supplementary data

Supplementary data related to this article can be found in the online version, at <http://dx.doi.org/10.1016/j.tet.2016.10.040>.

References and notes

1. Kaurasinghe, B. L.; Brown, J. *Chem. Commun.* **2005**, 4854–4857.
2. Guo, J.; Ju, J.; Li, J. *Anal. Bioanal. Chem.* **2012**, *392*, 1111–1117.
3. Shibuya, A.; Abe, H.; Fukukawa, K.; Yamada, S.; Ito, T. *Anal. Bioanal. Chem.* **2009**, *391*, 137–145.
4. Thurley, S.; Roglin, I.; Sutz, V. *J. Am. Chem. Soc.* **2007**, *129*, 2671–2680.
5. Tang, Z.; Mallikarjuny, P.; Tang, R.; Wan, X.; Wang, Z.; Wang, H. *Anal. Bioanal. Chem.* **2008**, *390*, 1233–1239.
6. Zhao, D.; Cheng, L. *Anal. Bioanal. Chem.* **2013**, *395*, 6231–6239.
7. Liu, Z.; Chen, S.; Liu, B.; Wu, J.; Zhou, Y.; Liu, L.; Dong, L. *Anal. Bioanal. Chem.* **2014**, *396*, 12229–12235.
8. Iyagi, S.; Kamen, R. *Nat. Biotechnol.* **1996**, *14*, 293–295.
9. Maras, S. A. P. *Mol. Biotechnol.* **2008**, *34*, 247–255.
10. Kashiwa, H.; Taketa, T.; Fujii, T.; Nakaguro, K.; Kame, W.; Nawa, E.; Takase, T.; Yoshida, Y.; Asahara, H. *Angew. Chem. Int. Ed.* **2009**, *48*, 8099–8103.
11. Holzhauser, E.; Wipflinger, H. *Chem. Commun.* **2011**, 7276–7278.
12. Li, Q.; Yuan, G.; Guo, J.; Tang, Y. *Anal. Bioanal. Chem.* **2002**, *382*, 100–105.
13. Kolpakchikov, D. M. *Chem. Rev.* **2010**, *110*, 4559–4570.
14. French, D. J.; Archard, A. E.; Brown, L. *Nucleic Acids Res.* **2001**, *29*, 363–374.
15. Venkatesan, N.; Chen, Y. L.; Kim, B. H. *Chem. Soc. Rev.* **2008**, *37*, 649–675.
16. Brunes, C.; Navarro, M. *Anal. Bioanal. Chem.* **2012**, *392*, 3071–3076.
17. Saito, O. *Angew. Chem. Int. Ed.* **2000**, *39*, 3249–3251.
18. Rubin, H.; Demidov, V. M.; Cullis, J. M.; Pambula, M. J.; Gildea, R. H.; Funt, I.; Neuvéglise, D. *J. Am. Chem. Soc.* **2002**, *124*, 1097–1103.
19. Benito, G.; Traga, S.; Libalaben, A.; Ruzova, I. *Proc. Natl. Acad. Sci. U.S.A.* **2009**, *106*, 6121–6126.

20. Söcher, E.; Bethge, L.; Knoll, A.; Jungnick, N.; Herrmann, A.; Seitz, D. *Angew. Chem., Int. Ed.* **2008**, *47*, 9555–9559.
21. Söcher, E.; Knoll, A.; Seitz, D. *Org. Biomol. Chem.* **2012**, *10*, 7363–7371.
22. Shinozuka, K.; Sato, Y.; Sawai, H. *J. Chem. Soc., Chem. Commun.* **1994**, 1377–1378.
23. Ranasinghe, R. T.; Brown, I. J.; Brown, I. *Chem. Commun.* **2001**, 1480–1481.
24. Kodama, S.; Azano, S.; Moriguchi, T.; Sawai, H.; Shinozuka, K. *Bioorg. Med. Chem. Lett.* **2006**, *16*, 2655–2658.
25. Yamane, K. *Nucleic Acids Res.* **2002**, *30*, e97.
26. Ikeda, S.; Okamoto, A. *Chem.–Asian J.* **2008**, *3*, 958–968.
27. Ikeda, S.; Kikuta, T.; Yuki, M.; Okamoto, A. *Angew. Chem., Int. Ed.* **2009**, *48*, 6486–6488.
28. Boonlua, C.; Ditmangkla, B.; Reenabthue, N.; Supaprom, C.; Poornak, N.; Siriwong, K.; Vilaivan, T. *RSC Adv.* **2014**, *4*, 8817–8827.
29. Ditmangkla, B.; Boonlua, C.; Supaprom, C.; Vilaivan, T. *Bioconjugate Chem.* **2013**, *24*, 614–625.
30. Boonlua, C.; Vilaivan, C.; Wagenknecht, H.-A.; Vilaivan, T. *Chem.–Asian J.* **2011**, *6*, 3251–3259.
31. Vilaivan, T. *Acc. Chem. Res.* **2015**, *48*, 1647–1656.
32. Kongpeth, J.; Jangpasa, S.; Chaitinplak, P.; Chaitinplak, O.; Vilaivan, T. *Talanta* **2016**, *145*, 318–325.
33. Bernacchi, S.; McJy, Y. *Nucleic Acids Res.* **2001**, *29*, e62.
34. Nazarenko, L.; Pres, B.; Lowe, B.; Obaidy, M.; Rashtchian, A. *Nucleic Acids Res.* **2002**, *30*, 2089–2193.
35. Johansson, M. K.; Hilder, H.; Dick, D.; Cook, R. M. *J. Am. Chem. Soc.* **2002**, *124*, 6950–6956.
36. Maras, S. A. E.; Kramer, E. R.; Fyng, S. *Nucleic Acids Res.* **2002**, *30*, v122.
37. Asseline, U.; Chassignol, M.; Auberta, Y.; Koiga, V. *Org. Biomol. Chem.* **2006**, *4*, 1949–1957.
38. Lohse, J.; Dohl, O.; Nielsen, P. E. *Proc. Natl. Acad. Sci. USA.* **1999**, *96*, 11804–11808.
39. Demidov, V. V.; Protopanova, E.; Irvinsky, K. I.; Price, C.; Nielsen, P. E.; Frank-Kamenetskii, M. D. *Proc. Natl. Acad. Sci. USA.* **2002**, *99*, 5953–5955.
40. Ishizuka, T.; Yoshida, J.; Yamamoto, Y.; Sumaeka, J.; Federich, T.; Gonzalez A.; Storza, S.; Komiyama, M. *Nucleic Acids Res.* **2008**, *36*, 1464–1471.



Contents lists available at ScienceDirect

Analytica Chimica Acta

journal homepage: www.elsevier.com/locate/aca

Electrochemical paper-based peptide nucleic acid biosensor for detecting human papillomavirus



Prinjaporn Teengam^a, Weena Siangproh^b, Adisorn Tuantranont^c, Charles S. Henry^c,
Tirayut Vilaivan^e, Orawon Chailapakul^{f,*,1}

^a Program in Petrochemistry, Faculty of Science, Chulalongkorn University, Pathumwan, Bangkok, 10330, Thailand

^b Department of Chemistry, Faculty of Science, Srinakharinwirot University, Bangkok, 10110, Thailand

^c Nanoelectronics and MEMS Laboratory, National Electronics and Computer Technology Center, Pathumthani, 12120, Thailand

^d Department of Chemistry, Colorado State University, Fort Collins, CO, 80523, United States

^e Organic Synthesis Research Unit, Department of Chemistry, Faculty of Science, Chulalongkorn University, Pathumwan, Bangkok, 10330, Thailand

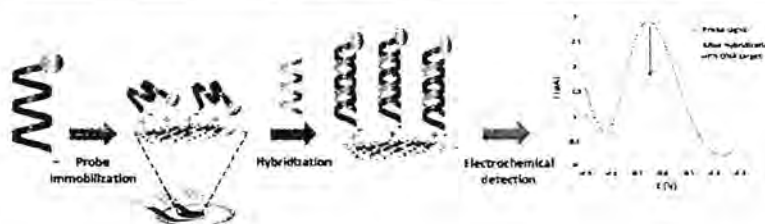
^f Electrochemistry and Optical Spectroscopy Research Unit, Department of Chemistry, Chulalongkorn University, Pathumwan, Bangkok, 10330, Thailand

^{*} Nanotec-CU Center of Excellence on Food and Agriculture, Bangkok, 10330, Thailand

HIGHLIGHTS

- A paper-based DNA biosensor using AQ-PNA probe and G-PANI modified electrode was first developed.
- This developed DNA biosensor was highly specific over the non-complementary DNA.
- This sensor was successfully applied to detect the HPV-DNA type 16 obtained from cancer cell lines.
- This sensor is inexpensive and disposable, which can be incinerated easily and safely after use.

GRAPHICAL ABSTRACT



ARTICLE INFO

Article history:

Received 23 July 2016

Received in revised form

21 October 2016

Accepted 29 November 2016

Available online 3 December 2016

Keywords:

Graphene

Polyaniline

Paper-based electrochemical DNA biosensor

acpcPNA

Electrochemical detection

Human papillomavirus

ABSTRACT

A novel paper-based electrochemical biosensor was developed using an anthraquinone-labeled pyrroli-dinyl peptide nucleic acid (acpcPNA) probe (AQ-PNA) and graphene-polyaniline (G-PANI) modified electrode to detect human papillomavirus (HPV). An inkjet printing technique was employed to prepare the paper-based G-PANI-modified working electrode. The AQ-PNA probe bearing a negatively charged amino acid at the N-terminus was immobilized onto the electrode surface through electrostatic attraction. Electrochemical impedance spectroscopy (EIS) was used to verify the AQ-PNA immobilization. The paper-based electrochemical DNA biosensor was used to detect a synthetic 14-base oligonucleotide target with a sequence corresponding to human papillomavirus (HPV) type 16 DNA by measuring the electrochemical signal response of the AQ label using square-wave voltammetry before and after hybridization. It was determined that the current signal significantly decreased after the addition of target DNA. This phenomenon is explained by the rigidity of PNA-DNA duplexes, which obstructs the accessibility of electron transfer from the AQ label to the electrode surface. Under optimal conditions, the detection limit of HPV type 16 DNA was found to be 2.3 nM with a linear range of 10–200 nM. The performance of this biosensor on real DNA samples was tested with the detection of PCR-amplified DNA samples from the SiHa cell line. The new method employs an inexpensive and disposable device, which

* Corresponding author. Electrochemistry and Optical Spectroscopy Research Unit, Department of Chemistry, Chulalongkorn University, Pathumwan, Bangkok, 10330, Thailand.

E-mail address: orawon.chailapakul@chula.ac.th (O. Chailapakul).

easily incinerated after use and is promising for the screening and monitoring of the amount of HPV-DNA type 16 to identify the primary stages of cervical cancer.

© 2016 Published by Elsevier B.V.

1. Introduction

The most important factors for diagnostic devices, especially for developing countries, are low cost, simplicity and speed of results for early screening and monitoring of disease biomarkers. To achieve this goal, paper-based analytical devices (PADs) have been widely used as an alternative device design for point-of-care (POC) applications [1–3]. Two detection modes that have been most frequently used with PADs include colorimetric and electrochemical detections. Since first reported by Dungchai et al. [4], PADs with electrochemical detection (ePADs) have increasingly attracted attention as they offer a combination of simplicity, low power requirements, low limits of detection, and ease of quantitation [5–8]. ePADs are therefore an ideal platform for developing sensitive, selective DNA biosensors for point-of-care applications.

In electrochemical DNA biosensors, many different electrode types have been used, including a gold [9–11], hanging mercury drop (HMDE) [12,13] and various carbon-based materials [14–17]. Carbon is considered a good electrode material due to its low cost, wide potential range, chemical inertness and low background current. Furthermore, carbon electrodes have a fast response time and can be easily fabricated in different configurations. These features make carbon suitable for use in ePAD DNA biosensors. However, the use of micro-scale electrodes as part of ePAD is a major obstacle due to limited sensitivity. To overcome this problem, graphene (G) has been used as a carbon-based nanomaterial and has achieved significant popularity due to the large specific surface area and unique electrochemical properties of G [18–20]. G-based electrodes exhibited superior performance compared to other carbon-based electrodes in terms of their electro-catalytic activity and electrical conductivity [21,22]. G has also been used in combination with various types of functional materials to fabricate high-performance electrodes. Among them, polyaniline (PANI) is a useful conducting polymer that has been widely used for electronic, optical and electrochemical applications such as enzyme-based biosensors and DNA assays due to its excellent environmental stability and unusual doping/dedoping chemistry [23–25]. Moreover, PANI improves the dispersion and reduces the agglomeration of the planar sp^2 -carbon of G [23,26]. PANI also possesses free amino groups, which can act as a handle for the covalent immobilization of suitable detection probes via amide bonds [27,28]. Finally, doped PANI possesses the positive charge of the amino group, which can immobilize negatively-charged probes via electrostatic interactions. Thus, it is a challenge to evaluate alternative systems for immobilization of various bio-recognition elements via electrostatic interaction.

For most electrochemical DNA biosensors, a probe that is designed to detect a specific sequence of target DNA is first immobilized on the electrode. Then, the electrochemical signal of an electroactive species, which was either covalently attached to the probe or added later as an indicator, is recorded and compared before and after the hybridization with the complementary DNA target [12,29]. The probe is a key parameter that determines the detection selectivity. While most DNA biosensors employ short oligodeoxynucleotide probes, several alternative probes have been used with great success. Peptide nucleic acid (PNA) [30,31], a synthetic DNA mimic with a peptide-like backbone of repeating N-(2-

aminoethyl)-glycine units replacing the sugar-phosphate in natural DNA or RNA, has attracted increasing interest as the probe for electrochemical DNA biosensors [12,32–34] due to its sequence-specific binding to DNA or RNA, resistance to nuclease and protease enzymes, and strong binding to the target DNA. Recently, Vilaivan's group [35–37] proposed a new conformationally constrained pyrrolidiny PNA system (known as acpcPNA) that possesses an α,β -peptide backbone derived from D -proline/2-aminocyclopentanecarboxylic acid. This new acpcPNA demonstrates a stronger binding affinity and higher specificity towards complementary DNA compared to DNA and Nielsen's PNA, and there are several applications of acpcPNA as a probe for DNA biosensors [38–40].

Human papillomavirus or HPV is the common virus that can be passed through any type of sexual contact. There are some high-risk types of HPV including type 16 and 18, which can cause abnormal changes to the cells of the cervix. These changes can lead to cervical cancer which, is one of the most important health problems for woman. The mortality occurring from cervical cancer has continuously increased especially in developing countries that have limited medical facilities [41].

In our previous work [33], the electrochemical sensor based-on acpcPNA probe for HPV detection was reported. Although the good limit of detection (LOD) was achieved, the use of PVC-based sensor was costly and the procedure relies on covalent method for probe immobilization was complicated and time-consuming. Cost is the most critical challenge for disposable POC electrochemical sensors. In this work, using PAD has potential to address all of challenges of disposable sensor in term of low-cost and simple fabrication. Electrostatic immobilization is also a key step of this work. This method eliminated the complicate steps of covalent process and significantly reduced time. Moreover, inkjet printing used for electrode modification step is advantageous due to it provided electrode reproducibility and high pattern resolution [42]. Inkjet-printing is scalable of mass production, while small amount of modifier is wasted in the modification process.

Here, we aim to develop a novel paper-based electrochemical DNA biosensor using an AQ-labeled acpcPNA probe in combination with a G-PANI modified electrode. In this new DNA biosensor, the acpcPNA probe labeled with anthraquinone (AQ) was first incorporated onto a G-PANI-modified ePAD using electrostatic immobilization. In the absence of complementary DNA, a strong signal was observed for the AQ. Hybridization with the complementary DNA target resulted in a decrease of the electrochemical signal that linearly correlated with the concentration of the target. The application of the biosensor to the sensitive detection of HPV DNA type 16 is demonstrated. The proposed method is applicable to the screening and monitoring of HPV-DNA type 16 in the primary stage of cervical cancer, a disease that leads to the death of women around the world, particularly in developing countries that have limited resources for public healthcare.

2. Materials and methods

2.1. Chemicals and materials

Graphene (G) was purchased from A.C.S (Medford, USA).

Polyaniline, camphor-10-sulfonic acid (C₁₀H₁₆O₄S), glutamic acid and N-methyl-2-pyrrolidone (NMP) were ordered from Sigma Aldrich (St.Louis, USA). Carbon and silver/silver chloride ink were obtained from Gwent group (Torfaen, United Kingdom). The screen-printed block was made by Chaiyaboon Co. Ltd. (Bangkok, Thailand). The labeling electroactive spices, 4-(anthraquinone-2-oxy)butyric acid, was synthesized as described previously [39]. Analytical grade reagents, including NaCl, KH₂PO₄, Na₂HPO₄ and KCl, were purchased from Merck and used without further purification. Synthetic oligonucleotides which correspond to partial sequences of HPV type 16 and other types of high risk HPV (HPV types 18, 31 and 33) used in the specificity test, were obtained from Pacific Science (Bangkok, Thailand). The sequences of the DNA oligonucleotides used are shown in Table 1.

The forward (5'-CACTATTITGGAGGACTGGA-3') and reverse primer (5'-GCCITAAATCCTGCTGTAG-3') used for the PCR cell-line samples were purchase from Pacific Science (Bangkok, Thailand). The cervical cancer cell-lines with (SiHa) HPV types 16 were obtained from the Human Genetics Research Group, Department of Botany, Faculty of Science, Chulalongkorn University.

2.2. Apparatus

The electrochemical measurements using square-wave voltammetry (SWV) were performed using a CHI232A electrochemical analyzer (CH Instruments, Inc., USA). A three electrode system was used and the working electrode was a G-PANI-modified screen-printed carbon electrode (4 mm in diameter). The electrochemical impedance spectroscopy (EIS) was carried out using PGSTAT 30 potentiostat (Metrohm Siam Company Ltd., Switzerland) in a solution of 1.0 mM [Fe(CN)₆]^{3-/4-} with the frequency range from 0.1 to 10⁻⁵ Hz. The Dimatix™ Materials Printer (DMP-2800, FUJIFILM Dimatix, Inc., Santa Clara, USA) was used for the electrode modification. JEM-2100 transmission electron microscope (Japan Electron Optics Laboratory Co., Ltd, Japan) was used for characterization of G-PANI composites. MALDI-TOF MS spectra was performed on a Microflex MALDI-TOF mass spectrometer (Bruker Daltonik GmbH, Bremen, Germany).

2.3. Fabrication of a paper-based electrochemical DNA sensor

A paper-based electrochemical DNA sensor was fabricated using the wax-printing method [43,44]. Initially, the patterned paper was designed using Adobe Illustrator and printed onto the filter paper (Whatman No.1) using a wax printer (Xerox Color Qube 8570, Japan). The printed paper was then placed on a hot plate (175 °C, 50 s) to melt the wax and create a hydrophobic barrier. For electrode fabrication, three electrode systems were prepared using an in-house screen-printing method. First, carbon ink was screened as a working electrode (WE) and counter electrode (CE). Afterward, silver/silver chloride was screened as a reference electrode (RE) and conductive pad. The basic design of the paper-based electrochemical DNA biosensor was shown in Fig. S1.

Table 1
List of oligonucleotides.

| Oligonucleotide | Sequence (5'-3') |
|---------------------------------------|----------------------|
| Complementary DNA (HPV type 16) | 5'-GCTGGAGGTGTATG-3' |
| Non-complementary DNA 1 (HPV type 18) | 5'-GGATGCTGCACCGG-3' |
| Non-complementary DNA 2 (HPV type 31) | 5'-CCAAAAGCCCAAGG-3' |
| Non-complementary DNA 3 (HPV type 33) | 5'-CACATCCACCGCA-3' |

2.4. Inkjet-printing of a G-PANI composite modified paper-based electrochemical DNA biosensor

Prior to electrode modification, a G-PANI composite was prepared using a physical mixing method following procedures extracted from relevant literature [45]. Graphene powder (10 mg) was dispersed in N-methyl-2-pyrrolidone (NMP) and sonicated for 20 h at room temperature. Subsequently, 20 mg of PANI (emeraldine base) was doped with 25 mg of camphor-10-sulfonic acid (CSA) to generate a positively charged amino group and also dissolved in 10 mL of NMP. For the preparation of the G-PANI conductive ink, the solutions of G and PANI were mixed together and stirred for 1 h. The mixture was centrifuged at 5000 rpm and filtered through a 0.43 μm filter membrane before use. The morphology of G-PANI conductive ink was characterized by transmission electron microscopy (TEM).

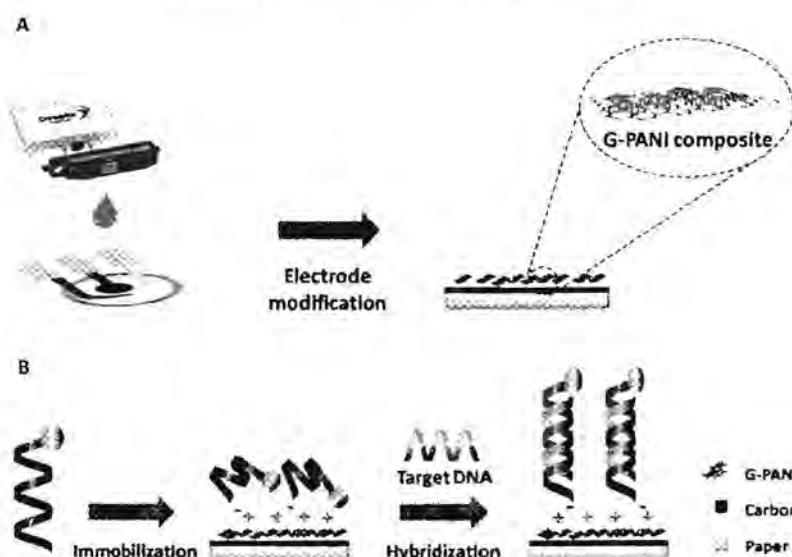
For electrode modification, the G-PANI composite solution was used as the ink for inkjet printing. The G-PANI conductive ink was loaded into a cartridge and printed onto the working electrode of the paper-based electrochemical DNA sensor using a Dimatix™ Materials Printer (DMP-2800, FUJIFILM Dimatix, Inc., Santa Clara, USA) at 30 °C, 20 V of applied voltage and 25 μm of drop spacing. Modification of the electrode is shown in Scheme 1A. Six layers of G-PANI composite solution were printed onto the surface area of the working electrode. Next, the modified electrode was heated at 65 °C for 30 min to dry the solvents from the G-PANI conductive ink.

2.5. Synthesis and labeling of the acpcPNA probe

The acpcPNA probe with the sequence Ac-(Glu)₃-CATA-CACCTCCAGC-Lys(AQ)NH₂ (written in the N→C direction, Ac = acetyl; AQ = anthraquinone; Glu = glutamic acid; Lys = lysine) was designed to detect 14 base synthetic oligonucleotide target with a sequence corresponding to human papillomavirus (HPV) type 16. The probe, referred to as AQ-PNA, was synthesized by solid-phase peptide synthesis using Fmoc chemistry as previously described [35]. The probe was modified with three glutamic acid residues at the N-terminus to incorporate the negative charge, which was followed by end-capping with an acetyl group. At the C-terminus, the acpcPNA probe was labeled with anthraquinone (AQ) via 4-(anthraquinone-2-oxy) butyric acid to the amino side chain of a C-terminal lysine residue. The progress of the reaction was monitored by MALDI-TOF-MS analysis on a Microflex MALDI-TOF mass spectrometer (Bruker Daltonik GmbH, Bremen, Germany). The modified PNA on the solid support was treated with 1:1 (v/v) aqueous ammonia:dioxane in a sealed tube at 60 °C overnight to remove the nucleobase protecting groups. Following cleavage from the solid support with trifluoroacetic acid (TFA), the AQ-PNA was purified by reverse-phase HPLC (C18 column, 0.1% (v/v) TFA in H₂O-MeOH gradient). The identity of AQ-PNA was verified by MALDI-TOF MS analysis, and the purity was confirmed to be >90% by reverse-phase HPLC.

2.6. Immobilization and hybridization of the PNA probe

First, the AQ-PNA probe (3 μL, 125 nM) was immobilized onto the G-PANI modified screen-printed carbon electrode surface by the drop-casting method and incubated for 15 min at room temperature. Next, 50 μL of PBS was placed onto the electrode surface. After immobilization of the probe, the AQ-PNA/G-PANI/SPCE modified electrode was hybridized with 3 μL of target DNA for 15 min. Then, the electrochemical signal response was measured using square-wave voltammetry. The immobilization and hybridization procedures are illustrated in Scheme 1B.



Scheme 1. Schematic illustration of (A) electrode modification and (B) immobilization and hybridization steps of paper-based electrochemical DNA biosensor.

2.7. PCR amplification of the cell line DNA sample

The SiHa (HPV type 16 positive) cell line DNA sample was amplified using PCR as previously reported [38]. Briefly, the amplification mixture containing 0.2 mM deoxynucleotide triphosphate mixture, $1 \times$ buffer (KCl, Tris) + 1.5 mM $MgCl_2$, 0.5 U of Taq polymerase, 0.4 μ M of each of the primers and 100 ng/ μ L of the cell line DNA sample was amplified at 95 °C for 10 min, follow by 30 cycles at 52 °C for 30 s and finally 72 °C for 7 min. The success of the PCR was confirmed by gel electrophoresis in 2% (w/v) agarose TBE gel followed by staining with ethidium bromide and visualization under a UV-transilluminator.

2.8. Electrochemical measurement

For electrochemical measurements, the square-wave voltammetry was used throughout the experiment using a potentiostat (CHI1232A). After the immobilization process, 50 μ L of PBS was dropped onto the modified working electrode, followed by adding the DNA target. Hybridization with AQ-PNA probe was done for 15 min. The electrochemical detection was performed under the optimal parameters including a frequency of 20 Hz, an amplitude of 100 mV and a step potential of 20 mV. The electrochemical signal after the hybridization was measured and compared with the signal in the absence of the DNA sample.

3. Results and discussion

3.1. Characterization of the G-PANI conductive ink

To confirm the success of the preparation of the G-PANI conductive ink, the morphology of the ink was characterized by transmission electron microscopy (TEM). Fig. 52A shows a TEM image of the G-PANI composite, which indicates a strong dispersion of G inside the composites without aggregation. Moreover, the electron diffraction pattern of G (Fig. 52B) matches very well with the standard, single crystal graphene.

The influence of the G-PANI ratio on the electrochemical conductivity of the modified electrodes was investigated. The anodic current of 1.0 mM $[Fe(CN)_6]^{3-/4-}$ in a 0.1 M KCl solution was measured using different proportions of G and PANI. Interestingly,

the anodic peak current of 1.0 mM $[Fe(CN)_6]^{3-/4-}$ increased with an increasing G:PANI ratio. The highest anodic current of $[Fe(CN)_6]^{3-/4-}$ was observed with the G-PANI modified electrode at the ratio of 1:2 indicating the optimal sensitivity of the modified sensor (Fig. S3). In addition, the peak currents gradually decrease for the higher G:PANI ratio, which could be due to the agglomeration of G within the G-PANI modifier [45]. Moreover, the effect of the number of printed G-PANI layers was also investigated as shown in Fig. S4. The anodic peak current of 1.0 mM $[Fe(CN)_6]^{3-/4-}$ tends to increase with an increase in the number of G-PANI layers. However, the current of the printed G-PANI modified electrode slightly decreased over 6 printing layers. We also believe that this phenomenon arises from the aggregation of excess G on the modified electrode surface causing a decrease in the anodic current response.

Next, the electroactive surface area (A) of SPCE and G-PANI modified electrode were determined to illustrate that the G-PANI conductive ink increases the surface area of the SPCE by solving the Randles-Sevcik equation (Equation (1)):

$$i_p = (2.69 \times 10^5) n^{3/2} A C D^{1/2} \nu^{1/2} \quad (1)$$

where i_p = current, n = number of electron transfer, C = concentration of electroactive species (mol cm^{-3}), D = diffusion coefficient ($\text{cm}^2 \text{s}^{-1}$) and ν = scan rate (V s^{-1}). As shown in Fig. S5, the cyclic voltammograms of 5.0 mM $[Fe(CN)_6]^{3-/4-}$ in a 0.1 M KCl solution for SPCE and G-PANI modified electrode were obtained. The current (i_p) is directly proportional to the square root of scan rate. According to the Randles-Sevcik equation, an approximate value of A was calculated to be 0.041 cm^2 and 0.222 cm^2 for SPCE and G-PANI modified electrode, respectively. This result provided a 5.4 times increase of electrode-electroactive surface area, thus, G-PANI conductive ink can improve the surface area of electrode, leading to enhance the sensitivity. As a result, the six G-PANI-layered modified electrode and the 1:2 ratio of G:PANI were considered to be the optimal conditions and were used for subsequent experiments.

3.2. Characterization of labeled acpPNA probe

In order to confirm the success of the synthesis and labeling of

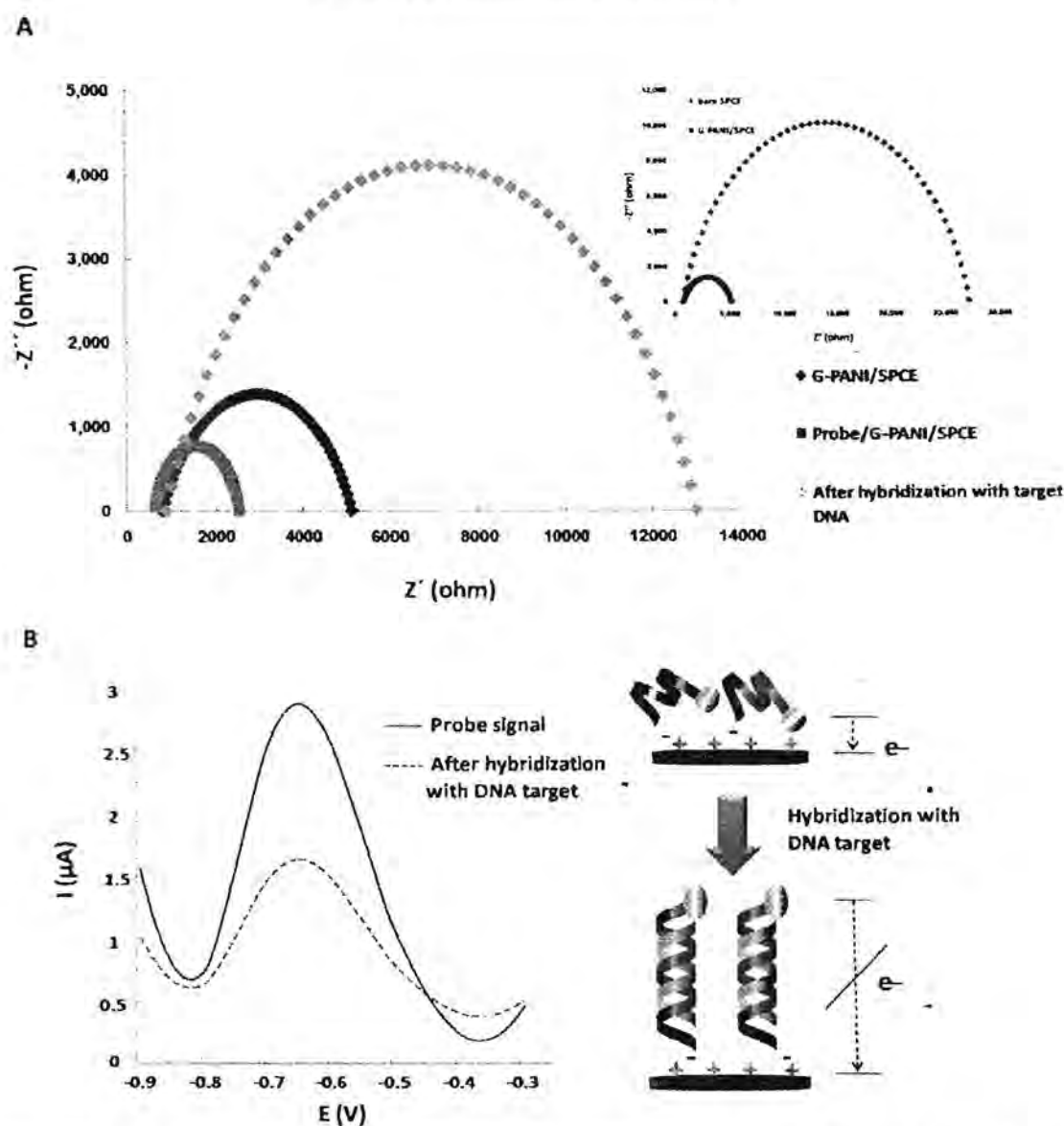


Fig. 1. (A) Nyquist plot of SPCE (inset), G-PANI/SPCE (inset), AQ-PNA/G-PANI/SPCE before and after hybridization with target DNA in 0.1 M $[\text{Fe}(\text{CN})_6]^{3-/4-}$. (B) Square-wave voltammograms of immobilized AQ-PNA probe on G-PANI/SPCE before and after hybridization with an equimolar concentration of target DNA.

the AQ-PNA probe, MALDI-TOF mass spectrometry was used to characterize the unlabeled and labeled acpcPNA probes. The 14-mers unlabeled acpcPNA showed a mass peak at 4754 m/z . After labeling, the mass increased to 5477 m/z . This increase of 723 m/z coincides with the mass of AQ and three glutamic acid residues plus an acetyl group. Therefore, the labeling of the acpcPNA probe with the electroactive species and the negatively charged polyglutamate was confirmed.

3.3. Electrochemical characterization

Electrochemical impedance spectroscopy (EIS) was used to characterize the AQ-PNA probe immobilization onto the working electrode. In general, the shape of the semicircle portion obtained from the EIS spectrum relates to either the electron transfer limited process or electron transfer resistance. Fig. 1A shows the Nyquist plots obtained from SPCE, G-PANI/SPCE and AQ-PNA/G-PANI/SPCE

before and after hybridization with the target DNA in a solution of 1.0 mM $[\text{Fe}(\text{CN})_6]^{3-/4-}$. Fig. 1A (inset) shows the Nyquist curve of unmodified SPCE (red line) with an R_{ct} value of 27.5 k Ω . This value is larger than that obtained from G-PANI/SPCE, and indicates that the unmodified SPCE has a higher charge-transfer resistance. Therefore, the decrease in R_{ct} to 5.08 k Ω of G-PANI/SPCE (blue line) indicates that G-PANI improves the electron transfer rates. After the immobilization step (Fig. 1A), the semicircular portion of AQ-PNA/G-PANI/SPCE (pink line) dramatically decreased with the R_{ct} value of 2.67 k Ω . This result can be explained theoretically as AQ is electroactive and can improve conductivity. Thus, the AQ-labeled PNA probe, which was immobilized onto the electrode surface, can facilitate the electron transfer process at the interface between the G-PANI/SPCE surface and the electrolyte. For this reason, the Nyquist curve of AQ-PNA/G-PANI/SPCE should have possessed the smallest semicircular portion. In order to confirm the success of the immobilization of the AQ-PNA probe, the heterogeneous electron-

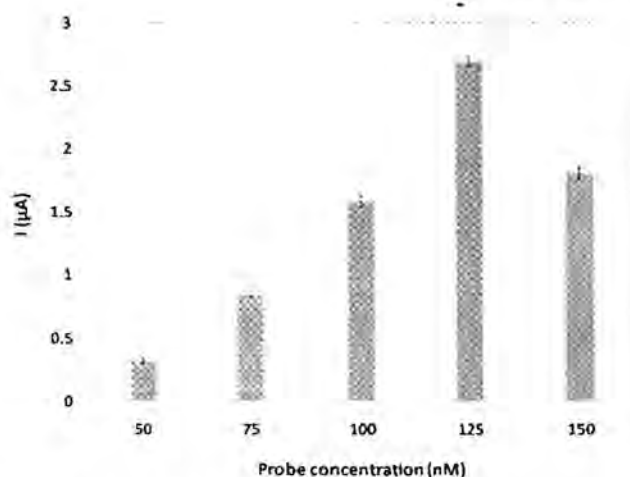


Fig. 2. The effect of AQ-PNA probe concentration on AQ electrochemical oxidation during the immobilization step.

transfer rate constant (K_{et}) value was obtained from Equation (2), which shows the relationship between R_{ct} and K_{et} .

$$K_{et} = \frac{RT}{n^2 F^2 R_{ct} A C_{redox}} \quad (2)$$

where n = number of electron transfer, F = faraday's constant ($KJ mol^{-1}$), A – electrode surface area (cm^2), C_{redox} = concentration of the redox couple ($mol cm^{-3}$). From the equation, the K_{et} values for SPCE, G-PANI/SPCE and AQ-PNA/G-PANI/SPCE were calculated to be $7.45 \times 10^{-5} cm s^{-1}$, $40.28 \times 10^{-5} cm s^{-1}$ and $76.70 \times 10^{-5} cm s^{-1}$, respectively. The increasing of K_{et} values inferred that the electron transfer process on AQ-PNA/G-PANI/SPCE is easier and faster than that on G-PANI/SPCE and SPCE. These results indicate that the negatively charged AQ-PNA probe was successfully immobilized

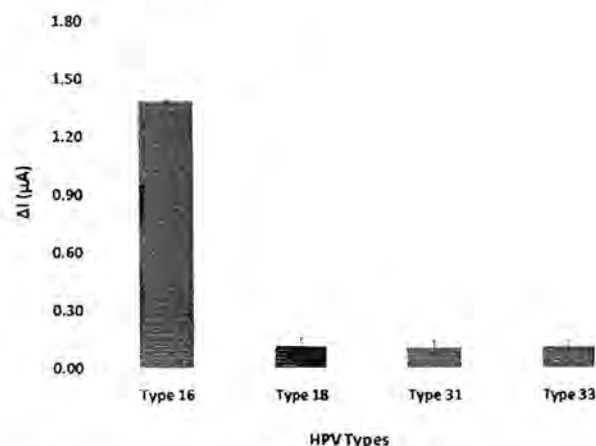


Fig. 4. The electrochemical signal response derived from AQ-PNA/G-PANI/SPCE probe after hybridized with various HPV types.

onto the positively charged G-PANI modified electrode surface through electrostatic attraction.

Next, the electrochemistry of the immobilized AQ-PNA/G-PANI/SPCE probe before and after hybridization with the DNA target were investigated using square-wave voltammetry (SWV), (Fig. 1B). The immobilization of the AQ-PNA/G-PANI/SPCE probe displayed a redox peak at approximately $-0.65 V$. After hybridization with an equimolar quantity of the complementary target DNA, the electrochemical response significantly decreased due to the increased rigidity of the PNA-DNA duplex relative to the native PNA probe. The rigidity hinders the electron transfer between the redox-active label (AQ) and the electrode surface [46,47].

3.4. Optimization of experimental variables

The experimental conditions were optimized next. The effect of

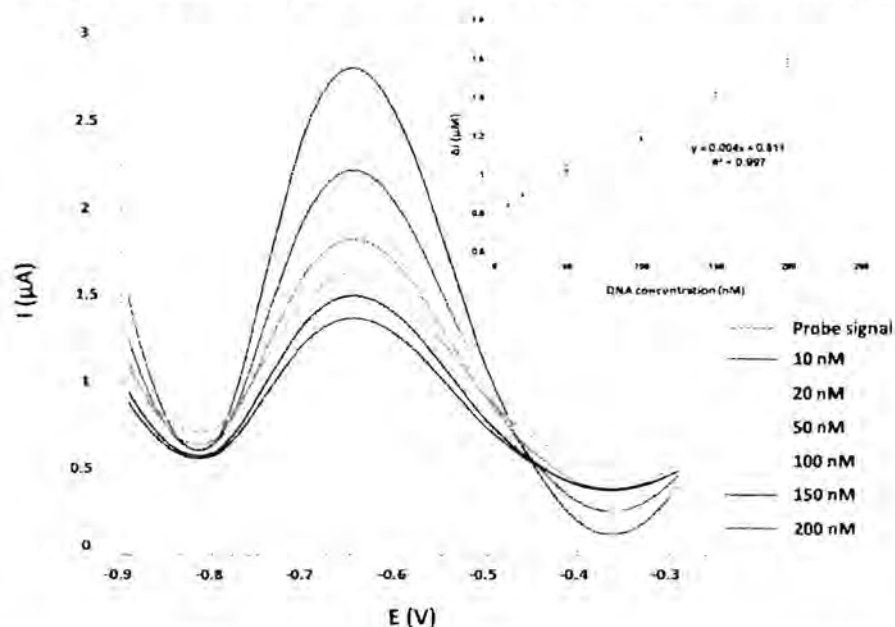


Fig. 3. Square-wave voltammograms of AQ-PNA/G-PANI/SPCE after hybridize with the target DNA in the concentration range of 10–200 nM and the calibration plots of the change in the probe electrochemical current (ΔI) versus the target DNA concentration (inset) at optimal condition: 125 nM of AQ-PNA probe concentration, a frequency of 20 Hz, an amplitude of 100 mV and a step potential of 20 mV.

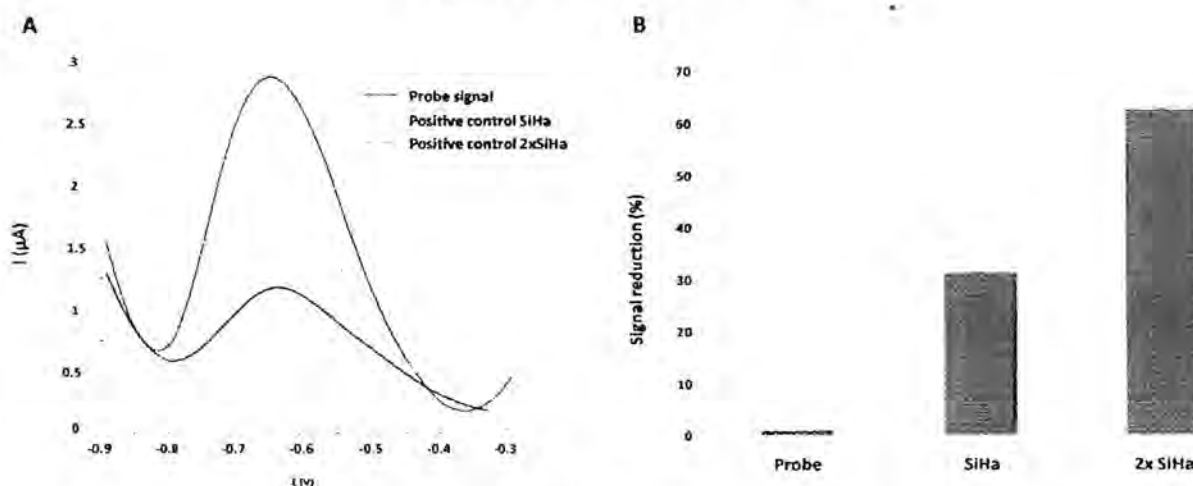


Fig. 5. Square-wave voltammograms of AQ-PNA/G-PANI/SPCE probe in the presence of PCR-amplified HPV type 16 positive sample from SiHa cell-line.

AQ-PNA probe concentration on AQ electrochemical oxidation was investigated first. The oxidation current obtained for different concentrations of the AQ-PNA probe measured by square wave voltammetry are shown in Fig. 2. The current continuously increased up to 125 nM. Above 125 nM, the current decreased significantly. The decrease in peak current at high AQ-PNA concentrations can potentially be caused do to an increased thickness of the organic layer [48,49], which leads to a lower electron transfer between AQ and the working electrode surface. Hence, the probe concentration of 125 nM was selected as the optimal concentration for further experiments.

For electrochemical detection using SWV, the variable parameters including frequency, step potential and amplitude were optimized using a 125 nM AQ-PNA probe concentration without DNA target shown in Fig. S6. The optimal parameters for electrochemical detection of this system was found to be 20 Hz of frequency, 100 mV of amplitude and 20 mV of step potential.

3.5. Analytical performance

To evaluate the analytical performance of the AQ-PNA/G-PANI/SPCE modified electrode, different concentrations of DNA target were determined using SWV analysis. Fig. 3 shows the voltammograms as well as the calibration curve (inset) as a function of target DNA concentrations. The calibration curve provided a linear range from 10 nM to 200 nM with a correlation coefficient of 0.997. The limit of detection (LOD) and limit of quantitation (LOQ), which were calculated as the concentration that produced a signal at 3 times and 10 times of the standard deviation of the blank ($N = 5$) [4], were found to be 2.3 nM and 7.7 nM, respectively. Our proposed method provides a wide linear range and sufficiently low detection limit for HPV detection. Table S1 shows a comparison of electrochemical performance between AQ-PNA/G-PANI/SPCE and the other modified electrodes used for HPV detection. It can be seen that a sufficiently low detection limit for HPV detection could be obtained from our proposed method. Importantly, this ePAD DNA biosensor can be easily and inexpensively prepared compared to the other HPV DNA biosensors [33,48,50].

3.6. Selectivity of the HPV type 16 detection

In order to investigate the selectivity of the acpcPNA probe, the current response obtained from the 14-nucleotide oligomer HPV

type 16 DNA target was compared to non-complementary 14-nucleotide oligomers, which originate from the other types of high risk HPV (types 18, 31 and 33), under the same experimental conditions. As shown in Fig. 4, a significantly different current was only obtained from the complementary DNA relative to the non-complementary DNA. Therefore, the immobilized AQ-PNA probe selectively binds to the HPV type 16 DNA target sequences. Accordingly, the proposed DNA biosensor demonstrated high selectivity to HPV type 16 DNA.

3.7. Reproducibility and stability of the paper-based electrochemical DNA biosensor

The electrode-to-electrode reproducibility and stability of the paper-based electrochemical DNA biosensor was examined. The relative standard deviations (RSDs) of five electrodes were tested in the concentration range of 10–200 nM. The % RSDs was determined to be between 2.16% and 7.79%. These results indicate that the proposed DNA biosensor offers acceptable reproducibility. Moreover, the storage stability is another important parameter for DNA biosensor development. The ePAD DNA biosensor was stored at room temperature (25 °C) for 2 weeks before recording the current response to 10 nM target DNA. It was determined that 90.2% of the initial current response was retained in the aged sensor compared to the response obtained from the freshly prepared sensor. The stability of this DNA sensor is mainly attributed to the environmental stability of PANI.

3.8. Detection of the PCR DNA sample

To test the ePAD biosensor, DNA was extracted from the SiHa cell line, HPV type 16 and amplified using PCR. Fig. 5A shows the SWV response of the proposed DNA biosensor in the presence of positive PCR products. It was observed that the current response decreased in the presence of the PCR product from the HPV type 16-positive cell line. Moreover, the current response decreased with increasing amounts of sample, as shown in Fig. 5B. These results indicate that the paper-based electrochemical DNA biosensor has potential for detecting HPV type 16 DNA in PCR samples in clinical samples in future work.

4. Conclusions

A novel paper-based electrochemical DNA biosensor was developed and used for the determination of high-risk HPV type 16 using AQ-PNA probe immobilized on a G-PANI/SPCE modified electrode. The AQ-PNA probe was modified with negatively charged amino acids at the C-terminus to enable electrostatic immobilization on the cationic G-PANI electrode. Using SWV, the electrochemical current decreased after hybridization with the complementary target DNA. Under optimal conditions, a linear range of 10–200 nM was obtained and the limit of detection was determined to be 2.3 nM. The proposed DNA sensor also exhibited very high selectivity against non-complementary 14-base oligonucleotides, including HPV types 18, 31 and 33 DNA. Finally, this sensing system was successfully applied to detect the PCR amplified DNA from HPV type 16 positive SiHa cells. As was demonstrated, several features make this highly sensitive ePAD DNA biosensor suited as an alternative tool for the diagnostic screening and detection of cervical cancer. First, the ePAD can provide a low-cost, disposable sensor for this POC application. Second, the immobilization through electrostatic attraction using G-PANI modified electrode is attractive relative to covalent immobilization because of its inherent simplicity. Third, the inkjet printing method for electrode modification process provides the potential for mass production while helping to reduce the variation among individual sensors, which is crucial for disposable sensor.

Acknowledgments

The authors gratefully appreciate the financial supports from Thailand Graduate Institute of Science and Technology (TGIST 01-55-014), the 90th Anniversary of Chulalongkorn University Fund (GCUGR1125582020D) and the Thailand Research Fund (DPG5780002). Also, this research was funded by the Ratchadapisek Sompoch Endowment Fund (2016), Chulalongkorn University (CU-59-008-HR). CSH acknowledges funding from Colorado State University.

Appendix A. Supplementary data

Supplementary data related to this article can be found at <http://dx.doi.org/10.1016/j.aca.2016.11.071>.

References

[1] J.C. Cunningham, N.J. Green, K.M. Crooks, Paper electrochemical device for detection of DNA and thrombin by target-induced conformational switching, *Anal. Chem.* **86** (2014) 6169–6170.

[2] T. Sengsarn, W. Dungsat, O. Chailapakul, W. Laitwattanapaisal, Novel, simple and low-cost alternative method for fabrication of paper-based microfluidic chip by ear-dipping, *Talanta* **85** (2015) 2587–2595.

[3] A. Apthor, M. Jangjai, W. Saangphub, N. Praphairakul, C. Henry, O. Chailapakul, Lab-on-Paper with dual electrochemical/colorimetric detection for simultaneous determination of gold and iron, *Anal. Chem.* **87** (2015) 1727–1732.

[4] W. Dungsat, O. Chailapakul, C.S. Henry, Electrochemical detection for paper-based microfluidics, *Anal. Chem.* **81** (2009) 5821–5826.

[5] J. Meekakunpuan, K. Boelke, E. Nantaphol, P. Teengam, J.A. Adkins, M. Srinivasan, C.S. Henry, Electrochemistry on paper-based analytical devices: a review, *Electroanalysis* **26** (2014) 1429–1446.

[6] C.-M. Ahn, R. T. Howe, Recent developments in electrochemical paper-based analytical devices, *Anal. Methods* **7** (2015) 1951–1960.

[7] Z. Ni, G.A. Nisany, J. Gong, X. Chen, A. Kumar, A.W. Martinez, M. Nanosystems, G.M. Whiteside, Electrochemical sensing on paper-based microfluidic devices, *Lab. Chip* **10** (2010) 427–467.

[8] J. Adkins, K. Boelke, C. Henry, Electrochemical paper-based microfluidic devices, *Electrophoresis* **36** (2015) 1811–1824.

[9] J. Zhang, S. Song, J. Wang, D. Pan, C. Fan, A gold nanoparticle-based electrochrometric DNA sensor for amplified detection of DNA, *Nat. Protoc.* **2** (2007) 2895–2899.

[10] B. Liu, S. Song, G. Wu, L. Wang, Z. Zhang, L. He, C. Fan, Electrochemical

interrogation of DNA molecules on gold surfaces, *Anal. Chem.* **77** (2005) 6475–6480.

[11] T. Garcia, M. Revenga-Parrá, I. Amargo, S. Arana, F. Pallares, E. Lorenzo, Disposable DNA biosensor based on thin-film gold electrodes for selective Salmonella detection, *Sens. Actuators B Chem.* **101** (2012) 9030–9037.

[12] P. Ozkan, P. Kara, K. Kerman, B. Meric, A. Erdem, F. Jelen, P.E. Nielsen, M. Ozsoz, DNA and PNA sensing on mercury and carbon electrodes by using methylene blue as an electrochemical label, *Bioelectrochemistry* **58** (2002) 119–126.

[13] P. Palaska, E. Arifonjati, S. Garosi, Sensitive detection of cyclophosphamide using DNA-modified carbon paste-pentyl graphite and hanging mercury drop electrode, *Talanta* **72** (2007) 1199–1205.

[14] H. Du, S. Guo, L. Tang, Y. Ning, Q. Yao, C.-J. Zhang, Graphene modified electrode for DNA detection via PNA-DNA hybridization, *Sens. Actuators B Chem.* **186** (2013) 563–570.

[15] L. Santiago-Rodríguez, G. Sánchez-Pomales, C.R. Cabrera, Electrochemical DNA sensing at single-walled carbon nanotubes chemically assembled on gold surfaces, *Electroanalysis* **22** (2010) 2817–2824.

[16] Z. Wang, J. Zhang, P. Chen, X. Zhou, Y. Yang, S. Wu, L. Sun, Y. Han, L. Wang, P. Chen, S. Boey, Q. Zhang, B. Liedberg, H. Zhang, Label-free, electrochemical detection of methicillin-resistant staphylococcus aureus DNA with reduced graphene oxide-modified electrodes, *Biosens. Bioelectron.* **26** (2011) 3881–3886.

[17] M. Zhou, Y. Zhai, S. Dong, Electrochemical sensing and biosensing platform based on chemically reduced graphene oxide, *Anal. Chem.* **81** (2009) 5602–5607.

[18] K.S. Kowalsow, M. Fathi, L. Colombo, P.R. Celliere, M.G. Schwab, K. Kim, A roadmap for graphene, *Nature* **499** (2012) 192–200.

[19] W. Choi, T. Jahn, R. Seelaboyina, Y.S. Kang, Synthesis of graphene and its applications: a review, *Crit. Rev. Solid State* **35** (2010) 72–77.

[20] M.A. Allen, V.C. Tung, R.E. Kaner, Honeycomb carbon: a review of graphene, *Chem. Rev.* **110** (2010) 132–145.

[21] J.R. Pates, D.R. Dreyer, C.W. Bielawski, R.S. Ruoff, Graphene-based polymer nanocomposites, *Polymer* **52** (2011) 9–25.

[22] A.K. Geim, K.S. Novoselov, The rise of graphene, *Nat. Mater.* **6** (2007) 183–191.

[23] X.-M. Feng, P.-M. Li, Y.-W. Ma, R.-F. Chen, X.-F. Shi, Q.-F. Song, W. Zhang, Gas-step electrochemical synthesis of graphene-polyaniline composite film and its applications, *Adv. Funct. Mater.* **21** (2011) 2989–2996.

[24] P. Manivel, M. Dhakshinamoorthy, A. Balasubramanian, N. Balakrishnan, D. Mangalaraj, C. Viswanathan, Conducting polyaniline-graphene oxide fibrous nanocomposites: preparation, characterization and simultaneous electrochemical detection of ascorbic acid (Dopamine) and urea acid, *RSC Adv.* **3** (2013) 14428–14433.

[25] N. Ruchira, R. Rangkapan, N. Kothongkham, O. Chailapakul, Novel paper-based electrochemical biosensor using graphene-polyvinylpyrrolidone-polyaniline nanocomposite, *Biosens. Bioelectron.* **52** (2014) 13–19.

[26] J.-D. Qiu, L. Shi, R.-P. Liang, G.-C. Wang, X. H. Guo, Controllable deposition of a platinum nanoparticle ensemble on a polyaniline-graphene hybrid as a novel electrode material for electrochemical sensing, *Chem. Lett.* **18** (2012) 2990–2995.

[27] Y. Ho, H. Yang, Y. Hu, T. Yao, Z. Huang, A novel electrochemical DNA biosensor based on graphene and polyaniline nanowires, *Electrochim. Acta* **56** (2011) 2676–2684.

[28] H. Chang, Y. Yuan, B. Shi, Y. Guan, Electrochemical DNA biosensor based on conducting polyaniline nanotube array, *Anal. Chem.* **78** (2006) 5111–5115.

[29] X. Luo, J. M. Qi, L. G. He, H. H. Huang, Immobilization-free sequence-specific electrochemical detection of DNA using boronic acid-labeled poly(2-vinylpyridine), *Anal. Chem.* **86** (2004) 7341–7346.

[30] M. Egholm, O. Richards, L. Christensen, J. Peterson, S.M. Fodor, S.A. Driver, R.H. Berg, S.K. Kim, E. Nordén, M. Nielsen, PNA hybridizes to complementary oligonucleotides obeying the Watson-Crick hydrogen-bonding rules, *Nucleic Acids Res.* **21** (1993) 566–568.

[31] P.E. Nielsen, M. Egholm, R.H. Berg, O. Richards, Sequence-selective recognition of DNA by strand displacement with a thymine-substituted polythiol, *Science* **297** (2002) 1499–1502.

[32] D. Ozkan, A. Ozdemir, P. Kara, K. Kerman, J. Jozsef, S. Yildirim, G. Sertkan, M. Bascak, Electrochemical detection of hydrogen, nitro, peroxide, amino acids and acetylcholine using an ion-assembly all-enzyme-immobilized porous gold electrode, *Electrochem Commun.* **4** (2003) 796–802.

[33] M. Steichen, S. Dezaem, E. Godfrin, A. Basso-Herman, Label-free PNA hybridization detection using peptide nucleic acids and RNA aptamers on gold electrodes, *Biosens. Bioelectron.* **22** (2007) 2237–2243.

[34] J. Wang, E. Palecek, P.E. Nielsen, L. Shao, X. Guo, H. Sun, J. N. J. Lin, P. H. P. Tan, P.A. M. Farias, Peptide nucleic acid probes for sequence-specific DNA biosensors, *J. Am. Chem. Soc.* **116** (1994) 2667–2670.

[35] E. Glysson, A. Sussanwattat, Hybridization of paraffinyl peptide nucleic acids and DNA: selective base-pairing specificity and direction of binding, *Org. Lett.* **6** (2004) 1897–1900.

[36] Y. Uchizawa, C. Srinivasan, C. Ananthanarayanan, S. Jayaraman, J. Kawakami, T. Yamaguchi, Y. Takaku, I. Vlassara, Peptidomimetic peptide nucleic acid with a β -peptide backbone: a conformationally constrained PNA with unusual hybridization properties, *Anal. DNA PNA RNA* **2** (2011) 90–96.

[37] E. Vlassara, Peptidomimetic PNA with a β -peptide backbone: from development to application, *Acc. Chem. Res.* **46** (2013) 1615–1626.

[38] S. Jaisriya, W. Kiatjarat, N. Kothongkham, W. Saangphub, E. Chailapakul

- T. Vilaivan, O. Chailapakul, Electrochemical detection of human papillomavirus DNA type 16 using a pyrrolidynyl peptide nucleic acid probe immobilized on screen-printed carbon electrodes, *Biosens. Bioelectron.* 54 (2014) 428–434.
- [39] J. Kengphet, S. Jampasa, P. Chaumpluk, O. Chailapakul, T. Vilaivan, Immobilization-free electrochemical DNA detection with anthraquinone-labeled pyrrolidynyl peptide nucleic acid probe, *Talanta* 146 (2016) 316–325.
- [40] N. Jirakitwong, N. Panyan, T. Nuanyai, T. Vilaivan, T. Phantennarat, Pyrrolidynyl peptide nucleic acids immobilised on cellulose paper as a DNA sensor, *RSC Adv.* 5 (2015) 24110–24114.
- [41] Global Burden of Disease Cancer Collaboration, The Global Burden of Cancer 2013, *JAMA Oncol.* 1 (2015) 505–527.
- [42] C. Karuwán, C. Suprachabwong, A. Wongsawat, D. Phokharatkul, P. Sritongkhon, A. Tuantanon, Inkjet-printed graphene-poly(3,4-ethylenedioxythiophene)/poly(styrene-sulfonate) modified on screen printed carbon electrode for electrochemical sensing of salbutamol, *Sens. Actuatur B Chem.* 161 (2012) 549–555.
- [43] M.M. Mendole, J. Cunningham, K. Koehler, J. Volckens, C.S. Henry, Microfluidic paper-based analytical device for particulate metals, *Anal. Chem.* 84 (2012) 4474–4480.
- [44] Y. Lu, W. Shi, J. Qin, B. Liu, Fabrication and characterization of paper-based microfluidics prepared in nitrocellulose membrane by wax printing, *Anal. Chem.* 82 (2010) 329–335.
- [45] C. Bardpho, P. Kaitanarat, W. Sangprad, O. Chailapakul, Ultra-high performance liquid chromatographic determination of antioxidants in teas using inkjet printed graphene-polyaniline electrode, *Talanta* 148 (2016) 672–679.
- [46] A. Abi, E.E. Ferapontova, Unmediated by DNA electron transfer in redox-labeled DNA duplexes end-tethered to gold electrodes, *J. Am. Chem. Soc.* 134 (2012) 14499–14507.
- [47] E. Farjami, L. Clima, X. Corbell, E.E. Ferapontova, “Off-on” electrochemical hairpin-DNA-based genosensor for cancer diagnostics, *Anal. Chem.* 83 (2011) 1554–1602.
- [48] D.S. Campos-ferreira, G.A. Nascimento, F.V.M. Souza, M.A. Soares-Mour, M.S. Arruda, D.M.L. Zanforlin, M.H.F. Feres, D. Brunoska, F.L. Lima Filho, Electrochemical DNA biosensor for human papillomavirus 16 detection in real samples, *Anal. Chim. Acta* 804 (2013) 256–263.
- [49] M.H. Fournagh-Azar, M.S. Hejazi, E. Alipour, Developing an electrochemical deoxyribonucleic acid (DNA) biosensor on the basis of human interleukin-2 gene using an electroactive label, *Anal. Chim. Acta* 570 (2006) 134–150.
- [50] L.D. Tran, D.T. Nguyen, B.H. Nguyen, G.P. Do, H. Le Nguyen, Development of interdigitated arrays coated with functional polyaniline/MWCNT for electrochemical biodetection: application for human papillomavirus, *Talanta* 85 (2011) 1560–1565.

Oxetin Synthesis

Enantioselective Synthesis of (2*S*,3*S*)-*epi*-Oxetin and Its Incorporation into Conformationally Constrained PyrrolidinyI PNA with an Oxetane BackbonePattarakiat Seankongsuk,^[a] Viwat Vchirawongkwin,^[b] Roderick W. Bates,^[c] Panuwat Padungros,^[a] and Tirayut Vilaivan^{*[a]}

In remembrance of His Majesty King Bhumibol Adulyadej (1927–2016), for his life-time dedication to Thailand.

Abstract: Fmoc-protected (2*S*,3*S*)-*epi*-oxetin was synthesized from (*E*)-4-(benzyloxy)but-2-enal via enantioselective organocatalytic epoxidation, epoxide ring opening with azide, alcohol activation and ring closure, followed by functional-group manipulation in eight steps with 12% overall yield and 94% ee. The amino acid was used as a building block for a new conformationally constrained pyrrolidinyI PNA with an oxetane-containing backbone. The unexpected sensitivity of the oxetane backbone posed considerable synthetic chal-

lenges under standard Fmoc-solid-phase peptide synthesis conditions, and a mechanism for acid-catalyzed degradation was proposed. In addition, the DNA- and RNA-binding properties of the oxetane PNA were investigated. The presence of an oxetane ring decreased the stability of the PNA-DNA and PNA-RNA duplexes when compared to PNA with a cyclobutane-containing backbone, which could be explained by the flattening of the oxetane ring, leading to a suboptimal torsional angle.

Introduction

Peptide nucleic acid (PNA) is a DNA mimic first introduced in 1990s by Nielsen and co-workers.^[1] The original PNA consists of an amide backbone derived from *N*-2-aminoethylglycine (aeg) and DNA bases, hence it is known as aegPNA. AegPNA recognizes DNA and RNA according to Watson–Crick base pairing rules; however, aegPNA-DNA duplexes are more stable, and the binding is more specific than that of natural nucleic acids.^[2] The electrostatically neutral polyamide backbone of PNA contributes to its remarkable nucleic acid binding proper-

ties, as well as to its resistance to proteases and nucleases.^[1] These properties led to various practical uses of PNA especially for diagnostic and therapeutic purposes.^[3]

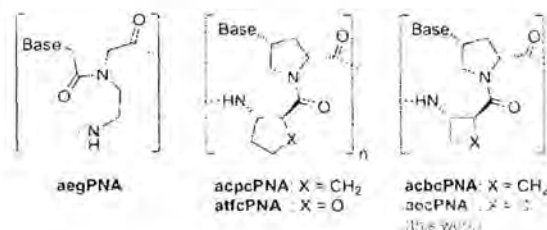
During the past 25 years, several research groups have proposed a number of structural modifications of aegPNA to increase the binding affinities and mismatch discrimination ability even further. One of the most successful approaches is by constraining the flexible backbone of aegPNA by incorporation of cyclic moieties or bulky substituents.^[4] Our laboratory developed a conformationally constrained pyrrolidinyI PNA derived from a nucleobase-modified proline and (1*S*,2*S*)-2-aminocyclopentane carboxylic acid dipeptide backbone (acpcPNA) that exhibited greater DNA binding affinity and specificity than aegPNA (Scheme 1).^[5] The structure and stereochemistry of the cyclic β -amino acid played a critical role in determining the DNA/RNA binding properties of the pyrrolidinyI PNA. For example, pyrrolidinyI PNA with a four-membered ring (1*S*,2*S*)-2-

[a] P. Seankongsuk, P. Padungros, T. Vilaivan
Department of Chemistry
Faculty of Science
Chulalongkorn University
Organic Synthesis Research Unit
Phayathai Road, Patumwan, Bangkok 10330 (Thailand)
E-mail: vtirayut@chula.ac.th

[b] V. Vchirawongkwin
Department of Chemistry
Faculty of Science
Chulalongkorn University
Phayathai Road, Patumwan, Bangkok 10330 (Thailand)

[c] R. W. Bates
Division of Chemistry and Biological Chemistry
School of Physical and Mathematical Sciences
Nanyang Technological University
21 Nanyang Link, Singapore 637371 (Singapore)

Supporting information and the ORCID identification number(s) for the author(s) of this article can be found under <http://dx.doi.org/10.1002/ajoc.201600575>.



Scheme 1. Structures of aegPNA (left), acpcPNA/atfcPNA (middle), and acbcPNA/aocPNA (right).

aminocyclobutanecarboxylic acid backbone (acbcPNA) formed even stronger hybrids with DNA and RNA than acpcPNA.^[6]

Although the affinity and specificity towards recognition of DNA/RNA have been enhanced, practical uses of PNAs are still limited by their poor water solubility and the tendency of non-specific interactions with hydrophobic materials. Ly and co-workers demonstrated that incorporation of polar groups into aegPNA (^RMP-γPNA) via a diethylene glycol side-chain can overcome the hydrophobicity problem without negative effects on PNA-DNA/RNA binding properties.^[7] In our recent work, the hydrophilicity of acpcPNA was enhanced by replacing the cyclopentane ring in acpcPNA with a tetrahydrofuran ring in (2*S*,3*S*)-3-aminotetrahydrofuran-2-carboxylic acid (atfcPNA) while the DNA/RNA binding affinities and sequence specificity were still retained.^[8]

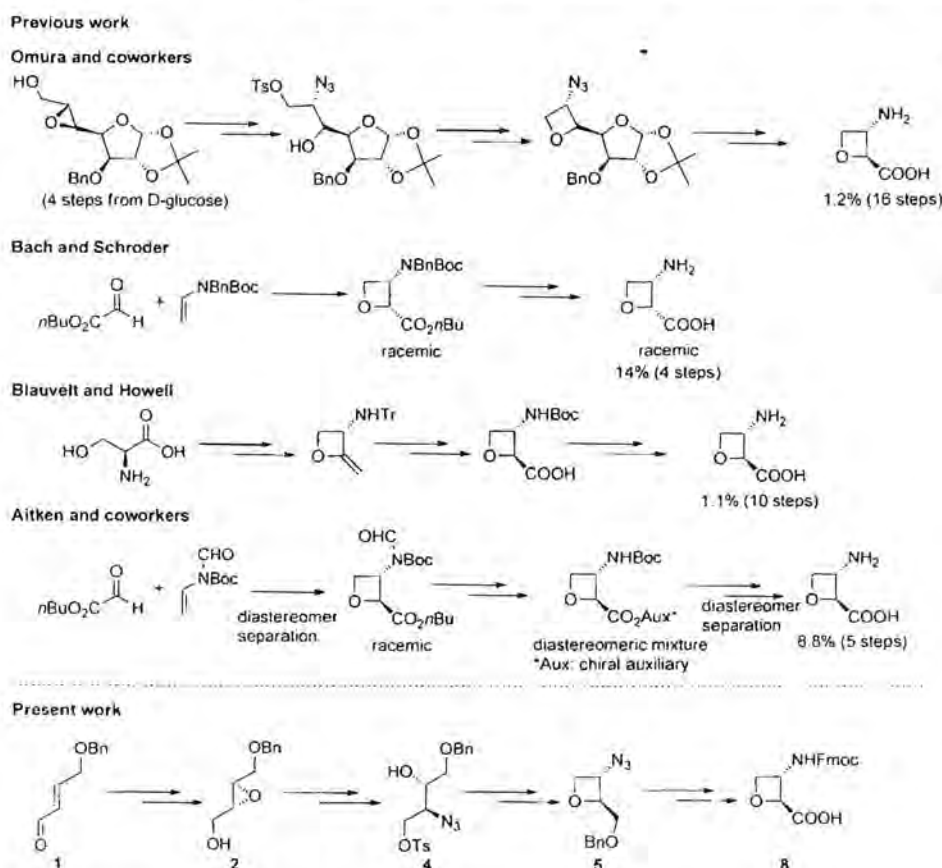
Oxetanes possess unique structural features and reactivities that make them useful as building blocks in medicinal chemistry^[9,10] and as intermediates for organic synthesis.^[11] Considering the beneficial effects of replacing the cyclopentane ring of acpcPNA with a cyclobutane in acbcPNA and with tetrahydrofuran in atfcPNA, herein we propose to combine both modifications into a novel pyrrolidinyl PNA with an oxetane-containing backbone derived from (2*S*,3*S*)-3-aminooxetane-2-carboxylic acid (aoc). The (2*S*,3*S*) enantiomer of the oxetane-containing β-amino acid, which is an epimer of a naturally occurring metabolite known as oxetin,^[12] was required as a building block.

In addition to showing some biological activity,^[12] oxetin, *epi*-oxetin and their ring-substituted derivatives are potentially useful as building blocks for novel foldamers.^[13] In this work, we report a concise enantioselective synthesis of (2*S*,3*S*)-*epi*-oxetin and its incorporation into a new pyrrolidinyl PNA (aocPNA) as well as DNA/RNA binding properties of the new aocPNA.

Results and Discussion

Synthesis of Fmoc-protected (2*S*,3*S*)-*epi*-oxetin

Fmoc-*trans*-(2*S*,3*S*)-*epi*-oxetin **8** is required as a key building block for the synthesis of aocPNA. The (2*S*,3*S*) configuration was chosen in accordance with the configurations of acpcPNA and acbcPNA that had been previously optimized in our research group.^[6] Syntheses of various stereoisomers of oxetin have been described in the literature (Scheme 2).^[12] Omura and co-workers reported the synthesis of all four diastereomers of oxetin by using *D*-glucose as a common precursor.^[14a] However, the syntheses were lengthy, had low stereoselectivity, and were non-atom-economical since only two carbon atoms from glucose remained in the final oxetin molecule. The overall yield of the *trans*-(2*S*,3*S*)-*epi*-oxetin from this 16-step synthesis was 1.2%.^[14a] Bach and Schröder reported the synthesis of racemic *cis*-oxetin via a concise four-step reaction sequence in



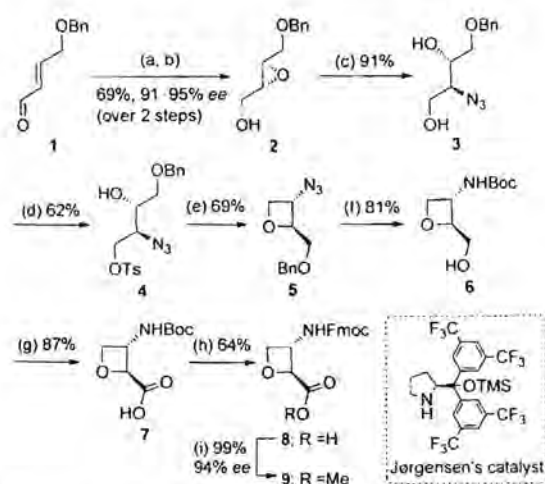
Scheme 2. Previous syntheses of oxetin and *epi*-oxetin, and the synthetic plan for the present work.

14% overall yield via a Paterno–Büchi reaction between butyl glyoxylate and a Boc-protected enamine.^[14b] More recently, Blauvelt and Howell reported a synthesis of (2*S*,3*S*)-*epi*-oxetin starting from ϵ -serine via a 10-step reaction sequence in 1.1% overall yield.^[14c] Very recently, Aitken and co-workers adapted Bach's procedure to synthesize all four stereoisomers of oxetin on gram scale by diastereomeric separation using a chiral oxazolidinone auxiliary, leading to (2*S*,3*S*)-*epi*-oxetin in 8.8% overall yield within a five-step reaction sequence.^[14d]

All of these previously reported syntheses have limitations. Thus, development of a concise enantioselective synthesis of Fmoc-protected (2*S*,3*S*)-*epi*-oxetin **8** is in our interest. The synthetic plan (Scheme 2) relying on the optically pure epoxyalcohol **2** as a key intermediate, is conceptually related to Omura's route.^[14a] However, the number of functional group transformations was shortened considerably by employing an organocatalytic asymmetric oxidation instead of using *D*-glucose as a source of chirality. Regioselective ring opening of the epoxide **2** with a suitable nitrogen nucleophile such as an azide, followed by selective activation of the primary OH group of intermediate **4**, ring closure and straightforward functional group transformation should provide the desired Fmoc-(2*S*,3*S*)-*epi*-oxetin **8**.

Enantioselective synthesis of the chiral epoxyalcohol **2** by catalytic asymmetric epoxidation is well-documented.^[15] While the Sharpless epoxidation has been reported to give the desired epoxide in as high as 97–98% ee,^[5c,d] in our hands it was difficult to achieve this level of enantioselectivity owing to several reaction parameters. Accordingly, we chose a more user-friendly organocatalytic epoxidation route reported by Jørgensen and co-workers in 2005.^[15e] Following the synthetic route outlined in Scheme 3, Jørgensen's organocatalytic epoxidation of (*E*)-4-(benzyloxy)but-2-enal (**1**)^[16] with aqueous hydrogen peroxide in the presence of 10 mol% (*S*)-2-(bis(3,5-bis(trifluoromethyl)phenyl)(trimethylsilyloxy)methyl) pyrrolidine (Jørgensen's catalyst) afforded an unstable epoxyaldehyde intermediate. It was immediately subjected to NaBH₄ reduction without further purification to give the epoxyalcohol **2** in 69% yield over two steps with ee values of 91–95%.^[15e] The absolute configuration was ascertained by comparison of the optical rotation with the literature.^[15a]

The azido moiety was introduced by a B(OMe)₃-mediated regioselective ring opening of the epoxyalcohol **2** with sodium azide to yield the azidoalcohol **3** in 91% yield.^[17] Next, the primary alcohol of **3** was activated in order to create a leaving group for ring closure. Under standard tosylation conditions (1 equiv TsCl, 2.2 equiv Et₃N and catalytic DMAP),^[18] the desired monotosylated **4** was observed in only 38% yield accompanied by 13% yield of ditosylated product. Several monotosylation attempts were performed without success. The best result was obtained only when 2-aminoethyldiphenylborinate (2-ADP) was employed as a catalyst in the presence of diisopropylethylamine (DIEA) as a base.^[19] Thus, in the presence of 10 mol% 2-ADP boron catalyst, the monotosylate intermediate **4** was obtained in 62% yield. Subsequent phase-transfer-catalyzed ring closure under basic conditions in the presence of tetrabutylammonium hydrogen sulfate (TBAHS)^[20] generated



Reagents and conditions: (a) (*S*)-2-(bis(3,5-bis(trifluoromethyl)phenyl)(trimethylsilyloxy)methyl) pyrrolidine (Jørgensen's catalyst, 10 mol%), 30% aq. H₂O₂, CH₂Cl₂, 10–20 °C, 4.5 h; (b) NaBH₄, MeOH, 0 °C, 30 min; (c) NaN₃, B(OMe)₃, DMF, 50 °C, 5 h; (d) TsCl, DIEA, 2-aminoethyl diphenylborinate (2-ADP, 10 mol%), MeCN, RT, 5 d; (e) NaOH, TBAHS (cat), toluene, H₂O, RT, 20 min; (f) Pd(OH)₂/C (cat), H₂ (1 atm), MeOH, Boc₂O, 7 d; (g) DAIB, TEMPO (cat), MeCN, H₂O, RT, 24 h; (h) i. TFA, CH₂Cl₂; ii. FmocOSu, NaHCO₃, MeCN, H₂O, RT, 24 h; (i) CH₂N₂ (generated from Diazald® and NaOH), EtOAc, RT, 30 min.

Scheme 3. Synthesis of Fmoc-(2*S*,3*S*)-*epi*-oxetin **8** starting from (*E*)-4-(benzyloxy)but-2-enal (**1**).

the azido-oxetane intermediate **5** in 69% yield. The remaining steps were straightforward functional group transformations, starting with catalytic hydrogenation to deprotect the benzyloxy ether and to reduce the azide group of **5** to the amino group, which was concomitantly protected in situ with di-*tert*-butyl dicarbonate to give the Boc-protected amino alcohol **6** in 81% yield. The alcohol **6** was then oxidized^[21] to the Boc-protected (2*S*,3*S*)-*epi*-oxetin **7** in 87% yield. Finally, removal of the Boc group followed by Fmoc installation yielded the desired Fmoc-(2*S*,3*S*)-*epi*-oxetin **8** in 64% yield. The ee of **8** was determined by chiral HPLC to be 94% from the corresponding methyl ester **9**, which was obtained by methylation of **8** with diazomethane. In conclusion, the target building block Fmoc-(2*S*,3*S*)-*epi*-oxetin **8** was successfully synthesized from the readily available (*E*)-4-(benzyloxy)but-2-enal (**1**) following an eight-step reaction sequence in 12% overall yield and high optical purity. As Aitken and co-workers reported a quantitative yield on Boc deprotection of Boc-(2*S*,3*S*)-*epi*-oxetin **7** to generate free (2*S*,3*S*)-oxetin,^[14d] the efficiency of the present synthesis of *epi*-oxetin should be calculated from the starting aldehyde **1** to Boc-(2*S*,3*S*)-oxetin **7**. This translated into 19% overall yield, which is higher than those reported by Omura (1.2%),^[12] Blauvelt (1.1%)^[14c] and Aitken (8.8%).^[14d]

Synthesis of aocPNA and its stability issues

For the synthesis of the aocPNA, the carboxylic acid moiety of Fmoc-(2*S*,3*S*)-*epi*-oxetin **8** was converted to a reactive pentafluorophenyl (Pfp) ester immediately, prior to use, by treatment with pentafluorophenyl trifluoroacetate (PfpOTf) in the presence of DIEA.^[6] A representative mix-sequence 10mer aocPNA

was synthesized from the corresponding Fmoc-protected pyrrolidiny PNA monomers (A^{Bz}, T, C^{Bz}, and G^{ibu}) and the Pfp-activated Fmoc-(2S,3S)-*epi*-oxetin **8**. The peptide syntheses were performed via Fmoc-solid phase peptide synthesis (Fmoc-SPSS) on Tentagel[®] 5 RAM resin according to the previously reported protocols for other pyrrolidiny PNAs.^{14,5a,31} The *N*-terminal amino group of the aocPNA was optionally capped by acetylation or benzylation. The overall coupling efficiency, as spectrophotometrically estimated from the final Fmoc deprotection, was 23%, which translates into 93% per coupling step. This value was only slightly lower than those typically obtained with acpcPNA or acbcPNA. In addition, the oxetane-containing aocPNA are much more susceptible towards degradation under both basic and acidic conditions. The nucleobase deprotection was initially performed on 10mer *N*-terminal benzoyl-capped aocPNA (Figure 1). The 10mer aocPNA sequence Bz-GTAGATCACT-LysNH₂ (m/z calcd for $[M+H]^+$ = 3501.4) was treated with 1:1 concentrated aqueous ammonia/dioxane at 60 °C for 12 h, which are standard conditions for other pyrrolidiny PNA deprotections.^{15a)} Unfortunately, these conditions caused extensive degradation of the aocPNA as shown by a very small signal in the MALDI-TOF mass spectrum at the expected m/z of 3501.4 and a series of peaks differing by one unit of proline-aoc "nucleotide" (Figure 1a, Table S1). These fragment peaks did not derive from incomplete coupling otherwise they would have carried an acetyl group from the final capping step. Stepwise degradation of aegPNA¹²⁾ and some pyrrolidiny PNA²³⁾ under basic conditions from the attack of the carbonyl by the free amino group at the *N*-terminus of the PNA is well known. A similar mechanism could also account for the observed degradation of aocPNA, although such degra-

ation had not been observed in related systems such as acpcPNA, atfcPNA and acbcPNA.

We hypothesized that the decomposition might be caused by the harsh deprotection conditions employed, thus milder deprotection and minimization of the reaction time were carried out. Milder deprotection conditions (1:1:2 *tert*-butylamine/MeOH/H₂O at 60 °C)^{12a)} provided better results. With short reaction times (1–2 h), the deprotection was incomplete, as shown by the signal of partially deprotected aocPNA at m/z = 3607.4 (Figure 1b). Extension of the reaction time up to 2.5 h led to some fragmentation of the aocPNA (Figure 1c). Thus, the optimal cleavage time of 2 h was chosen.

In addition to base sensitivity, the aocPNA was also susceptible to the standard trifluoroacetic acid (TFA) treatment required for cleavage of the PNA from the resin, as shown by MALDI-TOF mass spectrometric analyses. The degradation is evidenced on preparative scale whereby a long cleavage time was employed to ensure good recovery of the PNA from the solid support. The sensitivity of aocPNA to TFA was systematically evaluated on aocPNA with uncapped *N*-terminus (m/z calcd for $[M+H]^+$ = 3397.2) (Figure 2). A series of peaks with 18 mass units above the expected m/z of aocPNA were visible even after 10 minutes (Figure 2a) and the +18 m/z peaks became more pronounced, with additional degradation observed after prolonged acid treatment (Figure 2b). Addition of a carbocation scavenger, triisopropylsilane (TIPS), typically used in peptide cleavage mixtures,¹²⁵⁾ could not suppress this side reaction (Figure 2c). However, when a more dilute acid solution (1:1 TFA/CH₂Cl₂) was employed for less than 20 min, no water adducts or degradation was observed (Figure 2d). Prolonging the cleavage process and/or increasing the concentra-

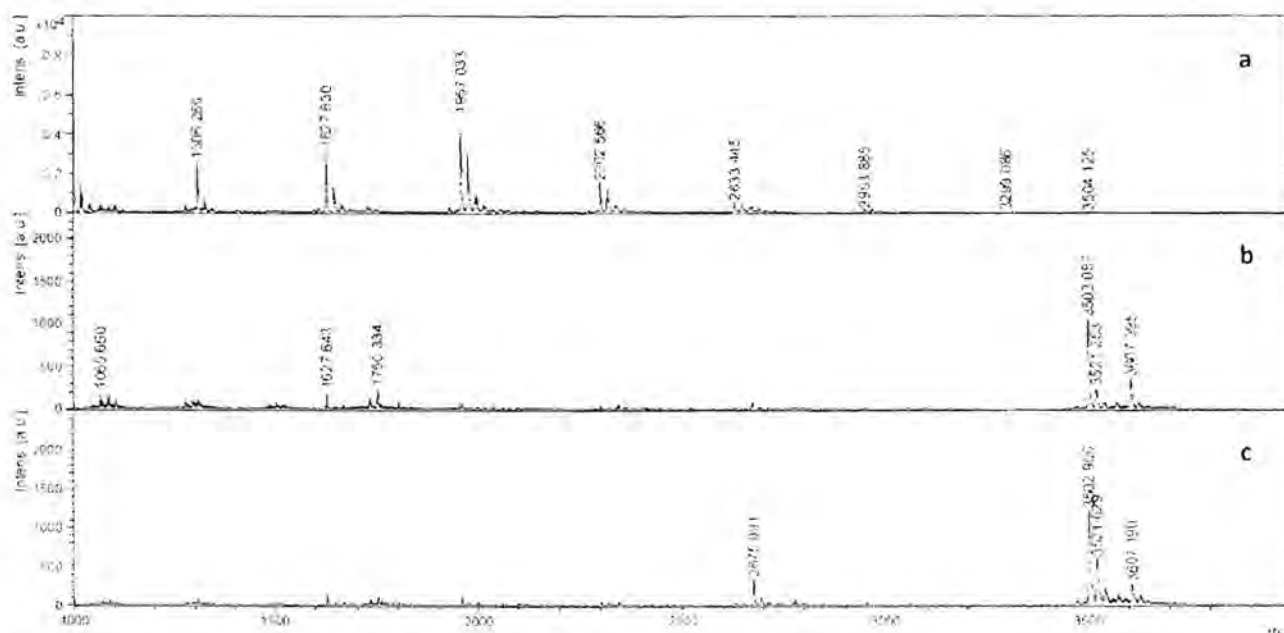


Figure 1. MALDI-TOF mass spectra of aocPNA under basic nucleobase deprotection conditions: a) 1:1 aqueous ammonia/dioxane at 60 °C for 12 h b) 1:1:2 *tert*-butylamine/MeOH/H₂O at 60 °C for 2 h and c) 1:1:2 *tert*-butylamine/MeOH/H₂O at 60 °C for 2.5 h. All PNAs (a–c) were cleaved from the solid support by treatment with TFA for 10 min at room temperature. The 10mer aocPNA in this study was Bz-GTAGATCACT-LysNH₂ (m/z calcd for $[M+H]^+$ = 3501.4).

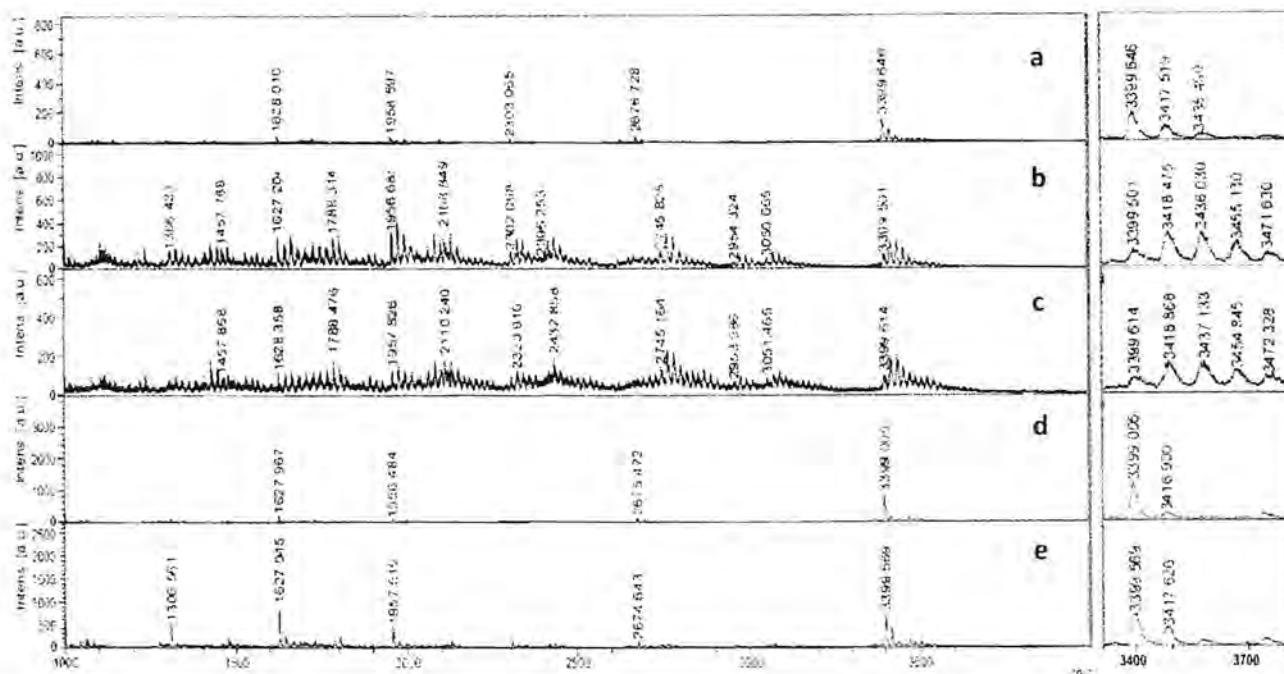


Figure 2. MALDI-TOF mass spectra of aocPNA in optimization of PNA cleavage from the solid support under various conditions: a) TFA at RT for 10 min b) TFA at RT for 3 h c) 1% TIPS in TFA at RT for 3 h d) 1:1 TFA/CH₂Cl₂ at RT for 20 min e) 4:1 TFA/CH₂Cl₂ at RT for 28 min. The 10mer aocPNA in this study was H-GTAGATCACT-LysNH₂ (m/z calcd for $[M+H]^+$ = 3397.2).

tion of TFA resulted in the formation of the +18 m/z peaks and other fragmentation products again (Figure 2e). The cleavage of aocPNA from the solid support was therefore accomplished by multiple treatments with 1:1 TFA/CH₂Cl₂ (2 min for each treatment). The completion of the cleavage was monitored by MALDI-TOF mass spectrometry. The cleavage mixture was immediately dried and precipitated with diethyl ether before being purified by reverse-phase HPLC. By this procedure, new aocPNA sequences H-GTAGATCACT-LysNH₂ (t_R = 25.9 min, m/z calcd for $M+H^+$ 3397.2; found 3397.1) and A-GTAGATCACT-LysNH₂ (t_R = 30.1 min, m/z calcd for $M+H^+$ 3439.3; found 3440.9) were successfully obtained. The low isolated yields (1.2% and 1.3%, respectively) could be attributed to the partial acid-induced degradation, resulting in poor recovery of the PNA during the final cleavage steps in addition to loss during HPLC purification (typical isolated yields of other pyrrolidiny PNA were 10–30%).^[4]

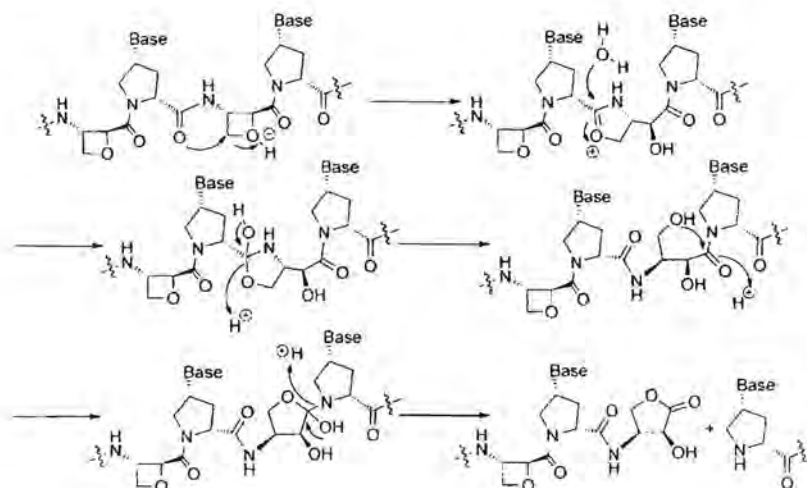
Since acpPNA and acbPNA are completely stable towards TFA treatment, the unprecedented acid sensitivity of aocPNA is proposed to be a direct consequence of the oxetane moiety of aoc in the PNA molecule. The mass increase by 18 m/z units accompanying the degradation products suggests that the aocPNA reacted with adventitious water to form a ring opened product followed by fragmentation. Such acid-catalyzed cleavage processes of oxetane ring are known in the literature,^[9,11,26] although, surprisingly, the Boc-deprotection of **7** by TFA does not result in ring cleavage of the *epi*-oxetane. This, together with the well-documented cases of acid-catalyzed ring opening of oxetane through intramolecular nucleophilic attack^[27] or neighboring group participation,^[28] led to a hypothesis that the ox-

tane ring cleavage in aocPNA was facilitated by the intramolecular attack by the amide carbonyl group. To support this hypothesis, the TFA-catalyzed ring cleavage of racemic *epi*-oxetane (*rac*-10) and its *N*-benzoyl derivative *rac*-12 (Scheme S1, Supporting Information) in D₂O were monitored by ¹H NMR spectroscopy (Figure S17). The results clearly showed that while *rac*-10 was stable in aqueous TFA, decomposition of *N*-benzoyl-*epi*-oxetane *rac*-12 was readily apparent in a matter of hours and was completed over a period of a few days.

Mass spectrometric studies (MALDI-TOF) of the remaining solution after TFA treatment for seven days confirmed the integrity of the acid-treated racemic *epi*-oxetane (*rac*-10, m/z = 117.0). It also confirmed the ring opening of *N*-benzoyl-*epi*-oxetane *rac*-12 by water as shown by the disappearance of the peak of *rac*-12 at m/z = 221.1 and formation of a new peak at m/z 239.1 (Figure S18). The mechanism for the acid-induced fragmentation of aocPNA was proposed as outlined in Scheme 4 based on the susceptibility of *N*-acyl-*epi*-oxetane to undergo amide-bond-assisted hydrolytic ring opening under acidic conditions, together with the fragmentation pattern of the aocPNA after acid treatment (Table S2).

DNA and RNA binding properties of aocPNA

Thermal denaturation experiments were next performed to evaluate the DNA and RNA binding properties of aocPNA by recording the UV absorption at 260 nm as a function of temperature. Sigmoidal melting curves indicated the cooperative binding with DNA and RNA. The stabilities of DNA and RNA hybrids of aocPNA, as shown by the melting temperatures (T_m) in



Scheme 4. A proposed mechanism for the acid-induced fragmentation of aocPNA.

Table 1, are considerably lower than the corresponding hybrids of acbcPNA, acpcPNA and atfcPNA (T_m decrease relative to DNA or RNA hybrids of acpcPNA: -19.8 , -7.0 and -6.2 °C for

should be noted that since the enantiomeric excess of the building block **8** was only 94%, which translated to 97% of the desired (2*S*,3*S*)-enantiomer of *epi*-oxetin, the aocPNA synthesized by repetitive addition of **8** may contain some diastereomeric impurities. However, it was estimated that the 10mer aocPNA should have still contained at least 74% of the desired all-(2*S*,3*S*)-enantiomer and therefore the presence of diastereomeric impurities should not have been the reason for the relatively poor DNA and RNA binding properties of aocPNA.

Table 1. Binding affinities of aocPNA to DNA/RNA compared to previously reported PNAs.

| Entry | X ^(a) | DNA/RNA ^(b) | T_m (°C) | | | |
|----------------|------------------|------------------------|---------------|------------------------|------------------------|------------------------|
| | | | aocPNA | acbcPNA ^(e) | acpcPNA ^(e) | atfcPNA ^(e) |
| 1 ^a | Ac | Dcom | 46.3 | 66.1 | 53.3 | 52.5 |
| 2 | H | Dcom | 46.1 | – | – | – |
| 3 | H | DsmC | > 20 (> 26.1) | 39.8 (26.3) | 23.8 (29.4) | 23.4 (29.1) |
| 4 | H | DsmG | > 20 (> 26.1) | 36.4 (29.7) | 23.9 (29.3) | 23.4 (29.1) |
| 5 | H | DsmT | 28.1 (18.0) | 46.6 (19.5) | 29.4 (23.8) | 25.4 (27.1) |
| 6 | Ac | Rcom | 31.3 | 58.2 | 42.3 | 36.0 |
| 7 | H | Rcom | 30.3 | – | – | – |

[a] aocPNA sequence: X-GTAGATCACT-LysNH₂. [b] DNA/RNA sequence: 5'-d(AGTGYTCTAC)-3'; Y = A (Dcom), C (DsmC), G (DsmG), T (DsmT) and 5'-r(AGUGAUCUAC)-3' (Rcom). [c] condition: 1.0 μM PNA, 1.0 μM DNA/RNA, 10 mM sodium phosphate buffer pH 7.0, 100 mM NaCl. Heating rate 1 °C min⁻¹. [d] values in parentheses are ΔT_m (T_m (complementary)– T_m (mismatch)). [e] Literature data for acetyl-capped PNAs with the same sequence under the same conditions.^{8,10}

Dcom, and -26.9 , -11.0 and -4.7 °C for Rcom, respectively). A strong preference for DNA binding over RNA was still observed similar to other pyrrolidinyl PNAs previously reported (Table 1, entries 1, 6 and 2, 7).^(b) No significant differences were observed in affinities of H-aocPNA and Ac-aocPNA towards complementary DNA and RNA (T_m difference between H-aocPNA and Ac-aocPNA was less than 1.0 °C, entries 1, 2 and 6, 7). The specificity of the DNA and RNA binding of aocPNA was confirmed by the low T_m or absence of melting in the cases of non-complementary hybrids of DNA and aocPNA (ΔT_m 18.0 to >26.1 °C) (Table 1, entries 1, 3–5). These T_m differences are comparable to acbcPNA (ΔT_m range = 19.5 – 29.7 °C), acpcPNA (ΔT_m range = 23.8 – 29.4 °C) and atfcPNA (ΔT_m range = 27.1 – 29.1 °C), which suggests a similar level of mismatch discrimination by aocPNA compared to other pyrrolidinyl PNA systems. It

Theoretical calculations

The effect of cyclobutane and oxetane on the binding affinity was investigated by ab initio calculations of the model compounds shown in Figure 3a. The energy profiles for each structure were computed by the optimized geometry with constraining of the torsional angle, which is the angle between the carbon and the nitrogen atoms bonding to the 4-membered ring, from 80 to 140 degrees with 1-degree steps. The relative energies for each model were then compared with the energy of the local minimum for the corresponding geometry. Figure 3b displays the optimized torsional angle at 95 and 110° for cyclobutane and oxetane amino acid, respectively. These results match with the values obtained from the full optimizations of 95.3 and 110.3° for the respective structures. The torsional angle value of the cyclobutane amino acid is also in good agreement with the value of 95–100° obtained from the X-ray structures of acbc-derived oligomers.⁽²⁰⁾ Since previous computational simulations suggest that the optimal torsional angle in acpcPNA-DNA hybrid was around 99–102°,⁽²⁰⁾ more conformational adjustment was required for the oxetane amino acid than for the cyclobutane amino acid in order to adopt the optimal DNA binding conformation. This may account for the observed lower stability of the aocPNA-DNA hybrids.⁽²¹⁾

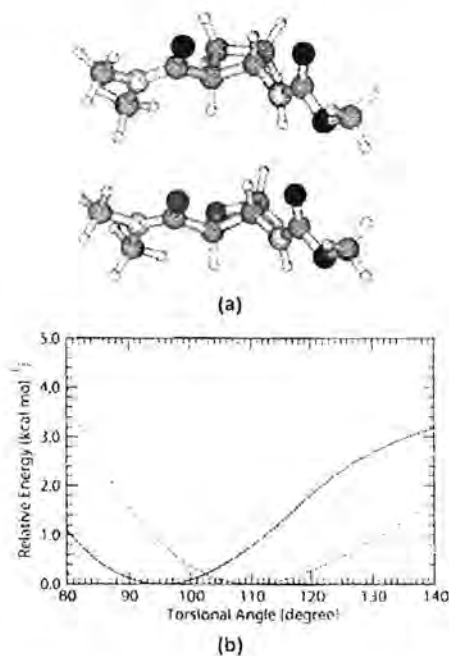


Figure 3. (a) The structures of cyclobutane (top) and oxetane amino acid (bottom) utilized as the models to investigate the torsional energy profiles. (b) Torsional energy profiles of cyclobutane (black line) and oxetane amino acid (red line).

Conclusions

In conclusion, we have reported an efficient and stereoselective synthesis of (2*S*,3*S*)-3-(9*H*-fluoren-9-ylmethoxycarbonylamino)oxetane-2-carboxylic acid [Fmoc-(2*S*,3*S*)-*epi*-oxetin] starting from (*E*)-4-(benzyloxy)but-2-enal in 12% overall yield and 94% ee over 8 steps. The Fmoc-protected (2*S*,3*S*)-*epi*-oxetin was successfully incorporated as a building block for the synthesis of a novel oxetane-containing pyrrolidiny PNA (aocPNA). However, the aocPNA was unstable under both basic and acidic conditions which are required for the nucleobase deprotection and cleavage of the PNA from the solid support, thus leading to low isolated yields. The degradation mechanism under acidic conditions was proposed to involve an amide-group-assisted hydrolysis of oxetane ring followed by cleavage of the amide linkage. The aocPNA binds sequence-specifically to both DNA and RNA, but the binding affinity of aocPNA to DNA and RNA was considerably lower than acbcPNA, acpcPNA and atfcPNA with the same base sequence as a result of a wider torsional angle compared to the optimal value required for the DNA-binding conformation of pyrrolidiny PNA. The information should be useful for future design of conformationally constrained PNA, and suggests that special care should be taken in handling of oxetane-containing foldamers.

Experimental Section

((2*R*,3*R*)-3-(Benzyloxymethyl)oxiran-2-yl)methanol (2). Aqueous hydrogen peroxide (30% w/v, 0.60 mL, 5.20 mmol) was added dropwise to a solution of **1** (0.7102 g, 4.0 mmol) and (5)-2-(bis(3,5-bis(trifluoromethyl)phenyl)(trimethylsilyloxy)methyl)pyrrolidine (Jor-

gensen's catalyst, 0.2300 g, 0.4 mmol) in CH₂Cl₂ (8 mL). The reaction mixture was stirred at 10–20 °C for 4.5 h and monitored by TLC (hexanes/EtOAc = 1:1, *R_f*, 0.29). After reaction completion, the organic layer was separated and the aqueous phase was extracted twice with CH₂Cl₂. The combined extracts was evaporated and re-dissolved in MeOH (8 mL), followed by addition of NaBH₄ (0.1529 g, 4.50 mmol) and stirring at 0 °C for 30 min. The reaction was completed as indicated by TLC (hexanes/EtOAc = 1:1, *R_f*, 0.22). Approximately 2–3 mL of water were added, followed by neutralization with citric acid and evaporated to dryness. The crude mixture was extracted from the residue by CH₂Cl₂ and subjected to column chromatography on silica gel to afford compound **2** as yellow oil (0.5391 g, 2.78 mmol, 69%). The enantiomeric excess was determined to be 91% by chiral HPLC (column: OJ-H chiral column, mobile phase: 15% *i*PrOH in *n*-hexane, flow rate: 0.6 mL min⁻¹, 210 nm, *t_R* major: 36.2 min, *t_R* minor: 41.7 min). [α]_D²³ = +17° (*c* = 0.5 in CHCl₃) ([α]_D²³ = +19.6° (*c* = 0.24 in CHCl₃), [α]_D¹⁵); ¹H NMR (400 MHz, CDCl₃): δ = 7.48–7.26 (m, 5H), 4.60 (ABq, *J*_{AB} = 11.9 Hz, 2H), 3.95 (dd, *J* = 12.7, 1.8 Hz, 1H), 3.79 (dd, *J* = 11.5, 3.0 Hz, 1H), 3.67 (dd, *J* = 12.5, 3.4 Hz, 1H), 3.55 (dd, *J* = 11.5, 5.5 Hz, 1H), 3.26 (dt, *J* = 5.4, 2.7 Hz, 1H), 3.12 ppm (dt, *J* = 4.5, 2.4 Hz, 1H); ¹³C NMR (100 MHz, CDCl₃): δ = 137.8, 128.5, 127.8, 127.7, 73.4, 69.7, 61.2, 55.8, 54.3 ppm; IR (thin film): $\tilde{\nu}$ = 3415, 2921, 2863, 1456, 1280, 1106 cm⁻¹; HRMS (ESI⁺): *m/z* calcd for C₁₁H₁₄O₃+Na⁺ 217.0841 [*M*+Na⁺]; found, 217.0838.

(2*S*,3*S*)-2-Azido-4-(benzyloxy)butane-1,3-diol (3). Trimethyl borate (1.18 mL, 10.5 mmol) was added to a solution of **2** (1.0234 g, 5.3 mmol) and NaN₃ (0.6862 g, 10.6 mmol) in anhydrous DMF (10 mL). The mixture was stirred vigorously under N₂ at 50 °C for 6 h and monitored by TLC (CH₂Cl₂/acetone = 9:1, *R_f*, 0.26). After completion, the reaction was cooled to 0 °C followed by addition of saturated aqueous NaHCO₃ (20 mL) and stirring for 30 min, and then extracted with EtOAc (3 × 20 mL). The combined organic layers were washed with water four times and the solvent was evaporated to obtain compound **3** as a yellow oil (1.1371 g, 4.79 mmol, 91%). [α]_D²³ = +22° (*c* = 1.0 in CHCl₃); ¹H NMR (400 MHz, CDCl₃): δ = 7.38–7.18 (m, 5H), 4.50 (s, 2H), 3.91–3.62 (m, 3H), 3.65–3.33 ppm (m, 3H); ¹³C NMR (100 MHz, CDCl₃): δ = 137.4, 128.6, 128.1, 127.9, 73.6, 71.0, 70.8, 63.9, 62.8 ppm; IR (thin film): $\tilde{\nu}$ = 3404, 2921, 2866, 2096, 1453, 1074 cm⁻¹; HRMS (ESI⁻): *m/z* calcd for C₁₁H₁₅N₃O₃+Na⁻ 260.1011 [*M*+Na⁻]; found, 260.1016.

(2*S*,3*S*)-2-Azido-4-(benzyloxy)-3-hydroxybutyl 4-methylbenzenesulfonate (4). DIEA (0.63 mL, 3.59 mmol) was added to a mixture of **3** (0.5657 g, 2.39 mmol), 2-aminoethyl diphenylborinate (2-ADP, 0.0535 g, 0.24 mmol), TsCl (0.5262 g, 2.76 mmol) and 4 Å molecular sieves (0.0619 g) in anhydrous MeCN (10 mL). The reaction was stirred under N₂ at 0 °C and was allowed to warm up to room temperature and left for 5 days. After the reaction was completed as indicated by TLC (hexanes/EtOAc = 1:1, *R_f*, 0.46), water was added and the mixture was extracted with EtOAc (3 × 20 mL) and evaporated to dryness. The crude reaction product was subjected to column chromatography on silica gel to afford compound **4** as a yellow oil (0.5830 g, 1.49 mmol, 62%). [α]_D²⁴ = -24° (*c* = 1.0 in CHCl₃); ¹H NMR (400 MHz, CDCl₃): δ = 7.74 (d, *J* = 8.2 Hz, 2H), 7.32–7.21 (m, 7H), 4.47 (s, 2H), 4.34 (dd, *J* = 10.6, 2.8 Hz, 1H), 4.06 (dd, *J* = 10.6, 7.4 Hz, 1H), 3.65 (ddd, *J* = 7.7, 7.5, 2.7 Hz, 1H), 3.61–3.54 (m, 1H), 3.53–3.50 (m, 2H), 2.37 ppm (s, 3H); ¹³C NMR (100 MHz, CDCl₃): δ = 145.1, 137.3, 132.7, 130.0, 128.6, 128.1, 128.0, 127.9, 73.6, 70.2, 69.6, 69.5, 61.6, 21.7 ppm; IR (thin film): $\tilde{\nu}$ = 3520, 2924, 2860, 2099, 1453, 1361, 1173 cm⁻¹; HRMS (ESI⁻): *m/z* calcd for C₁₈H₂₁N₃O₅+Na⁻ 414.1100 [*M*+Na⁻]; found, 414.1091.

(2*S*,3*S*)-3-Azido-2-(benzyloxymethyl)oxetane (5). A solution of **4** (1.3543 g, 3.46 mmol) in toluene (35 mL) was added dropwise to

a mixture of NaOH (5.6721 g, 141 mmol), TBAHS (0.1258 g, 0.37 mmol) and water (300 μ L). The reaction was stirred at room temperature for 20 min and monitored by TLC (hexanes/EtOAc 1:3, R_f 0.40). After completion of the reaction, the organic phase was separated, washed three times with water, and evaporated to dryness. The crude product was subjected to column chromatography on silica gel to afford compound 5 as a yellow oil (0.5198 g, 2.37 mmol, 69%). $[\alpha]_D^{25} = +49$ ($c = 1.0$ in CHCl_3); $^1\text{H NMR}$ (400 MHz, CDCl_3): $\delta = 7.43\text{--}7.30$ (m, 5H), 4.82 (m, 1H), 4.77–4.66 (m, 2H), 4.64–4.60 (m, 1H), 4.58–4.51 (m, 2H), 3.69 ppm (dd, $J = 3.5, 0.9$ Hz, 2H); $^{13}\text{C NMR}$ (100 MHz, CDCl_3): $\delta = 137.8, 128.5, 127.8, 127.7, 86.8, 73.8, 73.5, 70.4, 55.5$ ppm; IR (thin film): $\tilde{\nu} = 3062, 3025, 2954, 2929, 2855, 2846, 2102, 1259$ cm^{-1} ; HRMS (ESI $^-$): m/z calcd for $\text{C}_{11}\text{H}_{13}\text{N}_2\text{O}_2 + \text{Na}^+$ 242.0905 $[M + \text{Na}]^+$; found, 242.0901.

tert-Butyl (2S,3S)-2-(hydroxymethyl)oxetan-3-ylcarbamate (6). To a solution of 5 (0.4998 g, 2.28 mmol) in MeOH (3 mL), 10% Pd(OH) $_2$ /C (0.1008 g) and Boc $_2$ O (0.5451 g, 2.50 mmol) were added. The mixture was stirred vigorously under H_2 at room temperature. After the reaction was complete (TLC, EtOAc, R_f 0.44), the catalyst was filtered off and the filtrate evaporated to afford compound 6 as a yellow oil (0.3751 g, 1.85 mmol, 81%). $[\alpha]_D^{25} = -5$ ($c = 0.5$ in CHCl_3) ($[\alpha]_D^{25} = -5$ ($c = 1.0$ in CH_2Cl_2) 11k); $^1\text{H NMR}$ (400 MHz, CDCl_3): $\delta = 5.20$ (brm, 1H), 4.73–4.57 (m, 3H), 4.44 (t, $J = 6.4$ Hz, 1H), 3.86–3.70 (m, 2H), 1.46 ppm (s, 9H); $^{13}\text{C NMR}$ (100 MHz, CDCl_3): $\delta = 155.1, 89.8, 80.5, 74.2, 63.6, 47.3, 28.3$ ppm; IR (ATR): $\tilde{\nu} = 3328, 2973, 2929, 1688, 1530, 1166$ cm^{-1} ; HRMS (ESI $^+$): m/z calcd for $\text{C}_8\text{H}_{13}\text{NO}_4 + \text{Na}^+$ 226.1055 $[M + \text{Na}]^+$; found, 226.1051.

(2S,3S)-3-((tert-Butoxycarbonylamino)oxetane-2-carboxylic acid (7). 2,2,6,6-Tetramethylpiperidine *N*-oxide (TEMPO, 0.0320 g, 0.20 mmol) was added to a solution of 6 (0.1537 g, 0.76 mmol) and (diacetoxyiodo)benzene (DAIB, 0.5453 g, 1.69 mmol) in MeCN/water (1:1, 4 mL). The reaction was stirred at room temperature and monitored by TLC (hexanes/EtOAc 1:3, R_f 0.29). After completion, saturated aqueous NaHCO_3 was added to adjust the pH of the solution to ≈ 9 and the reaction mixture was extracted with Et $_2$ O (3 \times 5 mL). The aqueous phase was acidified with NaHSO_4 and re-extracted with EtOAc (3 \times 5 mL). The combined organic phases were evaporated to afford compound 7 as a yellow oil (0.1422 g, 0.65 mmol, 87%). $[\alpha]_D^{25} = -18$ ($c = 1.0$ in CHCl_3) ($[\alpha]_D^{25} = -36$ ($c = 0.5$ in CHCl_3) 14k); $^1\text{H NMR}$ (400 MHz, CDCl_3): $\delta = 5.60$ (brs, 1H), 5.09 (d, $J = 5.5$ Hz, 1H), 4.84–4.78 (m, 1H), 4.78–4.70 (m, 1H), 4.59 (t, $J = 6.0$ Hz, 1H), 1.48 ppm (s, 9H); $^{13}\text{C NMR}$ (100 MHz, CDCl_3): $\delta = 171.5, 156.1, 84.0, 82.1, 73.8, 49.2, 28.2$ ppm; IR (ATR): $\tilde{\nu} = 3325, 2978, 2926, 1713, 1688, 1524, 1158$ cm^{-1} ; HRMS (ESI $^+$): m/z calcd for $\text{C}_8\text{H}_{13}\text{NO}_4 + \text{Na}^+$ 240.0848 $[M + \text{Na}]^+$; found, 240.0843.

(2S,3S)-3-(((9H-Fluoren-9-yl)methoxy)carbonylamino)oxetane-2-carboxylic acid (8). Compound 7 (0.1322 g, 0.52 mmol) was dissolved in TFA/ CH_2Cl_2 (1:1, 2 mL) and stirred for 15 min followed by evaporation to dryness to give the TFA salt of (2S,3S)-*epi*-oxetan (10). The residue was dissolved in MeCN/H $_2$ O (1:1, 4 mL) containing NaHCO_3 (0.1255 g, 1.49 mmol), followed by addition of Fmoc *N*-hydroxysuccinimide (FmocOSu, 0.1748 g, 0.52 mmol). After stirring at ambient temperature for 20 h, saturated aqueous NaHCO_3 was added and the solution was washed with diethyl ether. The white solid precipitated in the aqueous phase was isolated by filtration and washed with 2 M HCl followed by water, affording compound 7 (0.1131 g, 0.33 mmol, 64%) after drying. m.p. 142–144 $^\circ\text{C}$; $[\alpha]_D^{25} = +20$ ($c = 0.5$ in DMSO); $^1\text{H NMR}$ (400 MHz, $[\text{D}_6]\text{DMSO}$): $\delta = 8.25$ (d, $J = 6.9$ Hz, 1H), 7.90 (d, $J = 7.5$ Hz, 2H), 7.75–7.65 (m, 2H), 7.43 (t, $J = 7.4$ Hz, 2H), 7.34 (t, $J = 7.3$ Hz, 2H), 4.93 (d, $J = 5.3$ Hz, 1H), 4.65–4.55 (m, 2H), 4.45–4.28 (m, 3H), 4.24 ppm (t, $J = 6.3$ Hz, 1H); $^{13}\text{C NMR}$ (100 MHz, $[\text{D}_6]\text{DMSO}$): $\delta = 171.5, 155.1, 143.8, 140.8, 127.6, 127.1, 125.0, 120.1, 83.4, 74.5, 65.6, 49.1, 46.6$ ppm; IR (ATR): $\tilde{\nu} =$

3325, 3065, 3016, 2953, 2888, 1693, 1530, 1262 cm^{-1} ; HRMS (ESI $^+$): m/z calcd for $\text{C}_{19}\text{H}_{17}\text{NO}_5 + \text{Na}^+$ 362.1004 $[M + \text{Na}]^+$; found, 362.1008.

Methyl (2S,3S)-3-(((9H-fluoren-9-yl)methoxy)carbonylamino)oxetane-2-carboxylate (9). A solution of compound 8 (0.0150 g, 0.044 mmol) in EtOAc (0.5 mL) was treated with diazomethane (generated by treatment of Diazald $^{\text{®}}$ (0.0287 g, 0.13 mmol) and 5 M NaOH (0.5 mL)). After 30 min, the reaction was complete as monitored by TLC (hexanes/EtOAc 1:1, R_f 0.34). After flushing off the excess diazomethane with a N_2 stream, the solvent was removed to obtain compound 9 as a white solid (0.0154 g, 0.43 mmol, 99%). The enantiomeric excess was determined to be 94% by chiral HPLC (column: OJ-H chiral column, mobile phase: 70% *i*PrOH in *n*-hexane, flow rate: 1.0 mL min $^{-1}$, 270 nm. t_R minor: 23.1 min, t_R major: 26.8 min). m.p. 157–159 $^\circ\text{C}$; $[\alpha]_D^{25} = -11$ ($c = 0.5$ in CHCl_3); $^1\text{H NMR}$ (400 MHz, CDCl_3): $\delta = 7.69$ (d, $J = 7.5$ Hz, 2H), 7.49 (d, $J = 6.5$ Hz, 2H), 7.33 (t, $J = 7.4$ Hz, 2H), 7.24 (t, $J = 7.3$ Hz, 2H), 5.34 (s, 1H), 4.95 (s, 1H), 4.75 (s, 2H), 4.35–4.50 (m, 3H), 4.13 (t, $J = 6.3$ Hz, 1H), 3.73 ppm (s, 3H); $^{13}\text{C NMR}$ (100 MHz, CDCl_3): $\delta = 170.3, 155.1, 143.6, 141.4, 127.8, 127.1, 124.9, 120.1, 84.4, 76.1, 67.0, 52.5, 49.7, 47.2$ ppm; IR (ATR): $\tilde{\nu} = 3303, 3063, 2954, 2891, 1737, 1695, 1540, 1264$ cm^{-1} ; HRMS (ESI $^+$): m/z calcd for $\text{C}_{19}\text{H}_{17}\text{NO}_5 + \text{Na}^+$ 376.1161 $[M + \text{Na}]^+$; found, 376.1176.

tert-Butyl-2-(Hydroxymethyl)oxetan-3-ylcarbamate (rac-6). Following the same protocol for the synthesis of (2S,3S)-6 using *rac*-2 as the starting material, compound *rac*-6 was obtained as a yellow oil (0.5226 g, 34% over four steps). $^1\text{H NMR}$ (400 MHz, CDCl_3): $\delta = 5.25$ (brs, 1H), 4.73–4.57 (m, 3H), 4.44 (t, $J = 6.3$ Hz, 1H), 3.83–3.65 (m, 2H), 1.45 ppm (s, 9H); $^{13}\text{C NMR}$ (100 MHz, CDCl_3): $\delta = 155.1, 89.8, 80.5, 74.3, 63.5, 47.2, 28.3$ ppm; IR (ATR): $\tilde{\nu} = 3310, 2973, 2927, 1681, 1529, 1168$ cm^{-1} .

Methyl trans-3-(((9H-fluoren-9-yl)methoxy)carbonylamino)oxetane-2-carboxylate (rac-9). Following the same protocol for the synthesis of (2S,3S)-9 starting from *rac*-6, compound *rac*-9 was obtained as a white solid (0.0480 g, 28% over three steps). m.p. 127–129 $^\circ\text{C}$; $^1\text{H NMR}$ (400 MHz, CDCl_3): $\delta = 7.68$ (d, $J = 7.5$ Hz, 2H), 7.49 (d, $J = 6.5$ Hz, 2H), 7.32 (t, $J = 7.4$ Hz, 2H), 7.23 (t, $J = 7.4$ Hz, 2H), 5.44 (d, $J = 6.1$ Hz, 1H), 4.94 (s, 1H), 4.74 (s, 2H), 4.52–4.27 (m, 3H), 4.12 (t, $J = 6.3$ Hz, 1H), 3.72 ppm (s, 3H); $^{13}\text{C NMR}$ (100 MHz, CDCl_3): $\delta = 170.3, 155.1, 143.7, 141.4, 127.8, 127.1, 124.9, 120.1, 84.4, 76.1, 67.0, 52.5, 49.7, 47.2$ ppm; IR (ATR): $\tilde{\nu} = 3302.4, 3066.9, 2951.8, 2886.0, 1734.9, 1697.0, 1541.7, 1262.1$ cm^{-1} ; HRMS (ESI $^-$): m/z calcd for $\text{C}_{19}\text{H}_{17}\text{NO}_5 + \text{Na}^+$ 376.1161 $[M + \text{Na}]^+$; found, 376.1167.

trans-N-(2-(Hydroxymethyl)oxetan-3-yl)benzamide (rac-11). Compound *rac*-6 (0.1002 g, 0.49 mmol) was dissolved in TFA/ CH_2Cl_2 (1:1, 1 mL) and stirred for 15 min. After removing the solvent, the crude reaction product was dissolved in CH_2Cl_2 (5 mL) followed by addition of triethylamine (70 μ L, 0.49 mmol) and Bz $_2$ O (0.1115 g, 0.49 mmol). The reaction was stirred at ambient temperature for 2 h. The reaction mixture was evaporated to dryness and the residue was purified by column chromatography on silica gel to obtain compound *rac*-11 as a colorless oil (0.0636 g, 45%). $^1\text{H NMR}$ (400 MHz, CDCl_3): $\delta = 7.82$ (d, $J = 7.5$ Hz, 2H), 7.54 (t, $J = 7.2$ Hz, 1H), 7.44 (t, $J = 7.5$ Hz, 2H), 7.20 (d, $J = 4.4$ Hz, 1H), 5.05–4.89 (m, 1H), 4.88–4.71 (m, 2H), 4.64 (t, $J = 6.5$ Hz, 1H), 3.85 ppm (qd, $J = 12.1, 3.9$ Hz, 2H); $^{13}\text{C NMR}$ (100 MHz, CDCl_3): $\delta = 167.8, 133.3, 132.1, 128.7, 127.1, 89.6, 73.7, 63.8, 47.4$ ppm; IR (ATR): $\tilde{\nu} = 3378, 3307, 3066, 2908, 1632, 1531, 1027, 953$ cm^{-1} ; HRMS (ESI $^-$): m/z calcd for $\text{C}_{11}\text{H}_{13}\text{NO}_3 + \text{H}^+$ 208.0974 $[M + \text{H}]^+$; found, 208.0998.

trans-3-Benzamidooxetane-2-carboxylic acid (rac-12). A mixture of TEMPO (0.0125 g, 0.35 mmol), *rac*-11 (0.0470 g, 0.23 mmol) and DAIB (0.1778 g, 0.55 mmol) was dissolved in MeCN/water (1:1, 1 mL). The reaction was stirred at room temperature for 72 h. After completion, saturated aqueous NaHCO_3 was added to adjust the

pH of the solution to ≈ 9 and the reaction mixture was extracted with EtOAc (3 \times 5 mL). The aqueous phase was acidified with NaHSO₄ and re-extracted with EtOAc (3 \times 5 mL). The combined organic phases were evaporated to give *rac*-12 as a colorless oil (0.0160 g, 44%). ¹H NMR (400 MHz, [D₆]DMSO): δ = 9.31 (d, *J* = 7.3 Hz, 1H), 7.90 (d, *J* = 7.4 Hz, 2H), 7.58 (t, *J* = 7.2 Hz, 1H), 7.51 (t, *J* = 7.4 Hz, 2H), 5.12 (d, *J* = 6.5 Hz, 1H), 5.08–4.99 (m, 1H), 4.69 (dd, *J* = 7.6, 6.2 Hz, 1H), 4.57 ppm (dd, *J* = 6.5, 6.1 Hz, 1H); ¹³C NMR (100 MHz, [D₆]DMSO): δ = 171.5, 165.9, 133.5, 131.6, 128.4, 127.3, 83.1, 74.5, 47.8 ppm; IR (ATR): $\tilde{\nu}$ = 3321, 3071, 2935, 2851, 1777, 1645, 1536, 970 cm⁻¹; HRMS (ESI+): *m/z* calcd for C₁₁H₁₁NO₆+H⁺ 222.0766 [*M*+H]⁺; found, 222.0782.

Synthesis of aocPNA

A representative mixed-sequence 10mer aocPNA was synthesized manually via Fmoc-solid-phase peptide synthesis (Fmoc-SPSS) on TentaGel³ S RAM resin on a 1.5 μ mol scale from the four Fmoc-protected pyrrolidinyl PNA monomers (A^{1c}, T, C^{2c} and G^{3m})^[5a] and the Pfp-activated *epi*-oxetin **8** following the previously reported protocols for other pyrrolidinyl PNAs.⁴ After completion, the *N*-terminal Fmoc was removed and the PNA was optionally capped by acetylation. Then, the aocPNA was treated with *tert*-butylamine/MeOH/H₂O (1:1:2) at 60 °C for 2 h whilst still attached to the solid support in order to remove the nucleobase protecting groups (Bz and Ibu). Cleavage from the solid support was carried out by a series of 2 min treatments with TFA/CH₂Cl₂ (1:1). The combined cleavage solutions were evaporated to dryness under a stream of nitrogen followed by precipitation with diethyl ether. The crude PNA was purified by reverse phase HPLC (C18 column, 4.6 \times 150 mm, 5 μ , gradient 0.1% TFA in H₂O/MeOH, 90:10, for 5 min, then a linear gradient to 10:90 over 60 min, flow rate: 0.5 mL min⁻¹, 270 nm). Fractions with the correct *m/z* according to MALDI-TOF analyses were neutralized with ammonium bicarbonate in order to minimize decomposition of aocPNA. Lastly, the combined fractions were freeze dried. The purity of the purified PNA was ascertained by reverse phase HPLC analysis (C18 column, 4.6 \times 50 mm, 3 μ , gradient 0.1% TFA in H₂O/MeOH, 90:10, for 5 min, then a linear gradient to 10:90 over 30 min, flow rate 0.5 mL min⁻¹).

Computational details

(1*S*,2*S*)-*N*-methoxycarbonyl-2-aminocyclobutanecarboxylic acid dimethylamide and (2*S*,3*S*)-*N*-methoxycarbonyl-2-aminoxetanecarboxylic acid dimethylamide were selected as model compounds. The effect of cyclobutane and oxetane on the binding affinity was investigated by ab initio calculations. The energy profiles for each structure were computed by using the optimized geometry with constraint of the torsional angle (the angle between the carbon and the nitrogen atoms bonding to the 4-membered ring) from 80 to 140 degrees, with 1-degree steps. All calculations were performed using the Gaussian 09 program package^[22] using a Pople basis set with a diffuse and polarization function on the heavy atoms (6-31+G(d)) at a density functional theory level with a Becke three-parameter hybrid exchange functional and Lee–Yang–Parr correlation functional (B3LYP). The implicit solvent model of conductor-like polarizable continuum model (CPCM) was also included, accounting for the effect of water molecules surrounding these structures.

Acknowledgements

This research is supported financially by The Thailand Research Fund and Chulalongkorn University (DPG5780002, for TV and PP), National Science and Technology Development Agency (NSTDA) (JSTP-06-57-06E, Junior Science Talent Project research grant, for PS) and Graduate School, Chulalongkorn University (Overseas Research Experience Scholarship for Graduate Student, for PS).

Keywords: amino acids · DNA recognition · foldamers · oxygen heterocycles · peptide nucleic acids

- [1] P. E. Nielsen, G. Haaima, *Chem. Soc. Rev.* **1997**, *26*, 73–78.
- [2] M. Egholm, O. Buchardt, L. Christensen, C. Behrens, S. M. Freier, D. A. Driver, R. H. Berg, S. K. Kim, B. Norden, P. E. Nielsen, *Nature* **1993**, *365*, 566–568.
- [3] a) V. V. Demidov, V. N. Potaman, M. D. Frank-Kamenetskii, M. Egholm, O. Buchardt, S. H. Sönnichsen, P. E. Nielsen, *Biochem. Pharmacol.* **1994**, *48*, 1310–1313; b) P. E. Nielsen, *Curr. Opin. Biotechnol.* **2001**, *12*, 16–20.
- [4] T. Vilaivan, *Acc. Chem. Res.* **2015**, *48*, 1645–1656.
- [5] a) T. Vilaivan, C. Srisuwannaket, *Org. Lett.* **2006**, *8*, 1897–1900; b) C. Ananthanawat, T. Vilaivan, V. P. Hoven, X. Su, *Biosens. Bioelectron.* **2010**, *25*, 1064–1069; c) C. Vilaivan, C. Srisuwannaket, C. Ananthanawat, C. Supparpprom, J. Kawakami, Y. Yamaguchi, Y. Tanaka, T. Vilaivan, *Artificial DNA PNA XNA* **2011**, *2*, 50–59.
- [6] W. Mansawaf, C. Vilaivan, A. Balázs, D. J. Aitken, T. Vilaivan, *Org. Lett.* **2012**, *14*, 1440–1443.
- [7] B. Sahu, I. Sacu, S. Rapireddy, K. J. Zanotti, R. Bahal, B. A. Armitage, D. H. Ly, *J. Org. Chem.* **2011**, *76*, 5614–5627.
- [8] P. Sriwarom, P. Padungros, T. Vilaivan, *J. Org. Chem.* **2015**, *80*, 7058–7065.
- [9] J. A. Bull, R. A. Croft, D. A. Davis, R. Doran, K. F. Morgan, *Chem. Rev.* **2016**, *116*, 12150–12233.
- [10] G. Wuitschik, E. M. Carreira, B. Wagner, H. Fischer, I. Parrilla, F. Schuler, M. Rogers-Evans, K. Müller, *J. Med. Chem.* **2010**, *53*, 3227–3446.
- [11] C. A. Malapit, A. R. Howell, *J. Org. Chem.* **2015**, *80*, 8489–8495.
- [12] S. Omura, M. Murata, N. Imamura, Y. Iwai, H. Tanaka, *J. Antibiot.* **1984**, *37*, 1324–1332.
- [13] a) S. F. Barker, D. Angus, C. Taillefumier, M. R. Probert, D. J. Watkin, M. P. Watterson, T. D. W. Claridge, N. L. Hungerford, G. W. J. Fleet, *Tetrahedron Lett.* **2001**, *42*, 4247–4250; b) T. D. W. Claridge, J. M. Goodman, A. Moreno, D. Angus, S. F. Barker, C. Taillefumier, M. P. Watterson, G. W. J. Fleet, *Tetrahedron Lett.* **2001**, *42*, 4251–4255.
- [14] a) Y. Kawahata, S. Takaysuto, N. Ikekawa, M. Murata, S. Omura, *Chem. Pharm. Bull.* **1986**, *34*, 3102–3110; b) T. Bach, J. Schröder, *Liebigs Ann.* **1997**, 2265–2267; c) M. L. Blauvelt, A. R. Howell, *J. Org. Chem.* **2008**, *73*, 517–521; d) A. F. Kassir, S. S. Ragab, T. A. M. Nguyen, F. Charnay-Pouget, R. Guillot, M. Scherrmann, T. Boddart, D. J. Aitken, *J. Org. Chem.* **2016**, *81*, 9983–9991.
- [15] a) M. P. Hayes, P. J. Hatala, B. A. Sherer, X. Tong, N. Zanatta, P. N. Borer, J. Kallmerten, *Tetrahedron* **2001**, *57*, 1515–1524; b) K. C. Nicolaou, R. A. Daines, J. Uenishi, W. S. Li, D. P. Papahatjis, T. K. Chakraborty, *J. Am. Chem. Soc.* **1988**, *110*, 4672–4685; c) J. M. Schomaker, V. R. Pulgam, B. Borhan, *J. Am. Chem. Soc.* **2004**, *126*, 13600–13601; d) G. V. Reddy, R. S. C. Kumar, B. Silva, K. S. Babu, J. M. Rao, *Synlett* **2012**, *23*, 2677–2681; e) M. Marigo, J. Franzen, T. B. Poulsen, W. Zhuang, K. A. Jorgensen, *J. Am. Chem. Soc.* **2005**, *127*, 6964–6965.
- [16] J. Fournier, S. Mathieu, A. B. Charette, *J. Am. Chem. Soc.* **2005**, *127*, 13140–13141.
- [17] M. Sasaki, K. Tanino, A. Hirai, M. Miyashita, *Org. Lett.* **2003**, *5*, 1789–1791.
- [18] J. J. Miller, S. Rajaram, C. Pfaffenroth, M. S. Sigman, *Tetrahedron* **2009**, *65*, 3110–3119.
- [19] D. Lee, C. L. Williamson, L. Chan, *J. Am. Chem. Soc.* **2012**, *134*, 8260–8267.

- [20] H. S. P. Rao, S. P. Senthikumar, *Proc. Indian Acad. Sci. Chem. Sci.* **2001**, *113*, 191–196.
- [21] J. B. Epp, T. S. Widlanski, *J. Org. Chem.* **1999**, *64*, 293–295.
- [22] S. A. Thomson, J. A. Josey, R. Cadilla, M. D. Gaul, C. F. Hassman, M. J. Luzzio, A. J. Pipe, K. L. Reed, D. J. Ricca, R. W. Wieth, S. A. Noble, *Tetrahedron* **1995**, *51*, 6179–6194.
- [23] G. Lowe, T. Vilaivan, *J. Chem. Soc. Perkin Trans. I* **1997**, 555–560.
- [24] R. S. Vinayak, L. G. Lee, K. B. Mullah, B. Rosenblum (Applera Corporation, Foster City, CA), US6835827B2, **2004**.
- [25] D. A. Pearson, M. Blanchette, M. L. Baker, C. A. Gundon, *Tetrahedron Lett.* **1989**, *30*, 2739–2742.
- [26] a) J. G. Pritchard, F. A. Long, *J. Am. Chem. Soc.* **1958**, *80*, 4162–4165; b) H. Xianming, R. M. Kellogg, *Tetrahedron: Asymmetry* **1995**, *6*, 1399–1408.
- [27] a) T. Bach, K. Kather, O. Krämer, *J. Org. Chem.* **1998**, *63*, 1910–1918; b) J. S. Yadav, V. K. Singh, P. Srihari, *Org. Lett.* **2014**, *16*, 836–839.
- [28] a) S. Kanoh, T. Nishimura, K. Ando, H. Senda, H. Ogawa, M. Motoi, *Macromolecules* **1998**, *31*, 7988–7991; b) T. Bach, J. Schröder, *Tetrahedron Lett.* **1997**, *38*, 3707–3710.
- [29] C. Fernandes, S. Faure, E. Pereira, V. Thery, V. Declerck, R. Guillot, D. J. Airken, *Org. Lett.* **2010**, *12*, 3606–3609.
- [30] W. Mansawat, C. Boonlua, K. Siri Wong, T. Vilaivan, *Tetrahedron* **2012**, *68*, 3988–3995.
- [31] The torsional angle of *trans*-oxetin derivative obtained from a recent X-ray structure (ref. 14d) was 123.5°, which confirmed that the conformation of the oxetane β -amino acid is very far from the optimal torsional angle required in acpcPNA-DNA and acbcPNA-DNA duplexes.
- [32] Gaussian 09, Revision C.01, M. J. Frisch, G. W. Trucks, H. B. Schlegel, G. E. Scuseria, M. A. Robb, J. R. Cheeseman, G. Scalmani, V. Barone, B. Mennucci, G. A. Petersson, H. Nakatsuji, M. Caricato, X. Li, H. P. Hratchian, A. F. Izmaylov, J. Bloino, G. Zheng, J. L. Sonnenberg, M. Hada, M. Ehara, K. Toyota, R. Fukuda, J. Hasegawa, M. Ishida, T. Nakajima, Y. Honda, O. Kitao, H. Nakai, T. Vreven, J. A. Montgomery, Jr., J. E. Peralta, F. Ogliaro, M. Bearpark, J. J. Heyd, E. Brothers, K. N. Kudin, V. N. Staroverov, R. Kobayashi, J. Normand, K. Raghavachari, A. Rendell, J. C. Burant, S. S. Iyengar, J. Tomasi, M. Cossi, N. Rega, J. M. Millam, M. Klene, J. E. Knox, J. B. Cross, V. Bakken, C. Adamo, J. Jaramillo, R. Gomperts, R. E. Stratmann, O. Yazyev, A. J. Austin, R. Cammi, C. Pomelli, J. W. Ochterski, R. L. Martin, K. Morokuma, V. G. Zakrzewski, G. A. Voth, P. Salvador, J. J. Dannenberg, S. Dapprich, A. D. Daniels, Ö. Farkas, J. B. Foresman, J. V. Ortiz, J. Cioslowski, D. J. Fox, Gaussian, Inc., Wallingford CT, **2009**.

Manuscript received: December 2, 2016

Revised: January 24, 2017

Accepted Article published: January 24, 2017

Final Article published: February 16, 2017



miR-21 promotes dengue virus serotype 2 replication in HepG2 cells



Sitthichai Kanokudom ^a, Tirayut Vilaivan ^b, Nitwara Wikan ^c, Chutima Thepparit ^c,
Duncan R. Smith ^c, Wanchai Assavalapsakul ^{a,*}

^a Department of Microbiology, Faculty of Science, Chulalongkorn University, Bangkok, 10330, Thailand

^b Organic Synthesis Research Unit, Department of Chemistry, Faculty of Science, Chulalongkorn University, Bangkok, 10330 Thailand

^c Institute of Molecular Biosciences, Mahidol University, Nakornpathom, 73170, Thailand

ARTICLE INFO

Article history:

Received 7 September 2016

Received in revised form

9 February 2017

Accepted 27 March 2017

Available online 30 March 2017

Keywords:

Dengue virus serotype 2 (DENV 2)

HepG2

MicroRNA (miRNA)

miRNA-21 (miR-21)

Anti-miRNA-21 oligonucleotide (AMO-21)

Peptide nucleic acid-21 (PNA-21)

ABSTRACT

Infection with the mosquito transmitted dengue virus (DENV) remains a significant worldwide public health problem. While the majority of infections are asymptomatic, infection can result in a range of symptoms. MicroRNAs (miRNAs) are small non-coding RNAs that regulate gene expression through repression or degradation of mRNAs. To understand the contribution of miRNAs to DENV 2 replication, we screened a number of candidate miRNAs for variations in expression levels during DENV 2 infection of HepG2 (liver) cells. Seven miRNAs were identified as differentially expressed, and one, miR-21, was differentially expressed at all time points examined. Interestingly, miR-21 was also differentially regulated in DENV 2 infection under conditions of antibody dependent enhancement of infection, and in direct Zika virus infection, but not in DENV 4 infection. The role of miR-21 during DENV infection was further examined by treating HepG2 cells with an anti-miR-21 (AMO-21) before DENV infection. The results showed a significant reduction in DENV 2 production, clearly suggesting that miR-21 plays a key role in DENV 2 replication. To further confirm the role of miR-21 in DENV infection, a peptide nucleic acid-21 (PNA-21) construct with a nucleotide sequence complementary to AMO-21, was co-administered with AMO-21 as an AMO-21/PNA-21 complex followed by DENV 2 infection. The results showed that AMO-21 significantly reduced DENV 2 titer, PNA-21 significantly increased DENV 2 titer and the combined AMO-21/PNA-21 showed no difference from non-treated infection controls. Taken together, the results show that miR-21 promotes DENV 2 replication, and this mechanism could serve as a possible therapeutic intervention point.

© 2017 Elsevier B.V. All rights reserved.

1. Introduction

Despite the recent introduction of a vaccine to protect against dengue virus (DENV) infection in selected countries (WHO, 2016), there remains no specific treatment for DENV infection. While the majority of DENV infections are asymptomatic (Runge-Ranzinger et al., 2014), the infection can lead to a range of symptoms from a mild fever to the more severe forms of the disease, dengue hemorrhagic fever and dengue shock syndrome (WHO, 2009). During infection, DENV manipulates the host cell machinery to facilitate its own replication (Walsh and Mohr, 2011) and as such targeting these processes offer the potential for the development of therapeutic agents.

RNA interference (RNAi) is a process by which small, non coding RNA molecules regulate gene expression through either attenuation of mRNA transcription or by targeting mRNAs for degradation (Felekis and Deltas, 2006). Currently, three classes of small RNAs associated with silencing pathways have been described in mammals, namely endogenous small interfering RNAs (endo-siRNAs), piwi-associated RNAs (piRNAs) and microRNAs (miRNAs). The first two classes of small RNAs are primarily involved in the repression of transposons as well as the nucleic acid of viruses (Larnell et al., 2007; Parazi et al., 2008), while the last class of small RNAs in particular regulates cellular gene expression (Felekis et al., 2010). miRNAs are generated through transcription to generate a primary miRNAs (pri-miRNA) that is composed of exonic and intronic regions (Borchert et al., 2006; Lee et al., 2004). The stem loop region of the pri-miRNA is processed by a complex of proteins to yield 70–80 nucleotide stem loop precursor miRNAs (pre-miRNA) (Hann et al., 2004; Landthaler et al., 2004; Lee et al., 2003), which are

* Corresponding author. Department of Microbiology, Faculty of Science, Chulalongkorn University, 254 Phayathai, Pathumwan, Bangkok, 10330, Thailand.
E-mail address: wanchai.assavalapsakul@chula.ac.th (W. Assavalapsakul).

further cleaved by DICER-1 and subsequently recognized by Argonaute protein to form miRNA-RNA Induced Silencing Complexes (miR-RISCs) (Lee et al., 2006; MacRae et al., 2008). The miR-RISC complex subsequently interacts with target sequences such as mRNA transcripts or DNA sequences in gene promoters, in order to modulate gene expression. miRNAs have been shown to modulate processes including cellular development, proliferation, apoptosis, the immune system and host-pathogen interactions (Bartel, 2004; Felekis and Deltas, 2006; Harfe, 2007).

Studies have increasingly shown that miRNAs have functional roles during viral infection. For example, Hepatitis C virus (HCV) infection leads to the induction and extracellular release of miR-122 and miR-885-5p without altering intracellular levels, whereas miR-494 accumulates intracellularly (El-Diwany et al., 2015). Moreover, miR-373 was shown to be significantly upregulated in HCV-infected primary human hepatocytes and HCV-infected liver biopsy specimens, which induces the negative regulation of the type I IFN signaling pathway by suppressing JAK1 and IRF9 (Mukherjee et al., 2015). Interestingly, the knockdown of miR-373 could inhibit HCV replication by up-regulating interferon-stimulated gene expression (Mukherjee et al., 2015). In addition, the up-regulation of miR-146a by Japanese encephalitis virus (JEV) infection in human brain microglial cells contributes to the suppression of NF- κ B activity and disruption of anti-viral JAK-STAT signaling which helps the virus to evade the cellular immune response (Sharma et al., 2015).

Although much attention has been paid to studying the interplay between miRNAs and viral infection, understanding the interaction of human miRNAs and dengue virus infection remains incomplete (Escalera-Cueto et al., 2015; Qi et al., 2013; Wu et al., 2013). Therefore, this work has investigated the differential expression of miRNAs during DENV 2 infection of HepG2 (liver) cells, with the candidate miRNAs being evaluated by RT-qPCR. While several miRNAs showed evidence of regulation during DENV infection, one miRNA, miR-21, showed differential expression at all time points examined. We further evaluated the role of miR-21 during DENV infection and established that miR-21 is a positive regulator of DENV 2 replication.

2. Materials and methods

2.1. Cells and culture conditions

The human liver cancer cell line HepG2 (ATCC[®] HB-8065[™]) was cultured in Dulbecco's modified Eagle's medium-DMEM (HyClone[™] Thermo Scientific, USA) with 10% heat-inactivated fetal bovine serum (FBS; Gibco[™] Invitrogen), at 37 °C, 5%CO₂. The human lung carcinoma epithelial cell line A549 (ATCC[®] CCL-185[™]) was cultured in MEM (HyClone[™] Thermo Scientific, USA) with 5% FBS at 37 °C. The human monocytic cell line U937 (ATCC CRL-1593.2) was cultured in RPMI 1640 medium (RPMI; Gibco[™] Invitrogen) supplemented with 10% FBS. The mosquito cell C6/36 (ATCC[®] CRL-1660[™]) was cultured in MEM (HyClone[™] Thermo Scientific, USA) with 10%FBS at 28 °C. The monkey kidney cell LLC-MK2 (ATCC[®] CCL-7[™]) was cultured in DMEM with 5% FBS at 37 °C, 5%CO₂. All media were supplemented with 100 units/ml of penicillin and 100 μ g/ml of streptomycin (HyClone[™] Thermo Scientific, USA).

2.2. Viruses

Dengue virus serotype 2 (DENV 2) strain 16681 and dengue virus serotype 4 (DENV 4) strain 1036 were propagated in C6/36 at a multiplicity of infection (MOI) of 1 at 28 °C for 6 days (Sakounwatanyoo et al., 2006) after which the culture medium was

centrifuged to remove cell debris and the supernatants were stored as stock virus at –80 °C. The viral titer was determined by plaque assay on LLC-MK2 cells as previously described (Panyasriwanit et al., 2011; Sithisarn et al., 2003). Zika virus (ZIKV) strain SV0010/15 used in this study was obtained from the Armed Forces Research Institute of Medical Sciences (AFRIMS) and The Department of Disease Control, Ministry of Public Health, Thailand. It was passaged 7 times through C6/36 cells.

2.3. Oligonucleotides

The anti-miRNA-21 oligonucleotide (AMO-21) employed in this study was modified at the 2'-OH position to generate 2'-O-methylation in the ribose residue of RNA (Supplementary Table S1, Integrated DNA technologies, Coralville, IA). AMO-21 was resuspended in nuclease-free water to obtain a 10 μ M final concentration stock which was stored at –80 °C until required.

Peptide nucleic acid-21 (PNA-21, Supplementary Table S1) was synthesized as previously described (Vilarvan et al., 2011; Vilarvan, 2015) to obtain 15 nucleotides in length of which all the sequence was identical to the first 15 nucleotides of hsa-miR-21-5p (MIMAT0000076). It was further modified at the N-terminus with a fluorescent label (FAM) to assist detection by fluorescence microscopy. HPLC-purified PNA-21 was subsequently resuspended in nuclease-free water to obtain a 10 μ M final concentration stock which was stored at –80 °C until required.

2.4. miR expression profile during DENV 2 replication

To investigate miR expression profiles, HepG2 cell were cultured and infected with DENV 2 as previously described (Suksumritsarn et al., 2009; Theppart et al., 2004). Briefly, HepG2 cells were seeded into 6-well plates at a density of 10⁶ cells/well and then cultured at 37 °C, 5%CO₂ overnight. Cells were mock infected or infected with DENV 2 at MOI of 10 for 2 h. Then, the culture medium was replaced with fresh medium and cells cultured for 6, 12, 24 and 48 h post infection (h.p.i.). At appropriate time points, all cells were harvested and total RNA extracted using the RiboZol[™] RNA Extraction Reagent (AMRESCO, LCC., USA). RNA was quantified using a Nanodrop 2000 (Thermo Scientific[™], USA) or a Quantity One (BIORAD Laboratory Inc., USA).

To determine miR expression, 150 ng of total RNA was used as the template for synthesizing cDNA with specific primers (Table S1) using RevertAid[™] Premium Reverse Transcriptase (Thermo Fisher Scientific inc., USA) as described by others (Varkonyi-Gaste et al., 2007). miRNAs were amplified with specific primers (Table S1) by quantitative PCR (qPCR) using IQ[™] SYBR Green Supermix (BIORAD Laboratory Inc., USA). The C_T values obtained from RT-qPCR were used to determine relative gene expression using the 2^{- $\Delta\Delta$ C_T} method (Livak and Schmittgen, 2001). All data was normalized against U6 small RNA. All nucleotide sequences of miRNAs are given in the supplementary information (Table S1).

To test the whether the miR-21 expression is specifically induced by DENV 2, two other viruses, DENV 4 and ZIKV were used to infect HepG2 cells at MOI of 20 and A549 cells at MOI of 2, respectively for 24 h following which total RNA was collected and analyzed for miR-21 using RT-qPCR as described above.

To determine whether miR-21 expression was specifically induced by DENV 2 under antibody-dependent enhancement (ADE) of infection, infection of U937 cells was undertaken as previously described (Klomporn et al., 2011). Briefly DENV 2 (16681) at MOI 20 or DENV 4 at MOI 1 was mixed with a 1:200 final dilution of a pan-specific anti-dengue E protein monoclonal antibody (HB114) in RPMI medium and incubated at 4 °C for 1 h with constant agitation. Then, the virus-antibody complexes were added to

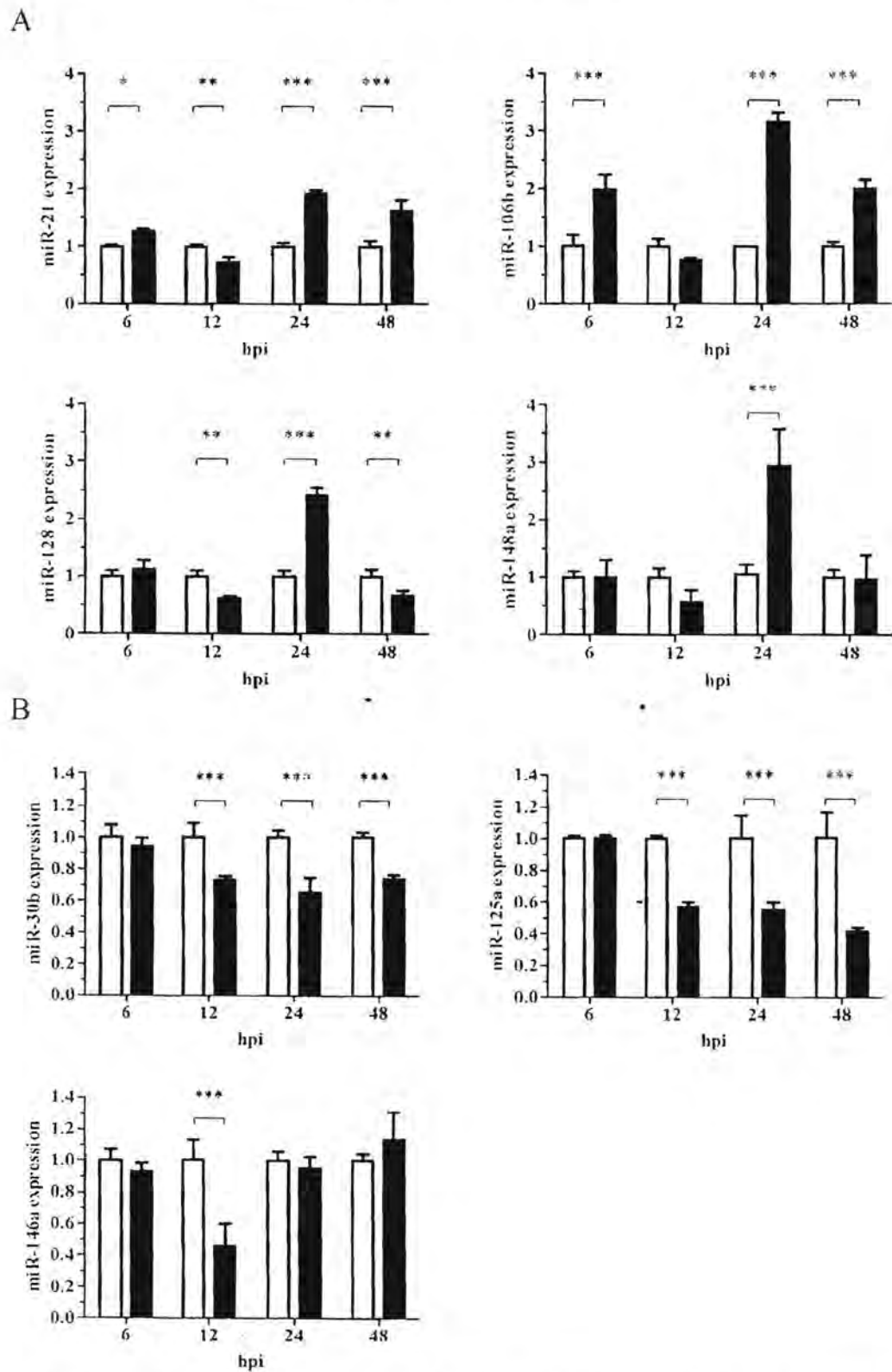


Fig. 1. miRNA expression profile upon DENV 2 infection. HepG2 cells were infected with DENV 2 at MOI of 10 for 6, 12, 24 and 48 h, respectively. miRNA expression was quantitated by RT-qPCR. (A) miRNAs (miR-21, miR-106b, miR-128 and miR-148a) showing up regulation at 24 h.p.i and (B) miRNAs (miR-30b, miR-125a and miR-146a) showing down-regulation at 12 h.p.i. Experiments were undertaken independently in triplicate. Data are shown as means with SD. The p -value < 0.05 (*); p -value < 0.01 (**); p -value < 0.001 (***) were considered to be statistically significant.

2×10^6 U937 cells in RPMI-1640 without FBS and incubated at 37 °C for 2 h with constant agitation. After incubation, the cells were resuspended to a final concentration of 3×10^5 cells/ml in RPMI-1640 supplemented with 10% FBS and further incubated at 37 °C 5% CO₂ until required. At 2 days post-infection, expression of miR-21 was determined by RT-qPCR as described above.

2.5. Nucleic acid binding properties of PNA-21

To ensure the complementary binding of nucleic acid between PNA-21 and AMO-21, AMO-21 alone (A), PNA-21 alone (P) and AMO-21 mixed with PNA-21 (AP) were prepared in culture medium and were analyzed by a gel mobility shift assay using 10% polyacrylamide gel electrophoresis (Das et al., 2012). After electrophoresis, the gel was stained with ethidium bromide.

2.6. Repression of miR-21 expression by AMO-21

To suppress miR-21 in HepG2 cells, reverse transfections were undertaken using the DharmaFECT4 reagent (Thermo Fisher Scientific Inc., USA) according to the manufacturer's protocol. Briefly, the requisite oligonucleotides and 1 μ l of DharmaFECT4 were prepared in 100 μ l of DMEM. All transfections were undertaken in a final volume of 500 μ l with either 100 nM of AMO-21(A), 200 nM of PNA-21(P) or mixture of AMO-21 and PNA-21 (AP). After a 40-min incubation at room temperature, transfection mixtures were added to a suspension of 1×10^5 HepG2 cells, and then the cell-complex mixtures were seeded to single wells of a 24 well-plate and cultured under standard conditions for 24 h. At 24 h post transfection, transfected HepG2 cells were harvested to extract total RNA and to determine the amount of miR-21 using qPCR as described above. In a parallel experiment cytotoxicity of the synthetic oligonucleotides was investigated by 3-(4,5-dimethylthiazol-2-yl)-2,5-diphenyl tetrazolium bromide (MTT) assays.

2.7. Expression of MYD88 and IRAK1 transcripts after miR-21 repression

To investigate whether miR-21 promotes DENV replication directly or indirectly by suppressing the type I interferon response, the expression of myeloid differentiation primary response 88 (MYD88) and Interleukin-1 receptor-associated kinase 1 (IRAK1) was investigated by RT-qPCR. Briefly, 150 ng of total RNA from transfected HepG2 cell was converted to cDNA by using ReverseAid™ Reverse Transcriptase (Thermo Fisher Scientific inc., USA). One microliter of cDNA was used as template to quantitate by qPCR using gene-specific primers (Table S1). The C_T values were normalized with glyceraldehyde-3-phosphate dehydrogenase (GADPH) and determined as previously described.

2.8. Influence of AMO-21 on DENV 2 replication

Approximately 10^5 HepG2 cells were reverse-transfected with appropriate concentrations of transfection mixtures as described above. At 24 h post transfections, the transfected cells were infected with DENV 2 at MOI of 10 for 2 h. At 24 h.p.i., the supernatants were harvested for determination of the DENV titers by standard plaque assay as previously described (Panyasrivanti et al., 2011).

2.9. Fluorescent microscopy

HepG2 cells were either transfected or non-transfected with oligonucleotides as described above (Method 2.7). At 24 h post-transfection, cells were washed twice with PBS. Transfected HepG2 cells were fixed with 4% formaldehyde for 10 min and then

washed twice with PBS. Cells were mounted with anti-fade Mowiol reagent (EMD Chemical Inc, Germany) and observed under a fluorescent microscope.

2.10. Statistical analysis

All analyses were performed using the GraphPad Prism program version 5.03 (GraphPadSoftware Inc., CA). Data were compared by Student's t-test or One-way ANOVA. The *p*-value < 0.05 (*); *p*-value < 0.01 (**); *p*-value < 0.001 (***) were considered to be statistically significant. Results are expressed as means \pm SD from at least three independent replicates.

3. Results

3.1. Regulation of miRNAs in DENV 2 infected HepG2 cells

To identify miRNAs with a possible role in DENV infection, a panel of miRNAs selected based on prior knowledge (miRbase and literature search) were evaluated for amplification from HepG2 cells. A number of candidate miRNAs failed optimization for reasons including multiple bands (e.g. miR-30a, miR-122, miR-155, miR-149, miR-218, and miR-375a) and failure to amplify (e.g. miR-23b and miR-221). However, seven miRNAs, namely miR-21, miR-106b, miR-128, miR-148a, miR-30b, miR-125a and miR-146a all gave optimized amplification profiles. To investigate the expression profile of these miRNAs during DENV infection, HepG2 cells were infected with DENV 2 or mock infected and at 6, 12, 24 and 48 h.p.i. the expression levels of 7 miRNAs assessed by RT-

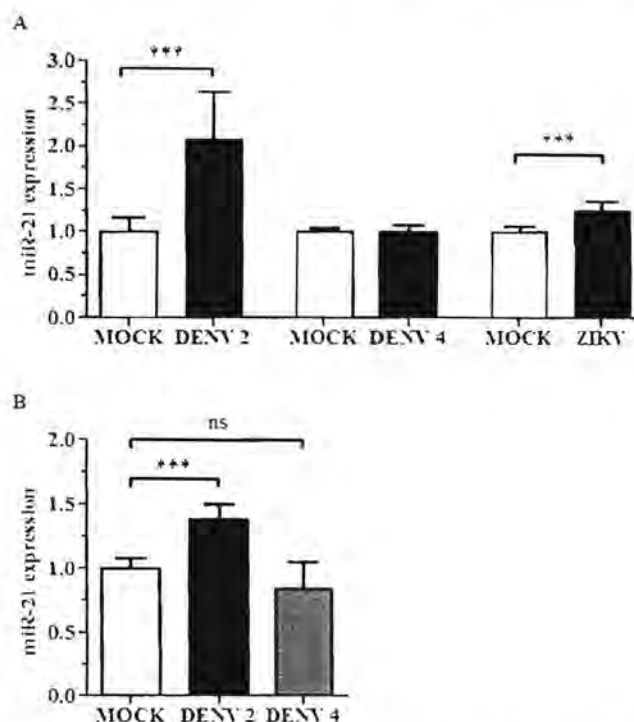


Fig. 2. miR-21 expression profile in different viral infected cells. (A) HepG2 cells were infected with DENV 2 (MOI of 10) or DENV4 (MOI of 20) for 24 h, whereas A549 cells were infected ZIKV (MOI of 2) for 24 h. (B) U937 cells were infected with DENV 2 (MOI of 20) or DENV 4 (MOI of 1) under conditions of ADE of infection for 48 h. miR-21 expression was quantitated by RT-qPCR. Experiments were undertaken independently in triplicate. Data are shown as means with SD. The *p*-value < 0.05 (*); *p*-value < 0.01 (**); *p*-value < 0.001 (***) were considered to be statistically significant.

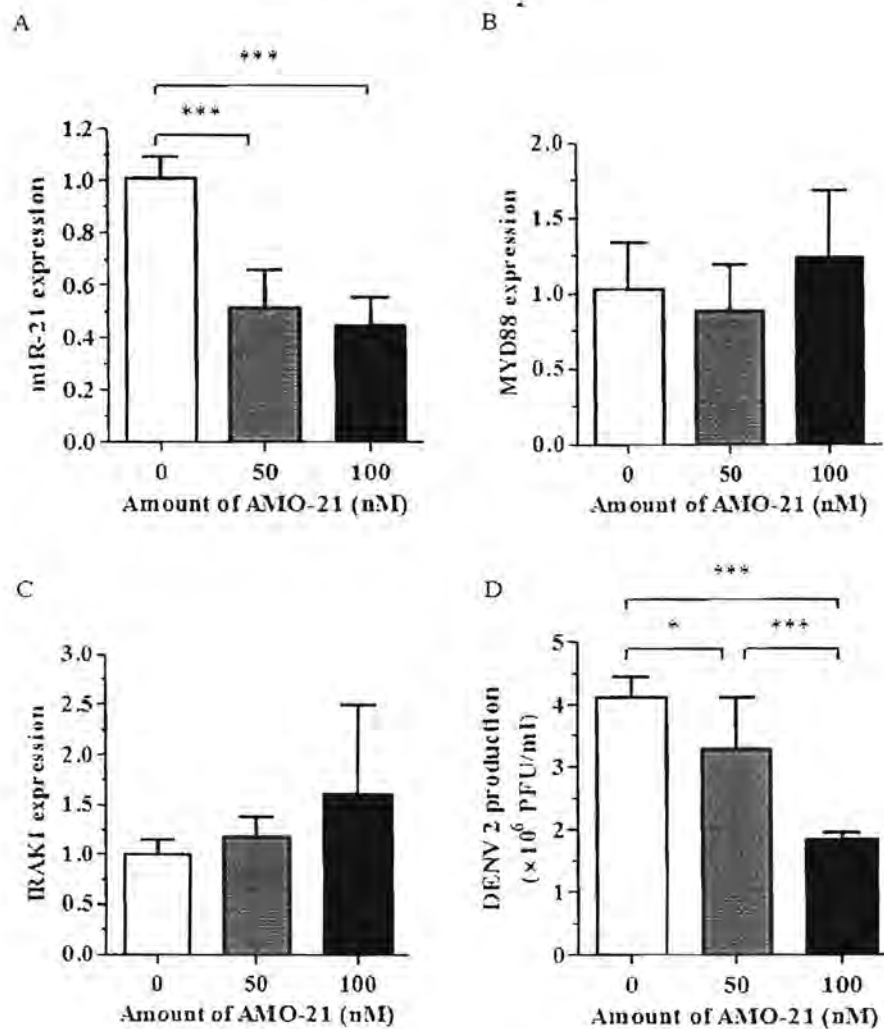


Fig. 3. Inhibition of DENV 2 replication by AMO-21. HepG2 cells were reverse-transfected with AMO-21 (0, 50 and 100 nM) for 24 h before DENV 2 infection. (A) miR-21 expression, (B) MYD88 expression and (C) IRAK1 expression of transfected HepG2 cells were assessed by RT-qPCR. (D) DENV 2 production was assessed by plaque assay. Experiments were undertaken independently in triplicate with duplicate plaque assay. Data are shown as mean with SD. The p -value < 0.05 (*); p -value < 0.01 (**); p -value < 0.001 (***) were considered to be statistically significant.

qPCR. The result revealed that all seven miRNAs were differentially expressed during infection (Fig. 1). The first four miRNAs (miR-21, miR-106b, miR-128 and miR-148a) generally showed up-regulation at 24 h.p.i. (Fig. 1A), while the three remaining miRNA (miR-30b, miR-125a, and miR-146a) were generally down-regulated at 12 h.p.i. (Fig. 1B). Surprisingly, only one miRNA, miR-21, exhibited significant changes in terms of gene expression level at every time point examined (Fig. 1A). Therefore, miR-21 was selected for further investigation into its function during DENV 2 infection.

3.2. Specificity of miR-21 up-regulation by DENV 2

To determine the specificity of the up-regulation of miR-21, total RNA of HepG2 cells infected with DENV 2, DENV 4 and ZIKV was isolated and used as a template for monitoring expression of miR-21. qPCR analysis showed that miR-21 was significantly up-regulated during DENV 2 infection (Fig. 2), consistent with the previous results (Fig. 1A). In ZIKV infection miR-21 was significantly up-regulated, albeit it to a lower extent than DENV 2, while no significant regulation of miR-21 was seen in DENV 4 infection

(Fig. 2A).

To determine whether the specific up-regulation of miR-21 also occur under conditions of ADE infection, U937 cells were infected with DENV 2 and DENV 4 separately under a previously established protocol (Klomporn et al., 2011). Results showed that consistent with direct infection of HepG2 cells, miR-21 was significantly up-regulated in ADE mediated infection of U937 cells during DENV 2 infection, but not in DENV 4 infection (Fig. 2B).

3.3. miR-21 promotes DENV 2 replication

To determine the role of miR-21 during DENV infection, we first established whether an anti-miR-21 oligonucleotide (AMO-21) with a nucleotide sequence complementary to the mature hsa-miR21-5p was able to reduce expression of miR-21. HepG2 cells were therefore transfected with 50 and 100 nM of AMO-21, and the expression of miR-21 quantified at 24 h post-transfection by RT-qPCR. The results showed that transfection with AMO-21 significantly reduced expression of miR-21 by approximately half (Fig. 3A), showing that AMO-21 can suppress miR-21 expression. To

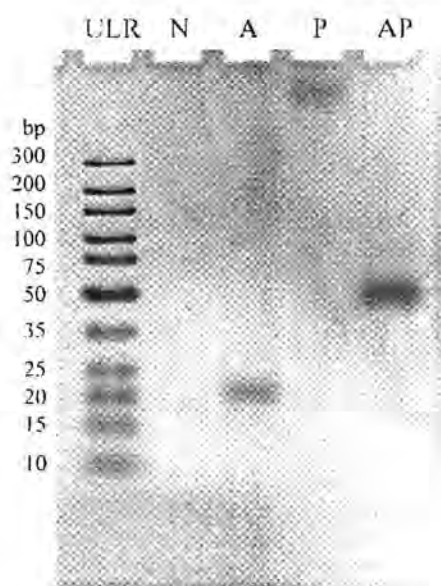


Fig. 4. Nucleic acid binding property of PNA-21. Oligonucleotide medium which used for transfection in HepG2 cells was analyzed by PAGE. lane N is no oligonucleotide control, lane A is 100 nM of AMO-21, lane P is 200 nM of PNA-21 and lane AP is a mixture of AMO-21 and PNA-21.

analyze the expression of possible miR-21 target genes, MYD88 and IRAK1, the relative expression of MYD88 and IRAK1 was measured by using RT-qPCR. Although AMO-21 could suppress miR-21 (Fig. 3A), the MYD88 and IRAK1 transcripts were not significantly changed after transfection in HepG2 cells (Fig. 3B and C, respectively). These results indicated that the MYD88 and IRAK1 are not directly affected as a result of miR-21 repression.

In order to determine if miR-21 is functionally involved in DENV 2 replication, AMO-21-transfected HepG2 cell was infected with DENV 2 in parallel with mock transfected cells, and at 24 h.p.i., the culture media were collected to determine DENV 2 titer by standard plaque assay. As shown in Fig. 3D, viral titers showed a significant and dose-dependent decrease in response to infection in the presence of AMO-21 (Fig. 3D).

3.4. Transfection of AMO-21, PNA-21, and AMO-21/PNA-21 in HepG2

Peptide nucleic acids (PNAs) are polynucleotides where the sugar-phosphate backbone has been substituted with electrostatically neutral peptide backbones (Nielsen, 2010). Many variants of PNA exists, and the PNA used in this work is the conformationally constrained pyrrolidinyl PNA with (2R,4R)-proline-2-aminocyclopentanecarboxylic acid backbone (acpcPNA) that reportedly shows stronger and more specific nucleic acid binding than the original PNA (Vilavain and Srisuwannaket, 2006; Vilavain, 2015). The peptide nucleic acid-21 (PNA-21) was synthesized to have a sequence complementary to AMO-21. To confirm that PNA-21 could hybridize with AMO-21, polyacrylamide gel electrophoresis (PAGE) was used to determine the mobility shift of the AMO-21/PNA-21 hybrid. As shown in Fig. 4, PNA-21 could specifically anneal to AMO-21 as shown by the mobility shift of the band (AP lane) at the position close to 50 bp. We next determined that the AMO-21/PNA-21 complex and PNA-21 *per se* can enter into HepG2 cell after transfection. As shown by fluorescent microscopy, specific internalization of AMO-21/PNA-21 and PNA-21 into HepG2 cells

was observed, while no internalization of AMO-21 alone was seen (Fig. 5A). Additionally, there is no signal observed with either PNA-21 and AMO-21/PNA-21 in the absence of the transfection reagent (Fig. 5B). These results indicated that synthetic PNA-21 can bind to AMO-21 and that the resultant complex can enter into HepG2 cells after transfection.

3.5. Specific inhibition of AMO-21 by PNA-21 in the DENV 2 infected HepG2 cell

To rule out any possibility that the oligonucleotide and the peptide nucleic acids were deleterious to cells, AMO-21 (A), PNA-21 (P), and AMO-21/PNA-21 (AP) were transfected into HepG2 cells, which were then assayed for cell cytotoxicity. The results showed that AMO-21, PNA-21, and AMO-21/PNA-21 did not exert significant cytotoxicity towards HepG2 cells (Fig. 6A). To determine if PNA-21 can specifically inhibit AMO-21, HepG2 cells were transfected with AMO-21, PNA-21, and AMO-21/PNA-21 separately. At 24 h post-transfection, cells were collected and levels of miR-21 quantitated by RT-qPCR. As shown in Fig. 6B, miR-21 expression in AMO-21 treated cells was significantly reduced, whereas miR-21 expression in PNA-21 treated cells was significantly increased. AMO-21/PNA-21 treated cells showed a slight, but non-significant increase in levels of miR-21 (Fig. 6B).

Finally, HepG2 cells transfected either with AMO-21, PNA-21 or AMO-21/PNA-21 were subsequently infected with DENV 2 at MOI 10. At 24 h.p.i., the culture media were collected and virus titer measured by standard plaque assay. Results (Fig. 6C) showed that AMO-21 treatment significantly reduced DENV titer to about 50%, consistent with the reduction in miR-21 expression (Fig. 6B), while PNA-21 significantly increased DENV titer, again consistent with the expression of miR-21. AMO-21/PNA-21 treatment had no significant effect on DENV titer, again consistent with the expression of miR-21 (Fig. 6).

4. Discussion

Since their discovery in *C. elegans* in 1993 (Lee et al., 1993), miRNAs have been shown to regulate a number of biological processes, and more than 2000 human miRNAs have been identified (Friedlander et al., 2014). miRNAs are known to exert their effects through regulation of mRNA translation (Felekis et al., 2010) as well as by interacting with mRNA binding proteins (Czajka and Galardi, 2013) resulting in the modulation of numerous biological processes (Felekis et al., 2010; Harlo, 2005).

The role of miRNAs in DENV infection remains poorly described. Previous studies have shown contradictory mechanisms, with specific miRNAs either enhancing (Wu et al., 2013) or suppressing (Zhu et al., 2014) DENV replication, and expression of specific miRNAs may be either increased (Qi et al., 2013; Wu et al., 2013; Zhu et al., 2014) or decreased (Castillo et al., 2016; Qi et al., 2013) during DENV infection. miRNAs that have been shown to suppress DENV replication include Let-7c (Escalera-Cueto et al., 2015) and miR-30e* (Zhu et al., 2014) which are both up-regulated during DENV infection whereas miR-133a (Castillo et al., 2016) and miR-233 (Wu et al., 2014) are decreased during DENV infection. miR-146a has been shown to be increased in DENV infection and expression facilitates DENV replication (Wu et al., 2013).

In this study we have shown that miR-21 is significantly increased upon DENV 2 infection and that expression of this miRNA promotes DENV replication, similar to the effect of miR-146a (Wu et al., 2013). Despite the limited number of studies of the role of miR-21 in terms of viral infection, our results are in congruence with the results of others as miR-21 was found to be up-regulated in serum from patient infected with DENV 1 (Cuvang et al., 2016),

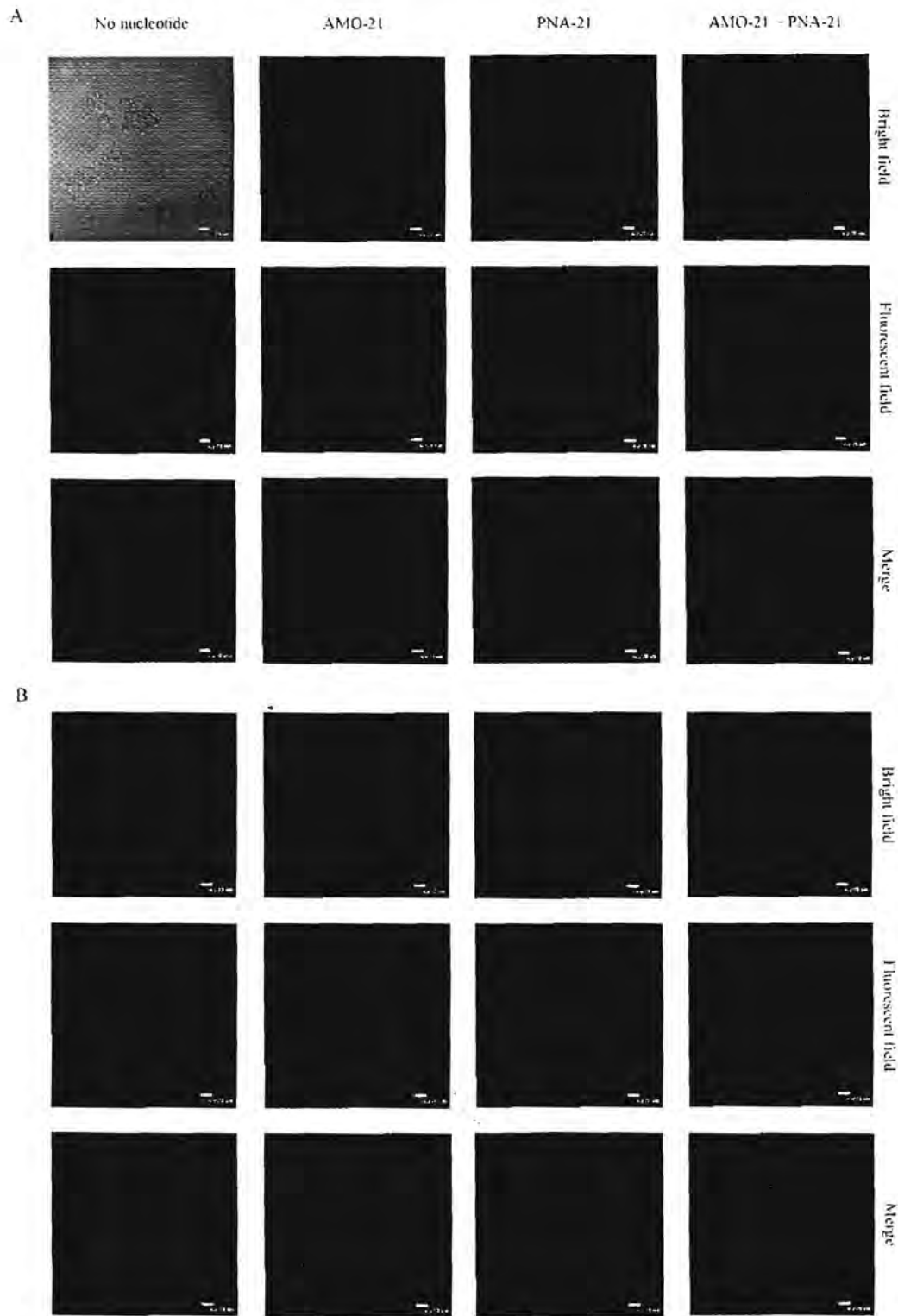


Fig. 5. Fluorescence microscopy of transfected HepG2 cells. HepG2 cells were either transfected (A) or non-transfected (B) with no nucleotide, AMO-21, PNA-21 and AMO-21/PNA-21 complex and were subsequently observed under a fluorescence microscope. Representative images are shown.

Interestingly, miR-21 was shown to be significantly increased in ZIKV infection, but not in DENV 4 infection. Moreover, miR-21 was also shown to be significantly up-regulated in ADE mediated

infection of monocytic U937 cells by DENV 2, but not by DENV 4. This would suggest that miR-21 has a broad involvement in flaviviral infections, but that this can be modulated by virus and strain

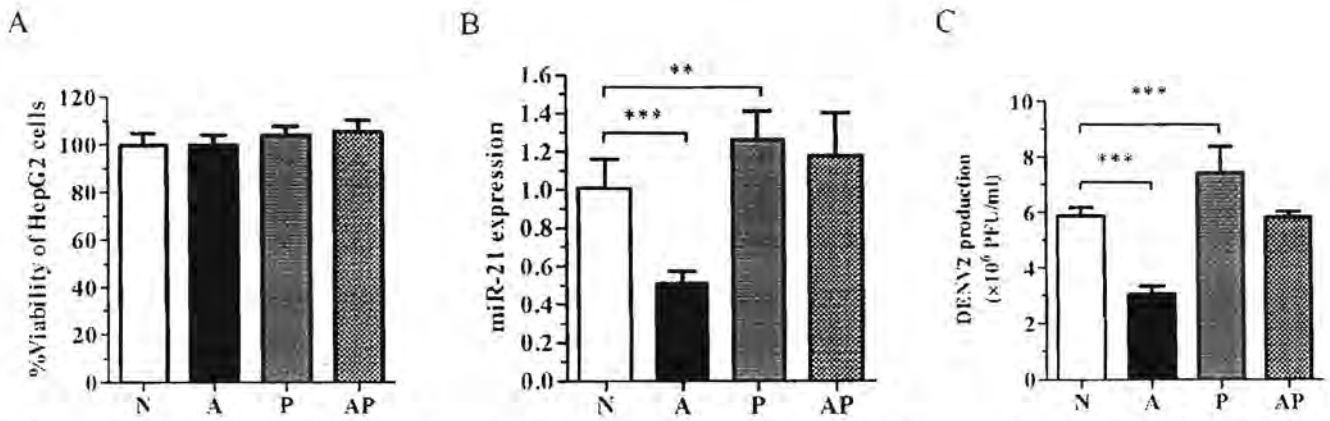


Fig. 6. Influence of miR-21 and AMO-21 on DENV 2 production in HepG2 cells. HepG2 cells were mock transfected (test N), or transfected with 100 nM of AMO-21 (test A), 200 nM of PNA-21 (test P) and a mixture of AMO-21/PNA-21 (test AP), respectively. The percentage viability after treatment (A), miR-21 expression (B) and DENV 2 production (C) were determined. Experiments were undertaken independently in triplicate with duplicate plaque assay. Data are shown as mean with SD. The *p*-value < 0.05 (*); *p*-value < 0.01 (**); *p*-value < 0.001 (***) were considered to be statistically significant.

type factors. Particularly for DENV the specific up-regulation of miR-21 in both primary and secondary DENV 2 infection, but not for DENV 4 under any conditions, may help explain the observed variations in pathogenicity seen between different DENVs (Rico-Hesse et al., 1997).

Recent studies have also shown that higher expression of miR-21 helped HCV mute the innate immune response by modulating IFN- α through inhibition of MYD88 and IRAK1, resulting in increased levels of the virus in the human hepatoma cell line Huh7 (Chen et al., 2013). In contrast, in our study, MYD88 and IRAK1 were not regulated by the repression of miR-21 via transfected AMO-21 in HepG2 cells, suggesting that this pathway is not the primary way in which miR-21 regulates DENV 2 replication in HepG2 cells. In addition to a role in HCV infection, miR-21 levels were significantly increased after infection by EBV, and miR-21 was responsible for facilitating EBV replication through enhancing pAKT expression (Anastasiadou et al., 2015; Rosato et al., 2012).

Previous studies have shown that miRNAs may modulate DENV infection through either directly targeting the DENV genome (Escalera-Cueeto et al., 2015) or by targeting innate immune response genes (Chen et al., 2014; Wu et al., 2013; Zhu et al., 2014). While the mechanism of how miR-21 enhances DENV replication remain unknown, it is possible that miR-21 may directly target NS1 sequences in the DENV 2 genome (Miranda et al., 2006) and Table S2. Interestingly, this particular region of the DENV 2 genome showed 100% conservation in more than 100 DENV 2 isolates when subjected to a BLAST search as of August 2016, reflecting the strong conservation of these sequences. The importance of miRNAs binding to the viral genome and enhancing replication has been described for other viruses. For example, the binding of miR-122 to the 5' region of the HCV genome promotes HCV genome stability and replication (Israelow et al., 2014; Mortimer and Doudna, 2013). In addition, miR-485 binds to the genomic IAV-PB1 of influenza virus in order to promote viral replication (Ingle et al., 2015). Interestingly, we observed that the miR-21 expression level was not affected by a 2 fold increase in the dose of AMO-21 (Fig. 3A), although there was a 50% decrease in the titer of DENV 2 (Fig. 3D), suggesting that AMO-21 could directly affect DENV 2 replication, and additionally given that there is an increase of miR-21 in response to transfection with PNA-21, it is possible that there is an endogenous inhibitor, such as an anti-miR-21 mediating some of the effect.

In summary, we have shown that miR-21 mediates DENV 2

infection by enhancing DENV replication. Knock down of miR-21 with AMO-21 reduced virus replication, suggesting that AMO-21 is a promising antiviral therapeutic agent against DENV infection.

Acknowledgement

This work was financially supported by the Royal Golden Jubilee Ph.D. Program (PHD/0239/2553 to S.K.), the Thailand Research Fund (RSA5580052) to W.A. and (DPG5780002 to T.V.), The Asahi Glass Foundation, Chulalongkorn University Centenary Academic Development Project to W.A.; The 90th Anniversary of Chulalongkorn University, Rachadapisek Sompote Fund and the Office of Higher Education Commission, Ministry of Education. We would like to thank Armed Forces Research Institute of Medical Sciences (AFRIMS) and the Department of Disease Control, Ministry of Public Health, Thailand for providing the Zika virus isolate used in this study.

Appendix A. Supplementary data

Supplementary data related to this article can be found at <http://dx.doi.org/10.1016/j.antiviral.2017.03.020>.

References

Anastasiadou, E., Garg, N., Egi, R., Yada, S., Campese, A.F., Lapenta, C., Pagan, M., Cuomo, L., Botta, A., Belandelli, F., Fran, I., Cecchetti, E., Pignatelli, A., Urra, G., 2015. Epstein-Barr virus infection induces miR-21 in terminally differentiated melanoid B cells. *Int. J. Cancer* 137 (9), 1491–1497.

Boutel, D.P., 2004. MicroRNA: genomic, biogenesis, mechanism, and function. *Curr. Opin. Cell Biol.* 16, 281–295.

Becherer, C.M., Lauer, W., Davidson, B.L., 2005. RNA polymerase II transcribes human miRNAs. *Nat. Struct. Mol. Biol.* 13 (12), 1003–1004.

Carmell, M.A., Guard, A., van de Kerk, H.J., Bourcous, D., Brumm, K.H., de Rooij, D.C., Hannon, G.J., 2007. miR21 is essential for spermatogenesis and repression of transcription in the mouse male germline. *Dev. Cell* 13, 502–514.

Castillo, J.A., Castellón, J.C., Torres, J.M., Betancor, J.V., Sánchez-Céspedes, J.M., Urcuzquiza, J.M., 2010. Complex interaction between dengue virus replication and expression of miR155. *BMC Infect. Dis.* 10, 29.

Chen, R.F., Yang, K.P., Jiao, X., Liu, J.W., Huang, C.H., Liu, G., Chen, Y.H., Chen, C.J., Wang, L., 2016. Augmented miR-155 expression associated with repressed SOCS1 expression involved in dengue haemorrhagic fever. *J. Infect.* 49 (3), 366–374.

Chen, Y., Chen, J., Wang, J., Shi, J., Wu, B., Liu, S., Liu, Y., Wu, J., 2012. Involvement of miR-21 in modulating host immune system by targeting MYD88 and IRAK1. *PLoS Pathog.* 8 (7), e1003348.

Clair, S.A., Galardi, S., 2013. microRNAs and RNA-binding proteins: a complex network of interaction and functional regulation. *Cancer Res.* 73 (1), 624–632.

- Dai, L., Desire, J., Monvar, D., Batsanne, I., Pandey, V.N., Decout, J.L., 2012. A peptide nucleic acid-aminoglycoside conjugate targeting transactivation response element of HIV-1 RNA genome shows a high bioavailability in human cells and strongly inhibits Tat-mediated transactivation of HIV-1 transcription. *J. Med. Chem.* 55 (11), 6021–6032.
- El-Dwany, K., Wasilowski, L., Witwer, K.W., Bailey, J.R., Page, K., Ray, S.C., Cox, A.L., Thomas, D.L., Balagopal, A., 2015. Acute hepatitis C virus infection induces consistent changes in circulating miRNAs that are associated with non-lytic hepatocyte release. *J. Virol.* 89 (18), 9454–9464.
- Escalera-Curiel, M., Medina-Martinez, L., del Angel, R.M., Berumen-Campos, J., Gutierrez-Escobedo, A.L., Yocupicio-Monroy, M., 2015. Let-7c overexpression inhibits dengue virus replication in human hepatoma Huh-7 cells. *Virus Res.* 196, 105–112.
- Farazi, T.A., Juranek, S.A., Tuschl, T., 2008. The growing catalog of small RNAs and their association with distinct Argonaute/Protein family members. *Development* 135 (7), 1201–1214.
- Felekis, K., Delias, C., 2006. RNA interference: a powerful laboratory tool and its therapeutic implications. *Hippokratia* 10 (3), 112–115.
- Felekis, K., Fouvana, E., Stefanou, Ch., Delias, C., 2010. microRNAs: a newly described class of encoded molecules that play a role in health and disease. *Hippokratia* 14 (4), 236–240.
- Friedlander, M.E., Lizano, E., Houben, A.J., Bezdán, D., Banez-Coronel, M., Andia, G., Mateo-Huertas, E., Ragerbauer, B., Gonzalez, J., Chen, K.C., LeProust, E.M., Marz, F., Kristil, A., 2014. Evidence for the biogenesis of more than 1000 novel human microRNAs. *Genome Biol.* 15 (6), R57.
- Han, J., Lee, Y., Yeom, K.H., Kim, Y.K., Jin, H., Kim, V.N., 2004. The Drosha-DGCR8 complex in primary microRNA processing. *Gene Dev.* 18, 3016–3027.
- Hartle, B.D., 2005. MicroRNAs in vertebrate development. *Curr. Opin. Genet. Dev.* 15, 419–425.
- Ingle, H., Kumar, S., Kaur, A.A., Mishra, A., Kulkarni, D.D., Kameyama, T., Takaoka, A., Arua, S., Kumar, H., 2015. The microRNA miR-485 targets hemagglutinin and influenza virus transcripts to regulate antiviral immunity and restrict viral replication. *Sci. Signal* 8 (146), ra126.
- Istaitieh, R., Mullokkandov, G., Agudo, J., Sourrisveanu, M., Bashir, A., Maldonado, A.Y., Dar, A.T., Brown, B.D., Evans, M.J., 2014. Hepatitis C virus genetics affects miR-122 requirements and response to miR-122 inhibitors. *Nat. Commun.* 5, 5408.
- Klemppert, C., Panyasrivant, M., Wikari, N., Smith, D.R., 2011. Dengue infection of monocyte cells activates ER stress pathways, but apoptosis is induced through both extrinsic and intrinsic pathways. *Virology* 409, 188–197.
- Landthaler, M., Yalcin, A., Tuschl, T., 2004. The human Dicer/syndrome critical region gene 8 and its *D. melanogaster* homolog are required for miRNA biogenesis. *Curr. Biol.* 14 (23), 2162–2167.
- Lee, K.C., Feinbaum, R.L., Ambros, V., 1993. The *C. elegans* heterochronic gene *lin-4* encodes small RNAs with antisense complementarity to *lin-14*. *Cell* 75, 843–854.
- Lee, Y., Ahn, C., Han, J., Choi, H., Kim, J., Yim, J., Lee, J., Provost, P., Rådmark, O., Kim, S., Kim, V.N., 2003. The nuclear kinase III Drosha initiates microRNA processing. *Nature* 425 (6956), 415–419.
- Lee, Y., Han, J., Park, S.Y., Kim, Y.K., Suh, M.R., Kim, V.N., 2006. The role of PACT in the RNA silencing pathway. *EMBO J.* 25 (3), 522–532.
- Lee, Y., Kim, M., Han, J., Yeom, K.H., Lee, S., Baek, S.H., Kim, V.N., 2004. MicroRNA genes are transcribed by RNA polymerase II. *EMBO J.* 23 (20), 4051–4060.
- Liak, K.J., Schmittgen, T.D., 2001. Analysis of relative gene expression data using real-time quantitative PCR and the 2^{-ΔΔCt} method. *Methods* 25 (4), 350–355.
- MacRae, I.J., Ma, F., Zhou, M., Robinson, C.V., Doudna, J.A., 2008. In vitro reconstitution of the human RISC-loading complex. *Proc. Natl. Acad. Sci. U.S.A.* 105 (2), 512–517.
- Miranda, K.C., Huynh, T., Tay, Y., Ang, Y.S., Tam, W.L., Thomson, A.M., Lim, B., Kloontjes, L., 2006. A pattern-based method for the identification of microRNA binding sites and their corresponding heteroduplexes. *Cell* 126 (6), 1203–1217.
- Montmercy, S.A., Doudna, J.A., 2013. Unconventional miR-122 binding stabilizes the HIV genome by forming a tripartite RNA structure. *Nucleic Acids Res.* 41 (7), 4280–4290.
- Muchmore, A., Di Biase, A.S., Ray, R.B., 2015. Hepatitis C virus-mediated enhancement of microRNA miR-373 impairs the Ikk-NF-κB signaling pathway. *J. Virol.* 89 (6), 3350–3365.
- Nielsen, P.E., 2010. Peptide nucleic acids (PNAs) in chemical biology and drug discovery. *Chem. Biodivers.* 7 (4), 785–804.
- Onyiah, K., Jiang, X., Gu, D., Zhang, Y., Kong, S.K., Jiang, C., Xie, W., 2010. High-yield serum miRNA profile and promising biomarker in dengue-infected patients. *Int. J. Med. Sci.* 13 (3), 193–205.
- Panyasrivant, M., Greenwood, M.P., Murphy, D., Isidoro, C., Auevarakul, P., Smith, D.R., 2011. Induced autophagy reduces virus output in dengue infected monocyte cells. *Virology* 418 (1), 74–84.
- Qi, Y., Li, Y., Zhang, L., Huang, J., 2013. microRNA expression profiling and bioinformatic analysis of dengue virus infection peripheral blood mononuclear cells. *Mol. Med. Rep.* 7 (3), 791–798.
- Rico-Hesse, R., Harrison, L.M., Salas, R.A., Tovar, J., Szabek, A., Komay, C., Boshell, J., de Mesa, M.L., Nogueira, R.M., da Foz, A.L., 1997. Origins of dengue type 2 viruses associated with increased pathogenicity in the Americas. *Virology* 230, 244–251.
- Rosato, P., Anastasiadou, I., Garg, N., Lewis, D., Roccellato, F., Vincenti, S., Severi, M., Corra, F.M., Bigli, R., Crocchi, M., Ferreri, E., Campese, A.E., Hummel, M., Hain, L., Prestori, C., Eggioni, A., Trivedi, P., 2012. Differential regulation of miR-21 and miR-146a by Epstein-Barr virus-encoded EBNA2. *Leukemia* 26 (11), 2362–2371.
- Runge-Kanzinger, S., McCall, P.J., Kroeger, A., Harsbick, G., 2014. Dengue disease surveillance: an updated systematic literature review. *Trop. Med. Int. Health* 19 (9), 1116–1160.
- Sakonowatanyee, P., Boonsanay, V., Smith, D.R., 2006. Growth and production of the dengue virus in C6/36 cells and identification of a laminin-binding protein as a candidate serotype 2 and 4 receptor protein. *Interferology* 49 (3), 161–172.
- Sharma, N., Verma, R., Kumari, R.L., Basu, A., Singh, S.K., 2017. miR-115a suppresses cellular immune response during Japanese encephalitis virus JAr5582 strain infection in human microglial cells. *J. Neuroinflammation* 12, 30.
- Sitharam, P., Suksanpaisan, I., Theppatt, C., Smith, D.R., 2003. Behavior of the dengue virus in solution. *J. Med. Virol.* 71 (4), 537–539.
- Suksanpaisan, I., Susantad, T., Smith, D.R., 2009. Characterization of dengue virus entry into HepG2 cells. *Biomol. Sci.* 18 (7).
- Theppatt, C., Phooltham, W., Suksanpaisan, I., Smith, D.R., 2006. Internalization and propagation of the dengue virus in human hepatoma HepG2 cells. *Interferology* 47 (2), 78–86.
- Varkonyi-Gasic, F., Wu, R., Wood, M., Walton, T.F., Hollen, K.P., 2007. Protocol: a highly sensitive RT-PCR method for detection and quantification of microRNA. *Plant Methods* 3, 12.
- Vilavain, C., Srisuwannaket, C., Ananthanawan, S., Supapittom, C., Kawakami, J., Yamaguchi, Y., Tanaka, Y., Vilavain, T., 2011. Perroliidynyl peptide nucleic acid with alpha/beta-peptide backbone: a conformationally constrained PNA with unusual hybridization properties. *Artif. DNA RNA XNA* 2 (2), 50–55.
- Vilavain, T., 2015. Perroliidynyl PNA with alpha/beta-dipeptide backbone: from development to applications. *Acc. Chem. Res.* 48 (5), 1643–1656.
- Vilavain, T., Srisuwannaket, C., 2006. Hybridization of perroliidynyl peptide nucleic acids and DNA: selectivity, base-pairing specificity, and direction of binding. *Org. Lett.* 8 (9), 1897–1900.
- Walsh, D., Mohr, I., 2011. Viral subversion of the host protein synthesis machinery. *Nat. Rev. Microbiol.* 9 (12), 860–875.
- World Health Organization, 2009. Dengue: Guidelines for Diagnosis, Treatment, Prevention and Control. New Edition WHO Technical Report Series 1069.
- World Health Organization, 2016. Dengue surveillance: WHO position statement 2016. *Wkly Epidemiol. Rec.* 91 (30), 349–354.
- Wu, N., Gao, N., Fan, D., Wei, J., Zhang, J., An, J., 2015. miR-271 inhibits dengue virus replication by negatively regulating the microtubule destabilizing protein STIM1 in F4H526 cells. *Microbes Infect.* 16 (1), 311–322.
- Wu, S., He, L., Li, Y., Wang, J., Feng, J., Jiang, J., Zhang, P., Huang, X., 2012. miR-146a facilitates replication of dengue virus by dampening interferon induction by targeting TRAF3. *J. Infect.* 67 (4), 339–344.
- Zhu, X., He, Z., Hu, Y., Wen, W., Lin, C., Yu, J., Fan, J., Li, K., Feng, H., Cao, S., Yuan, J., Wu, J., Li, J., Li, M., 2014. MicroRNAs-30c suppresses dengue virus replication by promoting NF-κB-dependent H2A production. *PLoS One* 9 (1), e83884.

Multiplex Paper-Based Colorimetric DNA Sensor Using Pyrrolidinyl Peptide Nucleic Acid-Induced AgNPs Aggregation for Detecting MERS-CoV, MTB, and HPV Oligonucleotides

Prinjaporn Teengam,[†] Weena Siangproh,[‡] Adisorn Tuantranont,[§] Tirayut Vilaivan,^{||} Orawon Chailapakul,^{*,†,¶} and Charles S. Henry^{*,○,§}

[†]Program in Petrochemistry, Faculty of Science, ^{||}Organic Synthesis Research Unit, Department of Chemistry, Faculty of Science, [‡]Electrochemistry and Optical Spectroscopy Research Unit, Department of Chemistry, and [§]National Center of Excellence for Petroleum, Petrochemicals, and Advanced Materials, Chulalongkorn University, Pathumwan, Bangkok, 10330, Thailand

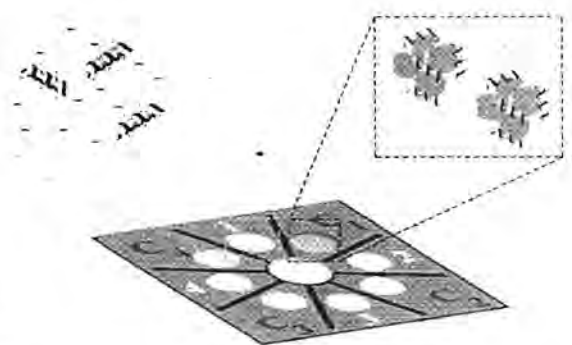
[‡]Department of Chemistry, Faculty of Science, Srinakharinwirot University, Bangkok, 10110, Thailand

[§]Nanoelectronics and MEMS Laboratory, National Electronics and Computer Technology Center, Pathumthani 12120, Thailand

[○]Departments of Chemistry and Chemical and Biological Engineering, Colorado State University, Fort Collins, Colorado 80523, United States

Supporting Information

ABSTRACT: The development of simple fluorescent and colorimetric assays that enable point-of-care DNA and RNA detection has been a topic of significant research because of the utility of such assays in resource limited settings. The most common motifs utilize hybridization to a complementary detection strand coupled with a sensitive reporter molecule. Here, a paper-based colorimetric assay for DNA detection based on pyrrolidinyl peptide nucleic acid (acpcPNA)-induced nanoparticle aggregation is reported as an alternative to traditional colorimetric approaches. PNA probes are an attractive alternative to DNA and RNA probes because they are chemically and biologically stable, easily synthesized, and hybridize efficiently with the complementary DNA strands. The acpcPNA probe contains a single positive charge from the lysine at C-terminus and causes aggregation of citrate anion-stabilized silver nanoparticles (AgNPs) in the absence of complementary DNA. In the presence of target DNA, formation of the anionic DNA-acpcPNA duplex results in dispersion of the AgNPs as a result of electrostatic repulsion, giving rise to a detectable color change. Factors affecting the sensitivity and selectivity of this assay were investigated, including ionic strength, AgNP concentration, PNA concentration, and DNA strand mismatches. The method was used for screening of synthetic Middle East respiratory syndrome coronavirus (MERS-CoV), *Mycobacterium tuberculosis* (MTB), and human papillomavirus (HPV) DNA based on a colorimetric paper-based analytical device developed using the aforementioned principle. The oligonucleotide targets were detected by measuring the color change of AgNPs, giving detection limits of 1.53 (MERS-CoV), 1.27 (MTB), and 1.03 nM (HPV). The acpcPNA probe exhibited high selectivity for the complementary oligonucleotides over single-base-mismatch, two-base-mismatch, and noncomplementary DNA targets. The proposed paper-based colorimetric DNA sensor has potential to be an alternative approach for simple, rapid, sensitive, and selective DNA detection.



Infectious diseases represent a major threat to human health in developed and developing countries alike. DNA alterations contribute to different types of diseases; therefore, the detection of specific DNA sequences plays a crucial role in the development method for early stage treatment and monitoring of genetic-related diseases. DNA diagnostics can provide sequence-specific detection, especially for single-nucleotide polymorphisms (SNPs),¹ which critical for a range of applications including the diagnosis of human diseases and bacterial/viral infections.

Middle East respiratory syndrome (MERS), tuberculosis (TB), and cervical cancers related to human papilloma virus

(HPV) are examples of infectious diseases caused by bacterial and viral infections that benefit greatly from DNA detection. TB is an infectious disease caused by mycobacteria, usually *M. tuberculosis* (MTB) in humans.² HPV has been shown to be a major cause of cervical cancer.³ Middle East Respiratory Syndrome coronavirus (MERS-CoV) has recently emerged as an infectious disease with a high fatality rate in humans.⁴

Received: January 20, 2017

Accepted: April 10, 2017

Published: April 10, 2017

Diagnostic methods developed for these infectious diseases include reverse transcription polymerase chain reaction (RT-PCR) for MERS-CoV,⁷ sputum smear microscopy, culture of bacilli, and molecular species diagnostics for MTB¹⁰⁻¹¹ and Digene Hybrid Capture assay (HC2) and Pap smear test for HPV.^{12,13} While these techniques have been used for successful detection, they are difficult to implement in point-of-care clinical diagnostics particularly in developing countries lacking specialized medical facilities and skilled personnel. Therefore, simple, rapid, low-cost, and highly accurate on-site diagnostic platforms amenable to nucleic acid detection remain a challenge for early detection of infectious diseases for better patient management and infection control. Although DNA amplification is still needed with the current method to provide high sensitivity, we seek to further improve selectivity and assay

simplicity to give immediate and quantitative responses in resource limited settings.

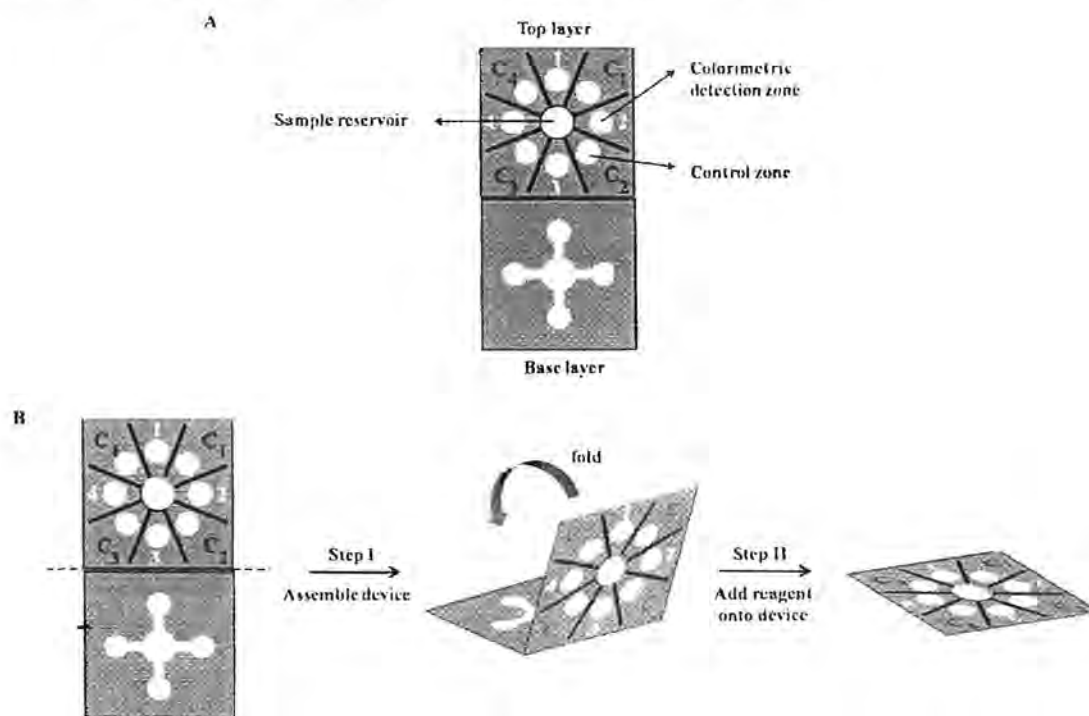
Paper-based analytical devices (PADs) are a point-of-use technology that recently received renewed interest because they are simple, inexpensive, portable, and disposable.¹⁴⁻¹⁶ To date, PADs have been extensively used for applications ranging from environmental analysis to clinical diagnostic assays.^{15,17,18} Colorimetric assays are particularly attractive when coupled with PADs due to their ease-of-use, lack of complicated external equipment and ability to provide semiquantitative results.¹⁹⁻²¹ Moreover, quantitative analysis of colorimetric assays can be accomplished using simple optical technologies such as digital cameras²²⁻²⁴ and office scanners^{21,25} combined with image processing software to carry out color, hue, and intensity measurements. In the field of clinical diagnostics, the advantages of simplicity, sensitivity, and low-cost are key reasons that make PADs coupled with colorimetric detection an effective diagnostic tool relative to traditional methods.

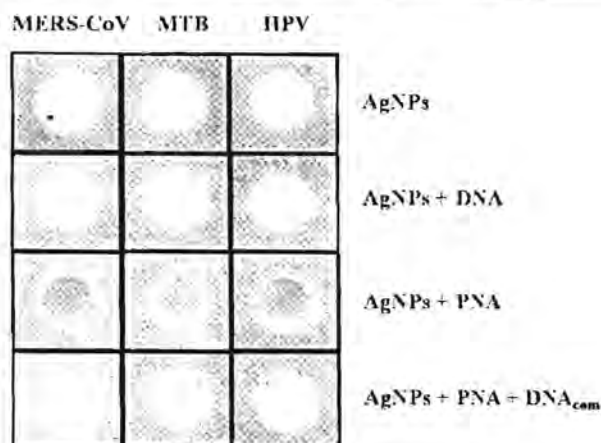
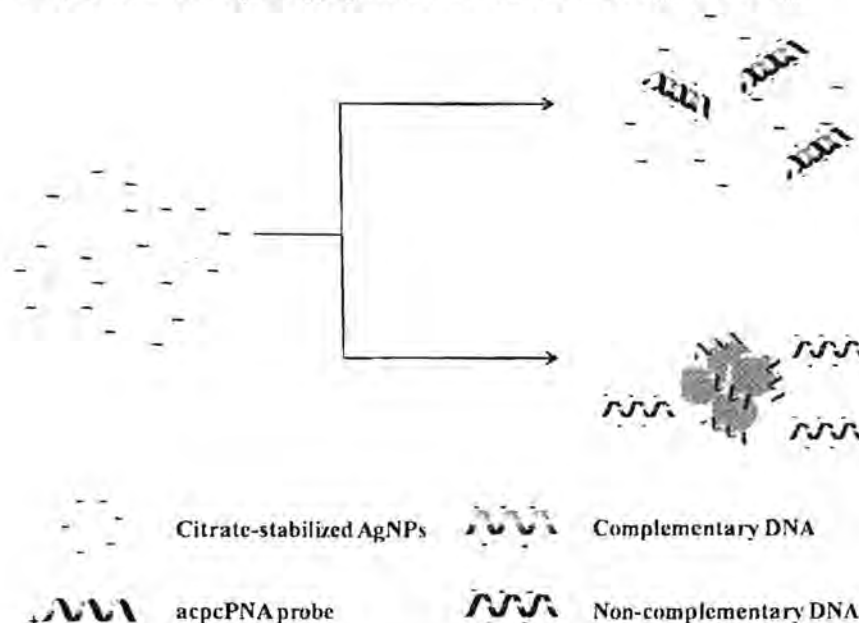
Colorimetric assays based on the aggregation of silver (AgNPs) and gold nanoparticles (AuNPs) have attracted increasing attention in biomedical applications. The optical properties of these nanomaterials depend on their size and shape.¹⁹⁻³¹ AgNPs are known to have a higher extinction coefficient compared to AuNPs,³²⁻³⁴ leading to improved optical sensitivity. Chemical reduction of silver salts is frequently used to synthesize AgNPs, while specific control of shape and size distribution is achieved by varying the reducing agents and stabilizers.³⁵⁻⁴⁷ Among stabilizing agents, negatively charged citrate has been widely used.^{7,31} Recently, colorimetric assays based on AgNPs aggregation for DNA detection has been reported.³¹ Colorimetric DNA detection using AgNPs usually involves modifying the particles with a DNA probe and mixing them with the DNA target containing the complementary

Table 1. List of Oligonucleotide Used in This Study

| oligonucleotide | sequence (5'-3') |
|--------------------------------------|-----------------------|
| MERS-CoV | |
| complementary DNA | 5'-CGATTATGTGAAGAG-3' |
| two-base-mismatch | 5'-CGATTATCTGAGGAG-3' |
| noncomplementary DNA | 5'-TTCGCACAGTGGTCA-3' |
| MTB | |
| complementary DNA | 5'-ATAACGTGTTTCTTG-3' |
| single-base-mismatch | 5'-ATAACGTCTTTCTTG-3' |
| noncomplementary DNA 1 | 5'-TGGCTAGCCGCTCCT-3' |
| noncomplementary DNA 2 | 5'-CACTTGCCCTACCCA-3' |
| HPV | |
| complementary DNA (HPV type 16) | 5'-GCTGGAGGTGTATG-3' |
| noncomplementary DNA 1 (HPV type 18) | 5'-GGATGCTGCACCGG-3' |
| noncomplementary DNA 2 (HPV type 31) | 5'-CCAAAAGCCCAAGG-3' |
| noncomplementary DNA 3 (HPV type 33) | 5'-CACATCCACCGCA-3' |

Scheme 1. (A) Design and (B) Operation of Multiplex Paper-Based Colorimetric Device



Scheme 2. Process of acpcPNA-Induced AgNP Aggregation in the Presence of DNA_{com} and DNA_{nc}Figure 1. Photograph of visual color changes obtained from detection of MERS-CoV, MTB, and HPV in the presence of DNA_{com}.

sequence. When the hybridization of probe and target DNA occurs, the AgNPs aggregate and change color.^{33,34} The assay principal has been further adopted using charge-neutral peptide nucleic acids (PNA)^{35,36} as the hybridization agent. PNA causes aggregation of metal nanoparticles in solution without immobilization, thus, simplifying the assay.^{37,38} Finally, PNA-based nanoparticle aggregation assays also provide a high hybridization efficiency of PNA-DNA duplexes leading to a rapid color change.

Recently, Vilaivan's group proposed a new conformationally constrained pyrrolidiny PNA system which possesses an α,β -peptide backbone derived from D-proline/2-aminocyclopentanecarboxylic acid (known as acpcPNA).^{44,45} Compared to Nielsen's PNA,³⁵ acpcPNA exhibits a stronger affinity and higher sequence specificity binding to DNA. acpcPNA exhibits the characteristic selectivity of antiparallel binding to the target DNA and low tendency to self-hybridize. Moreover, the

nucleobases and backbone of acpcPNA can be modified to increase molecular functionality. These combined properties make acpcPNA an attractive candidate as a probe for biological applications.^{46–48}

Here, the multiplex colorimetric PAD for DNA detection based on the aggregation of AgNPs induced by acpcPNA is reported. acpcPNA bearing a positively charged lysine modification at C-terminus was designed as the probe. The cationic PNA probe can interact with the negatively charged AgNPs leading to nanoparticle aggregation and a significant color change. This proposed sensor was used for simultaneous detection of MERS-CoV, MTB, and HPV. The developed paper-based DNA sensor has potential as an alternative diagnostic device for simple, rapid, sensitive, and selective DNA/RNA detection.

EXPERIMENTAL SECTION

Chemicals and Materials. Analytical grade reagents, including AgNO₃, NaBH₄, and sodium citrate from Sigma-Aldrich, KH₂PO₄ and KCl from Fisher Scientific, Na₂HPO₄ from Mallinckrodt, and NaCl from Macron, were used without further purification. A total of 18 M $\Omega\text{-cm}^{-1}$ resistance water was obtained from a Millipore Milli-Q water system. Synthetic DNA oligonucleotides were obtained from Biosearch Technologies. The sequences of DNA oligonucleotides are shown in Table 1.

Synthesis of AgNPs. The AgNPs were synthesized using the citrate-stabilization method.⁴⁹ Briefly, 4 mL of 12.6 mM sodium citrate and 50 mL of 0.3 mM AgNO₃ were mixed together. Then, 1 mL of 37 mM NaBH₄ was added to the mixture under vigorous stirring and the solution turned yellow. The formation of AgNPs and their size distribution were verified by dynamic light scattering measurement, and the average size of AgNPs was found to be 19 nm (Figure S1).

Synthesis of acpcPNA Probes. The acpcPNA probes were designed to detect the synthetic oligonucleotide targets

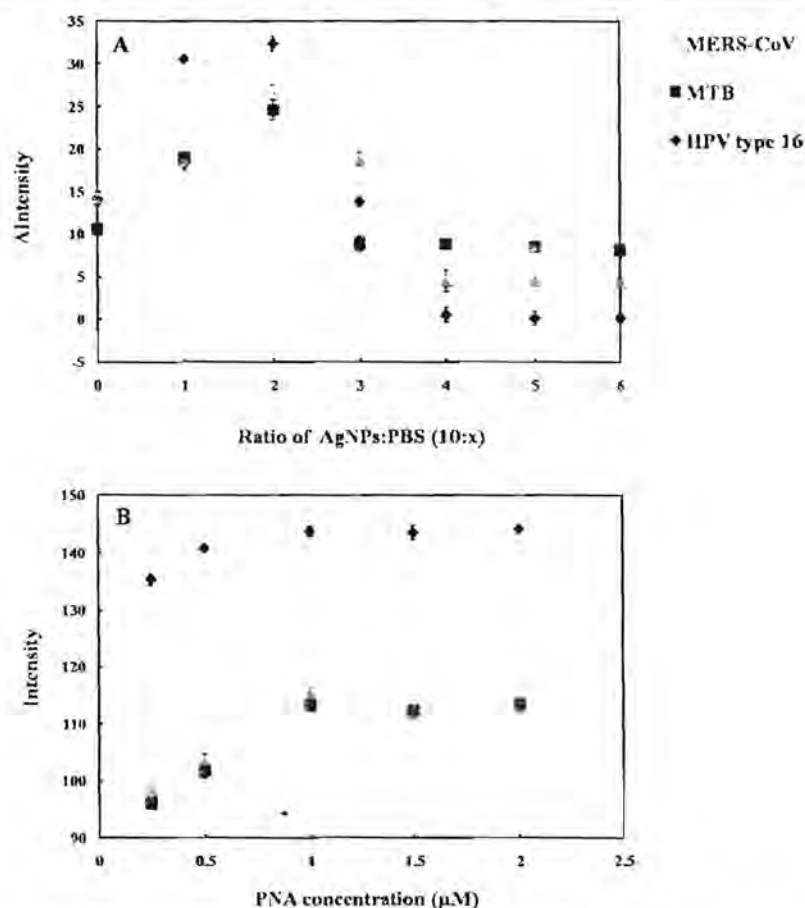


Figure 2. Influence of (A) AgNPs/PBS ratio and (B) acpcPNA probe concentration on color intensity for MERS-CoV, MTB, and HPV detection. The error bars represent one standard deviation (SD) obtained from three independent measurements ($n = 3$).

with sequences corresponding to MERS-CoV, MTB, and HPV type 16. The sequences of acpcPNA probes are as follows:

MERS-CoV: CTCTTCACATAATCG-LysNH₂

MTB: CAAGAAACACGTTAT-LysNH₂

HPV type 16: CATAACCTCCAGC-LysNH₂

*(written in the N → C direction)

The acpcPNA probe was synthesized by solid-phase peptide synthesis using Fmoc chemistry, as previously described.⁵⁴ At the C-terminus, lysinamide was included as a positively charged group that could induce nanoparticle aggregation. All PNA were purified by reverse-phase HPLC (C18 column, 0.1% (v/v) trifluoroacetic acid (TFA) in H₂O–MeOH gradient). The identity of the acpcPNA was verified by MALDI-TOF MS analysis (Figure S2), and the purity was confirmed to be >90% by reverse-phase HPLC.

Design and Operation of Paper-Based Multiplex DNA Sensor. A wax-printing technique was used to create PADs.⁵⁰ The sensor was designed using Adobe Illustrator. The wax colors were selected to be complementary to the colorimetric reactions to enhance visualization. For paper-based device fabrication, the wax design was printed onto Whatman grade 1 filter paper (VWR) using a wax printer (Xerox Phaser 8860). The wax pattern was subsequently melted at 175 °C for 50 s to generate the hydrophobic barriers and hydrophilic channels. The sensor was based on Origami concept consisting of two layers.^{5,52} As shown in Scheme 1A, the base layer contains four

wax-defined channels extending outward from the sample reservoir (6 mm i.d.) and the top layer contains four detection and control zones (4 mm i.d.). Scheme 1B illustrates operation of the multiplex sensor. First, the sample reservoir of the top layer was punched to provide a solution connection directly from the top to the bottom layer, and then the device was assembled by folding the top layer over the base layer to create the three-dimension origami paper-based device. A polydimethylsiloxane (PDMS) lid was used for holding the two layers together. The lid consisting of one 6 mm diameter hole over the sample reservoir and eight 4 mm diameter holes over the colorimetric detection and control zones was aligned over the device to provide consistent pressure across the surface of the device. Next, the acpcPNA probe and AgNPs solution were added onto the detection and control zones. Finally, the sample solution was added onto the sample reservoir and flow through the channels to wet the colorimetric detection zones.

Colorimetric Detection of MERS-CoV, MTB, and HPV DNA Target. According to the concept of PNA-induced AgNPs aggregation,^{47,48} acpcPNA was designed as a specific probe for quantitative detection of synthetic MERS-CoV, MTB, and HPV DNA targets. For colorimetric detection, the detection zone was prepared by adding 10 μL of AgNPs in 0.1 M phosphate buffer saline (PBS) pH 7.4 in a ratio of 5:1 (AgNPs: PBS), followed by 1 μL of specific acpcPNA probe. Control zones were prepared using the same conditions as the colorimetric

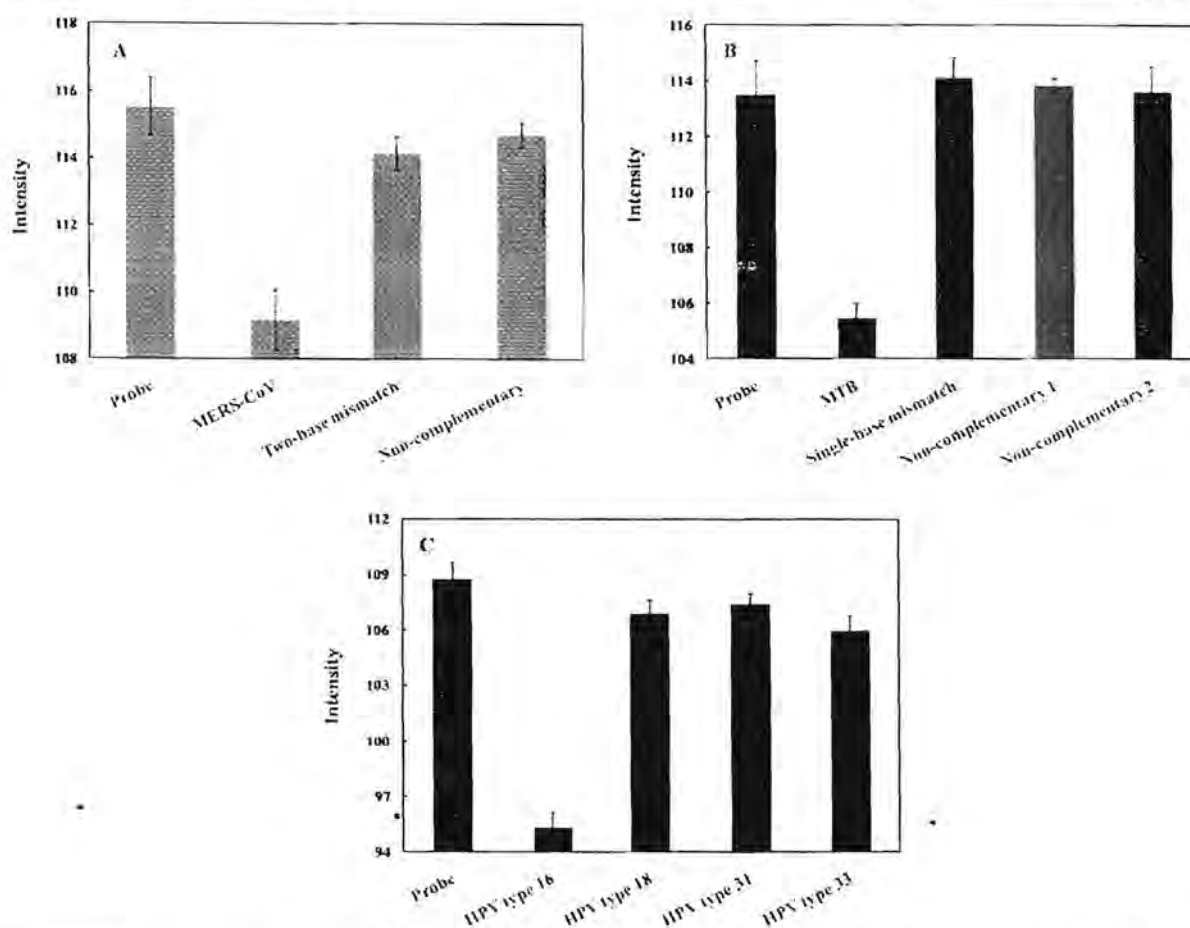


Figure 3. Color intensity of (A) MERS-CoV, (B) MTB, and (C) HPV detection after hybridization of DNA_{m1}, DNA_{m2}, and DNA_{nc}. The error bars represent one standard deviation (SD) obtained from three independent measurements ($n = 3$).

detection zones. Next, 25 μL of DNA target was added to the open sample reservoir. Upon sample addition, solution moved outward through the channels to wet the colorimetric detection zone of the top layer. Finally, the AgNPs aggregation occurred and the color intensity was measured.

Image Processing. The detection images were recorded using a scanner (XEROX DocuMate 3220) and saved in JPEG format at 600 dpi. ImageJ software (National Institutes of Health) was used to analyze the mean intensity of the color for each colorimetric reaction zone by applying a color threshold window for removing the blue background. Images were then inverted, and the mean intensity was measured.^{20,53}

RESULTS AND DISCUSSION

acpcPNA-Induced AgNPs Aggregation. The process of acpcPNA-induced AgNPs aggregation is shown in Scheme 2. The anionic AgNPs are initially well dispersed due to electrostatic repulsion. On addition of the cationic acpcPNA, the electrostatic repulsion is shielded, resulting in nanoparticle aggregation. When complementary DNA (DNA_{com}) is present, the specific PNA–DNA interaction outcompetes the less specific PNA–AgNPs interaction, resulting in a negatively charged PNA–DNA_{com} duplex and deaggregation of the anionic nanoparticles. Upon addition of noncomplementary DNA (DNA_{nc}), the acpcPNA should remain bound to the AgNPs and no color

change occurs. To prove the concept, we designed and synthesized acpcPNA probes to detect synthetic oligonucleotide targets with sequences corresponding to MERS-CoV, MTB, and HPV type 16. The photographs of the results are shown in Figure 1. The yellow AgNPs turned red when the acpcPNA was added. When the solution contained of the acpcPNA and DNA_{nc}, the color also changed to red due to aggregation of the AgNPs. On the other hand, the color changed from red (aggregated) to yellow (nonaggregated) in the presence of DNA_{com}, with the intensity dependent on the DNA concentration. Next, the sequence of adding the PNA probe and DNA target was investigated. As shown in Figure S3, when equimolar DNA_{com} was added either before or after the addition of acpcPNA probe into the AgNPs, the same color intensities were obtained indicating that the sequence of adding acpcPNA and DNA_{com} did not impact the final signal.

Critical Coagulation Concentration (CCC). The influence of electrolyte solution on the aggregation behavior of citrate-stabilized AgNPs was investigated based on the CCC. The CCC represents the electrolyte concentration required to cause aggregation of the nanoparticles in the absence of acpcPNA. In Figure S4, the color intensity of citrate-stabilized AgNPs in the absence of acpcPNA probe is shown as a function of NaCl concentration. The intensity and, therefore, the degree of aggregation, increased with the concentration of NaCl,

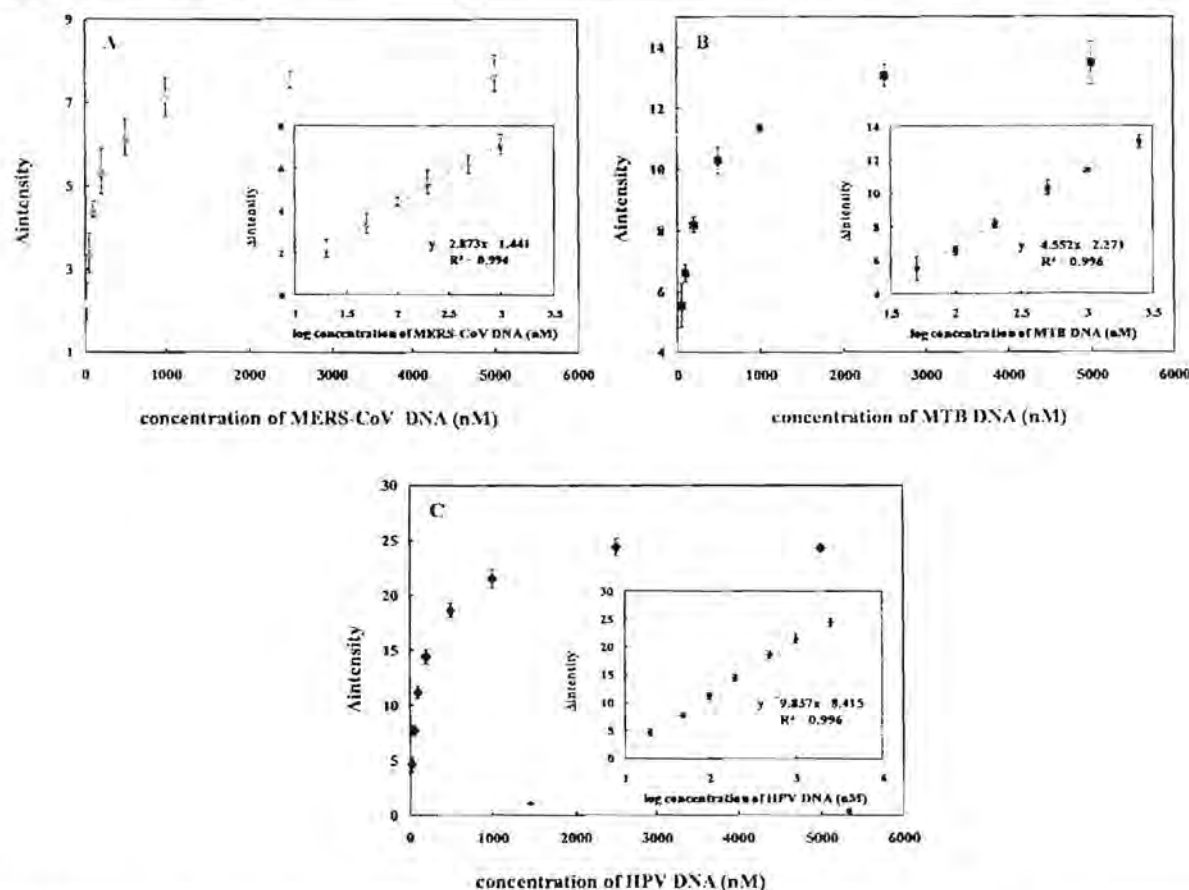


Figure 4. Change of probe color intensity vs DNA target concentration (ΔI) and calibration graph between ΔI and log DNA target concentration (inset) for (A) MERS-CoV, (B) MTB, and (C) HPV detection. The error bars represent standard deviation (SD) obtained from three independent measurement ($n = 3$).

Table 2. Summarized Analytical Performance of the Multiplexed 3DPAD for Colorimetric DNA Assay

| DNA target | linearity (nM) | LOD (nM) | %RSD ($n = 3$) |
|------------|----------------|----------|------------------|
| MERS-CoV | 20–1000 | 1.53 | 0.17–0.50 |
| MTB | 50–2500 | 1.27 | 0.12–0.67 |
| HPV | 20–2500 | 1.03 | 0.43–0.93 |

indicating that increasing ionic strength led to enhanced aggregation.⁵⁵ We believe that the ionic strength can decrease the electrostatic repulsion of citrate-stabilized AgNPs as a result of shielding, accelerating the AgNPs aggregation. The CCC was obtained when the degree of aggregation reached a maximum and became independent of NaCl concentration. In this experiment, the CCC of citrate-stabilized AgNPs was found to be 30 mM. Above this concentration, PNA-induced aggregation was not observed.

Optimization of Assay Parameters. For a colorimetric assay based on acpcPNA-induced AgNPs aggregation, assay parameters including 0.1 M PBS (pH 7.4) ratio and acpcPNA concentration were optimized using a simple paper-based design. The degree of AgNPs aggregation was determined by measuring the color intensity of the resulting solution in the presence of acpcPNA without target DNA. First, the impact of the PBS concentration on AgNPs aggregation was measured. The differential color intensity (Δ intensity, ΔI) obtained before and

after addition of acpcPNA as a function of AgNPs to PBS ratio is shown in Figure 2A. ΔI increased until the ratio of AgNPs/PBS reached 5:1 and then decreased until it plateaued at 5:2. Thus, the ratio of 5:1 AgNPs/PBS was selected as the optimal condition because it gave the largest ΔI . Another important aspect for the DNA assay is probe concentration. The influence of acpcPNA probe concentration on absolute intensity was studied. As shown in Figure 2B, the acpcPNA concentration was varied within a range of 0–2.5 μ M, and the highest aggregation was obtained at the concentration of 1.0 μ M. At this concentration, the aggregation became independent of acpcPNA concentration, which was desirable for simplifying the assay. Higher concentrations of AgNPs were not tested in order to minimize reagent consumption. As a result, the optimal conditions consisting of AgNPs/PBS ratio of 5:1 and acpcPNA concentration of 1.0 μ M were selected for further experiments.

Selectivity of MERS-CoV, MTB, and HPV Detection. To investigate the selectivity of this system, the color intensity obtained from the DNA_{com} of MERS-CoV, MTB, and HPV was compared to that of single-base mismatch (DNA_{m1}), two-base mismatch (DNA_{m2}), and DNA_{nc} sequences. The color intensity decreased significantly in the presence of DNA_{com}; whereas, the intensity did not change for the mismatched and noncomplementary targets (Figure 3). We believe the affinity of PNA–DNA hybridization was reduced due to the contribution of one- and two-base mismatches, leaving free PNA to aggregate

the nanoparticles. PNA–DNA_{com} complex can retard the ability of PNA to induce AgNPs aggregation as discussed above and result in different color intensities. These results suggest that the fully complementary DNA selectively hybridized the acpcPNA probe and yielded measurable signals. In addition, bovine serum albumin (BSA), which is commonly used in cell culture protocols, was used to investigate the protein interference of the proposed system. The DNA target was prepared in the presence of 3% BSA solution. It was observed that the color intensities of the DNA targets for MERS-CoV, MTB, and HPV in 3% BSA solution were statistically identical to the ones without BSA (Figure S5). Hence, common proteins should not negatively affect the analysis of this system.

Analytical Performance. To assess the sensitivity of the proposed method for DNA quantification, the intensity as a function of the target DNA concentration was determined. The color intensity decreases with the target DNA concentration. The calibration curves for each species are shown in Figure 4A, B, and C for MERS-CoV, MTB, and HPV, respectively. The linear range for each DNA target using a logarithmic DNA concentration and color intensity (Figure 4, inset) was also obtained. The analytical performances for all three DNA targets are summarized in Table 2. It can be seen that a sufficiently low detection limit could be obtained for MERS-CoV, MTB, and HPV detection without the need for multiple PCR cycles. Moreover, this multiplex system can provide sensitive and selective detection for simultaneous analysis of multiple DNA targets in a single device, which simplifies the analysis compared to traditional diagnostics.^{19,26–28}

Device Design. Next, a multiplex device (Scheme 1) was designed for simultaneous detection of MERS-CoV, MTB, and HPV. The top layer contained four detection zones and four control zones. Each zone contained AgNPs with a single acpcPNA probe to provide selectivity for DNA. The base layer contained four wax-defined channels extending outward from a sample inlet. After the device was folded and stacked together,

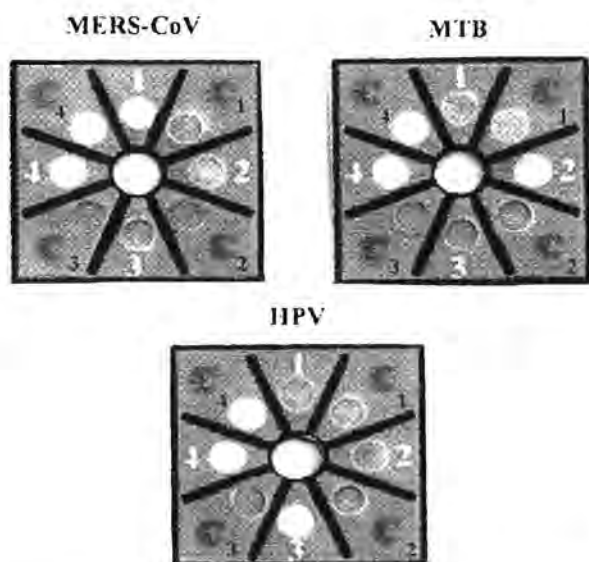


Figure 5. Selectivity of 100 nM MERS-CoV, MTB, and HPV detection using multiplex colorimetric PAD (1, C₁ = AgNPs + MERS-CoV acpcPNA probe; 2, C₂ = AgNPs + MTB acpcPNA probe; 3, C₃ = AgNPs + HPV acpcPNA probe).

the channels of the base layer were connected to four detection zones of the top layer. Upon sample addition, the solution moved outward through the channels of the base layer to wet the colorimetric detection zones of the top layer and lead to color change. Figure 5 illustrates the ability of the proposed sensor for detection of 100 nM MERS-CoV, MTB, and HPV. Only the colorimetric detection zones that contained the selective probes changed color compared to their control zones. This result indicated that the multiplex paper-based colorimetric sensor is promising for simultaneous determination of MERS-CoV, MTB, and HPV.

CONCLUSIONS

A multiplex colorimetric PAD was developed for simultaneous detection of DNA associated with viral and bacterial infectious diseases, including Middle East respiratory syndrome coronavirus (MERS-CoV), *Mycobacterium tuberculosis* (MTB), and human papillomavirus (HPV). AgNPs were used as a colorimetric reagent for DNA detection based on acpcPNA-induced nanoparticle aggregation. This colorimetric DNA sensor exhibited high selectivity against single-base mismatch, two-base mismatch and noncomplementary target DNA. Under the optimized condition, the limit of detection for MERS-CoV, MTB, and HPV were found to be 1.53, 1.27, and 1.03 nM, respectively. As a result, this developed multiplex colorimetric PAD could be a low-cost and disposable alternative tool for rapid screening and detecting in infectious diagnostics.

ASSOCIATED CONTENT

Supporting Information

The Supporting Information is available free of charge on the ACS Publications website at DOI: 10.1021/acs.analchem.7b00255.

Supporting Figures S1–S5 (PDF).

AUTHOR INFORMATION

Corresponding Authors

*E-mail: chuck.henry@colostate.edu.

*E-mail: corawon@chula.ac.th.

ORCID

Charles S. Henry: 0000-0002-3671-7725

Notes

The authors declare no competing financial interest.

ACKNOWLEDGMENTS

P.T. gratefully appreciates the financial supports from Thailand Graduate Institute of Science and Technology (TGIST 01-55-014) and The Thailand Research Fund (RTA5780005). C.S.H. acknowledges financial support from Colorado State University and the United States Department of Agriculture through the National Wildlife Research Center (1574000859CA). T.V. acknowledges technical assistance of Ms. Chotima Vilaivan (Organic Synthesis Research Unit, Chulalongkorn University) and the financial support from Thailand Research Fund (DPG5780002, to T.V.) for the PNA synthesis. The authors thank Dr. Yuanyuan Yang for assistance with manuscript editing. The authors also acknowledge important discussions with Dr. Christopher Ackerson surrounding the critical coagulation concentration.

REFERENCES

- (1) Wei, F.; Lillehoj, P. B.; Ho, C.-M. *Pediatr. Res.* **2010**, *67*, 458–468.
- (2) Smith, I. *Clin. Microbiol. Rev.* **2003**, *16*, 463–496.
- (3) Burd, E. M. *Clin. Microbiol. Rev.* **2003**, *16*, 1–17.
- (4) de Wit, E.; Rasmussen, A. L.; Falzarano, D.; Bushmaker, T.; Feldmann, F.; Brining, D. L.; Fischer, E. R.; Martellaro, C.; Okumura, A.; Chang, J.; Scott, D.; Benecke, A. G.; Katze, M. G.; Feldmann, H.; Munster, V. J. *Proc. Natl. Acad. Sci. U. S. A.* **2013**, *110*, 16598–16603.
- (5) Bhadra, S.; Jiang, Y. S.; Kumar, M. R.; Johnson, R. F.; Hensley, L. E.; Ellington, A. D. *PLoS One* **2015**, *10*, e0123126.
- (6) Davies, P. D. O.; Pai, M. *International Journal of Tuberculosis and Lung Disease* **2008**, *12*, 1226–1234.
- (7) Steingart, K. R.; Ng, V.; Henry, M.; Hopewell, P. C.; Ramsay, A.; Cunningham, J.; Urbanczik, R.; Perkins, M. D.; Aziz, M. A.; Pai, M. *Lancet Infect. Dis.* **2006**, *6*, 664–674.
- (8) Lee, J. J.; Suo, J.; Lin, C. B.; Wang, J. D.; Lin, T. Y.; Tsai, Y. C. *International Journal of Tuberculosis and Lung Disease* **2003**, *7*, 569–574.
- (9) Al-Zamel, F. A. *Expert Rev. Anti-Infect. Ther.* **2009**, *7*, 1099–1108.
- (10) Noordhoek, G. T.; Kolk, A. H.; Bjune, G.; Catty, D.; Dale, J. W.; Fine, P. E.; Godfrey-Faussett, P.; Cho, S. N.; Shinnick, T.; Svenson, S. B. *Journal of Clinical Microbiology* **1994**, *32*, 277–284.
- (11) Yang, Y.-C.; Lu, P.-L.; Huang, S. C.; Jenh, Y.-S.; Jou, R.; Chang, T. C. *Journal of Clinical Microbiology* **2011**, *49*, 797–801.
- (12) Lörcincz, A.; Anthony, J. *Papillomavirus Report* **2001**, *12*, 145–154.
- (13) Gravitt, P. E.; Jamshidi, R. *Infectious Disease Clinics of North America* **2005**, *19*, 439–458.
- (14) Martinez, A. W.; Phillips, S. T.; Butte, M. J.; Whitesides, G. M. *Angew. Chem., Int. Ed.* **2007**, *46*, 1318–1320.
- (15) Cate, D. M.; Adkins, J. A.; Mettakoonpitak, J.; Henry, C. S. *Anal. Chem.* **2015**, *87*, 19–41.
- (16) Yetisen, A. K.; Akram, M. S.; Lowe, C. R. *Lab Chip* **2013**, *13*, 2210–2251.
- (17) Adkins, J.; Boehle, K.; Henry, C. *Electrophoresis* **2015**, *36*, 1811–1824.
- (18) Mettakoonpitak, J.; Boehle, K.; Nantaphol, S.; Teengam, P.; Adkins, J. A.; Srisa-Art, M.; Henry, C. S. *Electroanalysis* **2016**, *28*, 1420–1436.
- (19) Nery, E. W.; Kubota, L. T. *Anal. Bioanal. Chem.* **2013**, *405*, 7573–7595.
- (20) Rattanarat, P.; Dungchai, W.; Cate, D.; Volckens, J.; Chailapakul, O.; Henry, C. S. *Anal. Chem.* **2014**, *86*, 3555–3562.
- (21) Liana, D. D.; Raguse, B.; Gooding, J. J.; Chow, E. *Sensors* **2012**, *12*, 11505.
- (22) Apilux, A.; Siangproh, W.; Praphairaksit, N.; Chailapakul, O. *Talanta* **2012**, *97*, 388–394.
- (23) Apilux, A.; Dungchai, W.; Siangproh, W.; Praphairaksit, N.; Henry, C. S.; Chailapakul, O. *Anal. Chem.* **2010**, *82*, 1727–1732.
- (24) Chaiyo, S.; Siangproh, W.; Apilux, A.; Chailapakul, O. *Anal. Chim. Acta* **2015**, *866*, 75–83.
- (25) Cate, D. M.; Nanthasurasak, P.; Riwkulkajorn, P.; L'Orange, C.; Henry, C. S.; Volckens, J. *Ann. Occup. Hyg.* **2014**, *58*, 413–423.
- (26) Shim, S.-Y.; Lim, D.-K.; Nam, J.-M. *Nanomedicine* **2008**, *3*, 215–232.
- (27) Baptista, P.; Pereira, E.; Eaton, P.; Doria, G.; Miranda, A.; Gomes, I.; Quaresma, P.; Franco, R. *Anal. Bioanal. Chem.* **2008**, *391*, 943–950.
- (28) Zhao, W.; Brook, M. A.; Li, Y. *ChemBioChem* **2008**, *9*, 2363–2371.
- (29) Thaxton, C. S.; Georganopoulou, D. G.; Mirkin, C. A. *Clin. Chim. Acta* **2006**, *363*, 120–126.
- (30) Li, H.; Cui, Z.; Han, C. *Sens. Actuators, B* **2009**, *143*, 87–92.
- (31) Vilela, D.; González, M. C.; Escarpa, A. *Anal. Chim. Acta* **2012**, *751*, 24–43.
- (32) Wei, H.; Chen, C.; Han, B.; Wang, E. *Anal. Chem.* **2008**, *80*, 7051–7055.
- (33) Lee, J.-S.; Lytton-Jean, A. K. R.; Hurst, S. J.; Mirkin, C. A. *Nano Lett.* **2007**, *7*, 2112–2115.
- (34) Thompson, D. G.; Enright, A.; Faulds, K.; Smith, W. E.; Graham, D. *Anal. Chem.* **2008**, *80*, 2805–2810.
- (35) Yeo, S. Y.; Lee, H. J.; Jeong, S. H. *J. Mater. Sci.* **2003**, *38*, 2143–2147.
- (36) Chimentao, R. J.; Kirm, I.; Medina, F.; Rodriguez, X.; Cesteros, Y.; Salagre, P.; Sueiras, J. E. *Chem. Commun.* **2004**, 846–847.
- (37) He, B.; Tan, J. J.; Liew, K. Y.; Liu, H. *J. Mol. Catal. A: Chem.* **2004**, *221*, 121–126.
- (38) Abou El-Nour, K. M. M.; Eftaiha, A. a.; Al-Warthan, A.; Ammar, R. A. A. *Arabian J. Chem.* **2010**, *3*, 135–140.
- (39) Irvani, S.; Korbekandi, H.; Mirmohammadi, S. V.; Zolfaghari, B. *Research in Pharmaceutical Sciences* **2014**, *9*, 385–406.
- (40) Nielsen, P.; Egholm, M.; Berg, R.; Buchardt, O. *Science (Washington, DC, U. S.)* **1991**, *254*, 1497–1500.
- (41) Egholm, M.; Buchardt, O.; Christensen, L.; Behrens, C.; Freier, S. M.; Driver, D. A.; Berg, R. H.; Kim, S. K.; Norden, B.; Nielsen, P. E. *Nature* **1993**, *365*, 566–568.
- (42) Su, X.; Kanjanawarut, R. *ACS Nano* **2009**, *3*, 2751–2759.
- (43) Kanjanawarut, R.; Su, X. *Anal. Chem.* **2009**, *81*, 6122–6129.
- (44) Vilaivan, T.; Srisuwannaket, C. *Org. Lett.* **2006**, *8*, 1897–1900.
- (45) Vilaivan, T. *Acc. Chem. Res.* **2015**, *48*, 1645–1656.
- (46) Jampasa, S.; Wonsawat, W.; Rodthongkum, N.; Siangproh, W.; Yanatatsaneejit, P.; Vilaivan, T.; Chailapakul, O. *Biosens. Bioelectron.* **2014**, *54*, 428–434.
- (47) Kongpeth, J.; Jampasa, S.; Chaumpluk, P.; Chailapakul, O.; Vilaivan, T. *Talanta* **2016**, *146*, 318–325.
- (48) Jirakittiwut, N.; Panyain, N.; Nuanyai, T.; Vilaivan, T.; Praneenarat, T. *RSC Adv.* **2015**, *5*, 24110–24114.
- (49) Laliwala, S. K.; Mehta, V. N.; Rohit, J. V.; Kailasa, S. K. *Sens. Actuators, B* **2014**, *197*, 254–263.
- (50) Carrilho, E.; Martinez, A. W.; Whitesides, G. M. *Anal. Chem.* **2009**, *81*, 7091–7095.
- (51) Liu, H.; Crooks, R. M. *J. Am. Chem. Soc.* **2011**, *133*, 17564–17566.
- (52) Liu, H.; Xiang, Y.; Lu, Y.; Crooks, R. M. *Angew. Chem.* **2012**, *124*, 7031–7034.
- (53) Mentele, M. M.; Cunningham, J.; Koehler, K.; Volckens, J.; Henry, C. S. *Anal. Chem.* **2012**, *84*, 4474–4480.
- (54) Huynh, K. A.; Chen, K. L. *Environ. Sci. Technol.* **2011**, *45*, 5564–5571.
- (55) Li, X.; Lenhart, J. J.; Walker, H. W. *Langmuir* **2010**, *26*, 16690–16698.
- (56) Shirato, K.; Yano, T.; Senba, S.; Akachi, S.; Kobayashi, T.; Nishinaka, T.; Notomi, T.; Matsuyama, S. *Virology* **2014**, *11*, 139–139.
- (57) Azhar, E. I.; Hashem, A. M.; El-Kafrawy, S. A.; Sohrab, S. S.; Aburizaiza, A. S.; Farraj, S. A.; Hassan, A. M.; Al-Saeed, M. S.; Jamjoom, G. A.; Madani, T. A. *mBio* **2014**, *5*, e01450.
- (58) Abreu, A. L. P.; Souza, R. P.; Gimenes, F.; Consolaro, M. E. L. *Virology* **2012**, *9*, 262–262.
- (59) Villa, L. L.; Denny, L. *Int. J. Gynecol. Obstet.* **2006**, *94*, S71–S80.

Hydrophilic and Cell-Penetrable Pyrrolidinyl Peptide Nucleic Acid via Post-synthetic Modification with Hydrophilic Side Chains

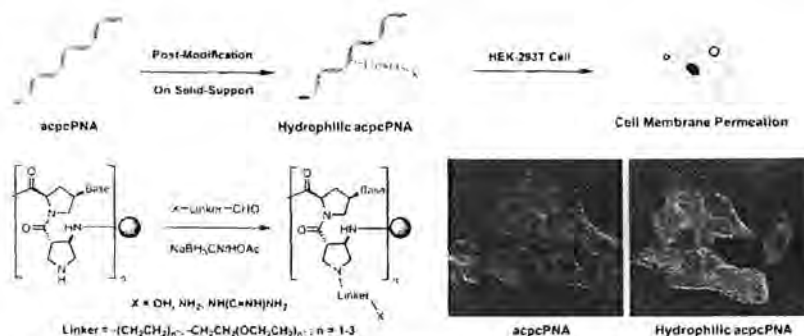
Haruthai Pansuwan,[†] Boonsong Ditmangklo,[‡] Chotima Vilaivan,[‡] Banphot Jiangchareon,[§] Porntip Pan-In,^{||} Supason Wanichwecharungruang,^{||} Tanapat Palaga,[⊥] Thanesuan Nuanyai,^{*,#} Chaturong Suparpprom,^{*,†} and Tirayut Vilaivan[‡]

[†]Department of Chemistry and Center of Excellence for Innovation in Chemistry, Faculty of Science, Naresuan University, Ta-Po District, Muang, Phitsanulok 65000, Thailand

[‡]Organic Synthesis Research Unit, Department of Chemistry, Faculty of Science, [§]Program in Biotechnology, Faculty of Science, ^{||}Department of Chemistry, Faculty of Science, and [⊥]Department of Microbiology, Faculty of Science, Chulalongkorn University, Phayathai Road, Patumwan, Bangkok 10330, Thailand

[#]Rajamankala University of Technology Rattanakosin, Wang Klai Kangwon Campus, Huahin, Prachuap Khiri Khan 77110, Thailand

Supporting Information



ABSTRACT: Peptide nucleic acid (PNA) is a nucleic acid mimic in which the deoxyribose–phosphate was replaced by a peptide-like backbone. The absence of negative charge in the PNA backbone leads to several unique behaviors including a stronger binding and salt independency of the PNA–DNA duplex stability. However, PNA possesses poor aqueous solubility and cannot directly penetrate cell membranes. These are major obstacles that limit in vivo applications of PNA. In previous strategies, the PNA can be conjugated to macromolecular carriers or modified with positively charged side chains such as guanidinium groups to improve the aqueous solubility and cell permeability. In general, a preformed modified PNA monomer was required. In this study, a new approach for post-synthetic modification of PNA backbone with one or more hydrophilic groups was proposed. The PNA used in this study was the conformationally constrained pyrrolidinyl PNA with prolyl-2-aminocyclopentanecarboxylic acid dipeptide backbone (acpcPNA) that shows several advantages over the conventional PNA. The aldehyde modifiers carrying different linkers (alkylene and oligo(ethylene glycol)) and end groups ($-\text{OH}$, $-\text{NH}_2$, and guanidinium) were synthesized and attached to the backbone of modified acpcPNA by reductive alkylation. The hybrids between the modified acpcPNAs and DNA exhibited comparable or superior thermal stability with base-pairing specificity similar to those of unmodified acpcPNA. Moreover, the modified acpcPNAs also showed the improvement of aqueous solubility (10–20 folds compared to unmodified PNA) and readily penetrate cell membranes without requiring any special delivery agents. This study not only demonstrates the practicality of the proposed post-synthetic modification approach for PNA modification, which could be readily applied to other systems, but also opens up opportunities for using pyrrolidinyl PNA in various applications such as intracellular RNA sensing, specific gene detection, and antisense and antigene therapy.

INTRODUCTION

Peptide nucleic acid (PNA) is an interesting DNA mimic that shows very strong and sequence-specific hybridization to complementary single-stranded DNA and RNA as well as to double-stranded DNA by triplex formation or duplex invasion.¹ These properties, together with excellent resistance to nucleases and proteases, make PNA useful for antigene and antisense

therapy, as tool for molecular biology, and as probe for DNA- or RNA-based diagnosis.^{2,3} The structure of PNA is chemically very different from DNA, whereby the deoxyribose phosphodiester

Received: June 3, 2017

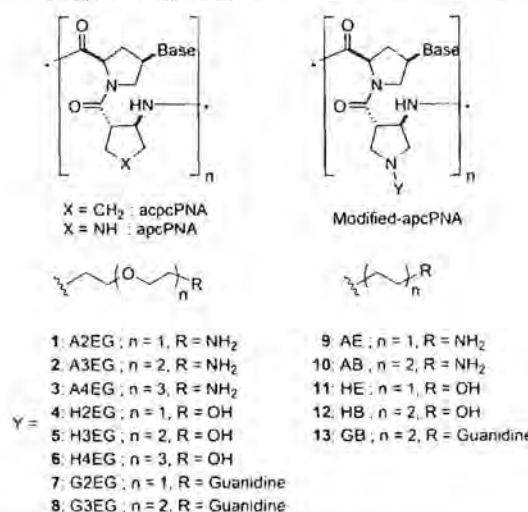
Revised: July 7, 2017

Published: July 13, 2017

backbone of DNA was replaced by a peptide-like backbone. Following the original design of *N*-2-aminoethylglycine (aeg) PNA backbone,¹ several other PNA structures have been proposed such as cyclopentyl,³ cyclohexyl,⁴ γ -position,⁵ pyrrolidinyl,⁶ pyrrolidine–amide oligonucleotide mimics,⁷ and pyrrolidinyl PNA with alternating proline and cyclic β -amino acids.^{10–12} These new PNAs displayed varying DNA binding affinities and selectivities, but only a few of them outperformed the original aegPNA, with γ -PNA⁵ and certain pyrrolidinyl PNA (acpcPNA¹³ and abcPNA)¹⁴ as the most notable examples. Although several applications of PNA have been demonstrated, one practical limitation that prevents widespread acceptance of PNA in various applications is its poor aqueous solubility relative to DNA as well as the tendency to exhibit nonspecific interactions with nonpolar molecules such as proteins and organic dyes.¹⁵ In addition, unmodified PNAs are not readily cell-penetrable,¹⁶ although lipophilic PNA can be delivered into cells using cationic lipids^{17,18} or amphipathic peptides¹⁹ as carriers. Alternatively PNA has been also conjugated to macromolecules such cell-penetrating peptides (CPP),^{20,21} polyethylene glycol (PEG),²² or DNA^{19,23} to improve the solubility along with the cellular membrane penetration. Other approaches to improving aqueous solubility and cellular uptake of PNA oligomers include terminal or internal modification with charged or hydrophilic moieties such as lysine or arginine.^{24,25} For example, γ PNA bearing a diethylene glycol side chain ($R^{MP}\gamma$ PNA)¹⁵ showed improved DNA and RNA hybridization and water solubility compared to the original PNA. Modification of γ PNA with cationic guanidinium group enables the PNA to traverse cell membrane²⁶ and has been used for targeting epidermal growth factor receptor (EGFR) in preclinical models.²⁷ Modified aegPNA carrying aminomethylene³⁰ or aminopropylene groups³¹ at α - or γ -positions have been recently reported. These amino-modified PNA showed enhanced DNA affinity due to the combination of electrostatic interaction and stereopreferred conformational preorganization and could also penetrate cells such as HeLa or MCF-7. Although displaying several favorable properties,¹⁰ the hydrophobic nature of acpcPNA contributes to its poor aqueous solubility (at least one order of magnitude less soluble than aegPNA,¹⁵ even with the inclusion of C-terminal lysine as a solubility enhancer). In addition, similar to other PNAs, unmodified acpcPNA is non-cell-permeable, and therefore, an external carrier such as carbon nanospheres³² or a commercial transfecting agent³³ is required to deliver acpcPNA for cellular applications. Accordingly, a reliable modification that can increase both water solubility and cellular uptake of acpcPNA is highly desirable. Recently, we reported the synthesis and the DNA- and RNA-binding properties of pyrrolidinyl PNA-carrying polar backbone by the replacement of the cyclopentane ring in the backbone of acpcPNA with tetrahydrofuran (atfcPNA),³⁴ oxetane (aocPNA),³⁵ or pyrrolidine (apcPNA) moieties.^{36,37} Among these modifications, the apcPNA bearing a pyrrolidine ring in place of the cyclopentane ring in acpcPNA is the most promising in terms of DNA-binding affinity. Importantly, the nitrogen atom of the pyrrolidine ring in the apc spacer provide a convenient handle for attaching label or other functional groups to the PNA backbone via acylation, reductive alkylation, or click chemistry.³⁸

In this study, we report the synthesis and DNA-binding properties of novel hydrophilic backbone-modified pyrrolidine PNA. The hydrophilic modifiers with different end groups ($-\text{OH}$, $-\text{NH}_2$, and guanidine) were attached to the backbone of pyrrolidinyl PNA via an alkylene or oligo(ethylene glycol) linker

Scheme 1. Structures of acpcPNA, apcPNA, and Hydrophilic Modified Pyrrolidinyl PNA

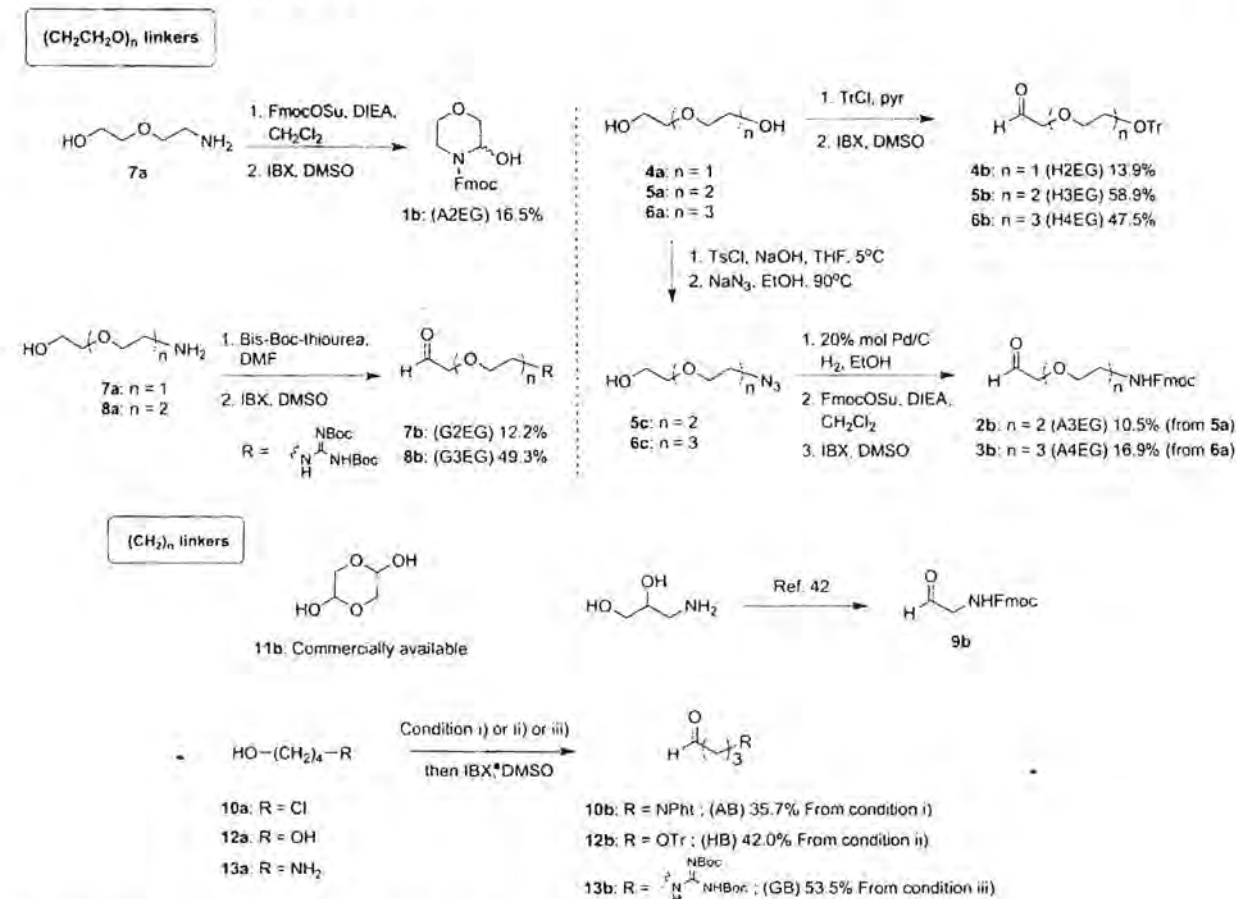


by reductive alkylation of the apc backbone, as shown in Scheme 1. Furthermore, water solubility and *in vitro* cellular uptake of modified PNA were also investigated.

RESULTS AND DISCUSSION

Synthesis of Hydrophilic Modifiers and Modification of PNA. The preparation of all hydrophilic modifiers started from commercially available α,ω -alkanediols (ethylene glycol and 1,4-butanediol) or oligo(ethylene glycol) ($n = 2-4$) (Scheme 2). Monoamino derivatives of oligo(ethylene glycol) were prepared by treatment of the parent diols with limited amounts of *p*-toluenesulfonyl chloride (TsCl), and the monotosylate was subsequently reacted with NaN₃ to afford the corresponding azido-alcohol derivatives (5c and 6c) following a modified literature protocol.³⁹ Hydrogenation over Pd/C catalyst followed by protection with Fmoc-OSu gave the corresponding *N*-Fmoc-amino alcohols. These were subsequently oxidized with 2-iodoxybenzoic acid (IBX) to get the desired novel Fmoc-protected amino aldehydes (2b and 3b). Compound 1b was synthesized starting from the commercially available 2-aminoethoxyethanol (7a) via Fmoc protection and oxidation.⁴¹ ¹H nuclear magnetic resonance (NMR) suggested that this is a cyclized product, but this compound underwent subsequent reductive alkylation without problems, presumably due to the presence of acetic acid in the reaction condition. However, Fmoc- or Boc-protected amino-C4 aldehyde could not be cleanly obtained by this procedure. The problem was solved by employing the phthalimido group, which completely blocked the nitrogen atom from the subsequent cyclization reaction. According to this method, 4-chloro-1-butanol was first reacted with phthalimide to give the known phthalimido alcohol⁴¹ and then subsequently oxidized to phthalimido aldehyde (10b)⁴¹ with IBX. The Fmoc-protected amino-C2 modifier (Fmoc-aminoacetaldehyde; 9b) was prepared from 3-amino-1,2-propanediol according to a literature procedure.⁴²

The guanidine derivatives (7b, 8b, and 13b)⁴³ were synthesized by the reaction of amino alcohol and bis-Boc-thiourea⁴⁴ followed by IBX oxidation. For the hydroxyl derivatives, alkanediol or poly(ethylene glycol) were protected with trityl chloride (TrCl) in pyridine under N₂ atmosphere to get the

Scheme 2. Synthesis of Hydrophilic Modifiers^a

^aReagents and conditions: (i) phthalimide, K₂CO₃, DMF; (ii) TrCl, pyridine, CH₂Cl₂; (iii) Bis-Boc-thiourea, DMF.

monoprotected diols by employing large excess of the diols.^{15,16} Oxidation of the alcohols in DMSO afforded the novel trityloxy-aldehyde derivatives (4b, 5b, and 12b)⁴³ ready for attachment to the backbone of apcPNA. Due to the instabilities of the aldehydes, some needed to be freshly prepared and used directly without further purification. The details of synthesis are reported in the Supporting Information. For the hydroxy-C2 modifier, the commercially available glycolaldehyde dimer (11b) was directly used as a masked aldehyde.

All PNAs were synthesized manually by Fmoc solid-phase peptide synthesis, as described previously.¹² To provide a handle for site-specific modification with the hydrophilic groups, the apc spacer of the apcPNA was site-specifically replaced with a Tfa-protected apc spacer.³⁶ The PNA sequence was end-capped by acetylation or benzoylation or with a fluorescence dye [5(6)-carboxyfluorescein]. Deprotection of the nucleobase side chain by ammonia treatment resulted in simultaneous deprotection of the Tfa group. This was followed by post-synthetic modification with the aldehyde-containing hydrophilic modifier via the reductive alkylation strategy previously reported by our group³¹ then by an appropriate treatment for the removal of the protecting group of the modifier (none for Boc, piperidine in DMF for Fmoc, and 40% aqueous methylamine solution for Ph₁). Analyses of crude products suggest that the reductive alkylation step was practically quantitative. Subsequent cleavage

from the solid support by treatment with trifluoroacetic acid (TFA) afforded 30 modified apcPNAs. The base sequences were either homothymine (T₉) or a mixed-base 10-mer sequence (GTAGATCACT). The number of modifier attached on the PNA sequence was varied between one and three per PNA sequence. The number and positions of the modification are arbitrarily chosen on the basis of the fact that multiple modifications are usually required to achieve cell permeability in other PNA systems^{27,47} to preliminarily explore whether the same strategy can increase the cellular uptake of apcPNA. A total of three PNA sequences with the apc spacer but without hydrophilic modification were also prepared as controls. These modified apcPNAs were purified by reverse-phase high-performance liquid chromatography (RP-HPLC). All unlabeled PNA sequences gave a single peak in their analytical HPLC chromatograms (estimated purity of >90%). Fluorescein-labeled PNA29–PNA33 carried two isomeric fluorescein labels, which should give the maximum of two peaks in the chromatogram. This is generally true except for PNA29 and PNA32, whereby additional minor peaks were observed in the HPLC chromatograms. The identities of all PNA sequences were confirmed by matrix-assisted laser desorption–ionization time-of-flight (MALDI-TOF) mass spectrometry, which showed the molecular ion peak that were in a good agreement with the expected values. The fact that MALDI-TOF analyses showed the correct mass for

Table 1. Base Sequence, MALDI-TOF Spectrometric, and Thermal Melting Data of the Modified apcPNA

| PNA | sequence (N → C) | modifier (X) | t_R min ^a | m/z (calcd) ^b | m/z (found) ^c | T_m ^d (°C) | ΔT_m ^e (°C) | T_m ^f (°C) | ΔT_m ^g (°C) |
|-------|--|--------------|------------------------|----------------------------|----------------------------|-------------------------|--------------------------------|-------------------------|--------------------------------|
| PNA1 | Ac-TTTT ^(NX) TTTT-LysNH ₂ | none | 36.2 | 3180.4 | 3180.3 | 77.7 | — | 71.9 | — |
| PNA2 | Ac-TTTT ^(NX) TTTT-LysNH ₂ | A2EG | 34.6 | 3267.5 | 3268.3 | 79.7 | +2.0 | 71.9 | 0.0 |
| PNA3 | Ac-TTTT ^(NX) TTTT-LysNH ₂ | A3EG | 35.2 | 3311.5 | 3309.5 | 78.7 | +1.0 | 72.9 | +1.0 |
| PNA4 | Ac-TTTT ^(NX) TTTT-LysNH ₂ | A4EG | 28.9 | 3355.5 | 3356.0 | 78.7 | +1.0 | 70.9 | -1.0 |
| PNA5 | Ac-TTTT ^(NX) TTTT-LysNH ₂ | AE | 31.1 | 3224.4 | 3228.0 | 81.9 | +4.2 | 73.8 | +1.9 |
| PNA6 | Ac-TTTT ^(NX) TTTT-LysNH ₂ | AB | 31.8 | 3251.5 | 3250.3 | 79.7 | +2.0 | 71.9 | 0.0 |
| PNA7 | Ac-TTTT ^(NX) TTTT-LysNH ₂ | H2EG | 34.8 | 3268.4 | 3266.4 | 71.9 | -5.8 | 68.0 | -3.9 |
| PNA8 | Ac-TTTT ^(NX) TTTT-LysNH ₂ | H3EG | 30.7 | 3312.5 | 3314.5 | 70.9 | -6.8 | 67.1 | -4.8 |
| PNA9 | Ac-TTTT ^(NX) TTTT-LysNH ₂ | H4EG | 36.5 | 3356.5 | 3355.5 | 70.9 | -6.8 | 67.1 | -4.8 |
| PNA10 | Ac-TTTT ^(NX) TTTT-LysNH ₂ | HE | 32.9 | 3225.4 | 3228.5 | 71.5 | -6.2 | 67.0 | -4.9 |
| PNA11 | Ac-TTTT ^(NX) TTTT-LysNH ₂ | HB | 31.9 | 3252.4 | 3253.5 | 71.9 | -5.8 | 67.1 | -4.8 |
| PNA12 | Ac-TTTT ^(NX) TTTT-LysNH ₂ | G2EG | 29.8 | 3309.5 | 3313.4 | 79.7 | +2.0 | 68.0 | -3.9 |
| PNA13 | Ac-TTTT ^(NX) TTTT-LysNH ₂ | G3EG | 28.6 | 3353.5 | 3351.6 | 79.7 | +2.0 | 70.9 | -1.0 |
| PNA14 | Ac-TTTT ^(NX) TTTT-LysNH ₂ | GB | 33.2 | 3293.5 | 3293.6 | 80.6 | +2.9 | 72.9 | +1.0 |
| PNA15 | Bz-GTAGA ^(NX) TCACCT-LysNH ₂ | none | 29.9 | 3621.9 | 3619.5 | 57.4 | — | 51.5 | — |
| PNA16 | Ac-GTAGA ^(NX) TCACCT-LysNH ₂ | A3EG | 29.2 | 3690.9 | 3691.3 | 63.2 | +5.8 | 55.4 | +3.9 |
| PNA17 | Ac-GTAGA ^(NX) TCACCT-LysNH ₂ | AE | 29.6 | 3603.8 | 3604.7 | 65.4 | +8.0 | 58.4 | +6.9 |
| PNA18 | Ac-GTAGA ^(NX) TCACCT-LysNH ₂ | AB | 25.2 | 3630.9 | 3628.1 | 66.1 | +8.7 | 58.3 | +6.8 |
| PNA19 | Ac-GTAGA ^(NX) TCACCT-LysNH ₂ | H3EG | 29.4 | 3691.9 | 3690.8 | 56.4 | -1.0 | 53.5 | +2.0 |
| PNA20 | Ac-GTAGA ^(NX) TCACCT-LysNH ₂ | HE | 29.8 | 3604.8 | 3605.4 | 58.7 | +1.3 | 54.2 | +2.7 |
| PNA21 | Ac-GTAGA ^(NX) TCACCT-LysNH ₂ | HB | 29.1 | 3631.9 | 3629.9 | 59.3 | +1.9 | 53.5 | +2.0 |
| PNA22 | Ac-GTAGA ^(NX) TCACCT-LysNH ₂ | GB | 29.7 | 3672.9 | 3671.0 | 67.1 | +9.7 | 58.3 | +6.8 |
| PNA23 | Bz-GT ^(NX) AGA ^(NX) TCA ^(NX) CT-LysNH ₂ | none | 28.5 | 3623.9 | 3617.2 | 60.3 | — | 52.5 | — |
| PNA24 | Ac-GT ^(NX) AGA ^(NX) TCA ^(NX) CT-LysNH ₂ | A3EG | 27.0 | 3954.7 | 3955.9 | 74.8 | +14.5 | 63.2 | +10.7 |
| PNA25 | Ac-GT ^(NX) AGA ^(NX) TCA ^(NX) CT-LysNH ₂ | AB | 29.9 | 3775.2 | 3776.9 | 78.7 | +18.4 | 65.1 | +12.6 |
| PNA26 | Ac-GT ^(NX) AGA ^(NX) TCA ^(NX) CT-LysNH ₂ | H3EG | 28.5 | 3958.0 | 3958.4 | 58.3 | -2.0 | 53.5 | +1.0 |
| PNA27 | Ac-GT ^(NX) AGA ^(NX) TCA ^(NX) CT-LysNH ₂ | HB | 27.4 | 3778.0 | 3779.2 | 61.2 | +0.9 | 54.4 | +1.9 |
| PNA28 | Ac-GT ^(NX) AGA ^(NX) TCA ^(NX) CT-LysNH ₂ | GB | 26.9 | 3901.1 | 3898.6 | 78.7 | +18.4 | 66.8 | +14.3 |
| PNA29 | Flu-GT ^(NX) AGA ^(NX) TCA ^(NX) CT-LysNH ₂ | H3EG | 30.9 | 4274.3 | 4274.9 | 50.0 | -10.3 | 46.7 | -3.8 |
| PNA30 | Flu-GT ^(NX) AGA ^(NX) TCA ^(NX) CT-LysNH ₂ | A3EG | 30.7 | 4271.3 | 4271.8 | 67.1 | +6.8 | 56.4 | +3.9 |
| PNA31 | Flu-GT ^(NX) AGA ^(NX) TCA ^(NX) CT-LysNH ₂ | HB | 30.3 | 4094.2 | 4095.9 | 53.5 | -6.8 | 48.6 | -3.9 |
| PNA32 | Flu-GT ^(NX) AGA ^(NX) TCA ^(NX) CT-LysNH ₂ | AB | 30.6 | 4091.3 | 4089.5 | 70.0 | +9.7 | 57.4 | +4.9 |
| PNA33 | Flu-GT ^(NX) AGA ^(NX) TCA ^(NX) CT-LysNH ₂ | GB | 29.6 | 4217.3 | 4217.3 | 68.0 | +7.7 | 56.4 | +3.9 |

^aHPLC conditions: C18 column, 4.6 × 150 mm, 3 μ, gradient 0.1% TFA in H₂O/MeOH 90:10 for 5 min then linear gradient to 10:90 over 30 min, flow rate 0.5 mL/min, 260 nm. ^bAverage mass of M + H⁺. ^cMALDI-TOF. ^dIsolated yield after HPLC purification, spectrophotometrically determined. ^eWith complementary DNA (dA₉ for PNA1–PNA14; dAGTGATCTAC for PNA15–PNA33). ^fConditions: 10 mM sodium phosphate buffer, pH 7.00, 0 mM NaCl, [PNA] = 1.0 μM, and [DNA] = 1.2 μM. ^g $\Delta T_m = T_m(\text{modified PNA}) - T_m(\text{unmodified PNA})$. Unmodified PNA refers to apc-modified apcPNA (X: none). ^hConditions: 10 mM sodium phosphate buffer, pH 7.00, 100 mM NaCl, [PNA] = 1.0 μM, and [DNA] = 1.2 μM.

PNA29 and PNA32 without other high-molecular-weight peaks suggests that the impurities are non-PNA related and should not interfere with the results. The sequences and characterization data of all modified apcPNA successfully synthesized are summarized in Table 1.

Thermal Stability of Modified apcPNA. Melting temperatures of the modified apcPNAs (PNA1–PNA33) are reported in Table 1. The simplest homothymine sequence (T₉) was chosen as a model sequence for initial studies. It should be noted that homothymine apcPNA binds to DNA to form only duplexes, and not as triplexes as observed in aegPNA.¹¹ Thermal stability (T_m) of hybrids between the homothymine PNA singly modified with hydroxyl modifiers attached to various linkers (PNA7–PNA11) and their complementary DNA sequence (dA₉) were in the range of 70.9–71.9 °C at a low salt concentration (0 mM NaCl) and 67.0–68.0 °C at a high salt concentration (100 mM NaCl), which were approximately 4–7 °C lower than that of unmodified apc/apcPNA (PNA1, 77.7 and 71.9 °C at 0 and 100 mM NaCl, respectively), irrespective of the nature of the linker. This could be explained by the steric effect of the modifiers that interferes with the DNA binding. However, amino-modified PNA (PNA2–PNA6) and

guanidine-modified PNA (PNA12–PNA14) showed comparable or even slightly increased T_m values compared to the unmodified PNA. This suggests that the amino and guanidino groups, which are likely to be fully protonated at neutral pH, can electrostatically interact with the negatively charged phosphate groups in the DNA backbone as previously observed in the case of similar cationic PNAs.^{27,30,51,57,68} This was confirmed by the salt dependence of T_m values. The amino and guanidino-modified PNAs showed much larger ΔT_m at low-salt than high-salt conditions ($\Delta T_m = +1.0$ to $+4.2$ °C at low salt and -3.9 to $+1.9$ °C at high salt). Much smaller difference was observed in the case of hydroxy-modified PNAs ($\Delta T_m = -6.8$ to -5.8 °C at low salt and -4.9 to -3.9 °C at high salt). At a high salt concentration, electrostatic interactions between the protonated amino and phosphate groups are expected to be diminished, which is fully consistent with the results. In view of a similar steric effect between the amino and hydroxyl modifiers, it is interesting to note that this electrostatic stabilization even dominated the steric effect, resulting in net stabilization of the PNA–DNA duplexes. The number of repeating units (2EG, 3EG, or 4EG) and type of linker ($-\text{CH}_2\text{CH}_2-$ or $-\text{OCH}_2\text{CH}_2-$) in the modifiers do not seem to have significant

effects to the thermal stability of PNA–DNA hybrids. In addition, CD spectra of complementary DNA hybrids of PNA6, PNA8, and PNA11 (Figure S56–S58) are similar to the CD spectra of unmodified PNA–DNA hybrids, suggesting that different modifiers did not significantly change the structures of the hybrids.

T_m data of singly modified mixed sequence PNA (GTA-GA^(NX)TCACT, PNA15–PNA22) with complementary DNA (Table 1) showed the same trend observed in homothymine PNAs (PNA1–PNA14), i.e., hydroxyl modifiers destabilize, whereas amino and guanidino modifiers stabilize the PNA–DNA duplexes. The data suggest the positively charged modifiers generally increase the binding affinity of the PNA to its complementary DNA regardless of sequence context. Importantly, the stabilizing effect is additive. As shown in a series of triply modified apcPNAs (PNA23–PNA28), increasing the number of amino or guanidino modifiers on the apcPNA backbone significantly increased the thermal stability of its DNA hybrids in comparison to singly modified PNA. For example, the DNA hybrids of triply amino-modified PNA25 (3 × AB) is thermally more stable than that of singly modified PNA18 (1 × AB) at both low- and high-salt conditions ($\Delta T_m = +12.6$ and $+6.8$ °C, respectively). Similarly, the DNA hybrid of PNA28 carrying three guanidino groups (3 × GB) is more thermally stable than that of PNA22 with only one guanidino group (1 × GB) ($\Delta T_m = +11.6$ and $+8.5$ °C, respectively). It could be noted that this additive effect is more clearly observed at low salt concentrations. However, triply and singly modified PNAs with hydroxy modifiers showed similar T_m values (Table 2).

Table 2. Thermal Melting Temperature (T_m) of Selected Singly and Triply-Modified Mixed-Sequence PNAs

| PNA ^a | modifiers (X) | 0 mM NaCl | | 100 mM NaCl | |
|------------------|---------------|-------------------------|--------------------------------|-------------------------|--------------------------------|
| | | T_m (°C) ^b | ΔT_m (°C) ^c | T_m (°C) ^b | ΔT_m (°C) ^c |
| PNA21 | HB | 59.3 | +1.9 | 53.5 | +0.9 |
| PNA27 | 3 × HB | 61.2 | | 54.4 | |
| PNA19 | H3EG | 56.4 | +1.9 | 53.5 | 0.0 |
| PNA26 | 3 × H3EG | 58.3 | | 53.5 | |
| PNA18 | AB | 66.1 | +12.6 | 58.3 | +6.8 |
| PNA25 | 3 × AB | 78.7 | | 65.1 | |
| PNA16 | A3EG | 63.2 | +11.6 | 55.4 | +7.8 |
| PNA24 | 3 × A3EG | 74.8 | | 63.2 | |
| PNA22 | GB | 67.1 | +11.6 | 58.3 | +8.5 |
| PNA28 | 3 × GB | 78.7 | | 66.8 | |

^aPNA sequence = Ac–GTAGA^(NX)TCACT–LysNH₂ or Ac–GT^(NX)AGA^(NX)TCA^(NX)CT–LysNH₂. ^bConditions: 10 mM sodium phosphate buffer, pH 7.00, 0, or 100 mM NaCl, [PNA] = 1.0 μM, and [DNA] = 1.2 μM. ^c $\Delta T_m = T_m(\text{triply modified PNA}) - T_m(\text{singly modified PNA})$.

Because the additional stabilization from electrostatic interaction in the cases of amino or guanidino-modified PNAs is nonspecific in nature, it was important to determine whether this may have negative impacts on the DNA binding specificity of the modified PNA. T_m values of hybrids between cationic PNAs with single mismatched DNA were also determined and compared with those of complementary DNA. From Figure 1, T_m of hybrids between the singly modified mixed sequence PNA with various linkers (butyl or ethylene glycol) and modification (hydroxy-, amino-, or guanidino-) (PNA16, PNA18, PNA19, PNA21, and PNA22) and single-mismatched DNA showed the same trend, whereby very low T_m values were observed

(the maximum T_m was 32.1 °C for some sequences). For triply modified PNA, the hydroxyl-modified PNA26 (H3EG) and PNA27 (HB) showed T_m of single mismatched hybrids of <30 °C, similar to singly modified PNA23. However, amino-modified PNA24 (A3EG), PNA25 (AB), and guanidino-modified PNA28 (GB) showed higher T_m values for single-mismatched hybrids (up to 46.8 °C). These results revealed that while amino- and guanidino-modified PNAs showed higher DNA affinity due to the electrostatic attraction, the same interaction can also stabilize the mismatched hybrids as well as the complementary hybrids. Nevertheless, when ΔT_m values were considered, it can be concluded that the modified PNA can still distinguish between full complementary and single mismatched in any cases with high specificity. This phenomenon was also observed in both low and high salt concentration (for the 0 mM NaCl result, see the Supporting Information). As shown in Figure 1, the presence of one mismatched base in the DNA strand resulted in substantial decrease in T_m values (ΔT_m range: –18.3 to –35.6 °C), indicating the high specificity of the DNA recognition by the modified PNA similar to unmodified PNA (ΔT_m range: –25.2 to –29.1 °C).

Solubility Measurement. The solubility of representative modified PNAs were evaluated by dissolving the PNA to a saturating concentration in water, and the concentration was determined by UV–vis spectrophotometry after centrifugation to remove excess PNA and appropriate dilution.¹⁵ Table 3 showed the saturating concentrations of representative modified PNAs compared to unmodified PNA. In general, all modified apcPNAs showed improved water solubility by more than 10-fold compared to unmodified apcPNA, although in some cases, the amount of PNA obtained was too small to obtain a saturating concentration; thus, only the lower limit of solubility was reported. To compare the influence of modifier to hydrophilicity, selected PNA with various modifiers were tested. Modified PNAs with poly(ethylene glycol) side chains (PNA3 and PNA8) were about 2-fold more soluble than the modified PNAs with alkyl side chains (PNA6, PNA11, and PNA14) regardless of end groups (amino or alcohol). It can therefore be concluded that the oligo(ethylene glycol) linker can enhance the water solubility more effectively than simple alkyl linkers. Thus, the modifier A3EG seems to be a good combination in terms of water solubility and DNA binding properties. This is in contrast to the case of atfcPNA,³¹ whereby the complete replacement of the cyclopentane ring in apcPNA by tetrahydrofuran ring in atfcPNA did not provide significant improvement in the water solubility.

In Vitro Cellular Uptake of Modified apcPNA. The cellular uptake of various modified PNAs carrying an *N*-terminal fluorescein label by HEK293T cells, a human embryonic kidney cell line, were observed by confocal laser scanning microscope (CLSM) and further quantified using flow cytometry. As shown in Figure 2, PNA33 with guanidinobutyl (GB) side chain showed the highest cellular uptake followed by PNA32 with aminobutyl (AB) modification. The CLSM image of the cells incubated with PNA33 in Figure 3 also showed an obvious green fluorescence signal of the fluorescein label in the cells, whereas the control cells (no PNA added) showed no detectable signal. The signal of the unmodified PNA sample was very weak, indicating a very low uptake level. Thus, the fluorescence images conformed well to the flow cytometry results.

CONCLUSIONS

In summary, we demonstrated a facile and general reductive alkylation strategy for post-synthetic modification of pyrrolidinyl

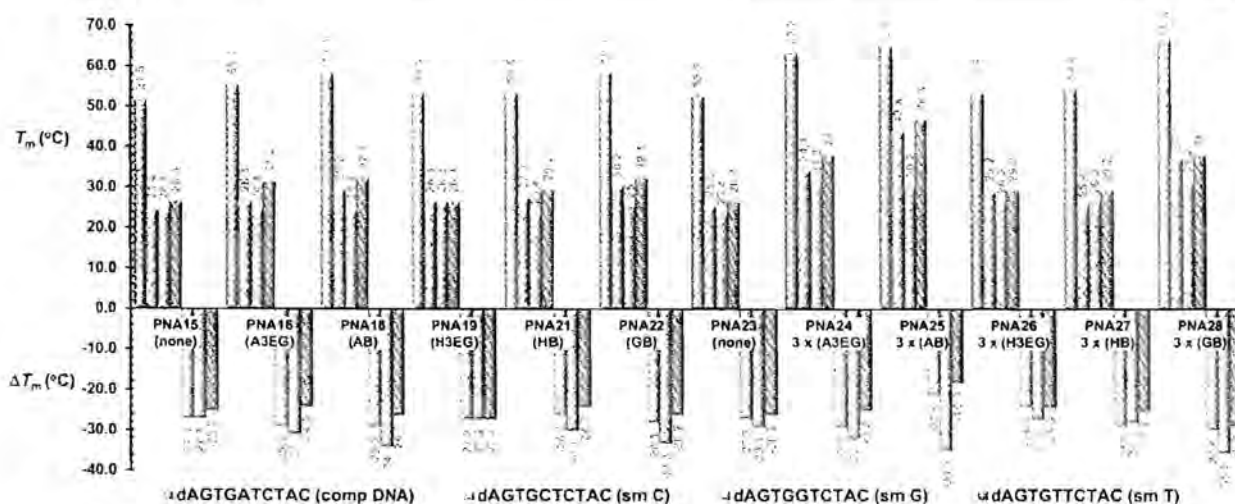


Figure 1. Thermal melting temperature (T_m) of modified acpcPNA (PNA15–PNA28) with complementary DNA (comp DNA) and single mismatched DNA (smC, smG, and smT). Conditions: 10 mM sodium phosphate buffer, pH 7.00, 100 mM NaCl, [PNA] = 1.0 μ M, [DNA] = 1.2 μ M, heating rate 1 $^{\circ}$ C/min; and $\Delta T_m = T_m - T_m(\text{complementary hybrid})$. Mismatch positions in the DNA sequences are indicated by underlining.

Table 3. Aqueous Solubility of Modified acpcPNAs

| PNA | modifier (X) | saturated concentration (mM) | saturated concentration (mg/mL) |
|-------------------------|--------------|------------------------------|---------------------------------|
| unmodified ^a | – | 3.3 \pm 0.2 | 10.5 \pm 0.6 |
| PNA3 | A3EG | 59.6 \pm 2.4 | 197.4 \pm 7.9 |
| PNA6 | AB | >12.0 \pm 0.2 | >39.0 \pm 0.7 |
| PNA8 | H3EG | 64.1 \pm 0.5 | 212.3 \pm 1.7 |
| PNA11 | HB | 31.8 \pm 0.9 | 103.4 \pm 2.9 |
| PNA14 | GB | >13.3 \pm 0.4 | >43.8 \pm 1.3 |

^aUnmodified acpcPNA; Ac–TTTTTTTT–LysNH₂.

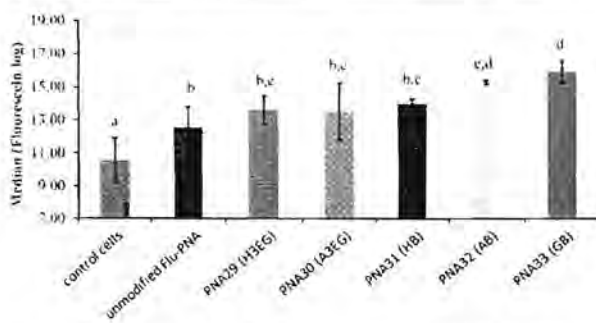


Figure 2. Cellular uptake levels of various PNA samples into the HEK293T cells after 6 h of incubation at the PNA concentration of 500 nM. In control cells, water was used in place of an aqueous PNA solution. PNA fluorescence intensity was obtained from flow cytometry analysis. Data represented means \pm SD ($n = 3$, from three independent experiments). Bar graphs with different superscript are significantly different ($p < 0.05$), per analysis by one-way analysis of variance with a Duncan test.

PNA backbone with hydrophilic modifiers consisting of a polar end group (hydroxy-, amino-, or guanidino-) and a linker (alkylene or oligo(ethylene glycol)) to provide a new class of hydrophilic pyrrolidinyl PNA. The advantage of this post-synthetic approach is that there is no need to separately synthesize new PNA building blocks, as generally required in other related reports,^{27,28,30,33} and various modifications can be

easily made without having to resynthesize the whole PNA sequence. The DNA binding affinities of these hydrophilic PNA were investigated by T_m measurement and compared with the unmodified PNA. The amino- and guanidino-modified PNAs bind more strongly to DNA than unmodified and hydroxyl-modified PNA, regardless of the linker type. This could be explained by electrostatic interaction between the positively charged protonated amino or guanidino groups and phosphate groups in the DNA, which was supported by the negative effect of salt concentration to the thermal stability of the PNA-DNA hybrids. The electrostatic interaction could also partly stabilize the mismatched hybrids, but the specificity of the DNA recognition by these modified PNAs is still retained as confirmed by the large decrease in T_m of mismatched compared to complementary hybrids in all cases. In addition, water solubility was increased by at least 10-fold in comparison to unmodified PNA. Furthermore, in vitro cellular uptake experiment demonstrated the cell permeable ability of these modified PNA. Triply modified PNA with positively charged guanidinobutyl (GB) and aminobutyl (AB) side chains showed enhanced cellular uptake relative to unmodified PNA or other triply modified PNAs. It can be further envisioned that a similar strategy can be used to add other functionalities to PNA and other related biomolecules. The ability to make small PNA that is intrinsically cell-penetrable without having to rely on other cell-permeable carrier would open up opportunities for pyrrolidinyl PNA to be used in cellular applications such as intracellular RNA sensing, specific gene detection, or antisense and antigen therapy.

EXPERIMENTAL SECTION

General Procedures. All reagent-grade chemicals and solvents were purchased from standard suppliers and were used without further purification. ¹H and ¹³C NMR spectra were recorded on Bruker Avance 400 NMR spectrometer operating at 400 MHz for ¹H and 100 MHz for ¹³C. RP-HPLC experiments were performed on a Waters Delta 600 HPLC system. Oligonucleotides were obtained from Pacific Science (Thailand) or BioDesign (Thailand).

Synthesis, Purification, and Characterization of Modified acpcPNA. The acp/acpcPNAs, Ac–TTTT^(apc)TTTT–LysNH₂,

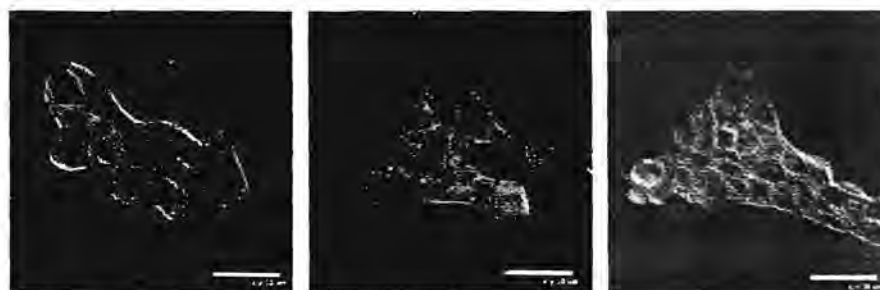


Figure 3. Confocal fluorescence images of HEK293T cells after being incubated with water (left), PNA33 (middle), and unmodified Flu-PNA (right) and then being fixed and stained with 4',6-diamidino-2-phenylindole (DAPI). Fluorescence detection was carried out with excitation and emission wavelengths of 405/450 (DAPI, shown in blue) and 488/525 nm (fluorescein-labeled PNA, shown in green); images shown are the merge of the bright field and the other two channels. Identical adjustments were applied to all images to allow a fair comparison. It should be noted that the DAPI staining was ineffective in the presence of a high concentration of PNA.

Bz-GTAGA^(apc)TCACT-LysNH₂, and Bz-GT^(apc)AGA^(apc)-TCA^(apc)CT-LysNH₂ were synthesized via solid-phase peptide synthesis on Tentagel S RAM resin according to the previously published protocol²⁷ (apc denotes substitution of apc with apc spacer). Lysinamide was also included at the C-terminus to allow a fair comparison with previous unmodified PNA. After the reaction was completed as monitored by MALDI-TOF mass spectrometry, the N-terminal Fmoc group was removed and the PNA was end-capped with acetyl or benzoyl group. In case of fluorescence-labeled PNA, the N-terminus of the PNA was coupled with 5(6)-carboxy-fluorescein N-hydroxysuccinimidyl ester on the solid-support. The nucleobase protecting groups (Bz, Ibu) for A, C, and G, and apc spacer protection (Tfa) were removed by heating with 1:1 aqueous ammonia-dioxane at 60 °C overnight. The apc/apcPNA was then reductively alkylated on the solid support with the aldehyde derivatives of modifier (X) in the presence of NaBH₃CN (2 equiv) and HOAc (2 equiv) in MeOH solution at rt for 4 h. The trityl- and Boc-protecting groups were deprotected in a cleavage step from solid support. The phthalimide protecting group was subsequently deprotected by 40% aqueous methylamine solution at rt for 3 h. The modified PNA was cleaved from the resin by treatment with trifluoroacetic acid (TFA) in dichloromethane and 10% triisopropylsilane (TIS) (500 μL × 30 min × 3). The cleavage solution was combined and dried under nitrogen gas, and the crude PNA was precipitated by addition of diethyl ether. The crude PNA was purified by RP-HPLC with linear gradient conditions using 9:1 of mobile phase A/B (A is 0.1% TFA in H₂O and B is 0.1% TFA in MeOH) for 5 min and gradient to 1:9 for 60 min. The combined purified PNA fractions were characterized by MALDI-TOF mass spectrometry (Microflex, BrukerDaltonics) using α-cyano-4-hydroxy-cinnamic acid (CCA) as a matrix.

UV Melting Experiments. The thermal stability (T_m) of all PNA-DNA hybrids was studied under the following conditions: [PNA], 1.0 μM and [DNA], 1.2 μM in 10 mM sodium phosphate buffer at pH 7.0 in the absence or presence of 100 mM NaCl. The A_{260} was measured on a CARY 100 Bio UV-vis spectrophotometer in steps from 20 to 90 °C with a temperature increment of 1.0 °C/min. The melting temperatures were obtained from first derivative plots between absorbance at 260 nm as a function of temperature.

Solubility Determination. The procedure for solubility determination was adapted from the literature.¹¹ The aqueous solubility was measured by adding a minimum amount of water into a microcentrifuge tube containing the lyophilized PNA at

20 °C, making sure that the solution is saturated with the PNA (some remaining insoluble solid was observed) and left until the dissolution reached equilibrium (the absorbance at 260 nm was no longer changed). Then, the sample was centrifuged at 14 000 rpm for 10 min to remove the excess insoluble PNA. The concentration of the supernatant was determined by measuring the UV absorption at 260 nm using a Nanodrop 2000 Spectrophotometer, and the solubility was calculated from the concentration and the initial volume of water added.

In Vitro Cellular Uptake of PNA. The cellular uptake of PNA into HEK293T cells was investigated using flow cytometry. HEK293T cells were seeded onto 24 well plates at a density of 7.5×10^4 cells per well and left to adhere overnight at 37 °C under 5% of CO₂ in the incubator. Then, the tested sample was added into the cells at final concentration of 500 nM and incubated at 37 °C for 6 h. After incubation, the old media was removed, and the cells were washed twice with phosphate-buffered saline (PBS). The cells were then harvested and resuspended in 500 μL of PBS. The suspension of cells was centrifuged at 3000g for 5 min at 4 °C. The supernatant was removed, and the cell pellet was resuspended with 100 μL of PBS. Finally, the obtained cell suspension was subjected to flow cytometry. The intracellular fluorescence signal of PNA was detected by flow cytometer (Cytomics FCS00MPL, Beckman Coulter Inc., NY) using $\lambda_{excite}/\lambda_{emit}$ values of 488/525 nm, of which 10 000 cells were being measured. The data were analyzed by FlowJo software (Tree Star, Inc.). Standard deviations were calculated from three replicates. Statistical analysis of data was performed by one-way analysis of variance with Duncan test (SPSS Inc., Chicago, IL). Differences were considered to be statistically significant at a level of $p < 0.05$.

To confirm the cellular uptake of PNA, the intracellular PNA was monitored using a CLSM. The HEK293T cells were seeded on an 8 well cell culture chamber slide at a density of 7.5×10^4 cells per well and left to adhere overnight. After that, the PNA sample was added into the cells at the final concentration of 500 nM and incubated at 37 °C for 6 h in the incubator. The cells were then washed twice with DMEM media containing 10% fetal bovine serum and fixed with 4% w/v paraformaldehyde for 10 min followed by washing with PBS. After that, 4',6-diamidino-2-phenylindole solution was added, and washing was carried out twice with PBS. Finally, intracellular PNA was imaged by CLSM (Nikon, Tokyo, Japan).

■ ASSOCIATED CONTENT

Supporting Information

The Supporting Information is available free of charge on the ACS Publications website at DOI: 10.1021/acs.bioconjchem.7b00308.

A table showing the sequence of modified PNA. Figures showing HPLC chromatograms, MALDI-TOF-MS analysis, UV-melting and first derivative plots, CD spectra, melting temperatures, and ^1H and ^{13}C NMR spectra. (PDF)

AUTHOR INFORMATION

Corresponding Authors

*E-mail: chaturongs@nu.ac.th. Phone: +66-55-963462. Fax: +66-55-963401.

*E-mail: thanesuan.nua@rmutr.ac.th. Phone: +66-81-4449908.

ORCID

Chaturong Suparpprom: 0000-0002-8885-3889

Notes

The authors declare no competing financial interest.

ACKNOWLEDGMENTS

We acknowledge financial supports from the Thailand Research Fund (DPG5780002 to T.V.), Research Fund for DPST Graduate with First Placement (grant no. 02/2555 to C.S.), and Ratchadapiseksomboj Endowment, Chulalongkorn University (postdoctoral fellowship to T.N.).

ABBREVIATIONS

peptide nucleic acid, PNA; aegPNA, *N*-2-aminoethylglycine PNA; acpcPNA, 2-amino cyclopentane carboxylic acid PNA; apcPNA, 3-aminopyrrolidine-4-carboxylic acid PNA; acbcPNA, 2-amino cyclobutane carboxylic acid PNA; atfcPNA, 2-amino tetrahydrofuran carboxylic acid PNA; aocPNA, 3-amino-oxetane-2-carboxylic acid PNA; $^{\text{R-MIP}}$ γ PNA, (*R*)-diethylene glycol ('mini-PEG') γ PNA; CPP, cell-penetrating peptides; EGFR, epidermal growth factor receptor; MCF-7, human breast adenocarcinoma cell line; Fmoc-OSu, *N*-(9-fluorenylmethoxycarbonyloxy) succinimide; IBX, 2-iodoxybenzoic acid; TrCl, trityl chloride; DMF, *N,N*-dimethylmethanamide; Pht, phthalimide group; Tfa, trifluoroacetyl group; Ibu, isobutryl group; Bz, benzoyl group; DAPI, 4',6'-diamidino-2-phenylindole; PBS, phosphate-buffered saline; TIS, triisopropylsilane; CCA, α -cyano-4-hydroxy-cinnamic acid; DMEM, Dulbecco's modified Eagle medium; CLSM, confocal laser scanning microscope; CD, circular dichroism; T_m , melting temperature; A260, absorbance at 260 nm

REFERENCES

- (1) Nielsen, P. E. (1999) Peptide nucleic acid. A molecule with two identities. *Acc. Chem. Res.* 32, 624–630.
- (2) Good, L., Sandberg, R., Larsson, O., Nielsen, P. E., and Wahlestedt, C. (2000) Antisense PNA effects in *Escherichia coli* are limited by the outer-membrane LPS layer. *Microbiology* 146, 2665–2670.
- (3) Gaglione, M., Milano, G., Chambery, A., Moggio, L., Romanelli, A., and Messere, A. (2011) PNA-based artificial nucleases as antisense and anti-miRNA oligonucleotide agents. *Mol. BioSyst.* 7, 2490–2499.
- (4) Egholm, M., Buchardt, O., Nielsen, P. E., and Berg, R. H. (1992) Peptide nucleic acids (PNA). Oligonucleotide analogs with an achiral peptide backbone. *J. Am. Chem. Soc.* 114, 1895–1897.
- (5) Pokorski, J. K., Witschi, M. A., Purnell, B. L., and Appella, D. H. (2004) *S,S*-trans-Cyclopentane-constrained peptide nucleic acids. A general backbone modification that improves binding affinity and sequence specificity. *J. Am. Chem. Soc.* 126, 15067–15073.
- (6) Govindaraju, T., Kumar, V. A., and Ganesh, K. N. (2005) (*SR/RS*)-Cyclohexanyl PNAs: Conformationally preorganized PNA analogues with unprecedented preference for duplex formation with RNA. *J. Am. Chem. Soc.* 127, 4144–4145.
- (7) Dragulescu-Andrasi, A., Rapireddy, S., Frezza, B. M., Gayathri, C., Gil, R. R., and Ly, D. H. (2006) A simple γ -backbone modification preorganizes peptide nucleic acid into a helical structure. *J. Am. Chem. Soc.* 128, 10258–10267.
- (8) Kitamatsu, M., Takahashi, A., Ohtsuki, T., and Sisido, M. (2010) Synthesis of pyrrolidine-based oxy-peptide nucleic acids carrying four types of nucleobases and their transport into cytoplasm. *Tetrahedron* 66, 9659–9666.
- (9) Worthington, R. J., and Micklefield, J. (2011) Biophysical and cellular-uptake properties of mixed-sequence pyrrolidine-amide oligonucleotide mimics. *Chem. - Eur. J.* 17, 14429–14441.
- (10) Vilaivan, T., Suparpprom, C., Harnyuttanakorn, P., and Lowe, G. (2001) Synthesis and properties of novel pyrrolidinyl PNA carrying-amino acid spacers. *Tetrahedron Lett.* 42, 5533–5536.
- (11) Vilaivan, C., Srisuwannaket, C., Ananthanawat, C., Suparpprom, C., Kawakami, J., Yamaguchi, Y., Tanaka, Y., and Vilaivan, T. (2011) Pyrrolidinyl peptide nucleic acid with α/β -peptide backbone: A conformationally constrained PNA with unusual hybridization properties. *Artif. DNA PNA XNA* 2, 50–59.
- (12) Vilaivan, T., and Srisuwannaket, C. (2006) Hybridization of pyrrolidinyl peptide nucleic acids and DNA: Selectivity, base-pairing specificity, and direction of binding. *Org. Lett.* 8, 1897–1900.
- (13) Vilaivan, T. (2015) Pyrrolidinyl PNA with α/β -dipeptide backbone: From development to applications. *Acc. Chem. Res.* 48, 1645–1656.
- (14) Mansawat, W., Vilaivan, C., Balázs, A., Aitken, D. J., and Vilaivan, T. (2012) Pyrrolidinyl peptide nucleic acid homologues: Effect of ring size on hybridization properties. *Org. Lett.* 14, 1440–1443.
- (15) Sahu, B., Sacui, I., Rapireddy, S., Zanotti, K. J., Bahal, R., Armitage, B. A., and Ly, D. H. (2011) Synthesis and characterization of conformationally preorganized, (*R*)-diethylene glycol-containing γ -peptide nucleic acids with superior hybridization properties and water solubility. *J. Org. Chem.* 76, 5614–5627.
- (16) Koppelhus, U., and Nielsen, P. E. (2003) Cellular delivery of peptide nucleic acid (PNA). *Adv. Drug Delivery Rev.* 55, 267–280.
- (17) Shiraishi, T., and Nielsen, P. E. (2012) Nanomolar cellular antisense activity of peptide nucleic acid (PNA) cholic acid ("umbrella") and cholesterol conjugates delivered by cationic lipids. *Bioconjugate Chem.* 23, 196–202.
- (18) Shiraishi, T., Bendifallah, N., and Nielsen, P. E. (2006) Cellular delivery of polyhetero aromatic-peptide nucleic acid conjugates mediated by cationic lipids. *Bioconjugate Chem.* 17, 189–194.
- (19) Morris, M. C., Gros, E., Aldrian-Herrada, G., Choob, M., Archdeacon, J., Heitz, F., and Divita, G. (2007) A non-covalent peptide-based carrier for in vivo delivery of DNA mimics. *Nucleic Acids Res.* 35, e49.
- (20) Shiraishi, T., and Nielsen, P. E. (2011) Peptide nucleic acid (PNA) cell penetrating peptide (CPP) conjugates as carriers for cellular delivery of antisense oligomers. *Artif. DNA PNA XNA* 2, 90–99.
- (21) Kilk, K., and Langel, U. (2005) Cellular delivery of peptide nucleic acid by cell-penetrating peptides. *Methods Mol. Biol.* 298, 131–141.
- (22) Bonora, G. M., Drioli, S., Ballico, M., Faccini, A., Corradini, R., Cogoi, S., and Xodo, L. (2007) PNA conjugated to high-molecular weight poly(ethylene glycol): Synthesis and properties. *Nucleosides, Nucleotides Nucleic Acids* 26, 661–664.
- (23) Bergmann, F., Bannwarth, W., and Tam, S. (1995) Solid phase synthesis of directly linked PNA-DNA-hybrids. *Tetrahedron Lett.* 36, 6823–6826.
- (24) Uhlmann, E., Will, D. W., Breipohl, G., Langner, D., and Rytte, A. (1996) Synthesis and properties of PNA/DNA chimeras. *Angew. Chem., Int. Ed. Engl.* 35, 2632–2635.
- (25) Finn, P. J., Gibson, N. J., Fallon, R., Hamilton, A., and Brown, T. (1996) Synthesis and properties of DNA-PNA chimeric oligomers. *Nucleic Acids Res.* 24, 3357–3363.
- (26) Van der Laan, A. C., Brill, R., Kuimelis, R. G., Kuyil-Yeheskiely, E., van Boom, J. H., Andrus, A., and Vinayak, R. (1997) A convenient automated solid-phase synthesis of PNA-(*5'*)-DNA-(*3'*)-PNA chimera. *Tetrahedron Lett.* 38, 2249–2252.

- (27) Zhou, P., Dragulescu-Andrasi, B., Bhattacharya, B., O'Keefe, H., Vatta, P., Hyldig-Nielsen, J., and Ly, D. H. (2006) Synthesis of cell-permeable peptide nucleic acids and characterization of their hybridization and uptake properties. *Bioorg. Med. Chem. Lett.* 16, 4931–4935.
- (28) Dragulescu-Andrasi, A., Zhou, P., He, G., and Ly, D. H. (2005) Cell-permeable GPNA with appropriate backbone stereochemistry and spacing binds sequence-specifically to RNA. *Chem. Commun.* 2, 244–246.
- (29) Thomas, S. M., Sahu, B., Rapireddy, S., Bahal, R., Wheeler, S. E., Procopio, E. M., Kim, J., Joyce, S. C., Contrucci, S., Wang, Y., et al. (2013) Antitumor effects of EGFR antisense guanidine-based peptide nucleic acids in cancer models. *ACS Chem. Biol.* 8, 345–352.
- (30) Mitra, R., and Ganesh, K. N. (2012) Aminomethylene peptide nucleic acid (am-PNA): Synthesis, regio-/stereospecific DNA binding, and differential cell uptake of (α/γ ,R/S)am-PNA analogues. *J. Org. Chem.* 77, 5696–5704.
- (31) Kumar, P., and Jain, D. R. (2015) C γ -Aminopropylene peptide nucleic acid (amp-PNA): chiral cationic PNAs with superior PNA:DNA/RNA duplex stability and cellular uptake. *Tetrahedron* 71, 3378–3384.
- (32) Arayachukiat, S., Seemork, J., Pan-In, P., Amornwachirabodee, K., Sangphech, N., Sansureerungsikul, T., Sathornsantikun, K., Vilaivan, C., Shigyou, K., Picnpinijtham, P., et al. (2015) Bringing macromolecules into cells and evading endosomes by oxidized carbon nanoparticles. *Nano Lett.* 15, 3370–3376.
- (33) Kanokudom, S., Vilaivan, T., Wikan, N., Thepparit, C., Smith, D. R., and Assavalapsakul, W. (2017) miR-21 promotes dengue virus serotype 2 replication in HepG2 cells. *Antiviral Res.* 142, 169–177.
- (34) Sriwarom, P., Padungros, P., and Vilaivan, T. (2015) Synthesis and DNA/RNA binding properties of conformationally constrained pyrrolidinyl PNA with a tetrahydrofuran backbone deriving from deoxyribose. *J. Org. Chem.* 80, 7058–7065.
- (35) Seankongsuk, P., Vchirawongkwin, V., Bates, R. W., Padungros, P., and Vilaivan, T. (2017) Enantioselective synthesis of (2S,3S)-epioxetin and its incorporation into conformationally constrained pyrrolidinyl PNA with an oxetane backbone. *Asian J. Org. Chem.* 6, 551–560.
- (36) Reenabthue, N., Boonlua, C., Vilaivan, C., Vilaivan, T., and Suparpprom, C. (2011) 3-Amino pyrrolidine-4-carboxylic acid as versatile handle for internal labeling of pyrrolidinyl PNA. *Bioorg. Med. Chem. Lett.* 21, 6465–6469.
- (37) Dangsoon, A., Poomsuk, N., Siriwong, K., Vilaivan, T., and Suparpprom, C. (2016) Synthesis and fluorescence properties of 3,6-diaminocarbazole-modified pyrrolidinyl peptide nucleic acid. *RSC Adv.* 6, 74314–74322.
- (38) Ditmangklo, B., Boonlua, C., Suparpprom, C., and Vilaivan, T. (2013) Reductive alkylation and sequential reductive alkylation-click chemistry for on-solid-support modification of pyrrolidinyl peptide nucleic acid. *Bioconjugate Chem.* 24, 614–625.
- (39) Strulson, M. K., Johnson, D. M., and Maurer, J. A. (2012) Increased stability of glycol-terminated self-assembled monolayers for long-term patterned cell culture. *Langmuir* 28, 4318–4324.
- (40) Nasopoulou, M., Georgiadis, D., Matziari, M., Dive, V., and Yiotakis, A. (2007) A versatile annulation protocol toward novel constrained phosphinic peptidomimetics. *J. Org. Chem.* 72, 7222–7228.
- (41) Eriks, J. C., van der Goot, H., Sterk, G. J., and Timmerman, H. (1992) Histamine H₂-receptor agonists. Synthesis, in vitro pharmacology, and qualitative structure-activity relationships of substituted 4- and 5-(2-aminoethyl)thiazoles. *J. Med. Chem.* 35, 3239–3246.
- (42) Ngamwiriawong, P., and Vilaivan, T. (2011) Synthesis and nucleic acids binding properties of diastereomeric aminoethylprolyl peptide nucleic acids (aepPNA). *Nucleosides, Nucleotides Nucleic Acids* 30, 97–112.
- (43) Shymanska, N. V., An, H. I., and Pierce, J. G. (2014) A rapid synthesis of 4-oxazolidinones: Total synthesis of synoxazolidinones A and B. *Angew. Chem., Int. Ed.* 53 (21), 5401–5404.
- (44) Expósito, A., Fernández-Suárez, M., Iglesias, T., Muñoz, L., and Riguera, R. (2001) Total synthesis and absolute configuration of minalemine A, a guanidine peptide from the marine tunicate *Didemnum rodriguessi*. *J. Org. Chem.* 66, 4206–4213.
- (45) Taura, Y., Tanaka, M., Wu, X.-M., Funakoshi, K., and Sakai, K. (1991) Asymmetric cyclization reactions. Cyclization of substituted 4-pentenals into cyclopentanone derivatives by rhodium(I) with chiral ligands. *Tetrahedron* 47, 4879–4888.
- (46) Menger, F. M., Lu, H., and Lundberg, D. (2007) A-B-A-B-A Block amphiphiles. Balance between hydrophilic and hydrophobic segmentation. *J. Am. Chem. Soc.* 129, 272–273.
- (47) Jain, D. R., Anandj V, L., Lahiri, M., and Ganesh, K. N. (2014) Influence of pendant chiral Cy-(alkylideneamino/guanidino) cationic side-chains of PNA backbone on hybridization with complementary DNA/RNA and cell permeability. *J. Org. Chem.* 79, 9567–9577.
- (48) Shrestha, A. R., Kotobuki, Y., Hari, Y., and Obika, S. (2014) Guanidine bridged nucleic acid (GuNA): An effect of a cationic bridged nucleic acid on DNA binding affinity. *Chem. Commun.* 50, 575–577.